DEVELOPMENT OF BACTERIAL TRANSCRIPTION INHIBITORS TARGETING THE RNA POLYMERASE CLAMP-HELICES REGION

ZHENG YINGBO

PhD

The Hong Kong Polytechnic University

2023

The Hong Kong Polytechnic University

Department of Applied Biology and Chemical Technology

Development of Bacterial Transcription Inhibitors Targeting the RNA Polymerase Clamp-Helices Region

ZHENG YINGBO

A thesis submitted in partial fulfillment of the requirements for the Degree of Doctor of Philosophy

June 2023

CERTIFICATE OF ORIGINALTIY

I hereby declare that this thesis is my own work and that, to the best of my knowledge and belief, it reproduces no material previously published or written nor material which has been accepted for the award of any other degree or diploma, except where due acknowledgement has been made in the text.

_____ _____ (Signed)

_____ZHENG YINGBO_____ (Name of student)

Acknowledgement

First of all, I would like to express my sincere gratitude to my supervisor, Dr. Ma Cong, for his kindness and patience on guiding and supporting me throughout my PhD career. Dr. Ma gave me valuable suggestion and advice on my research project, which helped me so much to achieve progress on research capacities in my PhD studies.

Nest then, I would like to thank my colleagues in Dr. Ma Cong's research group, including Dr. Tang Bocheng, Mr. Lam Long Yin, Mr. Chan King Hong, Mr. Chu Wai Chun, Mr. Liu Jiang and Miss. Ke Sinyu for your assistance on lab issues and suggestion on my research project.

Meanwhile, I would like to express gratitude to Prof. Yang Xiao and her team for their contribution and assistance on biological testing of my research project, especially to Prof. Yang Xiao for her kindness and care on my life in Hong Kong.

Finally, I would like to thank my parents and my girlfriend for their support and encourage during my PhD career.

Abstract

Bacterial infection has been identified as the primary cause of several common human diseases. Classic antibiotics, which experienced “the golden age” in the mid-twentieth century, have become inefficient due to the rapid development of antibiotic-resistant bacteria. N protein utilization substance G (NusG) is an essential bacterial factor that regulates transcription, including elongation and termination processes. As a conserved transcription factor, its interactions with RNA polymerase (RNAP) have been observed to maintain a consistent binding model across different bacteria. Considering these features, their interactions have the potential to serve as a novel and promising target for the discovery of small-molecule antibiotics.

The discovery and rational design of antibiotics targeting the protein-protein interactions (PPIs) between NusG and RNAP are based on the X-ray crystal structure of *E. coli* NusG in complex with RNAP. We generated four pharmacophores from predicted key residues on clamp helices of the β' subunit of RNAP (β'-CH) which contribute to the formation of PPIs with NusG. Using this pharmacophore model, we conducted the virtual screening to discover a promising lead compound, **AW00783**, from the drug-like MiniMaybridge database. Testing its antimicrobial activities revealed a minimum inhibitory concentration (MIC) value of 256 μg/mL against Gram-positive strains. Modifications to this lead compound have been classified into two categories: aminoethyl and aromatic derivatives. Seventy-two compounds have been synthesized and tested for their antimicrobial activities against selected Gram-positive and Gram-negative strains.

Among these derivatives, most exhibited antimicrobial activities against Gram-positive strains, while only specific compounds from the aminoethyl derivatives showed activities against Gram-negative strains. Compound **GI-36** from aminoethyl derivatives exhibited the best antimicrobial activity against Gram-negative *Escherichia Coli* with the MIC value of 8 μg/mL. Meanwhile, compound **GII-16** from aromatic derivatives showed the best activity with the MIC value of 1 μg/mL

against Gram-positive *Staphylococcus aureus*. SARs analysis was conducted on these derivatives, predicting the trifluoromethyl and hydroxy groups that contribute to interactions with RNAP. In silico docking simulation displayed the possible docking models of candidate compounds, including **GI-19**, **GI-36**, **GI-39** and **GII-16**. Although their docking models showed some differences, it provided structural evidence supporting the hypothesis of necessary functional groups targeting the clamp helices.

Further cytotoxicity assay and fluorescence microscopy experiment were conducted on candidate compounds from the aminoethyl derivatives. *In vitro* cytotoxicity assay demonstrated their mild cytotoxicity, with a 50% cytotoxic concentration (CC_{50}) value of 10-40 μM. Additionally, fluorescence microscopy demonstrated that these candidate compounds were capable of disrupting the normal localization of bacterial transcription complexes at the cellular level. They were also tested and found to exhibit good antimicrobial activities against selected *Bacillus subtilis* strains.

Abbreviation

CRBD, Comprehensive Antibiotic Resistance Database

WHO, World Health Organization

PDB, Protein Data Bank

CLSI, Clinical & Laboratory Standards Institute

RNA, ribonucleic acid

DNA, deoxyribonucleic acid

ntDNA, non-template DNA

mRNA, message RNA

rRNA, ribosomal RNA

RNAP, RNA polymerase

Pol II, RNA Polymerase II

β'-CH, the clamp helices of b' subunit of RNAP

β-GL, the gate loop of *b* subunit of RNAP

ops, operon polarity suppressor

nut, N protein utilization

PBS, primary RNA binding site

SBS, secondary RNA binding site

Nus, N protein utilization substance

TEC, transcription elongation complex

DSIF, DRB sensitivity-inducing factor

PPIs, protein-protein interactions

hGH, human growth hormone

hGHbp, extracellular domain of hGH's first bound receptor

IL-2, interleukin 2

IL2-αR, interleukin 2 α receptor

SC, sliding clamp

SSB, single-stranded DNA binding protein

Exo I, exonuclease I

Bam, *β*-barrel assembly machine

TA, toxin-antitoxin

PAINS, pan assay interference compounds

ADMET, absorption, distribution, metabolism, and excretion-toxicity in pharmacokinetics

cryo-EM, cryo-microscopy

CX-MS, crosslinking-mass spectrometry

HTS, high-throughput screening

SARs, structure-activity relationships

MIC, minimum inhibitory concentration

CC_{50}, 50% cytotoxic concentration

BBB, blood brain barrier

PPB, plasma protein binding

WT, wild type

Trp, tryptophan

Tyr, tyrosine

Arg, arginine

Ile, isoleucine

Phe, phenylalanine

Leu, leucine

Glu, glutamicacid

Gln, glutamine

Met, methionine

Asn, asparagine

Asp, asparticacid

His, histidine

Ser, serine

Lys, lysine

o-, *ortho-*

m-, *meta-*

p-, *para-*

DIPEA, N,N-diisopropylethylamine

EtOH, ethanol

THF, tetrahydrofuran

DMSO, dimethylsulfoxide

Et_3N, triethylamine

DCM, dichloromethane

DMF, dimethylformamide

X-Phos, dicyclohexyl[2′,4′,6′-tris(propan-2-yl)[1,1′-biphenyl]-2-yl]phosphane

TsOH, p-toluenesulfonic acid

MeOH, methanol

DEAD, diethyl azodicarboxylate

BINAP, 2,2′-bis(diphenylphosphino)-1,1′-binaphthyl

EDCI, 1-ethyl-3-(3-dimethylaminopropyl)carbodiimide

4-DMAP, 4-dimethylaminopyridine

Xantphos, (9,9-dimethyl-9H-xanthene-4,5-diyl)bis(diphenylphosphane)

TI, therapeutic index

GFP, green fluorescence protein

NMR, Nuclear Magnetic Resonance

HPLC, High Performance Liquid Chromatography

TBAB, tetrabutyl-ammonium bromide

EA, ethyl acetate

NMP, methylpyrrolidone

NBS, N-bromosuccinimide

$Pd_2(dba)_3$, tris(dibenzylideneacetone)dipalladium

CLSI, Clinical and Laboratory Standards Institute

MHB, Mueller–Hinton broth

ELISA, Enzyme-Linked Immunosorbent Assays

PK, pharmacokinetics

Table of Contents

Chapter I:

Introduction

1.1 History and predicament of the discovery on antibiotics

After the identification of bacteria as infectious agents of various diseases such as cholera, pulmonary tuberculosis, and tetanus in the late 19th century, scientists dedicated themselves to finding effective preventive and therapeutic approaches against these pathogens. From the 1940s to the 1960s, a multitude of antibiotics were successfully discovered, which continue to serve as fundamental therapies against bacterial infections to this day [1]. Currently, there are 22 approved categories of antibiotics for clinical treatment, classified based on their chemical structures and mechanisms of action against bacteria [2]. These antibiotics primarily function through three major mechanisms: disrupting membrane permeability, interfering with cell wall synthesis, and inhibiting the synthesis of functional proteins [3]. However, the discovery of novel antibiotics significantly slowed down after the 1960s and has made little progress in the 21st century.

Unfortunately, the widespread use of classical antibiotics has led to the emergence of antibiotic-resistant bacteria at an alarming rate, resulting in a noticeable decline in their effectiveness against these pathogens. The Comprehensive Antibiotic Resistance Database (CRBD) has identified resistance information for 377 pathogens and 21,079 chromosomes [4]. In 2017, the World Health Organization (WHO) published an essential list of antibiotic-resistant "priority pathogens," comprising 12 families of Gram-positive and Gram-negative bacteria. These pathogens have been proven to pose a severe threat to human health due to their resistance to multiple classical antibiotics [5]. Furthermore, modified derivatives of classical antibiotics often share the same mechanisms of action as their parent compounds, leading to multidrug resistance and cross-resistance when these derivatives are employed, further

diminishing their antimicrobial activities [6][7]. Consequently, there is a demand for novel antibiotics that target other essential cellular processes in bacteria. Compared to antibiotics derived from natural products, fluoroquinolones, a category of small-molecule antibiotics produced through chemical synthesis, exhibit superior membrane penetration and a broad spectrum of antimicrobial activity [8]. It is predicted that the rational design of small-molecule compounds targeting essential cellular processes in bacteria will be a preferred approach for the discovery of novel antibiotics.

1.2 Bacterial transcription and transcription factors

Transcription, the fundamental process of gene expression, occurs in all three domains of life: archaea, bacteria, and eukaryotes. It involves three main steps: initiation, elongation, and termination (**Figure 1**) [9]. During initiation, RNA polymerase (RNAP) recognizes the promoter region on the DNA template. Elongation involves the synthesis of the RNA molecule, and termination marks the release of the completed transcript from the DNA template. RNAP, is the key enzyme responsible for transcription and is composed of five subunits, termed as 2α, β, β' and ω. Two categories of antibiotics have been developed that target bacterial transcription: fidaxomicin and rifampicin. Fidaxomicin, derived from natural products, disrupts the formation of the promoter complex, thereby inhibiting the initiation process [10]. However, the precise binding model of fidaxomicin remains unknown, and its narrow antimicrobial spectrum limits its further optimization.

Rifampicin, another antibiotic targeting transcription, has been extensively studied. It binds to a cleft surrounding the active site of RNAP. Once bound, it blocks the construction of the third phosphodiester bond in the nascent RNA, effectively interrupting the elongation process [11]. However, rifampicin does not inhibit elongation when the RNA transcript has already become longer [12]. Despite its effectiveness, the widespread occurrence of antibiotic resistance and cross-resistance to its derivatives have posed significant limitations on further optimization and clinical use of rifampicin.

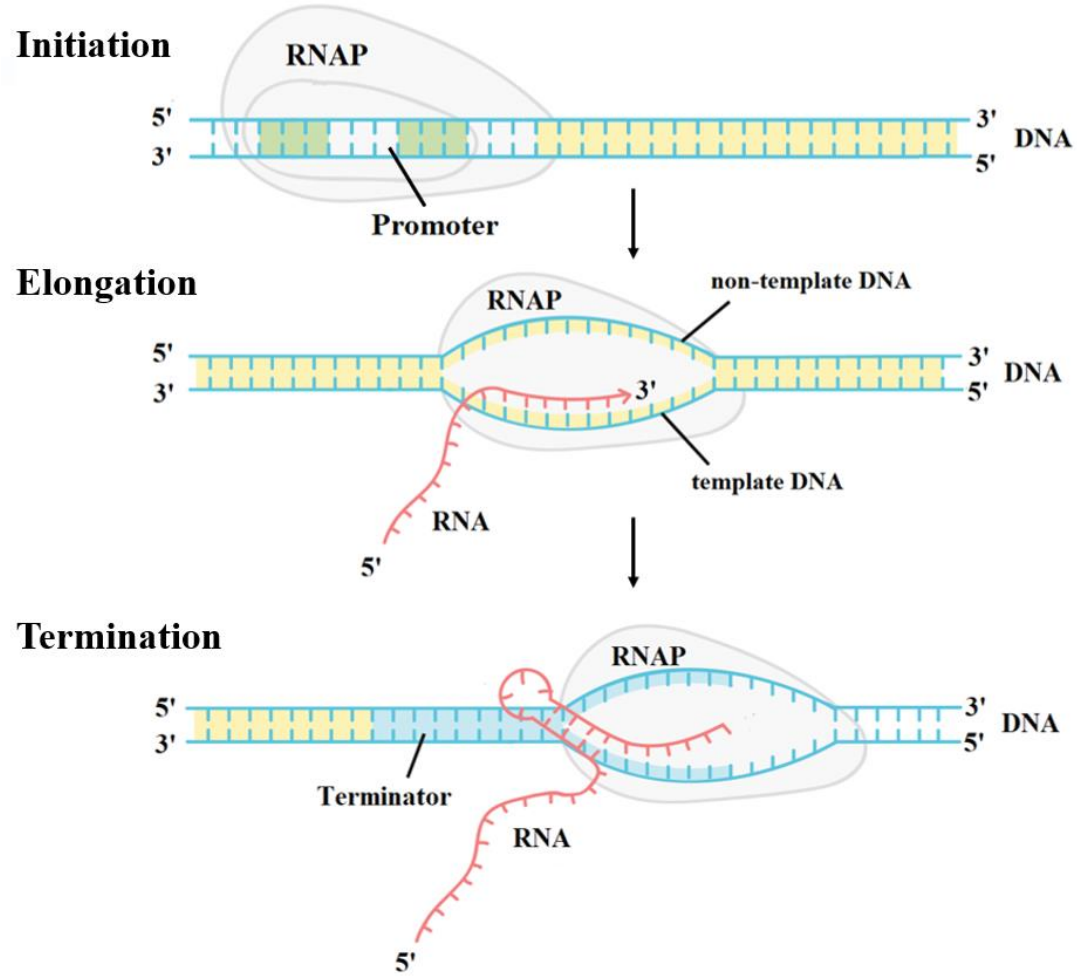

Figure 1. The three general steps of transcription.

Indeed, the proper functioning of RNA polymerase (RNAP), the key enzyme during transcription, relies on the formation of specific transcription complexes at each phase, which requires the recruitment of multiple transcription factors. These transcription factors represent promising targets for the rational design of novel small-molecule antibiotics.

1.3 NusG: a conserved transcription factor in bacteria

Through *in vitro* studies on transcription in bacteriophage lambda, it was observed that RNA transcript synthesis initiates at early promoters pL and pR An unfolded protein called N protein was identified to bind to the *boxB* sequence of the *nut* site in nascent P_L and P_R transcripts [13]. The proper function of the N protein requires several

transcription factors known as Nus factors, including NusA, NusB, NusE, and NusG, which participate in the formation of transcription complexes [14]. Among the Nus factors, NusG is the only conserved factor found in all three domains of life [15].

nusG gene was first sequenced in *Escherichia coli* in 1990, encoding a polypeptide consisting of 181 amino acids with a molecular weight of 20.5 kDa [16]. In 2002, the first crystallized NusG protein was purified from *Aquifex aeolicus* (PDB ID: 1M1G), exhibiting approximately 47% sequence identity to *E. coli* NusG [17]. NusG protein in *A. aeolicus*, apart from an 80-residue insertion compared to its *E. coli* homolog, consists of two conserved domains connected by a linker region, namely the N-terminal NGN domain and the C-terminal KOW domain (**Figure 2**). The NGN domain exhibits similarities to the ribonucleoprotein motif, forming an α-β sandwich structure composed of a four-stranded antiparallel β-sheet covered by two α-helices [18]. Meanwhile, the KOW domain consists of two major β-sheets and is homologous to the RL24 ribosomal protein identified by Kyrpides [19]. Over the following decades, NusG proteins purified from various bacteria demonstrated that these two conserved domains maintain the same crystal structures [20][21][22].

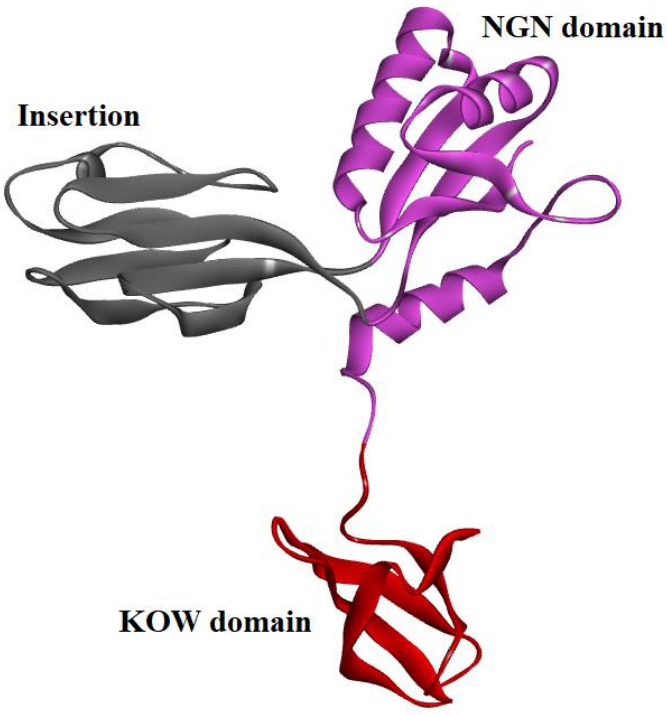

Figure 2. The three-dimensional structure of NusG protein purified from *A. aeolicus*. The conserved domains have been termed as NGN (in purple) and KOW (in red). Compared with NusG in *E. coli*, an 80-residue insertion was detected to build an extra domain, being colored in grey.

Afterward, there was a growing demand for obtaining crystal structures of NusG in complex with its target proteins to gain insights into its functional mechanisms. Subsequent research has revealed that the NGN domain of NusG interacts with two components of RNAP, the clamp helices on its β' subunit (β'-CH) [23] and the gate loop on its β subunit (β-GL) [24]. On the other hand, the KOW domain of NusG contacts a hydrophobic pocket in Rho, a hexameric helicase involved in transcription termination [25], as well as the NusE protein [26], which is also known as protein S10 in the 30S ribosomal subunit [27]. These essential interactions were possibly related with NusG's function on transcription processes, which would be described in the following sections together with crystallographic studies on NusG.

1.3.1 Contribution on the transcription elongation

In 2016, the first single-particle electron cryo-EM structure of RNAP in complex with NusG from *E. coli* was successfully crystalized, and its corresponding Protein Data Bank (PDB) ID is 5TBZ (**Figure 3A**) [28]. In addition to the expected interactions involving the NGN domain of NusG and RNAP, the structure revealed the presence of an additional α-helix in the linking region between the two conserved domains of NusG. This α-helix was found to contact the β-protrusion of RNAP **(Figure 3B and 3C)**. Notably, the α-helix within the NGN domain established interactions with the middle portion of the β'-CH helices of RNAP, potentially forming stable interactions between multiple residues from both polypeptides.

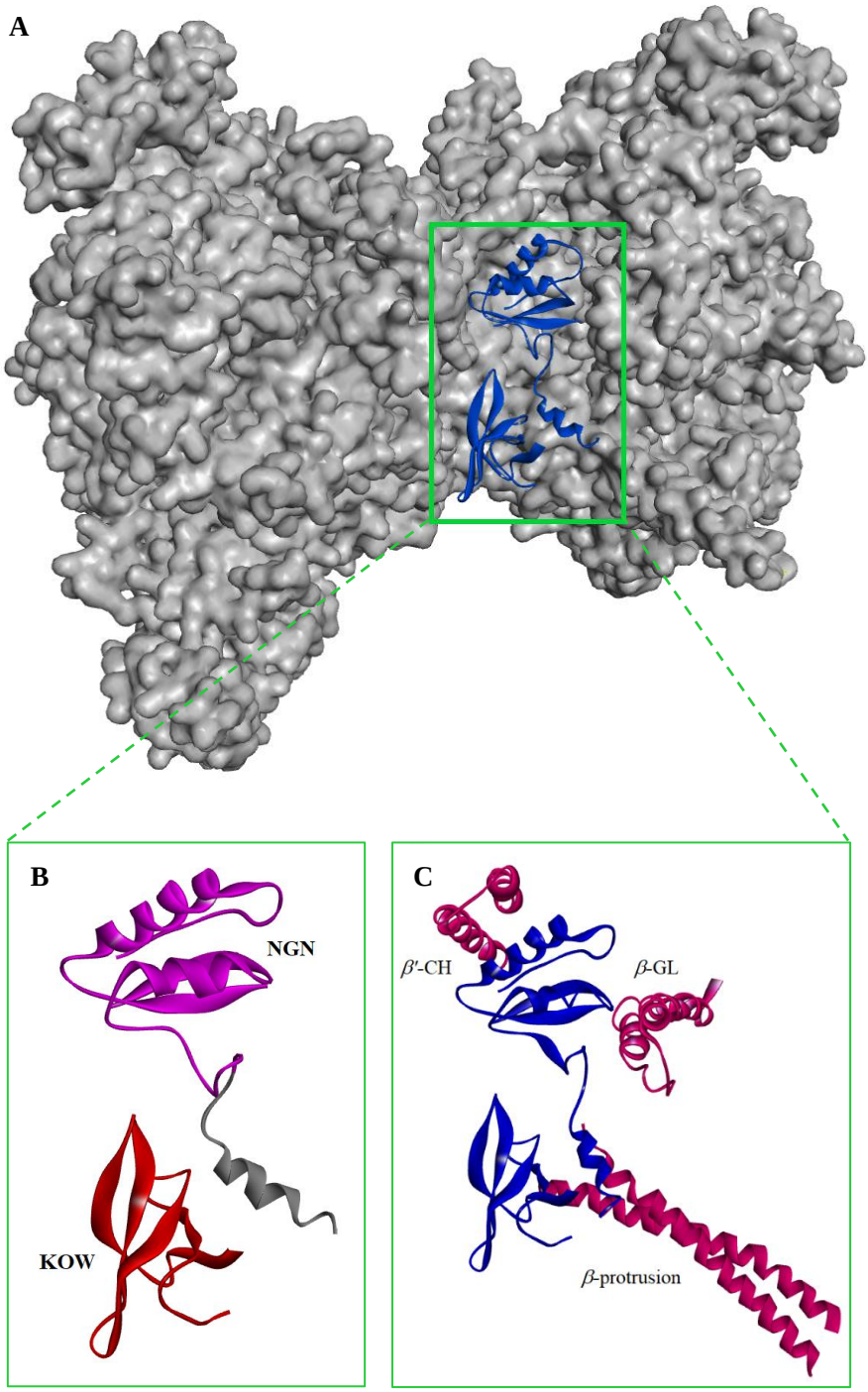

Figure 3. A): The cryo-EM crystal structure of *E. coli* RNAP (displayed with soft solid surface in grey) in complex with NusG (in blue). Their interacting region was marked in a green square; **B)**: NusG protein being isolated from the complex, displaying their conserved domains, NGN in purple and KOW in red. Apart from two conserved domains, the extra α-helix in the linking region was colored in grey; **C)**: The amplified contact region of NusG with RNAP (in magenta) being marked. The binding model with β'-CH displayed cross-like interactions on its middle

proportion. The other two components of RNAP interacting with NusG was also displayed.

The N protein has been identified as playing a role in transcription antitermination in most characterized lambdoid phages, except for phage HK022 [29]. When RNAP passes through the *nut* site on the nascent P_L and P_R mRNA transcripts, the N protein binds to this site and interacts with RNAP and transcription factors to form a transcription elongation complex (TEC) that is insensitive to downstream terminators [30]. However, it was necessary to investigate whether NusG also participates in the TEC through its interactions with RNAP to promote transcription antitermination.

Mason *et al.* conducted run-off transcription assays *in vitro*, to detect the mRNA transcript generation in the presence or absence of NusG within the entire TEC [31]. The results showed a significant decrease in the amount of mRNA fragments distal to the *nut* site when NusG was absent. This finding suggested that the recruitment of NusG into the TEC allows transcription to proceed over more base pairs downstream of the *nut* site, promoting processivity. In 2017, the transcription antitermination complex in phage lambda, consisting of double-stranded DNA and RNA transcript at the *nut* site was crystallized, and its corresponding PDB ID is 5MS0 (**Figure 4A**) [32]. This complex was also confirmed by chemical cross-linking mass spectrometry (CX-MS) analysis. The NGN domain of NusG, maintaining its α-β sandwich structure, was positioned near the entrance of the upstream DNA. Notably, compared to the previous complex (PDB ID: 5TBZ), the binding model with RNAP displayed some differences. The *α-β* sandwich structure underwent a rotation that caused the *a*-helix facing the *β′*-CH to move closer to the contact region of the *β*-GL with the upstream DNA **(Figure 4B)**. The linking *a*-helix moved towards the *β′*-CH rather than the *β*-protrusion. Additionally, the presence of the RNA-DNA hybrid caused the *β*-protrusion to be displaced away from NusG. Genome-wide studies have indicated that NusG is recruited by RNAP as transcription elongation progresses [33]. This suggests that NusG functions as an essential component in the formation of the TEC, contributing to the transcription antitermination mechanism.

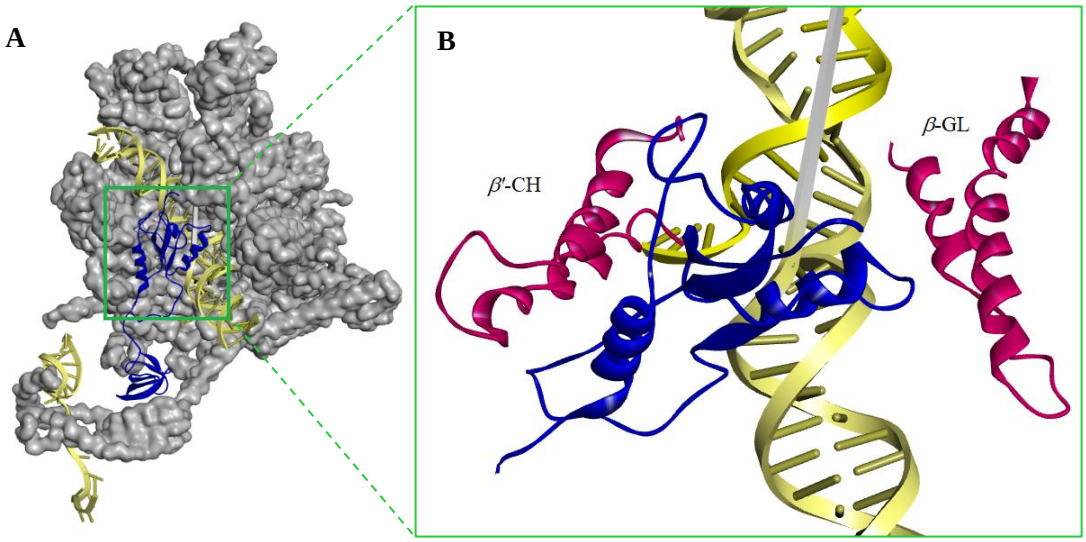

Figure 4. A): The X-ray crystal structure of the TEC in phage lambda with the existence of DNA-RNA hybrid. NusG was colored in blue, whose binding sites with RNAP (displayed with soft solid surface in grey) was marked in a green square. And the DNA-RNA hybrid was colored in pale yellow backbone with base pairs; **B)**: The amplified binding region of NGN domain with RNAP (in magenta) close to the entrance of upstream DNA. The α-helix on its linking region contacted with the β'-CH of RNAP while the α-β sandwich faced towards the β-GL.

During transcription elongation, RNAP can exist in two alternative conformational states: the active state and the paused state [34]. In the active state, RNAP efficiently synthesizes the RNA transcript and progresses along the DNA template. However, in the paused state, RNAP undergoes structural changes that result in a temporary halt in transcription. Further research and crystallographic studies are necessary to uncover the precise mechanisms by which NusG participates in transcription pausing and to provide a more comprehensive understanding of its functions in this process.

1.3.2 Inhibition of NusG on the backtracking pausing event

Once transcription is initiated, RNAP forms stable associations with the nascent RNA and elongates the transcription until it encounters pause sites. Pausing events during transcription can be classified into three major categories: elemental pause, backtracking of RNAP, and hairpin-dependent pause [35]. Elemental pause is a short-lived pause that occurs frequently in bacteria [36]. It involves transient isomerization of

RNAP on specific sites, which inhibits the loading of nucleotides into the transcription bubble. Elemental pauses do not have strong sequence specificity and are not typically the target for regulatory factors. However, they can potentially induce the formation of long-lived pauses in the other two categories [37]. Backtracking is a pausing mechanism where RNAP undergoes a reverse translocation along the template DNA, leading to the exclusion of the 3' end of the nascent RNA from the transcription site [38]. Transcription can only resume when the backtracked RNAP cleaves the old RNA and forms a new 3' end for the nascent RNA. Single-molecule studies of transcription by *E. coli* RNAP have shown that backtracking can result in long-lived pauses with lifetimes over 20 seconds [39]. Hairpin-dependent pause is characterized by the formation of a hairpin structure at specific nucleotide sequences upstream of the pause site on the nascent RNA. This hairpin structure interacts with RNAP, inhibiting the loading of nucleotides and promoting the release of the nascent RNA [40]. Unlike the first two pausing events, the formation of a hairpin structure is often associated with intrinsic termination in bacteria [41].

The study conducted by Herbet *et al.* [42] [43] using single-molecule transcription assays provided insights into the potential effects of NusG on transcription pausing. They compared the density and lifetime of pauses in the presence or absence of NusG, with specific external loads applied to eliminate backtracking. The results showed that the addition of NusG reduced the density of long-lived pauses, suggesting its role in modulating pausing events. In 2016, Turtola and Belogurov [44] identified two mismatches on the nucleotides located at positions 10 and 11 upstream of the template DNA, which were shown to prolong the lifetime of backtracking. By using photo-crosslinking techniques to label the template DNA with different probes, they observed that NusG prevented the DNA duplex with 11 upstream nucleotides from melting, providing a mechanism for NusG to inhibit backtracking pauses. Based on these studies, it is predicted that NusG can be recruited by RNAP as it passes through the pause site during bacterial transcription, and it exerts effects on pausing events.

In 2022, a crystallographic study revealed the structure of RNAP in complex with

NusG and a 9-base pair RNA-DNA hybrid [45]. This study compared the interactions between NusG and RNAP with or without swiveled subunits at different angles. Compared with its interactions with no-swiveled RNAP, which was proved active (PDB ID: 7PY8), it demonstrated that NusG could bind with RNAP in a swiveled conformation at an angle of up to 4.4° (PDB ID: 7PY0, **Figure 5A**), which is associated with a paused state [46]. In the binding model, it was observed that although the β-subunit of RNAP exhibited a rotation and moved away from NusG in the swiveled structure (**Figure 5B**), the location of the β' subunit and NGN domain remained conserved. The NGN domain of NusG occupied a cavity close to the entrance of the DNA duplex and was surrounded by β'-CH and β-GL of RNAP and the upstream DNA. This binding model resembled the interaction observed in the phage lambda system [32]. Facing the double-stranded DNA, the positively charged surface of the α-β sandwich structure in NGN was predicted to stabilize the upstream DNA. This suggests a potential mechanism for NusG in inhibiting backtracking pauses by stabilizing the DNA structure **(Figure 5C)**.

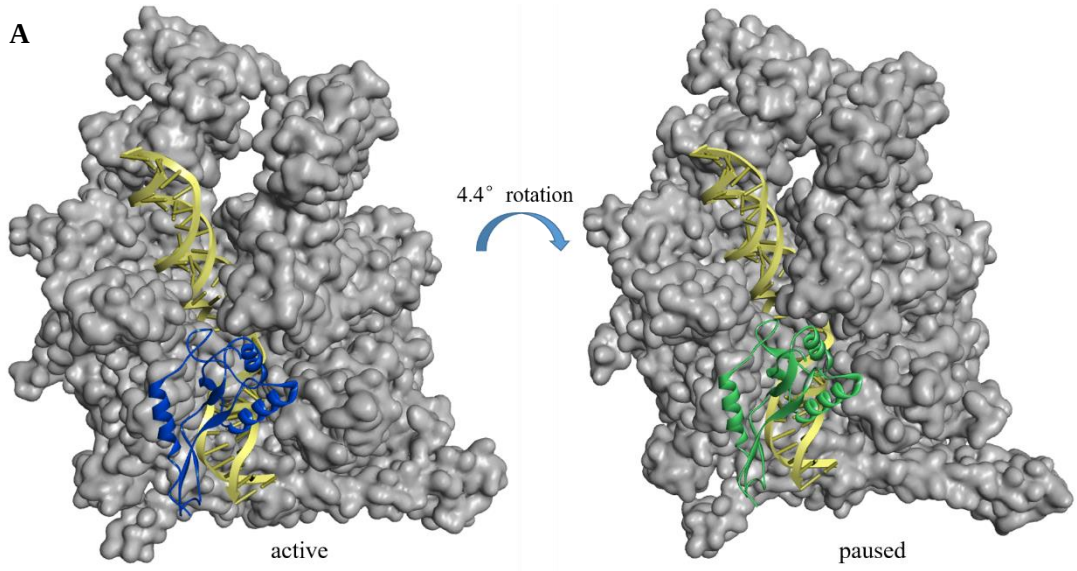

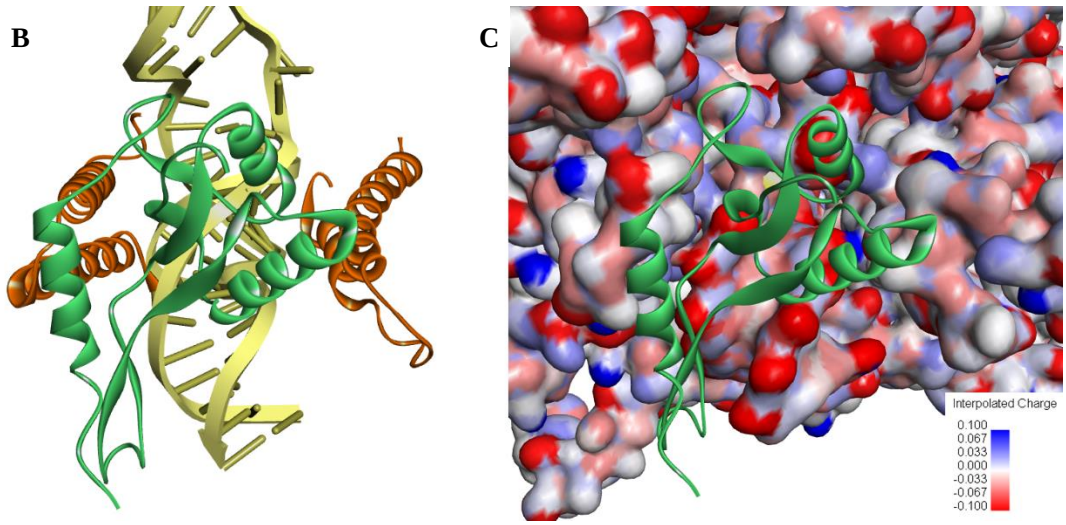

Figure 5. A): The three-dimensional crystal structure of the active and paused RNAP (both displayed with soft solid surface in grey) in complex with NusG. The paused RNAP was detected to swivel at the largest angle of 4.4° in comparison of the active one. The NusG proteins in both complexes (blue in the active one and green in the paused) showed the similar crystal structure and binding model; **B)**: The amplified binding model of NGN domain (in green) with paused RNAP (in brown). It was close to the entrance of duplex DNA (displayed in pale yellow backbone with base pairs) and contacted with β'-CH and β-GL of RNAP; **C)**: The cavity occupied by NGN domain, displaying negatively charged surface on the upstream DNA duplex. Surface of the cavity was colored by interpolated charge (negative in red and positive in blue) and the NGN domain was displayed in green ribbon. β'-CH and β-GL of RNAP together with DNA formed this cavity to fit for the NGN domain of NusG.

Previous studies have provided evidence that NusG is recruited by RNAP and plays a beneficial role in bacterial transcription elongation. Once recruited, the NGN domain of NusG interacts with the β'-CH and β-GL of RNAP, both in its active and paused state. The NGN domain of NusG adopts a conserved α-β sandwich structure, which maintains a stable configuration and stabilizes the positively charged surface of its binding cavity. Through these protein-protein interactions (PPIs), NusG functions as an essential factor within the transcription elongation complex (TEC) and exerts an inhibitory effect on backtracking pausing events.

1.3.3 Stimulation of NusG on Rho-dependent termination

Factor-dependent termination is a category of transcription termination that requires specific termination factors. One well-studied termination factor is Rho, which is an ATP-dependent hexameric helicase belonging to the RecA family [47]. Rho recognizes a specific site on the 3’ end of the nascent RNA, known as the *rut* site. Upon binding to the *rut* site, which contains cytosine-rich sequences, Rho initiates factor-dependent termination [48]. Rho undergoes an isomerization process, transitioning from an open-ring configuration to a closed state. It then moves along the RNA in the 5' to 3' direction until it encounters RNAP to terminate transcription [49]. Rho contains two RNA binding sites known as the primary RNA binding site (PBS) and the secondary RNA binding site (SBS) [50]. When Rho interacts with *rut* sites that have lower cytosine levels, referred to as suboptimal sites, the isomerization process slows down due to weaker interactions with the nascent RNA at the PBS. In such cases, additional elements are required to facilitate the termination process.

In 1992, Sullivan and Gottesman [51] utilized NusG deletion strains and mutants that induced premature termination at Rho-dependent sites. They observed that the deletion of NusG led to increased expression of promoters located upstream of Rho-dependent sites, indicating the indispensable role of NusG in Rho-dependent termination. Furthermore, Burns and Richardson [52] investigate the direct interaction between NusG and Rho and its effects on termination at specific sites. They focused on three Rho-dependent terminators, *tiZ1*, *tiZ2* and *tR1*. In the absence of NusG, Rho exhibited higher efficiency in releasing RNA from the complex at tR1 compared to *tiZ1*. Moreover, by using function-defective mutants of Rho, they found that NusG had no effect on *tiZ1*, *tiZ2*, or *tR1* when the levels of nucleoside triphosphates (NTPs) were high. However, when NTP levels were lowered, NusG specifically restored the termination efficiency at *tiZ1*. These findings suggest that the kinetic constraints of Rho at different termination sites account for the functional specificity of NusG. Additionally, it was observed that NusG accelerates the release of the transcript from the termination complex, contributing to termination efficiency.

Previous research has elucidated that the interactions between Rho and NusG are crucial for NusG's role in Rho-dependent termination. In 2018, the cryo-EM structure of Rho in complex with the KOW domain of NusG from *E. coli* was reported (PDB ID:6DUQ). This structure revealed that the KOW domain of NusG interacts with the last three α-helices of motor domain on Rho **(Figure 6)** [53]. In the absence of NusG, mutants with specific amino acid substitutions in these three helices exhibited a more rapid transition to the closed state compared to wild-type Rho. This suggests that these residues in wild-type Rho contribute to the formation of an autoinhibitory configuration that restricts isomerization but is remodeled upon NusG binding. The interactions between NusG and Rho activate Rho-dependent termination by facilitating the isomerization of Rho from an open-ring configuration to its closed state.

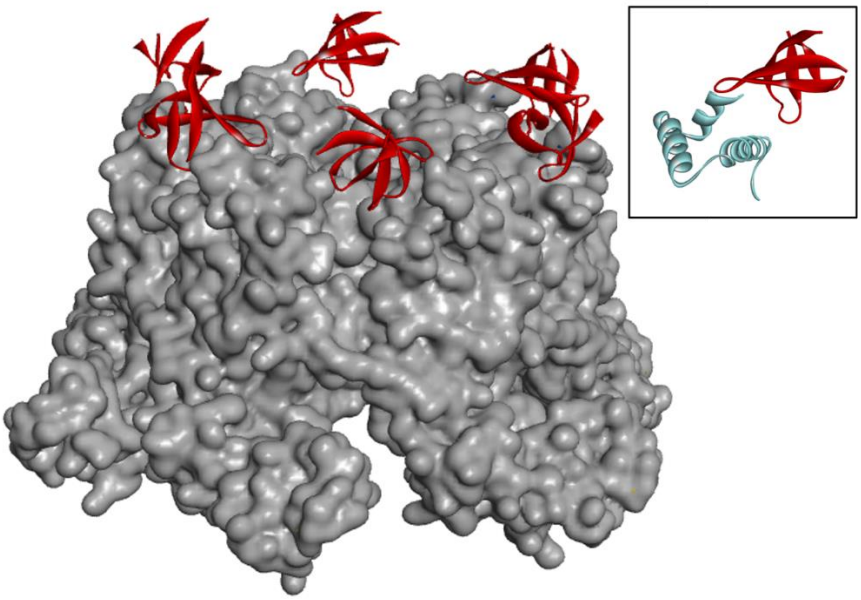

Figure 6. The cryo-EM structure of the KOW domain of NusG (in red) in complex with Rho (displayed with soft solid surface in grey). In the top right panel, one of motor domains in Rho (in cyan) was amplified to exhibit interactions with KOW.

Importantly, it has been demonstrated that the KOW domain of NusG interacts with NusE, also known as ribosomal protein S10, within the TEC isolated from phage

lambda [32]. This suggests that the KOW domain can dissociate from the TEC and subsequently bind to Rho when RNAP encounters the Rho-dependent termination site. Moreover, the interaction with NusE provides NusG with the potential to exert effects on protein translation.

1.3.4 NusG' s performance on transcription-translation coupling

Several decades ago, it was established that protein translation occurs in synchrony with transcription, facilitating the production of functional proteins based on mRNA [54]. This phenomenon, known as transcription-translation coupling, has been shown to play a vital role in regulating gene expression in bacteria. In 2018, the interaction between NusG and the mature 70S ribosome was detected using size exclusion chromatography and pelleting assays [55]. Additionally, based on the identified binding model between NusG and ribosomal protein S10, specific mutations were introduced in both proteins to demonstrate that NusG still interacts with S10 within this complex. Bailey *et al.* established an *in vitro* biochemical system using *E. coli* ribosomal subunit S30 (containing the S10 component) and a template DNA encoding luciferase reporter to investigate the transcription-translation coupling [56]. Comparing the WT NusG, the usage of purified NGN domain and a NusG mutant (carrying a mutation in the KOW domain) resulted in a significant decrease in luciferase reporter expression. Conversely, in a translation-only system where the DNA was replaced with an mRNA encoding the luciferase reporter, the purified NGN domain and the KOW mutant had minimal effect on luciferase expression. The inhibition of decoupled transcription-translation on transcription suggested that the interactions between NusG and ribosomal protein S10 are beneficial for transcription elongation but have no direct effect on translation. Further investigations are required to fully understand the mechanisms underlying transcription-translation coupling and NusG's impact on this process.

1.4 Homologs of NusG in eukaryotes

In the late 1990s, homologous proteins to NusG were identified in *Saccharomyces cerevisiae*, known as Spt5 [57], and in HeLa cells, where the Spt5 homolog functions as the p160 subunit in DSIF [58]. While these homologs in eukaryotes contain residues identical to NusG in prokaryotes, they exhibit an inhibitory effect on transcription elongation by stabilizing the eukaryotic RNA Polymerase II (Pol II) in a paused state [59]. Unlike NusG, Spt5 is composed of one NGN domain and five linked KOW motifs (six KOW motifs in its homologous p160 subunit) [60]. The NGN domain has been shown to interact with Spt4, also known as the p14 subunit in DSIF, near the transcription bubble. Additionally, the KOW domains of Spt5 interact with distinct regions on Pol II [61]. Since 2017, multiple X-ray crystal structures of the Pol II in complex with Spt5 had been reported, comprising different categories of transcription factors. In the complex without other factors (PDB ID: 5OIK), the α-β sandwich structure remains conserved as observed in bacterial homologs. However, it faces the upstream DNA and forms a clamp structure with KOW1 to trap the upstream DNA. [62]. KOW4 and KOW5 are positioned close to the exit tunnel of the nascent RNA and occupy a cleft formed by a stalk-like subunit of Pol II, along with KOW2 and KOW3. Crystal structures purified in complex with other transcription factors reveal additional binding sites of Spt5 with these additional factors [63] [64] [65]. The crystallographic studies on Spt5 suggest that the eukaryotic homologs of NusG exhibit more complex binding models and exert additional unknown effects when recruited by Pol II.

1.5 The discovery of PPIs inhibitors

1.5.1 The potential of PPIs acting as targets for novel drugs

Protein-protein interactions (PPIs) play crucial roles in various biological processes and have emerged as promising targets for the development of new drugs. However,

the discovery of small-molecule drugs targeting PPIs has historically been challenging due to the often large and flat interfaces of PPIs [66]. Furthermore, unlike enzymes with well-defined active sites for natural ligands, identifying binding sites on PPIs for potential drugs has been difficult in early studies. In 1995, Clackson and Wells conducted mutational studies on specific residues in the binding domain of hGH and hGHbp and found that only a few mutations reduced the binding affinity between these proteins [67]. This observation suggested that certain key residues play a critical role in PPIs, rather than all residues in the binding domain. Key residues are typically found in the core domain of PPIs and can form a binding pocket of approximately 300-500 $Å^2$ for small-molecule compounds [68]. Analysis of a database of alanine mutants in heterodimeric protein-protein complexes revealed that specific amino acids such as Trp, Tyr, and Arg are more likely to act as key residues [69]. These residues often engage in various interactions with small-molecule compounds, including hydrogen bonds, electrostatic interactions, and π stackings. Studies on inhibitors targeting the PPI between interleukin 2 (IL-2) and interleukin 2 α receptor (IL2-αR) have shown that a small-molecule compound called **SP4206** exhibits affinity for key residues on IL-2 similar to IL2-αR [70]. Over the subsequent decades, significant progress has been made in the discovery of novel inhibitors targeting various types of PPIs.

Strategies for discovering novel drugs targeting PPIs vary depending on the participation domains of the proteins involved and can be categorized into three groups (**Figure 7**) [71]. In cases where the partner protein contributes to the PPI by a linear sequence of six to nine amino acid residues, the interface is more accessible for small-molecule compounds [72]. However, many PPIs are formed through the secondary structure of the partner protein, such as *α*-helix or *β*-sheet [73]. Key residues in these PPIs may not be adjacent to each other in the primary sequence. The potential binding pocket based on these key residues is often more flexible than the primary epitopes [74]. Moreover, when the partner protein interacts with the main protein in discontinuous binding sites, it is considered a tertiary epitope, which represents the

most challenging targets for drug design [75]. Several novel inhibitors targeting PPIs have been approved or have entered clinical trials, with many of them being developed as anti-tumor agents. These inhibitors, whether small molecules or natural products, tend to be highly lipophilic molecules.

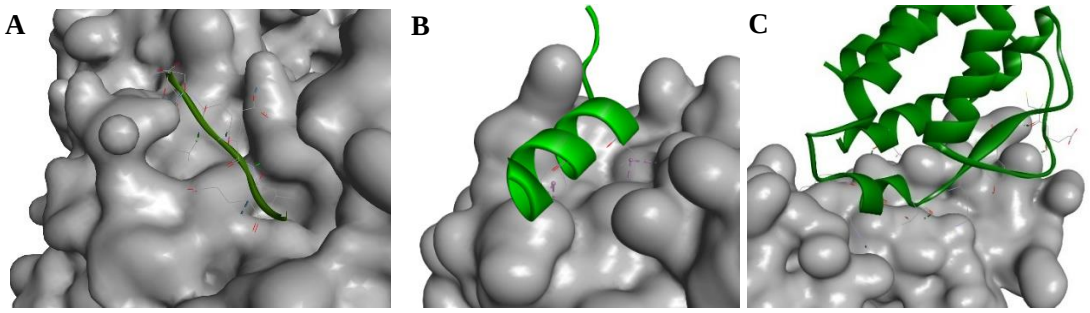

Figure 7. The three categories of partner protein participating in PPIs. **A**): a primary epitope with a linear sequence in 9 residues of DNA polymerase III (in dark green) binding with the SC (PDB ID: 3D1F) shown with soft solid surface in grey; **B**): a secondary epitope with an a-helix of FtsZ (in light green) constructing the PPIs with ZipA (PDB ID: 1F47) shown with soft solid surface in grey; **C**): a tertiary epitope in which continuous binding sites between IL-2 (in grass green) and IL2-αR shown with soft solid surface in grey were detected (PDB ID: 1Z92).

1.5.2 Progress on the discovery of antibiotics targeting on PPIs

PPIs also play essential roles in bacterial growth and division. Thousands of PPIs have been identified in well-studied bacteria such as *Escherichia coli*, *Pseudomonas aeruginosa*, *Synechocystis spp*., *Bacillus subtilis* and *Streptococcus pneumoniae*. The discovery of novel antibiotics targeting PPIs has evolved through five approaches in recent years: (i) bacterial division, (ii) DNA replication, (iii) bacterial membrane function, (iv) translation agents, (v) bacterial transcription. A brief introduction to the first four categories was presented in this session.

(i) Bacterial division: Multiple PPIs involved in bacterial division are unique to prokaryotes. Cell division involves the cooperative invagination of the cytoplasmic membrane and the reconstruction of the peptidoglycan cell wall. PPIs between FtsZ and ZipA play an essential role in this bacterial process. Inhibition of these PPIs has

been found to block cell division and the association of protofilaments into bundles [76]. Analysis of the X-ray crystal structure of FtsZ binding with ZipA (PDB ID: 1F47) revealed that an *a*-helix of FtsZ forms PPIs with ZipA through three key residues, Ile374, Phe377 and Leu378 [77]. Through high-throughput screening (HTS) and subsequent modifications, Kenny *et al.* discovered candidate compounds exhibiting moderate antimicrobial activities [78]. However, off-target activity was detected through fluorescence polarization studies, limiting the further clinical trials of these inhibitors.

(ii) Bacterial DNA replication: DNA replication requires multiple proteins to replicate chromosomal information, separate the double-stranded DNA, terminate replication, and repair replication errors. Previous research has focused on the sliding clamp (SC) protein hub and single-stranded DNA binding protein (SSB). In bacteria, the SC surrounds the double-stranded DNA and recruits multiple DNA polymerases, including polymerases I, II, III, IV and V [79], to form a protein hub with multiple PPIs. Although the SC is conserved in bacteria, it differs from its eukaryotic homolog [80], providing possibilities for discovering novel antibiotics that target PPIs in this SC protein hub. The X-ray crystal structure of SC binding with DNA polymerase III, crystallized in 2008, revealed that a conserved primary sequence of polymerase III comprising 9 residues, participates in the PPIs (PDB ID: 3D1F) [81]. Through HTS, one rhodanine-like compound was obtained and co-crystallized with the SC from *E. coli*. It was found that this compound occupied a similar binding site to the linear sequence of DNA polymerase III (PDB ID: 3D1G). However, the rhodanine-like structure has been identified as a PAINS structure that causes cytotoxicity to normal cells [82]. Nonetheless, this discovery holds promising prospects for the development of inhibitors targeting PPIs in the SC protein hub. Further screening based on the binding site of the rhodanine-like compound led to the identification of multiple small-molecule and peptide inhibitors.

Another essential protein in DNA replication is SSB, which binds to single-stranded DNA to prevent replication from stalling [83] and also recruits multiple partner proteins,

such as exonuclease I (Exo I) [84]. PPIs between Exo I and two linear sequences on the C-terminal of SSB were identified through co-crystallization (PDB ID:3C94) , and their function in replication was found to be associated with DNA mismatch repair [85]. Keck *et al.* employed high-throughput fluorescence polarization screening and identified four hits, termed as **CFAM**, **BCBP**, **BOTP** and **MPTA** [86]. Co-crystallization of these compounds with Exo I was conducted and yielded two X-ray structures of **CFAM** and **BCBP**. They were found to occupy the binding site B between Exo I and SSB, although alanine mutations on the primary sequence indicated that this site is not necessary for PPI construction [87]. While these compounds exhibited inhibition of Exo I activity, further research is required to understand their inhibitory mechanism on the PPIs between Exo I and SSB.

(iii) Bacterial membrane function: Gram-negative bacteria possess an outer membrane that acts as a selective permeation barrier, leading to intrinsic resistance to antibiotics [88]. A network of β-barrel outer membrane proteins is transported to the outer membrane through various pathways, involving PPIs between functional proteins. PPIs in the β-barrel assembly machine (Bam) complex have been targeted on the discovery of novel antibiotics. In Bam complex, BamA was found to bind conservatively with BamD in the Gram-negative bacteria [89]. Two binding sites were identified through X-ray structure co-crystallization of BamA with BamD (PDB ID:5D0Q), both formed by secondary structures of BamD [90]. The binding site surrounded by residues Ser769 to Trp776 of BamA was shown to be necessary for interactions with BamD [91]. In 2020, Li Y *et al.* conducted a yeast two-hybrid assay to screen over 25,000 compounds and identified a promising inhibitor named **IMB-H4**, with the MIC value ranging from 4 to 32 μg/mL against different *E. coli* strains. However, further testing is required to determine its direct inhibition of the PPIs between BamA and BamD.

(iv) Translation agents: The discovery of novel antibiotics targeting bacterial translation has been associated with toxin-antitoxin (TA) systems in recent years. TA systems are known to regulate self-inhibition of cell growth in bacteria, and certain

TA systems also function in bacterial translation to exert effects, including VapBC family, HicBA, PemK-like protein family, and HipAB [92]. Peptide antibiotics targeting PPIs between toxins and antitoxins have been discovered based on crystal structures of these TA systems. Unlike small-molecule antibiotics, peptide inhibitors mimic the binding interface of partner proteins to competitively disrupt the formation of PPIs.

1.5.3 Discovery of novel antibiotics targeting on PPIs in bacterial transcription

As mentioned above, RNAP serves as a key enzyme that regulates bacterial transcription in conjunction with various transcription factors. During the initiation step, the Sigma factor (σ) is essential for recognizing specific promoters by interacting with RNAP [93]. While bacteria exhibit multiple paralogs, the major σ factor has been identified as conserved in both Gram-positive and Gram-negative bacteria, lacking homologs in eukaryotes [94]. Targeting the PPIs between σ and RNAP holds promise for the discovery of novel antibiotics with a broad antibacterial spectrum. In the complex of σ factor with RNAP in *Thermus thermophilus*, it has been observed that the N-terminal domain-2 of the σ factor binds to the *β'* subunit of RNAP (PDB ID: 1IW7, **Figure 8A**) [95]. ELISA-based binding tests have identified Glu166, Gln165, and Met169 on the σ factor as key residues contributing to these PPIs [96]. Similarly, Arg264, Arg267, and Arg270 on the *β'* subunit of RNAP have also been found to be essential. Notably, Arg264 and Arg267 form hydrogen bonds with key residues on the σ factor, while Arg270, along with Leu271 and Ile280, creates a hydrophobic pocket. Lewis *et al.* constructed a pharmacophore model based on the key residues of the σ factor and conducted screening, resulting in the identification of three hits with an indole-like structure. Through gel electrophoresis and isothermal titration calorimetry experiments *in vitro*, a compound called **GKL003** (**Figure 8B**) was found to competitively bind to the *β'* subunit of RNAP, thereby disrupting the PPIs. However, **GKL003** exhibited poor inhibition of cell growth in both Gram-positive and Gram-negative bacteria (＞1mM). Building upon this study, Ma C *et al.*

optimized the pharmacophores based on key residues of the *β'* subunit of RNAP and performed virtual screening on the MiniMaybridge database, which contains 530,000 compounds [97]. Among the 27 hits obtained from the screening, compound **C5** exhibited the most potent inhibitory activity against the PPIs in the ELISA-based binding assay. Furthermore, compound **C3** (**Figure 8C**), which showed lower inhibitory activity than **C5**, was selected for further modifications due to its chemical structure [98]. The substituted aromatic rings in **C3** provided ideal sites for modification, and structure-activity relationship (SARs) studies were conducted. Rational design involving the substitution of isosteres and bioisosteres was employed to modify the substituted aromatic rings and linking regions.

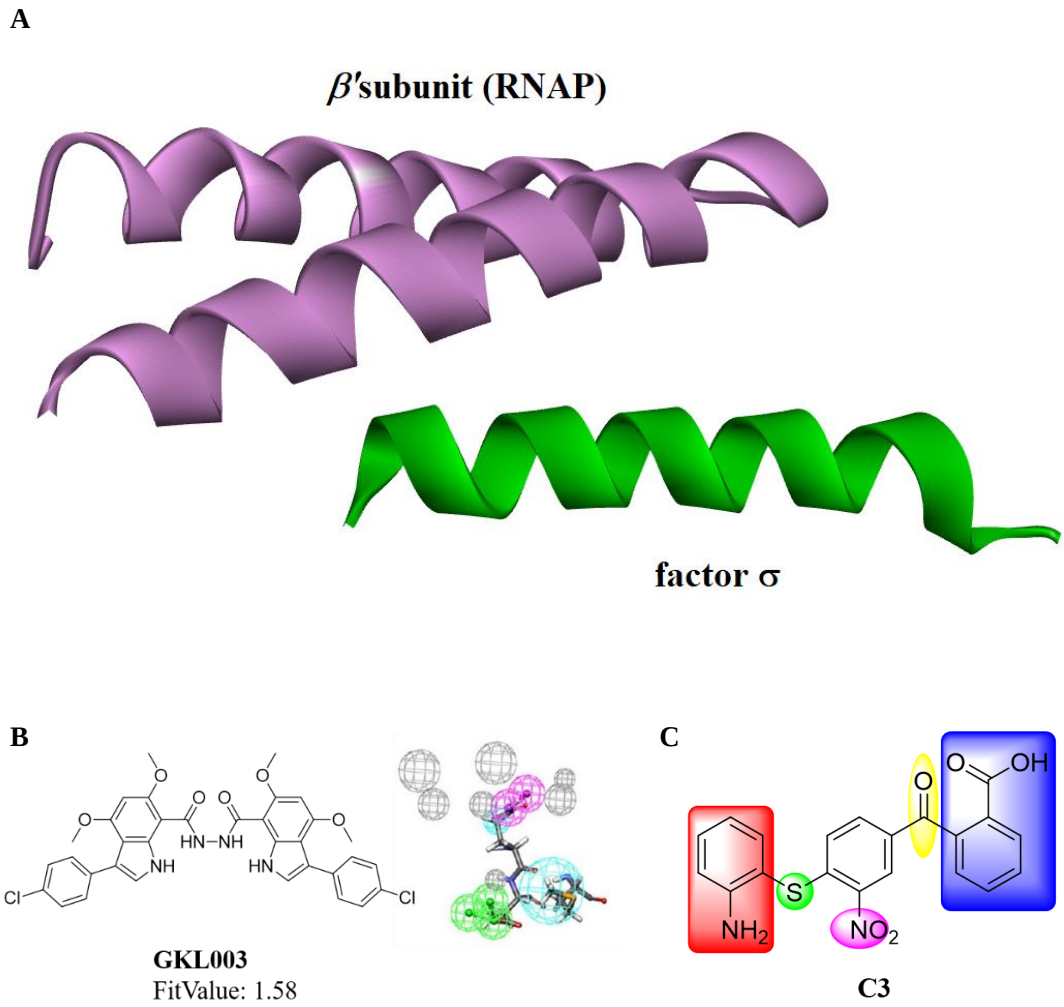

Figure 8. **A**): The identified PPIs constructed by *β'* subunit of RNAP (in magenta) and factor σ (in green). **B**): compound **GKL003** achieved by the virtual screening and how it fitted into the

pharmacophore model generated by Lewis *et al.* [96] The pharmacophores included hydrogen-bond acceptor (in green) and donor (in pink), hydrophobic group (in cyan) and exclusion zone (in grey). **C**): compound **C3** reported Ma C *et al.* and its potential sites for modifications, including substituted aromatic rings (in red, blue and purple separately) and linking regions (in green and yellow).

Additionally, Sartini *et al.* developed a bioluminescence resonance energy transfer assay in yeast to evaluate 4,960 candidate compounds from the screening, based on the known compounds **GKL003** and **C5** [99]. Subsequently, an ELISA-based binding assay and antimicrobial activity test were conducted on seven promising hits. The results demonstrated that four hits exhibited moderate inhibition compared to **GKL003**. Notably, the authors also constructed a pharmacophore model based on these hits and **GKL003**, using another X-ray crystal structure of factor σ interacting with RNAP in *E. coli* (PDB ID: 4YG2). The pharmacophores revealed some differences from those reported by Lewis, as certain residues, such as Asn294 and Glu295 on the *β'* subunit of RNAP, were identified as key residues for hydrogen bonding with inhibitors. These differences could potentially be attributed to variations in residue participation in the PPIs across different bacterial categories.

Apart from factor σ, another potential target for the discovery of novel antibiotics in bacterial transcription is the PPIs formed by NusB and NusE, which play a crucial role in the formation of the nucleation complex for antitermination, a process necessary for rRNA transcription [100]. The interface of these PPIs is composed of the α1-helix of NusE and a pocket in NusB. Key residues involved in this interaction have been identified as His15, Arg16, and Asp19 of NusE, as well as Tyr18, Arg76, and Glu81 of NusB (PDB ID: 3R2C) [101]. These residues form five essential hydrogen bonds that contribute to stabilizing the PPIs. Cossar *et al.* performed sequence alignment of NusE and NusB from various bacterial categories and demonstrated a highly conserved sequence in the α1-helix of NusE, suggesting its potential for the discovery of novel antibiotics with a broad antimicrobial spectrum. Based on the key residues in the α1-helix of NusE, they constructed a pharmacophore model and

conducted virtual screening on the MiniMaybridge database. Through modifications of the lead compound identified during the screening, they eventually obtained a promising candidate compound, referred to as compound **22**, which exhibited favorable inhibition of the PPIs (55% at 25 μM) and demonstrated antimicrobial activity against selected Gram-positive strains (MIC ≤ 3 μg/mL) [102]. Although compound **22** displayed significant cytotoxicity in tested human cell lines, it indicates the potential for discovering novel antibiotics targeting the PPIs of the NusB-NusE heterodimer.

1.5.4 Commonly utilized screening strategies on the discovery of novel antibiotics targeting on PPIs

In previous studies focused on discovering novel antibiotics targeting PPIs, the initial step involved defining the structure of the PPI interface and identifying the key residues involved in its formation. If the potential binding site formed by these key residues was suitable for small-molecule compounds, a rational screening strategy was necessary to identify promising hits from known compounds. High-throughput screening, fragment screening and virtual screening were commonly employed as screening strategies.

HTS has proven effective in the discovery of drugs targeting traditional targets. However, the compound libraries for HTS were typically built based on compounds that fit the binding model of traditional receptor-ligand drug targets. The distinct characteristics of the potential binding pocket on PPIs and the inhibitors targeting them resulted in lower hit rates for HTS [104]. Fragment screening, on the other hand, was favored for the discovery of PPI inhibitors. This method involves screening fragment libraries to identify fragments that exhibit weak to moderate affinity for the key residues on the PPIs [105]. These fragment hits are subsequently linked rationally to generate lead compounds. However, the expensive detection instruments and the requirement for crystalized target proteins limit the widespread use of fragment screening [106].

Considering the drawbacks of the other two screening strategies, virtual screening has been widely employed in the discovery of promising compounds targeting PPIs, particularly when X-ray crystal structures of the PPIs are available. Virtual screening offers high screening rates and consumes fewer biological assay resources [107]. Virtual screening methods can be classified into two approaches: structure-based and ligand-based. Structure-based screening relies on docking simulations of target proteins with compounds from selected libraries [108]. A scoring function, which is a mathematical algorithm, evaluates the docking fitness of the compounds. Structure-based virtual screening requires significant effort, as compound libraries typically contain thousands of compounds. Ligand-based screening, on the other hand, utilizes the structural and physicochemical properties of ligands for the target protein and inactive molecules to identify molecular similarities [109]. Pharmacophore modeling, based on the general configurations or spatial arrangements of molecules, is employed to define chemical features that interact with target proteins [110]. Given the absence of a natural ligand, pharmacophore modeling based on the key residues involved in the target PPIs has become a valuable and effective method for virtual screening of novel compounds [111].

1.6 Potential of PPIs between NusG and RNAP on acting as a target for small-molecule antibiotics

In this chapter, it has been demonstrated that the function of NusG in bacterial transcription relies on its interactions with various enzymatic proteins involved in the process. The NGN domain of NusG directly binds to RNAP, the key enzyme in transcription. The NGN domain maintains a highly conserved α-β sandwich structure in prokaryotes. Upon recruitment, NusG acts as an essential component in the TEC. Inhibition of the backtracking pause by NusG has been shown to be beneficial for transcription elongation in bacteria universally. It is predicted that NusG stabilizes the positively charged surface of its binding region with RNAP. Interactions between the KOW domain of NusG and NusE, the ribosomal S10 protein, have also been

identified in purified TECs. However, studies on its role in transcription-translation coupling have not detected a direct effect on mRNA translation. In Rho-dependent transcription termination, NusG has been found to accelerate the isomerization of Rho, thereby stimulating the termination process through interactions between its KOW domain and the motor domain of Rho. These protein-protein interactions provide opportunities for targeting NusG as a potential strategy for the discovery of novel small-molecule antibiotics. Disrupting the PPIs between NusG and RNAP/Rho with antibiotics may exhibit promising antimicrobial activities against antibiotic-resistant pathogens. Analysis of the X-ray structures of NusG in complex with RNAP and Rho has identified the PPIs between them. In comparison to its stimulation of specific Rho-dependent termination sites, NusG is observed to universally inhibit the backtracking pause in bacteria through its PPIs with RNAP. Furthermore, the distinct binding site of the NGN domain with Pol II in eukaryotes provides selectivity for potential antibiotics targeting this PPI in bacteria. In the pursuit of discovering broad-spectrum antibiotics, the PPIs between the NGN domain and RNAP hold potential for the discovery of novel small-molecule antibiotics. Since no antibiotics targeting these PPIs have been reported, virtual screening based on pharmacophores constructed by key residues is a favorable strategy for identifying promising lead compounds for further modification and biological testing. The next chapter will provide a detailed description of the procedures involved in the discovery and rational design of these novel antibiotics.

Chapter II:

The discovery, synthesis and SARs analysis on novel small-molecular antibiotics targeting on PPIs between NusG and RNAP

2.1 Definition on key residues of PPIs between NusG and RNAP

To investigate the interaction model of NusG with RNAP, the X-ray crystal structure of the NusG-RNAP complex from *E. coli* (PDB ID: 5TBZ) was obtained from the Protein Data Bank (PDB) [112]. The complex was prepared using the *Clean Protein* module of Discovery Studio 2016. Among the three identified binding sites in this complex, it was observed that interactions between the linking α-helix of NusG and β-protrusion of RNAP were easily disrupted upon loading of the DNA duplex during transcription [32]. Therefore, the focus was directed towards the other two sites, we defined NusG as the partner protein to detect its interactions with the β'-CH and β-GL of RNAP. Previous studies have demonstrated the conservation of certain residues on these subunits, which were selected as key residues for pharmacophore modeling [96][113]. **Figure 9** illustrates the interactions formed by Arg270, Arg271, Arg278 and Arg281 on the β'-CH, as well as Arg470, Arg473, Lys496 and Glu504 on the β-GL**.** Since arginine residues often play a crucial role in PPIs, particular attention was given to the interactions involving arginine. Arg270, Arg278 and Arg281 on the β'-CH formed three hydrogen bonds with shorter bond lengths (2.53, 2.58 and 2.71 Å) compared to the hydrogen bond formed by Arg470 (2.72 Å) on the β-GL. Additionally, Arg470 and Arg473 on the β-GL contributed to two hydrophobic interactions. (5.28 Å and 4.52 Å). Furthermore, Arg271 on the β'-CH formed an electrostatic interaction. These findings suggest that the four arginine residues on the β'-CH play a more significant role in the construction of PPIs. Moreover, these four arginine residues contribute to the formation of a potential pocket capable of accommodating small-

molecule inhibitors. Considering the pharmacophore modeling, Arg270, Arg278, and Arg281 were considered as hydrogen bond acceptors or donors to generate the binding site as receptors.

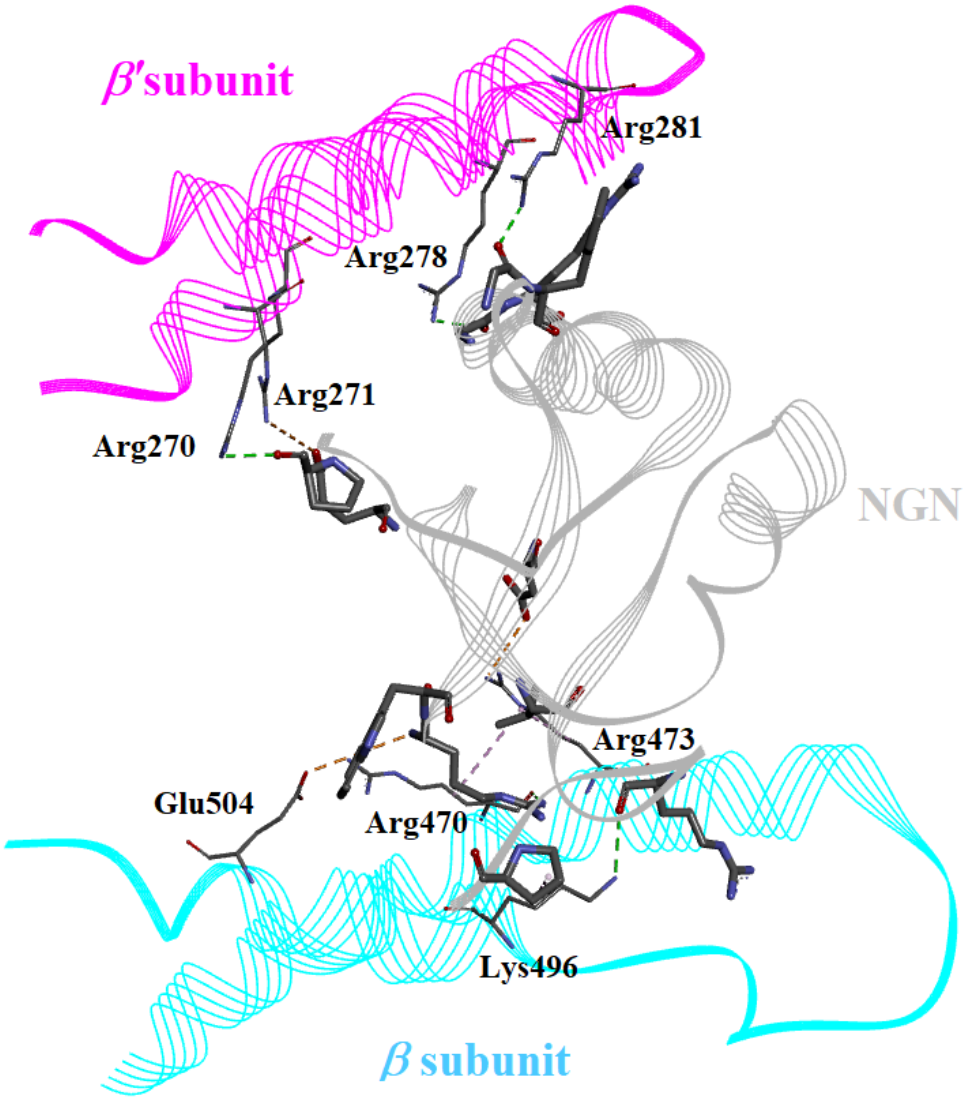

Figure 9: The binding model of NGN domain (displayed in grey mesh) with the *β*'-CH (displayed in purple mesh) and *β*-GL (displayed in blue mesh) of RNAP. There are three residues on the *β*'-CH being marked with Arg270, Arg278 and Arg 281, which build conventional hydrogen-bonds (green dotted line) in the length of 2.53 to 2.71 Å, while Arg271 forms an electrostatic interaction (orange dotted line). In comparison, the length of hydrogen-bond constructed by Arg470 on the *β*-GL is 2.72 Å and hydrophobic interactions (pink dotted line) formed by Arg470 and Arg473 are 5.28 Å and 4.52 Å. Extra hydrophobic interactions, electrostatic interactions and hydrogen-bonds

being formed by other conserved residues on the β-GL, Lys496 and Glu504, were also displayed but predicted to be unnecessary for the PPIs construction.

2.2 Discovery of the lead compound through the Virtual Screening

Using the receptor definition of the β'-CH of RNAP, we employed the *Receptor-Ligand Pharmacophore Generation* in the *Pharmacophore* module to generate pharmacophores. These pharmacophores were categorized into hydrophobic, hydrogen bond donor, and hydrogen bond acceptor features. To refine the generated pharmacophores, we eliminated the excluded volume model and performed clustering analysis. This process allowed us to retain only the relevant and effective pharmacophores associated with the key arginine residues. The resulting pharmacophore model, which is suitable for subsequent virtual screening, is shown in **Figure 10**.

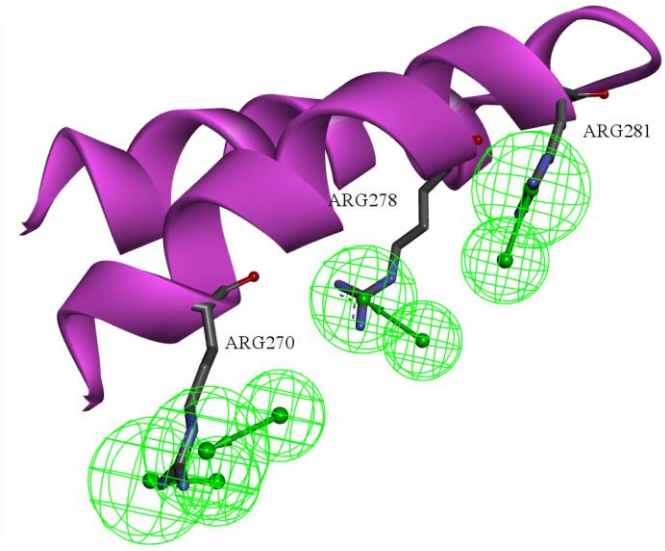

Figure 10. Pharmacophores being generated when defining Arg270, Arg278 and Arg 281 on the β' subunit of RNAP (displayed in magenta ribbon) as the potential binding site. These selected pharmacophores based on three key residues contributed on the formation of hydrogen-bonds with NusG, being defined as hydrogen bond acceptor (in green sphere).

Following the generation of the pharmacophore model, virtual screening was

performed using the *Search 3D Database* in the *Pharmacophore* module. The MiniMaybridge database was utilized, resulting in 57 hits with FitValues ranging from 2.8656 to 0.086479. To filter the hits, ADMET prediction was conducted to assess their drug-likeness and pharmacokinetic properties, which include absorption, distribution, metabolism, excretion, and toxicity [114]. The *ADMET Descriptors* in *Small Molecules* module of Discovery Studio 2016 was employed to grade each property and identify favorable levels for the hits. Based on the FitValue and favorable drug-like ADMET properties (not shown), the top ten hits were selected for antimicrobial activity evaluation. For the antimicrobial activity evaluation, a panel of bacteria was used, including seven pathogens from the "WHO priority pathogens list for guiding R&D of new antibiotics" [5]. The panel consisted of three Gram-positive pathogens: *Enterococcus faecalis*, *Staphylococcus aureus*, *Streptococcus pneumonia*; and four Gram-negative ones: *Acinetobacter baumannii*, *Pseudomonas aeruginosa*, *Enterobacter spp. and Escherichia coli*. Antibiotic susceptibility testing was performed using standard strains based on the Clinical & Laboratory Standards Institute (CLSI) guideline. The positive controls included multiple broad-spectrum antibiotics such as vancomycin, oxacillin, gentamicin, rifampicin, ciprofloxacin, and colistin. The MIC values, shown in **Table 1**, revealed that only **AW00783** exhibited acceptable antimicrobial activity against *Streptococcus pneumonia*, with a MIC value of 256 μg/mL. This compound also demonstrated a promising FitValue and favorable ADMET properties based on previous studies. Therefore, **AW00783** was selected as the lead compound for further modifications.

Table 1. Antimicrobial activities of hits against typical pathogens (MIC μg/mL).

No.	Name	EFAE	SAUR[a]	SAUR[b]	SPNE	ABAU	PAER	ECLO	ECOL
1	**KM06753**	>256	>256	>256	>256	>256	>256	>256	>256
2	**AW00783**	>256	>256	>256	256	>256	>256	>256	>256
3	**RF00627**	>256	>256	>256	>256	>256	>256	>256	>256

4	**NRB00386**	>256	>256	>256	>256	>256	>256	>256	>256
5	**SP00883**	>256	>256	>256	>256	>256	>256	>256	>256
6	**JFD03984**	>256	>256	>256	>256	>256	>256	>256	>256
7	**RH01573**	>256	>256	>256	>256	>256	>256	>256	>256
8	**NRB03988**	>256	>256	>256	>256	>256	>256	>256	>256
9	**SPB01943**	>256	>256	>256	>256	>256	>256	>256	>256
10	**RDR01935**	>256	>256	>256	>256	>256	>256	>256	>256
	Vancomycin	1	2	0.5	1	>64	>64	>64	>64
	Oxacillin	32	1	1	2	>64	>64	≥64	≥64
	Gentamicin	16	0.5	2	16	32	2	1	1
	Rifampicin	4	0.015625	≤0.0625	≤0.0625	4	32	≥64	64
	Ciprofloxacin	4	2	2	2	0.5	0.25	≤0.0625	0.0625
	Colistin					0.5	≤64	>256	≤16

EFAE: *Enterococcus faecalis* ATCC® 19433, SAUR[a]: *Staphylococcus. aureus* ATCC® 25923, SAUR[b]: *S. aureus* ATCC® 29213, SPNE: *Streptococcus pneumonia* ATCC® 49619, ABAU: *Acinetobacter baumannii* ATCC® 19606, PAER: *Pseudomonas aeruginosa* ATCC® 27853, ECLO: *Enterobacter cloacae* ATCC® 13047, ECOL: *E. Coli* ATCC® 25922.

2.3 Modifications based on the lead compound

The modifications of the lead compound were guided by the analysis of its binding model with the β'-CH of RNAP. **AW00783** had three components that fit into the pharmacophore model (**Figure 11A**). When defined as the ligand to generate

interactions, the nitro group on its benzene ring, which fit into two pharmacophores, also formed an electrostatic interaction with Arg270 (**Figure 11B**). Additionally, one nitrogen atom of the pyrimidine acted as a hydrogen bond acceptor, binding with Arg281. The substituted aromatic rings were easily modifiable and amenable to SARs analysis. However, the hydroxy group, which fit into the pharmacophore formed by Arg278, did not form direct interactions. Furthermore, Asn274 was found to create a π-donor interaction with the benzene ring and an additional hydrogen-bond with the nitrogen atom on the linking region. It appeared that Arg278 and Arg281 formed bottom region of the potential binding pocket, which could be expanded due to the flexible side-chain of Arg270 (**Figure 11C**). Therefore, the flexible linear linker between the terminal aromatic rings could also be modified and elongated. Following classical drug-design strategies, the four-atom linker adjacent to the hydroxy group could be replaced by a six-membered aromatic ring, while maintaining the relative position of other components on the linking region (**Figure 11D**). Based on these considerations, derivatives of the lead compound were classified into two categories based on the linking region, referred to as "aminoethyl derivatives" and "aromatic derivatives".

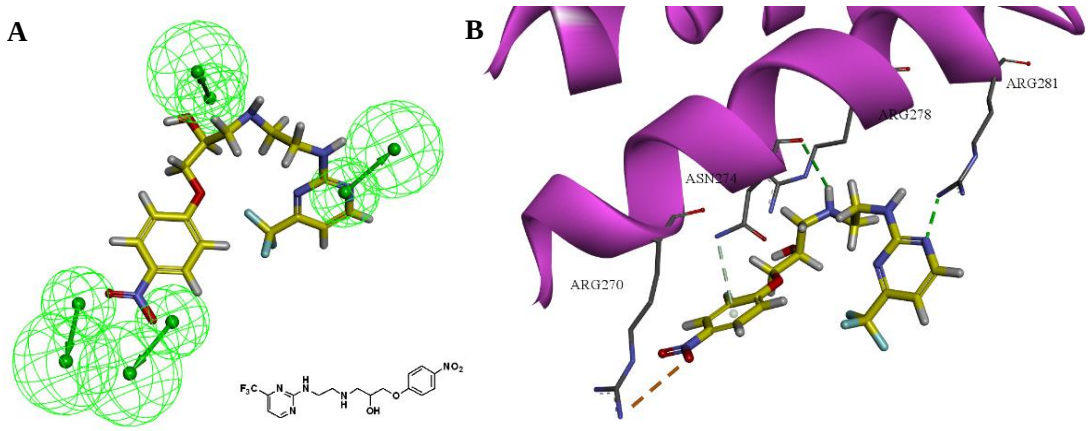

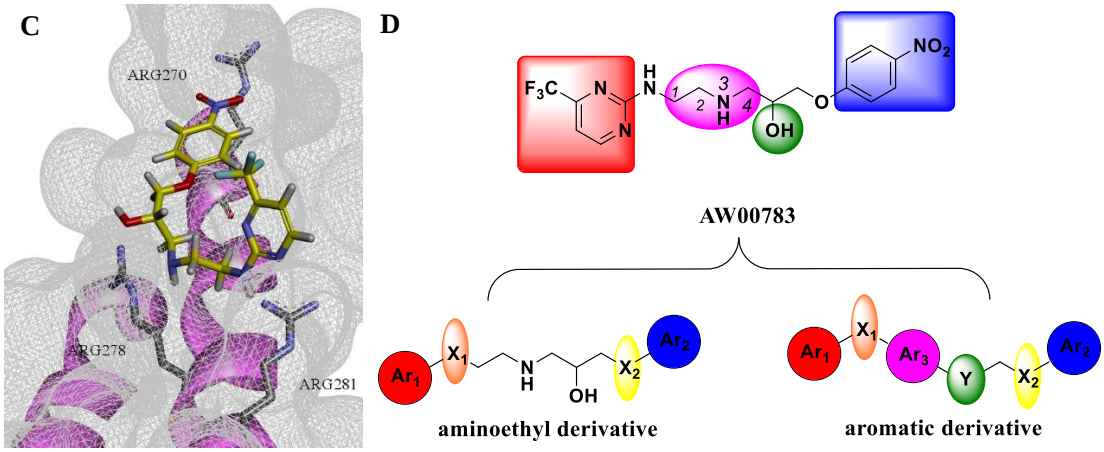

Figure 11. A): The chemical structure of **AW00783**, fitting into the pharmacophore model; **B)**: The binding model of **AW00783** with the *β'*-CH. Its interactions with key residues included an electrostatic interaction with Arg270 and a hydrogen-bond with Arg281. While a π-donor interaction (grey dotted line) and an extra hydrogen-bond were detected to be constructed by Asn274; **C)**: The configuration of **AW00783** inside the binding pocket whose surface was exhibited in mesh; **D)**: Two categories of derivatives being modified from **AW00783**. Modified components were marked in different colors, including the terminal aromatic rings (Ar_1 colored in red; Ar_2 colored in blue), moieties adjacent to terminal rings (X_1 colored in orange; X_2 colored in yellow), hydroxy group on the linking region (in green) and a four-atoms proportion of the linker (modified by aromatic ring Ar_3, colored in purple).

In aminoethyl derivatives, we selected substituted 2'-pyrimidine, 2'-pyridine, 3'-pyridine and benzene rings as the terminal rings, each with various substitution groups. These substitutions included electron-withdrawing or -donating groups, as well as hydrogen-bond donors or acceptors, all targeting the positively charged guanidine side-chain of arginine. We maintained the central structure of the aminoethyl linker, which contributed to the formation of hydrogen bonds and fit into the pharmacophore model. However, we modified the moieties adjacent to the terminal rings for SARs analysis. In the aromatic derivatives, except for similar modifications on terminal rings and moieties adjacent to them, the middle ring was determined as aromatic, heteroaromatic or substituted aromatic. Additionally, we substituted the hydroxy group with carbonyl, acylamino or sulfonamino for SARs

analysis, as the increased rigidity of aromatic derivatives might result in alterations to their binding models with the *β'*-CH. Furthermore, it appeared that the binding pocket could expand due to the flexible side-chain of arginine and accommodate more rigid structures (**Figure 11C)**. Cyclization of the hydroxy group with the terminal aromatic ring was also conducted, while preserving a hydrogen bond donor to maintain the hydrogen bonds with Arg278 and Arg270. In **Scheme 1**, we listed modifications on different components in both categories and provided examples of typical substitution groups utilized.

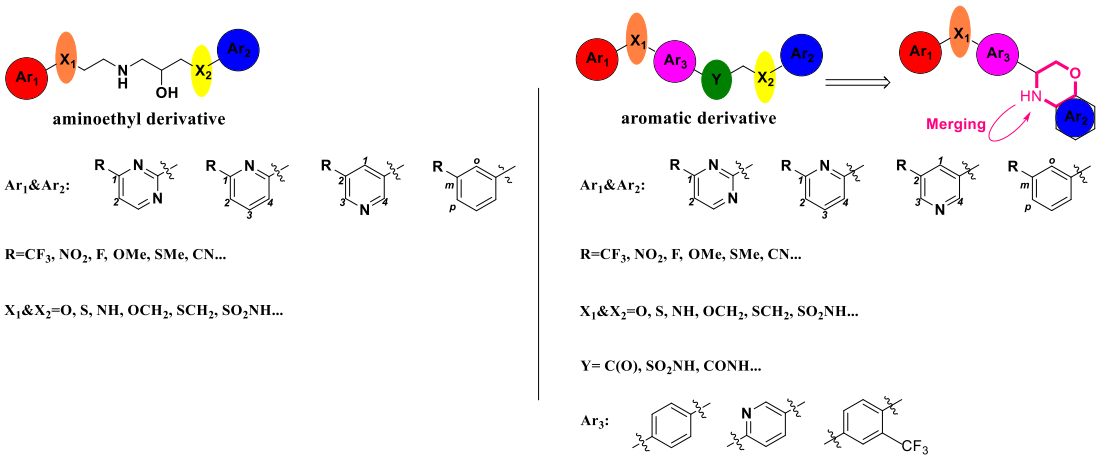

Scheme 1. Modifications on aminoethyl and aromatic derivatives. The modified components were marked in different colors and typical substitution groups were listed.

2.3.1 Synthetic routes of aminoethyl derivatives

Aminoethyl derivatives were prepared by nucleophilic substitution reaction of a substrate in Formula (**A**) with the other one in Formula (**B**) in ethanol (**Scheme 2**). The synthetic routes of different substrate **A** and **B** were displayed in the following schemes.

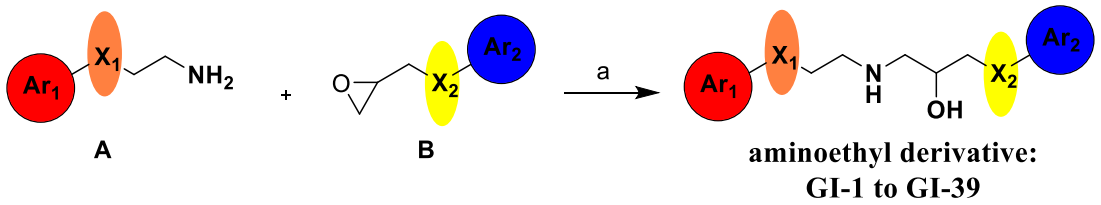

Scheme 2. Synthesis of aminoethyl derivatives. Reagent and condition: (a) DIPEA, EtOH, reflux,

8h.

The synthetic routes of substrates **A** have been classified into four categories based on the structure of their aromatic rings and adjacent components (**Scheme 3**). Starting materials, which are substituted compounds, undergo reactions either with ethylenediamine monohydrate or 2-(Boc-amino)ethyl bromide to yield the desired products.

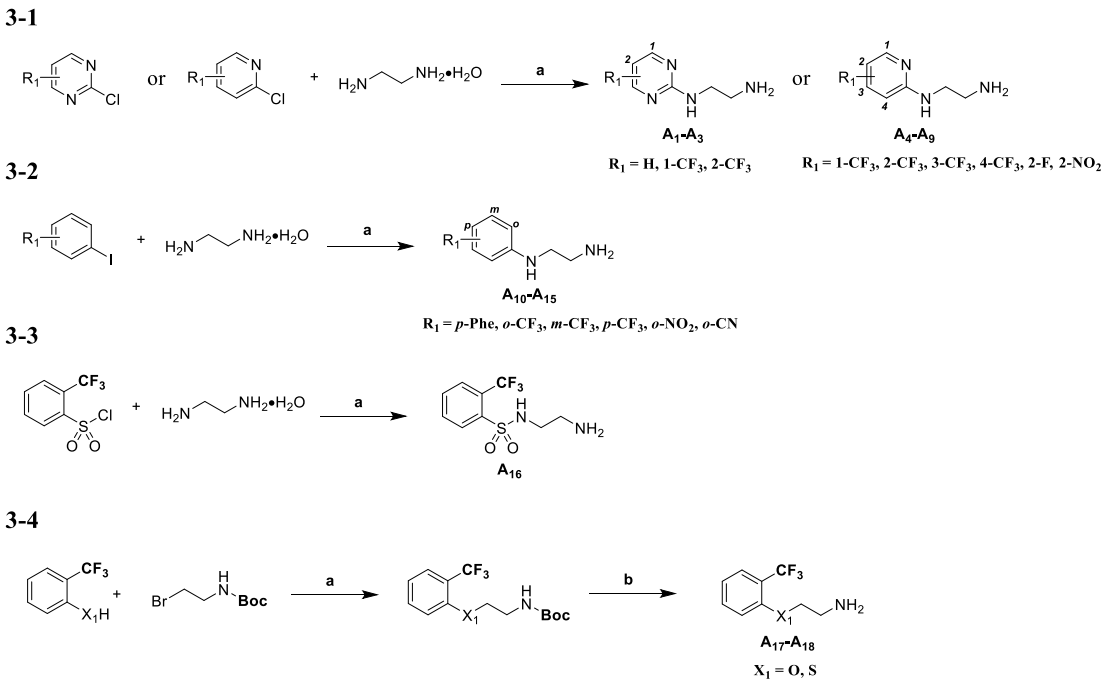

Scheme 3. Synthesis of substrates **A**. **1):** Reagent and condition: K_2CO_3, THF, reflux, overnight; **2):** Reagents and conditions: CuCl, Cs_2CO_3, DMSO, 120 ℃, 8h; **3):** Reagent and condition: Et_3N, DCM, rt, overnight; **4):** Reagents and conditions: (a): K_2CO_3, DMF, 65 ℃, 8h; (b): CF_3COOH, DCM, reflux, 8h.

Substrates **B** were synthesized through a substitution reaction between starting materials containing different nucleophilic groups and epichlorohydrin (**Scheme 4**). The reactions were carried out under diverse conditions, which were selected based on the reactivity of the specific nucleophiles involved.

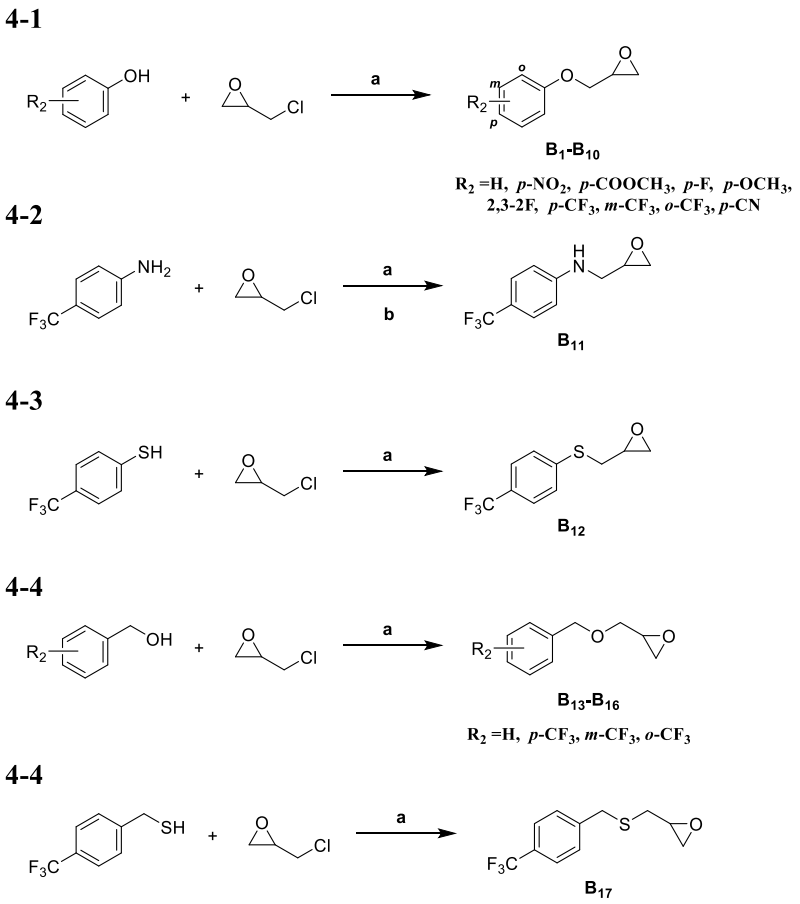

Scheme 4. Synthesis of substrates **B**. **1):** Reagent and condition: KI, Cs_2CO_3, DMF, 80 ℃, overnight; **2):** Reagent and condition: (a): $Zn(SO_3CF_3)_2$, $CHCl_3$, 60 ℃, 12h; (b): KI, MeCN, 80 ℃, 6h. **3):** Reagent and condition: K_2CO_3, MeCN, 85 ℃, 8h; **4):** Reagent and condition: TBAB, 1M NaOH aqueous solution, rt, 18h; **5):** Reagent and condition: KOH, water : dioxane = 1: 1, rt, 8h.

2.3.2 Synthetic routes of aromatic derivatives

The general synthetic route of aromatic derivatives is illustrated in **Scheme 5**. It involves a palladium-catalyzed coupling reaction between substituted chloropyridine or iodobenzene and aminoacetophenone. This coupling reaction generates intermediate **C**. Subsequently, halogenation is performed on intermediate **C**, resulting in the formation of intermediates **D**. These intermediates **D** then undergo reactions with the nucleophilic group present in the substituted aromatic reactants. Finally, the carbonyl group in intermediates **E** is reduced, leading to the formation of the desired target compounds.

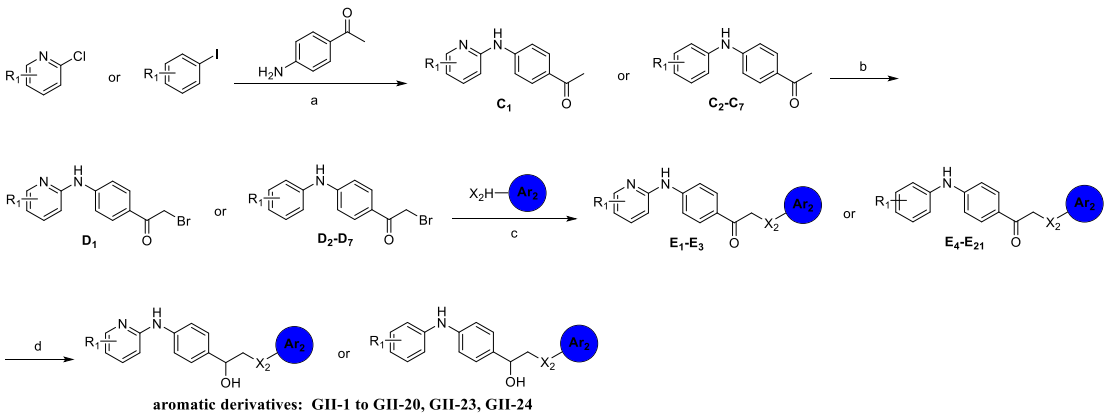

Scheme 5: The synthetic route of aromatic derivatives initiating from a palladium-catalysed coupling reaction. Reagents and conditions: (a) $Pd(OAc)_2$, X-Phos, Cs_2CO_3, toluene, 120 ℃, 8h; (b) $CuBr_2$, $CHCl_3$: EA = 1 : 1, 60 ℃, overnight; (c) K_2CO_3, acetone, reflux, 6h; (d) $NaBH_4$, MeOH, rt, 8h.

The synthetic route for aromatic derivatives with alternative X_1 or Ar_3 moieties exhibits variations in the initial step, as depicted in **Scheme 6**. Depending on the specific substitution requirements, two distinct approaches were employed. In **Scheme 6-1**, nucleophilic aromatic substitution reactions were employed for the substitution on X_1, utilizing either oxygen or sulfur nucleophiles. The subsequent halogenation step was carried out under more rigorous conditions to enhance the overall yield. In **Scheme 6-2**, bromide starting materials with alternative Ar_3 moieties were utilized for the palladium-catalyzed coupling reaction. After the formation of intermediates **C**, the subsequent steps followed a similar pattern to the general synthetic route.

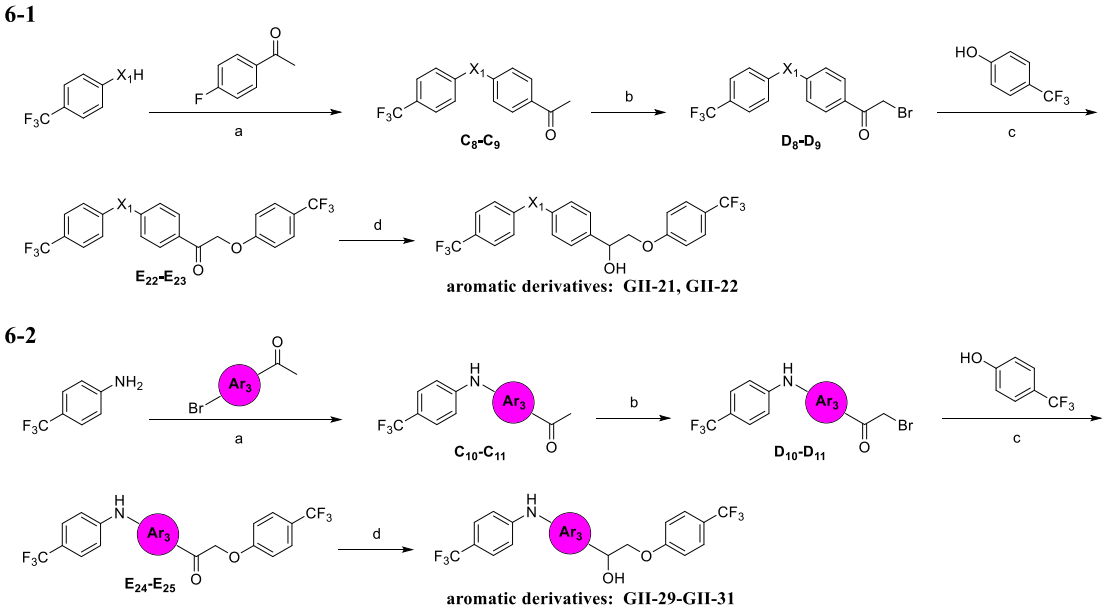

Scheme 6: The synthetic route of aromatic derivatives with alternative X_1 or Ar_3 components. **1):** Reagents and conditions: (a) Cs_2CO_3, NMP, 120℃, overnight; (b) NBS, TsOH, MeCN, 90 ℃, 8h; (c) K_2CO_3, acetone, reflux, 6h; (d) $NaBH_4$, MeOH, rt, 8h; **2):** Reagents and conditions: (a) $Pd_2(dba)_3$, Cs_2CO_3, X-Phos, toluene, 80 ℃, 24h; (b) $CuBr_2$, $CHCl_3$: EA = 1 : 1, 60 ℃, overnight; (c) K_2CO_3, acetone, reflux, 6h; (d) $NaBH_4$, MeOH, rt, 8h.

Aromatic derivatives with modification on the hydroxy group were synthesized through three distinct synthetic routes, as depicted in **Scheme 7**. Synthetic routes were designed for derivatives without a hydroxy group or with substitution by a sulfonamino group. In **Scheme 7-1** and **7-3**, the synthesis begins with a substitution reaction, followed by a hydrolysis reaction. These reactions generate substituted aniline intermediates, which serve as substrates for the final step: a palladium-catalyzed coupling reaction, leading to the formation of the target compounds. In contrast, the synthetic route for derivatives substituted by an acylamino group follows a reverse sequence. It initiates with a palladium-catalyzed coupling reaction, followed by hydrolysis and subsequent substitution reactions (**Scheme 7-2)**.

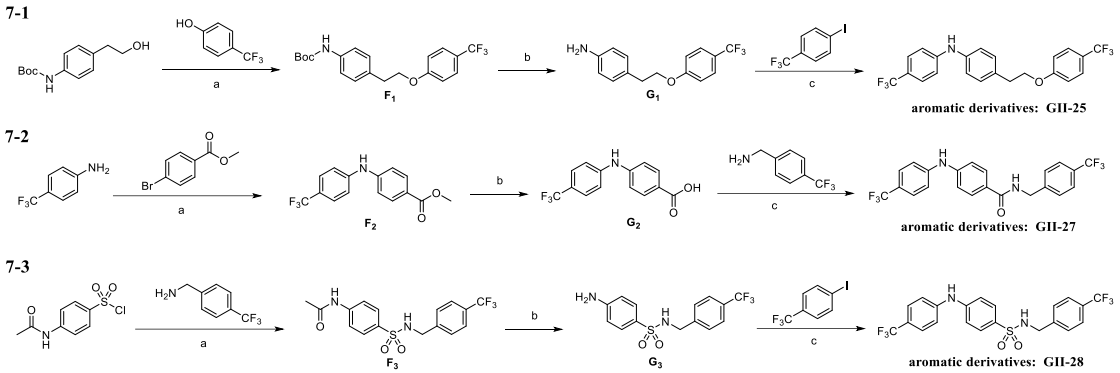

Scheme 7: The synthetic route of aromatic derivatives with alternative X_1 or Ar_3 components. **1):** Reagents and conditions: (a) PPh_3, DEAD, anhydrous THF, rt, overnight; (b) CF_3COOH, DCM, reflux, 8h; (c) $Pd(OAc)_2$, Cs_2CO_3, X-Phos, toluene, 120 ℃, 8h; **2):** Reagents and conditions: (a) $Pd(OAc)_2$, K_2CO_3, BINAP, toluene, 80 ℃, 24h; (b) NaOH, EtOH, reflux, 4h; (c) EDCI, 4-DMAP, DCM, rt, 24h; **3):** Reagents and conditions: (a) Et_3N, DCM, rt, 12h; (b) HCl, EtOH, 70 ℃, 4h; (c) $Pd_2(dba)_3$, Xantphos, NaO*t*Bu, toluene, 110 ℃, 24h.

The synthetic route for aromatic derivatives with cyclization is illustrated in **Scheme 8**. The reaction involves the utilization of intermediate **D_1** or **D_2**, which undergoes a reaction with 2-amino-4-nitrophenol to generate Schiff base intermediates. The synthesis of these derivatives involves two key processes: a condensation reaction and a nucleophilic substitution reaction. The condensation reaction occurs between the carbonyl group of intermediate **D1** or **D2** and the amino group of 2-amino-4-nitrophenol, resulting in the formation of the Schiff base intermediates.

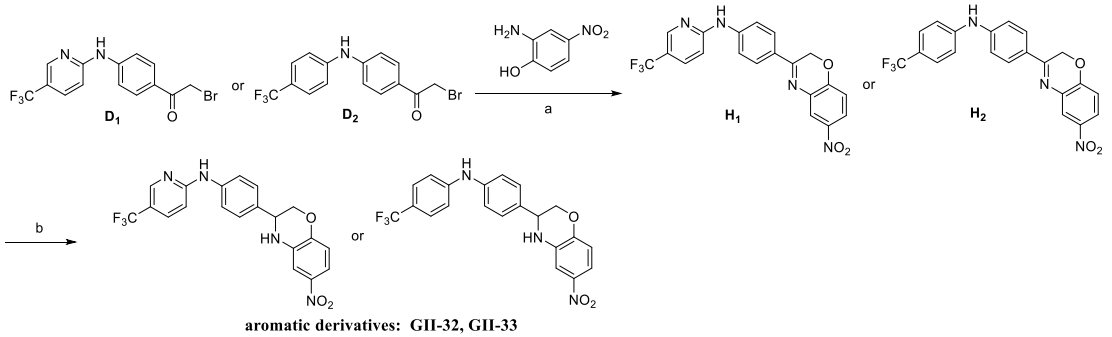

Scheme 7: The synthetic route of aromatic derivatives with further cyclization. Reagents and conditions: (a) Tetrabutylammonium hydrogen sulfate, K_2CO_3, DCM, reflux, 6h; (b) $NaBH_4$, MeOH, rt, 8h.

2.4 Antimicrobial activity tests and SARs analysis

In our study, we employed the same strains that were previously used for testing the hits in antibiotic susceptibility testing. Upon evaluation, several derivatives displayed enhanced antimicrobial activity against both Gram-positive and Gram-negative strains, surpassing that of the lead compound. Based on their favorable antimicrobial activity, we carefully selected promising candidate compounds specifically targeting Gram-positive and Gram-negative strains for further biological testing. Additionally, we performed a comprehensive analysis of SARs on these selected compounds. This analysis helped us identify key structural features and modifications that contribute to their enhanced antimicrobial properties.

2.4.1 SARs analysis on aminoethyl derivatives

Modifications were initially carried out on the two terminal aromatic rings of the lead compound, focusing on aminoethyl derivatives. Compound **GI-1**, lacking a substitution group on Ar_1, exhibited no antimicrobial activities according to **Table 2-1**. This observation suggests that the presence of the trifluoromethyl group on Ar_1 might contribute to the formation of a hydrogen bond with Arg281, rather than the nitrogen atom of pyrimidine. This hypothesis was confirmed by the moderate activities of compound **GI-8**, where the benzene ring substituted Ar_1. Furthermore, compounds **GI-2** to **GI-6**, with a trifluoromethyl substitution on the pyridine ring, indicated that the position of the substitution group on the aromatic ring was also influential in terms of antimicrobial activity. Among these derivatives, **GI-4** and **GI-8** exhibited promising activity and were selected for further modifications. Simultaneously, the evaluation of derivatives with different substitution groups on Ar_2 demonstrated that trifluoromethyl remained the preferred choice compared to other hydrogen-bond acceptors, as shown in **Table 2-2**. The decreased activities of compounds **GI-10** to **GI-13**, with alternative hydrogen-bond acceptors, suggested that the steric bulk of the substitution group influenced its compatibility within the pharmacophore formed by

Arg270. Although the nitro group contributed to both hydrogen bonding and electrostatic interactions, it exhibited weaker affinity for the *β'*-CH compared to the trifluoromethyl group, as observed in the binding model of **AW00783**. Additionally, these three selected derivatives (**GI-4**, **GI-8** and **GI-14**) demonstrated improved antimicrobial activities against Gram-negative strains compared to the lead compound.

Table 2: The antimicrobial activity evaluation on aminoethyl derivatives with different terminal aromatic rings (MIC μg/mL)

1.

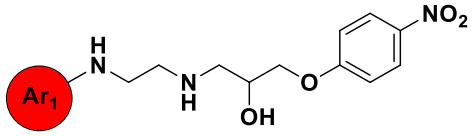

Ar_1	R_1	Compd.	EFAE	SAUR[a]	SAUR[b]	SPNE	ABAU	PAER	ECLO	ECOL
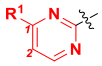	/	**GI-1**	>256	>256	>256	>256	>256	>256	>256	>256
	2-CF_3	**GI-2**	>256	256	256	128	>256	>256	>256	>256
	1-CF_3	**GI-3**	128	128	64	32	256	>256	256	256
	2-CF_3	**GI-4**	128	32	32	64	128	>256	128	128
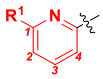	3-CF_3	**GI-5**	128	128	128	64	>256	>256	256	>256
	4-CF_3	**GI-6**	256	128	128	64	>256	>256	>256	>256
	2-F	**GI-7**	>256	>256	>256	>256	>256	>256	>256	>256
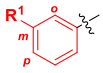	*o*-CF_3	**GI-8**	128	64	64	64	128	>256	128	128

2.

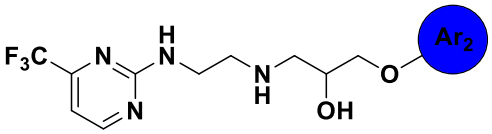

Ar_2	R_2	Compd.	EFAE	SAUR[a]	SAUR[b]	SPNE	ABAU	PAER	ECLO	ECOL
	/	**GI-9**	>256	>256	>256	128	>256	>256	>256	>256
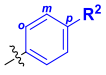	*p*-$COOCH_3$	**GI-10**	>256	>256	>256	256	>256	>256	>256	>256
	p-F	**GI-11**	>256	>256	256	128	>256	>256	>256	>256

m, *p*-2F	**GI-12**	256	256	256	64	256	>256	256	128
p-OMe	**GI-13**	>256	>256	>256	256	>256	>256	>256	>256
p-CF_3	**GI-14**	256	64	64	32	128	>256	>256	>256

Further modifications were conducted on the substitution group of Ar_1 when it was substituted with trifluoromethyl on Ar_2. Compound **GI-19**, with trifluoromethyl on the *o*-position of the benzene ring, exhibited the most potent antimicrobial activities against Gram-positive strains, particularly with a MIC value of 4 μg/mL against SPNE, as shown in **Table 3-1**. In contrast, when the cyano group, known for its role as a hydrogen-bond acceptor and commonly used in rational drug design [115], was substituted on the same position, antimicrobial activities of compound **GI-21** declined. Meanwhile, modifications on substitution groups of Ar_2 in compound **GI-19** did not yield more promising derivatives, as indicated in **Table 3-2**. This finding suggests that the trifluoromethyl group at a specific position, acting as a hydrogen-bond acceptor, is the optimal substitution group on the terminal aromatic rings.

Table 3: The antimicrobial activity evaluation on further modifications based on **GI-4**, **GI-8** and **GI-14** (MIC μg/mL)

1.

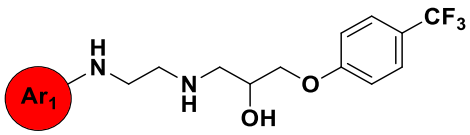

Ar_1	R_1	Compd.	EFAE	SAUR[a]	SAUR[b]	SPNE	ABAU	PAER	ECLO	ECOL
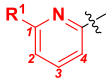	2-CF_3	**GI-15**	64	64	32	16	64	>256	>256	64
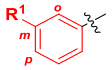	*p*-Ph	**GI-16**	>256	>256	256	>256	>256	>256	>256	>256
	p-CF_3	**GI-17**	≥32	64	32	8	256	>256	256	≥128
	m-CF_3	**GI-18**	>256	>256	>256	>256	>256	>256	>256	>256
	o-CF_3	**GI-19**	64	32	32	4	256	>256	128	128
	o-NO_2	**GI-20**	128	128	128	32	>256	>256	128	>256

	o-CN	**GI-21**	128	128	128	64	128	>256	128	16

2.

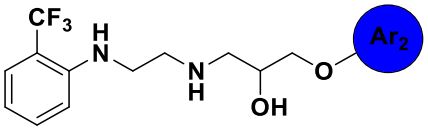

Ar_2	R_2	Compd.	EFAE	SAUR[a]	SAUR[b]	SPNE	ABAU	PAER	ECLO	ECOL
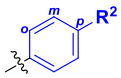	*m*-CF_3	**GI-22**	16	32	32	16	32	>256	32	32
	o-CF_3	**GI-23**	32	64	32	32	64	>256	64	64
	p-CN	**GI-24**	>256	>256	≥128	128	>256	>256	>256	>256

In addition to the modifications on Ar1 and Ar2, we also investigated the impact of lengthening the aminoethyl linker and modifying moieties adjacent to Ar_2, as indicated in **Table 4**. To lengthen the linker, we inserted one methylene group between the X_2 atom and Ar_2. However, compared to the activity of **GI-19**, these derivatives with the inserted methylene group showed a decline in antimicrobial activity. Furthermore, we conducted substitutions on the oxygen atom based on the principle of isosterism [116]. When comparing it with **GI-15**, which exhibited the best antimicrobial activities among the previous pyridine derivatives, compound **GI-30** with thioether substitution in the linking region stood out as the only exception. It displayed improved activities against both Gram-positive and Gram-negative strains, as shown in **Table 4-1**.

Table 4: The antimicrobial activity evaluation on derivatives with modifications on the moiety adjacent to Ar_2 (MIC μg/mL)

1.

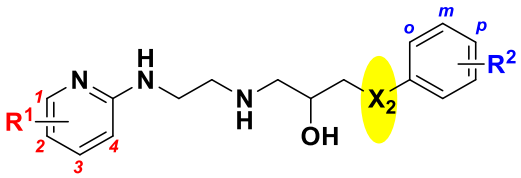

R_1	X_2	R_2	Compd.	EFAE	SAUR[a]	SAUR[b]	SPNE	ABAU	PAER	ECLO	ECOL
2-CF_3	NH	*p*-CF_3	**GI-25**	≥16	128	32	16	32	>256	64	64
	OCH_2	/	**GI-26**	256	256	128	128	>256	>256	256	256

		p-CF_3	**GI-27**	32	32	32	16	64	>256	256	128
		m-CF_3	**GI-28**	≥64	64	32	32	≥128	>256	≥256	64
		o-CF_3	**GI-29**	≥128	64	64	64	≥128	>256	≥128	128
	SCH_2	*p*-CF_3	**GI-30**	32	16	8	16	≥32	>256	≥64	32
2-NO_2	OCH_2	*p*-CF_3	**GI-31**	128	128	64	64	128	>256	128	128

2.

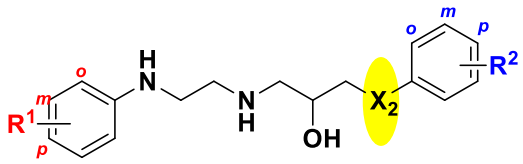

R_1	X_2	R_2	Compd.	EFAE	SAUR[a]	SAUR[b]	SPNE	ABAU	PAER	ECLO	ECOL
		p-CF_3	**GI-32**	64	64	64	32	64	>256	128	64
o-CF_3	OCH_2	*m*-CF_3	**GI-33**	>256	>256	≥128	128	>256	>256	>256	>256
		o-CF_3	**GI-34**	>256	>256	≥128	128	>256	>256	>256	>256

In addition to the modifications on the moiety adjacent to Ar_2, similar modifications were conducted on the moiety adjacent to Ar_1, as shown in **Table 5**. We initially modified it with sulfonamino, a moiety widely used in multiple small-molecular drugs [117]. With thioether on the linking region, compounds **GI-37**, **GI-38** and **GI-39** exhibited slightly improved antimicrobial activities compared to **GI-19**, with the best MIC value of 4 μg/mL against SPNE. The presence of a sulfide in drugs has been shown to establish non-bonding interactions with nitrogen or oxygen atoms, as well as intermolecular interactions with aromatic rings and sulfur atoms in residues [118]. Additionally, the bond length and angle of thioether differ from those of amino and ether, which can alter the configuration of these derivatives to facilitate their binding within the target site. Furthermore, compound **GI-36**, modified with oxygen on the X_1, displayed increased activities against Gram-negative strains, particularly with a MIC value of 8 μg/mL against ECOL, as shown in **Table 5-1**. This improvement in activity may be attributed to enhanced penetration through the bacterial membrane. However, further biological testing is required to validate this hypothesis.

Table 5): The antimicrobial activity evaluation on derivatives with further modifications on the aminoethyl linker (MIC μg/mL)

1.

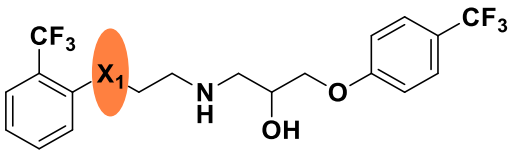

X_1	Compd.	EFAE	SAUR[a]	SAUR[b]	SPNE	ABAU	PAER	ECLO	ECOL
SO_2NH	**GI-35**	64	64	64	32	≥64	>256	128	64
O	**GI-36**	16	32	16	8	≥16	>256	≥32	8
S	**GI-37**	8	16	8	4	≥32	>256	128	16

2.

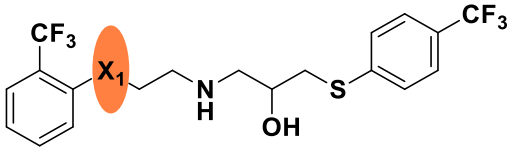

X_1	Compd.	EFAE	SAUR[a]	SAUR[b]	SPNE	ABAU	PAER	ECLO	ECOL
NH	**GI-38**	16	32	16	≥4	≥32	>256	≥64	16
S	**GI-39**	32	32	16	4	>256	>256	>256	>256

In conclusion, based on the conducted modifications on the terminal aromatic rings of aminoethyl derivatives, it was determined that substituting benzene with a trifluoromethyl group at a specific position is the optimal choice. This trifluoromethyl group acts as a hydrogen-bond acceptor, enabling interactions with Arg270 and Arg281. The decreased antimicrobial activities observed in derivatives with other hydrogen-bond acceptors and a lengthened linker indicate that the steric bulk and configuration of the derivatives play a role in their occupancy within the binding pocket and their ability to form interactions with key residues. The favorable activities observed in derivatives with a thioether on the linker further support this hypothesis.

2.4.2 SARs analysis on aromatic derivatives

Based on the SAR analysis of aminoethyl derivatives, it is likely that the

configuration of aromatic compounds occupying the target site undergoes some changes due to increased rigidity in the chemical structure. Modifications were made to the terminal aromatic rings and substitution groups on them. In comparison to other hydrogen-bond acceptors such as nitro, cyano, fluoride, and methoxy, compounds with trifluoromethyl-substituted aromatic rings demonstrated good activities against Gram-positive strains, as shown in **Table 6**. Among these derivatives, compound **GII-16** showed the most potent antimicrobial activities against SAUR[a] and SAUR[b], with the MIC value of 1 μg/mL. However, modifications on the trifluoromethyl group with a thioether substitution resulted in reduced antimicrobial activities (**GII-11** and **GII-18**). This suggests that the construction of hydrogen bonds may also contribute to the binding of aromatic derivatives with the target protein. Furthermore, compound **GII-20**, with a trifluoromethyl-substituted thiazole acting as Ar_1, exhibited no antimicrobial activities **(Table 6-3)**. This indicates that the presence of a six-membered aromatic ring is necessary for the construction of hydrogen bonds. Moreover, these aromatic derivatives showed no activities against Gram-negative strains, which may be attributed to decreased penetration due to increased rigidity in their chemical structures.

Table 6: The antimicrobial activity evaluation on aromatic derivatives with modified aromatic rings, Ar_1 and Ar_2 (MIC μg/mL)

1.

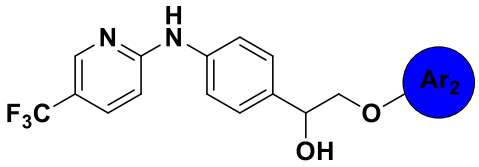

Ar_2	Compd.	EFAE	SAUR[a]	SAUR[b]	SPNE	ABAU	PAER	ECLO	ECOL
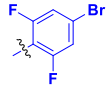	**GII-1**	32	>256	8	32	>256	>256	>256	>256
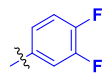	**GII-2**	64	32	16	8	>256	>256	>256	>256
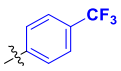	**GII-3**	64	16	4	4	>256	>256	>256	>256

2.

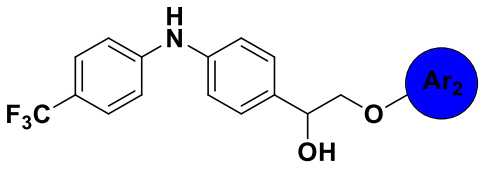

Ar_2	Compd.	EFAE	SAUR[a]	SAUR[b]	SPNE	ABAU	PAER	ECLO	ECOL
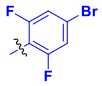	**GII-4**	64	>256	64	16	>256	>256	>256	>256
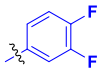	**GII-5**	32	32	32	8	>256	>256	>256	>256
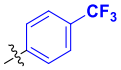	**GII-6**	32	8	4	16	>256	>256	>256	>256
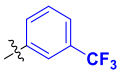	**GII-7**	16	8	8	4	>256	>256	>256	>256
	**GII-8**	>256	64	32	8	>256	>256	>256	>256
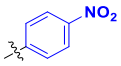	**GII-9**	>256	>256	8	4	>256	>256	>256	>256
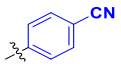	**GII-10**	>256	>256	64	8	>256	>256	>256	>256
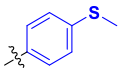	**GII-11**	>256	>256	128	16	>256	>256	>256	>256
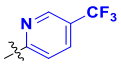	**GII-12**	>256	16	8	16	>256	>256	>256	>256
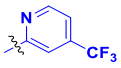	**GII-13**	>256	>256	>256	128	>256	>256	>256	>256
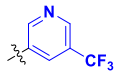	**GII-14**	>256	32	16	8	>256	>256	>256	>256

3.

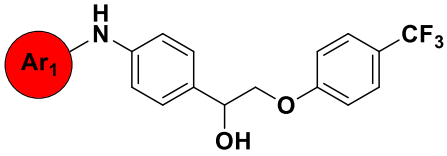

Ar_2	Compd.	EFAE	SAUR[a]	SAUR[b]	SPNE	ABAU	PAER	ECLO	ECOL
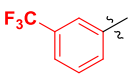	**GII-15**	≥16	8	4	4	>256	>256	>256	>256
	**GII-16**	8	1	1	≥8	≥32	>256	>256	>256
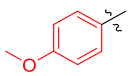	**GII-17**	>256	>256	>256	>256	>256	>256	>256	>256

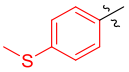	**GII-18**	>256	>256	>256	32	>256	>256	>256	>256
	**GII-19**	>256	>256	>256	16	>256	>256	>256	>256
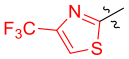	**GII-20**	>256	>256	>256	>256	>256	>256	>256	>256

Further modifications were performed based on **GII-6**, which displayed moderate antimicrobial activities. Similar to the strategy employed for aminoethyl derivatives, modifications were made to the linking moiety adjacent to Ar_1 and Ar_2, as shown in **Table 7**. However, these derivatives exhibited decreased antimicrobial activities compared to **GII-6**. The alterations made to the bond length and angle in these derivatives led to changes in their configuration, which hindered their occupation within the binding pocket. These structural changes likely impacted the interactions with key residues and affected the overall antimicrobial activity.

Table 7: The antimicrobial activity evaluation on aromatic derivatives with modifications on the moiety adjacent to Ar_1 and Ar_2 (MIC μg/mL)

1.

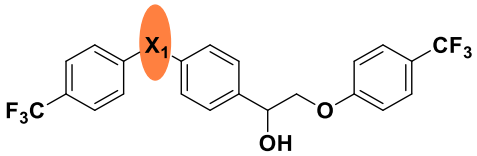

X_1	Compd.	EFAE	SAUR[a]	SAUR[b]	SPNE	ABAU	PAER	ECLO	ECOL
O	**GII-21**	>256	>256	>256	16	>256	>256	>256	>256
S	**GII-22**	>256	>256	>256	32	>256	>256	>256	>256

2.

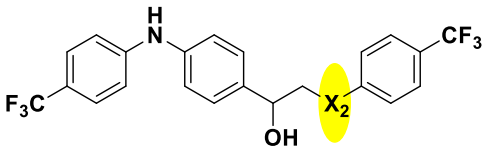

X_2	Compd.	EFAE	SAUR[a]	SAUR[b]	SPNE	ABAU	PAER	ECLO	ECOL
OCH_2	**GII-23**	>256	>256	16	4	>256	>256	>256	>256
S	**GII-24**	32	≥128	64	16	>256	>256	>256	>256

Modifications were made to the hydroxy group in order to investigate its role in binding with the β'-CH, as shown in **Table 8**. In the docking model of lead compound, the hydroxy group was observed to fit into the pharmacophore formed by Arg278 but did not form direct interactions. Compound **GII-25** exhibited poor antimicrobial activities, and **GII-26** showed no activity at all. This suggests that the hydroxy group is essential in the linking region for maintaining antimicrobial activity. Additionally, the linking moiety Y was modified with acylamino and sulfonamino groups, which can act as both hydrogen bond acceptors and donors. Compounds **GII-27** and **GII-28** exhibited moderate but still reduced antimicrobial activities. These modifications with carbonyl, acylamino, and sulfonamino groups altered the configuration of the derivatives. It is speculated that the hydroxy group functions as a hydrogen-bond donor to interact with key residues on the target protein, contributing to the overall binding affinity and antimicrobial activity.

Table 8: The antimicrobial activity evaluation on aromatic derivatives with modifications on the linker between Ar_2 and Ar_3 (MIC μg/mL)

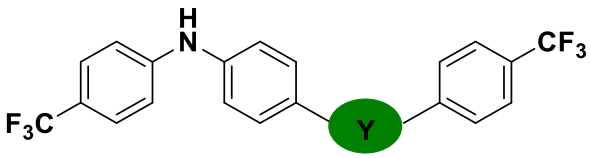

Y	Compd.	EFAE	SAUR[a]	SAUR[b]	SPNE	ABAU	PAER	ECLO	ECOL
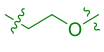	**GII-25**	>256	>256	>256	128	>256	>256	>256	>256
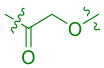	**GII-26**	>256	>256	>256	>256	>256	>256	>256	>256
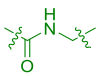	**GII-27**	>256	>256	32	32	>256	>256	>256	>256
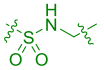	**GII-28**	>256	128	64	16	>256	>256	>256	>256

Modifications were made on Ar3, including the addition of substitution groups and the replacement with heteroaromatic rings, as shown in **Table 9**. Among these compounds, compound **GII-29** with a pyridine substitution exhibited slightly

decreased activities compared to **GII-6**. This suggests that the nitrogen atom in the pyridine ring is unnecessary for binding with the target protein. However, when Ar_3 was substituted with a trifluoromethyl group, a decline in activities was observed. This indicates that the additional hydrogen-bond acceptor displayed hindrance in interactions with the target protein due to steric effects. Furthermore, compound **GII-31**, in which the linking region was translocated to the *m*-position, only exhibited moderate activities against SPNE. The translocation of the hydroxy group also imposed steric hindrance due to changes in configuration.

Table 9: The antimicrobial activity evaluation on aromatic derivatives with modifications on Ar_3 (MIC μg/mL)

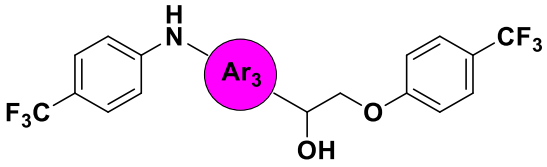

Ar_3	Compd.	EFAE	SAUR[a]	SAUR[b]	SPNE	ABAU	PAER	ECLO	ECOL
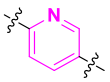	**GII-29**	32	32	32	8	>256	>256	>256	>256
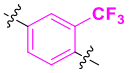	**GII-30**	64	>256	>256	32	>256	>256	>256	>256
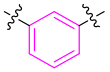	**GII-31**	>256	>256	>256	8	>256	>256	>256	>256

In the final stage of modifications, derivatives with further cyclization were evaluated, and it was found that these compounds exhibited minimal to no antimicrobial activities against all tested strains, except for SPNE (**Table 10**).

Table 10: The antimicrobial activity evaluation on aromatic derivatives with further cyclization (MIC μg/mL)

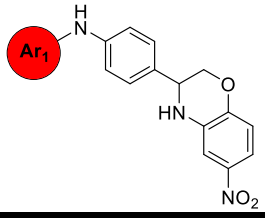

Ar_1	Compd.	EFAE	SAUR[a]	SAUR[b]	SPNE	ABAU	PAER	ECLO	ECOL
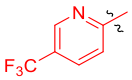	**GII-32**	>256	>256	>256	32	>256	>256	>256	>256
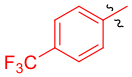	**GII-33**	>256	>256	>256	4	>256	>256	>256	>256

Based on the analysis of SARs for aromatic derivatives, it was found that the trifluoromethyl group exhibited the most favorable substitution on the terminal aromatic rings. However, the configuration of the aromatic derivatives played a crucial role in their antimicrobial activities and could be easily influenced by the linking region and middle aromatic ring. The hydroxy group was identified as an essential component for stabilizing the binding with the target protein by acting as a hydrogen bond donor. Introducing other linking moieties with hydrogen bond donors or acceptors, as well as additional substitution groups on the middle ring, led to a decrease in antimicrobial activities. This suggests that the middle aromatic ring offered a promising configuration for establishing interactions with key residues on the β'-CH of RNAP, although these interactions were not direct. In comparison to the aminoethyl derivatives, the moderately rigid nature of aromatic derivatives appeared to be advantageous for binding with the β'-CH and exhibiting improved antimicrobial activities against Gram-positive strains. Conversely, aminoethyl derivatives with a flexible linker demonstrated good activities against Gram-negative strains, possibly due to their ability to penetrate the bacterial membrane effectively. Based on their antimicrobial activities, four promising candidate compounds were selected for further investigation: **GI-19**, **GI-36**, **GI-39** from aminoethyl derivatives and **GII-16** from aromatic derivatives. These compounds underwent in silico docking simulations and subsequent biological testing to explore their binding interactions and evaluate their antimicrobial efficacy.

Chapter III:

In-silico analysis, cytotoxicity and fluorescence microscopy testing on candidate compounds

3.1 Docking simulation and prediction on ADMET properties

To predict the binding models of the candidate compounds, in silico docking simulations were performed using the *CDocker* module in Discovery Studio 2016 to simulate the docking models of these candidate compounds with the β'-CH of RNAP. The binding site was defined based on key residues, namely Arg270, Arg278, and Arg281, which were known to establish essential interactions with NusG. The candidate compounds were prepared using *Prepare Ligands* and *Full Minimization* modules with default parameters. During the *CDocker* module operation, the *Pose Cluster Radius* parameter was set to 0.5 to ensure diversity in the configurations of the candidate compounds in their docking models. Based on the *CDocker* energy and *CDocker* interaction energy, promising docking models were obtained for the four compounds (**Figure 12**). These docking models exhibited some differences compared to the lead compound. In the binding model of **GI-19**, hydrogen-bonds were formed by its trifluoromethyl and hydroxy groups with Asn274, Arg275, Arg278, and Arg281, which aligned with the SARs analysis on aminoethyl derivatives. Additionally, electrostatic and hydrophobic interactions were observed with Arg271 (**Figure 12A**). Compared with the binding model of **GI-19**, compound **GI-36** also constructed hydrogen-bonds with Asn274 and Arg278, along with a hydrophobic interaction with Arg271. However, it only formed an electrostatic interaction with Arg281 because its trifluoromethyl group on Ar_2 was positioned far away from Arg281 (**Figure 12B**). On the other hand, compound **GI-39** exhibited a distinct binding model with only one hydrogen bond formed between its hydroxy group and Arg278. Its configuration in this binding model changed to create an additional hydrophobic interaction with

Leu292 due to the presence of the thioether linker (**Figure 12C**). Unlike the binding models of aminoethyl derivatives, the hydroxy group of **GII-16** moved futher away from Arg278 due to the steric effect of middle aromatic ring (**Figure 12D**). Although the hydroxy group approached Arg270 closely, no direct interactions were detected between them. However, the trifluoromethyl groups on its terminal aromatic rings still formed hydrogen bonds with Arg275, Asn277, and Arg278. Hydrophobic interactions with Arg270 and Arg271 were also observed in this binding model. In summary, the binding models of these candidate compounds all exhibited non-covalent interactions with the identified key residues on the β'-CH of RNAP. In summary, the binding models of these candidate compounds all exhibited non-covalent interactions with the identified key residues on the β'-CH. This supports the hypothesis presented in the previous chapter that the trifluoromethyl and hydroxy groups contribute to stabilizing the binding of these compounds with RNAP and exhibit antimicrobial activities. It is important to note that the docking simulations were conducted without considering the dynamic flexibility of the target protein in the physiological environment. The flexible side-chain of key arginine residues probably build a binding pocket for inhibitors which was difficult to be predicted by the docking simulation.

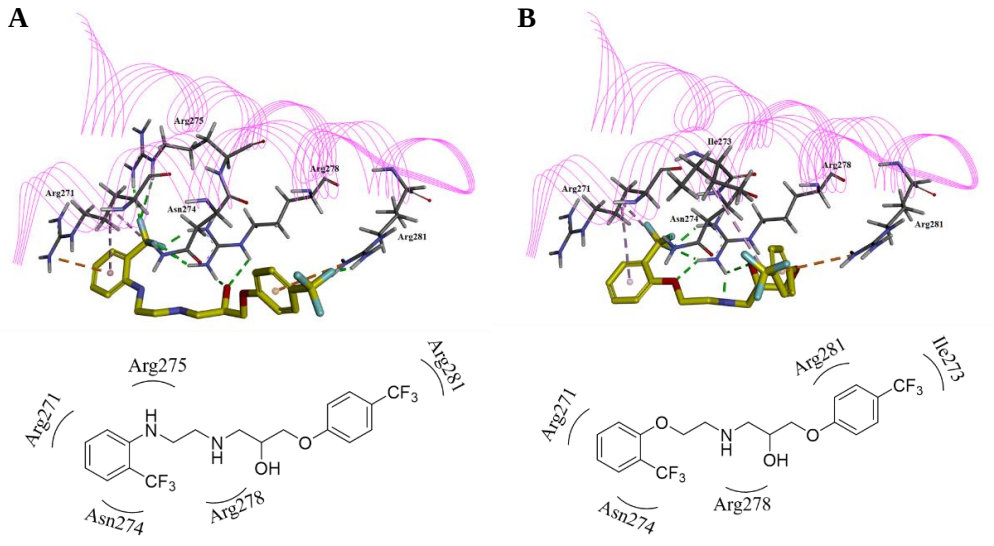

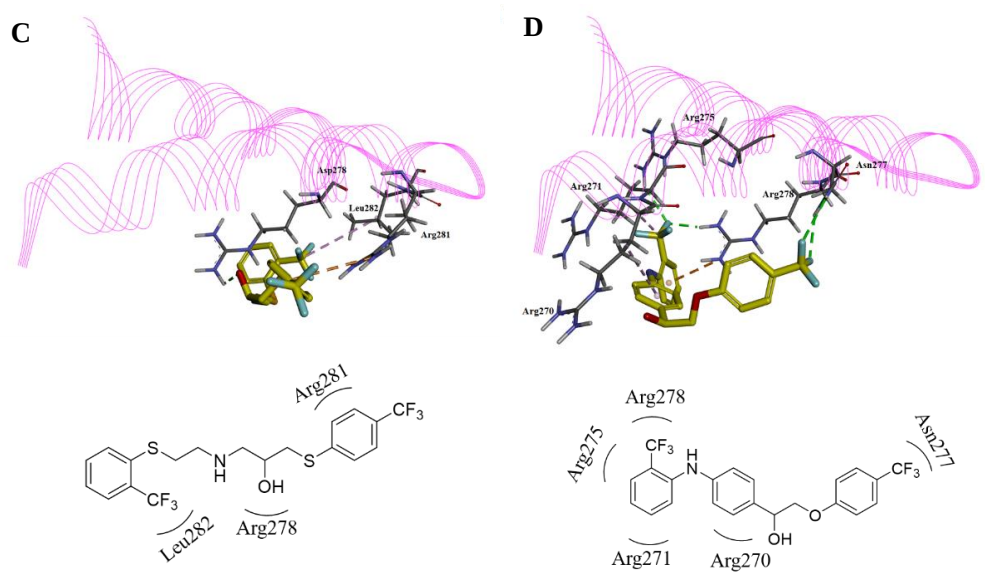

Figure 12. The binding models of compound **GI-19 (A), GI-36 (B), GI-39 (C)** and **GII-16 (D)**. The ligand and residues interacting with them were displayed in stick and the carbon atoms of ligands were colored in yellow. Essential non-covalent interactions being formed was displayed in dotted lines including hydrogen-bonds (in green), hydrophobic interactions (in pink) and electrostatic interactions (in orange). Chemical structure of candidate compounds was displayed with their relative position in the binding pocket, which was marked by residues interacting with them.

We also performed ADMET properties prediction on these candidate compounds, and the results are summarized in **Table 11**. All these derivatives exhibited high lipophilicity and low aqueous solubility, as indicated by their log(Sw) values . These characteristics are commonly observed in reported inhibitors of PPIs. In terms of absorption, these compounds displayed favorable oral absorption and bioavailability. However, they exhibited a high level of plasma protein binding (PPB), which suggests potential limitations in their distribution in vivo according to the free drug hypothesis [119]. Prediction of their inhibition on CYP2D6 indicated that these compounds acted as CYP2D6 inhibitors. The CYP2D6 enzyme is known to play a crucial role in the metabolism of many clinical drugs [120]. Inhibiting this enzyme suggests that the candidate compounds may have a longer half-life *in vivo* , but there is a potential for toxic accumulation. Additionally, the prediction of blood-brain barrier (BBB)

permeability and hepatotoxicity indicated that these compounds had the potential for central nervous system toxicity but not hepatotoxicity. Overall, the docking simulation and prediction of ADMET properties demonstrated that these candidate compounds possess drug-like properties and show potential for further *in vivo* testing.

Table 11: The ADMET properties prediction on **GI-19, GI-36, GI-39** and **GII-16**

Principal descriptors	**GI-19**	**GI-36**	**GI-39**	**GII-16**	**Standard Range**
log(Sw)	-5.602	-5.386	-6.354	-7.215	< -6.0 very low, < -4.1 low
Absorption level	0	0	0	1	0 (good absorption), 1 (moderate absorption)
EXT PPB	True	True	True	True	true (highly bound), false (not highly bound)
EXT CYP2D6#Prediction	True	True	True	True	true (CYP2D6 inhibitor), false (no inhibition on CYP2D6)
BBB level	1	1	0	0	0 (brain-blood ratio higher than 5:1), 1 (brain-blood ratio between 1:1 and 5:1)
EXT Hepatotoxic#Prediction	False	False	False	False	true (hepatotoxic), false (no hepatotoxic)

3.2 *In vitro* cytotoxicity assay

We have conducted an *in vitro* cytotoxicity assay on the candidate compounds derived from the aminoethyl derivative. The human lung carcinoma cell line A549 and human keratinocytes HaCaT were utilized in this assay. And the CC_{50}, defined as the concentration of the selected compound at which it reduced cell viability by 50%, was determined to assess their cytotoxicity. As shown in **Table 12**, compound **GI-19** exhibited mild cytotoxicity at concentrations of 10-17 μM. This finding is consistent with previous reports that aniline derivatives possess cytotoxic properties [121]. By

replacing the amino group of the linker, compounds **GI-36** and **GI-39** showed a moderate improvement in CC_{50} values, ranging from 14 to 40 μM. Additionally, the therapeutic index (TI) was calculated to compare the cytotoxicity of candidate compounds with antimicrobial activity. Compounds with higher TI values are predicted to be more effective and safer for further *in vivo* testing. Compound **GI-39** exhibited a preferred TI value of 5-6, compared to compounds **GI-19** and **GI-36**, which had TI values of 2-4**.** It is important to note that cell-based cytotoxicity assays provide preliminary testing and further evaluation through *in vivo* toxicity assays, along with pharmacokinetic studies, is necessary to fully assess the toxicity profile of these compounds.

Table 12: cytotoxicity of **GI-19, GI-36** and **GI-39** against human A549 and HaCaT cell lines.

Cpd.	MIC[a] (μg/ml)	CC_{50} (μM)		Therapeutic Index[b]	
		A549	HaCaT	A549	HaCaT
GI-19	4	10.47±0.70	17.12±2.33	2	4
GI-36	8	14.87±2.69	38.42±5.02	2	4
GI-39	4	20.78±3.18	24.91±2.67	5	6
DDP[c]		7.70±0.58	7.83±0.66		

[a] *S. pneumonia* ATCC® 49619

[b] Calculated by CC_{50} (μM)/ ½ MIC (μM)

[c] DDP: cisplatin

3.3 Fluorescence microscopy

The cellular effects of compounds **GI-19**, **GI-36** and **GI-39** were investigated through fluorescence microscopy experiments. The *B. subtilis* strain BS1048 was used, which

carries the green fluorescence protein (GFP)-tagged *β'*-subunit of RNAP due to the fusion of *gfp* to the *rpoC* gene. When observed under a microscope, the fluorescent signal was localized to the nucleoid region, which is the central chromosome-containing area of the cell (**Figure 13A-BLK**) [122]. As a positive control, the fluorescent signal became delocalized in rifampicin-treated cells (**Figure 13A-Pos. Ctrl**). Similar delocalization was observed in cells treated with the candidate compounds, and their antimicrobial activities against BS1048 strains were evaluated separately. The minimum inhibitory concentration (MIC) values for the candidate compounds were determined as follows: 16 μg/mL for **GI-19** (**Figure 13B**), 8 μg/mL for **GI-36** (**Figure 13C**) and 2 μg/mL for **GI-39** (**Figure 13D)**. Compared to the untreated cells, delocalization of the fluorescent signal was already observed in cells treated with lower concentrations of the candidate compounds (**Figure 13B-4 μg/mL, C-4 μg/mL** and **D-1 μg/mL**). This indicates that the compounds affect the localization of the GFP-tagged β'-subunit of RNAP in the cells.

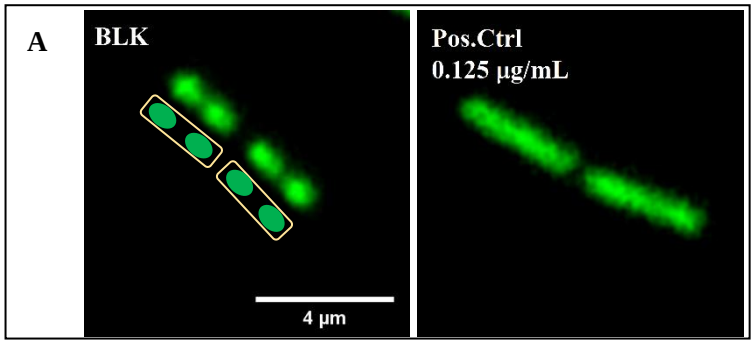

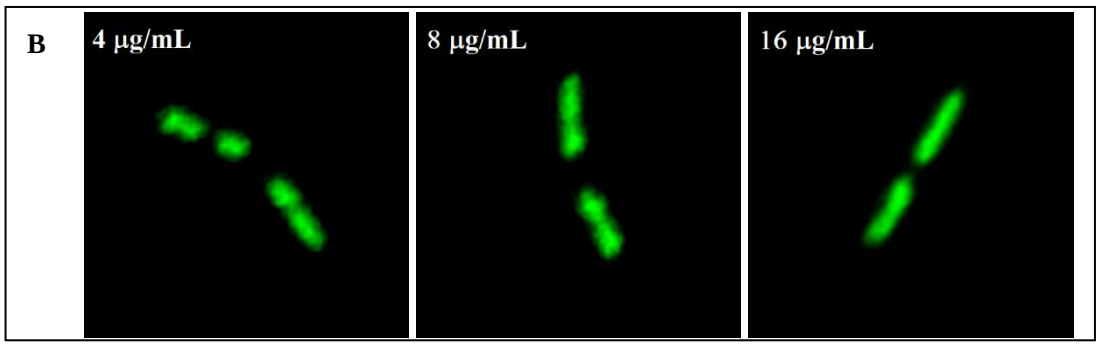

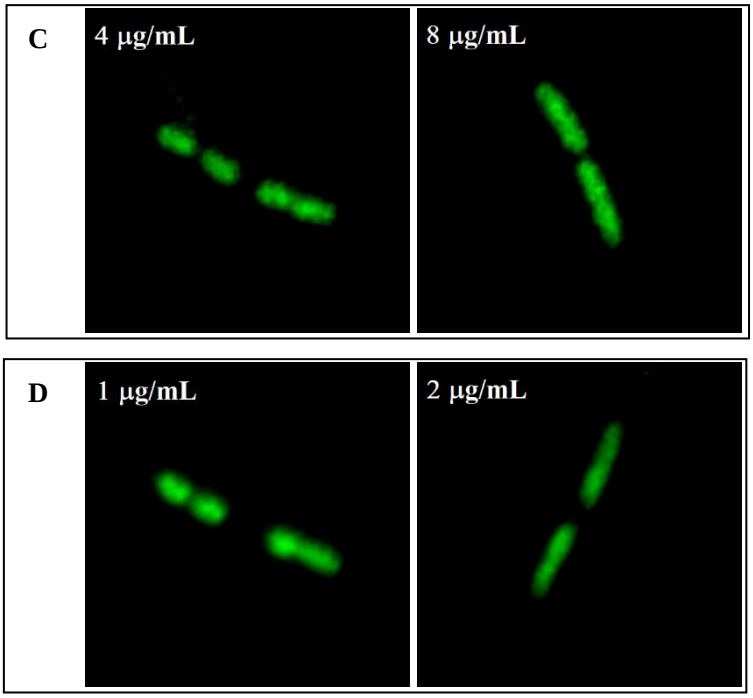

Figure 13. The confocal microscopy results of BS1048 cells with GFP-tagged RNAP. **A**): untreated cells and the positive control which was treated by rifampicin at the concentration of 0.125 μg/mL. **B**): **GI19**-treated cells with compound at the concentration of 4, 8, 16 μg/mL. **C**): **GI36**-treated cells with compound at the concentration of 4, 8 μg/mL. **D**): **GI39**-treated cells with compound at the concentration of 1, 2 μg/mL.

In addition, the strain BS128 carries the GFP-targeted NusG expressed through the fusion of the *gfp* gene with the *nusG* gene [123]. In untreated BS128 cells, the fluorescent signal exhibited a similar localization pattern to that observed in BS1048 cells, which is consistent with the known function of NusG in bacterial transcription (**Figure 14A-BLK**). As a positive control, rifampicin-treated cells were used, and the antimicrobial activities against BS128 strains were evaluated. The MIC values of **GI-19** and **GI-36** showed a decline to 4 μg/mL, following a similar trend to rifampicin treatment (**Figure 14B and C**). However, compound **GI-39** exhibited decreased but still moderate activities, with a MIC value of 8 μg/mL (**Figure 14D**). Similar to the observations in BS1048 cells, treatment with these candidate compounds at lower concentrations resulted in delocalization of the fluorescent signal in cells (**Figure 14B-1 μg/mL, C-1 μg/mL** and **D-2 μg/mL**). As the concentration increased, the diffusion of the fluorescent signal outside the nucleoid region became more

pronounced. These results from the fluorescence microscopy experiment demonstrate that these three candidate compounds have the ability to disrupt the normal localization of the bacterial transcription complex when assessed at the cellular level.

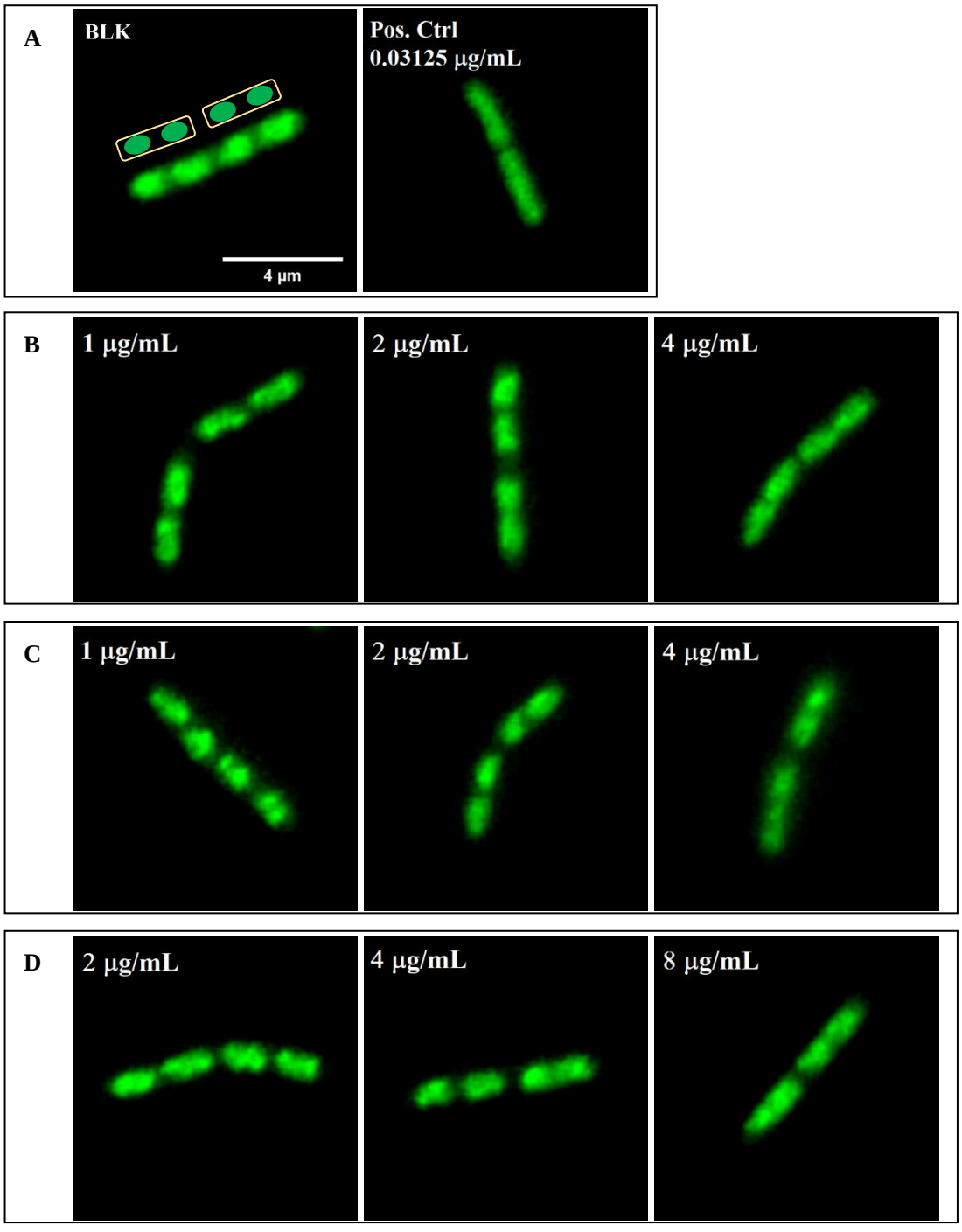

Figure 14. The confocal microscopy results of BS128 cells with GFP-tagged NusG. **A**): untreated cells and the positive control which was treated with rifampicin at the concentration of 0.03125 μg/mL. **B**): **GI19**-treated cells with compound at the concentration of 1, 2, 4 μg/mL. **C**): **GI36-**

treated cells with compound at the concentration of 1, 2, 4 μg/mL. **D**): **GI39**-treated cells with compound at the concentration of 2, 4, 8 μg/mL.

Chapter IV:

Conclusion and Prospect

In this project, we employed a rational drug discovery strategy to identify small-molecule antibiotics targeting the PPIs between the NGN domain of the NusG protein and the β' subunit of RNAP. We conducted virtual screening using a pharmacophore model based on key residues involved in these PPIs. The screening was performed on the MiniMaybridge database, resulting in 57 hits. Further evaluation through antibiotic susceptibility testing led us to discover a promising lead compound named **AW00783**. Based on this lead compound, we carried out modifications to generate 72 compounds classified into two categories: aminoethyl derivatives and aromatic derivatives. We evaluated the antimicrobial activity of these compounds against selected Gram-positive and Gram-negative strains to analyze the SARs analysis o within each category. Through SARs analysis, we selected four candidate compounds, **GI-19**, **GI-36**, **GI-39** and **GII-16** for further studies.

As first-in-class small-molecule antibiotics targeting the PPIs between RNAP and NusG, further testing of our candidate compounds was deemed necessary. In silico docking simulations confirmed that the candidate compounds formed non-covalent interactions with multiple residues on the β'-subunit in their binding models. Consistent with the SAR analysis, certain functional groups such as trifluoromethyl on terminal aromatic rings and hydroxy on the linking region were identified as necessary for interacting with key residues. Further biological testing was required to identify the key residues involved in the PPIs and accurately determine the binding sites of the candidate compounds. *In vitro* cytotoxicity testing and in silico ADMET properties prediction demonstrated that the candidate compounds possessed drug-like properties, despite showing mild cytotoxicity *in vitro*. Therefore, further *in vitro* and *in vivo* PK testing was necessary to assess their drug-like properties for further modifications.

In conclusion, we have successfully employed a rational drug discovery strategy to generate small-molecule antibiotics that target the β'-CH of RNAP through a rational drug-discovery strategy (**Figure 15**). These candidate compounds exhibited promising antimicrobial activities against both Gram-positive and -negative pathogens. However, further biological testing is required to validate their efficacy and safety profiles.

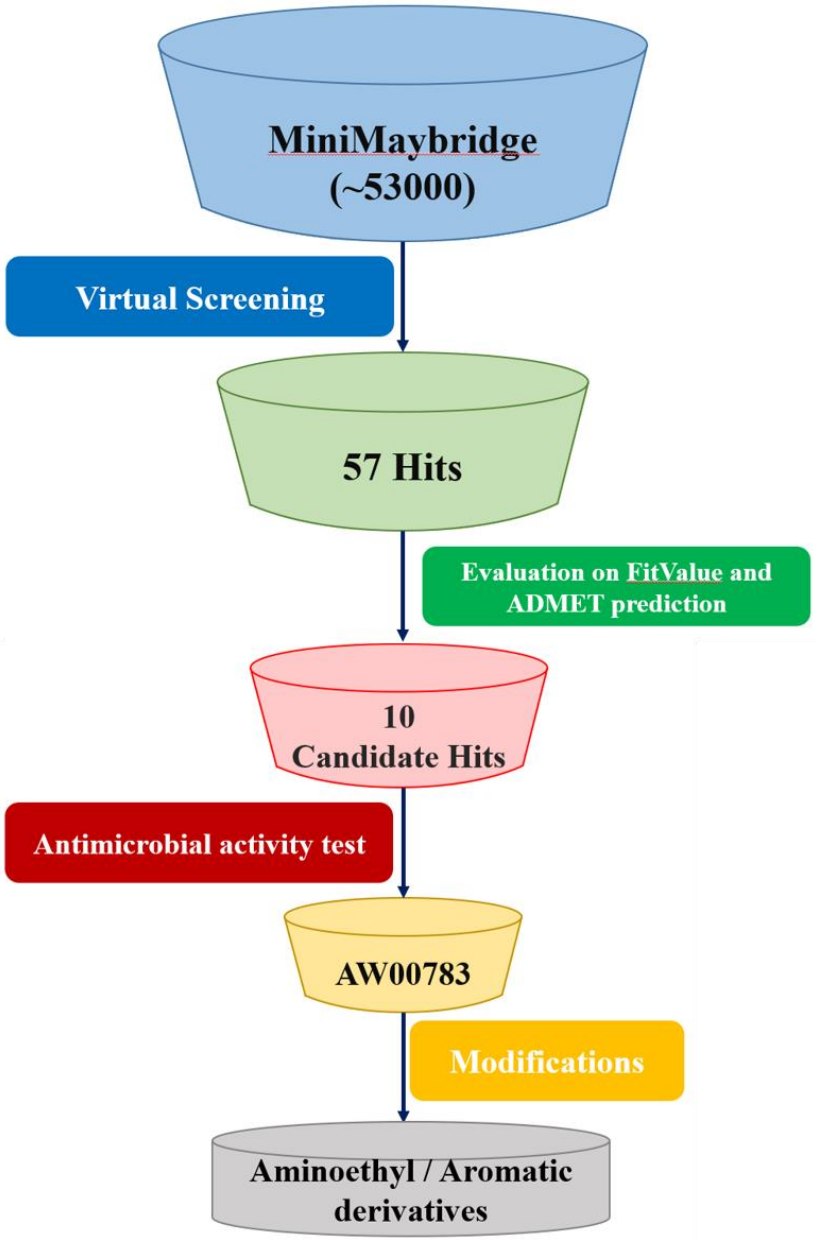

Figure 15. The procedure on the discovery of novel small-molecular antibiotic targeting on the β'-CH of RNAP.

Chapter V:

Experimental Section

5.1 Chemistry

Chemicals and reagents being utilized in synthesis, unless otherwise stated, were in commercial grade and required no purification. All reactions were monitored by thin-layer chromatography (TLC) on glass sheets (Silica gel F254) which were visualized under UV light. And flash chromatography purification was conducted by using silica gel (200-300 mesh) column. ^{1}H-NMR (400 MHz or 600 MHz) and ^{13}C-NMR (100 MHz or 150 MHz) spectra were measured on Bruker Advance-III spectrometer with TMS as an internal standard. Chemical shifts were presented in δ (ppm) and coupling constants (J) in Hz. High resolution mass spectrometry (HRMS) spectra were measured by Agilent 6540 liquid chromatography-electrospray ionization (LC-EI) QTOF Mass spectrometer. HPLC analysis was performed on Waters HPLC system including 2535 quaternary gradient module, 2707 autosampler and 2998 photodiode array (PDA) detector with a XBridge C18, 4.6×100 mm, 5 μM column.

5.1.1 The synthesis on substrates of aminoethyl derivatives

N^{1}-(pyrimidin-2-yl)ethane-1,2-diamine (A_1)

To a solution of 2-chloropyrimidine (50 mg, 0.44 mmol) and K_2CO_3 (72.4 mg, 0.52 mmol) in THF, ethylenediamine monohydrate (170.5 mg, 2.18 mmol) was added at room temperature. The mixture was stirred at reflux for overnight and monitored to react completely. After cooling to room temperature and filtration, the filtrate was concentrated and purified by column chromatography on silica gel with the elution fluid of DCM/MeOH (50:1-20:1, with additional drops of aqueous ammonia). Pale yellow solid was achieved in 50.1 mg with 83.1% yield. ^{1}H NMR (600 MHz, DMSO-d_6) δ 8.24 (d, J = 4.8 Hz, 2H), 7.24 (t, J = 5.7 Hz, 1H), 6.53 (t, J = 4.8 Hz, 1H), 3.30

(q, *J* = 6.2 Hz, 2H), 2.72 (t, *J* = 6.5 Hz, 2H).

N^1-(5-(trifluoromethyl)pyrimidin-2-yl)ethane-1,2-diamine (A_2)

To a solution of 2-chloro-5-(trifluoromethyl)pyrimidine (50 mg, 0.27 mmol) and K_2CO_3 (45.4 mg, 0.33 mmol) in THF, ethylenediamine monohydrate (107 mg, 1.37 mmol) was added at room temperature. The mixture was stirred at reflux for overnight and monitored to react completely. After cooling to room temperature and filtration, the filtrate was concentrated and purified by column chromatography on silica gel with the elution fluid of DCM/MeOH (50:1-20:1, with additional drops of aqueous ammonia). Pale yellow solid was achieved in 49.7 mg with 87.9% yield. ^{1}H NMR (400 MHz, DMSO-d_6) δ 8.62-8.52 (m, 2H), 8.12 (t, *J* = 5.7 Hz, 1H), 3.37 (s, 2H), 2.74 (d, *J* = 12.9 Hz, 2H).

N^1-(4-(trifluoromethyl)pyrimidin-2-yl)ethane-1,2-diamine (A_3)

To a solution of 2-chloro-4-(trifluoromethyl)pyrimidine (50 mg, 0.27 mmol) and K_2CO_3 (45.4 mg, 0.33 mmol) in THF, ethylenediamine monohydrate (107 mg, 1.37 mmol) was added at room temperature. The mixture was stirred at reflux for overnight and monitored to react completely. After cooling to room temperature and filtration, the filtrate was concentrated and purified by column chromatography on silica gel with the elution fluid of DCM/MeOH (50:1-20:1, with additional drops of aqueous ammonia). Pale yellow solid was achieved in 48.2 mg with 85.4% yield. ^{1}H NMR (600 MHz, DMSO-d_6) δ 8.59 (d, *J* = 26.5 Hz, 1H), 7.87 (d, *J* = 29.7 Hz, 1H), 6.95 (d, *J* = 4.9 Hz, 1H), 3.58 (s, 4H).

N^1-(6-(trifluoromethyl)pyridin-2-yl)ethane-1,2-diamine (A_4)

To a solution of 2-chloro-6-(trifluoromethyl)pyridine (50 mg, 0.28 mmol) and K_2CO_3 (45.7 mg, 0.34 mmol) in THF, ethylenediamine monohydrate (107.6 mg, 1.38 mmol) was added at room temperature. The mixture was stirred at reflux for overnight and monitored to react completely. After cooling to room temperature and filtration, the filtrate was concentrated and purified by column chromatography on silica gel with

the elution fluid of DCM/MeOH (100:1-30:1, with additional drops of aqueous ammonia). Pale yellow oil was achieved in 48.1 mg with 85.1% yield. ^{1}H NMR (600 MHz, Chloroform-*d*) δ 7.52 (t, *J* = 7.9 Hz, 1H), 6.92 (d, *J* = 7.2 Hz, 1H), 6.57 (d, *J* = 8.5 Hz, 1H), 5.18 (s, 1H), 3.42 (q, *J* = 5.8 Hz, 2H), 2.97 (t, *J* = 5.9 Hz, 2H).

N^1-(5-(trifluoromethyl)pyridin-2-yl)ethane-1,2-diamine (A_5)

To a solution of 2-chloro-5-(trifluoromethyl)pyridine (50 mg, 0.28 mmol) and K_2CO_3 (45.7 mg, 0.34 mmol) in THF, ethylenediamine monohydrate (107.6 mg, 1.38 mmol) was added at room temperature. The mixture was stirred at reflux for overnight and monitored to react completely. After cooling to room temperature and filtration, the filtrate was concentrated and purified by column chromatography on silica gel with the elution fluid of DCM/MeOH (100:1-30:1, with additional drops of aqueous ammonia). Pale yellow oil was achieved in 47.6 mg with 84.2% yield. ^{1}H NMR (400 MHz, Chloroform-*d*) δ 8.34 (d, *J* = 2.2 Hz, 1H), 7.58 (dd, *J* = 8.8, 2.4 Hz, 1H), 6.46 (d, *J* = 8.8 Hz, 1H), 5.38 (s, 1H), 3.45 (q, *J* = 5.8 Hz, 2H), 2.99 (s, 2H).

N^1-(4-(trifluoromethyl)pyridin-2-yl)ethane-1,2-diamine (A_6)

To a solution of 2-chloro-4-(trifluoromethyl)pyridine (50 mg, 0.28 mmol) and K_2CO_3 (45.7 mg, 0.34 mmol) in THF, ethylenediamine monohydrate (107.6 mg, 1.38 mmol) was added at room temperature. The mixture was stirred at reflux for overnight and monitored to react completely. After cooling to room temperature and filtration, the filtrate was concentrated and purified by column chromatography on silica gel with the elution fluid of DCM/MeOH (100:1-30:1, with additional drops of aqueous ammonia). Pale yellow oil was achieved in 48.4 mg with 85.6% yield. ^{1}H NMR (600 MHz, Chloroform-*d*) δ 8.22 (d, *J* = 5.3 Hz, 1H), 6.75 (dd, *J* = 5.3, 1.4 Hz, 1H), 6.61 (s, 1H), 5.23 (s, 1H), 3.43 (q, *J* = 5.8 Hz, 2H), 2.99 (t, *J* = 5.9 Hz, 2H).

N^1-(3-(trifluoromethyl)pyridin-2-yl)ethane-1,2-diamine (A_7)

To a solution of 2-chloro-3-(trifluoromethyl)pyridine (50 mg, 0.28 mmol) and K_2CO_3 (45.7 mg, 0.34 mmol) in THF, ethylenediamine monohydrate (107.6 mg, 1.38 mmol)

was added at room temperature. The mixture was stirred at reflux for overnight and monitored to react completely. After cooling to room temperature and filtration, the filtrate was concentrated and purified by column chromatography on silica gel with the elution fluid of DCM/MeOH (100:1-30:1, with additional drops of aqueous ammonia). Pale yellow oil was achieved in 46.4 mg with 82.2% yield. ^{1}H NMR (600 MHz, Chloroform-*d*) δ 8.28-8.24 (m, 1H), 7.66 (dd, *J* = 7.6, 1.7 Hz, 1H), 6.63 (dd, *J* = 7.5, 5.0 Hz, 1H), 5.38 (s, 1H), 3.58 (q, *J* = 5.7 Hz, 2H), 2.98 (t, *J* = 6.0 Hz, 2H).

N^1-(5-fluoropyridin-2-yl)ethane-1,2-diamine (A_8)

To a solution of 2-chloro-5-fluoropyridine (50 mg, 0.38 mmol) and K_2CO_3 (63 mg, 0.46 mmol) in THF, ethylenediamine monohydrate (148.5 mg, 1.9 mmol) was added at room temperature. The mixture was stirred at reflux for overnight and monitored to react completely. After cooling to room temperature and filtration, the filtrate was concentrated and purified by column chromatography on silica gel with the elution fluid of DCM/MeOH (100:1-30:1, with additional drops of aqueous ammonia). Pale yellow oil was achieved in 46.1 mg with 78.2% yield. 1H NMR (600 MHz, DMSO-d_6) δ 7.73 (s, 1H), 7.14 (d, *J* = 8.7 Hz, 1H), 7.01 (d, *J* = 8.7 Hz, 1H), 6.15 (s, 1H), 3.07-3.00 (m, 2H), 2.72 (d, *J* = 6.8 Hz, 2H).

N^1-(5-nitropyridin-2-yl)ethane-1,2-diamine (A_9)

To a solution of 2-chloro-5-nitropyridine (50 mg, 0.32 mmol) and K_2CO_3 (52.3 mg, 0.38 mmol) in THF, ethylenediamine monohydrate (123.2 mg, 1.58 mmol) was added at room temperature. The mixture was stirred at reflux for overnight and monitored to react completely. After cooling to room temperature and filtration, the filtrate was concentrated and purified by column chromatography on silica gel with the elution fluid of DCM/MeOH (100:1-30:1, with additional drops of aqueous ammonia). Yellow oil was achieved in 49.2 mg with 85.6% yield. ^{1}H NMR (600 MHz, DMSO-d_6) δ 8.91 (d, *J* = 2.8 Hz, 1H), 8.15-8.05 (m, 1H), 6.62 (d, *J* = 9.3 Hz, 1H), 3.50 (s, 2H), 2.85 (t, *J* = 6.2 Hz, 2H).

N^1-(2-(trifluoromethyl)phenyl)ethane-1,2-diamine (A_{10})

To a solution of 1-iodo-2-(trifluoromethyl)benzene (50 mg, 0.18 mmol), CuCl (3.6 mg, 0.038 mmol) and Cs_2CO_3 (119.8 mg, 0.37 mmol) in DMSO, ethylenediamine monohydrate (71.8 mg, 0.92 mmol) was added at room temperature. The mixture was stirred at 120 ℃ for 8 hours and monitored to react completely. After cooling to room temperature and filtration, water was added and the filtrate was extracted with ethyl acetate for three times and washed with saturated brine. The combined organic layer was dried over anhydrous Na_2SO_4 and purified by column chromatography on silica gel with the elution fluid of DCM/MeOH (200:1-100:1, with additional drops of aqueous ammonia). Pale yellow oil was achieved in 26.4 mg with 70.3% yield. ^{1}H NMR (400 MHz, Chloroform-*d*) δ 7.46 (d, J = 7.7 Hz, 1H), 7.38 (t, J = 7.9 Hz, 1H), 6.79-6.71 (m, 2H), 4.79 (s, 1H), 3.27 (q, J = 5.7 Hz, 2H), 3.02 (t, J = 5.9 Hz, 2H).

N^1-([1,1'-biphenyl]-4-yl)ethane-1,2-diamine (A_{11})

To a solution of 4-iodo-1,1'-biphenyl (50 mg, 0.18 mmol), CuCl (3.5 mg, 0.037 mmol) and Cs_2CO_3 (116.3 mg, 0.36 mmol) in DMSO, ethylenediamine monohydrate (69.7 mg, 0.89 mmol) was added at room temperature. The mixture was stirred at 120 ℃ for 8 hours and monitored to react completely. After cooling to room temperature and filtration, water was added and the filtrate was extracted with ethyl acetate for three times and washed with saturated brine. The combined organic layer was dried over anhydrous Na_2SO_4 and purified by column chromatography on silica gel with the elution fluid of DCM/MeOH (200:1-100:1, with additional drops of aqueous ammonia). Pale yellow oil was achieved in 28.5 mg with 75.2% yield. ^{1}H NMR (400 MHz, Chloroform-*d*) δ 8.26 (d, J = 1.6 Hz, 1H), 7.57-7.54 (m, 2H), 7.49-7.46 (m, 2H), 7.42 (t, J = 7.7 Hz, 2H), 7.31 (d, J = 1.3 Hz, 2H), 6.75-6.70 (m, 2H), 3.62 (q, J = 6.0 Hz, 2H), 3.40 (t, J = 5.8 Hz, 2H).

N^1-(4-(trifluoromethyl)phenyl)ethane-1,2-diamine (A_{12})

To a solution of 1-iodo-4-(trifluoromethyl)benzene (50 mg, 0.18 mmol), CuCl (3.6 mg, 0.038 mmol) and Cs_2CO_3 (119.8 mg, 0.37 mmol) in DMSO, ethylenediamine monohydrate (71.8 mg, 0.92 mmol) was added at room temperature. The mixture was

stirred at 120 ℃ for 8 hours and monitored to react completely. After cooling to room temperature and filtration, water was added and the filtrate was extracted with ethyl acetate for three times and washed with saturated brine. The combined organic layer was dried over anhydrous Na_2SO_4 and purified by column chromatography on silica gel with the elution fluid of DCM/MeOH (200:1-100:1, with additional drops of aqueous ammonia). Pale yellow oil was achieved in 27.1 mg with 72.2% yield. ^{1}H NMR (400 MHz, Chloroform-*d*) δ 8.27 (s, 1H), 7.43 (d, J = 8.4 Hz, 2H), 6.64 (d, J = 8.4 Hz, 2H), 5.89 (s, 1H), 4.50 (s, 1H), 3.61 (q, J = 6.0 Hz, 2H), 3.37 (q, J = 5.6 Hz, 2H).

N^1-(3-(trifluoromethyl)phenyl)ethane-1,2-diamine (A_{13})

To a solution of 1-iodo-3-(trifluoromethyl)benzene (50 mg, 0.18 mmol), CuCl (3.6 mg, 0.038 mmol) and Cs_2CO_3 (119.8 mg, 0.37 mmol) in DMSO, ethylenediamine monohydrate (71.8 mg, 0.92 mmol) was added at room temperature. The mixture was stirred at 120 ℃ for 8 hours and monitored to react completely. After cooling to room temperature and filtration, water was added and the filtrate was extracted with ethyl acetate for three times and washed with saturated brine. The combined organic layer was dried over anhydrous Na_2SO_4 and purified by column chromatography on silica gel with the elution fluid of DCM/MeOH (200:1-100:1, with additional drops of aqueous ammonia). Pale yellow oil was achieved in 28.1 mg with 74.8% yield. ^{1}H NMR (400 MHz, Chloroform-*d*) δ 7.26 (d, J = 7.9 Hz, 1H), 6.95 (d, J = 7.6 Hz, 1H), 6.84 (d, J = 2.4 Hz, 1H), 6.79 (dd, J = 8.2, 2.3 Hz, 1H), 4.34 (s, 1H), 3.22 (t, J = 5.8 Hz, 2H), 3.00 (t, J = 5.8 Hz, 2H).

N^1-(2-nitrophenyl)ethane-1,2-diamine (A_{14})

To a solution of 1-iodo-2-nitrobenzene (50 mg, 0.2 mmol), CuCl (4 mg, 0.041 mmol) and Cs_2CO_3 (130.9 mg, 0.4 mmol) in DMSO, ethylenediamine monohydrate (76.4 mg, 1 mmol) was added at room temperature. The mixture was stirred at 120 ℃ for 8 hours and monitored to react completely. After cooling to room temperature and filtration, water was added and the filtrate was extracted with ethyl acetate for three

times and washed with saturated brine. The combined organic layer was dried over anhydrous Na_2SO_4 and purified by column chromatography on silica gel with the elution fluid of DCM/MeOH (200:1-100:1, with additional drops of aqueous ammonia). Yellow oil was achieved in 27.8 mg with 76.4% yield. ^{1}H NMR (400 MHz, Chloroform-*d*) δ 8.27 (s, 1H), 8.18 (dt, *J* = 8.6, 2.8 Hz, 1H), 7.44 (m, *J* = 8.9, 5.3, 2.1 Hz, 1H), 6.88 (dd, *J* = 8.7, 2.6 Hz, 1H), 6.65 (m, *J* = 8.8, 7.3, 3.5 Hz, 1H), 3.44-3.36 (m, 2H), 3.07 (td, *J* = 6.1, 3.1 Hz, 2H).

2-((2-aminoethyl)amino)benzonitrile (A_{15})

To a solution of 2-iodobenzonitrile (50 mg, 0.22 mmol), CuCl (4.3 mg, 0.044 mmol) and Cs_2CO_3 (142.3 mg, 0.44 mmol) in DMSO, ethylenediamine monohydrate (83.1 mg, 1.1 mmol) was added at room temperature. The mixture was stirred at 120 ℃ for 8 hours and monitored to react completely. After cooling to room temperature and filtration, water was added and the filtrate was extracted with ethyl acetate for three times and washed with saturated brine. The combined organic layer was dried over anhydrous Na_2SO_4 and purified by column chromatography on silica gel with the elution fluid of DCM/MeOH (200:1-100:1, with additional drops of aqueous ammonia). Pale yellow oil was achieved in 27.6 mg with 78.5% yield. ^{1}H NMR (600 MHz, Chloroform-*d*) δ 7.40 (td, *J* = 7.6, 1.5 Hz, 2H), 6.72-6.68 (m, 2H), 3.40 (t, *J* = 5.8 Hz, 2H), 3.07 (t, *J* = 5.8 Hz, 2H).

***N*-(2-aminoethyl)-2-(trifluoromethyl)benzenesulfonamide (A_{16})**

To a solution of ethylenediamine monohydrate (16 mg, 0.2 mmol) and triethylamine (62.1 mg, 0.61 mmol) in DCM, 2-(trifluoromethyl)benzenesulfonyl chloride (50 mg, 0.2 mmol) was added dropwise in ice bath. After warming to room temperature, the mixture was stirred for overnight and monitored to react completely. The mixture was concentrated and purified by column chromatography on silica gel with the elution fluid of DCM/MeOH (200:1-50:1, with additional drops of aqueous ammonia). Yellow oil was achieved in 50.5 mg with 92.1% yield. ^{1}H NMR (400 MHz, Methanol-d_4) δ 8.23-8.17 (m, 1H), 7.98 (dd, *J* = 6.9, 2.2 Hz, 1H), 7.83 (m, *J* = 6.1, 5.3, 2.7 Hz,

2H), 3.05 (t, *J* = 6.2 Hz, 2H), 2.78 (t, *J* = 6.2 Hz, 2H).

2-(2-(trifluoromethyl)phenoxy)ethan-1-amine (A_{17})

To a solution of 2-(trifluoromethyl)phenol (50 mg, 0.31 mmol) and K_2CO_3 (426.3 mg, 3.08 mmol) in DMF, *tert*-butyl (2-bromoethyl)carbamate (82.9 mg, 0.37 mmol) was added at room temperature. The mixture was stirred at 65 ℃ for 8 hours and monitored to react completely. After cooling to room temperature and filtration, water was added and the filtrate was extracted with ethyl acetate for three times and washed with saturated brine. The combined organic layer was dried over anhydrous Na_2SO_4 and purified by column chromatography on silica gel with the elution fluid of Hexane/EA (10:1-5:1). *tert*-butyl (2-(2-(trifluoromethyl)phenoxy)ethyl)carbamate was achieved in 83.6 mg with 88.8% yield. ^{1}H NMR (400 MHz, Methanol-d_4) δ 7.55 (m, *J* = 14.0, 7.7, 1.7 Hz, 2H), 7.16 (d, *J* = 8.3 Hz, 1H), 7.06 (t, *J* = 7.6 Hz, 1H), 4.13 (t, *J* = 5.9 Hz, 2H), 3.48 (m, *J* = 5.9, 4.6 Hz, 2H), 1.45 (s, 9H).

To a solution of *tert*-butyl (2-(2-(trifluoromethyl)phenoxy)ethyl)carbamate (50 mg, 0.16 mmol) in DCM, TFA (186.7 mg, 1.64 mmol) was added at room temperature. The mixture was stirred at reflux for 8 hours and monitored to react completely. After cooling to room temperature, NaOH aqueous (1M) solution was added in ice bath to regulate the pH value ranging from 8 to 10. The mixture was extracted with DCM for three times and washed with saturated brine. The combined organic layer was dried over anhydrous Na_2SO_4 and concentrated. Pale yellow oil was achieved in 32.1 mg with 95.6% yield. ^{1}H NMR (600 MHz, Chloroform-*d*) δ 7.62 (dd, *J* = 7.8, 1.5 Hz, 1H), 7.56-7.52 (m, 1H), 7.11 (t, *J* = 7.6 Hz, 1H), 7.01 (d, *J* = 8.3 Hz, 1H), 4.22 (t, *J* = 5.0 Hz, 2H), 3.86 (q, *J* = 5.4 Hz, 2H).

2-((2-(trifluoromethyl)phenyl)thio)ethan-1-amine (A_{18})

To a solution of 2-(trifluoromethyl)benzenethiol (50 mg, 0.28 mmol) and K_2CO_3 (387.8 mg, 2.81 mmol) in DMF, tert-butyl (2-bromoethyl)carbamate (75.5 mg, 0.34 mmol) was added at room temperature. The mixture was stirred at 65 ℃ for 8 hours and monitored to react completely. After cooling to room temperature and filtration,

water was added and the filtrate was extracted with ethyl acetate for three times and washed with saturated brine. The combined organic layer was dried over anhydrous Na_2SO_4 and purified by column chromatography on silica gel with the elution fluid of Hexane/EA (10:1-5:1). *tert*-butyl (2-((2-(trifluoromethyl)phenyl)thio)ethyl)carbamate was achieved in 58.8 mg with 65.2% yield. ^{1}H NMR (400 MHz, Methanol-d_4) δ 7.67 (t, J = 7.8 Hz, 2H), 7.55 (t, J = 7.8 Hz, 1H), 7.33 (t, J = 7.7 Hz, 1H), 4.85 (d, J = 1.9 Hz, 1H), 3.32-3.24 (m, 2H), 3.11 (dd, J = 8.3, 6.1 Hz, 2H), 1.44 (s, 9H).

To a solution of *tert*-butyl (2-((2-(trifluoromethyl)phenyl)thio)ethyl)carbamate (50 mg, 0.15 mmol) in DCM, TFA (177.4 mg, 1.56 mmol) was added at room temperature. The mixture was stirred at reflux for 8 hours and monitored to react completely. After cooling to room temperature, NaOH aqueous (1M) solution was added in ice bath to regulate the pH value ranging from 8 to 10. The mixture was extracted with DCM for three times and washed with saturated brine. The combined organic layer was dried over anhydrous Na_2SO_4 and concentrated. Pale yellow oil was achieved in 33.1 mg with 96.3% yield. ^{1}H NMR (600 MHz, Chloroform-d) δ 7.67-7.63 (m, 1H), 7.53 (d, J = 7.9 Hz, 1H), 7.47 (t, J = 7.7 Hz, 1H), 7.29 (d, J = 15.3 Hz, 1H), 3.07 (td, J = 6.3, 1.6 Hz, 2H), 2.92 (td, J = 6.3, 1.7 Hz, 2H).

2-((4-nitrophenoxy)methyl)oxirane (B_1)

The solution of 4-nitrophenol (50 mg, 0.36 mmol), Cs_2CO_3 (175.7 mg, 0.54 mmol) and KI (11.9 mg, 0.072 mmol) in DMF being stirred at room temperature for 30 minutes, 2-(chloromethyl)oxirane (99.8 mg, 1.08 mmol) was added at room temperature. The solution was stirred at 80 ℃ for overnight and monitored to react completely. After cooling to room temperature and filtration, water was added and the filtrate was extracted with ethyl acetate for three times and washed with saturated brine. The combined organic layer was dried over anhydrous Na_2SO_4 and purified by column chromatography on silica gel with the elution fluid of Hexane/EA (200:1-50:1). Yellow oil was achieved in 57.9 mg with 82.6% yield. ^{1}H NMR (400 MHz, DMSO-d_6) δ 8.25-8.19 (m, 2H), 7.22-7.16 (m, 2H), 4.53 (dd, J = 11.5, 2.5 Hz, 1H),

4.00 (dd, *J* = 11.5, 6.6 Hz, 1H), 3.39 (m, *J* = 6.8, 5.0, 2.6 Hz, 1H), 2.88 (t, *J* = 4.6 Hz, 1H), 2.75 (dd, *J* = 5.1, 2.6 Hz, 1H).

2-(phenoxymethyl)oxirane (B_2)

The solution of phenol (50 mg, 0.53 mmol), Cs_2CO_3 (259.7 mg, 0.8 mmol) and KI (17.6 mg, 0.072 mmol) in DMF being stirred at room temperature for 30 minutes, 2-(chloromethyl)oxirane (147.5 mg, 1.59 mmol) was added at room temperature. The solution was stirred at 80 ℃ for overnight and monitored to react completely. After cooling to room temperature and filtration, water was added and the filtrate was extracted with ethyl acetate for three times and washed with saturated brine. The combined organic layer was dried over anhydrous Na_2SO_4 and purified by column chromatography on silica gel with the elution fluid of Hexane/EA (200:1-50:1). Pale yellow oil was achieved in 67.2 mg with 84.2% yield. ^{1}H NMR (400 MHz, Chloroform-*d*) δ 7.36-7.30 (m, 2H), 7.04-6.94 (m, 3H), 4.25 (dd, *J* = 11.0, 3.1 Hz, 1H), 3.97 (dd, *J* = 11.0, 5.7 Hz, 1H), 3.38 (m, *J* = 5.7, 4.1, 2.8 Hz, 1H), 2.92 (t, *J* = 4.5 Hz, 1H), 2.78 (dd, *J* = 5.0, 2.7 Hz, 1H).

methyl 4-(oxiran-2-ylmethoxy)benzoate (B_3)

The solution of methyl 4-hydroxybenzoate (50 mg, 0.33 mmol), Cs_2CO_3 (160.6 mg, 0.49 mmol) and KI (10.9 mg, 0.066 mmol) in DMF being stirred at room temperature for 30 minutes, 2-(chloromethyl)oxirane (91.2 mg, 0.99 mmol) was added at room temperature. The solution was stirred at 80 ℃ for overnight and monitored to react completely. After cooling to room temperature and filtration, water was added and the filtrate was extracted with ethyl acetate for three times and washed with saturated brine. The combined organic layer was dried over anhydrous Na_2SO_4 and purified by column chromatography on silica gel with the elution fluid of Hexane/EA (200:1-50:1). Pale yellow oil was achieved in 54 mg with 78.9% yield. ^{1}H NMR (600 MHz, Chloroform-*d*) δ 8.00-7.98 (m, 2H), 6.95-6.92 (m, 2H), 4.30 (dd, *J* = 11.0, 3.0 Hz, 1H), 3.98 (dd, *J* = 11.0, 5.9 Hz, 1H), 3.88 (s, 3H), 3.38 (m, *J* = 5.7, 4.0, 2.7 Hz, 1H), 2.93 (t, *J* = 4.5 Hz, 1H), 2.77 (dd, *J* = 4.9, 2.6 Hz, 1H).

2-((4-fluorophenoxy)methyl)oxirane (B_4)

The solution of 4-fluorophenol (50 mg, 0.45 mmol), Cs_2CO_3 (218 mg, 0.67 mmol) and KI (14.8 mg, 0.089 mmol) in DMF being stirred at room temperature for 30 minutes, 2-(chloromethyl)oxirane (123.8 mg, 1.34 mmol) was added at room temperature. The solution was stirred at 80 ℃ for overnight and monitored to react completely. After cooling to room temperature and filtration, water was added and the filtrate was extracted with ethyl acetate for three times and washed with saturated brine. The combined organic layer was dried over anhydrous Na_2SO_4 and purified by column chromatography on silica gel with the elution fluid of Hexane/EA (200:1-50:1). Pale yellow oil was achieved in 62.6 mg with 83.5% yield. ^{1}H NMR (400 MHz, Chloroform-*d*) δ 7.56 (d, *J* = 8.3 Hz, 2H), 7.00 (d, *J* = 8.3 Hz, 2H), 4.32 (m, *J* = 11.1, 2.0 Hz, 1H), 3.98 (m, *J* = 11.1, 6.0, 1.9 Hz, 1H), 3.38 (m, *J* = 2.5 Hz, 1H), 2.98-2.91 (m, 1H), 2.78 (m, *J* = 4.6, 2.1 Hz, 1H).

2-((3,4-difluorophenoxy)methyl)oxirane (B_5)

The solution of 3,4-difluorophenol (50 mg, 0.38 mmol), Cs_2CO_3 (187.8 mg, 0.58 mmol) and KI (12.8 mg, 0.077 mmol) in DMF being stirred at room temperature for 30 minutes, 2-(chloromethyl)oxirane (106.7 mg, 1.15 mmol) was added at room temperature. The solution was stirred at 80 ℃ for overnight and monitored to react completely. After cooling to room temperature and filtration, water was added and the filtrate was extracted with ethyl acetate for three times and washed with saturated brine. The combined organic layer was dried over anhydrous Na_2SO_4 and purified by column chromatography on silica gel with the elution fluid of Hexane/EA (200:1-50:1). Pale yellow oil was achieved in 58.6 mg with 81.9% yield. ^{1}H NMR (600 MHz, Chloroform-*d*) δ 7.07 (q, *J* = 9.3 Hz, 1H), 6.76 (m, *J* = 11.9, 6.5, 3.0 Hz, 1H), 6.63 (m, *J* = 8.5, 3.2, 1.7 Hz, 1H), 4.23 (dd, *J* = 11.0, 2.8 Hz, 1H), 3.87 (dd, *J* = 11.0, 5.9 Hz, 1H), 3.35 (m, *J* = 6.0, 4.0, 2.8 Hz, 1H), 2.93 (t, *J* = 4.5 Hz, 1H), 2.76 (dd, *J* = 4.8, 2.6 Hz, 1H).

2-((4-methoxyphenoxy)methyl)oxirane (B_6)

The solution of 4-methoxyphenol (50 mg, 0.4 mmol), Cs_2CO_3 (196.9 mg, 0.6 mmol) and KI (13.4 mg, 0.08 mmol) in DMF being stirred at room temperature for 30 minutes, 2-(chloromethyl)oxirane (111.8 mg, 1.21 mmol) was added at room temperature. The solution was stirred at 80 ℃ for overnight and monitored to react completely. After cooling to room temperature and filtration, water was added and the filtrate was extracted with ethyl acetate for three times and washed with saturated brine. The combined organic layer was dried over anhydrous Na_2SO_4 and purified by column chromatography on silica gel with the elution fluid of Hexane/EA (200:1-50:1). Yellow oil was achieved in 55.3 mg with 76.2% yield. ^{1}H NMR (400 MHz, Chloroform-*d*) δ 7.28 (t, *J* = 3.4 Hz, 2H), 6.92-6.87 (m, 2H), 4.23 (dd, *J* = 11.1, 3.1 Hz, 1H), 3.96 (dd, *J* = 11.1, 5.7 Hz, 1H), 3.39-3.33 (m, 1H), 2.93 (t, *J* = 4.5 Hz, 1H), 2.77 (dd, *J* = 4.9, 2.7 Hz, 1H), 2.47 (s, 3H).

2-((4-(trifluoromethyl)phenoxy)methyl)oxirane (B_7)

The solution of 4-(trifluoromethyl)phenol (50 mg, 0.31 mmol), Cs_2CO_3 (150.7 mg, 0.46 mmol) and KI (10.2 mg, 0.062 mmol) in DMF being stirred at room temperature for 30 minutes, 2-(chloromethyl)oxirane (85.6 mg, 0.93 mmol) was added at room temperature. The solution was stirred at 80 ℃ for overnight and monitored to react completely. After cooling to room temperature and filtration, water was added and the filtrate was extracted with ethyl acetate for three times and washed with saturated brine. The combined organic layer was dried over anhydrous Na_2SO_4 and purified by column chromatography on silica gel with the elution fluid of Hexane/EA (200:1-50:1). Pale yellow oil was achieved in 57.4 mg with 85.3% yield. ^{1}H NMR (400 MHz, Chloroform-*d*) δ 7.60-7.49 (m, 2H), 7.04-6.93 (m, 2H), 4.30 (m, *J* = 11.1, 2.2 Hz, 1H), 3.94 (m, *J* = 10.9, 5.9, 3.1 Hz, 1H), 3.35 (m, *J* = 5.6, 4.1, 2.6 Hz, 1H), 2.90 (dd, *J* = 5.7, 3.3 Hz, 1H), 2.75 (m, *J* = 4.8, 2.5 Hz, 1H).

2-((3-(trifluoromethyl)phenoxy)methyl)oxirane (B_8)

The solution of 3-(trifluoromethyl)phenol (50 mg, 0.31 mmol), Cs_2CO_3 (150.7 mg, 0.46 mmol) and KI (10.2 mg, 0.062 mmol) in DMF being stirred at room temperature

for 30 minutes, 2-(chloromethyl)oxirane (85.6 mg, 0.93 mmol) was added at room temperature. The solution was stirred at 80 ℃ for overnight and monitored to react completely. After cooling to room temperature and filtration, water was added and the filtrate was extracted with ethyl acetate for three times and washed with saturated brine. The combined organic layer was dried over anhydrous Na_2SO_4 and purified by column chromatography on silica gel with the elution fluid of Hexane/EA (200:1-50:1). Pale yellow oil was achieved in 55 mg with 81.8% yield. ^{1}H NMR (400 MHz, Chloroform-*d*) δ 7.41 (t, *J* = 8.0 Hz, 1H), 7.25 (s, 1H), 7.17 (d, *J* = 2.1 Hz, 1H), 7.12 (dd, *J* = 8.3, 2.5 Hz, 1H), 4.31 (dt, *J* = 10.9, 2.2 Hz, 1H), 3.97 (m, *J* = 11.1, 5.9, 1.5 Hz, 1H), 3.39 (m, *J* = 8.7, 4.4, 2.1, 1.7 Hz, 1H), 2.94 (td, *J* = 4.5, 1.4 Hz, 1H), 2.79 (dt, *J* = 4.4, 2.0 Hz, 1H).

2-((2-(trifluoromethyl)phenoxy)methyl)oxirane (B_9)

The solution of 2-(trifluoromethyl)phenol (50 mg, 0.31 mmol), Cs_2CO_3 (150.7 mg, 0.46 mmol) and KI (10.2 mg, 0.062 mmol) in DMF being stirred at room temperature for 30 minutes, 2-(chloromethyl)oxirane (85.6 mg, 0.93 mmol) was added at room temperature. The solution was stirred at 80 ℃ for overnight and monitored to react completely. After cooling to room temperature and filtration, water was added and the filtrate was extracted with ethyl acetate for three times and washed with saturated brine. The combined organic layer was dried over anhydrous Na_2SO_4 and purified by column chromatography on silica gel with the elution fluid of Hexane/EA (200:1-50:1). Pale yellow oil was achieved in 56.2 mg with 83.5% yield. ^{1}H NMR (400 MHz, Chloroform-*d*) δ 7.59 (dd, *J* = 7.6, 1.6 Hz, 1H), 7.50 (td, *J* = 8.0, 1.6 Hz, 1H), 7.05 (t, *J* = 8.4 Hz, 2H), 4.35 (dd, *J* = 11.2, 2.9 Hz, 1H), 4.12 (dd, *J* = 11.2, 5.0 Hz, 1H), 3.39 (m, *J* = 5.0, 2.9 Hz, 1H), 2.92 (t, *J* = 4.6 Hz, 1H), 2.85 (dd, *J* = 5.0, 2.6 Hz, 1H).

4-(oxiran-2-ylmethoxy)benzonitrile (B_{10})

The solution of 4-hydroxybenzonitrile (50 mg, 0.42 mmol), Cs_2CO_3 (205.1 mg, 0.63 mmol) and KI (13.9 mg, 0.084 mmol) in DMF being stirred at room temperature for 30 minutes, 2-(chloromethyl)oxirane (116.5 mg, 1.26 mmol) was added at room

temperature. The solution was stirred at 80 ℃ for overnight and monitored to react completely. After cooling to room temperature and filtration, water was added and the filtrate was extracted with ethyl acetate for three times and washed with saturated brine. The combined organic layer was dried over anhydrous Na_2SO_4 and purified by column chromatography on silica gel with the elution fluid of Hexane/EA (200:1-50:1). Pale yellow oil was achieved in 60.9 mg with 82.8% yield. ^{1}H NMR (400 MHz, Chloroform-*d*) δ 7.63-7.54 (m, 2H), 7.02-6.95 (m, 2H), 4.34 (dd, *J* = 11.1, 2.8 Hz, 1H), 3.96 (dd, *J* = 11.2, 5.9 Hz, 1H), 3.37 (m, *J* = 6.8, 5.5, 2.8 Hz, 1H), 2.93 (t, *J* = 4.5 Hz, 1H), 2.77 (dd, *J* = 4.8, 2.6 Hz, 1H).

_N_-(oxiran-2-ylmethyl)-4-(trifluoromethyl)aniline (B_{11})

The solution of 4-(trifluoromethyl)aniline (50 mg, 0.31 mmol) and $Zn(SO_3CF_3)_2$ (13.3 mg, 0.062 mmol) in $CHCl_3$, 2-(chloromethyl)oxirane (28.7 mg, 0.31 mmol) was added dropwise in ice bath. The solution was stirred at 60 ℃ for 12 hours and monitored to react completely. After cooling to room temperature and filtration, water was added and the filtrate was extracted with ethyl acetate for three times and washed with saturated brine. The combined organic layer was dried over anhydrous Na_2SO_4 and concentrated to achieve the crude product. The solution of 1-chloro-3-((4-(trifluoromethyl)phenyl)amino)propan-2-ol (67.3 mg, 0.27 mmol) and KI (8 mg, 0.05 mmol) in MeCN was stirred at 80 ℃ for 6 hours. and monitored to react completely. After cooling to room temperature and filtration, water was added and the filtrate was extracted with ethyl acetate for three times and washed with saturated brine. The combined organic layer was dried over anhydrous Na_2SO_4 and purified by column chromatography on silica gel with the elution fluid of DCM/MeOH (200:1-100:1). Yellow oil was achieved in 42.5 mg with 73.8% yield. ^{1}H NMR (400 MHz, Chloroform-*d*) δ 7.44 (d, *J* = 8.5 Hz, 2H), 6.67 (d, *J* = 8.4 Hz, 2H), 4.23 (s, 1H), 3.63 (m, *J* = 13.8, 5.8, 2.7 Hz, 1H), 3.35-3.18 (m, 2H), 2.86 (t, *J* = 4.3 Hz, 1H), 2.71 (dd, *J* = 4.8, 2.6 Hz, 1H).

2-(((4-(trifluoromethyl)phenyl)thio)methyl)oxirane (B_{12})

The solution of 4-(trifluoromethyl)benzenethiol (50 mg, 0.28 mmol) and K_2CO_3 (58.2 mg, 0.42 mmol) in MeCN, 2-(chloromethyl)oxirane (51.9 mg, 0.56 mmol) was added at room temperature. The solution was stirred at 85 ℃ for 8 hours and monitored to react completely. After cooling to room temperature and filtration, water was added and the filtrate was extracted with ethyl acetate for three times and washed with saturated brine. The combined organic layer was dried over anhydrous Na_2SO_4 and purified by column chromatography on silica gel with the elution fluid of Hexane/EA (200:1-50:1). Yellow oil was achieved in 53.8 mg with 81.8% yield. ^{1}H NMR (400 MHz, Chloroform-*d*) δ 7.55 (d, J = 8.3 Hz, 2H), 7.48 (d, J = 8.3 Hz, 2H), 3.25-3.18 (m, 2H), 3.12 (dd, J = 15.5, 6.5 Hz, 1H), 2.86-2.82 (m, 1H), 2.64 (dd, J = 4.9, 2.3 Hz, 1H).

2-((benzyloxy)methyl)oxirane (B_{13})

The solution of 2-(chloromethyl)oxirane (51.3 mg, 0.56 mmol) and TBAB (16.3 mg, 0.023 mmol) in 1M NaOH aqueous solution, benzyl alcohol (50 mg, 0.46 mmol) was added dropwise in ice bath. After warming to room temperature, the solution was stirred for 18 hours and monitored to react completely. The reaction was quenched with iced water and extracted with ethyl acetate for three times and washed with saturated brine. The combined organic layer was dried over anhydrous Na_2SO_4 and purified by column chromatography on silica gel with the elution fluid of Hexane/EA (200:1-100:1). Pale yellow oil was achieved in 68.1 mg with 89.7% yield.

2-(((4-(trifluoromethyl)benzyl)oxy)methyl)oxirane (B_{14})

The solution of 2-(chloromethyl)oxirane (31.5 mg, 0.34 mmol) and TBAB (10 mg, 0.014 mmol) in 1M NaOH aqueous solution, (4-(trifluoromethyl)phenyl)methanol (50 mg, 0.28 mmol) was added dropwise in ice bath. After warming to room temperature, the solution was stirred for 18 hours and monitored to react completely. The reaction was quenched with iced water and extracted with ethyl acetate for three times and washed with saturated brine. The combined organic layer was dried over anhydrous Na_2SO_4 and purified by column chromatography on silica gel with the elution fluid of

Hexane/EA (200:1-50:1). Pale yellow oil was achieved in 59.5 mg with 90.2% yield. ^{1}H NMR (400 MHz, Chloroform-*d*) δ 7.56 (d, *J* = 8.5 Hz, 2H), 7.00 (d, *J* = 8.5 Hz, 2H), 4.31 (dd, *J* = 11.1, 2.8 Hz, 1H), 3.99-3.91 (m, 1H), 3.38 (m, *J* = 5.5, 3.9, 2.7 Hz, 1H), 2.93 (t, *J* = 4.5 Hz, 1H), 2.78 (dd, *J* = 4.9, 2.6 Hz, 1H).

2-(((3-(trifluoromethyl)benzyl)oxy)methyl)oxirane (B_{15})

The solution of 2-(chloromethyl)oxirane (31.5 mg, 0.34 mmol) and TBAB (10 mg, 0.014 mmol) in 1M NaOH aqueous solution, (3-(trifluoromethyl)phenyl)methanol (50 mg, 0.28 mmol) was added dropwise in ice bath. After warming to room temperature, the solution was stirred for 18 hours and monitored to react completely. The reaction was quenched with iced water and extracted with ethyl acetate for three times and washed with saturated brine. The combined organic layer was dried over anhydrous Na_2SO_4 and purified by column chromatography on silica gel with the elution fluid of Hexane/EA (200:1-50:1). Pale yellow oil was achieved in 57.7 mg with 87.6% yield. ^{1}H NMR (400 MHz, Chloroform-*d*) δ 7.56 (tt, *J* = 24.8, 5.9 Hz, 4H), 4.66 (m, *J* = 12.3, 5.2 Hz, 2H), 3.86 (m, *J* = 11.5, 2.9 Hz, 1H), 3.47 (dt, *J* = 11.4, 5.7 Hz, 1H), 3.23 (m, *J* = 6.1, 3.0 Hz, 1H), 2.84 (q, *J* = 5.1 Hz, 1H), 2.65 (dt, *J* = 5.1, 2.7 Hz, 1H).

2-(((2-(trifluoromethyl)benzyl)oxy)methyl)oxirane (B_{16})

The solution of 2-(chloromethyl)oxirane (31.5 mg, 0.34 mmol) and TBAB (10 mg, 0.014 mmol) in 1M NaOH aqueous solution, (2-(trifluoromethyl)phenyl)methanol (50 mg, 0.28 mmol) was added dropwise in ice bath. After warming to room temperature, the solution was stirred for 18 hours and monitored to react completely. The reaction was quenched with iced water and extracted with ethyl acetate for three times and washed with saturated brine. The combined organic layer was dried over anhydrous Na_2SO_4 and purified by column chromatography on silica gel with the elution fluid of Hexane/EA (200:1-50:1). Pale yellow oil was achieved in 60.1 mg with 91.2% yield. ^{1}H NMR (400 MHz, Chloroform-*d*) δ 7.78-7.55 (m, 3H), 7.40 (t, *J* = 7.7 Hz, 1H), 4.85-4.73 (m, 2H), 3.86 (dd, *J* = 11.3, 3.0 Hz, 1H), 3.52 (dd, *J* = 11.4, 5.9 Hz, 1H), 3.25 (m, *J* = 5.9, 4.1, 2.8 Hz, 1H), 2.85 (t, *J* = 4.6 Hz, 1H), 2.68 (dd, *J* = 5.0, 2.7 Hz,

1H).

2-(((4-(trifluoromethyl)benzyl)thio)methyl)oxirane (B_{17})

The solution of 2-(chloromethyl)oxirane (72.2 mg, 0.78 mmol) and KOH (43.8 mg, 0.78 mmol) in dioxane and water (1:1), (4-(trifluoromethyl)phenyl)methanethiol (50 mg, 0.26 mmol) was added dropwise in ice bath. The solution was warmed to room temperature for 8 hours and monitored to react completely. The mixture was extracted with ethyl acetate for three times and washed with saturated brine. The combined organic layer was dried over anhydrous Na_2SO_4 and purified by column chromatography on silica gel with the elution fluid of Hexane/EA (200:1-100:1). Yellow oil was achieved in 52.8 mg with 81.8% yield. ^{1}H NMR (400 MHz, Chloroform-*d*) δ 7.60 (d, *J* = 8.0 Hz, 2H), 7.49 (d, *J* = 8.0 Hz, 2H), 3.93-3.82 (m, 2H), 3.14 (m, *J* = 6.3, 4.2, 2.7 Hz, 1H), 2.79 (t, *J* = 4.4 Hz, 1H), 2.66-2.51 (m, 3H).

5.1.2 The synthesis on aminoethyl derivatives

1-(4-nitrophenoxy)-3-((2-(pyrimidin-2-ylamino)ethyl)amino)propan-2-ol (GI-1)

To a solution of **A_1** (30 mg, 0.22 mmol) and **B_1** (42.4 mg, 0.22 mmol) in ethanol, DIPEA (56.1 mg, 0.43 mmol) was added at room temperature. The solution was stirred at reflux for 8 hours and monitored to react completely. After warming to room temperature, the mixture was concentrated and purified by column chromatography on silica gel with the elution fluid of DCM/MeOH (100:1-50:1, with additional drops of aqueous ammonia). Pale yellow solid was achieved in 52.9 mg with 73.2% yield. ^{1}H NMR (400 MHz, Chloroform-*d*) δ 8.27 (d, *J* = 4.8 Hz, 2H), 8.23-8.18 (m, 2H), 7.00-6.95 (m, 2H), 6.55 (dd, *J* = 5.4, 4.3 Hz, 1H), 5.46 (s, 1H), 4.11-4.08 (m, 3H), 3.57 (q, *J* = 5.8 Hz, 2H), 2.97-2.91 (m, 3H), 2.86-2.80 (m, 1H); ^{13}C NMR (101 MHz, Chloroform-*d*) δ 163.6, 162.5, 158.1, 141.8, 125.9, 114.6, 110.8, 71.1, 68.2, 51.3, 49.1, 41.2. HRMS(ESI): calcd for $C_{15}H_{19}N_5O_4$, $[M + H]^+$ 334.1515; found, 334.1514. HPLC purity: 97.06%.

1-(4-nitrophenoxy)-3-((2-((5-(trifluoromethyl)pyrimidin-2-

yl)amino)ethyl)amino)propan-2-ol (GI-2)

To a solution of **A2** (30 mg, 0.15 mmol) and **B1** (28.4 mg, 0.15 mmol) in ethanol, DIPEA (37.6 mg, 0.29 mmol) was added at room temperature. The solution was stirred at reflux for 8 hours and monitored to react completely. After warming to room temperature, the mixture was concentrated and purified by column chromatography on silica gel with the elution fluid of DCM/MeOH (100:1-50:1, with additional drops of aqueous ammonia). Yellow solid was achieved in 41.5 mg with 70.8% yield. ^{1}H NMR (400 MHz, Chloroform-*d*) δ 8.47 (s, 2H), 8.25-8.17 (m, 2H), 7.01-6.95 (m, 2H), 6.01 (s, 1H), 4.14-4.07 (m, 3H), 3.62 (q, *J* = 5.8 Hz, 2H), 2.95 (m, *J* = 9.5, 3.8, 3.0 Hz, 3H), 2.84 (dd, *J* = 12.3, 7.3 Hz, 1H), 2.39 (s, 2H). ^{13}C NMR (101 MHz, Chloroform-*d*) δ 163.5, 163.4, 155.8, 155.8, 155.8, 155.7, 141.8, 125.9, 125.3, 114.5, 114.2, 71.0, 68.3, 51.3, 48.6, 41.2. HRMS(ESI): calcd for $C_{16}H_{18}F_3N_5O_4$, $[M + H]^+$ 402.1389; found, 402.1382. HPLC purity: 97.06%.

1-(4-nitrophenoxy)-3-((2-((6-(trifluoromethyl)pyridin-2-yl)amino)ethyl)amino)propan-2-ol (GI-3)

To a solution of **A4** (30 mg, 0.15 mmol) and **B1** (28.5 mg, 0.15 mmol) in ethanol, DIPEA (37.8 mg, 0.29 mmol) was added at room temperature. The solution was stirred at reflux for 8 hours and monitored to react completely. After warming to room temperature, the mixture was concentrated and purified by column chromatography on silica gel with the elution fluid of DCM/MeOH (100:1-50:1, with additional drops of aqueous ammonia). Yellow solid was achieved in 38.9 mg with 66.2% yield. ^{1}H NMR (400 MHz, Chloroform-*d*) δ 8.18 (d, *J* = 8.9 Hz, 2H), 7.50 (t, *J* = 7.9 Hz, 1H), 6.94 (dd, *J* = 15.7, 8.1 Hz, 3H), 6.54 (d, *J* = 8.5 Hz, 1H), 5.16 (t, *J* = 5.6 Hz, 1H), 4.09 (d, *J* = 7.0 Hz, 3H), 3.48 (q, *J* = 5.8 Hz, 2H), 2.93 (dd, *J* = 9.6, 4.4 Hz, 3H), 2.82 (dd, *J* = 12.3, 7.2 Hz, 1H). ^{13}C NMR (101 MHz, Chloroform-*d*) δ 163.6, 158.6, 146.6, 146.3, 141.7, 138.1, 125.9, 123.0, 120.3, 114.5, 110.3, 109.1, 109.1, 71.1, 68.2, 51.3, 48.8, 41.5. HRMS(ESI): calcd for $C_{17}H_{19}F_3N_4O_4$, $[M + H]^+$ 401.1437; found, 401.1431. HPLC purity: 92.9%.

1-(4-nitrophenoxy)-3-((2-((5-(trifluoromethyl)pyridin-2-yl)amino)ethyl)amino)propan-2-ol (GI-4)

To a solution of **A_5** (30 mg, 0.15 mmol) and **B_1** (28.5 mg, 0.15 mmol) in ethanol, DIPEA (37.8 mg, 0.29 mmol) was added at room temperature. The solution was stirred at reflux for 8 hours and monitored to react completely. After warming to room temperature, the mixture was concentrated and purified by column chromatography on silica gel with the elution fluid of DCM/MeOH (100:1-50:1, with additional drops of aqueous ammonia). Yellow solid was achieved in 37.7 mg with 64.7% yield. ^{1}H NMR (400 MHz, Chloroform-*d*) δ 8.29 (s, 1H), 8.15 (d, *J* = 8.8 Hz, 2H), 7.55 (d, *J* = 8.8 Hz, 1H), 6.93 (d, *J* = 8.8 Hz, 2H), 6.42 (d, *J* = 8.8 Hz, 1H), 5.59 (t, *J* = 5.7 Hz, 1H), 4.19-4.04 (m, 3H), 3.49 (q, *J* = 5.3, 4.8 Hz, 2H), 2.97-2.89 (m, 3H), 2.83 (dd, *J* = 12.3, 7.9 Hz, 1H). ^{13}C NMR (101 MHz, Chloroform-*d*) δ 163.6, 160.3, 145.9, 145.8, 141.7, 134.4, 125.9, 123.2, 115.6, 115.3, 114.5, 106.6, 71.2, 68.3, 51.5, 48.6, 41.4. HRMS(ESI): calcd for $C_{17}H_{19}F_3N_4O_4$, $[M + H]^+$ 401.1437; found, 401.1433. HPLC purity: 91.7%.

1-(4-nitrophenoxy)-3-((2-((4-(trifluoromethyl)pyridin-2-yl)amino)ethyl)amino)propan-2-ol (GI-5)

To a solution of **A_6** (30 mg, 0.15 mmol) and **B_1** (28.5 mg, 0.15 mmol) in ethanol, DIPEA (37.8 mg, 0.29 mmol) was added at room temperature. The solution was stirred at reflux for 8 hours and monitored to react completely. After warming to room temperature, the mixture was concentrated and purified by column chromatography on silica gel with the elution fluid of DCM/MeOH (100:1-50:1, with additional drops of aqueous ammonia). Yellow solid was achieved in 42.1 mg with 71.9% yield. ^{1}H NMR (400 MHz, Chloroform-*d*) δ 8.25-8.16 (m, 3H), 6.97 (dd, *J* = 9.0, 1.5 Hz, 2H), 6.75 (d, *J* = 5.3 Hz, 1H), 6.58 (s, 1H), 5.15 (s, 1H), 4.14-4.07 (m, 3H), 3.49 (q, *J* = 5.7 Hz, 2H), 3.00-2.91 (m, 3H), 2.84 (dd, *J* = 12.4, 7.1 Hz, 1H). ^{13}C NMR (101 MHz, Chloroform-*d*) δ 163.5, 158.9, 149.4, 141.8, 139.8, 139.5, 125.9, 124.4, 121.6, 114.5, 108.2, 108.2, 71.0, 68.3, 51.4, 48.7, 41.7. HRMS(ESI): calcd for $C_{17}H_{19}F_3N_4O_4$, [M +

H]$^+$ 401.1437; found, 401.1431. HPLC purity: 98.44%.

1-(4-nitrophenoxy)-3-((2-((3-(trifluoromethyl)pyridin-2-yl)amino)ethyl)amino)propan-2-ol (GI-6)

To a solution of **A$_7$** (30 mg, 0.15 mmol) and **B$_1$** (28.5 mg, 0.15 mmol) in ethanol, DIPEA (37.8 mg, 0.29 mmol) was added at room temperature. The solution was stirred at reflux for 8 hours and monitored to react completely. After warming to room temperature, the mixture was concentrated and purified by column chromatography on silica gel with the elution fluid of DCM/MeOH (100:1-50:1, with additional drops of aqueous ammonia). Yellow solid was achieved in 40.1 mg with 68.5% yield. ^{1}H NMR (400 MHz, Chloroform-*d*) δ 8.28-8.15 (m, 3H), 7.65 (d, *J* = 7.6 Hz, 1H), 7.00-6.93 (m, 2H), 6.62 (dd, *J* = 7.6, 5.0 Hz, 1H), 5.41 (d, *J* = 5.4 Hz, 1H), 4.11 (q, *J* = 3.9 Hz, 3H), 3.63 (q, *J* = 5.6 Hz, 2H), 2.97 (m, *J* = 12.4, 10.4, 4.8 Hz, 3H), 2.84 (dd, *J* = 12.3, 6.5 Hz, 1H), 2.57(s, 2H). ^{13}C NMR (101 MHz, Chloroform-*d*) δ 163.6, 154.7, 151.6, 141.7, 135.2, 135.1, 135.1, 135.0, 125.9, 125.8, 123.1, 120.4, 114.5, 111.5, 108.8, 108.5, 108.2, 71.0, 68.3, 51.1, 48.6, 40.9. HRMS(ESI): calcd for $C_{17}H_{19}F_3N_4O_4$, [M + H]$^+$ 401.1437; found, 401.143. HPLC purity: 98.7%.

1-((2-((5-fluoropyridin-2-yl)amino)ethyl)amino)-3-(4-nitrophenoxy)propan-2-ol (GI-7)

To a solution of **A$_8$** (30 mg, 0.19 mmol) and **B$_1$** (37.7 mg, 0.19 mmol) in ethanol, DIPEA (49.9 mg, 0.39 mmol) was added at room temperature. The solution was stirred at reflux for 8 hours and monitored to react completely. After warming to room temperature, the mixture was concentrated and purified by column chromatography on silica gel with the elution fluid of DCM/MeOH (100:1-50:1, with additional drops of aqueous ammonia). Yellow solid was achieved in 47.1 mg with 69.5% yield. ^{1}H NMR (400 MHz, Chloroform-*d*) δ 8.25-8.13 (m, 4H), 7.01-6.94 (m, 2H), 5.50 (t, *J* = 5.7 Hz, 1H), 4.09 (s, 3H), 3.53 (q, *J* = 5.8 Hz, 2H), 2.96-2.90 (m, 3H), 2.82 (dd, *J* = 12.3, 6.8 Hz, 1H), 2.30 (s, 2H). ^{13}C NMR (101 MHz, Chloroform-*d*) δ 163.6, 159.5, 153.4, 150.9, 145.7, 145.4, 141.8, 125.9, 114.5, 71.1, 68.2, 51.3, 48.9, 41.8.

HRMS(ESI): calcd for $C_{15}H_{18}FN_5O_4$, $[M + H]^+$ 352.1469; found, 352.1478. HPLC purity: 95.72%.

1-(4-nitrophenoxy)-3-((2-((2-(trifluoromethyl)phenyl)amino)ethyl)amino)propan-2-ol (GI-8)

To a solution of **A_{10}** (30 mg, 0.15 mmol) and **B_1** (28.7 mg, 0.15 mmol) in ethanol, DIPEA (38 mg, 0.29 mmol) was added at room temperature. The solution was stirred at reflux for 8 hours and monitored to react completely. After warming to room temperature, the mixture was concentrated and purified by column chromatography on silica gel with the elution fluid of DCM/MeOH (200:1-100:1, with additional drops of aqueous ammonia). Yellow solid was achieved in 42.8 mg with 73.1% yield. ^{1}H NMR (400 MHz, Chloroform-*d*) δ 8.25-8.17 (m, 2H), 7.46 (d, *J* = 7.6 Hz, 1H), 7.39 (t, *J* = 7.9 Hz, 1H), 7.01-6.95 (m, 2H), 6.76 (dd, *J* = 8.2, 5.2 Hz, 2H), 4.91 (s, 1H), 4.13 (s, 3H), 3.30 (m, *J* = 6.8, 3.4 Hz, 2H), 3.08-2.94 (m, 3H), 2.89-2.82 (m, 1H). ^{13}C NMR (101 MHz, Chloroform-*d*) δ 163.6, 145.7, 145.7, 141.8, 133.2, 129.3, 126.8, 126.7, 126.7, 126.6, 125.9, 123.9, 121.2, 116.1, 114.5, 114.0, 113.7, 113.4, 113.1, 111.9, 71.0, 68.5, 51.0, 48.0, 42.8. HRMS(ESI): calcd for $C_{18}H_{20}F_3N_3O_4$, $[M + H]^+$ 400.1484; found, 400.1491. HPLC purity: 95.37%.

1-phenoxy-3-((2-((4-(trifluoromethyl)pyrimidin-2-yl)amino)ethyl)amino)propan-2-ol (GI-9)

To a solution of **A_3** (30 mg, 0.15 mmol) and **B_2** (21.9 mg, 0.15 mmol) in ethanol, DIPEA (37.6 mg, 0.29 mmol) was added at room temperature. The solution was stirred at reflux for 8 hours and monitored to react completely. After warming to room temperature, the mixture was concentrated and purified by column chromatography on silica gel with the elution fluid of DCM/MeOH (100:1-50:1, with additional drops of aqueous ammonia). Pale yellow solid was achieved in 38.6 mg with 74.5% yield. ^{1}H NMR (400 MHz, Chloroform-*d*) δ 8.44 (s, 1H), 7.27 (d, *J* = 7.6 Hz, 2H), 6.99-6.84 (m, 3H), 6.77 (s, 1H), 6.53 (s, 1H), 4.15 (s, 1H), 3.98 (s, 2H), 3.59 (s, 2H), 2.96-2.80 (m, 4H). ^{13}C NMR (101 MHz, Chloroform-*d*) δ 162.5, 160.4, 158.6, 156.9, 156.5,

156.2, 155.8, 129.5, 121.9, 121.1, 119.2, 116.4, 114.5, 105.3, 70.6, 68.7, 51.8, 48.6, 41.1. HRMS(ESI): calcd for $C_{16}H_{19}F_3N_4O_2$, $[M + H]^+$ 357.1538; found, 357.153. HPLC purity: 97.91%.

methyl 4-(2-hydroxy-3-((2-((4-(trifluoromethyl)pyrimidin-2-yl)amino)ethyl)amino)propoxy)benzoate (GI-10)

To a solution of **A_3** (30 mg, 0.15 mmol) and **B_3** (30.3 mg, 0.15 mmol) in ethanol, DIPEA (37.6 mg, 0.29 mmol) was added at room temperature. The solution was stirred at reflux for 8 hours and monitored to react completely. After warming to room temperature, the mixture was concentrated and purified by column chromatography on silica gel with the elution fluid of DCM/MeOH (100:1-50:1, with additional drops of aqueous ammonia). Pale yellow solid was achieved in 41.4 mg with 68.3% yield. ^{1}H NMR (400 MHz, Chloroform-*d*) δ 8.40 (s, 1H), 7.91 (d, *J* = 8.5 Hz, 2H), 6.84 (d, *J* = 8.5 Hz, 2H), 6.74 (d, *J* = 4.9 Hz, 1H), 6.50 (t, *J* = 5.9 Hz, 1H), 4.12 (m, *J* = 9.3, 4.9 Hz, 1H), 4.02-3.95 (m, 2H), 3.84 (s, 3H), 3.56 (q, *J* = 5.8 Hz, 4H), 2.92-2.83 (m, 3H), 2.79 (dd, *J* = 12.1, 8.1 Hz, 1H). ^{13}C NMR (101 MHz, Chloroform-*d*) δ 166.7, 162.5, 162.3, 160.3, 156.8, 156.5, 156.1, 131.5, 122.8, 121.8, 119.1, 114.0, 105.4, 105.3, 105.3, 70.7, 68.4, 51.8, 51.6, 48.6, 41.0. HRMS(ESI): calcd for $C_{18}H_{21}F_3N_4O_4$, $[M + H]^+$ 415.1593; found, 415.1586. HPLC purity: 98.5%.

1-(4-fluorophenoxy)-3-((2-((4-(trifluoromethyl)pyrimidin-2-yl)amino)ethyl)amino)propan-2-ol (GI-11)

To a solution of **A_3** (30 mg, 0.15 mmol) and **B_4** (24.5 mg, 0.15 mmol) in ethanol, DIPEA (37.6 mg, 0.29 mmol) was added at room temperature. The solution was stirred at reflux for 8 hours and monitored to react completely. After warming to room temperature, the mixture was concentrated and purified by column chromatography on silica gel with the elution fluid of DCM/MeOH (100:1-50:1, with additional drops of aqueous ammonia). Pale yellow solid was achieved in 39.4 mg with 72.1% yield. ^{1}H NMR (400 MHz, Chloroform-*d*) δ 8.46 (s, 1H), 6.96 (t, *J* = 8.4 Hz, 2H), 6.90-6.72 (m, 3H), 6.17 (s, 1H), 4.15-4.04 (m, 1H), 3.95 (d, *J* = 5.2 Hz, 2H), 3.60 (q, *J* = 6.0 Hz,

2H), 3.10-2.52 (m, 6H). ^{13}C NMR (101 MHz, Chloroform-*d*) δ 162.5, 160.4, 158.6, 157.0, 156.6, 156.2, 155.9, 154.7, 154.7, 121.9, 119.1, 116.4, 115.9, 115.7, 115.6, 115.5, 105.5, 105.5, 71.2, 68.6, 51.6, 48.6, 41.1. HRMS(ESI): calcd for $C_{16}H_{18}F_4N_4O_2$, $[M + H]^+$ 375.1444; found, 375.1438. HPLC purity: 98.74%.

1-(3,4-difluorophenoxy)-3-((2-((4-(trifluoromethyl)pyrimidin-2-yl)amino)ethyl)amino)propan-2-ol (GI-12)

To a solution of **A$_3$** (30 mg, 0.15 mmol) and **B$_5$** (27.1 mg, 0.15 mmol) in ethanol, DIPEA (37.6 mg, 0.29 mmol) was added at room temperature. The solution was stirred at reflux for 8 hours and monitored to react completely. After warming to room temperature, the mixture was concentrated and purified by column chromatography on silica gel with the elution fluid of DCM/MeOH (100:1-50:1, with additional drops of aqueous ammonia). Pale yellow solid was achieved in 42.2 mg with 73.3% yield. ^{1}H NMR (400 MHz, Chloroform-*d*) δ 8.46 (d, *J* = 4.9 Hz, 1H), 7.04 (q, *J* = 9.4 Hz, 1H), 6.81 (d, *J* = 4.9 Hz, 1H), 6.72 (m, *J* = 12.1, 6.6, 3.0 Hz, 1H), 6.60 (dd, *J* = 8.9, 4.2 Hz, 1H), 6.18 (t, *J* = 5.8 Hz, 1H), 4.09 (m, *J* = 9.1, 4.7 Hz, 1H), 3.93 (d, *J* = 5.1 Hz, 2H), 3.60 (q, *J* = 5.8 Hz, 2H), 2.95-2.70 (m, 6H). ^{13}C NMR (101 MHz, Chloroform-*d*) δ 162.5, 160.4, 157.0, 156.6, 156.2, 154.9, 154.9, 154.9, 154.8, 151.7, 151.6, 149.2, 149.1, 146.4, 146.3, 144.0, 143.9, 124.6, 121.8, 119.1, 117.3, 117.3, 117.1, 117.1, 116.4, 109.8, 109.8, 109.8, 109.7, 105.6, 105.5, 105.5, 104.3, 104.1, 71.3, 68.4, 51.5, 48.6, 41.1. HRMS(ESI): calcd for $C_{16}H_{17}F_5N_4O_2$, $[M + H]^+$ 393.135; found, 393.1343. HPLC purity: 98.98%.

1-(4-methoxyphenoxy)-3-((2-((4-(trifluoromethyl)pyrimidin-2-yl)amino)ethyl)amino)propan-2-ol (GI-13)

To a solution of **A$_3$** (30 mg, 0.15 mmol) and **B$_6$** (26.2 mg, 0.15 mmol) in ethanol, DIPEA (37.6 mg, 0.29 mmol) was added at room temperature. The solution was stirred at reflux for 8 hours and monitored to react completely. After warming to room temperature, the mixture was concentrated and purified by column chromatography on silica gel with the elution fluid of DCM/MeOH (100:1-50:1, with additional drops

of aqueous ammonia). Pale yellow solid was achieved in 40.1 mg with 71.3% yield. ^{1}H NMR (400 MHz, Chloroform-*d*) δ 8.52-8.41 (m, 1H), 6.82 (m, *J* = 11.8, 3.7 Hz, 5H), 6.14 (s, 1H), 4.09 (m, *J* = 9.0, 5.1 Hz, 1H), 3.94 (d, *J* = 5.2 Hz, 2H), 3.77 (s, 3H), 3.59 (q, *J* = 5.8 Hz, 2H), 2.95-2.87 (m, 3H), 2.81 (m, *J* = 12.1, 7.8 Hz, 1H). ^{13}C NMR (101 MHz, Chloroform-*d*) δ 162.5, 160.4, 156.6, 156.2, 154.1, 152.7, 121.9, 119.1, 115.5, 114.7, 105.5, 105.5, 71.3, 68.8, 55.7, 51.7, 48.6, 41.2. HRMS(ESI): calcd for $C_{17}H_{21}F_3N_4O_3$, $[M + H]^+$ 387.1644; found, 387.1644. HPLC purity: 99.02%.

1-(4-(trifluoromethyl)phenoxy)-3-((2-((4-(trifluoromethyl)pyrimidin-2-yl)amino)ethyl)amino)propan-2-ol (GI-14)

To a solution of **A$_3$** (30 mg, 0.15 mmol) and **B$_7$** (31.8 mg, 0.15 mmol) in ethanol, DIPEA (37.6 mg, 0.29 mmol) was added at room temperature. The solution was stirred at reflux for 8 hours and monitored to react completely. After warming to room temperature, the mixture was concentrated and purified by column chromatography on silica gel with the elution fluid of DCM/MeOH (100:1-50:1, with additional drops of aqueous ammonia). Pale yellow solid was achieved in 41.5 mg with 67.2% yield. ^{1}H NMR (400 MHz, Chloroform-*d*) δ 8.46 (s, 1H), 7.53 (d, *J* = 8.6 Hz, 2H), 6.96 (d, *J* = 8.6 Hz, 2H), 6.81 (d, *J* = 4.9 Hz, 1H), 6.20 (t, *J* = 5.7 Hz, 1H), 4.14 (m, *J* = 9.2, 5.0 Hz, 1H), 4.03 (d, *J* = 5.1 Hz, 2H), 3.61 (q, *J* = 5.7 Hz, 2H), 3.08-2.74 (m, 6H). ^{13}C NMR (101 MHz, Chloroform-*d*) δ 162.5, 161.0, 160.4, 156.6, 156.2, 127.0, 126.9, 126.9, 126.9, 125.7, 123.4, 123.1, 123.0, 121.8, 119.1, 114.5, 105.6, 105.5, 70.6, 68.4, 51.5, 48.7, 41.1. HRMS(ESI): calcd for $C_{17}H_{18}F_6N_4O_2$, $[M + H]^+$ 425.1412; found, 425.1406. HPLC purity: 96.47%.

1-(4-(trifluoromethyl)phenoxy)-3-((2-((5-(trifluoromethyl)pyridin-2-yl)amino)ethyl)amino)propan-2-ol (GI-15)

To a solution of **A$_5$** (30 mg, 0.15 mmol) and **B$_7$** (31.9 mg, 0.15 mmol) in ethanol, DIPEA (37.8 mg, 0.29 mmol) was added at room temperature. The solution was stirred at reflux for 8 hours and monitored to react completely. After warming to room temperature, the mixture was concentrated and purified by column chromatography

on silica gel with the elution fluid of DCM/MeOH (100:1-50:1, with additional drops of aqueous ammonia). Pale yellow solid was achieved in 42.2 mg with 68.7% yield. ^{1}H NMR (400 MHz, Chloroform-*d*) δ 8.36-8.27 (m, 1H), 7.55 (t, *J* = 8.7 Hz, 3H), 6.96 (d, *J* = 8.5 Hz, 2H), 6.41 (d, *J* = 8.8 Hz, 1H), 5.28 (s, 1H), 4.10 (m, *J* = 10.0, 5.8, 2.8 Hz, 1H), 4.06-4.00 (m, 2H), 3.49 (q, *J* = 5.7 Hz, 2H), 2.97-2.89 (m, 3H), 2.82 (dd, *J* = 12.2, 7.7 Hz, 1H). ^{13}C NMR (101 MHz, Chloroform-*d*) δ 161.0, 160.3, 146.1, 146.1, 146.0, 146.0, 134.4, 134.4, 134.3, 130.9, 127.0, 127.0, 126.9, 126.9, 125.9, 125.7, 123.5, 123.2, 123.0, 115.8, 115.4, 114.5, 106.6, 70.5, 68.5, 51.4, 48.6, 41.5. HRMS(ESI): calcd for $C_{18}H_{19}F_6N_3O_2$, $[M + H]^+$ 424.146; found, 424.1454. HPLC purity: 99.4%.

1-((2-([1,1'-biphenyl]-4-ylamino)ethyl)amino)-3-(4-(trifluoromethyl)phenoxy)propan-2-ol (GI-16)

To a solution of **A$_{11}$** (30 mg, 0.14 mmol) and **B$_7$** (30.8 mg, 0.14 mmol) in ethanol, DIPEA (36.5 mg, 0.28 mmol) was added at room temperature. The solution was stirred at reflux for 8 hours and monitored to react completely. After warming to room temperature, the mixture was concentrated and purified by column chromatography on silica gel with the elution fluid of DCM/MeOH (200:1-100:1, with additional drops of aqueous ammonia). White solid was achieved in 42.2 mg with 70.6% yield. ^{1}H NMR (400 MHz, Chloroform-*d*) δ 7.56 (d, *J* = 8.1 Hz, 4H), 7.47 (d, *J* = 8.2 Hz, 2H), 7.43 (d, *J* = 7.6 Hz, 2H), 7.29 (d, *J* = 8.2 Hz, 1H), 6.99 (d, *J* = 8.4 Hz, 2H), 6.73 (d, *J* = 8.3 Hz, 2H), 4.16-4.03 (m, 4H), 3.33 (q, *J* = 5.1 Hz, 2H), 3.01-2.91 (m, 3H), 2.85 (dd, *J* = 12.2, 7.5 Hz, 1H). ^{13}C NMR (101 MHz, Chloroform-*d*) δ 161.0, 147.6, 141.1, 130.6, 128.7, 128.0, 127.0, 127.0, 127.0, 126.9, 126.3, 126.1, 125.7, 123.5, 123.1, 123.0, 114.5, 113.2, 70.6, 68.5, 51.5, 48.8, 43.7. HRMS(ESI): calcd for $C_{24}H_{25}F_3N_2O_2$, $[M + H]^+$ 431.1946; found, 431.1939. HPLC purity: 99.02%.

1-(4-(trifluoromethyl)phenoxy)-3-((2-((4-(trifluoromethyl)phenyl)amino)ethyl)amino)propan-2-ol (GI-17)

To a solution of **A$_{12}$** (30 mg, 0.15 mmol) and **B$_7$** (32.1 mg, 0.15 mmol) in ethanol,

DIPEA (37.8 mg, 0.29 mmol) was added at room temperature. The solution was stirred at reflux for 8 hours and monitored to react completely. After warming to room temperature, the mixture was concentrated and purified by column chromatography on silica gel with the elution fluid of DCM/MeOH (200:1-100:1, with additional drops of aqueous ammonia). White solid was achieved in 42.2 mg with 68.8% yield. ^{1}H NMR (400 MHz, Chloroform-*d*) δ 7.54 (d, *J* = 8.5 Hz, 2H), 7.39 (d, *J* = 8.3 Hz, 2H), 6.95 (d, *J* = 8.4 Hz, 2H), 6.61 (d, *J* = 8.3 Hz, 2H), 4.47 (t, *J* = 5.5 Hz, 1H), 4.12 (m, *J* = 9.9, 7.8, 4.3 Hz, 1H), 4.06-3.98 (m, 2H), 3.28 (q, *J* = 5.5 Hz, 2H), 2.97-2.87 (m, 3H), 2.82 (dd, *J* = 12.2, 7.8 Hz, 1H). ^{13}C NMR (101 MHz, Chloroform-*d*) δ 160.9, 150.7, 128.4, 127.0, 127.0, 127.0, 126.9, 126.7, 126.6, 126.6, 126.6, 126.3, 125.7, 123.6, 123.5, 123.2, 123.0, 119.1, 118.7, 114.5, 111.9, 70.5, 68.5, 51.5, 48.4, 43.0. HRMS(ESI): calcd for $C_{19}H_{20}F_6N_2O_2$, $[M + H]^+$ 423.1507; found, 423.1503. HPLC purity: 97.3%.

1-(4-(trifluoromethyl)phenoxy)-3-((2-((3-(trifluoromethyl)phenyl)amino)ethyl)amino)propan-2-ol (GI-18)

To a solution of **A$_{13}$** (30 mg, 0.15 mmol) and **B$_7$** (32.1 mg, 0.15 mmol) in ethanol, DIPEA (37.8 mg, 0.29 mmol) was added at room temperature. The solution was stirred at reflux for 8 hours and monitored to react completely. After warming to room temperature, the mixture was concentrated and purified by column chromatography on silica gel with the elution fluid of DCM/MeOH (200:1-100:1, with additional drops of aqueous ammonia). White solid was achieved in 44.3 mg with 71.1% yield. ^{1}H NMR (400 MHz, Chloroform-*d*) δ 7.57 (d, *J* = 8.4 Hz, 2H), 7.29 (d, *J* = 4.4 Hz, 1H), 6.98 (t, *J* = 8.8 Hz, 3H), 6.88-6.74 (m, 2H), 4.29 (s, 1H), 4.17-4.02 (m, 3H), 3.30 (s, 2H), 3.06-2.81 (m, 4H). ^{13}C NMR (101 MHz, Chloroform-*d*) δ 161.0, 148.4, 131.8, 131.4, 131.1, 129.6, 128.4, 127.0, 127.0, 126.9, 126.9, 125.7, 123.5, 123.2, 123.0, 116.0, 114.5, 114.0, 113.9, 113.9, 113.9, 108.9, 108.9, 108.9, 70.5, 68.5, 51.4, 48.5, 43.3. HRMS(ESI): calcd for $C_{19}H_{20}F_6N_2O_2$, $[M + H]^+$ 423.1507; found, 423.1520. HPLC purity: 98.83%.

1-(4-(trifluoromethyl)phenoxy)-3-((2-((2-(trifluoromethyl)phenyl)amino)ethyl)amino)propan-2-ol (GI-19)

To a solution of **A$_{10}$** (30 mg, 0.15 mmol) and **B$_7$** (32.1 mg, 0.15 mmol) in ethanol, DIPEA (37.8 mg, 0.29 mmol) was added at room temperature. The solution was stirred at reflux for 8 hours and monitored to react completely. After warming to room temperature, the mixture was concentrated and purified by column chromatography on silica gel with the elution fluid of DCM/MeOH (200:1-100:1, with additional drops of aqueous ammonia). White solid was achieved in 41.3 mg with 66.1% yield. ^{1}H NMR (400 MHz, Chloroform-*d*) δ 7.56 (d, *J* = 8.5 Hz, 2H), 7.46 (d, *J* = 7.8 Hz, 1H), 7.39 (t, *J* = 7.8 Hz, 1H), 6.99 (d, *J* = 8.5 Hz, 2H), 6.76 (d, *J* = 7.8 Hz, 2H), 4.93 (d, *J* = 5.2 Hz, 1H), 4.15-4.05 (m, 3H), 3.30 (q, *J* = 6.0 Hz, 2H), 3.07-2.93 (m, 3H), 2.85 (dd, *J* = 12.3, 6.6 Hz, 1H). ^{13}C NMR (101 MHz, Chloroform-*d*) δ 161.0, 145.7, 133.1, 127.0, 126.9, 116.1, 114.5, 111.9, 70.5, 68.7, 51.2, 48.1, 42.9. HRMS(ESI): calcd for $C_{19}H_{20}F_6N_2O_2$, $[M + H]^+$ 423.1507; found, 423.1503. HPLC purity: 92.86%.

1-((2-((2-nitrophenyl)amino)ethyl)amino)-3-(4-(trifluoromethyl)phenoxy)propan-2-ol (GI-20)

To a solution of **A$_{14}$** (30 mg, 0.17 mmol) and **B$_7$** (36.1 mg, 0.17 mmol) in ethanol, DIPEA (42.8 mg, 0.33 mmol) was added at room temperature. The solution was stirred at reflux for 8 hours and monitored to react completely. After warming to room temperature, the mixture was concentrated and purified by column chromatography on silica gel with the elution fluid of DCM/MeOH (200:1-100:1, with additional drops of aqueous ammonia). Yellow solid was achieved in 41.9 mg with 63.9% yield. ^{1}H NMR (600 MHz, Chloroform-*d*) δ 8.40 (d, *J* = 5.1 Hz, 1H), 8.19 (dd, *J* = 8.6, 1.5 Hz, 1H), 7.55 (d, *J* = 8.4 Hz, 2H), 7.45 (m, *J* = 8.5, 7.0, 1.5 Hz, 1H), 7.01 (d, *J* = 8.5 Hz, 2H), 6.86 (d, *J* = 8.6 Hz, 1H), 6.67 (m, *J* = 8.4, 6.9, 1.1 Hz, 1H), 4.12 (m, *J* = 16.0, 8.2, 4.4 Hz, 3H), 3.44 (q, *J* = 5.9 Hz, 2H), 3.13-2.97 (m, 3H), 2.88 (dd, *J* = 12.2, 6.2 Hz, 1H). ^{13}C NMR (101 MHz, Chloroform-*d*) δ 161.0, 145.4, 136.2, 132.1, 127.0, 127.0, 126.9, 126.9, 125.7, 123.4, 123.1, 123.0, 115.4, 114.5, 113.8, 70.4, 68.7, 51.1,

47.9, 42.4. HRMS(ESI): calcd for $C_{18}H_{20}F_3N_3O_4$, $[M + H]^+$ 400.1484; found, 400.1490. HPLC purity: 99.68%.

2-((2-((2-hydroxy-3-(4-(trifluoromethyl)phenoxy)propyl)amino)ethyl)amino)benzonitrile(GI-21)

To a solution of **A_{15}** (30 mg, 0.19 mmol) and **B_7** (40.6 mg, 0.19 mmol) in ethanol, DIPEA (48.1 mg, 0.37 mmol) was added at room temperature. The solution was stirred at reflux for 8 hours and monitored to react completely. After warming to room temperature, the mixture was concentrated and purified by column chromatography on silica gel with the elution fluid of DCM/MeOH (200:1-100:1, with additional drops of aqueous ammonia). White solid was achieved in 47.4 mg with 66.4% yield. ^{1}H NMR (600 MHz, Chloroform-*d*) δ 7.56 (d, *J* = 8.5 Hz, 2H), 7.40 (m, *J* = 7.5, 5.9, 1.8 Hz, 2H), 7.02 (d, *J* = 8.5 Hz, 2H), 6.73-6.67 (m, 2H), 5.13 (d, *J* = 5.9 Hz, 1H), 4.12 (m, *J* = 13.1, 4.1 Hz, 3H), 3.33 (m, *J* = 5.6, 2.0 Hz, 2H), 3.06-2.95 (m, 3H), 2.86 (dd, *J* = 12.2, 6.5 Hz, 1H). ^{13}C NMR (151 MHz, Chloroform-*d*) δ 161.0, 150.4, 134.3, 132.8, 127.0, 127.0, 126.9, 126.9, 125.3, 123.5, 123.4, 123.2, 118.0, 116.7, 114.6, 110.8, 96.0, 70.5, 68.8, 51.2, 48.1, 42.7. HRMS(ESI): calcd for $C_{19}H_{20}F_3N_3O_2$, $[M + H]^+$ 380.1586; found, 380.1593. HPLC purity: 98.38%.

1-(3-(trifluoromethyl)phenoxy)-3-((2-((2-(trifluoromethyl)phenyl)amino)ethyl)amino)propan-2-ol (GI-22)

To a solution of **A_{10}** (30 mg, 0.15 mmol) and **B_8** (32.1 mg, 0.15 mmol) in ethanol, DIPEA (37.8 mg, 0.29 mmol) was added at room temperature. The solution was stirred at reflux for 8 hours and monitored to react completely. After warming to room temperature, the mixture was concentrated and purified by column chromatography on silica gel with the elution fluid of DCM/MeOH (200:1-100:1, with additional drops of aqueous ammonia). White solid was achieved in 42.4 mg with 68.6% yield. ^{1}H NMR (600 MHz, Chloroform-*d*) δ 7.49-7.44 (m, 1H), 7.40 (m, *J* = 10.6, 7.9 Hz, 2H), 7.27 (d, *J* = 20.1 Hz, 1H), 7.17 (t, *J* = 2.0 Hz, 1H), 7.10 (dd, *J* = 8.3, 2.5 Hz, 1H), 6.78-6.73 (m, 2H), 4.93 (s, 1H), 4.15-4.05 (m, 3H), 3.31 (h, *J* = 5.8, 5.1 Hz, 2H),

3.06-2.94 (m, 3H), 2.85 (dd, *J* = 12.2, 6.9 Hz, 1H). ^{13}C NMR (101 MHz, Chloroform-*d*) δ 158.7, 145.7, 133.1, 132.1, 131.7, 130.0, 127.9, 126.8, 126.7, 126.6, 126.6, 125.2, 123.9, 122.5, 121.2, 117.9, 117.8, 117.8, 117.7, 116.0, 114.0, 113.7, 113.5, 111.9, 111.4, 111.4, 111.4, 111.3, 70.6, 68.7, 51.2, 48.1, 42.9. HRMS(ESI): calcd for $C_{19}H_{20}F_6N_3O_2$, $[M + H]^+$ 423.1507; found, 423.1518. HPLC purity: 96.63%.

1-(2-(trifluoromethyl)phenoxy)-3-((2-((2-(trifluoromethyl)phenyl)amino)ethyl)amino)propan-2-ol (GI-23)

To a solution of **A$_{10}$** (30 mg, 0.15 mmol) and **B$_9$** (32.1 mg, 0.15 mmol) in ethanol, DIPEA (37.8 mg, 0.29 mmol) was added at room temperature. The solution was stirred at reflux for 8 hours and monitored to react completely. After warming to room temperature, the mixture was concentrated and purified by column chromatography on silica gel with the elution fluid of DCM/MeOH (200:1-100:1, with additional drops of aqueous ammonia). White solid was achieved in 40.6 mg with 65.2% yield. ^{1}H NMR (400 MHz, Chloroform-*d*) δ 7.59 (d, *J* = 7.7 Hz, 1H), 7.51 (t, *J* = 8.0 Hz, 1H), 7.45 (d, *J* = 7.8 Hz, 1H), 7.38 (t, *J* = 7.9 Hz, 1H), 7.08-7.00 (m, 2H), 6.74 (t, *J* = 8.3 Hz, 2H), 4.96 (s, 1H), 4.14 (d, *J* = 2.5 Hz, 3H), 3.29 (q, *J* = 5.3 Hz, 2H), 3.04-2.94 (m, 3H), 2.90 (dd, *J* = 10.9, 4.1 Hz, 1H). ^{13}C NMR (101 MHz, Chloroform-*d*) δ 156.4, 145.8, 133.4, 133.1, 129.3, 127.1, 127.1, 127.0, 127.0, 126.7, 126.6, 126.6, 126.5, 125.1, 123.9, 122.4, 120.5, 118.9, 118.6, 115.9, 113.7, 113.4, 113.1, 112.9, 111.9, 71.0, 68.6, 51.0, 48.1, 42.8. HRMS(ESI): calcd for $C_{19}H_{20}F_6N_3O_2$, $[M + H]^+$ 423.1507; found, 423.1509. HPLC purity: 96.79%.

4-(2-hydroxy-3-((2-((2-(trifluoromethyl)phenyl)amino)ethyl)amino)propoxy)benzonitrile(GI-24)

To a solution of **A$_{10}$** (30 mg, 0.15 mmol) and **B$_{10}$** (25.7 mg, 0.15 mmol) in ethanol, DIPEA (37.8 mg, 0.29 mmol) was added at room temperature. The solution was stirred at reflux for 8 hours and monitored to react completely. After warming to room temperature, the mixture was concentrated and purified by column chromatography on silica gel with the elution fluid of DCM/MeOH (200:1-100:1, with additional

drops of aqueous ammonia). White solid was achieved in 42.1 mg with 75.4% yield. ^{1}H NMR (400 MHz, Chloroform-*d*) δ 7.63-7.57 (m, 2H), 7.46 (d, *J* = 7.8 Hz, 1H), 7.39 (t, *J* = 7.9 Hz, 1H), 7.00-6.95 (m, 2H), 6.79-6.72 (m, 2H), 4.91 (s, 1H), 4.15-4.06 (m, 3H), 3.34-3.25 (m, 2H), 3.07-2.93 (m, 3H), 2.84 (dd, *J* = 12.3, 6.3 Hz, 1H). ^{13}C NMR (101 MHz, Chloroform-*d*) δ 161.8, 145.7, 145.7, 134.0, 133.2, 126.8, 126.7, 126.7, 126.6, 123.9, 119.1, 116.1, 115.2, 113.7, 113.4, 111.9, 104.4, 70.6, 68.5, 51.1, 48.1, 42.9. HRMS(ESI): calcd for $C_{19}H_{20}F_3N_3O_2$, $[M + H]^+$ 380.1586; found, 380.1590. HPLC purity: 96.25%.

1-((4-(trifluoromethyl)phenyl)amino)-3-((2-((5-(trifluoromethyl)pyridin-2-yl)amino)ethyl)amino)propan-2-ol (GI-25)

To a solution of **A$_5$** (30 mg, 0.15 mmol) and **B$_{11}$** (31.8 mg, 0.15 mmol) in ethanol, DIPEA (37.8 mg, 0.29 mmol) was added at room temperature. The solution was stirred at reflux for 8 hours and monitored to react completely. After warming to room temperature, the mixture was concentrated and purified by column chromatography on silica gel with the elution fluid of DCM/MeOH (100:1-50:1, with additional drops of aqueous ammonia). Pale yellow solid was achieved in 36.2 mg with 58.8% yield. ^{1}H NMR (400 MHz, Chloroform-*d*) δ 8.32 (s, 1H), 7.59 (d, *J* = 8.8 Hz, 1H), 7.40 (d, *J* = 8.3 Hz, 2H), 6.62 (d, *J* = 8.3 Hz, 2H), 6.42 (d, *J* = 8.9 Hz, 1H), 5.40 (t, *J* = 5.7 Hz, 1H), 4.58 (s, 1H), 3.94 (m, *J* = 8.0, 3.8 Hz, 1H), 3.48 (q, *J* = 5.8 Hz, 2H), 3.30 (dd, *J* = 12.9, 3.7 Hz, 1H), 3.13 (dd, *J* = 12.8, 7.1 Hz, 1H), 2.99-2.39 (m, 6H). ^{13}C NMR (101 MHz, Chloroform-*d*) δ 160.3, 150.7, 146.0, 146.0, 145.9, 134.5, 134.4, 128.9, 126.7, 126.6, 126.6, 126.6, 126.2, 125.9, 123.6, 123.2, 119.3, 119.0, 118.6, 115.9, 115.5, 115.2, 112.1, 106.5, 68.3, 52.8, 52.8, 48.7, 47.3, 47.3, 41.6. HRMS(ESI): calcd for $C_{18}H_{21}F_6N_4O$, $[M + H]^+$ 423.1620; found, 423.1614. HPLC purity: 98.89%.

1-(benzyloxy)-3-((2-((5-(trifluoromethyl)pyridin-2-yl)amino)ethyl)amino)propan-2-ol (GI-26)

To a solution of **A$_5$** (30 mg, 0.15 mmol) and **B$_{13}$** (24 mg, 0.15 mmol) in ethanol, DIPEA (37.8 mg, 0.29 mmol) was added at room temperature. The solution was

stirred at reflux for 8 hours and monitored to react completely. After warming to room temperature, the mixture was concentrated and purified by column chromatography on silica gel with the elution fluid of DCM/MeOH (100:1-50:1, with additional drops of aqueous ammonia). Pale yellow solid was achieved in 39.9 mg with 73.3% yield. ^{1}H NMR (400 MHz, Chloroform-*d*) δ 8.33 (d, *J* = 2.1 Hz, 1H), 7.57 (dd, *J* = 8.9, 2.4 Hz, 1H), 7.41-7.29 (m, 5H), 6.42 (d, *J* = 8.8 Hz, 1H), 5.42 (s, 1H), 4.57 (s, 2H), 3.94 (m, *J* = 7.6, 4.1 Hz, 1H), 3.57-3.44 (m, 4H), 2.91 (t, *J* = 5.8 Hz, 2H), 2.75 (m, *J* = 12.2, 5.8 Hz, 2H). ^{13}C NMR (101 MHz, Chloroform-*d*) δ 160.3, 146.0, 146.0, 145.9, 137.8, 134.3, 134.2, 134.2, 134.2, 128.5, 127.9, 127.8, 125.9, 123.3, 115.6, 115.3, 106.8, 73.5, 72.7, 69.0, 51.7, 48.5, 41.3. HRMS(ESI): calcd for $C_{18}H_{22}F_3N_3O_2$, $[M + H]^+$ 370.1742; found, 370.1734. HPLC purity: 95.09%.

1-((4-(trifluoromethyl)benzyl)oxy)-3-((2-((5-(trifluoromethyl)pyridin-2-yl)amino)ethyl)amino)propan-2-ol (GI-27)

To a solution of **A$_5$** (30 mg, 0.15 mmol) and **B$_{14}$** (33.9 mg, 0.15 mmol) in ethanol, DIPEA (37.8 mg, 0.29 mmol) was added at room temperature. The solution was stirred at reflux for 8 hours and monitored to react completely. After warming to room temperature, the mixture was concentrated and purified by column chromatography on silica gel with the elution fluid of DCM/MeOH (100:1-50:1, with additional drops of aqueous ammonia). Pale yellow solid was achieved in 37.1 mg with 58.7% yield. ^{1}H NMR (400 MHz, Chloroform-*d*) δ 8.32 (d, *J* = 2.3 Hz, 1H), 7.65-7.53 (m, 3H), 7.44 (d, *J* = 8.0 Hz, 2H), 6.41 (d, *J* = 8.8 Hz, 1H), 5.50 (t, *J* = 5.5 Hz, 1H), 4.61 (s, 2H), 3.95 (m, *J* = 7.8, 6.1, 3.9 Hz, 1H), 3.58-3.49 (m, 2H), 3.45 (q, *J* = 5.7 Hz, 2H), 2.90 (t, *J* = 5.8 Hz, 2H), 2.80-2.69 (m, 2H). ^{13}C NMR (101 MHz, Chloroform-*d*) δ 160.3, 146.0, 145.9, 142.0, 134.3, 134.3, 130.1, 129.8, 127.6, 125.9, 125.4, 125.4, 125.4, 125.3, 123.2, 122.7, 115.6, 115.2, 106.6, 73.2, 72.6, 69.1, 51.7, 48.5, 41.4. HRMS(ESI): calcd for $C_{19}H_{21}F_6N_3O_2$, $[M + H]^+$ 438.1616; found, 438.1612. HPLC purity: 97.4%.

1-((3-(trifluoromethyl)benzyl)oxy)-3-((2-((5-(trifluoromethyl)pyridin-2-

yl)amino)ethyl)amino)propan-2-ol (GI-28)

To a solution of **A5** (30 mg, 0.15 mmol) and **B15** (33.9 mg, 0.15 mmol) in ethanol, DIPEA (37.8 mg, 0.29 mmol) was added at room temperature. The solution was stirred at reflux for 8 hours and monitored to react completely. After warming to room temperature, the mixture was concentrated and purified by column chromatography on silica gel with the elution fluid of DCM/MeOH (100:1-50:1, with additional drops of aqueous ammonia). Pale yellow solid was achieved in 33.8 mg with 53.5% yield. ^{1}H NMR (400 MHz, Chloroform-*d*) δ 8.33 (d, *J* = 2.3 Hz, 1H), 7.61-7.46 (m, 5H), 6.42 (d, *J* = 8.8 Hz, 1H), 5.36 (s, 1H), 4.62 (s, 2H), 3.95 (m, *J* = 7.9, 6.3, 3.9 Hz, 1H), 3.59-3.52 (m, 2H), 3.47 (q, *J* = 5.7 Hz, 2H), 2.92 (t, *J* = 5.8 Hz, 2H), 2.83-2.69 (m, 2H). ^{13}C NMR (101 MHz, Chloroform-*d*) δ 160.3, 139.0, 130.8, 128.9, 124.6, 124.2, 115.3, 73.1, 72.7, 69.1, 51.7, 48.5, 41.4. HRMS(ESI): calcd for $C_{19}H_{21}F_6N_3O_2$, $[M + H]^+$ 438.1616; found, 438.1629. HPLC purity: 93.05%

1-((2-(trifluoromethyl)benzyl)oxy)-3-((2-((5-(trifluoromethyl)pyridin-2-yl)amino)ethyl)amino)propan-2-ol (GI-29)

To a solution of **A5** (30 mg, 0.15 mmol) and **B16** (33.9 mg, 0.15 mmol) in ethanol, DIPEA (37.8 mg, 0.29 mmol) was added at room temperature. The solution was stirred at reflux for 8 hours and monitored to react completely. After warming to room temperature, the mixture was concentrated and purified by column chromatography on silica gel with the elution fluid of DCM/MeOH (100:1-50:1, with additional drops of aqueous ammonia). Pale yellow solid was achieved in 34.2 mg with 54.1% yield. ^{1}H NMR (600 MHz, Chloroform-*d*) δ 8.33-8.30 (m, 1H), 7.66 (t, *J* = 7.6 Hz, 2H), 7.58-7.53 (m, 2H), 7.40 (t, *J* = 7.7 Hz, 1H), 6.42 (d, *J* = 8.8 Hz, 1H), 5.49 (s, 1H), 4.74 (s, 2H), 3.97 (m, *J* = 10.1, 7.5, 3.2 Hz, 1H), 3.59 (dd, *J* = 9.6, 3.9 Hz, 1H), 3.55 (dd, *J* = 9.6, 6.3 Hz, 1H), 3.48-3.44 (m, 2H), 2.91 (t, *J* = 5.8 Hz, 2H), 2.79 (dd, *J* = 12.2, 3.7 Hz, 1H), 2.74 (dd, *J* = 12.2, 8.0 Hz, 1H). ^{13}C NMR (151 MHz, Chloroform-*d*) δ 160.3, 146.0, 146.0, 146.0, 145.9, 136.5, 134.3, 134.2, 134.2, 134.2, 132.0, 129.1, 128.0, 127.8, 127.6, 127.4, 127.3, 127.0, 125.9, 125.9, 125.9, 125.8, 125.5, 125.2,

123.7, 123.4, 121.9, 121.6, 115.7, 115.5, 115.2, 115.0, 73.4, 69.5, 69.1, 51.7, 48.5, 41.4. HRMS(ESI): calcd for $C_{19}H_{21}F_6N_3O_2$, $[M + H]^+$ 438.1616; found, 438.1628. HPLC purity: 94.01%

1-((4-(trifluoromethyl)benzyl)thio)-3-((2-((5-(trifluoromethyl)pyridin-2-yl)amino)ethyl)amino)propan-2-ol (GI-30)

To a solution of **A_5** (30 mg, 0.15 mmol) and **B_{17}** (36.3 mg, 0.15 mmol) in ethanol, DIPEA (37.8 mg, 0.29 mmol) was added at room temperature. The solution was stirred at reflux for 8 hours and monitored to react completely. After warming to room temperature, the mixture was concentrated and purified by column chromatography on silica gel with the elution fluid of DCM/MeOH (100:1-50:1, with additional drops of aqueous ammonia). Yellow solid was achieved in 43.7 mg with 65.9% yield. ^{1}H NMR (400 MHz, Chloroform-*d*) δ 8.38-8.28 (m, 1H), 7.58 (dd, *J* = 8.6, 3.2 Hz, 3H), 7.45 (d, *J* = 8.0 Hz, 2H), 6.43 (d, *J* = 8.8 Hz, 1H), 5.38 (s, 1H), 3.81 (s, 3H), 3.46 (q, *J* = 5.7 Hz, 2H), 2.89 (m, *J* = 5.7, 1.4 Hz, 2H), 2.78 (dd, *J* = 12.1, 3.3 Hz, 1H), 2.65-2.51 (m, 3H). ^{13}C NMR (101 MHz, Chloroform-*d*) δ 160.3, 146.1, 146.0, 146.0, 146.0, 142.3, 134.4, 134.3, 134.3, 134.3, 129.6, 129.3, 129.2, 125.9, 125.6, 125.5, 125.5, 125.5, 125.4, 123.2, 122.7, 115.7, 115.3, 106.6, 68.7, 53.9, 48.5, 41.5, 36.3, 36.2. HRMS(ESI): calcd for $C_{19}H_{21}F_6N_3OS$, $[M + H]^+$ 454.1388; found, 454.1385. HPLC purity: 93.19%.

1-((2-((5-nitropyridin-2-yl)amino)ethyl)amino)-3-((4-(trifluoromethyl)benzyl)oxy)propan-2-ol (GI-31)

To a solution of **A_9** (30 mg, 0.16 mmol) and **B_{14}** (38.2 mg, 0.16 mmol) in ethanol, DIPEA (42.6 mg, 0.33 mmol) was added at room temperature. The solution was stirred at reflux for 8 hours and monitored to react completely. After warming to room temperature, the mixture was concentrated and purified by column chromatography on silica gel with the elution fluid of DCM/MeOH (100:1-50:1, with additional drops of aqueous ammonia). Yellow solid was achieved in 43.1 mg with 69.7% yield. ^{1}H NMR (600 MHz, Chloroform-*d*) δ 9.02 (d, *J* = 2.7 Hz, 1H), 8.18 (d, *J* = 9.1 Hz, 1H),

7.63 (d, *J* = 8.0 Hz, 2H), 7.46 (d, *J* = 7.9 Hz, 2H), 6.38 (d, *J* = 9.2 Hz, 1H), 5.95 (s, 1H), 4.63 (s, 2H), 3.96 (m, *J* = 10.4, 3.8 Hz, 1H), 3.59-3.50 (m, 4H), 2.95 (t, *J* = 5.8 Hz, 2H), 2.81 (dd, *J* = 12.2, 3.7 Hz, 1H), 2.74 (dd, *J* = 12.2, 7.9 Hz, 1H). ^{13}C NMR (151 MHz, Chloroform-*d*) δ 161.1, 147.0, 141.9, 135.8, 130.2, 129.9, 127.6, 125.5, 125.4, 125.4, 125.4, 125.0, 123.2, 121.4, 73.1, 72.7, 69.2, 51.6, 48.2, 41.5. HRMS(ESI): calcd for $C_{18}H_{21}F_3N_4O_4$, $[M + H]^+$ 415.1593; found, 415.1601. HPLC purity: 98.35%.

1-((4-(trifluoromethyl)benzyl)oxy)-3-((2-((2-(trifluoromethyl)phenyl)amino)ethyl)amino)propan-2-ol (GI-32)

To a solution of **A$_{10}$** (30 mg, 0.15 mmol) and **B$_{14}$** (34.1 mg, 0.15 mmol) in ethanol, DIPEA (37.8 mg, 0.29 mmol) was added at room temperature. The solution was stirred at reflux for 8 hours and monitored to react completely. After warming to room temperature, the mixture was concentrated and purified by column chromatography on silica gel with the elution fluid of DCM/MeOH (200:1-100:1, with additional drops of aqueous ammonia). White solid was achieved in 39.9 mg with 62.2% yield. ^{1}H NMR (600 MHz, Chloroform-*d*) δ 7.61 (d, *J* = 8.0 Hz, 2H), 7.46 (d, *J* = 7.9 Hz, 3H), 7.41-7.36 (m, 1H), 6.75 (d, *J* = 7.9 Hz, 2H), 4.94 (d, *J* = 5.4 Hz, 1H), 4.62 (s, 2H), 3.94 (m, *J* = 6.8, 4.0 Hz, 1H), 3.56 (m, *J* = 9.7, 5.1 Hz, 2H), 3.27 (q, *J* = 5.6 Hz, 2H), 3.00-2.92 (m, 2H), 2.81 (m, *J* = 11.9, 4.1, 1.5 Hz, 1H), 2.73 (m, *J* = 12.1, 7.3, 1.1 Hz, 1H). ^{13}C NMR (151 MHz, Chloroform-*d*) δ 145.8, 142.1, 133.1, 120.0, 129.8, 127.6, 126.7, 126.7, 126.6, 126.6, 126.1, 125.4, 125.4, 125.4, 125.3, 125.0, 124.3, 123.2, 115.9, 113.6, 113.4, 111.9, 73.1, 72.6, 69.3, 51.4, 48.0, 42.9. HRMS(ESI): calcd for $C_{20}H_{22}F_6N_2O_2$, $[M + H]^+$ 437.1664; found, 437.1669. HPLC purity: 92.05%.

1-((3-(trifluoromethyl)benzyl)oxy)-3-((2-((2-(trifluoromethyl)phenyl)amino)ethyl)amino)propan-2-ol (GI-33)

To a solution of **A$_{10}$** (30 mg, 0.15 mmol) and **B$_{15}$** (34.1 mg, 0.15 mmol) in ethanol, DIPEA (37.8 mg, 0.29 mmol) was added at room temperature. The solution was stirred at reflux for 8 hours and monitored to react completely. After warming to room

temperature, the mixture was concentrated and purified by column chromatography on silica gel with the elution fluid of DCM/MeOH (200:1-100:1, with additional drops of aqueous ammonia). White solid was achieved in 38.1 mg with 59.4% yield. ^{1}H NMR (600 MHz, Chloroform-*d*) δ 7.62 (s, 1H), 7.57 (d, *J* = 7.8 Hz, 1H), 7.53 (d, *J* = 7.7 Hz, 1H), 7.49-7.44 (m, 2H), 7.40-7.36 (m, 1H), 6.74 (t, *J* = 8.1 Hz, 2H), 4.94 (t, *J* = 5.1 Hz, 1H), 4.61 (s, 2H), 3.94 (m, *J* = 7.9, 6.5, 4.0 Hz, 1H), 3.57 (m, *J* = 9.7, 5.1 Hz, 2H), 3.26 (q, *J* = 5.7 Hz, 2H), 2.96 (h, *J* = 5.9 Hz, 2H), 2.81 (dd, *J* = 12.1, 4.1 Hz, 1H), 2.72 (dd, *J* = 12.1, 7.3 Hz, 1H). ^{13}C NMR (101 MHz, Chloroform-*d*) δ 145.8, 145.8, 145.8, 139.1, 133.1, 130.8, 130.6, 128.9, 128.8, 126.7, 126.6, 126.6, 126.5, 125.5, 124.6, 124.5, 124.5, 124.5, 124.4, 124.3, 124.3, 124.2, 124.2, 123.9, 122.8, 115.9, 113.9, 113.7, 113.6, 113.4, 113.3, 113.1, 111.9, 111.8, 73.1, 72.7, 69.2, 51.4, 48.0, 42.8. HRMS(ESI): calcd for $C_{20}H_{22}F_6N_2O_2$, $[M + H]^+$ 437.1664; found, 437.1664. HPLC purity: 98.51%.

1-((2-(trifluoromethyl)benzyl)oxy)-3-((2-((2-(trifluoromethyl)phenyl)amino)ethyl)amino)propan-2-ol (GI-34)

To a solution of **A$_{10}$** (30 mg, 0.15 mmol) and **B$_{16}$** (34.1 mg, 0.15 mmol) in ethanol, DIPEA (37.8 mg, 0.29 mmol) was added at room temperature. The solution was refluxed for 3 hours and monitored to react completely. The mixture was concentrated and purified by column chromatography on silica gel with the elution fluid of DCM/MeOH (200:1-100:1, with additional drops of aqueous ammonia). White solid was achieved in 42.9 mg with 67.6% yield. ^{1}H NMR (400 MHz, Chloroform-*d*) δ 7.67 (d, *J* = 7.9 Hz, 2H), 7.56 (t, *J* = 7.6 Hz, 1H), 7.42 (m, *J* = 24.0, 7.9 Hz, 3H), 6.74 (t, *J* = 8.1 Hz, 2H), 4.94 (d, *J* = 5.3 Hz, 1H), 4.76 (s, 2H), 3.96 (m, *J* = 6.2, 4.1 Hz, 1H), 3.60 (h, *J* = 5.8 Hz, 2H), 3.27 (q, *J* = 5.6 Hz, 2H), 2.97 (m, *J* = 5.7, 2.0 Hz, 2H), 2.86-2.71 (m, 2H). ^{13}C NMR (101 MHz, Chloroform-*d*) δ 145.8, 145.8, 145.8, 136.7, 136.7, 133.1, 132.0, 129.3, 129.1, 128.4, 128.2, 127.9, 127.6, 127.3, 126.7, 126.7, 126.6, 126.6, 126.5, 125.9, 125.9, 125.8, 125.8, 125.7, 123.9, 123.0, 120.2, 115.9, 114.0, 113.7, 113.4, 113.1, 111.9, 73.3, 69.5, 69.2, 51.5, 48.0, 42.9. HRMS(ESI): calcd for $C_{20}H_{22}F_6N_2O_2$, $[M + H]^+$ 437.1664; found, 437.1663. HPLC purity: 99.4%.

***N*-(2-((2-hydroxy-3-(4-(trifluoromethyl)phenoxy)propyl)amino)ethyl)-2-(trifluoromethyl)benzenesulfonamide (GI-35)**

To a solution of **A_{16}** (30 mg, 0.11 mmol) and **B_{16}** (24.4 mg, 0.11 mmol) in ethanol, DIPEA (28.9 mg, 0.22 mmol) was added at room temperature. The solution was stirred at reflux for 8 hours and monitored to react completely. After warming to room temperature, the mixture was concentrated and purified by column chromatography on silica gel with the elution fluid of DCM/MeOH (100:1-50:1, with additional drops of aqueous ammonia). White solid was achieved in 37.7 mg with 69.3% yield. ^{1}H NMR (600 MHz, DMSO-d_6) δ 8.11 (dd, J = 8.1, 3.0 Hz, 1H), 7.98 (dd, J = 8.1, 2.6 Hz, 1H), 7.89 (t, J = 7.7 Hz, 1H), 7.83 (t, J = 7.7 Hz, 1H), 7.63 (dd, J = 9.0, 2.8 Hz, 2H), 7.11 (d, J = 8.5 Hz, 2H), 5.06 (s, 1H), 4.02 (m, J = 9.9, 4.4, 1.6 Hz, 1H), 3.93 (m, J = 9.3, 6.2, 2.5 Hz, 1H), 3.84 (h, J = 5.6 Hz, 1H), 2.99-2.93 (m, 2H), 2.61 (m, J = 12.9, 5.1, 4.2 Hz, 3H), 2.54 (m, J = 10.7, 6.5, 3.7 Hz, 1H). ^{13}C NMR (151 MHz, DMSO-d_6) δ 162.0, 140.0, 133.7, 133.7, 133.2, 133.2, 130.4, 128.9, 128.9, 128.8, 128.8, 127.4, 127.3, 127.3, 127.3, 126.7, 126.5, 126.5, 126.1, 125.9, 124.3, 124.1, 122.5, 121.8, 121.5, 121.3, 121.3, 115.4, 71.4, 68.5, 52.3, 49.2, 43.3. HRMS(ESI): calcd for $C_{19}H_{20}F_6N_2O_4S$, $[M + H]^+$ 487.1126; found, 487.1132. HPLC purity: 99.23%.

1-(4-(trifluoromethyl)phenoxy)-3-((2-(2-(trifluoromethyl)phenoxy)ethyl)amino)propan-2-ol (GI-36)

To a solution of **A_{17}** (30 mg, 0.15 mmol) and **B_7** (31.9 mg, 0.15 mmol) in ethanol, DIPEA (37.8 mg, 0.29 mmol) was added at room temperature. The solution was stirred at reflux for 8 hours and monitored to react completely. After warming to room temperature, the mixture was concentrated and purified by column chromatography on silica gel with the elution fluid of DCM/MeOH (200:1-100:1, with additional drops of aqueous ammonia). White solid was achieved in 37.4 mg with 60.3% yield. ^{1}H NMR (600 MHz, DMSO-d_6) δ 7.62 (dd, J = 16.9, 8.2 Hz, 4H), 7.27 (d, J = 8.4 Hz, 1H), 7.10 (t, J = 8.2 Hz, 3H), 5.09 (d, J = 5.0 Hz, 1H), 4.16 (t, J = 5.6 Hz, 2H), 4.04 (dd, J = 9.8, 4.5 Hz, 1H), 3.96 (dd, J = 9.8, 6.1 Hz, 1H), 3.90 (t, J = 5.9 Hz, 1H), 2.94

(t, *J* = 5.6 Hz, 2H), 2.76 (dd, *J* = 12.0, 4.8 Hz, 1H), 2.68 (dd, *J* = 11.9, 6.7 Hz, 1H). ^{113}C NMR (151 MHz, DMSO-d_6) δ 162.0, 156.9, 134.7, 130.1, 127.4, 127.4, 127.3, 127.3, 127.1, 127.1, 127.1, 126.0, 125.2, 124.2, 123.4, 121.5, 121.3, 120.7, 117.8, 117.6, 117.4, 115.4, 114.1, 71.4, 69.0, 68.5, 52.5, 48.6. HRMS(ESI): calcd for $C_{19}H_{19}F_6NO_3$, $[M + H]^+$ 424.1347; found, 424.1355. HPLC purity: 95.69%.

1-(4-(trifluoromethyl)phenoxy)-3-((2-((2-(trifluoromethyl)phenyl)thio)ethyl)amino)propan-2-ol (GI-37)

To a solution of **A$_{18}$** (30 mg, 0.14 mmol) and **B$_7$** (29.6 mg, 0.14 mmol) in ethanol, DIPEA (35.1 mg, 0.27 mmol) was added at room temperature. The solution was stirred at reflux for 8 hours and monitored to react completely. After warming to room temperature, the mixture was concentrated and purified by column chromatography on silica gel with the elution fluid of DCM/MeOH (200:1-100:1, with additional drops of aqueous ammonia). White solid was achieved in 34.5 mg with 58.1% yield. ^{1}H NMR (400 MHz, Chloroform-*d*) δ 7.68 (d, *J* = 7.9 Hz, 1H), 7.59-7.46 (m, 4H), 7.33 (t, *J* = 7.6 Hz, 1H), 6.99 (d, *J* = 8.4 Hz, 2H), 4.08-4.01 (m, 3H), 3.17 (m, *J* = 6.4, 2.2 Hz, 2H), 2.99-2.87 (m, 3H), 2.83-2.76 (m, 1H). ^{13}C NMR (101 MHz, Chloroform-*d*) δ 161.1, 135.4, 132.0, 131.6, 130.6, 130.3, 127.0, 127.0, 127.0, 126.9, 126.9, 126.9, 126.3, 125.7, 125.1, 123.4, 123.1, 123.0, 122.4, 120.3, 114.5, 70.5, 68.2, 51.1, 47.9, 35.2. HRMS(ESI): calcd for $C_{19}H_{19}F_6NO_2S$, $[M + H]^+$ 440.1119; found, 440.1120. HPLC purity: 98.46%.

1-((2-((2-(trifluoromethyl)phenyl)amino)ethyl)amino)-3-((4-(trifluoromethyl)phenyl)thio)propan-2-ol (GI-38)

To a solution of **A$_{10}$** (30 mg, 0.15 mmol) and **B$_{12}$** (34.4 mg, 0.15 mmol) in ethanol, DIPEA (37.8 mg, 0.29 mmol) was added at room temperature. The solution was stirred at reflux for 8 hours and monitored to react completely. After warming to room temperature, the mixture was concentrated and purified by column chromatography on silica gel with the elution fluid of DCM/MeOH (200:1-100:1, with additional drops of aqueous ammonia). White solid was achieved in 34.3 mg with 70.7% yield.

^{1}H NMR (400 MHz, Chloroform-*d*) δ 7.53 (d, *J* = 8.2 Hz, 2H), 7.42 (m, *J* = 15.6, 7.9 Hz, 4H), 6.75 (dd, *J* = 8.1, 5.4 Hz, 2H), 4.87 (s, 1H), 3.86 (m, *J* = 7.3, 3.9 Hz, 1H), 3.34-3.22 (m, 2H), 3.20-3.09 (m, 2H), 3.03-2.88 (m, 3H), 2.72 (dd, *J* = 12.2, 7.5 Hz, 1H). ^{13}C NMR (101 MHz, Chloroform-*d*) δ 145.7, 145.7, 141.3, 133.1, 128.4, 128.1, 128.0, 127.7, 126.8, 126.7, 126.7, 126.6, 126.6, 125.8, 125.8, 125.7, 125.7, 125.4, 123.9, 122.7, 116.1, 113.7, 113.4, 111.9, 68.5, 53.4, 48.0, 42.9, 37.7. HRMS(ESI): calcd for $C_{19}H_{20}F_6N_2OS$, $[M + H]^+$ 439.1279; found, 439.1279. HPLC purity: 96.13%.

1-((4-(trifluoromethyl)phenyl)thio)-3-((2-((2-(trifluoromethyl)phenyl)thio)ethyl)amino)propan-2-ol (GI-39)

To a solution of **A_{18}** (30 mg, 0.14 mmol) and **B_{12}** (31.8 mg, 0.14 mmol) in ethanol, DIPEA (35.1 mg, 0.27 mmol) was added at room temperature. The solution was stirred at reflux for 8 hours and monitored to react completely. After warming to room temperature, the mixture was concentrated and purified by column chromatography on silica gel with the elution fluid of DCM/MeOH (200:1-100:1, with additional drops of aqueous ammonia). Pale yellow solid was achieved in 46.8 mg with 66.4% yield. ^{1}H NMR (600 MHz, Chloroform-*d*) δ 7.70 -7.67 (m, 1H), 7.54 (t, *J* = 8.6 Hz, 3H), 7.49 (t, *J* = 7.7 Hz, 1H), 7.43 (d, *J* = 8.2 Hz, 2H), 7.33 (t, *J* = 7.6 Hz, 1H), 3.82 (m, *J* = 12.0, 6.1, 3.6 Hz, 1H), 3.18-3.10 (m, 4H), 2.93-2.84 (m, 3H), 2.65 (dd, *J* = 12.2, 8.1 Hz, 1H). ^{13}C NMR (151 MHz, Chloroform-*d*) δ 141.5, 135.4, 132.0, 131.6, 130.6, 130.4, 127.9, 127.9, 127.7, 127.5, 127.0, 127.0, 126.9, 126.9, 126.3, 125.8, 125.8, 125.7, 125.7, 125.0, 124.6, 123.2, 122.8, 68.2, 53.3, 47.8, 37.5, 35.2. HRMS(ESI): calcd for $C_{19}H_{19}F_6NOS_2$, $[M + H]^+$ 456.0890; found, 456.0893. HPLC purity: 95.63%.

5.1.3 The synthesis on intermediates of aromatic derivatives

1-(4-((5-(trifluoromethyl)pyridin-2-yl)amino)phenyl)ethan-1-one (C1)

To a solution of 2-chloro-5-(trifluoromethyl)pyridine (1 g, 5.51 mmol), 1-(4-aminophenyl)ethan-1-one (893.5 mg, 6.61 mmol) in toluene, $Pd(OAc)_2$ (224.5 mg,

1.1 mmol), X-Phos (525.2 mg, 1.1 mmol) and Cs_2CO_3 (2.7 g, 8.26 mmol) was added. The mixture was stirred under nitrogen at 120 ℃ for 8 hours. After cooling to room temperature and filtration with diatomite, water was added and the filtrate was extracted with ethyl acetate for three times and washed with saturated brine. The combined organic layer was dried over anhydrous Na_2SO_4 and purified by column chromatography on silica gel with the elution fluid of Hexane/EA (100:1-50:1). Pale yellow solid was achieved in 1.35 g with 87.8% yield. ^{1}H NMR (600 MHz, Chloroform-*d*) δ 8.44 (d, *J* = 2.7 Hz, 1H), 8.02 (d, *J* = 8.6 Hz, 1H), 7.60 (d, *J* = 8.4 Hz, 2H), 7.53 (dd, *J* = 8.7, 2.7 Hz, 1H), 7.25 (d, *J* = 8.3 Hz, 2H), 6.64-6.53 (m, 1H), 2.70 (s, 3H).

1-(4-((4-(trifluoromethyl)phenyl)amino)phenyl)ethan-1-one (C2)

To a solution of 1-iodo-4-(trifluoromethyl)benzene (1 g, 3.68 mmol), 1-(4-aminophenyl)ethan-1-one (596.3 mg, 4.41 mmol) in toluene, $Pd(OAc)_2$ (165.1 mg, 0.74 mmol), X-Phos (350.5 mg, 0.74 mmol) and Cs_2CO_3 (1.8 g, 5.51 mmol) was added. The mixture was stirred under nitrogen at 120 ℃ for 8 hours. After cooling to room temperature and filtration with diatomite, water was added and the filtrate was extracted with ethyl acetate for three times and washed with saturated brine. The combined organic layer was dried over anhydrous Na_2SO_4 and purified by column chromatography on silica gel with the elution fluid of Hexane/EA (200:1-100:1). Pale yellow solid was achieved in 867.3 mg with 84.2% yield. ^{1}H NMR (600 MHz, Chloroform-*d*) δ 7.96-7.92 (m, 2H), 7.58 (d, *J* = 8.3 Hz, 2H), 7.24 (d, *J* = 8.3 Hz, 2H), 7.15-7.11 (m, 2H), 6.47 (s, 1H), 2.58 (s, 3H).

1-(4-((3-(trifluoromethyl)phenyl)amino)phenyl)ethan-1-one (C3)

To a solution of 1-iodo-3-(trifluoromethyl)benzene (1 g, 3.68 mmol), 1-(4-aminophenyl)ethan-1-one (596.3 mg, 4.41 mmol) in toluene, $Pd(OAc)_2$ (165.1 mg, 0.74 mmol), X-Phos (350.5 mg, 0.74 mmol) and Cs_2CO_3 (1.8 g, 5.51 mmol) was added. The mixture was stirred under nitrogen at 120 ℃ for 8 hours. After cooling to room temperature and filtration with diatomite, water was added and the filtrate was

extracted with ethyl acetate for three times and washed with saturated brine. The combined organic layer was dried over anhydrous Na_2SO_4 and purified by column chromatography on silica gel with the elution fluid of Hexane/EA (200:1-100:1). Pale yellow solid was achieved in 889.9 mg with 86.4% yield. ^{1}H NMR (400 MHz, Chloroform-*d*) δ 7.96-7.91 (m, 2H), 7.49-7.42 (m, 2H), 7.38-7.30 (m, 2H), 7.10-7.04 (m, 2H), 6.21 (s, 1H), 2.58 (s, 3H).

1-(4-((2-(trifluoromethyl)phenyl)amino)phenyl)ethan-1-one (C4)

To a solution of 1-iodo-2-(trifluoromethyl)benzene (1 g, 3.68 mmol), 1-(4-aminophenyl)ethan-1-one (596.3 mg, 4.41 mmol) in toluene, $Pd(OAc)_2$ (165.1 mg, 0.74 mmol), X-Phos (350.5 mg, 0.74 mmol) and Cs_2CO_3 (1.8 g, 5.51 mmol) was added. The mixture was stirred under nitrogen at 120 ℃ for 8 hours. After cooling to room temperature and filtration with diatomite, water was added and the filtrate was extracted with ethyl acetate for three times and washed with saturated brine. The combined organic layer was dried over anhydrous Na_2SO_4 and purified by column chromatography on silica gel with the elution fluid of Hexane/EA (200:1-100:1). Pale yellow solid was achieved in 869.3 mg with 84.4% yield. ^{1}H NMR (400 MHz, Chloroform-*d*) δ 7.77 (dd, *J* = 8.6, 1.3 Hz, 2H), 7.55 (d, *J* = 7.9 Hz, 1H), 7.42-7.37 (m, 2H), 7.07 (dt, *J* = 8.4, 4.1 Hz, 1H), 6.90 (dd, *J* = 8.6, 1.3 Hz, 2H), 6.56 (s, 1H), 2.43 (d, *J* = 1.2 Hz, 3H).

1-(4-((4-methoxyphenyl)amino)phenyl)ethan-1-one (C5)

To a solution of 1-iodo-4-methoxybenzene (1 g, 4.27 mmol), 1-(4-aminophenyl)ethan-1-one (693.1 mg, 5.13 mmol) in toluene, $Pd(OAc)_2$ (191.9 mg, 0.85 mmol), X-Phos (407.4 mg, 0.85 mmol) and Cs_2CO_3 (2.09 g, 6.41 mmol) was added. The mixture was stirred under nitrogen at 120 ℃ for 8 hours. After cooling to room temperature and filtration with diatomite, water was added and the filtrate was extracted with ethyl acetate for three times and washed with saturated brine. The combined organic layer was dried over anhydrous Na_2SO_4 and purified by column chromatography on silica gel with the elution fluid of Hexane/EA (200:1-100:1). Pale

yellow solid was achieved in 787.9 mg with 76.5% yield. ^{1}H NMR (400 MHz, Chloroform-*d*) δ 7.89-7.81 (m, 2H), 7.19-7.14 (m, 2H), 6.96-6.91 (m, 2H), 6.86-6.81 (m, 2H), 6.05-5.97 (m, 1H), 3.85 (s, 3H), 2.53 (s, 3H).

1-(4-((4-(methylthio)phenyl)amino)phenyl)ethan-1-one (C6)

To a solution of (4-iodophenyl)(methyl)sulfane (1 g, 4 mmol), 1-(4-aminophenyl)ethan-1-one (648.5 mg, 4.8 mmol) in toluene, $Pd(OAc)_2$ (179.5 mg, 0.79 mmol), X-Phos (381.2 mg, 0.79 mmol) and Cs_2CO_3 (1.95 g, 6 mmol) was added. The mixture was stirred under nitrogen at 120 ℃ for 8 hours. After cooling to room temperature and filtration with diatomite, water was added and the filtrate was extracted with ethyl acetate for three times and washed with saturated brine. The combined organic layer was dried over anhydrous Na_2SO_4 and purified by column chromatography on silica gel with the elution fluid of Hexane/EA (200:1-100:1). Pale yellow solid was achieved in 748.8 mg with 72.7% yield. ^{1}H NMR (400 MHz, Chloroform-*d*) δ 7.88-7.83 (m, 2H), 7.29-7.24 (m, 2H), 7.14-7.10 (m, 2H), 7.01 (s, 1H), 6.98-6.94 (m, 2H), 6.73 (s, 1H), 2.54 (s, 3H), 2.49 (s, 3H).

2-((4-acetylphenyl)amino)benzonitrile (C7)

To a solution of 2-iodobenzonitrile (1 g, 4.37 mmol), 1-(4-aminophenyl)ethan-1-one (708.2 mg, 5.24 mmol) in toluene, $Pd(OAc)_2$ (196.1 mg, 0.87 mmol), X-Phos (416.3 mg, 0.87 mmol) and Cs_2CO_3 (2.13 g, 6.55 mmol) was added. The mixture was stirred under nitrogen at 120 ℃ for 8 hours. After cooling to room temperature and filtration with diatomite, water was added and the filtrate was extracted with ethyl acetate for three times and washed with saturated brine. The combined organic layer was dried over anhydrous Na_2SO_4 and purified by column chromatography on silica gel with the elution fluid of Hexane/EA (100:1-50:1). Pale yellow solid was achieved in 672.6 mg with 65.3% yield. ^{1}H NMR (400 MHz, Chloroform-*d*) δ 8.00-7.96 (m, 2H), 7.61 (dd, J = 7.7, 1.5 Hz, 1H), 7.54-7.44 (m, 2H), 7.20 (d, J = 8.7 Hz, 2H), 7.07-7.02 (m, 1H), 6.55 (s, 1H), 2.60 (s, 3H).

1-(4-(4-(trifluoromethyl)phenoxy)phenyl)ethan-1-one (C8)

To a solution of 4-(trifluoromethyl)phenol (1 g, 6.17 mmol) in NMP, 1-(4-fluorophenyl)ethan-1-one (852.1 mg, 6.17 mmol) and Cs_2CO_3 (4.02 g, 12.34 mmol) was added. The mixture was stirred at 120 ℃ under nitrogen for overnight and monitored to react completely. After cooling to room temperature and filtration with diatomite, water was added and the filtrate was extracted with ethyl acetate for three times and washed with saturated brine. The combined organic layer was dried over anhydrous Na_2SO_4 and purified by column chromatography on silica gel with the elution fluid of Hexane/EA (200:1-100:1). Pale yellow solid was achieved in 1.54 g with 89.1% yield. ^{1}H NMR (400 MHz, Chloroform-*d*) δ 8.03-7.99 (m, 2H), 7.66 (d, *J* = 8.5 Hz, 2H), 7.15 (d, *J* = 8.3 Hz, 2H), 7.11-7.07 (m, 2H), 2.62 (s, 3H).

1-(4-((4-(trifluoromethyl)phenyl)thio)phenyl)ethan-1-one (C9)

To a solution of 4-(trifluoromethyl)benzenethiol (1 g, 5.61 mmol) in NMP, 1-(4-fluorophenyl)ethan-1-one (775.3 mg, 5.61 mmol) and Cs_2CO_3 (3.66 g, 11.23 mmol) was added. The mixture was stirred at 120 ℃ under nitrogen for overnight and monitored to react completely. After cooling to room temperature and filtration with diatomite, water was added and the filtrate was extracted with ethyl acetate for three times and washed with saturated brine. The combined organic layer was dried over anhydrous Na_2SO_4 and purified by column chromatography on silica gel with the elution fluid of Hexane/EA (200:1-100:1). Yellow solid was achieved in 1.03 g with 62.3% yield. ^{1}H NMR (400 MHz, Chloroform-*d*) δ 7.94-7.90 (m, 2H), 7.61 (d, *J* = 8.5 Hz, 2H), 7.49 (d, *J* = 8.2 Hz, 2H), 7.42-7.38 (m, 2H), 2.61 (s, 3H).

1-(6-((4-(trifluoromethyl)phenyl)amino)pyridin-3-yl)ethan-1-one (C10)

To a solution of 4-(trifluoromethyl)aniline (1 g, 6.21 mmol) and 1-(6-bromopyridin-3-yl)ethan-1-one (1.24 g, 6.21 mmol) in toluene, $Pd_2(dba)_3$ (1.14 g, 1.24 mmol), X-Phos (1.18 g, 2.48 mmol) and Cs_2CO_3 (3.03 g, 9.31 mmol) was added. The mixture was stirred under nitrogen at 80 ℃ for 24 hours. After cooling to room temperature and filtration with diatomite, water was added and the filtrate was extracted with ethyl acetate for three times and washed with saturated brine. The combined organic layer

was dried over anhydrous Na_2SO_4 and purified by column chromatography on silica gel with the elution fluid of Hexane/EA (100:1-50:1). Pale yellow solid was achieved in 1.48 g with 85.5% yield. ^{1}H NMR (400 MHz, Chloroform-*d*) δ 8.88 (s, 1H), 8.15 (dd, *J* = 8.8, 2.2 Hz, 1H), 7.63 (s, 4H), 7.18 (s, 1H), 6.88 (d, *J* = 8.8 Hz, 1H), 2.59 (s, 3H).

1-(2-(trifluoromethyl)-4-((4-(trifluoromethyl)phenyl)amino)phenyl)ethan-1-one (C11)

To a solution of 4-(trifluoromethyl)aniline (1 g, 6.21 mmol), 1-(4-bromo-2-(trifluoromethyl)phenyl)ethan-1-one (1.66 g, 6.21 mmol) in toluene, $Pd_2(dba)_3$ (1.14 g, 1.24 mmol), X-Phos (1.18 g, 2.48 mmol) and Cs_2CO_3 (3.03 g, 9.31 mmol) was added. The mixture was stirred under nitrogen at 80 ℃ for 24 hours. After cooling to room temperature and filtration with diatomite, water was added and the filtrate was extracted with ethyl acetate for three times and washed with saturated brine. The combined organic layer was dried over anhydrous Na_2SO_4 and purified by column chromatography on silica gel with the elution fluid of Hexane/EA (200:1-100:1). White solid was achieved in 1.98 g with 92.1% yield. ^{1}H NMR (400 MHz, DMSO-d_6) δ 9.39 (s, 1H), 7.89 (d, *J* = 8.4 Hz, 1H), 7.66 (d, *J* = 8.4 Hz, 2H), 7.47 (d, *J* = 7.5 Hz, 2H), 7.33 (d, *J* = 8.4 Hz, 2H).

1-(4-((4-(trifluoromethyl)thiazol-2-yl)amino)phenyl)ethan-1-one (C12)

To a solution of 4-(trifluoromethyl)thiazol-2-amine (1 g, 5.95 mmol), 1-(4-bromophenyl)ethan-1-one (1.18 g, 5.95 mmol) in toluene, $Pd_2(dba)_3$ (1.09 g, 1.19 mmol), X-Phos (1.13 g, 2.38 mmol) and Cs_2CO_3 (2.91 g, 8.92 mmol) was added. The mixture was stirred under nitrogen at 80 ℃ for 24 hours. After cooling to room temperature and filtration with diatomite, water was added and the filtrate was extracted with ethyl acetate for three times and washed with saturated brine. The combined organic layer was dried over anhydrous Na_2SO_4 and purified by column chromatography on silica gel with the elution fluid of Hexane/EA (100:1-50:1). Pale yellow solid was achieved in 999.6 mg with 58.8% yield. ^{1}H NMR (400 MHz,

Chloroform-*d*) δ 8.05-8.01 (m, 2H), 7.55 (s, 1H), 7.50-7.46 (m, 2H), 7.21 (s, 1H), 2.61 (s, 3H).

1-(3-((2-(trifluoromethyl)phenyl)amino)phenyl)ethan-1-one (C13)

To a solution of 1-iodo-2-(trifluoromethyl)benzene (1 g, 3.68 mmol), 1-(3-aminophenyl)ethan-1-one (596.3 mg, 4.41 mmol) in toluene, $Pd(OAc)_2$ (165.1 mg, 0.74 mmol), X-Phos (350.5 mg, 0.74 mmol) and Cs_2CO_3 (1.8 g, 5.51 mmol) was added. The mixture was stirred under nitrogen at 120 ℃ for 8 hours. After cooling to room temperature and filtration with diatomite, water was added and the filtrate was extracted with ethyl acetate for three times and washed with saturated brine. The combined organic layer was dried over anhydrous Na_2SO_4 and purified by column chromatography on silica gel with the elution fluid of Hexane/EA (200:1-100:1). Pale yellow solid was achieved in 855.9 mg with 83.1% yield. ^{1}H NMR (400 MHz, Chloroform-*d*) δ 7.69 (t, *J* = 2.0 Hz, 1H), 7.61 (m, *J* = 6.3, 4.4, 3.1 Hz, 2H), 7.46-7.39 (m, 2H), 7.36 (d, *J* = 8.3 Hz, 1H), 7.31 (m, *J* = 8.0, 2.4, 1.1 Hz, 1H), 7.04 (t, *J* = 7.6 Hz, 1H), 6.15 (s, 1H), 2.62 (s, 3H).

2-bromo-1-(4-((5-(trifluoromethyl)pyridin-2-yl)amino)phenyl)ethan-1-one (D1)

To a solution of **C1** (500 mg, 1.78 mmol) in a mixture of $CHCl_3$ and EA (1:1), $CuBr_2$ (438.3 mg, 1.96 mmol) was added. The mixture was stirred at 60 ℃ for overnight and monitored to react completely**.** After cooling to room temperature and filtration with diatomite, the filtrate was concentrated and purified by column chromatography on silica gel with the elution fluid of Hexane/EA (100:1-50:1). Yellow solid was achieved in 316.5 mg with 49.4% yield. ^{1}H NMR (600 MHz, Chloroform-*d*) δ 8.57 (s, 1H), 8.04-8.01 (m, 2H), 7.80 (dd, *J* = 8.8, 2.4 Hz, 1H), 7.65-7.62 (m, 2H), 7.16 (s, 1H), 6.97 (dd, *J* = 8.9, 4.3 Hz, 1H), 4.45 (s, 2H).

2-bromo-1-(4-((4-(trifluoromethyl)phenyl)amino)phenyl)ethan-1-one (D2)

To a solution of **C2** (500 mg, 1.79 mmol) in a mixture of $CHCl_3$ and EA (1:1), $CuBr_2$ (439.9 mg, 1.97 mmol) was added. The mixture was stirred at 60 ℃ for overnight and

monitored to react completely**.** After cooling to room temperature and filtration with diatomite, the filtrate was concentrated and purified by column chromatography on silica gel with the elution fluid of Hexane/EA (200:1-150:1). Yellow solid was achieved in 284.1 mg with 44.3% yield. ^{1}H NMR (400 MHz, Chloroform-*d*) δ 7.97 (d, *J* = 8.4 Hz, 2H), 7.61 (d, *J* = 8.3 Hz, 2H), 7.27 (d, *J* = 8.0 Hz, 2H), 7.14 (d, *J* = 8.5 Hz, 2H), 6.34 (s, 1H), 4.41 (s, 2H).

2-bromo-1-(4-((3-(trifluoromethyl)phenyl)amino)phenyl)ethan-1-one (D3)

To a solution of **C3** (500 mg, 1.79 mmol) in a mixture of $CHCl_3$ and EA (1:1), $CuBr_2$ (439.9 mg, 1.97 mmol) was added. The mixture was stirred at 60 ℃ for overnight and monitored to react completely**.** After cooling to room temperature and filtration with diatomite, the filtrate was concentrated and purified by column chromatography on silica gel with the elution fluid of Hexane/EA Hexane/EA (200:1-150:1). Yellow solid was achieved in 262.3 mg with 40.9% yield. ^{1}H NMR (400 MHz, Chloroform-*d*) δ 7.97 (d, *J* = 2.0 Hz, 1H), 7.95 (d, *J* = 2.1 Hz, 1H), 7.52-7.44 (m, 2H), 7.41-7.34 (m, 2H), 7.07 (d, *J* = 2.0 Hz, 1H), 7.06 (d, *J* = 2.0 Hz, 1H), 6.27 (s, 1H), 4.41 (s, 2H).

2-bromo-1-(4-((2-(trifluoromethyl)phenyl)amino)phenyl)ethan-1-one (D4)

To a solution of **C4** (500 mg, 1.79 mmol) in a mixture of $CHCl_3$ and EA (1:1), $CuBr_2$ (439.9 mg, 1.97 mmol) was added. The mixture was stirred at 60 ℃ for overnight and monitored to react completely**.** After cooling to room temperature and filtration with diatomite, the filtrate was concentrated and purified by column chromatography on silica gel with the elution fluid of Hexane/EA (200:1-150:1). Yellow solid was achieved in 278.9 mg with 43.5% yield. ^{1}H NMR (400 MHz, Chloroform-*d*) δ 8.24 (d, *J* = 2.1 Hz, 1H), 7.81 (dt, *J* = 8.7, 2.1 Hz, 1H), 7.75 (dd, *J* = 8.0, 1.5 Hz, 1H), 7.63-7.57 (m, 1H), 7.54 (d, *J* = 8.2 Hz, 1H), 7.35-7.30 (m, 1H), 7.07 (dd, *J* = 8.6, 1.9 Hz, 1H), 6.89 (s, 1H), 4.36 (d, *J* = 2.0 Hz, 2H).

2-bromo-1-(4-((4-methoxyphenyl)amino)phenyl)ethan-1-one (D5)

To a solution of **C5** (500 mg, 2.07 mmol) in a mixture of $CHCl_3$ and EA (1:1), $CuBr_2$

(509.1 mg, 2.28 mmol) was added. The mixture was stirred at 60 ℃ for overnight and monitored to react completely**.** After cooling to room temperature and filtration with diatomite, the filtrate was concentrated and purified by column chromatography on silica gel with the elution fluid of Hexane/EA (200:1-150:1). Yellow solid was achieved in 244.2 mg with 36.8% yield. ^{1}H NMR (600 MHz, Chloroform-*d*) δ 7.78 (d, *J* = 8.7 Hz, 2H), 7.10-7.06 (m, 2H), 6.87-6.83 (m, 2H), 6.76-6.72 (m, 2H), 4.28 (s, 2H), 3.76 (s, 3H).

2-bromo-1-(4-((4-(methylthio)phenyl)amino)phenyl)ethan-1-one (D6)

To a solution of **C6** (500 mg, 1.94 mmol) in a mixture of $CHCl_3$ and EA (1:1), $CuBr_2$ (477.3 mg, 2.14 mmol) was added. The mixture was stirred at 60 ℃ for overnight and monitored to react completely**.** After cooling to room temperature and filtration with diatomite, the filtrate was concentrated and purified by column chromatography on silica gel with the elution fluid of Hexane/EA (200:1-150:1). Yellow solid was achieved in 223.4 mg with 34.2% yield.

2-((4-(2-bromoacetyl)phenyl)amino)benzonitrile (D7)

To a solution of **C7** (500 mg, 2.12 mmol) in a mixture of $CHCl_3$ and EA (1:1), $CuBr_2$ (519.9 mg, 2.33 mmol) was added. The mixture was stirred at 60 ℃ for overnight and monitored to react completely**.** After cooling to room temperature and filtration with diatomite, the filtrate was concentrated and purified by column chromatography on silica gel with the elution fluid of Hexane/EA (100:1-50:1). Yellow solid was achieved in 259.4 mg with 38.9% yield. ^{1}H NMR (400 MHz, Chloroform-*d*) δ 7.99-7.94 (m, 2H), 7.78-7.75 (m, 1H), 7.67-7.64 (m, 1H), 7.47 (td, *J* = 7.7, 1.2 Hz, 1H), 7.39-7.35 (m, 3H), 4.43 (s, 2H).

2-bromo-1-(4-(4-(trifluoromethyl)phenoxy)phenyl)ethan-1-one (D8)

To a solution of **C8** (500 mg, 1.78 mmol) and TsOH (307.2 mg, 1.78 mmol) in acetonitrile, NBS (349.3 mg, 1.96 mmol) was added in ice bath. After warming to room temperature, the mixture was stirred at 90 ℃ for 8 hours and monitored to react

completely. After cooling to room temperature, the solution was concentrated and purified by column chromatography on silica gel with the elution fluid of Hexane/EA (200:1-150:1). Yellow solid was achieved in 437.6 mg with 68.3% yield. ^{1}H NMR (400 MHz, Chloroform-*d*) δ 8.08-8.02 (m, 2H), 7.69 (d, *J* = 8.5 Hz, 2H), 7.18 (d, *J* = 8.4 Hz, 2H), 7.12-7.08 (m, 2H), 4.44 (s, 2H).

2-bromo-1-(4-((4-(trifluoromethyl)phenyl)thio)phenyl)ethan-1-one (D9)

To a solution of **C9** (500 mg, 1.69 mmol) and TsOH (290.6 mg, 1.69 mmol) in acetonitrile, NBS (330.4 mg, 1.86 mmol) was added in ice bath. After warming to room temperature, the mixture was stirred at 90 ℃ for 8 hours and monitored to react completely. After cooling to room temperature, the solution was concentrated and purified by column chromatography on silica gel with the elution fluid of Hexane/EA (200:1-150:1). Yellow solid was achieved in 410.3 mg with 64.8% yield. ^{1}H NMR (600 MHz, Chloroform-*d*) δ 7.48 (d, *J* = 8.2 Hz, 2H), 7.43-7.40 (m, 2H), 7.32 (d, *J* = 8.1 Hz, 2H), 7.28 (d, *J* = 2.0 Hz, 2H), 4.14 (s, 2H).

2-bromo-1-(6-((4-(trifluoromethyl)phenyl)amino)pyridin-3-yl)ethan-1-one (D10)

To a solution of **C10** (500 mg, 1.78 mmol) in a mixture of $CHCl_3$ and EA (1:1), $CuBr_2$ (438.3 mg, 1.96 mmol) was added. The mixture was stirred at 60 ℃ for overnight and monitored to react completely**.** After cooling to room temperature and filtration with diatomite, the filtrate was concentrated and purified by column chromatography on silica gel with the elution fluid of Hexane/EA (100:1-50:1). Yellow solid was achieved in 228.1 mg with 35.6% yield. ^{1}H NMR (600 MHz, Chloroform-*d*) δ 8.87 (d, *J* = 2.3 Hz, 1H), 8.14 (dd, *J* = 8.8, 2.3 Hz, 1H), 7.65-7.59 (m, 4H), 7.19 (s, 1H), 6.89 (d, *J* = 8.8 Hz, 1H), 4.61 (s, 2H).

2-bromo-1-(2-(trifluoromethyl)-4-((4-(trifluoromethyl)phenyl)amino)phenyl)ethan-1-one (D11)

To a solution of **C11** (500 mg, 1.44 mmol) in a mixture of $CHCl_3$ and EA (1:1), $CuBr_2$ (353.8 mg, 1.58 mmol) was added. The mixture was stirred at 60 ℃ for overnight and

monitored to react completely**.** After cooling to room temperature and filtration with diatomite, the filtrate was concentrated and purified by column chromatography on silica gel with the elution fluid of Hexane/EA (200:1-150:1). Pale yellow solid was achieved in 279.2 mg with 45.5% yield. ^{1}H NMR (600 MHz, Chloroform-*d*) δ 7.62 (dd, *J* = 13.1, 8.4 Hz, 3H), 7.42 (d, *J* = 2.3 Hz, 1H), 7.31-7.28 (m, 1H), 7.25 (d, *J* = 8.3 Hz, 2H), 6.47 (s, 1H), 4.39 (s, 2H).

2-bromo-1-(4-((4-(trifluoromethyl)thiazol-2-yl)amino)phenyl)ethan-1-one (D12)

To a solution of **C12** (500 mg, 1.75 mmol) in a mixture of $CHCl_3$ and EA (1:1), $CuBr_2$ (429.1 mg, 1.92 mmol) was added. The mixture was stirred at 60 ℃ for overnight and monitored to react completely**.** After cooling to room temperature and filtration with diatomite, the filtrate was concentrated and purified by column chromatography on silica gel with the elution fluid of Hexane/EA (200:1-150:1). Yellow solid was achieved in 190.1 mg with 29.8% yield. ^{1}H NMR (600 MHz, DMSO-d_6) δ 11.11 (d, *J* = 2.1 Hz, 1H), 8.03 (d, *J* = 8.6 Hz, 2H), 7.81 (d, *J* = 4.6 Hz, 1H), 7.74 (dd, *J* = 8.7, 1.5 Hz, 2H), 4.84 (d, *J* = 1.6 Hz, 2H).

2-bromo-1-(3-((2-(trifluoromethyl)phenyl)amino)phenyl)ethan-1-one (D13)

To a solution of **C13** (500 mg, 1.79 mmol) in a mixture of $CHCl_3$ and EA (1:1), $CuBr_2$ (439.9 mg, 1.97 mmol) was added. The mixture was stirred at 60 ℃ for overnight and monitored to react completely**.** After cooling to room temperature and filtration with diatomite, the filtrate was concentrated and purified by column chromatography on silica gel with the elution fluid of Hexane/EA (200:1-150:1). Yellow solid was achieved in 283.4 mg with 44.2% yield. ^{1}H NMR (600 MHz, Chloroform-*d*) δ 7.71 (t, *J* = 2.0 Hz, 1H), 7.65-7.60 (m, 2H), 7.45 (q, *J* = 8.1 Hz, 2H), 7.39 (d, *J* = 8.3 Hz, 1H), 7.33 (dd, *J* = 8.1, 2.4 Hz, 1H), 7.07 (t, *J* = 7.6 Hz, 1H), 6.16 (s, 1H), 4.45 (s, 2H).

2-(4-bromo-2,6-difluorophenoxy)-1-(4-((5-(trifluoromethyl)pyridin-2-yl)amino)phenyl)ethan-1-one (E1)

To a solution of 4-bromo-2,6-difluorophenol (87.3 mg, 0.42 mmol) in acetone, K_2CO_3

(76.9 mg, 0.56 mmol) was added. The mixture was stirred at room temperature for 30 minutes. With the following addition of **D1** (100 mg, 0.28 mmol), it was stirred at reflux for 6 hours and monitored to react completely**.** After cooling to room temperature and filtration, the filtrate was concentrated and purified by column chromatography on silica gel with the elution fluid of Hexane/EA (20:1-10:1). Pale yellow solid was achieved in 122.4 mg with 90.2% yield. ^{1}H NMR (600 MHz, DMSO-d_6) δ 10.13 (s, 1H), 8.62-8.58 (m, 1H), 7.97 (dd, J = 8.9, 2.4 Hz, 1H), 7.91 (q, J = 9.0 Hz, 4H), 7.50 (dd, J = 8.4, 1.4 Hz, 2H), 7.07 (d, J = 8.9 Hz, 1H), 5.64 (s, 2H).

2-(3,4-difluorophenoxy)-1-(4-((5-(trifluoromethyl)pyridin-2-yl)amino)phenyl)ethan-1-one (E2)

To a solution of 3,4-difluorophenol (54.3 mg, 0.42 mmol) in acetone, K_2CO_3 (76.96 mg, 0.56 mmol) was added. The mixture was stirred at room temperature for 30 minutes. With the following addition of **D1** (100 mg, 0.28 mmol), it was stirred at reflux for 6 hours and monitored to react completely**.** After cooling to room temperature and filtration, the filtrate was concentrated and purified by column chromatography on silica gel with the elution fluid of Hexane/EA (20:1-10:1). Pale yellow solid was achieved in 103.8 mg with 91.3% yield. ^{1}H NMR (600 MHz, DMSO-d_6) δ 10.12 (s, 1H), 8.61 (d, J = 2.4 Hz, 1H), 8.01-7.96 (m, 3H), 7.91 (d, J = 8.6 Hz, 2H), 7.35 (q, J = 9.6 Hz, 1H), 7.15 (m, J = 12.7, 6.7, 3.0 Hz, 1H), 7.07 (d, J = 8.9 Hz, 1H), 6.82 (dd, J = 8.6, 4.2 Hz, 1H), 5.54 (s, 2H).

2-(4-(trifluoromethyl)phenoxy)-1-(4-((5-(trifluoromethyl)pyridin-2-yl)amino)phenyl)ethan-1-one (E3)

To a solution of 4-(trifluoromethyl)phenol (67.7 mg, 0.42 mmol) in acetone, K_2CO_3 (76.9 mg, 0.56 mmol) was added. The mixture was stirred at room temperature for 30 minutes. With the following addition of **D1** (100 mg, 0.28 mmol), it was stirred at reflux for 6 hours and monitored to react completely**.** After cooling to room temperature and filtration, the filtrate was concentrated and purified by column chromatography on silica gel with the elution fluid of Hexane/EA (20:1-10:1). Pale

yellow solid was achieved in 111.1 mg with 90.6% yield. ^{1}H NMR (600 MHz, DMSO-d_6) δ 10.13 (s, 1H), 8.60 (d, J = 2.5 Hz, 1H), 8.02-7.95 (m, 3H), 7.92 (d, J = 8.8 Hz, 2H), 7.64 (d, J = 8.5 Hz, 2H), 7.14 (d, J = 8.5 Hz, 2H), 7.08 (d, J = 8.9 Hz, 1H), 5.65 (s, 2H).

2-(4-bromo-2,6-difluorophenoxy)-1-(4-((4-(trifluoromethyl)phenyl)amino)phenyl)ethan-1-one (E4)

To a solution of 4-bromo-2,6-difluorophenol (87.5 mg, 0.42 mmol) in acetone, K_2CO_3 (77.2 mg, 0.56 mmol) was added. The mixture was stirred at room temperature for 30 minutes. With the following addition of **D2** (100 mg, 0.28 mmol), it was stirred at reflux for 6 hours and monitored to react completely**.** After cooling to room temperature and filtration, the filtrate was concentrated and purified by column chromatography on silica gel with the elution fluid of Hexane/EA (50:1-20:1). Pale yellow solid was achieved in 123.3 mg with 90.8% yield. ^{1}H NMR (400 MHz, Chloroform-d) δ 7.94-7.89 (m, 2H), 7.60 (d, J = 8.5 Hz, 2H), 7.25 (d, J = 8.4 Hz, 2H), 7.16-7.08 (m, 4H), 6.37 (s, 1H), 5.40 (s, 2H).

2-(3,4-difluorophenoxy)-1-(4-((4-(trifluoromethyl)phenyl)amino)phenyl)ethan-1-one (E5)

To a solution of 3,4-difluorophenol (54.5 mg, 0.42 mmol) in acetone, K_2CO_3 (77.2 mg, 0.56 mmol) was added. The mixture was stirred at room temperature for 30 minutes. With the following addition of **D2** (100 mg, 0.28 mmol), it was stirred at reflux for 6 hours and monitored to react completely**.** After cooling to room temperature and filtration, the filtrate was concentrated and purified by column chromatography on silica gel with the elution fluid of Hexane/EA (50:1-20:1). Pale yellow solid was achieved in 100.8 mg with 88.6% yield. ^{1}H NMR (400 MHz, Chloroform-d) δ 7.96 (d, J = 8.5 Hz, 2H), 7.61 (d, J = 8.3 Hz, 2H), 7.26 (d, J = 8.4 Hz, 2H), 7.15 (d, J = 8.5 Hz, 2H), 7.08 (q, J = 9.4 Hz, 1H), 6.79 (m, J = 11.8, 6.4, 3.0 Hz, 1H), 6.68-6.63 (m, 1H), 6.42 (s, 1H), 5.21 (s, 2H).

2-(4-(trifluoromethyl)phenoxy)-1-(4-((4-

(trifluoromethyl)phenyl)amino)phenyl)ethan-1-one (E6/GII-26)

To a solution of 4-(trifluoromethyl)phenol (67.9 mg, 0.42 mmol) in acetone, K_2CO_3 (77.2 mg, 0.56 mmol) was added. The mixture was stirred at room temperature for 30 minutes. With the following addition of **D2** (100 mg, 0.28 mmol), it was stirred at reflux for 6 hours and monitored to react completely**.** After cooling to room temperature and filtration, the filtrate was concentrated and purified by column chromatography on silica gel with the elution fluid of Hexane/EA (50:1-20:1). Pale yellow solid was achieved in 111.6 mg with 91% yield. ^{1}H NMR (400 MHz, Chloroform-*d*) δ 7.99 (d, *J* = 8.7 Hz, 2H), 7.59 (dd, *J* = 17.4, 8.4 Hz, 4H), 7.27 (d, *J* = 8.0 Hz, 2H), 7.18-7.12 (m, 2H), 7.02 (d, *J* = 8.5 Hz, 2H), 6.35 (s, 1H), 5.30 (s, 2H). ^{13}C NMR (151 MHz, Chloroform-*d*) δ 191.72 160.5, 147.5, 143.7, 130.5, 127.2, 127.0, 127.0, 127.0, 126.9, 126.9, 125.2, 123.8, 123.6, 123.4, 118.9, 118.8, 116.0, 116.0, 114.8, 114.7, 70.5, 29.7. HRMS(ESI): calcd for $C_{22}H_{15}F_6NO$, $[M - H]^-$ 438.0929; found, 438.0938. HPLC purity: 99.06%.

2-(3-(trifluoromethyl)phenoxy)-1-(4-((4-(trifluoromethyl)phenyl)amino)phenyl)ethan-1-one (E7)

To a solution of 3-(trifluoromethyl)phenol (67.9 mg, 0.42 mmol) in acetone, K_2CO_3 (77.2 mg, 0.56 mmol) was added. The mixture was stirred at room temperature for 30 minutes. With the following addition of **D2** (100 mg, 0.28 mmol), it was stirred at reflux for 6 hours and monitored to react completely**.** After cooling to room temperature and filtration, the filtrate was concentrated and purified by column chromatography on silica gel with the elution fluid of Hexane/EA (50:1-20:1). Pale yellow solid was achieved in 110 mg with 89.7% yield. ^{1}H NMR (400 MHz, Chloroform-*d*) δ 8.04-7.96 (m, 2H), 7.61 (d, *J* = 8.3 Hz, 2H), 7.42 (t, *J* = 8.0 Hz, 1H), 7.27 (d, *J* = 8.3 Hz, 3H), 7.24-7.10 (m, 4H), 6.36 (s, 1H), 5.28 (s, 2H).

2-(2-(trifluoromethyl)phenoxy)-1-(4-((4-(trifluoromethyl)phenyl)amino)phenyl)ethan-1-one (E8)

To a solution of 2-(trifluoromethyl)phenol (67.9 mg, 0.42 mmol) in acetone, K_2CO_3

(77.2 mg, 0.56 mmol) was added. The mixture was stirred at room temperature for 30 minutes. With the following addition of **D2** (100 mg, 0.28 mmol), it was stirred at reflux for 6 hours and monitored to react completely**.** After cooling to room temperature and filtration, the filtrate was concentrated and purified by column chromatography on silica gel with the elution fluid of Hexane/EA (50:1-20:1). Pale yellow solid was achieved in 109.4 mg with 89.2% yield. ^{1}H NMR (400 MHz, Chloroform-*d*) δ 8.05-7.99 (m, 2H), 7.63-7.57 (m, 3H), 7.49-7.43 (m, 1H), 7.25 (d, *J* = 8.3 Hz, 2H), 7.15-7.09 (m, 2H), 7.05 (t, *J* = 7.6 Hz, 1H), 6.94 (d, *J* = 8.4 Hz, 1H), 6.40 (d, *J* = 5.0 Hz, 1H), 5.29 (s, 2H).

2-(4-nitrophenoxy)-1-(4-((4-(trifluoromethyl)phenyl)amino)phenyl)ethan-1-one (E9)

To a solution of 4-nitrophenol (58.3 mg, 0.42 mmol) in acetone, K_2CO_3 (77.2 mg, 0.56 mmol) was added. The mixture was stirred at room temperature for 30 minutes. With the following addition of **D2** (100 mg, 0.28 mmol), it was stirred at reflux for 6 hours and monitored to react completely**.** After cooling to room temperature and filtration, the filtrate was concentrated and purified by column chromatography on silica gel with the elution fluid of Hexane/EA (50:1-20:1). Yellow solid was achieved in 108.6 mg with 93.4% yield. ^{1}H NMR (400 MHz, Chloroform-*d*) δ 8.27-8.18 (m, 2H), 7.97 (d, *J* = 8.7 Hz, 2H), 7.62 (d, *J* = 8.3 Hz, 2H), 7.26 (s, 2H), 7.20-7.11 (m, 2H), 7.08-6.96 (m, 2H), 6.36 (s, 1H), 5.38 (s, 2H).

4-(2-oxo-2-(4-((4-(trifluoromethyl)phenyl)amino)phenyl)ethoxy)benzonitrile (E10)

To a solution of 4-hydroxybenzonitrile (49.9 mg, 0.42 mmol) in acetone, K_2CO_3 (77.2 mg, 0.56 mmol) was added. The mixture was stirred at room temperature for 30 minutes. With the following addition of **D2** (100 mg, 0.28 mmol), it was stirred at reflux for 6 hours and monitored to react completely**.** After cooling to room temperature and filtration, the filtrate was concentrated and purified by column chromatography on silica gel with the elution fluid of Hexane/EA (20:1-10:1). Pale yellow solid was achieved in 104.3 mg with 94.2% yield. ^{1}H NMR (600 MHz,

Chloroform-*d*) δ 7.96 (d, *J* = 8.2 Hz, 2H), 7.61 (dd, *J* = 8.3, 5.2 Hz, 4H), 7.27 (d, *J* = 8.1 Hz, 2H), 7.15 (d, *J* = 8.4 Hz, 2H), 7.00 (d, *J* = 8.6 Hz, 2H), 6.45 (s, 1H), 5.33 (s, 2H).

2-(4-(methylthio)phenoxy)-1-(4-((4-(trifluoromethyl)phenyl)amino)phenyl)ethan-1-one (E11)

To a solution of 4-(methylthio)phenol (58.7 mg, 0.42 mmol) in acetone, K_2CO_3 (77.2 mg, 0.56 mmol) was added. The mixture was stirred at room temperature for 30 minutes. With the following addition of **D2** (100 mg, 0.28 mmol), it was stirred at reflux for 6 hours and monitored to react completely**.** After cooling to room temperature and filtration, the filtrate was concentrated and purified by column chromatography on silica gel with the elution fluid of Hexane/EA (50:1-20:1). Pale yellow solid was achieved in 104.1 mg with 89.32% yield. ^{1}H NMR (400 MHz, Chloroform-*d*) δ 8.02-7.97 (m, 2H), 7.60 (d, *J* = 8.4 Hz, 2H), 7.28-7.23 (m, 4H), 7.16-7.12 (m, 2H), 6.94-6.89 (m, 2H), 6.33 (s, 1H), 5.21 (s, 2H), 2.46 (s, 3H).

1-(4-((4-(trifluoromethyl)phenyl)amino)phenyl)-2-((5-(trifluoromethyl)pyridin-2-yl)oxy)ethan-1-one (E12)

To a solution of 5-(trifluoromethyl)pyridin-2-ol (68.3 mg, 0.42 mmol) in acetone, K_2CO_3 (77.2 mg, 0.56 mmol) was added. The mixture was stirred at room temperature for 30 minutes. With the following addition of **D2** (100 mg, 0.28 mmol), it was stirred at reflux for 6 hours and monitored to react completely**.** After cooling to room temperature and filtration, the filtrate was concentrated and purified by column chromatography on silica gel with the elution fluid of Hexane/EA (20:1-10:1). Pale yellow solid was achieved in 112.5 mg with 91.5% yield. ^{1}H NMR (400 MHz, DMSO-d_6) δ 9.38 (s, 1H), 8.38 (s, 1H), 7.99 (d, *J* = 8.6 Hz, 2H), 7.76 (d, *J* = 7.7 Hz, 1H), 7.66 (d, *J* = 8.4 Hz, 2H), 7.37 (d, *J* = 8.4 Hz, 2H), 7.27 (d, *J* = 8.5 Hz, 2H), 6.60 (d, *J* = 9.7 Hz, 1H), 5.50 (s, 2H).

1-(4-((4-(trifluoromethyl)phenyl)amino)phenyl)-2-((4-(trifluoromethyl)pyridin-2-yl)oxy)ethan-1-one (E13)

To a solution of 4-(trifluoromethyl)pyridin-2-ol (68.3 mg, 0.42 mmol) in acetone, K_2CO_3 (77.2 mg, 0.56 mmol) was added. The mixture was stirred at room temperature for 30 minutes. With the following addition of **D2** (100 mg, 0.28 mmol), it was stirred at reflux for 6 hours and monitored to react completely**.** After cooling to room temperature and filtration, the filtrate was concentrated and purified by column chromatography on silica gel with the elution fluid of Hexane/EA (20:1-10:1). Pale yellow solid was achieved in 114.7 mg with 93.3% yield. ^{1}H NMR (600 MHz, DMSO-d_6) δ 9.39 (s, 1H), 8.01-7.98 (m, 2H), 7.93 (d, J = 7.0 Hz, 1H), 7.66 (d, J = 8.4 Hz, 2H), 7.36 (d, J = 8.4 Hz, 2H), 7.29-7.26 (m, 2H), 6.85 (d, J = 2.1 Hz, 1H), 6.58 (dd, J = 7.1, 2.0 Hz, 1H), 5.51 (s, 2H).

1-(4-((4-(trifluoromethyl)phenyl)amino)phenyl)-2-((5-(trifluoromethyl)pyridin-3-yl)oxy)ethan-1-one (E14)

To a solution of 5-(trifluoromethyl)pyridin-3-ol (68.3 mg, 0.42 mmol) in acetone, K_2CO_3 (77.2 mg, 0.56 mmol) was added. The mixture was stirred at room temperature for 30 minutes. With the following addition of **D2** (100 mg, 0.28 mmol), it was stirred at reflux for 6 hours and monitored to react completely**.** After cooling to room temperature and filtration, the filtrate was concentrated and purified by column chromatography on silica gel with the elution fluid of Hexane/EA (20:1-10:1). Pale yellow solid was achieved in 110.5 mg with 89.9% yield. ^{1}H NMR (400 MHz, Chloroform-*d*) δ 8.54 (d, J = 2.3 Hz, 2H), 7.95 (d, J = 8.5 Hz, 2H), 7.61 (d, J = 8.3 Hz, 2H), 7.45-7.41 (m, 1H), 7.26 (s, 2H), 7.16 (d, J = 8.6 Hz, 2H), 6.61 (t, J = 8.3 Hz, 1H), 5.39 (s, 2H).

2-(4-(trifluoromethyl)phenoxy)-1-(4-((3-(trifluoromethyl)phenyl)amino)phenyl)ethan-1-one (E15)

To a solution of 4-(trifluoromethyl)phenol (67.9 mg, 0.42 mmol) in acetone, K_2CO_3 (77.2 mg, 0.56 mmol) was added. The mixture was stirred at room temperature for 30 minutes. With the following addition of **D3** (100 mg, 0.28 mmol), it was stirred at reflux for 6 hours and monitored to react completely**.** After cooling to room

temperature and filtration, the filtrate was concentrated and purified by column chromatography on silica gel with the elution fluid of Hexane/EA (50:1-20:1). Pale yellow solid was achieved in 110.5 mg with 90.1% yield. ^{1}H NMR (400 MHz, Chloroform-*d*) δ 7.94 (dd, *J* = 14.8, 8.6 Hz, 2H), 7.54 (d, *J* = 8.5 Hz, 1H), 7.45 (dd, *J* = 15.2, 7.5 Hz, 2H), 7.40-7.28 (m, 2H), 7.11-6.98 (m, 3H), 5.31 (s, 1H), 2.58 (s, 2H).

2-(4-(trifluoromethyl)phenoxy)-1-(4-((2-(trifluoromethyl)phenyl)amino)phenyl)ethan-1-one (E16)

To a solution of 4-(trifluoromethyl)phenol (67.9 mg, 0.42 mmol) in acetone, K_2CO_3 (77.2 mg, 0.56 mmol) was added. The mixture was stirred at room temperature for 30 minutes. With the following addition of **D4** (100 mg, 0.28 mmol), it was stirred at reflux for 6 hours and monitored to react completely**.** After cooling to room temperature and filtration, the filtrate was concentrated and purified by column chromatography on silica gel with the elution fluid of Hexane/EA (50:1-20:1). Pale yellow solid was achieved in 113.6 mg with 92.6% yield. ^{1}H NMR (400 MHz, Chloroform-*d*) δ 7.99-7.93 (m, 2H), 7.70 (d, *J* = 7.8 Hz, 1H), 7.59-7.52 (m, 4H), 7.23 (m, *J* = 8.3, 4.4 Hz, 1H), 7.03 (dd, *J* = 11.1, 8.5 Hz, 4H), 6.34 (s, 1H), 5.29 (s, 2H).

1-(4-((4-methoxyphenyl)amino)phenyl)-2-(4-(trifluoromethyl)phenoxy)ethan-1-one (E17)

To a solution of 4-(trifluoromethyl)phenol (75.9 mg, 0.47 mmol) in acetone, K_2CO_3 (86.3 mg, 0.62 mmol) was added. The mixture was stirred at room temperature for 30 minutes. With the following addition of **D5** (100 mg, 0.31 mmol), it was stirred at reflux for 6 hours and monitored to react completely**.** After cooling to room temperature and filtration, the filtrate was concentrated and purified by column chromatography on silica gel with the elution fluid of Hexane/EA (50:1-20:1). Pale yellow solid was achieved in 111 mg with 88.6% yield. ^{1}H NMR (400 MHz, Chloroform-*d*) δ 7.90-7.83 (m, 2H), 7.53 (d, *J* = 8.5 Hz, 2H), 7.18-7.12 (m, 2H), 6.99 (d, *J* = 8.5 Hz, 2H), 6.95-6.90 (m, 2H), 6.85-6.79 (m, 2H), 6.01 (s, 1H), 5.24 (s, 2H), 3.83 (s, 3H).

1-(4-((4-(methylthio)phenyl)amino)phenyl)-2-(4-(trifluoromethyl)phenoxy)ethan-1-one (E18)

To a solution of 4-(trifluoromethyl)phenol (72.3 mg, 0.45 mmol) in acetone, K_2CO_3 (82.2 mg, 0.59 mmol) was added. The mixture was stirred at room temperature for 30 minutes. With the following addition of **D6** (100 mg, 0.3 mmol), it was stirred at reflux for 6 hours and monitored to react completely**.** After cooling to room temperature and filtration, the filtrate was concentrated and purified by column chromatography on silica gel with the elution fluid of Hexane/EA (50:1-20:1). Yellow solid was achieved in 115.1 mg with 92.7% yield. ^{1}H NMR (400 MHz, Chloroform-*d*) δ 7.95-7.90 (m, 2H), 7.56 (d, *J* = 8.5 Hz, 2H), 7.31 (d, *J* = 8.5 Hz, 2H), 7.16 (d, *J* = 8.4 Hz, 2H), 7.00 (dd, *J* = 13.8, 8.6 Hz, 4H), 6.13 (s, 1H), 5.28 (s, 2H), 2.52 (s, 3H).

2-((4-(2-(4-(trifluoromethyl)phenoxy)acetyl)phenyl)amino)benzonitrile (E19)

To a solution of 4-(trifluoromethyl)phenol (77.2 mg, 0.47 mmol) in acetone, K_2CO_3 (87.7 mg, 0.63 mmol) was added. The mixture was stirred at room temperature for 30 minutes. With the following addition of **D7** (100 mg, 0.32 mmol), it was stirred at reflux for 6 hours and monitored to react completely**.** After cooling to room temperature and filtration, the filtrate was concentrated and purified by column chromatography on silica gel with the elution fluid of Hexane/EA (20:1-10:1). Pale yellow solid was achieved in 116.1 mg with 92.3% yield. ^{1}H NMR (400 MHz, Chloroform-*d*) δ 8.04-7.98 (m, 2H), 7.64 (dd, *J* = 7.9, 1.5 Hz, 1H), 7.59-7.48 (m, 4H), 7.23-7.19 (m, 2H), 7.13-7.07 (m, 1H), 7.02 (d, *J* = 8.6 Hz, 2H), 6.66 (s, 1H), 5.31 (s, 2H).

2-((4-(trifluoromethyl)benzyl)oxy)-1-(4-((4-(trifluoromethyl)phenyl)amino)phenyl)ethan-1-one (E20)

To a solution of (4-(trifluoromethyl)phenyl)methanol (73.8 mg, 0.42 mmol) in acetone, K_2CO_3 (77.2 mg, 0.56 mmol) was added. The mixture was stirred at room temperature for 30 minutes. With the following addition of **D2** (100 mg, 0.28 mmol), it was stirred at reflux for 6 hours and monitored to react completely**.** After cooling to

room temperature and filtration, the filtrate was concentrated and purified by column chromatography on silica gel with the elution fluid of Hexane/EA (50:1-20:1). Pale yellow solid was achieved in 114.8 mg with 90.7% yield. ^{1}H NMR (600 MHz, Chloroform-*d*) δ 7.85-7.81 (m, 2H), 7.55 (d, *J* = 8.0 Hz, 2H), 7.50 (d, *J* = 8.3 Hz, 2H), 7.45 (d, *J* = 8.0 Hz, 2H), 7.15 (d, *J* = 8.3 Hz, 2H), 7.04-7.02 (m, 2H), 6.22 (s, 1H), 4.68 (d, *J* = 2.5 Hz, 4H).

1-(4-((4-(trifluoromethyl)phenyl)amino)phenyl)-2-((4-(trifluoromethyl)phenyl)thio)ethan-1-one (E21)

To a solution of 4-(trifluoromethyl)benzenethiol (74.6 mg, 0.42 mmol) in acetone, K_2CO_3 (77.2 mg, 0.56 mmol) was added. The mixture was stirred at room temperature for 30 minutes. With the following addition of **D2** (100 mg, 0.28 mmol), it was stirred at reflux for 6 hours and monitored to react completely**.** After cooling to room temperature and filtration, the filtrate was concentrated and purified by column chromatography on silica gel with the elution fluid of Hexane/EA (50:1-20:1). Pale yellow solid was achieved in 103.2 mg with 81.2% yield. ^{1}H NMR (400 MHz, Chloroform-*d*) δ 7.98-7.93 (m, 2H), 7.61 (d, *J* = 8.4 Hz, 2H), 7.54 (d, *J* = 8.4 Hz, 2H), 7.48 (d, *J* = 8.3 Hz, 2H), 7.27-7.24 (m, 2H), 7.15-7.12 (m, 2H), 6.32 (s, 1H), 4.33 (s, 2H).

2-(4-(trifluoromethyl)phenoxy)-1-(4-(4-(trifluoromethyl)phenoxy)phenyl)ethan-1-one (E22)

To a solution of 4-(trifluoromethyl)phenol (67.7 mg, 0.42 mmol) in acetone, K_2CO_3 (76.9 mg, 0.56 mmol) was added. The mixture was stirred at room temperature for 30 minutes. With the following addition of **D8** (100 mg, 0.28 mmol), it was stirred at reflux for 6 hours and monitored to react completely**.** After cooling to room temperature and filtration, the filtrate was concentrated and purified by column chromatography on silica gel with the elution fluid of Hexane/EA (50:1-20:1). Pale yellow solid was achieved in 106.3 mg with 86.7% yield. ^{1}H NMR (400 MHz, Chloroform-*d*) δ 7.99 (d, *J* = 8.6 Hz, 2H), 7.55 (d, *J* = 8.5 Hz, 2H), 7.42 (t, *J* = 7.8 Hz,

2H), 7.11- 6.97 (m, 6H), 5.29 (s, 2H).

2-(4-(trifluoromethyl)phenoxy)-1-(4-((4-(trifluoromethyl)phenyl)thio)phenyl)ethan-1-one (E23)

To a solution of 4-(trifluoromethyl)phenol (64.8 mg, 0.39 mmol) in acetone, K_2CO_3 (73.7 mg, 0.53 mmol) was added. The mixture was stirred at room temperature for 30 minutes. With the following addition of **D9** (100 mg, 0.26 mmol), it was stirred at reflux for 6 hours and monitored to react completely**.** After cooling to room temperature and filtration, the filtrate was concentrated and purified by column chromatography on silica gel with the elution fluid of Hexane/EA (50:1-20:1). Pale yellow solid was achieved in 111.4 mg with 91.6% yield. ^{1}H NMR (400 MHz, Chloroform-*d*) δ 7.97-7.93 (m, 2H), 7.65 (d, *J* = 8.2 Hz, 2H), 7.56 (dd, *J* = 8.4, 5.8 Hz, 4H), 7.41-7.37 (m, 2H), 7.01 (d, *J* = 8.5 Hz, 2H), 5.30 (s, 2H).

2-(4-(trifluoromethyl)phenoxy)-1-(6-((4-(trifluoromethyl)phenyl)amino)pyridin-3-yl)ethan-1-one (E24)

To a solution of 4-(trifluoromethyl)phenol (67.7 mg, 0.42 mmol) in acetone, K_2CO_3 (76.9 mg, 0.56 mmol) was added. The mixture was stirred at room temperature for 30 minutes. With the following addition of **D10** (100 mg, 0.28 mmol), it was stirred at reflux for 6 hours and monitored to react completely**.** After cooling to room temperature and filtration, the filtrate was concentrated and purified by column chromatography on silica gel with the elution fluid of Hexane/EA (20:1-10:1). Pale yellow solid was achieved in 96.4 mg with 78.6% yield. ^{1}H NMR (400 MHz, Chloroform-*d*) δ 8.95 (s, 1H), 8.20 (dd, *J* = 8.9, 2.0 Hz, 1H), 7.69-7.55 (m, 7H), 7.03 (d, *J* = 8.6 Hz, 2H), 6.93 (d, *J* = 8.9 Hz, 1H), 5.24 (s, 2H).

1-(2-(trifluoromethyl)-4-((4-(trifluoromethyl)phenyl)amino)phenyl)-2-(4-(trifluoromethyl)phenoxy)ethan-1-one (E25)

To a solution of 4-(trifluoromethyl)phenol (57.1 mg, 0.35 mmol) in acetone, K_2CO_3 (64.9 mg, 0.47 mmol) was added. The mixture was stirred at room temperature for 30

minutes. With the following addition of **D11** (100 mg, 0.23 mmol), it was stirred at reflux for 6 hours and monitored to react completely**.** After cooling to room temperature and filtration, the filtrate was concentrated and purified by column chromatography on silica gel with the elution fluid of Hexane/EA (50:1-20:1). White solid was achieved in 96.8 mg with 81.3% yield. ^{1}H NMR (400 MHz, Chloroform-*d*) δ 7.61 (dd, *J* = 8.4, 6.1 Hz, 3H), 7.55 (d, *J* = 8.6 Hz, 2H), 7.42 (d, *J* = 2.3 Hz, 1H), 7.29 (dd, *J* = 8.6, 2.3 Hz, 1H), 7.24 (d, *J* = 8.4 Hz, 2H), 6.97 (d, *J* = 8.6 Hz, 2H), 6.51 (s, 1H), 5.12 (s, 2H).

2-(4-(trifluoromethyl)phenoxy)-1-(4-((4-(trifluoromethyl)thiazol-2-yl)amino)phenyl)ethan-1-one (E26)

To a solution of 4-(trifluoromethyl)phenol (66.6 mg, 0.41 mmol) in acetone, K_2CO_3 (75.7 mg, 0.55 mmol) was added. The mixture was stirred at room temperature for 30 minutes. With the following addition of **D12** (100 mg, 0.27 mmol), it was stirred at reflux for 6 hours and monitored to react completely**.** After cooling to room temperature and filtration, the filtrate was concentrated and purified by column chromatography on silica gel with the elution fluid of Hexane/EA (50:1-20:1). Pale yellow solid was achieved in 108.4 mg with 88.7% yield. ^{1}H NMR (400 MHz, Chloroform-*d*) δ 8.07 (d, *J* = 8.7 Hz, 2H), 7.68 (s, 1H), 7.57 (dd, *J* = 8.8, 5.2 Hz, 4H), 7.24 (s, 1H), 7.02 (d, *J* = 8.5 Hz, 2H), 5.33 (s, 2H).

2-(4-(trifluoromethyl)phenoxy)-1-(3-((2-(trifluoromethyl)phenyl)amino)phenyl)ethan-1-one (E27)

To a solution of 4-(trifluoromethyl)phenol (67.9 mg, 0.42 mmol) in acetone, K_2CO_3 (77.2 mg, 0.56 mmol) was added. The mixture was stirred at room temperature for 30 minutes. With the following addition of **D13** (100 mg, 0.28 mmol), it was stirred at reflux for 6 hours and monitored to react completely**.** After cooling to room temperature and filtration, the filtrate was concentrated and purified by column chromatography on silica gel with the elution fluid of Hexane/EA (50:1-20:1). Pale yellow solid was achieved in 113.1 mg with 92.2% yield. ^{1}H NMR (400 MHz,

Chloroform-*d*) δ 7.70 (t, *J* = 2.0 Hz, 1H), 7.66-7.55 (m, 4H), 7.45 (td, *J* = 7.8, 2.9 Hz, 2H), 7.40-7.34 (m, 2H), 7.08 (t, *J* = 7.5 Hz, 1H), 7.01 (d, *J* = 8.5 Hz, 2H), 6.16 (s, 1H), 5.34 (s, 2H).

tert-butyl (4-(2-(4-(trifluoromethyl)phenoxy)ethyl)phenyl)carbamate (F1)

To a solution of *tert*-butyl (4-(2-hydroxyethyl)phenyl)carbamate (1 g, 4.21 mmol), 4-(trifluoromethyl)phenol (683.2 mg, 4.21 mmol) and triphenylphosphine (1.33 g, 5.06 mmol) in anhydrous THF, DEAD (880.7 mg, 5.06 mmol) was added in ice bath. The mixture was stirred in ice bath for 1 hour and was warmed to room temperature for overnight. When being monitored to react completely, it was concentrated and purified by column chromatography on silica gel with the elution fluid of Hexane/EA (20:1-10:1). White solid was achieved in 1.11 g with 69.2% yield.

methyl 4-((4-(trifluoromethyl)phenyl)amino)benzoate (F2)

To a solution of 4-(trifluoromethyl)aniline (1 g, 6.21 mmol) and methyl 4-bromobenzoate (1.6 g, 7.45 mmol) in toluene, $Pd(OAc)_2$ (83.6 mg, 0.37 mmol), BINAP (772.9 mg, 1.24 mmol) and K_2CO_3 (2.57 g, 18.62 mmol) was added. The mixture was stirred under nitrogen at 80 ℃ for 24 hours. After cooling to room temperature and filtration with diatomite, water was added and the filtrate was extracted with ethyl acetate for three times and washed with saturated brine. The combined organic layer was dried over anhydrous Na_2SO_4 and purified by column chromatography on silica gel with the elution fluid of Hexane/EA (200:1-100:1). White solid was achieved in 1.38 mg with 75.5% yield. ^{1}H NMR (400 MHz, Chloroform-*d*) δ 8.01-7.97 (m, 2H), 7.57 (d, *J* = 8.4 Hz, 2H), 7.22 (d, *J* = 8.4 Hz, 2H), 7.15-7.10 (m, 2H), 6.31 (s, 1H), 3.92 (s, 3H).

N-(4-(N-(4-(trifluoromethyl)benzyl)sulfamoyl)phenyl)acetamide (F3)

To a solution of (4-(trifluoromethyl)phenyl)methanamine (749.6 mg, 4.28 mmol) and triethylaminemethyl (1.3 g, 12.84 mmol) in anhydrous DCM, 4-acetamidobenzenesulfonyl chloride (1 g, 4.28 mmol) was added. The mixture was

stirred at room temperature for 12 hours and monitored to react completely. It was concentrated and purified by column chromatography on silica gel with the elution fluid of Hexane/EA (10:1-5:1). Pale yellow solid was achieved in 1.31 g with 82.8% yield. ^{1}H NMR (400 MHz, Chloroform-*d*) δ 7.82 (d, *J* = 8.8 Hz, 2H), 7.67 (d, *J* = 8.5 Hz, 2H), 7.56 (d, *J* = 8.1 Hz, 2H), 7.36 (d, *J* = 8.2 Hz, 3H), 4.75 (t, *J* = 6.5 Hz, 1H), 4.24 (d, *J* = 6.4 Hz, 2H), 2.26 (s, 3H).

4-(2-(4-(trifluoromethyl)phenoxy)ethyl)aniline (G1)

To a solution of **F1** (500 mg, 1.31 mmol) in DCM, TFA (1.49 g, 13.11 mmol) was added. The mixture was stirred at reflux for 8 hours and monitored to react completely. After cooling to room temperature, 1M NaOH aqueous solution was added in ice bath to regulate the pH value ranging from 8 to 10. The mixture was extracted with DCM for three times and washed with saturated brine. The combined organic layer was dried over anhydrous Na_2SO_4 and purified by column chromatography on silica gel with the elution fluid of Hexane/EA (5:1-2:1, with additional drops of aqueous ammonia). Pale yellow oil was achieved in 352.9 mg with 95.7% yield. ^{1}H NMR (400 MHz, Chloroform-*d*) δ 7.56 (d, *J* = 8.6 Hz, 2H), 7.14-7.07 (m, 2H), 6.97 (d, *J* = 8.6 Hz, 2H), 6.71-6.66 (m, 2H), 4.17 (t, *J* = 7.2 Hz, 2H), 3.66 (s, 2H), 3.04 (t, *J* = 7.2 Hz, 2H).

4-((4-(trifluoromethyl)phenyl)amino)benzoic acid (G2)

To a solution of **F2** (500 mg, 1.69 mmol) in EtOH, NaOH (338.6 mg, 8.47 mmol) was added. The mixture was stirred at reflux for 4 hours and monitored to react completely. After cooling to room temperature and being concentrated under vacuum, dilute hydrochloric acid (~10%) was added in ice bath to regulate the pH value ranging from 3 to 5. The mixture was extracted with DCM for three times and washed with saturated brine. The combined organic layer was dried over anhydrous Na_2SO_4 and purified by column chromatography on silica gel with the elution fluid of Hexane/EA (10:1-5:1, with additional drops of acetic acid). Pale yellow solid was achieved in 465.3 mg with 97.7% yield. ^{1}H NMR (400 MHz, DMSO-d_6) δ 12.48 (s, 1H), 9.13 (s,

1H), 7.85 (d, *J* = 8.6 Hz, 2H), 7.58 (d, *J* = 8.4 Hz, 2H), 7.29 (d, *J* = 8.4 Hz, 2H), 7.19 (d, *J* = 8.6 Hz, 2H).

4-amino-N-(4-(trifluoromethyl)benzyl)benzenesulfonamide (G3)

To a solution of **F3** (500 mg, 1.34 mmol) in EtOH, dilute hydrochloric acid (~10%, 170 mL) was added in ice bath. After warming to the room temperature, the mixture was stirred at 70 ℃ for 4 hours and monitored to react completely. After cooling to room temperature and being concentrated under vacuum, 1M NaOH aqueous solution was added in ice bath to regulate the pH value ranging from 8 to 10. The mixture was extracted with DCM for three times and washed with saturated brine. The combined organic layer was dried over anhydrous Na_2SO_4 and purified by column chromatography on silica gel with the elution fluid of Hexane/EA (5:1-2:1, with additional drops of aqueous ammonia). Pale yellow solid was achieved in 421.8 mg with 95.1% yield. ^{1}H NMR (400 MHz, Chloroform-*d*) δ 7.68-7.62 (m, 2H), 7.56 (d, *J* = 8.0 Hz, 2H), 7.37 (d, *J* = 7.9 Hz, 2H), 6.72-6.66 (m, 2H), 4.67 (d, *J* = 6.4 Hz, 1H), 4.20 (d, *J* = 6.5 Hz, 2H).

N-(4-(6-nitro-2H-benzo[b][1,4]oxazin-3-yl)phenyl)-5-(trifluoromethyl)pyridin-2-amine (H1)

To a solution of 2-amino-4-nitrophenol (64.4 mg, 0.42 mmol) in DCM, tetrabutylammonium hydrogen sulfate (18.9 mg, 0.06 mmol) and K_2CO_3 (76.9 mg, 0.56 mmol) was added. The mixture was stirred at room temperature for 2 hours. With the following adding of **D1** (100 mg, 0.28 mmol), the solution was stirred at reflux for 6 hours and monitored to react completely. After cooling to room temperature and filtration, it was concentrated and purified by column chromatography on silica gel with the elution fluid of Hexane/EA (20:1-10:1). Orange solid was achieved in 90.2 mg with 78.2% yield. ^{1}H NMR (600 MHz, DMSO-d_6) δ 10.09 (s, 1H), 8.59 (d, *J* = 3.0 Hz, 1H), 8.08 (t, *J* = 2.5 Hz, 1H), 8.06-8.00 (m, 3H), 7.96-7.91 (m, 3H), 7.14 (dd, *J* = 9.0, 3.2 Hz, 1H), 7.07 (t, *J* = 7.7 Hz, 1H), 5.41 (d, *J* = 3.2 Hz, 2H).

4-(6-nitro-2H-benzo[b][1,4]oxazin-3-yl)-N-(4-(trifluoromethyl)phenyl)aniline (H2)

To a solution of 2-amino-4-nitrophenol (64.6 mg, 0.42 mmol) in DCM, tetrabutylammonium hydrogen sulfate (19 mg, 0.06 mmol) and K_2CO_3 (77.2 mg, 0.56 mmol) was added. The mixture was stirred at room temperature for 2 hours. With the following adding of **D2** (100 mg, 0.28 mmol), the solution was stirred at reflux for 6 hours and monitored to react completely. After cooling to room temperature and filtration, it was concentrated and purified by column chromatography on silica gel with the elution fluid of Hexane/EA (50:1-20:1). Orange solid was achieved in 89.8 mg with 77.9% yield. ^{1}H NMR (600 MHz, DMSO-d_6) δ 9.27 (s, 1H), 8.08-7.98 (m, 4H), 7.63 (d, J = 8.4 Hz, 2H), 7.32 (d, J = 8.4 Hz, 2H), 7.28 (d, J = 8.6 Hz, 2H), 7.14 (d, J = 8.8 Hz, 1H), 5.39 (s, 2H).

5.1.4 The synthesis on aminoethyl derivatives

2-(4-bromo-2,6-difluorophenoxy)-1-(4-((5-(trifluoromethyl)pyridin-2-yl)amino)phenyl)ethan-1-ol (GII-1)

To a solution of **E1** (50 mg, 0.1 mmol) in MeOH, $NaBH_4$ (7.8 mg, 0.2 mmol) was added in ice bath. After warming to room temperature, the mixture was stirred for 8 hours and monitored to react completely. It was concentrated and purified by column chromatography on silica gel with the elution fluid of Hexane/EA (2:1-1:1). Pale yellow solid was achieved in 38.3 mg with 76.3% yield. ^{1}H NMR (400 MHz, Chloroform-d) δ 8.46 (s, 1H), 7.69 (dd, J = 9.0, 2.5 Hz, 1H), 7.47-7.36 (m, 4H), 7.15 (t, J = 6.1 Hz, 2H), 6.94 (s, 1H), 6.85 (d, J = 8.6 Hz, 1H), 5.14-5.05 (m, 1H), 4.30 (dd, J = 10.3, 3.2 Hz, 1H), 4.13 (t, J = 9.5 Hz, 1H), 3.04 (s, 1H). ^{13}C NMR (101 MHz, Chloroform-d) δ 158.0, 157.0, 154.5, 154.5, 139.0, 134.9, 134.6, 127.5, 121.4, 116.3, 116.3, 116.2, 116.1, 114.7, 114.6, 114.5, 107.4, 79.5, 72.4. HRMS(ESI): calcd for $C_{20}H_{14}BrF_5N_2O_2$, $[M + H]^+$ 489.0237; found, 489.0235. HPLC purity: 99.72%.

2-(3,4-difluorophenoxy)-1-(4-((5-(trifluoromethyl)pyridin-2-yl)amino)phenyl)ethan-1-ol (GII-2)

To a solution of **E2** (50 mg, 0.12 mmol) in MeOH, $NaBH_4$ (9.3 mg, 0.24 mmol) was

added in ice bath. After warming to room temperature, the mixture was stirred for 8 hours and monitored to react completely. It was concentrated and purified by column chromatography on silica gel with the elution fluid of Hexane/EA (2:1-1:1). Pale yellow solid was achieved in 39 mg with 77.7% yield. ^{1}H NMR (400 MHz, Chloroform-*d*) δ 8.47 (s, 1H), 7.70 (dd, *J* = 8.8, 2.4 Hz, 1H), 7.50-7.39 (m, 4H), 7.09 (q, *J* = 9.3 Hz, 1H), 6.97 (s, 1H), 6.87 (d, *J* = 8.8 Hz, 1H), 6.77 (m, *J* = 11.8, 6.5, 3.0 Hz, 1H), 6.69-6.61 (m, 1H), 5.13 (dd, *J* = 8.4, 3.4 Hz, 1H), 4.09-3.98 (m, 2H), 2.88 (s, 1H). ^{13}C NMR (101 MHz, Chloroform-*d*) δ 158.0, 154.7, 154.6, 151.8, 151.6, 149.2, 146.6, 146.5, 144.2, 144.1, 139.1, 135.1, 134.9, 134.9, 127.4, 125.5, 122.8, 121.4, 117.4, 117.2, 109.9, 109.9, 109.9, 109.9, 104.5, 104.3, 73.9, 72.1. HRMS(ESI): calcd for $C_{20}H_{15}F_5N_2O_2$, $[M + H]^+$ 411.1132; found, 411.1131. HPLC purity: 99.85%.

2-(4-(trifluoromethyl)phenoxy)-1-(4-((5-(trifluoromethyl)pyridin-2-yl)amino)phenyl)ethan-1-ol (GII-3)

To a solution of **E3** (50 mg, 0.11 mmol) in MeOH, $NaBH_4$ (8.6 mg, 0.23 mmol) was added in ice bath. After warming to room temperature, the mixture was stirred for 8 hours and monitored to react completely. It was concentrated and purified by column chromatography on silica gel with the elution fluid of Hexane/EA (2:1-1:1). Pale yellow solid was achieved in 37.6 mg with 74.9% yield. ^{1}H NMR (400 MHz, Chloroform-*d*) δ 8.45 (s, 1H), 7.69 (dd, *J* = 8.8, 2.4 Hz, 1H), 7.57 (d, *J* = 8.5 Hz, 2H), 7.48 (d, *J* = 8.2 Hz, 2H), 7.40 (d, *J* = 8.5 Hz, 2H), 7.00 (d, *J* = 8.5 Hz, 2H), 6.87 (d, *J* = 8.8 Hz, 1H), 5.17 (dd, *J* = 8.2, 3.6 Hz, 1H), 4.19-4.08 (m, 2H), 3.22 (s, 1H). ^{13}C NMR (101 MHz, Chloroform-*d*) δ 160.8, 158.1, 139.2, 135.3, 135.0, 135.0, 134.9, 134.9, 128.2, 127.5, 127.1, 127.0, 127.0, 127.0, 125.7, 125.5, 123.7, 123.4, 123.0, 122.8, 121.5, 117.9, 117.5, 114.6, 107.5, 73.3, 72.0. HRMS(ESI): calcd for $C_{21}H_{16}F_6N_2O_2$, $[M + H]^+$ 443.1194; found, 443.1187. HPLC purity: 99.59%.

2-(4-bromo-2,6-difluorophenoxy)-1-(4-((4-(trifluoromethyl)phenyl)amino)phenyl)ethan-1-ol (GII-4)

To a solution of **E4** (50 mg, 0.1 mmol) in MeOH, $NaBH_4$ (7.8 mg, 0.2 mmol) was

added in ice bath. After warming to room temperature, the mixture was stirred for 8 hours and monitored to react completely. It was concentrated and purified by column chromatography on silica gel with the elution fluid of Hexane/EA (5:1-2:1). Dark yellow oil was achieved in 46.8 mg with 93.2% yield. ^{1}H NMR (400 MHz, Chloroform-*d*) δ 7.50 (d, *J* = 8.4 Hz, 2H), 7.42-7.35 (m, 2H), 7.20-7.10 (m, 4H), 7.06 (d, *J* = 8.4 Hz, 2H), 5.99 (s, 1H), 5.10-5.03 (m, 1H), 4.30 (dd, *J* = 10.2, 3.1 Hz, 1H), 4.13 (t, *J* = 9.6 Hz, 1H), 2.95 (s, 1H). ^{13}C NMR (101 MHz, Chloroform-*d*) δ 157.1, 157.0, 154.6, 154.5, 146.4, 141.3, 135.0, 134.9, 134.8, 133.0, 127.6, 126.8, 126.7, 126.7, 126.7, 125.9, 123.2, 122.1, 121.8, 121.5, 119.7, 116.3, 116.3, 116.2, 116.1, 115.6, 114.7, 114.6, 114.5, 79.6, 72.4. HRMS(ESI): calcd for $C_{21}H_{15}BrF_5NO_2$, $[M + H]^+$ 488.0285; found, 488.0273. HPLC purity: 99.19%.

2-(3,4-difluorophenoxy)-1-(4-((4-(trifluoromethyl)phenyl)amino)phenyl)ethan-1-ol (GII-5)

To a solution of **E5** (50 mg, 0.12 mmol) in MeOH, $NaBH_4$ (9.3 mg, 0.24 mmol) was added in ice bath. After warming to room temperature, the mixture was stirred for 8 hours and monitored to react completely. It was concentrated and purified by column chromatography on silica gel with the elution fluid of Hexane/EA (5:1-2:1). Dark yellow oil was achieved in 45.4 mg with 90.4% yield. ^{1}H NMR (600 MHz, Chloroform-*d*) δ 7.51 (d, *J* = 8.4 Hz, 2H), 7.44-7.40 (m, 2H), 7.21-7.17 (m, 2H), 7.12-7.07 (m, 3H), 6.78 (m, *J* = 11.8, 6.5, 3.0 Hz, 1H), 6.65 (m, *J* = 8.6, 3.2, 1.7 Hz, 1H), 6.04-5.99 (m, 1H), 5.11 (dd, *J* = 8.7, 3.2 Hz, 1H), 4.08-3.98 (m, 2H), 2.76-2.69 (m, 1H). ^{13}C NMR (151 MHz, Chloroform-*d*) δ 154.7, 154.7, 154.7, 154.6, 151.3, 151.3, 149.7, 149.6, 146.4, 146.2, 146.1, 144.6, 144.5, 141.4, 133.5, 127.6, 126.8, 126.8, 126.7, 126.7, 125.4, 123.6, 122.1, 121.9, 119.7, 117.4, 117.3, 115.6, 110.0, 109.9, 109.9, 109.9, 104.5, 104.3, 74.0, 72.1. HRMS(ESI): calcd for $C_{21}H_{16}F_5NO_2$, $[M + H]^+$ 410.1179; found, 410.1178. HPLC purity: 98.75%.

2-(4-(trifluoromethyl)phenoxy)-1-(4-((4-(trifluoromethyl)phenyl)amino)phenyl)ethan-1-ol (GII-6)

To a solution of **E6** (50 mg, 0.11 mmol) in MeOH, $NaBH_4$ (8.6 mg, 0.23 mmol) was added in ice bath. After warming to room temperature, the mixture was stirred for 8 hours and monitored to react completely. It was concentrated and purified by column chromatography on silica gel with the elution fluid of Hexane/EA (5:1-2:1). Dark yellow oil was achieved in 46.6 mg with 92.9% yield. ^{1}H NMR (400 MHz, Chloroform-*d*) δ 7.58 (d, *J* = 8.5 Hz, 2H), 7.51 (d, *J* = 8.3 Hz, 2H), 7.44 (d, *J* = 8.4 Hz, 2H), 7.22-7.16 (m, 2H), 7.09 (d, *J* = 8.4 Hz, 2H), 7.02 (d, *J* = 8.5 Hz, 2H), 6.06 (s, 1H), 5.15 (dd, *J* = 8.5, 3.4 Hz, 1H), 4.19-4.08 (m, 2H), 2.88 (d, *J* = 7.0 Hz, 1H). ^{13}C NMR (101 MHz, Chloroform-*d*) δ 160.8, 146.4, 141.5, 133.5, 127.6, 127.1, 127.0, 127.0, 127.0, 126.8, 126.8, 126.7, 126.7, 125.9, 125.7, 123.7, 123.3, 123.2, 123.0, 122.2, 121.9, 121.5, 119.7, 115.7, 114.6, 73.3, 72.1. HRMS(ESI): calcd for $C_{22}H_{17}F_6NO_2$, $[M - H]^-$ 440.1085; found, 440.1080. HPLC purity: 98.04%.

2-(3-(trifluoromethyl)phenoxy)-1-(4-((4-(trifluoromethyl)phenyl)amino)phenyl)ethan-1-ol (GII-7)

To a solution of **E7** (50 mg, 0.11 mmol) in MeOH, $NaBH_4$ (8.6 mg, 0.23 mmol) was added in ice bath. After warming to room temperature, the mixture was stirred for 8 hours and monitored to react completely. It was concentrated and purified by column chromatography on silica gel with the elution fluid of Hexane/EA (5:1-2:1). Dark yellow oil was achieved in 46.3 mg with 92.2% yield. ^{1}H NMR (400 MHz, Chloroform-*d*) δ 7.51 (d, *J* = 8.4 Hz, 2H), 7.44 (d, *J* = 8.2 Hz, 3H), 7.28 (d, *J* = 2.0 Hz, 1H), 7.19 (dd, *J* = 9.0, 2.4 Hz, 3H), 7.13 (dd, *J* = 8.3, 2.5 Hz, 1H), 7.09 (d, *J* = 8.4 Hz, 2H), 6.03 (s, 1H), 5.14 (dd, *J* = 8.6, 3.3 Hz, 1H), 4.18-4.07 (m, 2H), 2.81 (s, 1H). ^{13}C NMR (101 MHz, Chloroform-*d*) δ 158.5, 146.4, 141.4, 133.6, 132.4, 132.1, 131.8, 131.5, 130.1, 127.6, 126.8, 126.8, 126.7, 126.7, 125.9, 125.2, 123.2, 122.5, 122.2, 121.8, 121.5, 119.7, 118.2, 118.1, 118.0, 115.6, 111.4, 111.3, 73.4, 72.2. HRMS(ESI): calcd for $C_{22}H_{17}F_6NO_2$, $[M - H]^-$ 440.1085; found, 440.1093. HPLC purity: 99.44%.

2-(2-(trifluoromethyl)phenoxy)-1-(4-((4-(trifluoromethyl)phenyl)amino)phenyl)ethan-1-ol (GII-8)

To a solution of **E8** (50 mg, 0.11 mmol) in MeOH, $NaBH_4$ (8.6 mg, 0.23 mmol) was added in ice bath. After warming to room temperature, the mixture was stirred for 8 hours and monitored to react completely. It was concentrated and purified by column chromatography on silica gel with the elution fluid of Hexane/EA (5:1-2:1). Pale yellow solid was achieved in 46.4 mg with 92.4% yield. ^{1}H NMR (600 MHz, Chloroform-*d*) δ 7.63 (dd, *J* = 7.8, 1.6 Hz, 1H), 7.50 (d, *J* = 8.3 Hz, 3H), 7.46-7.43 (m, 2H), 7.20-7.17 (m, 2H), 7.08 (dd, *J* = 8.0, 4.9 Hz, 3H), 7.00 (d, *J* = 8.3 Hz, 1H), 6.01 (s, 1H), 5.17 (dd, *J* = 8.6, 3.3 Hz, 1H), 4.25 (dd, *J* = 9.1, 3.3 Hz, 1H), 4.09 (t, *J* = 8.9 Hz, 1H), 2.93 (s, 1H). ^{13}C NMR (151 MHz, Chloroform-*d*) δ 156.2, 146.5, 141.3, 133.4, 127.7, 127.3, 127.2, 127.2, 127.2, 126.8, 126.7, 126.7, 126.7, 125.5, 124.7, 123.7, 122.9, 122.0, 121.8, 120.8, 119.8, 119.0, 118.8, 115.6, 113.1, 74.0, 71.9. HRMS(ESI): calcd for $C_{22}H_{17}F_6NO_2$, $[M - H]^-$ 440.1085; found, 440.1092. HPLC purity: 99.58%.

2-(4-nitrophenoxy)-1-(4-((4-(trifluoromethyl)phenyl)amino)phenyl)ethan-1-ol (GII-9)

To a solution of **E9** (50 mg, 0.12 mmol) in MeOH, $NaBH_4$ (9.1 mg, 0.24 mmol) was added in ice bath. After warming to room temperature, the mixture was stirred for 8 hours and monitored to react completely. It was concentrated and purified by column chromatography on silica gel with the elution fluid of Hexane/EA (5:1-2:1). Yellow solid was achieved in 37.4 mg with 74.5% yield. ^{1}H NMR (600 MHz, Chloroform-*d*) δ 8.24 (d, *J* = 9.0 Hz, 2H), 7.51 (d, *J* = 8.4 Hz, 2H), 7.44 (d, *J* = 8.1 Hz, 2H), 7.20 (d, *J* = 8.1 Hz, 2H), 7.10 (d, *J* = 8.4 Hz, 2H), 7.02 (d, *J* = 8.9 Hz, 2H), 6.03 (s, 1H), 5.17 (dd, *J* = 8.4, 3.4 Hz, 1H), 4.22-4.13 (m, 2H), 2.68 (s, 1H). ^{13}C NMR (151 MHz, Chloroform-*d*) δ 163.4, 146.2, 141.9, 141.6, 133.2, 127.6, 127.2, 126.8, 126.8, 126.8, 126.7, 126.0, 125.4, 123.6, 122.5, 122.3, 122.1, 119.6, 115.8, 114.6, 73.7, 72.1. HRMS(ESI): calcd for $C_{21}H_{17}F_3N_2O_4$, $[M - H]^-$ 417.1062; found, 417.1067. HPLC purity: 100%.

4-(2-hydroxy-2-(4-((4-(trifluoromethyl)phenyl)amino)phenyl)ethoxy)benzonitrile

(GII-10)

To a solution of **E10** (50 mg, 0.13 mmol) in MeOH, $NaBH_4$ (9.5 mg, 0.25 mmol) was added in ice bath. After warming to room temperature, the mixture was stirred for 8 hours and monitored to react completely. It was concentrated and purified by column chromatography on silica gel with the elution fluid of Hexane/EA (2:1-1:1). White solid was achieved in 42.1 mg with 83.8% yield. ^{1}H NMR (600 MHz, DMSO-d_6) δ 8.72 (s, 1H), 7.77-7.73 (m, 2H), 7.51 (d, J = 8.6 Hz, 2H), 7.42-7.38 (m, 2H), 7.18-7.15 (m, 2H), 7.14-7.10 (m, 4H), 5.66 (d, J = 4.6 Hz, 1H), 4.91 (dt, J = 7.3, 4.6 Hz, 1H), 4.15-4.09 (m, 2H). ^{13}C NMR (151 MHz, DMSO-d_6) δ 162.5, 148.1, 141.1, 135.8, 134.6, 128.0, 127.0, 127.0, 127.0, 126.9, 126.3, 124.5, 119.6, 119.3, 119.1, 118.9, 118.7, 118.4, 116.2, 114.9, 103.2, 73.7, 70.8. HRMS(ESI): calcd for $C_{22}H_{17}F_3N_2O_2$, $[M - H]^-$ 397.1164; found, 397.1173. HPLC purity: 97.74%.

2-(4-(methylthio)phenoxy)-1-(4-((4-(trifluoromethyl)phenyl)amino)phenyl)ethan-1-ol (GII-11)

To a solution of **E11** (50 mg, 0.12 mmol) in MeOH, $NaBH_4$ (9.1 mg, 0.24 mmol) was added in ice bath. After warming to room temperature, the mixture was stirred for 8 hours and monitored to react completely. It was concentrated and purified by column chromatography on silica gel with the elution fluid of Hexane/EA (5:1-2:1). Pale yellow solid was achieved in 45.3 mg with 90.1% yield. ^{1}H NMR (600 MHz, Chloroform-d) δ 7.50 (d, J = 8.4 Hz, 2H), 7.44-7.40 (m, 2H), 7.30-7.27 (m, 2H), 7.19-7.16 (m, 2H), 7.07 (d, J = 8.4 Hz, 2H), 6.92-6.89 (m, 2H), 6.06 (s, 1H), 5.11 (dd, J = 8.8, 3.1 Hz, 1H), 4.10 (dd, J = 9.5, 3.3 Hz, 1H), 4.03 (t, J = 9.1 Hz, 1H), 2.95 (s, 1H), 2.47 (s, 3H). ^{13}C NMR (151 MHz, Chloroform-d) δ 156.9, 146.5, 141.3, 133.8, 129.9, 129.7, 127.6, 126.8, 126.8, 126.7, 126.7, 125.5, 123.7, 122.0, 121.7, 119.7, 115.6, 115.4, 73.4, 72.2, 17.8. HRMS(ESI): calcd for $C_{22}H_{20}F_3NO_2S$, $[M - H]^-$ 418.1089; found, 418.1097. HPLC purity: 96.22%.

1-(4-((4-(trifluoromethyl)phenyl)amino)phenyl)-2-((5-(trifluoromethyl)pyridin-2-yl)oxy)ethan-1-ol (GII-12)

To a solution of **E12** (50 mg, 0.11 mmol) in MeOH, $NaBH_4$ (8.6 mg, 0.22 mmol) was added in ice bath. After warming to room temperature, the mixture was stirred for 8 hours and monitored to react completely. It was concentrated and purified by column chromatography on silica gel with the elution fluid of Hexane/EA (2:1-1:1). Pale yellow solid was achieved in 46.4 mg with 92.4% yield. ^{1}H NMR (400 MHz, DMSO-d_6) δ 8.72 (s, 1H), 8.15 (d, J = 2.7 Hz, 1H), 7.67 (dd, J = 9.6, 2.8 Hz, 1H), 7.50 (d, J = 8.4 Hz, 2H), 7.33 (d, J = 8.5 Hz, 2H), 7.15 (dd, J = 18.0, 8.3 Hz, 4H), 6.57 (d, J = 9.5 Hz, 1H), 5.68 (d, J = 4.9 Hz, 1H), 4.80 (dt, J = 8.9, 4.2 Hz, 1H), 4.24 (dd, J = 12.9, 3.6 Hz, 1H), 3.90 (dd, J = 12.9, 9.2 Hz, 1H). ^{13}C NMR (101 MHz, DMSO-d_6) δ 161.6, 148.0, 141.3, 136.0, 135.7, 127.4, 126.9, 126.9, 126.7, 125.7, 124.0, 123.0, 120.4, 119.4, 119.1, 118.7, 115.0, 107.0, 106.7, 79.7, 79.4, 79.1, 69.7, 56.7. HRMS(ESI): calcd for $C_{21}H_{16}F_6N_2O_2$, $[M - H]^-$ 441.1038; found, 441.1047. HPLC purity: 99.56%.

1-(4-((4-(trifluoromethyl)phenyl)amino)phenyl)-2-((4-(trifluoromethyl)pyridin-2-yl)oxy)ethan-1-ol (GII-13)

To a solution of **E13** (50 mg, 0.11 mmol) in MeOH, $NaBH_4$ (8.6 mg, 0.22 mmol) was added in ice bath. After warming to room temperature, the mixture was stirred for 8 hours and monitored to react completely. It was concentrated and purified by column chromatography on silica gel with the elution fluid of Hexane/EA (2:1-1:1). Pale yellow solid was achieved in 46 mg with 91.6% yield. ^{1}H NMR (400 MHz, Chloroform-d) δ 7.50 (d, J = 8.4 Hz, 2H), 7.39 (dd, J = 10.2, 7.7 Hz, 3H), 7.17 (s, 2H), 7.07 (d, J = 8.4 Hz, 2H), 6.88 (s, 1H), 6.31 (dd, J = 7.1, 1.9 Hz, 1H), 6.06 (s, 1H), 5.12 (d, J = 8.3 Hz, 1H), 4.49 (dd, J = 13.4, 3.0 Hz, 1H), 3.88 (dd, J = 13.4, 8.4 Hz, 1H), 3.40 (d, J = 3.6 Hz, 1H). ^{13}C NMR (101 MHz, Chloroform-d) δ 162.5, 146.3, 141.9, 141.6, 141.4, 140.6, 134.9, 127.0, 126.8, 126.7, 123.4, 123.2, 122.2, 121.9, 119.7, 118.1, 115.6, 101.1, 101.1, 72.1, 58.0. HRMS(ESI): calcd for $C_{21}H_{16}F_6N_2O_2$, $[M - H]^-$ 441.1038; found, 441.1050. HPLC purity: 99.45%.

1-(4-((4-(trifluoromethyl)phenyl)amino)phenyl)-2-((5-(trifluoromethyl)pyridin-3-yl)oxy)ethan-1-ol (GII-14)

To a solution of **E14** (50 mg, 0.11 mmol) in MeOH, $NaBH_4$ (8.6 mg, 0.22 mmol) was added in ice bath. After warming to room temperature, the mixture was stirred for 8 hours and monitored to react completely. It was concentrated and purified by column chromatography on silica gel with the elution fluid of Hexane/EA (2:1-1:1). Pale yellow solid was achieved in 46.7 mg with 92.9% yield. ^{1}H NMR (600 MHz, Chloroform-*d*) δ 8.51 (q, *J* = 3.0 Hz, 2H), 7.50 (d, *J* = 8.4 Hz, 2H), 7.45-7.41 (m, 3H), 7.19 (d, *J* = 8.1 Hz, 2H), 7.09 (d, *J* = 8.3 Hz, 2H), 6.11 (q, *J* = 4.3, 3.8 Hz, 1H), 5.16 (dd, *J* = 7.6, 4.2 Hz, 1H), 4.21-4.16 (m, 2H), 3.20-3.02 (m, 1H). ^{13}C NMR (151 MHz, Chloroform-*d*) δ 154.5, 146.2, 141.7, 139.0, 138.9, 138.9, 138.9, 133.3, 127.6, 127.3, 127.1, 126.8, 126.8, 126.7, 126.7, 125.4, 124.1, 123.6, 122.3, 122.2, 122.0, 121.8, 119.6, 117.9, 117.9, 117.8, 117.8, 115.8, 73.7, 72.1. HRMS(ESI): calcd for $C_{21}H_{16}F_6N_2O_2$, $[M + H]^+$ 443.1194; found, 443.1191. HPLC purity: 99.11%.

2-(4-(trifluoromethyl)phenoxy)-1-(4-((3-(trifluoromethyl)phenyl)amino)phenyl)ethan-1-ol (GII-15)

To a solution of **E15** (50 mg, 0.11 mmol) in MeOH, $NaBH_4$ (8.6 mg, 0.23 mmol) was added in ice bath. After warming to room temperature, the mixture was stirred for 8 hours and monitored to react completely. It was concentrated and purified by column chromatography on silica gel with the elution fluid of Hexane/EA (5:1-2:1). Dark yellow oil was achieved in 46.1 mg with 91.7% yield. ^{1}H NMR (400 MHz, Chloroform-*d*) δ 7.58 (d, *J* = 8.4 Hz, 2H), 7.39 (dd, *J* = 18.9, 8.1 Hz, 3H), 7.30 (d, *J* = 10.9 Hz, 1H), 7.24-7.12 (m, 4H), 7.02 (d, *J* = 8.4 Hz, 2H), 5.99 (s, 1H), 5.13 (dd, *J* = 8.4, 3.5 Hz, 1H), 4.17-4.10 (m, 2H), 2.91 (s, 1H). ^{13}C NMR (101 MHz, Chloroform-*d*) δ 171.4, 160.9, 143.7, 142.1, 132.9, 132.3, 131.9, 131.6, 131.3, 129.9, 128.4, 127.7, 127.1, 127.0, 127.0, 126.9, 125.7, 125.4, 123.9, 123.6, 123.3, 123.0, 122.7, 120.3, 120.1, 118.7, 117.3, 117.3, 117.3, 117.2, 114.6, 113.5, 113.5, 113.5, 113.4, 73.3, 72.2. HRMS(ESI): calcd for $C_{21}H_{16}F_6N_2O_2$, $[M - H]^-$ 440.1085; found, 440.1095. HPLC purity: 96.82%.

2-(4-(trifluoromethyl)phenoxy)-1-(4-((2-

(trifluoromethyl)phenyl)amino)phenyl)ethan-1-ol (GII-16)

To a solution of **E16** (50 mg, 0.11 mmol) in MeOH, $NaBH_4$ (8.6 mg, 0.23 mmol) was added in ice bath. After warming to room temperature, the mixture was stirred for 8 hours and monitored to react completely. It was concentrated and purified by column chromatography on silica gel with the elution fluid of Hexane/EA (5:1-2:1). Pale yellow solid was achieved in 45.4 mg with 90.5% yield. ^{1}H NMR (400 MHz, Chloroform-*d*) δ 7.60 (dd, *J* = 10.4, 8.1 Hz, 3H), 7.45-7.36 (m, 4H), 7.16 (d, *J* = 8.5 Hz, 2H), 7.04-6.98 (m, 3H), 6.12 (s, 1H), 5.14 (dd, *J* = 8.5, 3.4 Hz, 1H), 4.18-4.07 (m, 2H), 2.75 (s, 1H). ^{13}C NMR (101 MHz, Chloroform-*d*) δ 160.8, 142.0, 141.7, 133.3, 132.7, 127.6, 127.1, 127.0, 127.0, 127.0, 126.0, 125.7, 123.6, 123.3, 123.0, 120.3, 119.8, 118.3, 118.2, 117.9, 114.6, 73.3, 72.1. HRMS(ESI): calcd for $C_{21}H_{16}F_6N_2O_2$, $[M - H]^-$ 440.1085; found, 440.1097. HPLC purity: 98.82%.

1-(4-((4-methoxyphenyl)amino)phenyl)-2-(4-(trifluoromethyl)phenoxy)ethan-1-ol (GII-17)

To a solution of **E17** (50 mg, 0.12 mmol) in MeOH, $NaBH_4$ (9.4 mg, 0.25 mmol) was added in ice bath. After warming to room temperature, the mixture was stirred for 8 hours and monitored to react completely. It was concentrated and purified by column chromatography on silica gel with the elution fluid of Hexane/EA (5:1-2:1). Pale yellow solid was achieved in 44.1 mg with 87.8% yield. ^{1}H NMR (400 MHz, Chloroform-*d*) δ 7.57 (d, *J* = 8.6 Hz, 2H), 7.31 (d, *J* = 8.1 Hz, 2H), 7.15-6.98 (m, 4H), 6.92 (dd, *J* = 13.0, 8.9 Hz, 4H), 5.08 (d, *J* = 6.4 Hz, 1H), 4.14-4.07 (m, 2H), 3.83 (s, 3H). ^{13}C NMR (101 MHz, Chloroform-*d*) δ 160.9, 155.6, 145.6, 135.3, 130.1, 127.5, 127.0, 127.0, 127.0, 126.9, 125.7, 123.5, 123.2, 123.0, 122.9, 122.6, 115.4, 114.7, 114.6, 73.4, 72.2, 55.6. HRMS(ESI): calcd for $C_{22}H_{20}F_3NO_3$, $[M + H]^+$ 404.1474; found, 404.1466. HPLC purity: 98.89%.

1-(4-((4-(methylthio)phenyl)amino)phenyl)-2-(4-(trifluoromethyl)phenoxy)ethan-1-ol (GII-18)

To a solution of **E18** (50 mg, 0.12 mmol) in MeOH, $NaBH_4$ (9.1 mg, 0.24 mmol) was

added in ice bath. After warming to room temperature, the mixture was stirred for 8 hours and monitored to react completely. It was concentrated and purified by column chromatography on silica gel with the elution fluid of Hexane/EA (5:1-2:1). Pale yellow solid was achieved in 44.8 mg with 89.3% yield. ^{1}H NMR (600 MHz, Chloroform-*d*) δ 7.58 (d, *J* = 8.4 Hz, 2H), 7.36 (d, *J* = 8.2 Hz, 2H), 7.28-7.25 (m, 2H), 7.09-6.99 (m, 6H), 5.77 (s, 1H), 5.11 (dd, *J* = 8.6, 3.3 Hz, 1H), 4.16-4.07 (m, 2H), 2.69 (s, 1H), 2.49 (s, 3H). ^{13}C NMR (151 MHz, Chloroform-*d*) δ 160.9, 143.4, 140.8, 131.6, 129.7, 129.7, 127.5, 127.0, 127.0, 127.0, 127.0, 126.4, 125.2, 123.5, 123.4, 123.3, 120.1, 119.0, 117.4, 114.6, 73.4, 72.2, 17.7. HRMS(ESI): calcd for $C_{22}H_{20}F_3NO_2S$, $[M - H]^-$ 418.1089; found, 418.1094. HPLC purity: 92.71%.

2-((4-(1-hydroxy-2-(4-(trifluoromethyl)phenoxy)ethyl)phenyl)amino)benzonitrile (GII-19)

To a solution of **E19** (50 mg, 0.12 mmol) in MeOH, $NaBH_4$ (9.5 mg, 0.25 mmol) was added in ice bath. After warming to room temperature, the mixture was stirred for 8 hours and monitored to react completely. It was concentrated and purified by column chromatography on silica gel with the elution fluid of Hexane/EA (2:1-1:1). White solid was achieved in 47.5 mg with 94.6% yield. ^{1}H NMR (600 MHz, Chloroform-*d*) δ 9.61 (s, 1H), 7.58 (d, *J* = 8.5 Hz, 2H), 7.50 (dd, *J* = 7.9, 1.4 Hz, 1H), 7.42 (d, *J* = 8.2 Hz, 2H), 7.37 (d, *J* = 8.3 Hz, 1H), 7.33 (dd, *J* = 8.3, 6.7 Hz, 1H), 7.27 (d, *J* = 8.2 Hz, 2H), 7.02 (d, *J* = 8.5 Hz, 2H), 6.81 (t, *J* = 7.5 Hz, 1H), 5.14 (d, *J* = 8.6 Hz, 1H), 4.17-4.09 (m, 2H), 2.74 (d, *J* = 2.5 Hz, 1H). ^{13}C NMR (151 MHz, Chloroform-*d*) δ 171.6, 160.9, 146.1, 141.5, 133.4, 133.0, 129.9, 129.9, 128.3, 127.4, 127.0, 127.0, 127.0, 127.0, 126.5, 125.2, 123.7, 123.5, 123.4, 123.3, 121.2, 117.9, 116.1, 115.4, 114.6, 73.4, 72.2. HRMS(ESI): calcd for $C_{22}H_{17}F_3N_2O_2$, $[M + H]^+$ 399.1320; found, 399.1320. HPLC purity: 96.16%.

2-(4-(trifluoromethyl)phenoxy)-1-(4-((4-(trifluoromethyl)thiazol-2-yl)amino)phenyl)ethan-1-ol (GII-20)

To a solution of **E26** (50 mg, 0.11 mmol) in MeOH, $NaBH_4$ (8.5 mg, 0.22 mmol) was

added in ice bath. After warming to room temperature, the mixture was stirred for 8 hours and monitored to react completely. It was concentrated and purified by column chromatography on silica gel with the elution fluid of Hexane/EA (5:1-2:1). White solid was achieved in 45.3 mg with 90.2% yield. ^{1}H NMR (400 MHz, DMSO-d_6) δ 10.59 (s, 1H), 7.66-7.60 (m, 3H), 7.59-7.54 (m, 2H), 7.44 (d, J = 8.5 Hz, 2H), 7.13 (d, J = 8.6 Hz, 2H), 5.67 (d, J = 4.5 Hz, 1H), 4.91 (q, J = 5.5 Hz, 1H), 4.09 (d, J = 5.8 Hz, 2H). ^{13}C NMR (101 MHz, DMSO-d_6) δ 165.8, 161.9, 140.1, 136.3, 127.7, 127.4, 117.5, 115.5, 73.6, 70.8. HRMS(ESI): calcd for $C_{19}H_{14}F_6N_2O_2S$, $[M - H]^-$ 447.0602; found, 447.0611. HPLC purity: 99.27%.

2-(4-(trifluoromethyl)phenoxy)-1-(4-(4-(trifluoromethyl)phenoxy)phenyl)ethan-1-ol (GII-21)

To a solution of **E22** (50 mg, 0.11 mmol) in MeOH, $NaBH_4$ (8.6 mg, 0.22 mmol) was added in ice bath. After warming to room temperature, the mixture was stirred for 8 hours and monitored to react completely. It was concentrated and purified by column chromatography on silica gel with the elution fluid of Hexane/EA (5:1-2:1). Pale yellow oil was achieved in 46 mg with 91.6% yield. ^{1}H NMR (400 MHz, Chloroform-d) δ 7.64-7.46 (m, 6H), 7.14-6.98 (m, 6H), 5.19 (dd, J = 8.5, 3.3 Hz, 1H), 4.20-4.07 (m, 2H), 2.81 (s, 1H). ^{13}C NMR (101 MHz, Chloroform-d) δ 160.7, 160.2, 155.8, 135.4, 128.1, 127.2, 127.2, 127.2, 127.1, 127.1, 127.1, 127.0, 125.6, 125.5, 125.3, 125.0, 123.8, 123.4, 122.9, 122.8, 120.0, 118.0, 114.6, 73.3, 72.0. HRMS(ESI): calcd for $C_{22}H_{16}F_6O_3$, $[M - H]^-$ 441.0925; found, 441.0926. HPLC purity: 94.17%.

2-(4-(trifluoromethyl)phenoxy)-1-(4-((4-(trifluoromethyl)phenyl)thio)phenyl)ethan-1-ol (GII-22)

To a solution of **E23** (50 mg, 0.11 mmol) in MeOH, $NaBH_4$ (8.3 mg, 0.22 mmol) was added in ice bath. After warming to room temperature, the mixture was stirred for 8 hours and monitored to react completely. It was concentrated and purified by column chromatography on silica gel with the elution fluid of Hexane/EA (5:1-2:1). Pale yellow solid was achieved in 45 mg with 89.7% yield. ^{1}H NMR (600 MHz,

Chloroform-*d*) δ 7.58 (d, *J* = 8.6 Hz, 2H), 7.52 (d, *J* = 9.1 Hz, 6H), 7.32 (d, *J* = 8.2 Hz, 2H), 7.01 (d, *J* = 8.5 Hz, 2H), 5.20 (dt, *J* = 8.6, 2.6 Hz, 1H), 4.18 (dd, *J* = 9.4, 3.3 Hz, 1H), 4.09 (t, *J* = 9.0 Hz, 1H), 2.82 (d, *J* = 6.6 Hz, 1H). ^{13}C NMR (151 MHz, Chloroform-*d*) δ 160.7, 142.3, 139.8, 133.4, 132.9, 128.7, 128.4, 128.2, 127.6, 127.1, 127.1, 127.1, 127.0, 127.0, 125.9, 125.9, 125.9, 125.9, 125.2, 124.9, 123.8, 123.6, 123.4, 123.1, 114.6, 73.2, 72.0. HRMS(ESI): calcd for $C_{22}H_{16}F_6O_2S$, $[M - H]^-$ 457.0697; found, 457.0707. HPLC purity: 98.94%.

2-((4-(trifluoromethyl)benzyl)oxy)-1-(4-((4-(trifluoromethyl)phenyl)amino)phenyl)ethan-1-ol (GII-23)

To a solution of **E20** (50 mg, 0.11 mmol) in MeOH, $NaBH_4$ (8.3 mg, 0.22 mmol) was added in ice bath. After warming to room temperature, the mixture was stirred for 8 hours and monitored to react completely. It was concentrated and purified by column chromatography on silica gel with the elution fluid of Hexane/EA (5:1-2:1). Pale yellow solid was achieved in 43.7 mg with 87.1% yield. ^{1}H NMR (600 MHz, Chloroform-*d*) δ 7.64 (d, *J* = 8.0 Hz, 2H), 7.51-7.47 (m, 4H), 7.38-7.35 (m, 2H), 7.17-7.13 (m, 2H), 7.06 (d, *J* = 8.4 Hz, 2H), 5.96 (s, 1H), 4.95 (dd, *J* = 8.8, 3.2 Hz, 1H), 4.73-4.66 (m, 2H), 3.68 (dd, *J* = 9.7, 3.3 Hz, 1H), 3.58 (t, *J* = 9.3 Hz, 1H), 2.77 (s, 1H). ^{13}C NMR (151 MHz, Chloroform-*d*) δ 146.5, 141.8, 141.0, 134.4, 129.9, 127.7, 127.5, 126.7, 126.7, 125.5, 119.8, 115.4, 76.0, 72.6. HRMS(ESI): calcd for $C_{23}H_{19}F_6NO_2$, $[M - H]^-$ 454.1242; found, 454.1248. HPLC purity: 99.03%.

1-(4-((4-(trifluoromethyl)phenyl)amino)phenyl)-2-((4-(trifluoromethyl)phenyl)thio)ethan-1-ol (GII-24)

To a solution of **E21** (50 mg, 0.11 mmol) in MeOH, $NaBH_4$ (8.3 mg, 0.22 mmol) was added in ice bath. After warming to room temperature, the mixture was stirred for 8 hours and monitored to react completely. It was concentrated and purified by column chromatography on silica gel with the elution fluid of Hexane/EA (5:1-2:1). Dark yellow oil was achieved in 46.7 mg with 93.1% yield. ^{1}H NMR (400 MHz, Chloroform-*d*) δ 7.56 (d, *J* = 8.1 Hz, 2H), 7.49 (dd, *J* = 15.5, 8.3 Hz, 4H), 7.35 (d, *J* =

8.2 Hz, 2H), 7.15 (d, *J* = 8.2 Hz, 2H), 7.07 (d, *J* = 8.3 Hz, 2H), 6.00 (s, 1H), 4.82 (dd, *J* = 8.8, 4.0 Hz, 1H), 3.40 (dd, *J* = 13.7, 4.1 Hz, 1H), 3.27 (dd, *J* = 13.7, 8.7 Hz, 1H), 2.71 (s, 1H). ^{13}C NMR (101 MHz, Chloroform-*d*) δ 146.3, 141.3, 140.8, 136.1, 128.6, 128.4, 128.3, 128.1, 128.0, 127.7, 127.2, 126.8, 126.8, 126.7, 126.7, 125.9, 125.9, 125.8, 125.8, 125.4, 123.2, 122.7, 122.5, 122.2, 121.9, 121.5, 119.7, 115.6, 71.8, 42.3. HRMS(ESI): calcd for $C_{22}H_{17}F_6NOS$, $[M - H]^-$ 456.0857; found, 456.0862. HPLC purity: 98.74%.

4-(trifluoromethyl)-N-(4-(2-(4-(trifluoromethyl)phenoxy)ethyl)phenyl)aniline (GII-25)

To a solution of 1-iodo-4-(trifluoromethyl)benzene (48.3 mg, 0.18 mmol) and **G1** (50 mg, 0.18 mmol) in toluene, $Pd(OAc)_2$ (7.9 mg, 0.04 mmol), X-Phos (16.9 mg, 0.04 mmol) and Cs_2CO_3 (86.9 mg, 0.27 mmol) was added. The mixture was stirred under nitrogen at 120 ℃ for 8 hours. After cooling to room temperature and filtration with diatomite, water was added and the filtrate was extracted with ethyl acetate for three times and washed with saturated brine. The combined organic layer was dried over anhydrous Na_2SO_4 and purified by column chromatography on silica gel with the elution fluid of Hexane/EA (20:1-10:1). Pale yellow oil was achieved in 67.4 mg with 89.2% yield. ^{1}H NMR (400 MHz, Chloroform-*d*) δ 7.57 (d, *J* = 8.5 Hz, 2H), 7.50 (d, *J* = 8.4 Hz, 2H), 7.29 (d, *J* = 4.8 Hz, 2H), 7.15 (d, *J* = 8.1 Hz, 2H), 7.05 (d, *J* = 8.4 Hz, 2H), 7.00 (d, *J* = 8.5 Hz, 2H), 5.92 (s, 1H), 4.24 (t, *J* = 6.9 Hz, 2H), 3.13 (t, *J* = 6.9 Hz, 2H). ^{13}C NMR (101 MHz, Chloroform-*d*) δ 161.3, 146.9, 139.7, 132.6, 130.1, 128.5, 127.0, 126.9, 126.9, 126.8, 126.8, 126.7, 126.7, 126.6, 126.0, 125.8, 123.4, 123.3, 123.1, 123.1, 122.8, 122.0, 121.7, 121.4, 120.5, 115.1, 114.5, 68.9, 35.0. HRMS(ESI): calcd for $C_{22}H_{17}F_6NO$, $[M - H]^-$ 424.1136; found, 424.1144. HPLC purity: 100%.

N-(4-(trifluoromethyl)benzyl)-4-((4-(trifluoromethyl)phenyl)amino)benzamide (GII-27)

To a solution of **G2** (50 mg, 0.18 mmol), EDCI (82.8 mg, 0.53 mmol) and 4-DMAP (2.2 mg, 0.02 mmol) in DCM, (4-(trifluoromethyl)phenyl)methanamine (31.1 mg,

0.18 mmol) was added dropwise in ice bath. After warming to room temperature, the mixture was stirred for 24 hours and monitored to react completely. It was concentrated and purified by column chromatography on silica gel with the elution fluid of Hexane/EA (50:1-20:1). Pale yellow solid was achieved in 69.1 mg with 88.6% yield. ^{1}H NMR (400 MHz, Chloroform-*d*) δ 7.80-7.74 (m, 2H), 7.56 (dd, *J* = 22.6, 8.2 Hz, 4H), 7.45 (d, *J* = 8.0 Hz, 2H), 7.19-7.10 (m, 4H), 6.70 (t, *J* = 5.9 Hz, 1H), 6.43 (s, 1H), 4.69 (d, *J* = 5.9 Hz, 2H). ^{13}C NMR (101 MHz, Chloroform-*d*) δ 167.0, 145.2, 144.8, 142.5, 129.9, 129.6, 129.3, 128.8, 127.9, 126.8, 126.8, 126.8, 126.7, 126.6, 125.7, 125.7, 125.6, 125.6, 125.4, 123.6, 123.2, 123.0, 122.7, 117.4, 117.1, 43.5. HRMS(ESI): calcd for $C_{22}H_{16}F_6N_2O$, $[M + H]^+$ 439.1245; found, 439.1245. HPLC purity: 99.26%.

N-(4-(trifluoromethyl)benzyl)-4-((4-(trifluoromethyl)phenyl)amino)benzamide (GII-28)

To a solution of 1-iodo-4-(trifluoromethyl)benzene (41.2 mg, 0.15 mmol) and **G3** (50 mg, 0.15 mmol) in toluene, $Pd_2(dba)_3$ (13.9 mg, 0.02 mmol), XantPhos (17.5 mg, 0.03 mmol) and NaO*t*Bu (29.1 mg, 0.3 mmol) was added. The mixture was stirred under nitrogen at 110 ℃ for 24 hours. After cooling to room temperature and filtration with diatomite, water was added and the filtrate was extracted with ethyl acetate for three times and washed with saturated brine. The combined organic layer was dried over anhydrous Na_2SO_4 and purified by column chromatography on silica gel with the elution fluid of Hexane/EA (20:1-10:1). White solid was achieved in 49.8 mg with 69.4% yield. ^{1}H NMR (400 MHz, DMSO-d_6) δ 9.21 (s, 1H), 8.11 (t, *J* = 6.4 Hz, 1H), 7.69-7.59 (m, 6H), 7.48 (d, *J* = 8.1 Hz, 2H), 7.29 (d, *J* = 8.4 Hz, 2H), 7.25-7.20 (m, 2H), 4.10-4.05 (m, 2H). ^{13}C NMR (151 MHz, DMSO-d_6) δ 146.2, 145.7, 142.9, 131.4, 128.9, 128.7, 128.3, 128.1, 127.3, 127.01, 127.0, 127.0, 125.9, 125.5, 125.5, 125.5, 125.4, 125.4, 124.1, 123.7, 121.4, 121.2, 117.6, 116.6, 45.9. HRMS(ESI): calcd for $C_{21}H_{16}F_6N_2O_2S$, $[M - H]^-$ 473.0758; found, 473.0762. HPLC purity: 97.15%.

2-(4-(trifluoromethyl)phenoxy)-1-(6-((4-(trifluoromethyl)phenyl)amino)pyridin-

3-yl)ethan-1-ol (GII-29)

To a solution of **E24** (50 mg, 0.11 mmol) in MeOH, $NaBH_4$ (8.6 mg, 0.23 mmol) was added in ice bath. After warming to room temperature, the mixture was stirred for 8 hours and monitored to react completely. It was concentrated and purified by column chromatography on silica gel with the elution fluid of Hexane/EA (2:1-1:1). Pale yellow solid was achieved in 27.8 mg with 55.4% yield. ^{1}H NMR (600 MHz, Chloroform-*d*) δ 8.33 (s, 1H), 7.72 (dd, *J* = 8.6, 2.2 Hz, 1H), 7.61-7.55 (m, 4H), 7.52-7.48 (m, 2H), 6.98 (dd, *J* = 27.0, 8.5 Hz, 4H), 5.13 (dd, *J* = 8.0, 3.8 Hz, 1H), 4.16-4.10 (m, 2H). ^{13}C NMR (151 MHz, Chloroform-*d*) δ 160.6, 154.8, 146.5, 143.5, 136.3, 127.2, 127.1, 127.1, 127.1, 127.0, 127.0, 126.6, 126.6, 126.5, 126.5, 125.2, 125.2, 124.0, 123.8, 123.6, 123.4, 123.4, 118.4, 114.6, 109.8, 72.9, 70.2. HRMS(ESI): calcd for $C_{21}H_{16}F_6N_2O_2$, $[M + H]^+$ 443.1194; found, 473.1198. HPLC purity: 97.69%.

1-(2-(trifluoromethyl)-4-((4-(trifluoromethyl)phenyl)amino)phenyl)-2-(4-(trifluoromethyl)phenoxy)ethan-1-ol (GII-30)

To a solution of **E25** (50 mg, 0.09 mmol) in MeOH, $NaBH_4$ (7.5 mg, 0.19 mmol) was added in ice bath. After warming to room temperature, the mixture was stirred for 8 hours and monitored to react completely. It was concentrated and purified by column chromatography on silica gel with the elution fluid of Hexane/EA (5:1-2:1). White solid was achieved in 38.2 mg with 76.2% yield. ^{1}H NMR (600 MHz, Chloroform-*d*) δ 7.83 (d, *J* = 8.4 Hz, 1H), 7.58 (t, *J* = 9.2 Hz, 4H), 7.43-7.38 (m, 2H), 7.14 (d, *J* = 8.3 Hz, 2H), 7.02 (d, *J* = 8.4 Hz, 2H), 6.13 (s, 1H), 5.53 (d, *J* = 8.7 Hz, 1H), 4.18 (dd, *J* = 9.6, 2.7 Hz, 1H), 4.03 (t, *J* = 9.2 Hz, 1H), 2.85 (s, 1H). ^{13}C NMR (151 MHz, Chloroform-*d*) δ 160.7, 145.0, 141.9, 130.8, 130.0, 129.9, 129.0, 128.8, 128.6, 127.1, 127.1, 127.0, 127.0, 127.0, 127.0, 126.9, 125.2, 125.2, 124.8, 123.9, 123.7, 123.5, 123.5, 123.4, 123.4, 123.3, 123.0, 121.6, 116.7, 115.6, 115.6, 115.5, 115.5, 114.6, 72.9, 67.9. HRMS(ESI): calcd for $C_{23}H_{16}F_9NO_2$, $[M - H]^-$ 508.0959; found, 508.0975. HPLC purity: 99.25%.

2-(4-(trifluoromethyl)phenoxy)-1-(3-((2-

(trifluoromethyl)phenyl)amino)phenyl)ethan-1-ol (GII-31)

To a solution of **E27** (50 mg, 0.11 mmol) in MeOH, $NaBH_4$ (8.6 mg, 0.23 mmol) was added in ice bath. After warming to room temperature, the mixture was stirred for 8 hours and monitored to react completely. It was concentrated and purified by column chromatography on silica gel with the elution fluid of Hexane/EA (5:1-2:1). Dark yellow oil was achieved in 46.4 mg with 92.4% yield. ^{1}H NMR (400 MHz, Chloroform-*d*) δ 7.59 (dd, *J* = 11.5, 8.2 Hz, 3H), 7.44-7.32 (m, 3H), 7.24 (t, *J* = 1.9 Hz, 1H), 7.14-7.09 (m, 2H), 7.01 (d, *J* = 8.4 Hz, 3H), 6.13 (s, 1H), 5.14 (dd, *J* = 8.6, 3.2 Hz, 1H), 4.20-4.07 (m, 2H), 2.77 (s, 1H). ^{13}C NMR (101 MHz, Chloroform-*d*) δ 160.8, 142.3, 141.6, 141.0, 132.7, 129.8, 127.1, 127.0, 127.0, 127.0, 126.0, 125.7, 123.7, 123.4, 123.3, 123.0, 120.3, 120.3, 119.5, 118.3, 118.2, 117.9, 117.5, 114.6, 73.4, 72.3. HRMS(ESI): calcd for $C_{22}H_{17}F_6NO_2$, $[M - H]^-$ 440.1085; found, 440.1093. HPLC purity: 98.59%.

N-(4-(6-nitro-3,4-dihydro-2H-benzo[b][1,4]oxazin-3-yl)phenyl)-5-(trifluoromethyl)pyridin-2-amine (GII-32)

To a solution of **H1** (50 mg, 0.12 mmol) in MeOH, $NaBH_4$ (9.13 mg, 0.24 mmol) was added in ice bath. After warming to room temperature, the mixture was stirred for overnight and monitored to react completely. It was concentrated and purified by column chromatography on silica gel with the elution fluid of Hexane/EA (10:1-5:1). Yellow solid was achieved in 32.5 mg with 64.8% yield. ^{1}H NMR (400 MHz, Chloroform-*d*) δ 8.49 (s, 1H), 7.72 (dd, *J* = 8.7, 2.4 Hz, 1H), 7.66 (dt, *J* = 8.5, 2.5 Hz, 1H), 7.60 (d, *J* = 2.6 Hz, 1H), 7.48 (d, *J* = 8.4 Hz, 2H), 7.41 (d, *J* = 8.3 Hz, 2H), 6.94-6.81 (m, 3H), 4.58-4.52 (m, 1H), 4.41 (dt, *J* = 10.7, 2.5 Hz, 1H), 4.33 (s, 1H), 4.08 (dd, *J* = 10.8, 8.5 Hz, 1H). ^{13}C NMR (151 MHz, Chloroform-*d*) δ 157.7, 148.8, 146.1, 146.1, 142.1, 139.7, 134.9, 134.9, 133.9, 133.0, 129.9, 129.9, 128.2, 125.0, 121.3, 118.1, 117.9, 116.5, 115.2, 110.2, 107.9, 71.1, 53.1. HRMS(ESI): calcd for $C_{20}H_{15}F_3N_4O_3$, $[M + H]^+$ 417.1175; found, 417.1164. HPLC purity: 94.68%.

4-(6-nitro-3,4-dihydro-2H-benzo[b][1,4]oxazin-3-yl)-N-(4-

(trifluoromethyl)phenyl)aniline (GII-33)

To a solution of **H2** (50 mg, 0.12 mmol) in MeOH, $NaBH_4$ (9.15 mg, 0.24 mmol) was added in ice bath. After warming to room temperature, the mixture was stirred for overnight and monitored to react completely. It was concentrated and purified by column chromatography on silica gel with the elution fluid of Hexane/EA (20:1-10:1). Yellow solid was achieved in 31.8 mg with 63.3% yield. ^{1}H NMR (400 MHz, Chloroform-*d*) δ 7.65 (dd, *J* = 8.8, 2.6 Hz, 1H), 7.59 (d, *J* = 2.6 Hz, 1H), 7.52 (d, *J* = 8.4 Hz, 2H), 7.35 (d, *J* = 8.3 Hz, 2H), 7.22-7.18 (m, 2H), 7.11 (d, *J* = 8.4 Hz, 2H), 6.92 (d, *J* = 8.8 Hz, 1H), 6.02 (s, 1H), 4.52 (dd, *J* = 8.6, 3.0 Hz, 1H), 4.40 (dt, *J* = 10.8, 2.4 Hz, 1H), 4.32 (s, 1H), 4.08 (dd, *J* = 10.8, 8.6 Hz, 1H). ^{13}C NMR (101 MHz, Chloroform-*d*) δ 148.8, 146.0, 142.1, 141.9, 134.0, 131.6, 128.3, 126.8, 126.8, 119.6, 116.4, 116.0, 115.2, 110.2, 71.2, 53.1. HRMS(ESI): calcd for $C_{21}H_{17}F_3N_3O_3$, $[M + H]^+$ 416.1222; found, 416.1218. HPLC purity: 92.43%.

5.2 Biology

5.2.1 Bacterial strains and antibiotic controls

The bacterial strains used in this study for microdilution assay were as follows: *Enterococcus faecalis* ATCC® 19433, SAUR[a]: *S. aureus* ATCC® 25923, SAUR[b]: *S. aureus* ATCC® 29213, SPNE: *Streptococcus pneumonia* ATCC® 49619, ABAU: *Acinetobacter baumannii* ATCC® 19606, PAER: *Pseudomonas aeruginosa* ATCC® 27853, ECLO: *Enterobacter cloacae* ATCC® 13047, ECOL: *Escherichia coli* ATCC® 25922. (The American Type Culture Collection, Manassas, Virginia, United States). The antibiotic controls were purchased from Sigma-Aldrich (St. Louis, Missouri, United States).

5.2.2 Determination of MIC value

The antimicrobial activity of the compounds was determined by broth microdilution according to the Clinical and Laboratory Standards Institute (CLSI) guidelines [124].

The test medium was cation-adjusted Mueller–Hinton broth (MHB) if not specified elsewhere. Serial twofold dilutions of the tested compound were performed starting from 256 to 0.5 μg/mL, and the bacterial cell inoculum was adjusted to approximately 5×10^5 CFU per mL. Results were taken after 20 hours of incubation at 37 °C. The MIC value was defined as the lowest concentration of antibiotic with no visible growth. Experiments were performed in at least duplicates.

5.2.3 Cytotoxicity assay

Human HepG2 liver cancer and A549 lung carcinoma cell lines were used in this study. The cells were seeded at 2.5×10^5 per well. After 24 hours of incubation, the tested compounds will be added in a twofold serial dilution ranging from 1.562 to 50 μM. The plates were incubated at 37 °C. At 48 h and 72 h after adding the compound, the MTT assay was performed as described previously [103]. Cisplatin was used as the positive control, and DMSO was used as the negative control.

5.2.4 Fluorescence microscopy

B. subtilis strain BS1048 (RNAP *β′*-GFP) and *B. subtilis* strain BS128 (NusG-GFP) was grown on an LB agar plate and selected by chloramphenicol (5 μg/mL). A single colony was incubated in an LB medium at 37 °C until OD600 ~ 0.6. The compounds at gradient final concentrations were then added to the culture and allowed to incubate for further 15 min. The cell culture (2.5 μL) was placed onto 1.2% freshly made agarose plate and covered with a coverslip prior to imaging. A Nikon Eclipse Ti2-E Live-cell Fluorescence Imaging System equipped with a 60×/1.4 oil objective and multi-wavelength LED illumination system was used to capture the fluorescence images. The fluorescence images were processed with Nikon NIS-Elements Image Analysis software.

Reference

[1] Davies J, Davies D. “Origins and evolution of antibiotic resistance.” *Microbiol Mol Biol Rev*, vol. 74, no. 3, pp. 417-433, 2010.

[2] Walesch S, Birkelbach J, Jézéquel G, Haeckl F.P.J, Hegemann J.D, Hesterkamp T, Hirsch A.K.H, Hammann P, Müller R. “Fighting antibiotic resistance-strategies and (pre)clinical developments to find new antibacterials.” *EMBO Rep*. vol. 24, no. 1, pp. e56033-e56033, 2023.

[3] https://www.merckmanuals.com/professional/infectious-diseases/bacteria-and-antibacterial-drugs/overview-of-antibacterial-drugs

[4] https://card.mcmaster.ca/

[5] WHO. “WHO publishes list of bacteria for which new antibiotics are urgently needed, 2017.” WHO, Geneva, Switzerland.

[6] Huang W, Zhang Q, Li W, Yuan M, Zhou J, Hua L, Chen Y, Ye C, Ma Y. “Development of novel nanoantibiotics using an outer membrane vesicle-based drug efflux mechanism.” *J. Control. Release*, vol. 317, pp. 1-22, 2020.

[7] Hobson C, Chan A.N, Wright G.D. “The antibiotic resistome: a guide for the discovery of natural products as antimicrobial agents.” *Chem Rev*, vol. 121, pp. 3464-3494, 2021.

[8] Oliphant C.M, Green G. “Quinolones: a comprehensive review.” *Am Fam*, vol. 65, no. 3, pp. 455-464, 2002.

[9] Cramer P. “Multisubunit RNA polymerases.” *Curr Opin Struct Biol*, vol. 12, pp. 89-97, 2002.

[10] Babakhani F, Seddon J, Sears P. “Comparative microbiological studies of transcription inhibitors fidaxomicin and the rifamycins in Clostridium difficile.” *Antimicrob Agents Chemother*, vol.58, no. 5, pp. 2934-2937, 2014.

[11] Campbell E.A, Korzheva N, Mustaev A, Murakami K, Nair S, Goldfarb A, Darst S.A. “Structural mechanism for rifampicin inhibition of bacterial rna polymerase.” *Cell*, vol. 104, no. 6, pp. 901-912, 2001.

[12] McClure W.R, Cech C.L. “On the mechanism of rifampicin inhibition of RNA synthesis.” *J. Biol. Chem*, vol. 253, pp. 8949-8956, 1978.

[13] Van Gilst M.R, von Hippel P.H. “Assembly of the N-dependent antitermination complex of phage lambda: NusA and RNA bind independently to different unfolded domains of the N protein.”

J Mol Biol, vol. 274, no. 2, pp. 160-173, 1997.

[14] Sen R, Chalissery J, Muteeb G. “Nus Factors of Escherichia coli.” *EcoSal Plus*, vol. 3, no. 1, 2008.

[15] Tomar, S.K, Artsimovitch I. “NusG-Spt5 proteins-Universal tools for transcription modification and communication.” *Chemical reviews*, vol. 113, no. 11, pp. 8604-8619, 2013.

[16] Downing W.L, Sullivan S.L, Gottesman M.E, Dennis P.P. “Sequence and transcriptional pattern of the essential Escherichia coli secE-nusG operon.” *J Bacteriol*, vol. 172, no. 3, pp. 1621-1627, 1990.

[17] Steiner T, Kaiser J.T, Marinkoviç S, Huber R, Wahl M.C. “Crystal structures of transcription factor NusG in light of its nucleic acid- and protein-binding activities.” *EMBO J*, vol. 21, no. 17, pp. 4641-4653, 2002.

[18] Varani G, Nagai K. “RNA recognition by RNP proteins during RNA processing.” *Annu Rev Biophys Biomol Struc*, vol. 27, pp. 407-445, 1998.

[19] Kyrpides N.C, Woese C.R, Ouzounis C.A. “KOW: a novel motif linking a bacterial transcription factor with ribosomal proteins.” *Trends Biochem Sci*, vol. 21, no. 11, pp. 425-426, 1996.

[20] Reay P, Yamasaki K, Terada T, Kuramitsu S, Shirouzu M, Yokoyama S. “Structural and sequence comparisons arising from the solution structure of the transcription elongation factor NusG from Thermus thermophilus.” *Proteins*, vol. 56, no. 1, pp. 40-51, 2004.

[21] Mooney R.A, Schweimer K, Rösch P, Gottesman M, Landick R. “Two structurally independent domains of *E. coli* NusG create regulatory plasticity via distinct interactions with RNA polymerase and regulators.” *J Mol Biol*, vol. 391, no. 2, pp. 341-358, 2009.

[22] Drögemüller J, Stegmann C.M, Mandal A, Steiner T, Burmann B.M, Gottesman M.E, Wöhrl B.M, Rösch P, Wahl M.C, Schweimer K. “An autoinhibited state in the structure of Thermotoga maritima NusG.” *Structure*, vol. 21, no. 3, pp. 365-375, 2013.

[23] Martinez-Rucobo F.W, Sainsbury S, Cheung A.C, Cramer P. “Architecture of the RNA polymerase-Spt4/5 complex and basis of universal transcription processivity.” *The EMBO journal*, vol. 30, no. 7, pp. 1302-1310, 2011.

[24] Sevostyanova A, Belogurov G.A, Mooney R.A, Landick R, Artsimovitch I. “The β subunit

gate loop is required for RNA polymerase modification by RfaH and NusG." *Mol Cell*, vol. 43, no. 2, pp. 253-262, 2011.

[25] Chalissery J, Muteeb G, Kalarickal N.C, Mohan S, Jisha V, Sen R. "Interaction surface of the transcription terminator Rho required to form a complex with the C-terminal domain of the antiterminator NusG." *J Mol Biol*, vol. 405, no. 1, pp. 49-64, 2011.

[26] Drögemüller J, Strauß M, Schweimer K, Jurk M, Rösch P, Knauer S.H. "Determination of RNA polymerase binding surfaces of transcription factors by NMR spectroscopy." *Sci Rep*, vol. 5, pp. 16428-16428, 2015.

[27] Burmann B.M, Schweimer K, Luo X, Wahl M.C, Stitt B.L, Gottesman M.E, Rösch P. "A NusE:NusG complex links transcription and translation." *Science*, vol. 328, no. 5977, pp. 501-504, 2010.

[28] Liu B, Steitz T.A. "Structural insights into NusG regulating transcription elongation." *Nucleic Acids Res*, vol. 45, no. 2, pp. 968-974, 2017.

[29] Casjens S.R, Hendrix R.W. "Bacteriophage lambda: Early pioneer and still relevant." *Virology*, vol. 479-480, pp. 310-330, 2015.

[30] Cheeran A, Babu Suganthan R, Swapna G, Bandey I, Achary M.S, Nagarajaram H.A, Sen R. "*Escherichia coli* RNA polymerase mutations located near the upstream edge of an RNA:DNA hybrid and the beginning of the RNA-exit channel are defective for transcription antitermination by the N protein from lambdoid phage H-19B." *J. Mol. Biol*, vol. 352, pp. 28-43, 2005.

[31] Mason S.W, Li J, Greenblatt J. "Host factor requirements for processive antitermination of transcription and suppression of pausing by the N protein of bacteriophage lambda." *J Biol Chem*, vol. 267, no. 27, pp. 19418-19426, 1992.

[32] Said N, Krupp F, Anedchenko E, Santos K.F, Dybkov O, Huang Y.H, Lee C.T, Loll B, Behrmann E, Bürger J, Mielke T, Loerke J, Urlaub H, Spahn C.M.T, Weber G, Wahl M.C. "Structural basis for λN-dependent processive transcription antitermination." *Nat Microbiol*, vol. 2, pp. 17062-17062, 2017.

[33] Mooney R.A, Davis S.E, Peters J.M, Rowland J.L, Ansari A.Z, Landick R. "Regulator trafficking on bacterial transcription units in vivo." *Mol Cell*, vol. 33, pp. 97-108, 2009.

[34] Kang J.Y, Mishanina T.V, Bellecourt M.J, Mooney R.A, Darst S.A, Landick R. "RNA

Polymerase Accommodates a Pause RNA Hairpin by Global Conformational Rearrangements that Prolong Pausing." *Mol Cell*, vol. 69, no. 5, pp. 802-815.e5, 2018

[35] Landick R. "The regulatory roles and mechanism of transcriptional pausing." *Biochem Soc Trans*, vol. 34, no. Pt 6, pp. 1062-1066, 2006.

[36] Larson M.H, Mooney R.A, Peters J.M, Windgassen T, Nayak D, Gross C.A, Block S.M, Greenleaf W.J, Landick R, Weissman J.S. "A pause sequence enriched at translation start sites drives transcription dynamics *in vivo*." *Science*, vol. 344, no. 6187, pp. 1042-1047, 2014.

[37] Zhang J, Landick R. "A Two-Way Street: Regulatory Interplay between RNA Polymerase and Nascent RNA Structure." *Trends in biochemical sciences*, vol. 41, no. 4, pp. 293-310, 2016.

[38] Nudler E. "RNA polymerase backtracking in gene regulation and genome instability." *Cell*, vol. 149, no. 7, pp. 1438-1445, 2012.

[39] Shaevitz J.W, Abbondanzieri E.A, Landick R, Block S.M. "Backtracking by single RNA polymerase molecules observed at near-base-pair resolution." *Nature*, vol. 426, no. 6967, pp. 684-687, 2003.

[40] Chan C.L, Wang D, Landick R. "Multiple interactions stabilize a single paused transcription intermediate in which hairpin to 3' end spacing distinguishes pause and termination pathways." *J Mol Biol*, vol. 268, no. 1, pp. 54-68, 1997.

[41] Uptain S.M, Kane C.M, Chamberlin M.J. "Basic mechanisms of transcript elongation and its regulation." *Annu Rev Biochem*, vol. 66, pp. 117-172, 1997.

[42] Herbert K.M, Zhou J, Mooney R.A, Porta A.L, Landick R, Block S.M. "*E. coli* NusG inhibits backtracking and accelerates pause-free transcription by promoting forward translocation of RNA polymerase." *J Mol Biol*, vol. 399, no. 1, pp. 17-30, 2010.

[43] Herbert K.M, La Porta A, Wong B.J, Mooney R.A, Neuman K.C, Landick R, Block S.M. "Sequence-resolved detection of pausing by single RNA polymerase molecules." *Cell*, vol. 125, pp. 1083-1094, 2006.

[44] Turtola M, Belogurov G.A. "NusG inhibits RNA polymerase backtracking by stabilizing the minimal transcription bubble." *Elife*, vol. 5, pp. e18096-e18096, 2016.

[45] Zhu C, Guo X, Dumas P, Takacs M, Abdelkareem M, Vanden Broeck A, Saint-André C, Papai G, Crucifix C, Ortiz J, Weixlbaumer A. "Transcription factors modulate RNA polymerase

conformational equilibrium." *Nat Commun*, vol. 13, no. 1, pp. 1546-1546, 2022.

[46] Guo X, Myasnikov A.G, Chen J, Crucifix C, Papai G, Takacs M, Schultz P, Weixlbaumer A. "Structural Basis for NusA Stabilized Transcriptional Pausing." *Mol Cell*, vol. 69, no. 5, pp. 816-827.e4, 2018.

[47] Skordalakes E, Berger J.M. "Structure of the Rho transcription terminator: mechanism of mRNA recognition and helicase loading." *Cell*, vol. 114, pp. 135-146, 2003.

[48] Morgan W.D, Bear D.G, Litchman B.L, von Hippel P.H. "RNA sequence and secondary structure requirements for rho-dependent transcription termination." *Nucleic Acids Res*, vol. 13, pp. 3739-3754, 1985.

[49] Park J.S, Roberts J.W. "Role of DNA bubble rewinding in enzymatic transcription termination." *Proc Natl Acad Sci USA*, vol. 103, pp. 4870-4875, 2006.

[50] Qayyum M.Z, Dey D, and Sen R. "Transcription elongation factor NusA is a negative regulator of Rho-dependent termination." *J. Biol. Chem*, vol. 291, pp. 8090-8108, 2016.

[51] Sullivan S.L, Gottesman M.E. "Requirement for *E. coli* NusG protein in factor-dependent transcription termination." *Cell*, vol. 68, no. 5, pp. 989-994, 1992.

[52] Burns C.M, Nowatzke W.L, Richardson J.P. "Activation of Rho-dependent transcription termination by NusG. Dependence on terminator location and acceleration of RNA release." *J Biol Chem*, vol. 274, no. 8, pp. 5245-5251, 1999.

[53] Lawson M.R, Ma W, Bellecourt M.J, Artsimovitch I, Martin A, Landick R, Schulten K, Berger J.M. "Mechanism for the Regulated Control of Bacterial Transcription Termination by a Universal Adaptor Protein." *Molecular cell*, vol. 71, no. 6, pp. 911-922, 2018.

[54] Das H.K, Goldstein A, Lowney L.I. "Attachment of ribosomes to nascent messenger RNA in *Escherichia coli*." *J Mol Biol*, vol. 24, no. 2, pp. 231-245, 1967.

[55] Saxena S, Myka K.K, Washburn R, Costantino N, Court D.L, Gottesman M.E. "*Escherichia coli* transcription factor NusG binds to 70S ribosomes." *Mol Microbiol*, vol. 108, no. 5, pp. 495-504, 2018.

[56] Bailey E.J, Gottesman M.E, Gonzalez R.L. Jr. "NusG-mediated Coupling of Transcription and Translation Enhances Gene Expression by Suppressing RNA Polymerase Backtracking." *J Mol Biol*, vol. 434, no. 2, pp. 167330-167330, 2022.

[57] Hartzog G.A, Wada T, Handa H, Winston F. “Evidence that Spt4, Spt5, and Spt6 control transcription elongation by RNA polymerase II in *Saccharomyces cerevisiae*.” *Genes & development*, vol. 12, no. 3, pp. 357-369, 1998.

[58] Wada T, Takagi T, Yamaguchi Y, Ferdous A, Imai T, Hirose S, Sugimoto S, Yano K, Hartzog G.A, Winston F, Buratowski S, Handa H. “DSIF, a novel transcription elongation factor that regulates RNA polymerase II processivity, is composed of human Spt4 and Spt5 homologs.” *Genes & development*, vol. 12, no. 3, pp. 343-356, 1998.

[59] Renner D.B, Yamaguchi Y, Wada T, Handa H, Price D.H. “A highly purified RNA polymerase II elongation control system.” *J Biol Chem*, vol. 276, no. 45, pp. 42601-42609, 2001.

[60] Ponting C.P. “Novel domains and orthologues of eukaryotic transcription elongation factors.” *Nucleic Acids Res*, vol. 30, no. 17, pp. 3643-3652, 2002.

[61] Meyer P.A, Li S, Zhang M, Yamada K, Takagi Y, Hartzog G.A, Fu J. “Structures and Functions of the Multiple KOW Domains of Transcription Elongation Factor Spt5.” *Mol Cell Biol*, vol. 35, no. 19, pp. 3354-3369, 2015.

[62] Bernecky C, Plitzko J.M, Cramer P. “Structure of a transcribing RNA polymerase II-DSIF complex reveals a multidentate DNA-RNA clamp.” *Nat Struct Mol Biol*, vol. 24, no. 10, pp. 809-815, 2017.

[63] Filipovski M, Soffers J.H.M, Vos S.M, Farnung L. “Structural basis of nucleosome retention during transcription elongation.” *Science*, vol. 376, no. 6599, pp. 1313-1316, 2022.

[64] Vos S.M, Farnung L, Boehning M, Wigge C, Linden A, Urlaub H, Cramer P. “Structure of activated transcription complex Pol II-DSIF-PAF-SPT6.” vol. 560, no. 7720, pp. 607-612, 2018.

[65] Ehara H, Kujirai T, Shirouzu M, Kurumizaka H, Sekine S.I. “Structural basis of nucleosome disassembly and reassembly by RNAPII elongation complex with FACT.” *Science*, vol. 377, no. 6611, pp. eabp9466-eabp9466, 2022.

[66] Hwang H, Vreven T, Janin J, Weng Z. “Protein-protein docking benchmark version 4.0.” *Proteins*, vol. 78, pp. 3111-3114, 2010.

[67] Clackson T, Wells J.A. “A hot spot of binding energy in a hormone-receptor interface.” *Science*, vol. 377, no. 6611, pp. 383-386, 1995.

[68] Sperandio O, Reynès C.H, Camproux A, Villoutreix B.O. “Rationalizing the chemical space

of protein-protein interaction inhibitors." *Drug Discov Today*, vol. 15, pp. 220-229, 2010.

[69] Bogan A.A, Thorn K.S. "Anatomy of hot spots in protein interfaces." *J Mol Biol*, vol. 280, no. 1, pp.1-9, 1998.

[70] Thanos C.D, DeLano W.L, Wells J.A. "Hot-spot mimicry of a cytokine receptor by a small molecule." *Proc Natl Acad Sci USA*, vol. 103, no. 42, pp. 15422-15427, 2006.

[71] Arkin M.R, Tang Y, Wells J.A. "Small-molecule inhibitors of protein-protein interactions: progressing toward the reality." *Chem Biol*, vol. 21, no. 9, pp. 1102-1114, 2014.

[72] Perkins J.R, Diboun I, Dessailly B.H, Lees J.G, Orengo C. "Transient protein-protein interactions: structural, functional, and network properties." *Structure*, vol. 18, pp. 1233-1243, 2010.

[73] Raj M, Bullock B.N, Arora P.S. "Plucking the high hanging fruit: a systematic approach for targeting protein-protein interactions." *Bioorganic & medicinal chemistry*. vol. 21, pp. 4051-4057, 2013.

[74] Johnson D.K, Karanicolas J. "Druggable Protein Interaction Sites Are More Predisposed to Surface Pocket Formation than the Rest of the Protein Surface." *PLoS Computational Biology*, vol. 9, no. 3, pp. e1002951-e1002951, 2013.

[75] Arkin M.R, Tang Y, Wells J.A. "Small-molecule inhibitors of protein-protein interactions: progressing toward the reality." *Chem Biol*, vol. 21, pp. 1102-1114, 2014.

[76] Erickson H.P, Anderson D.E, Osawa M. "FtsZ in Bacterial Cytokinesis: Cytoskeleton and Force Generator All in One." *Microbiology and Molecular Biology Reviews*, vol. 74, no. 4, pp. 504-528, 2010.

[77] Rush T.S, Grant J.A, Mosyak L, Nicholls A. "A Shape-Based 3-D Scaffold Hopping Method and Its Application to a Bacterial Protein−Protein Interaction." *Journal of Medicinal Chemistry*, vol. 9, no. 3, pp. 1489-1495, 2005.

[78] Kenny C.H, Ding W, Kelleher K, Benard S, Dushin E.G, Sutherland A.G, Mosyak L, Kriz R, Ellestad G. "Development of a fluorescence polarization assay to screen for inhibitors of the FtsZ/ZipA interaction." *Anal Biochem*, vol. 323, no. 2, pp. 224-233, 2003.

[79] Cossar P.J, Lewis P.J, McCluskey A. "Protein-protein interactions as antibiotic targets: A medicinal chemistry perspective." *Medicinal Research Reviews*, vol. 40, no. 2, pp. 469-494, 2020.

[80] Yin Z, Wang Y, Whittell L.R, Jergic S, Liu M, Harry E, Dixon N.E, Kelso M.J, Beck J.L, Oakley A.J. “DNA replication is the target for the antibacterial effects of nonsteroidal antiinflammatory drugs.” *Chem Biol*, vol. 21, pp. 481-487, 2014.

[81] Georgescu R.E, Yurieva O, Kim S.S, Kuriyan J, Kong X.P, O'Donnell M. “Structure of a small-molecule inhibitor of a DNA polymerase sliding clamp.” *Proc Natl Acad Sci USA*, vol. 105, no. 32, pp. 11116-11121, 2008.

[82] Baell J.B, Holloway G.A. “New Substructure Filters for Removal of Pan Assay Interference Compounds (PAINS) from Screening Libraries and for Their Exclusion in Bioassays.” *Journal of Medicinal Chemistry*, vol. 53, no. 7, pp. 2719-2740, 2010.

[83] Marceau A.H. “Ammonium sulfate co-precipitation of SSB and interacting proteins.” *Methods Mol Biol*. vol. 922, pp. 151-153, 2012.

[84] Lu D, Keck J.L. “Structural basis of Escherichia coli single-stranded DNA-binding protein stimulation of exonuclease I.” *Proc Natl Acad Sci USA*, vol. 105, no. 27, pp. 9169-9174, 2008.

[85] Iyer R.R, Pluciennik A, Burdett V, Modrich P.L. “DNA mismatch repair: Functions and mechanisms.” *Chem Rev*, vol. 106, pp. 302-323, 2006.

[86] Lu D, Bernstein D.A, Satyshur K.A, Keck J.L. “Small-molecule tools for dissecting the roles of SSB/protein interactions in genome maintenance.” *Proc Natl Acad Sci USA*, vol. 107, no. 2, pp. 633-638, 2010.

[87] Lu D, Keck J.L. “Structural basis of *Escherichia coli* single-stranded DNA-binding protein stimulation of exonuclease I.” *Proc Natl Acad Sci USA*, vol. 105, no. 27, pp. 9169-9174, 2008.

[88] Nikaido H. “Molecular basis of bacterial outer membrane permeability revisited.” *Microbiol Mol Biol Rev*, vol. 67, no. 4, pp. 593-656, 2003.

[89] Ricci D.P, Hagan C.L, Kahne D, Silhavy T.J. “Activation of the Escherichia coli β-barrel assembly machine (Bam) is required for essential components to interact properly with substrate.” *Proc Natl Acad Sci USA*, vol. 109, no. 9, pp. 3487-3491, 2012.

[90] Gu Y, Li H, Dong H, Zeng Y, Zhang Z, Paterson N.G, Stansfeld P.J, Wang Z, Zhang Y, Wang W, Dong C. “Structural basis of outer membrane protein insertion by the BAM complex.” *Nature*, vol. 531, no. 7592, pp. 64-69, 2016.

[91] Hagan C.L, Wzorek J.S, Kahne D. “Inhibition of the β-barrel assembly machine by a peptide

that binds BamD." *Proc Natl Acad Sci USA*, vol. 112, no. 7, pp. 2011-2016, 2015.

[92] Jurėnas D, Van Melderen L. "The Variety in the Common Theme of Translation Inhibition by Type II Toxin-Antitoxin Systems." *Front Genet*, vol. 11, pp. 262-262, 2020.

[93] Lee J, Borukhov S. "Bacterial RNA Polymerase-DNA Interaction-The Driving Force of Gene Expression and the Target for Drug Action." *Front Mol Biosci*, vol. 3, pp. 73-73, 2016.

[94] Werner F, Grohmann D. "Evolution of multisubunit RNA polymerases in the three domains of life." *Nat Rev Microbiol*, vol. 9, no. 2, pp. 85-98, 2011.

[95] Vassylyev D.G, Sekine S, Laptenko O, Lee J, Vassylyeva M.N, Borukhov S, Yokoyama S. "Crystal structure of a bacterial RNA polymerase holoenzyme at 2.6 Å resolution." *Nature*, vol. 417, no. 6890, pp. 712-749, 2002.

[96] Ma C, Yang X, Kandemir H, Mielczarek M, Johnston E.B, Griffith R, Kumar N, Lewis P.J. "Inhibitors of bacterial transcription initiation complex formation." *ACS Chem Biol*, vol. 8, no. 9, pp. 1972-1980, 2013.

[97] Ma C, Yang X, Lewis P.J. "Bacterial Transcription Inhibitor of RNA Polymerase Holoenzyme Formation by Structure-Based Drug Design: From in Silico Screening to Validation." *ACS Infect Dis*, vol. 2, no. 1, pp. 39-46, 2016.

[98] Ye J, Chu A.J, Lin L, Yang X, Ma C. "First-In-Class Inhibitors Targeting the Interaction between Bacterial RNA Polymerase and Sigma Initiation Factor Affect the Viability and Toxin Release of *Streptococcus pneumoniae*." *Molecules*, vol. 24, no. 16, pp. 2902-2902, 2019.

[99] Sartini S, Levati E, Maccesi M, Guerra M, Spadoni G, Bach S, Benincasa M, Scocchi M, Ottonello S, Rivara S, Montanini B. "New Antimicrobials Targeting Bacterial RNA Polymerase Holoenzyme Assembly Identified with an *in Vivo* BRET-Based Discovery Platform." *ACS Chem Biol*, vol. 14, no. 8, pp. 1727-1736, 2019.

[100] Greive S.J, Lins A.F, von Hippel P.H. "Assembly of an RNA-protein complex. Binding of NusB and NusE (S10) proteins to boxA RNA nucleates the formation of the antitermination complex involved in controlling rRNA transcription in *Escherichia coli*." *J Biol Chem*, vol. 280, no. 43, pp. 36397-36408, 2005.

[101] Cossar P.J, Ma C, Gordon C.P, Ambrus J.I, Lewis P.J, McCluskey A. "Identification and validation of small molecule modulators of the NusB-NusE interaction." *Bioorg Med Chem Lett*,

vol. 27, no. 2, pp. 162-167, 2017.

[102] Cossar P.J, Abdel-Hamid M.K, Ma C, Sakoff J.A, Trinh T.N, Gordon C.P, Lewis P.J, McCluskey A. “Small-Molecule Inhibitors of the NusB-NusE Protein-Protein Interaction with Antibiotic Activity.” *ACS Omega*, vol. 2, no. 7, pp. 3839-3857, 2017.

[103] Yang X, Luo M.J, Yeung A.C.M, Lewis P.J, Chan P.K.S, Ip M, Ma C. “First-In-Class Inhibitor of Ribosomal RNA Synthesis with Antimicrobial Activity against *Staphylococcus aureus*.” *Biochemistry*, vol. 56, no. 38, pp. 5049-5052, 2017.

[104] Sheng C, Dong G, Miao Z, Zhang W, Wang W. “State-of-the-art strategies for targeting protein–protein interactions by small-molecule inhibitors.” *Chemical Society Reviews*, vol. 44, no. 22, pp. 8238-8259, 2015.

[105] Schuffenhauer A, Ruedisser S, Marzinzik A.L, Jahnke W, Blommers M, Selzer P, Jacoby E. “Library design for fragment based screening.” *Curr Top Med Chem*, vol. 5, no. 8, pp. 751-762, 2005.

[106] Warr W.A. “Silver threads.” *J Comput Aided Mol Des*, vol. 26, no. 1, pp. 151-152, 2012.

[107] Hou T, Xu X. “Recent development and application of virtual screening in drug discovery: An overview.” *Curr Pharm Des*, vol. 10, no. 9, pp. 1011-1033, 2004.

[108] Cheng T, Li Q, Zhou Z, Wang Y, Bryant S.H. “Structure-based virtual screening for drug discovery: a problem-centric review.” *AAPS J*, vol. 14, no. 1, pp. 133-141, 2012.

[109] Suay-García B, Bueso-Bordils J.I, Falcó A, Antón-Fos G.M, Alemán-López P.A. “Virtual Combinatorial Chemistry and Pharmacological Screening: A Short Guide to Drug Design.” *Int J Mol Sci*, vol. 23, no. 3, pp. 1620-1620,2022.

[110] Li S, Zhang S, Chen D, Jiang X, Liu B, Zhang H, Rachakunta M, Zuo Z. “Identification of Novel TRPC5 Inhibitors by Pharmacophore-Based and Structure-Based Approaches.” *Comput Biol Chem*, vol. 87, pp. 107302-107302, 2020.

[111] Voet A, Banwell E.F, Sahu K.K, Heddle J.G, Zhang K.Y.J. “Protein Interface Pharmacophore Mapping Tools for Small Molecule Protein: Protein Interaction Inhibitor Discovery.” *Current Topics in Medicinal Chemistry*, vol. 13, no. 9, pp. 989-1001, 2013.

[112] https://www.rcsb.org/

[113] Iyer L.M, Koonin E.V, Aravind L. “Evolution of bacterial RNA polymerase: implications for

large-scale bacterial phylogeny, domain accretion, and horizontal gene transfer." *Gene*, vol. 335, pp. 73-88, 2004.

[114] Ntie-Kang F. "An in silico evaluation of the ADMET profile of the StreptomeDB database." *Springerplus*, vol. 2, pp. 353, 2013.

[115] Fleming F.F, Yao L, Ravikumar P.C, Funk L, Shook B.C. "Nitrile-containing pharmaceuticals: efficacious roles of the nitrile pharmacophore." *J Med Chem*, vol. 53, no. 22, pp. 7902-7917, 2010.

[116] Patani G.A, LaVoie E.J. "Bioisosterism: A Rational Approach in Drug Design." *Chem Rev*, vol. 96, no. 8, pp. 3147-3176, 1996.

[117] Carta F, Scozzafava A, Supuran C.T. "Sulfonamides: a patent review (2008-2012)." *Expert Opin Ther Pat*, vol. 22, no. 7, pp. 747-758, 2012.

[118] Surur A.S, Schulig L, Link A. "Interconnection of sulfides and sulfoxides in medicinal chemistry." *Arch Pharm (Weinheim)*, vol. 23, no. 3, pp. e1800248-e1800248, 2019.

[119] Summerfield S.G, Yates J.W.T, Fairman D.A. "Free Drug Theory-No Longer Just a Hypothesis?" *Pharm Res*, vol. 23, no. 3, pp. 213-222, 2022.

[120] Martignoni M, Groothuis G.M.M, de Kanter R. "Species differences between mouse, rat, dog, monkey and human CYP-mediated drug metabolism, inhibition and induction." *Expert Opinion on Drug Metabolism & Toxicology*, vol. 2, no. 6, pp. 875-894, 2006.

[121] Qiu Y, Chan S.T, Lin L, Shek T.L, Tsang T.F, Barua N, Zhang Y, Ip M, Chan P.K, Blanchard N, Hanquet G, Zuo Z, Yang X, Ma C. "Design, synthesis and biological evaluation of antimicrobial diarylimine and -amine compounds targeting the interaction between the bacterial NusB and NusE proteins." *Eur J Med Chem*, vol. 178, pp. 214-231, 2019.

[122] Lewis P.J, Thaker S.D, Errington J. "Compartmentalization of transcription and translation in *Bacillus subtilis*." *EMBO J*, vol. 19, no. 4, pp. 710-718, 2000.

[123] Doherty G.P, Meredith D.H, Lewis P.J. "Subcellular partitioning of transcription factors in *Bacillus subtilis*." *J Bacteriol*, vol. 188, no. 11, pp. 4101-4110, 2006.

[124] Clinical and Laboratory Standards Institute. Performance Standards for Antimicrobial Susceptibility Testing, 29th ed. (M100Ed29); Clinical and Laboratory Standards Institute: Wayne, PA, 2018.

Appendix I

NMR spectra of compounds

GI-1

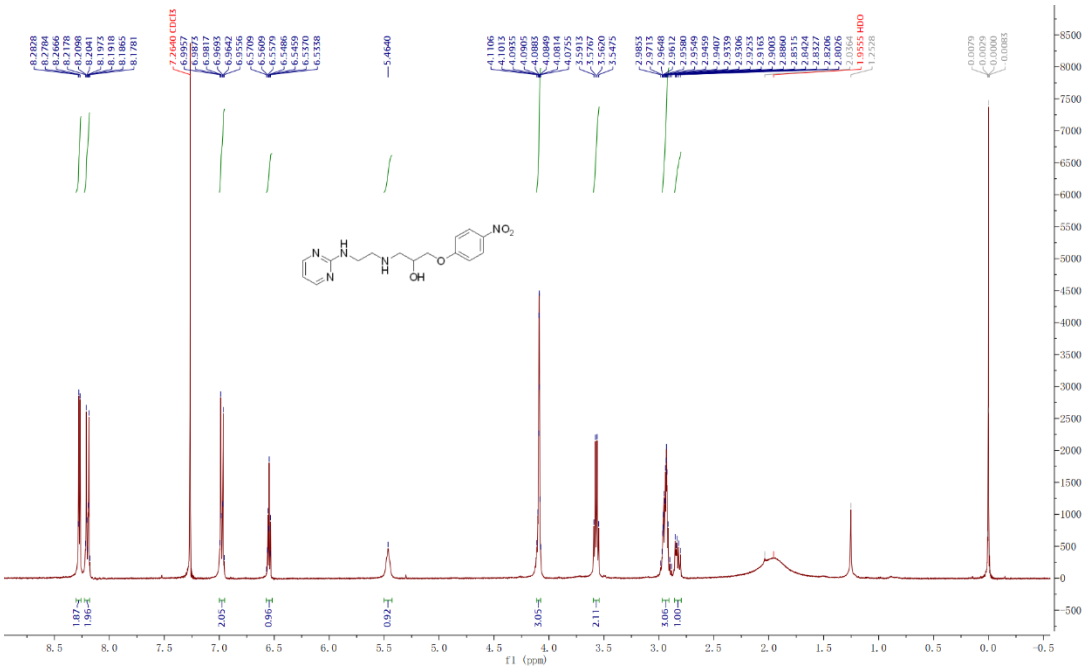

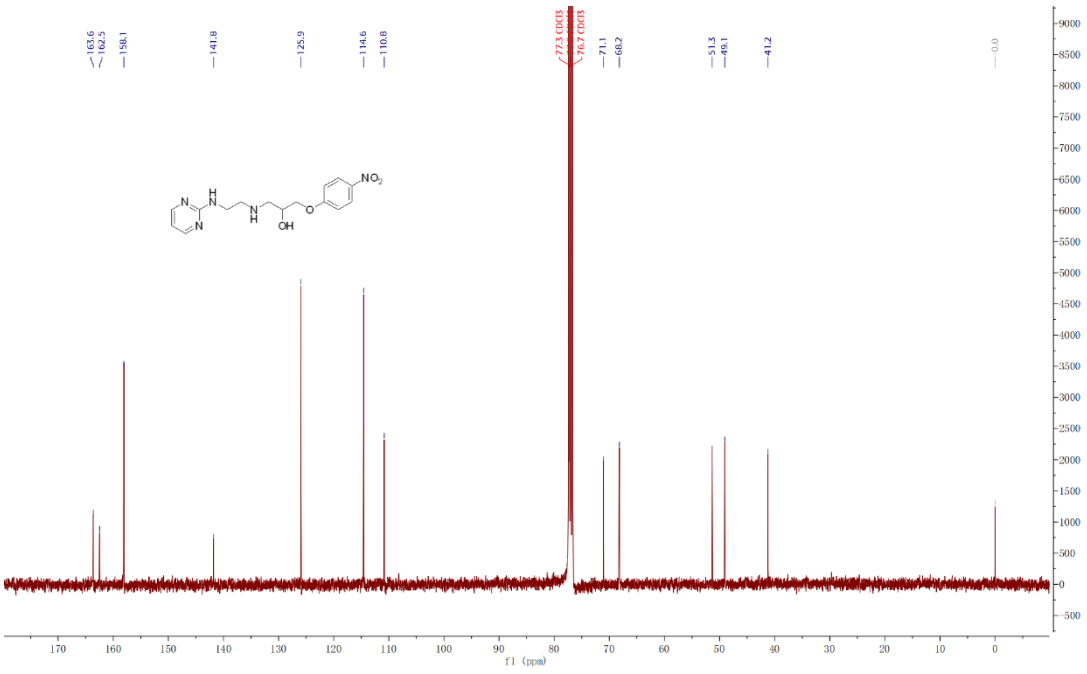

GI-2

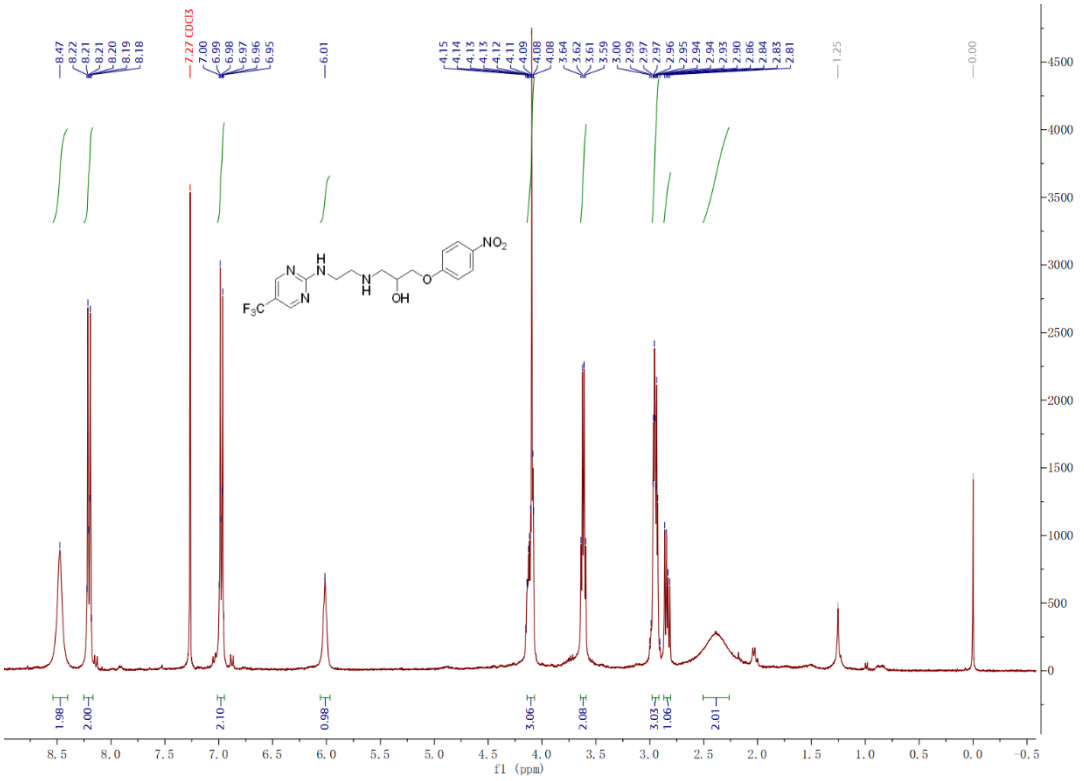
8.47
8.22
8.21
8.21
8.20
8.19
8.18
7.27 CDCl3
7.00
6.99
6.98
6.97
6.96
6.95
6.01
4.15
4.14
4.13
4.13
4.12
4.11
4.09
4.08
4.08
3.64
3.62
3.61
3.59
3.00
2.99
2.97
2.97
2.96
2.95
2.94
2.94
2.93
2.90
2.86
2.84
2.83
2.81
1.25
0.00
NO2
H
N
N
N
O
OH
F3C
1.98
2.00
2.10
0.98
3.06
2.08
3.03
1.06
2.01
f1 (ppm)

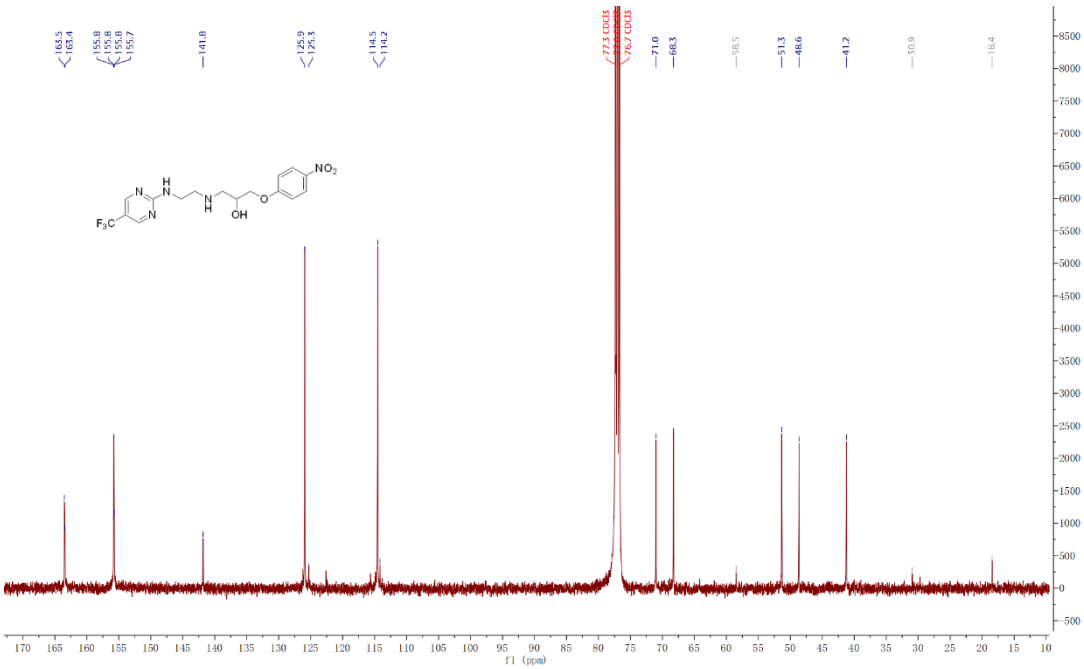
164.5
163.4
155.8
155.8
155.8
155.7
141.8
125.9
125.3
114.5
114.2
77.3 CDCl3
76.7 CDCl3
71.0
68.3
58.5
51.3
48.6
41.2
30.9
18.4
NO2
H
N
N
N
O
OH
F3C
f1 (ppm)

GI-3

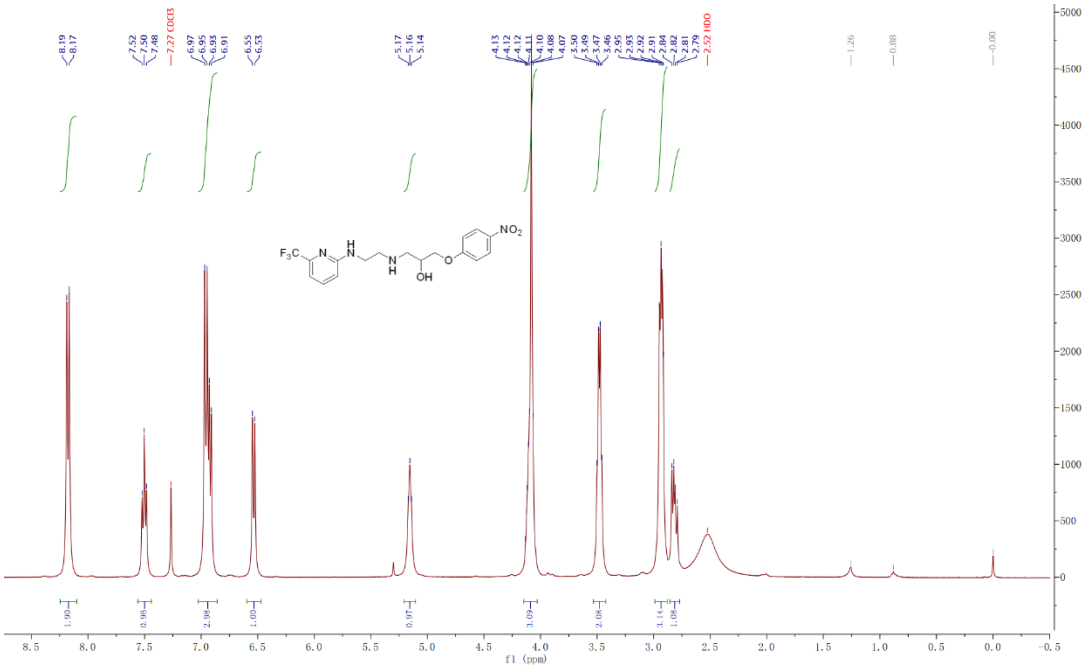
8.19
8.17
7.52
7.50
7.48
7.27 CDCl3
6.97
6.95
6.93
6.91
6.55
6.53
5.17
5.16
5.14
4.13
4.12
4.12
4.11
4.10
4.08
4.07
3.50
3.49
3.47
2.96
2.95
2.92
2.91
2.84
2.82
2.81
2.79
2.52 HDO
1.26
0.88
0.00
F3C
N
H
N
H
O
OH
NO2
f1 (ppm)

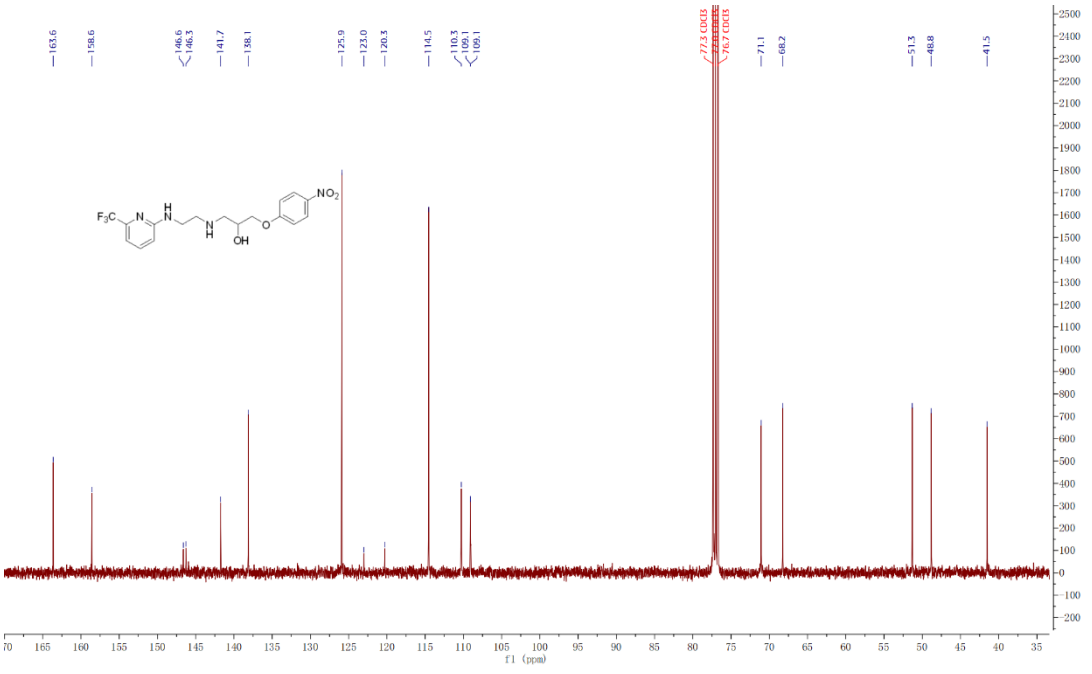
163.6
158.6
146.6
146.3
141.7
138.1
125.9
123.0
120.3
114.5
110.3
109.1
108.1
77.3 CDCl3
77.0
76.7 CDCl3
71.1
68.2
51.3
48.8
41.5
F3C
N
H
N
H
O
OH
NO2
f1 (ppm)

GI-4

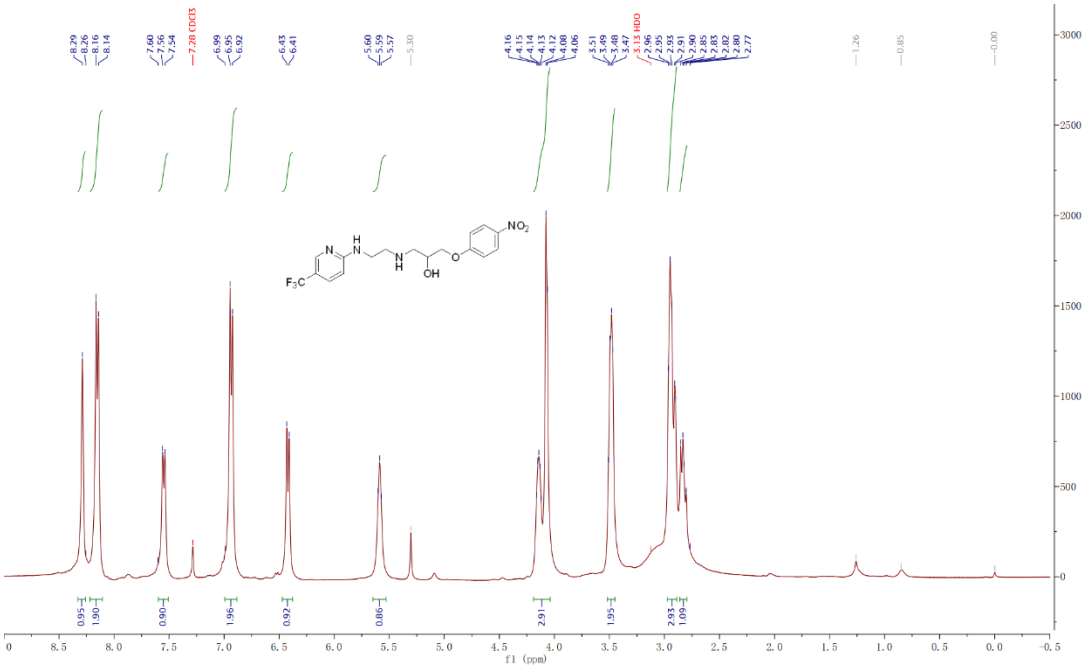
8.29
8.26
8.16
8.14
7.60
7.56
7.54
7.26 CDCl3
6.99
6.95
6.92
6.43
6.41
5.60
5.59
5.57
5.30
4.16
4.15
4.14
4.13
4.12
4.08
4.06
3.51
3.49
3.48
3.47
3.15 HDO
2.96
2.95
2.93
2.91
2.90
2.85
2.83
2.82
2.80
2.77
1.26
0.85
0.00
NO2
F3C
OH
0.95
1.90
0.90
1.96
0.92
0.86
2.91
1.95
2.93
1.09
f1 (ppm)

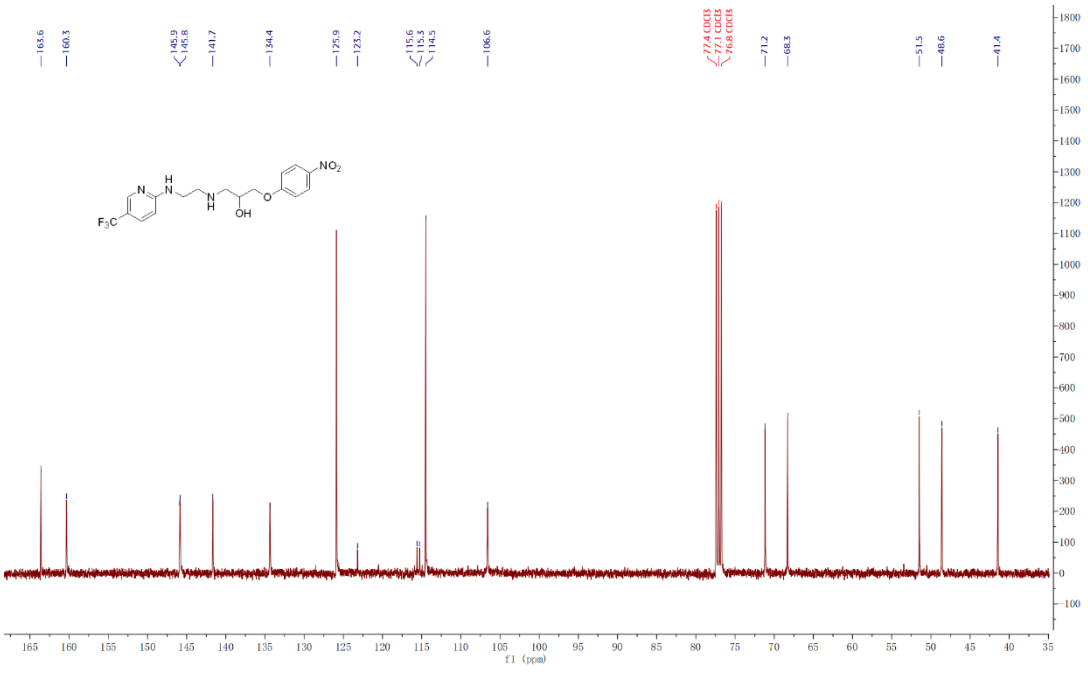
163.6
160.3
145.9
145.8
141.7
134.4
125.9
123.2
115.6
115.5
114.5
106.6
77.4 CDCl3
77.1 CDCl3
76.8 CDCl3
71.2
68.3
51.5
48.6
41.4
NO2
F3C
OH
f1 (ppm)

GI-5

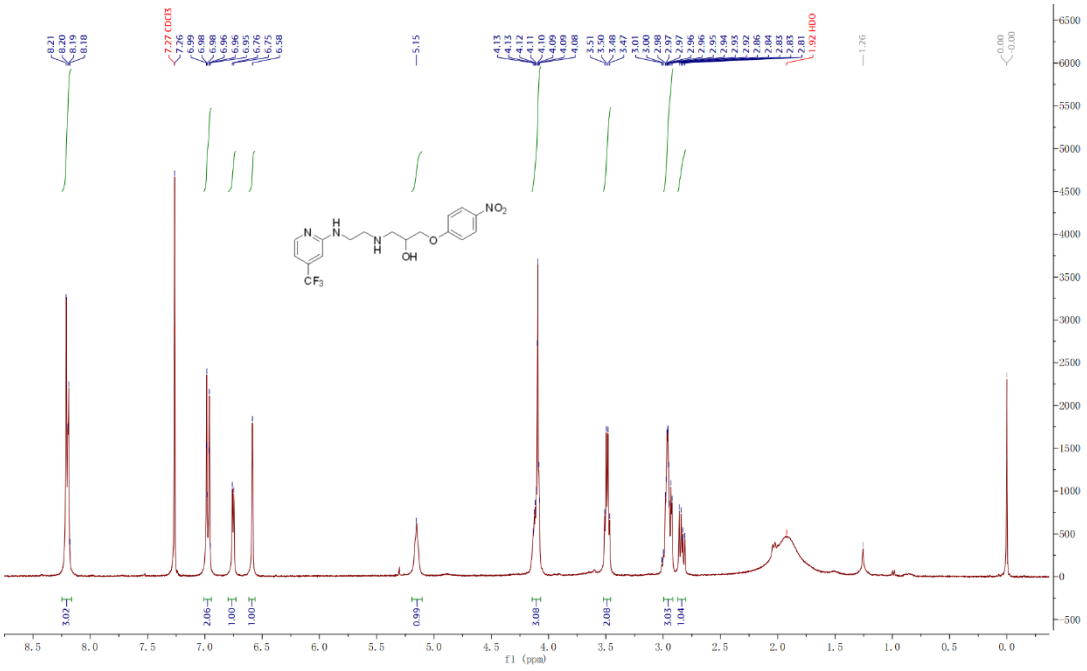

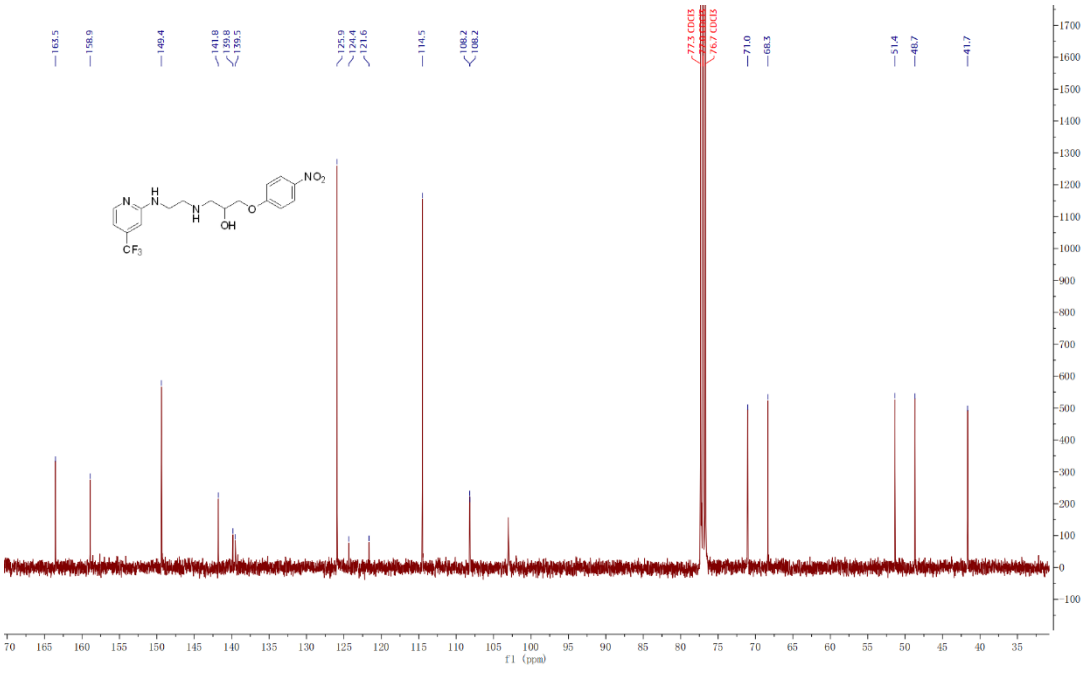

GI-6

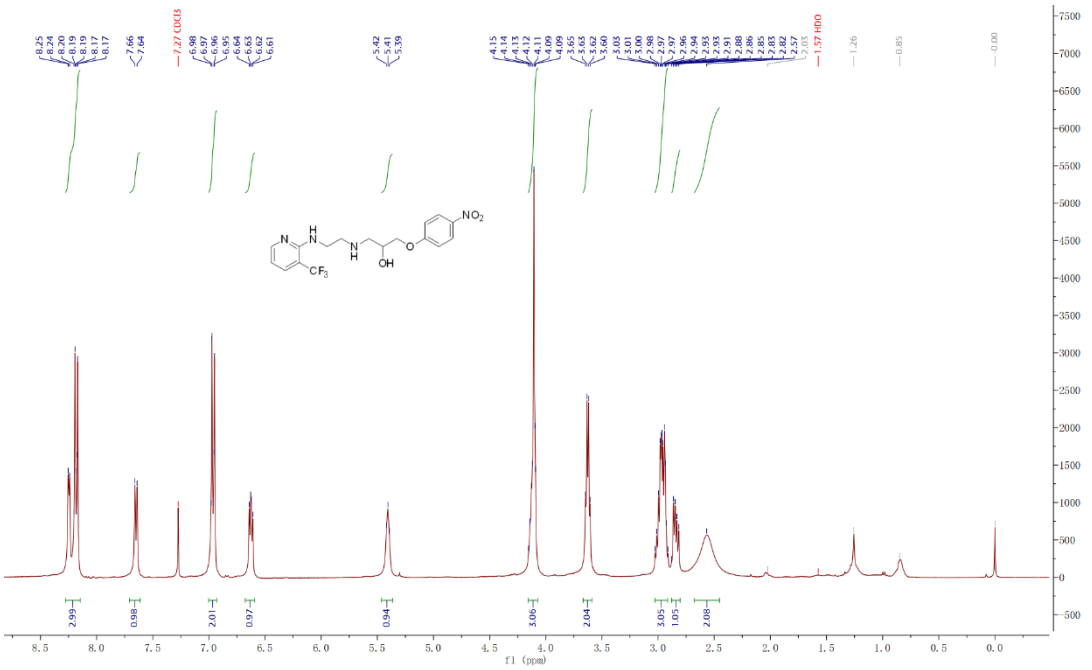
8.25
8.24
8.20
8.19
8.19
8.17
8.17
7.66
7.64
7.27 CDCl3
6.98
6.97
6.96
6.95
6.64
6.63
6.62
6.61
5.42
5.41
5.39
4.15
4.14
4.13
4.12
4.11
4.09
4.08
3.65
3.63
3.62
3.60
3.05
3.01
3.00
2.98
2.97
2.97
2.96
2.94
2.93
2.91
2.88
2.86
2.85
2.84
2.82
2.57
1.57 HDO
1.26
0.85
0.00
NO2
N
H
N
H
O
OH
CF3
2.99
0.98
2.01
0.97
0.94
3.06
2.04
3.05
1.05
2.08
f1 (ppm)

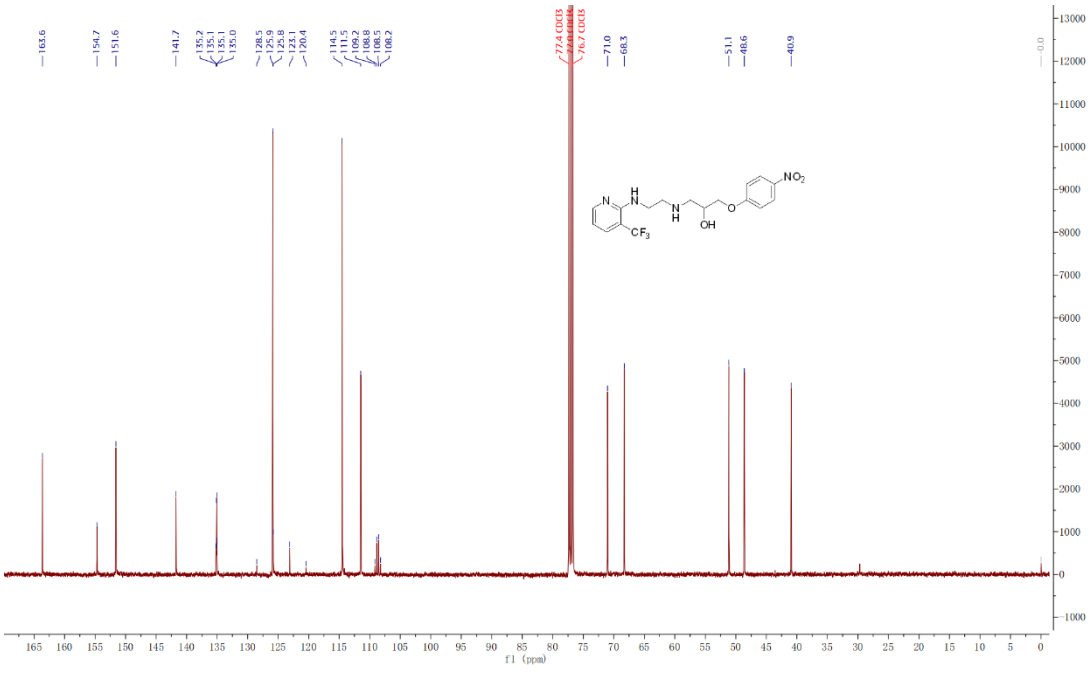
165.6
154.7
151.6
141.7
135.2
135.1
135.1
135.0
128.5
125.9
123.8
123.1
120.4
114.5
111.5
109.2
108.8
108.5
108.2
77.4 CDCl3
77.0
76.7 CDCl3
71.0
68.3
51.1
48.6
40.9
0.0
NO2
N
H
N
H
O
OH
CF3
f1 (ppm)

GI-7

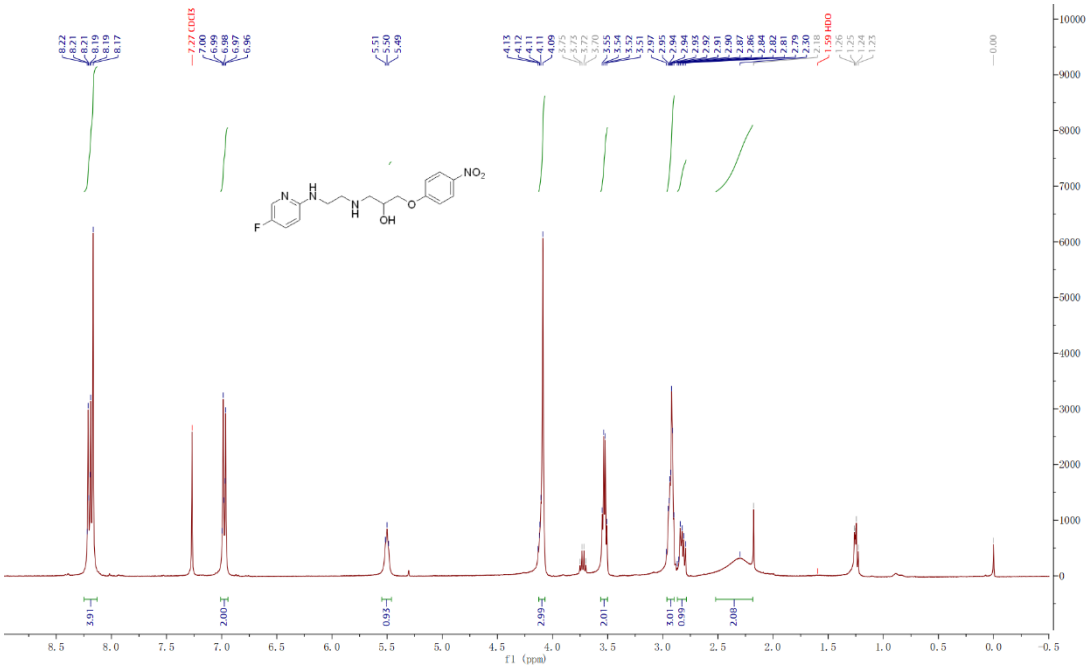
8.22
8.21
8.21
8.19
8.19
8.17
7.27 CDCl3
7.00
6.99
6.98
6.98
6.97
6.96
5.51
5.50
5.49
4.13
4.12
4.11
4.11
4.09
3.75
3.72
3.70
3.55
3.54
3.52
3.51
2.97
2.95
2.94
2.94
2.93
2.92
2.91
2.90
2.89
2.87
2.86
2.84
2.82
2.81
2.79
2.30
2.18
1.99 HDO
1.26
1.25
1.24
1.23
0.00
3.91
2.00
0.93
2.99
2.01
3.01
0.99
2.08
f1 (ppm)

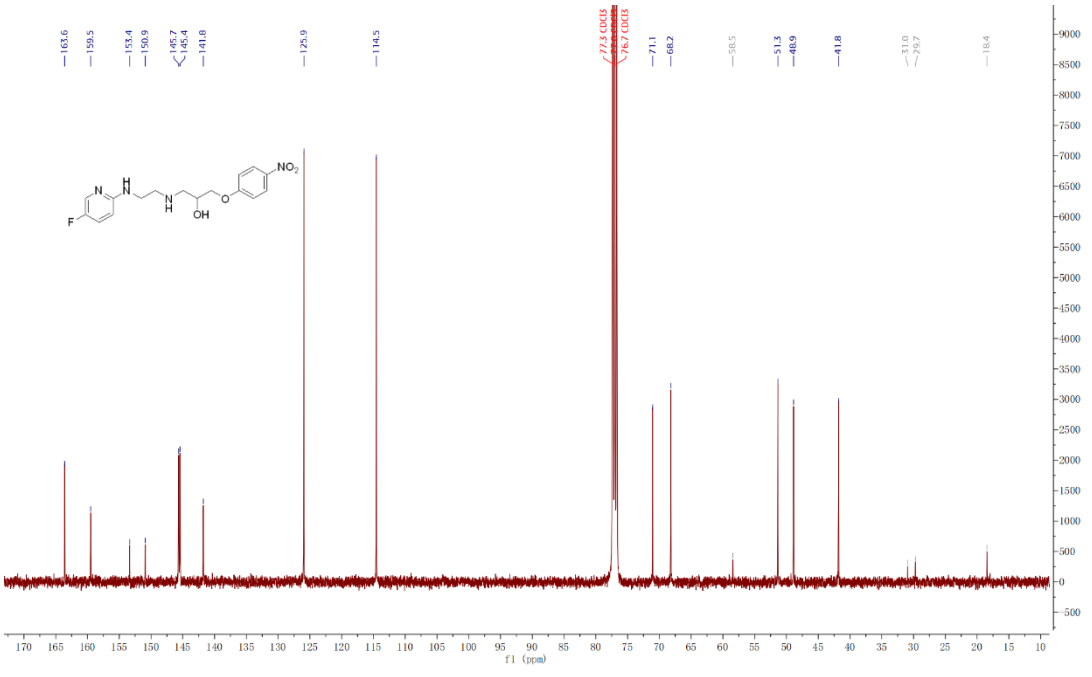
163.6
159.5
153.4
150.9
145.7
145.4
141.8
125.9
114.5
77.5 CDCl3
77.2
76.7 CDCl3
71.1
68.2
58.5
51.3
48.9
41.8
31.0
29.7
18.4
f1 (ppm)

GI-8

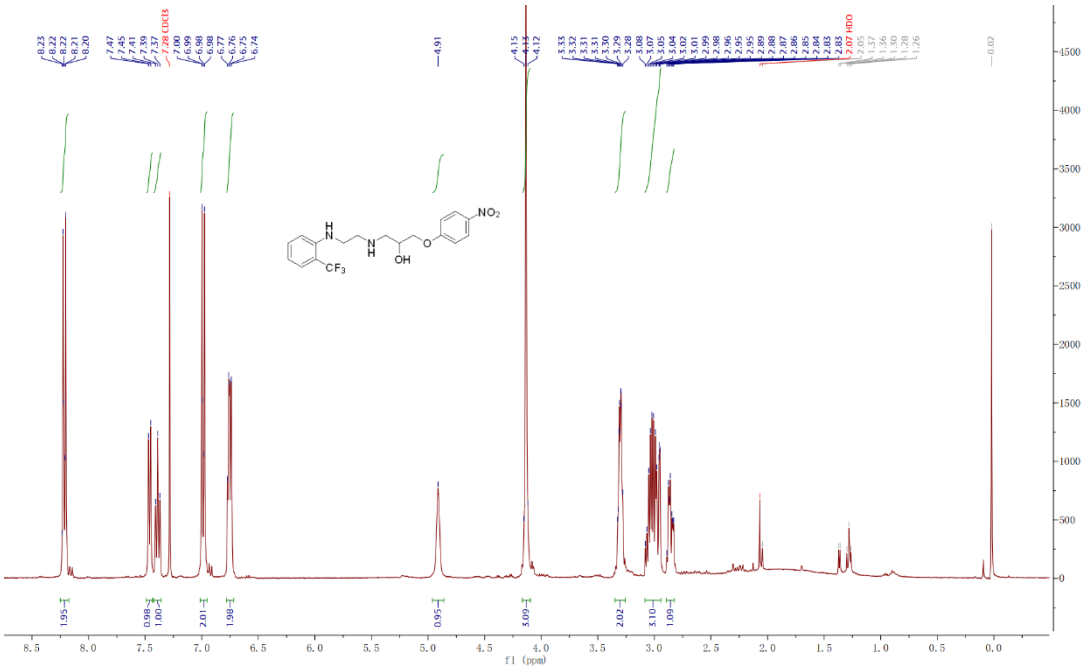

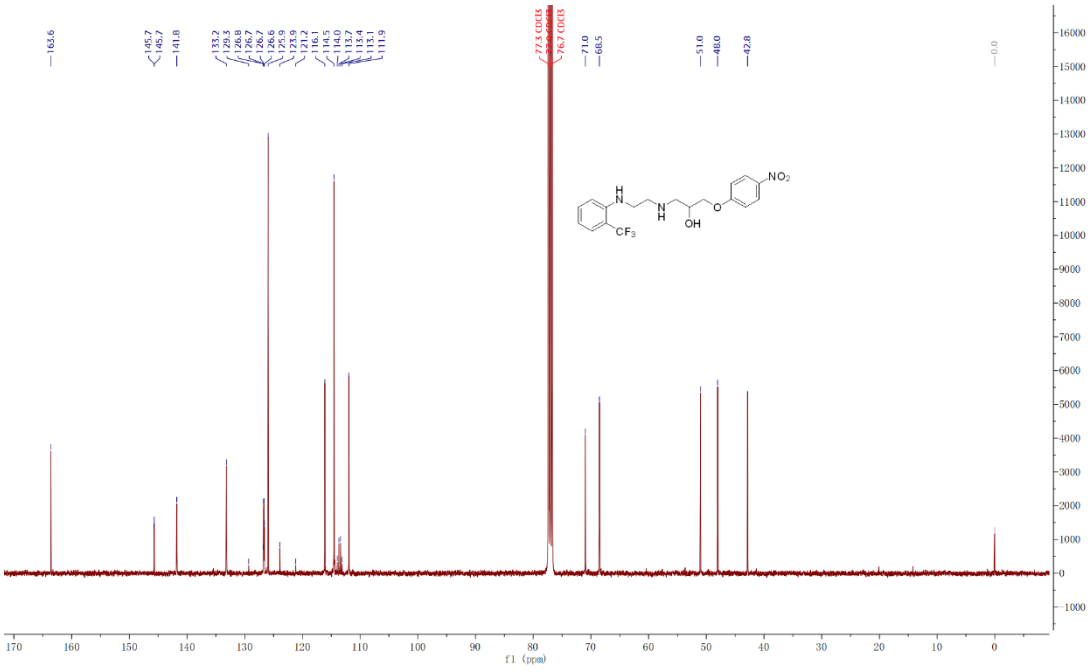

GI-9

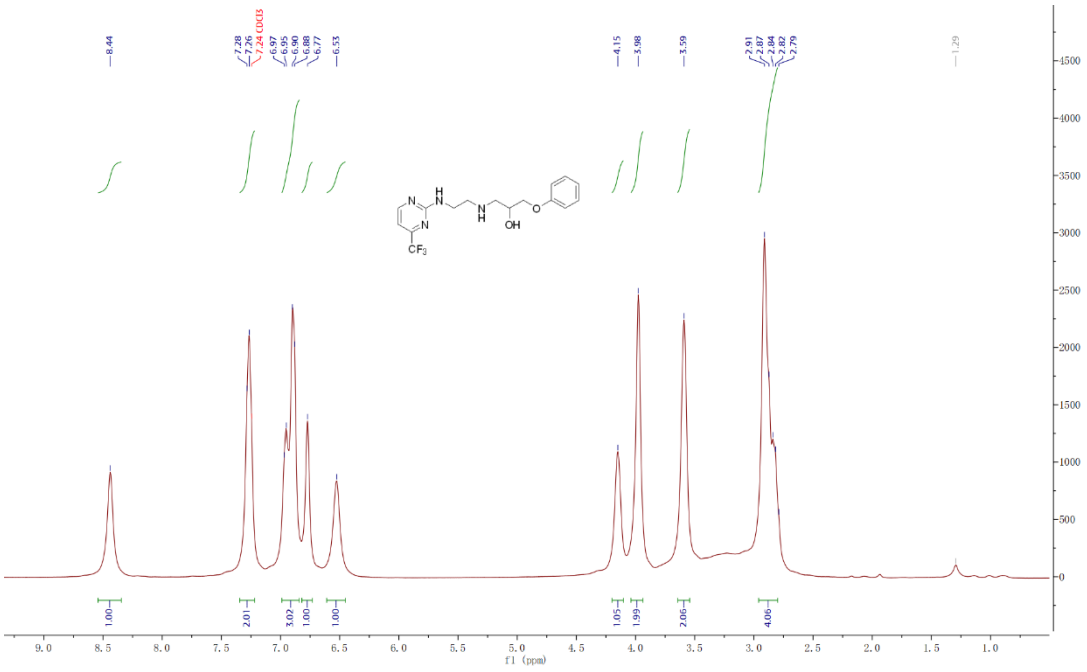
8.44
7.28
7.26
7.24 CDCl3
6.97
6.95
6.90
6.88
6.77
6.53
4.15
3.98
3.59
2.91
2.87
2.84
2.82
2.79
1.29
1.00
2.01
3.02
1.00
1.00
1.05
1.99
2.06
4.05
f1 (ppm)

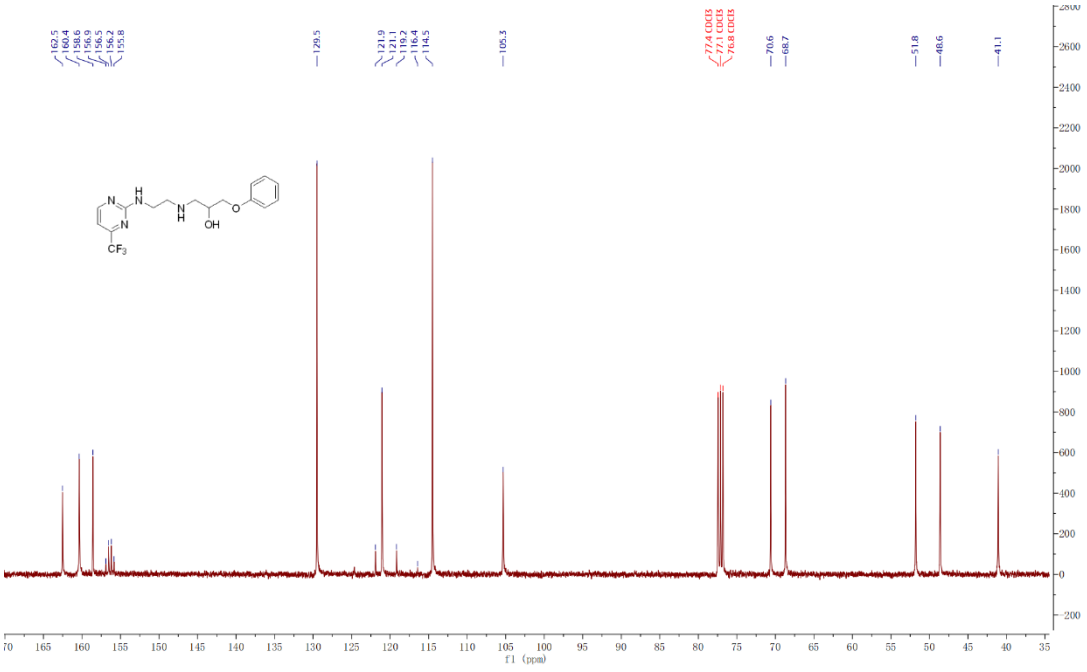
162.5
160.4
158.6
156.9
156.5
156.2
155.8
129.5
121.9
121.1
119.2
116.4
114.5
105.3
77.4 CDCl3
77.1 CDCl3
76.8 CDCl3
70.6
68.7
51.8
48.6
41.1
f1 (ppm)

GI-10

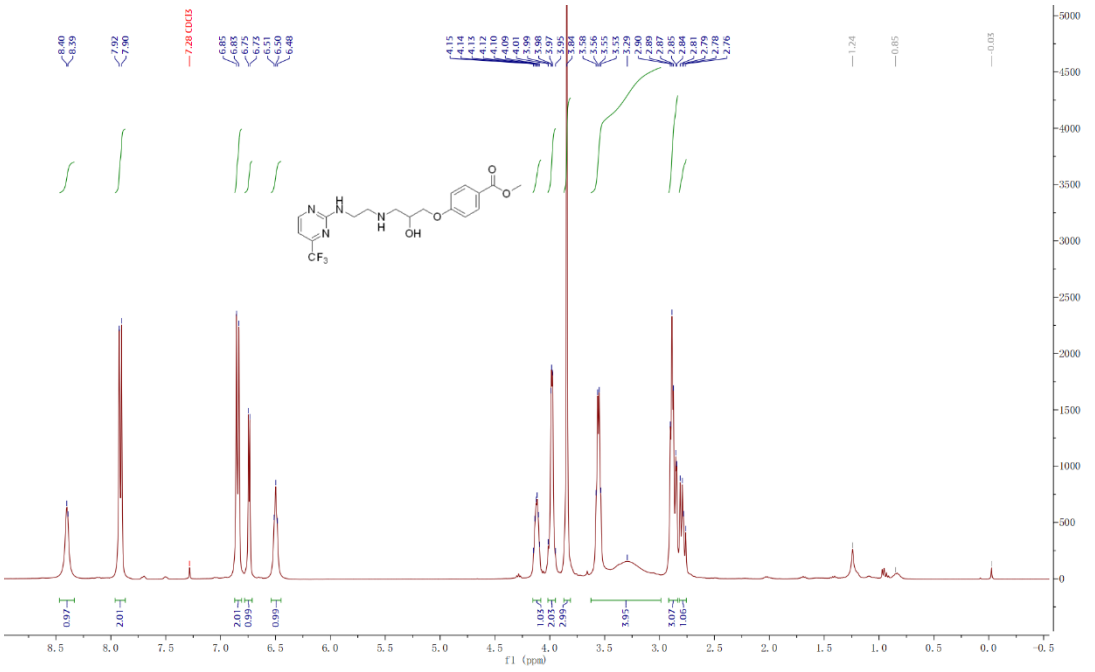

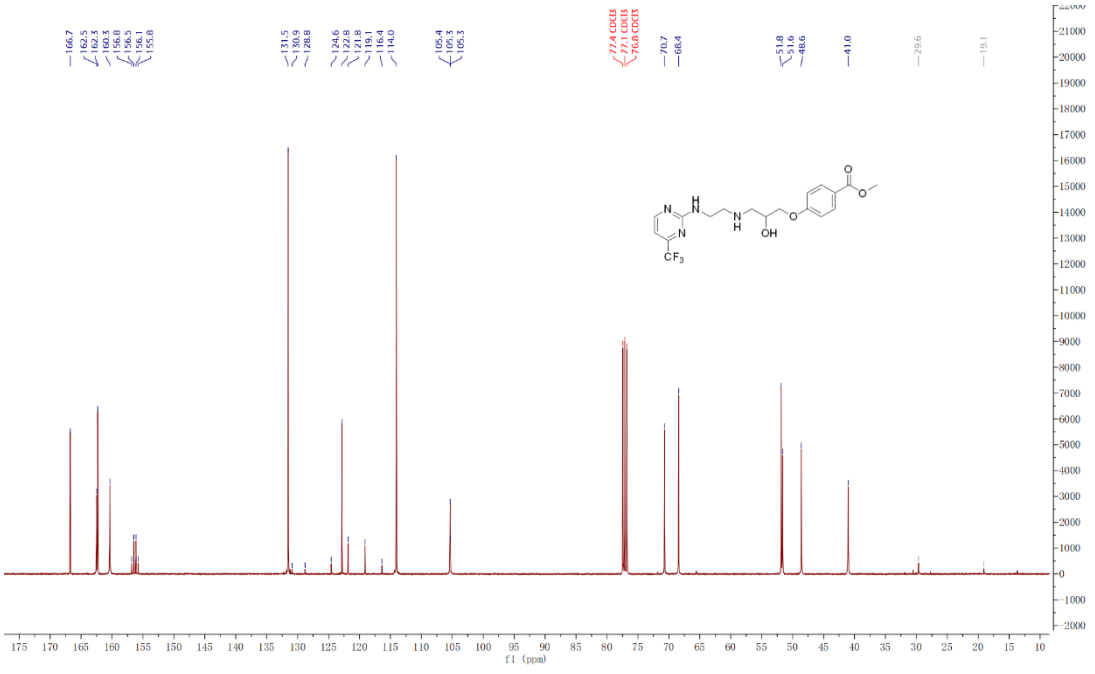

GI-11

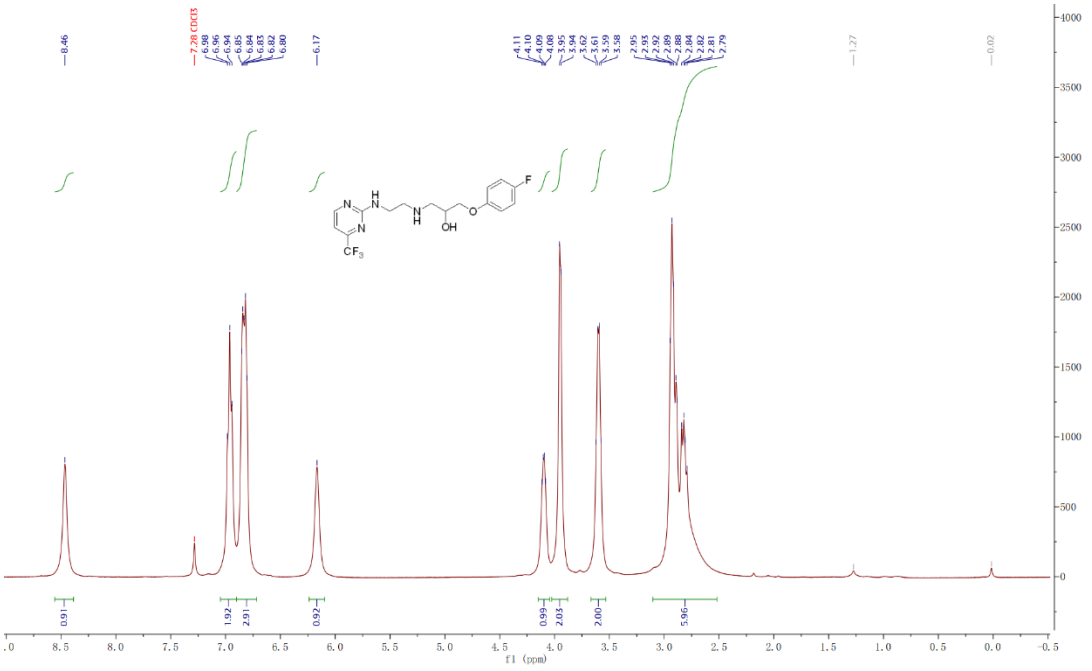
8.46
7.28 CDCl3
6.98
6.96
6.94
6.85
6.84
6.83
6.82
6.80
6.17
4.11
4.10
4.09
4.08
3.95
3.94
3.62
3.61
3.59
3.58
2.95
2.93
2.92
2.89
2.88
2.84
2.82
2.81
2.79
1.27
0.02
0.91
1.92
2.91
0.92
0.99
2.03
2.00
5.96
f1 (ppm)

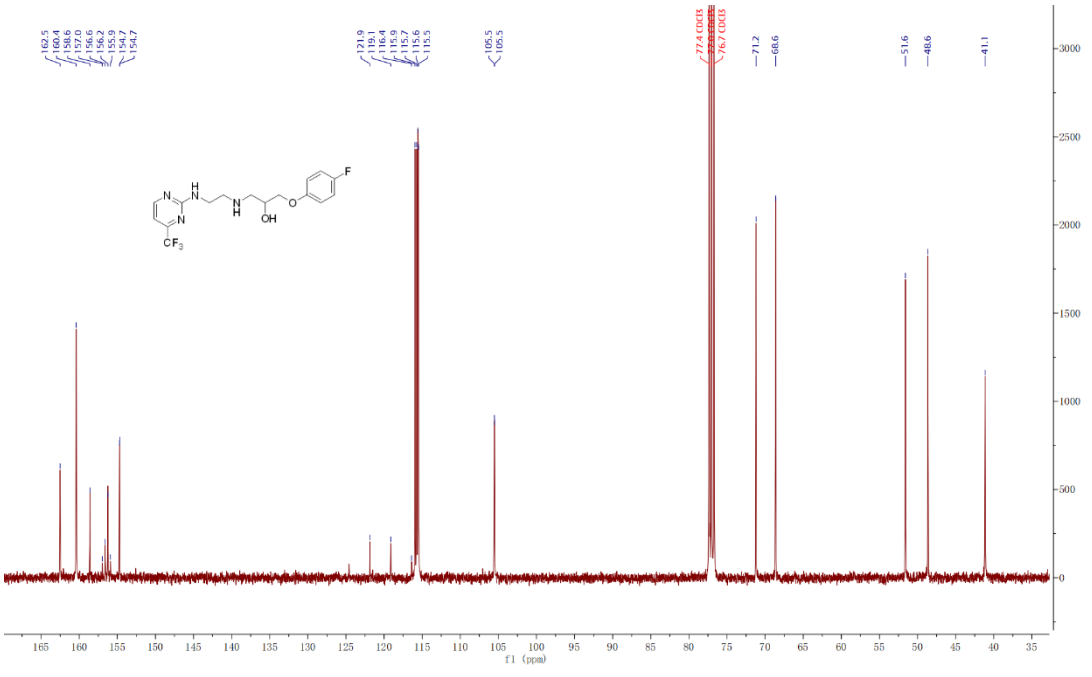
162.5
160.4
158.6
157.0
156.6
156.2
155.9
154.7
154.7
121.9
119.1
116.4
116.0
115.7
115.6
115.3
105.5
105.5
77.4 CDCl3
76.7 CDCl3
71.2
68.6
51.6
48.6
41.1
f1 (ppm)

GI-12

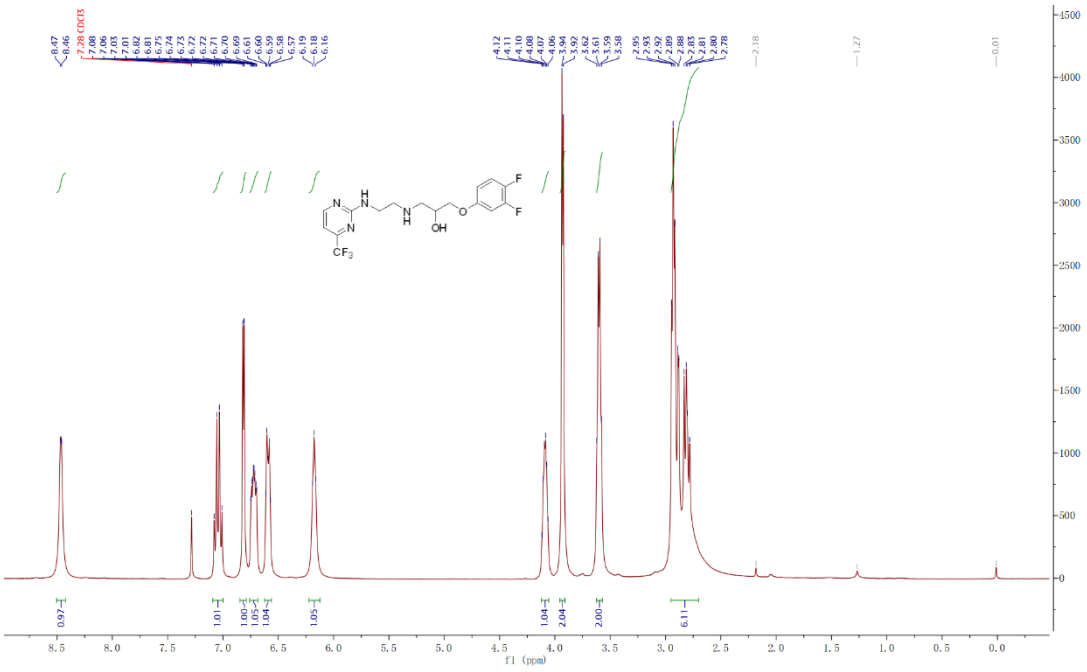

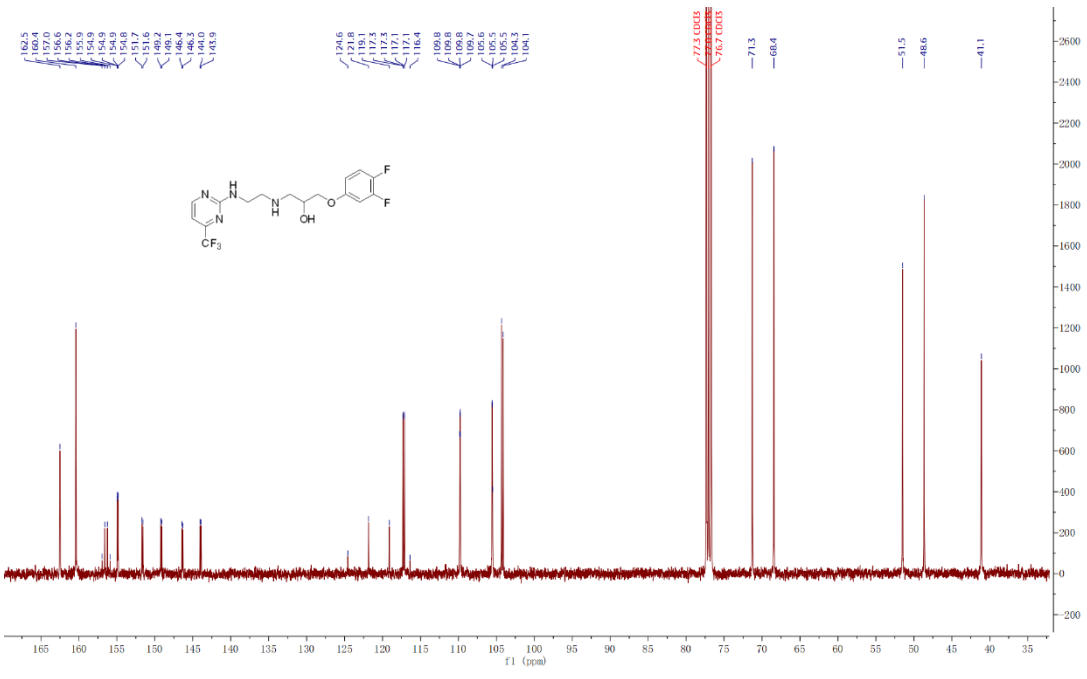

GI-13

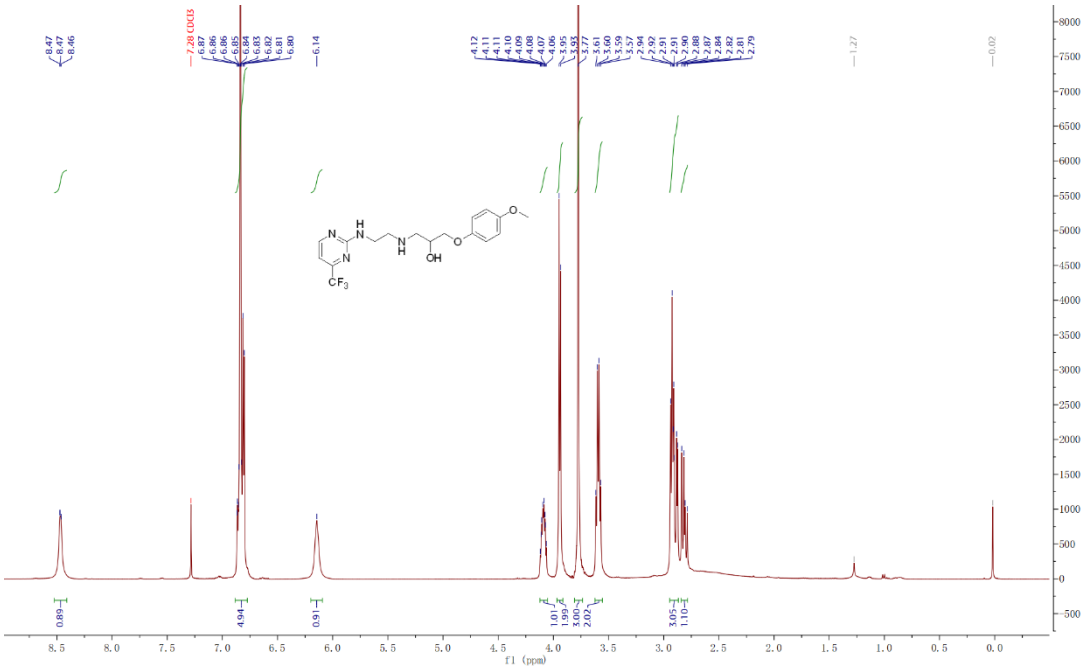

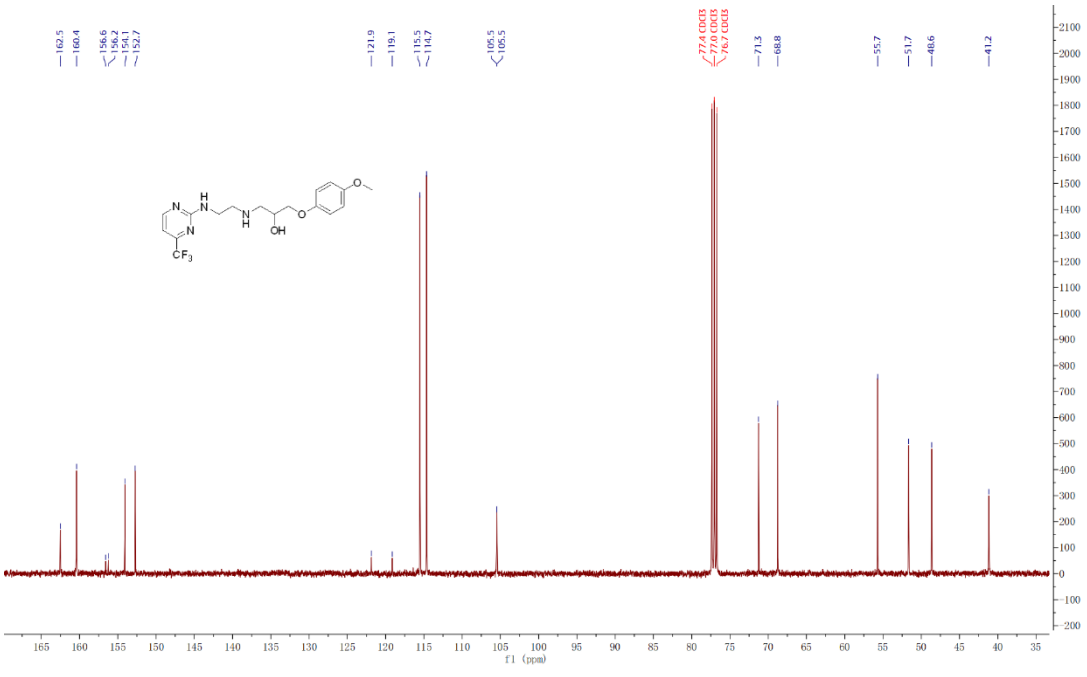

GI-14

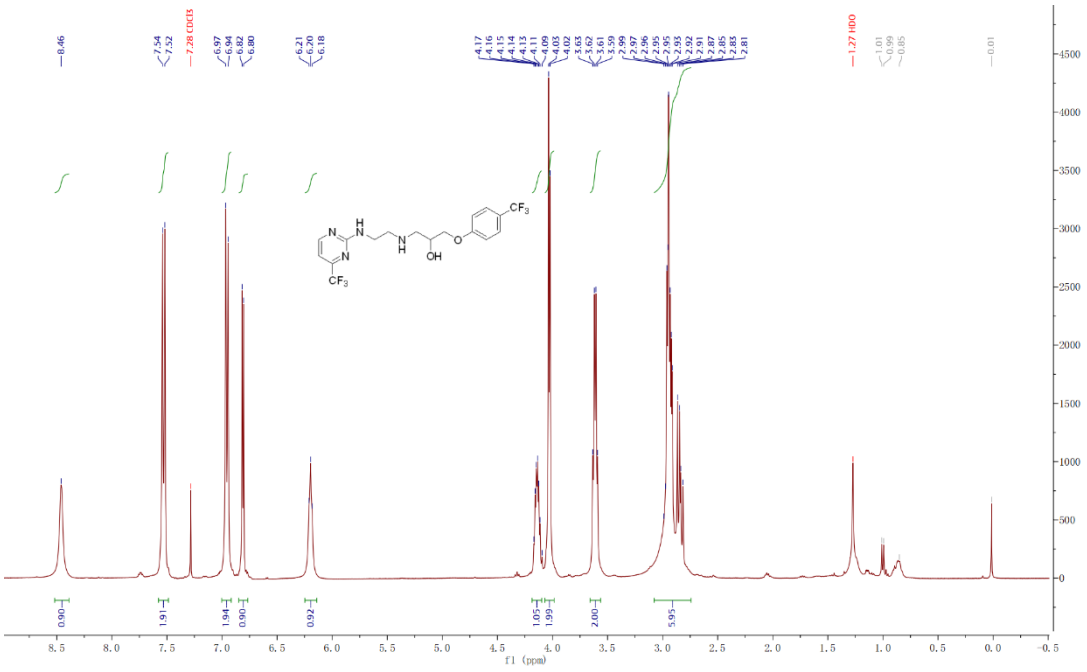
8.46
7.54
7.32
7.28 CDCl3
6.97
6.94
6.82
6.80
6.21
6.20
6.18
4.17
4.16
4.15
4.14
4.13
4.11
4.09
4.03
4.02
3.63
3.62
3.61
3.59
2.99
2.97
2.96
2.95
2.95
2.93
2.92
2.91
2.87
2.85
2.83
2.81
1.27 H2O
1.01
0.99
0.85
0.01
0.90
1.91
1.94
0.90
0.92
1.05
1.99
2.00
5.95
f1 (ppm)

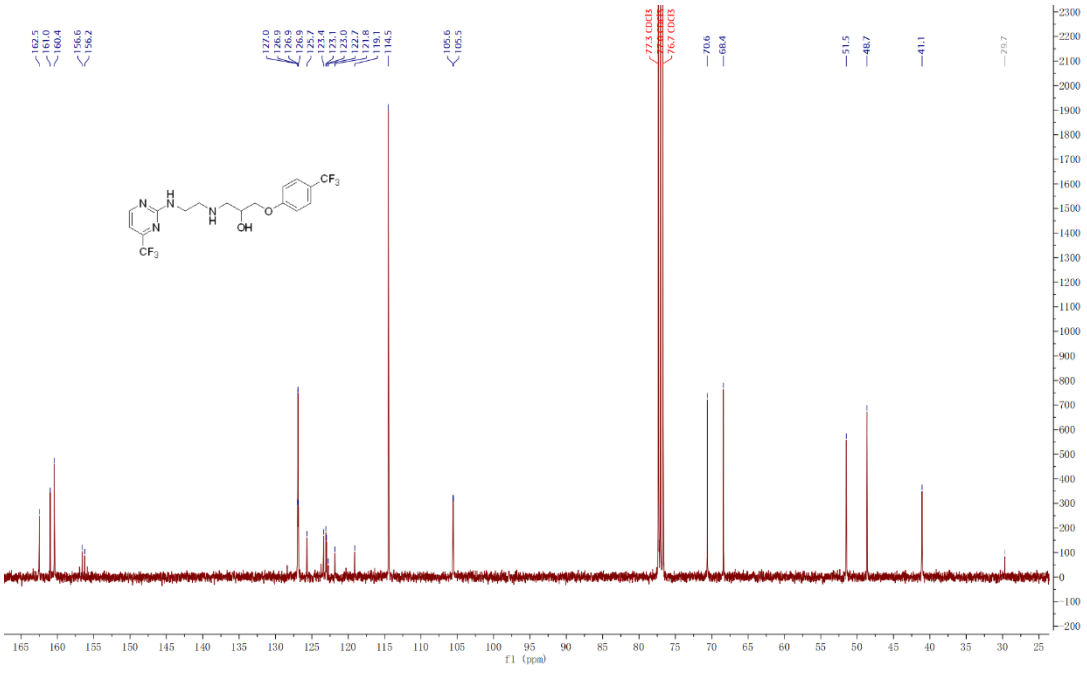
162.5
161.0
160.4
156.6
156.2
127.0
126.9
126.9
126.9
125.7
123.4
123.1
123.0
122.7
122.6
119.1
114.5
105.6
105.5
77.3 CDCl3
77.0
76.7 CDCl3
70.6
68.4
51.5
48.7
41.1
29.7
f1 (ppm)

GI-15

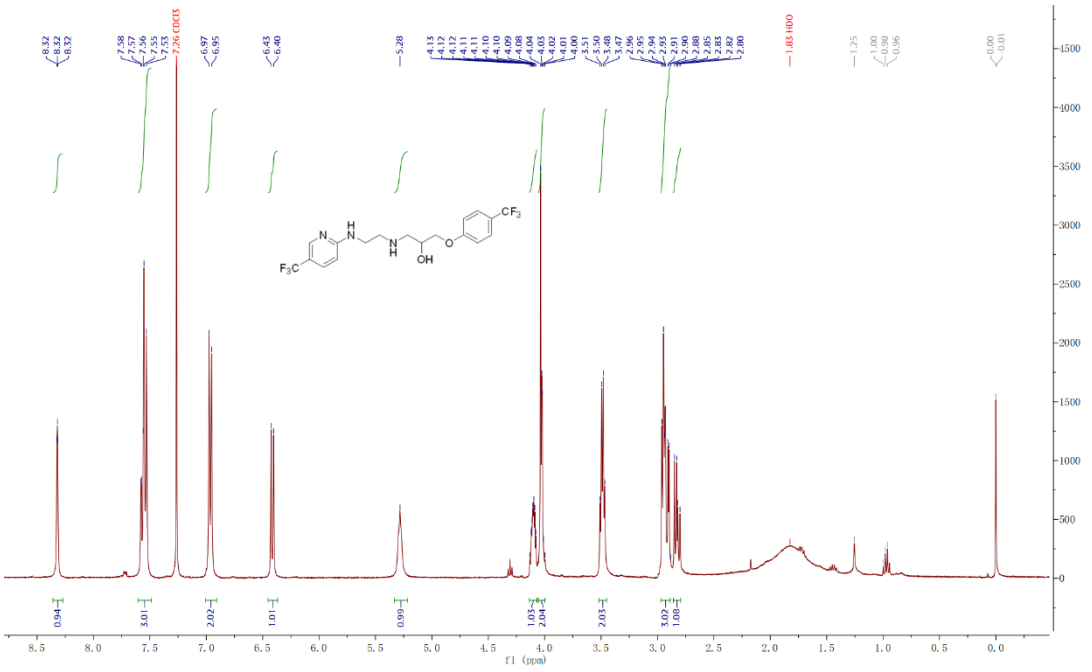

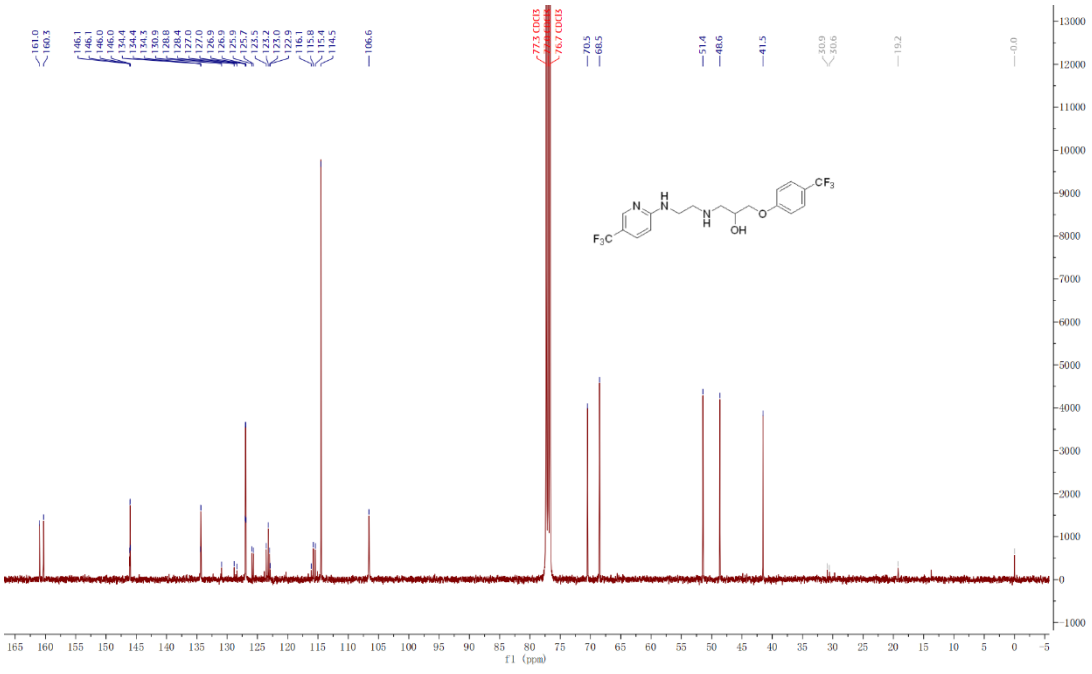

GI-16

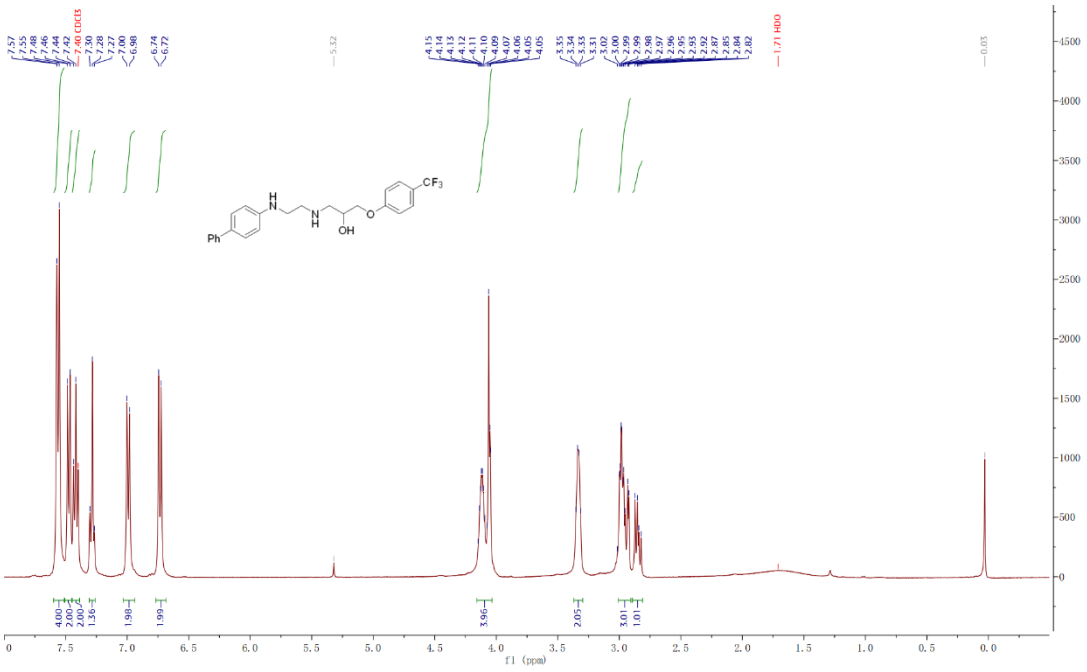
7.57
7.55
7.48
7.46
7.44
7.42
7.40 CDCl3
7.30
7.28
7.27
7.00
6.98
6.74
6.72
5.32
4.15
4.14
4.13
4.12
4.11
4.10
4.09
4.07
4.06
4.05
3.35
3.34
3.33
3.31
3.00
2.99
2.98
2.97
2.96
2.95
2.93
2.92
2.87
2.85
2.84
2.82
1.71 H2O
0.03
CF3
H
N
N
H
O
OH
Ph
4.00
2.00
2.00
1.36
1.98
1.99
3.96
2.05
3.01
1.01
f1 (ppm)

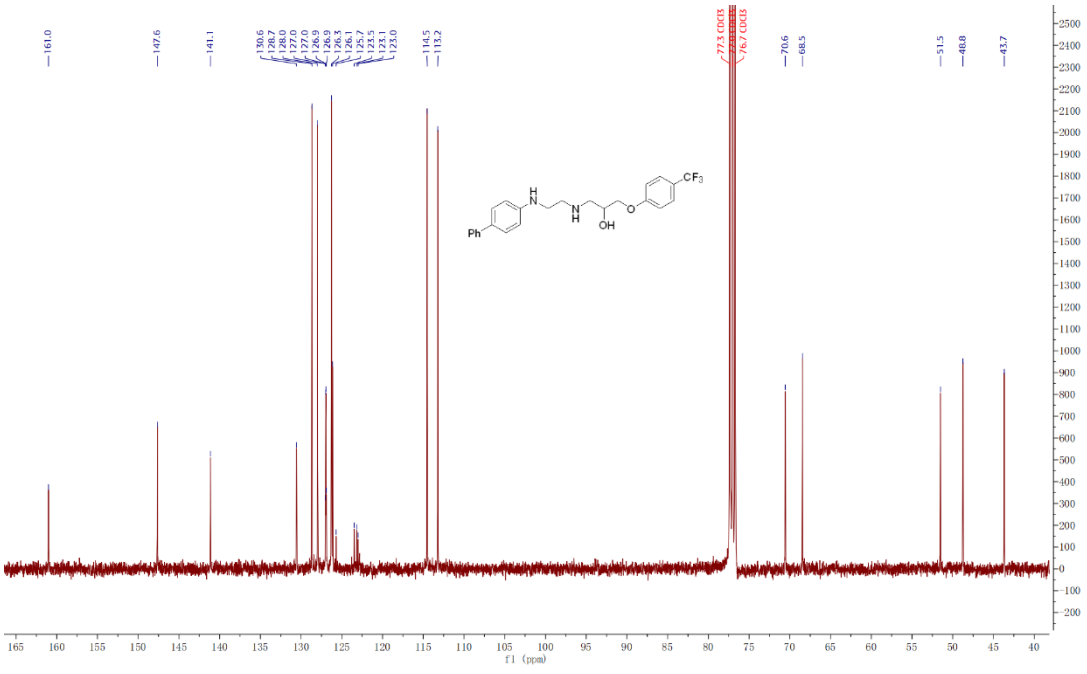
161.0
147.6
141.1
130.6
128.7
128.0
127.0
127.0
126.9
126.5
126.3
126.1
125.7
123.5
123.1
123.0
114.5
113.2
77.3 CDCl3
77.0
76.7 CDCl3
70.6
68.5
51.5
48.8
43.7
CF3
H
N
N
H
O
OH
Ph
f1 (ppm)

GI-17

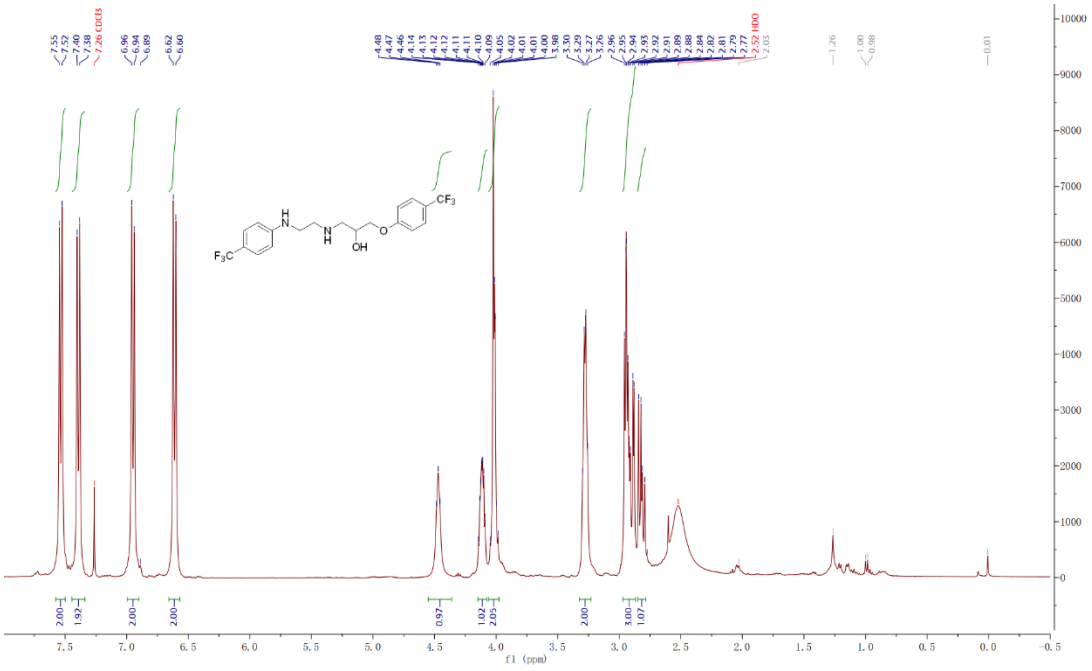
7.55
7.52
7.40
7.38
7.26 CDCl3
6.96
6.94
6.89
6.62
6.60
4.48
4.47
4.46
4.14
4.13
4.12
4.11
4.10
4.09
4.05
4.02
4.01
4.01
4.00
3.98
3.30
3.29
3.27
3.26
2.96
2.95
2.94
2.93
2.92
2.91
2.89
2.88
2.84
2.82
2.81
2.79
2.77
2.52 HDO
2.03
1.26
1.00
0.98
0.01
CF3
F3C
H
N
N
H
O
OH
2.00
1.97
2.00
2.00
0.97
1.02
2.05
2.00
3.00
1.07
f1 (ppm)

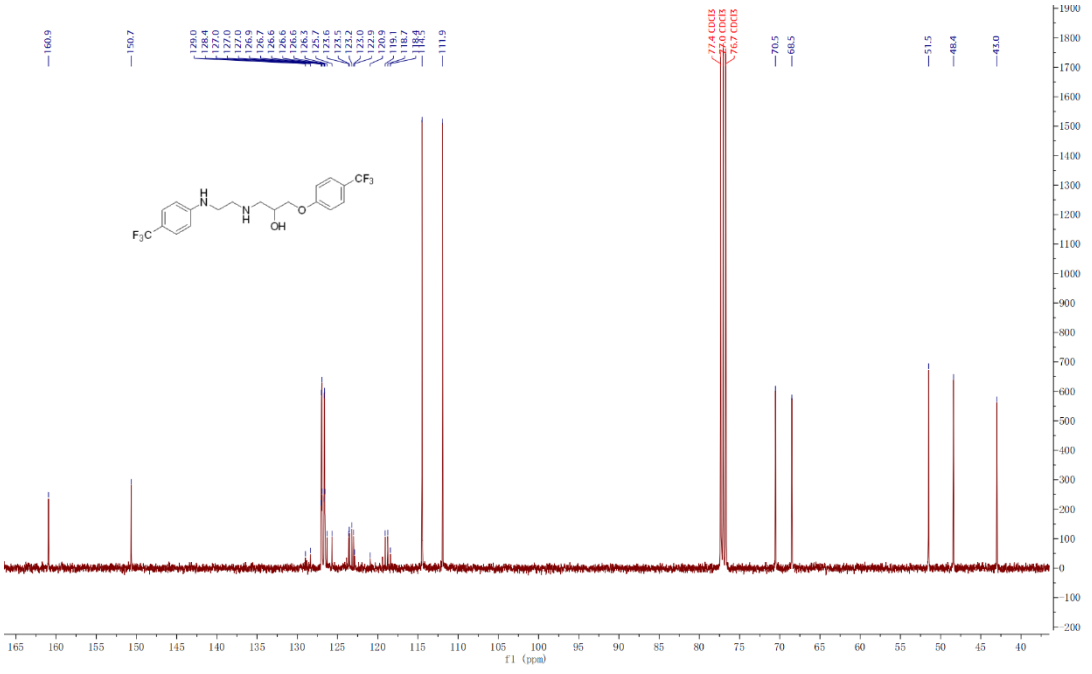
160.9
150.7
129.0
128.4
127.0
127.0
127.0
126.9
126.7
126.6
126.6
126.6
126.3
125.7
123.6
123.5
123.2
123.0
122.9
120.9
119.1
118.7
118.4
118.3
111.9
77.4 CDCl3
77.0 CDCl3
76.7 CDCl3
70.5
68.5
51.5
48.4
43.0
CF3
F3C
H
N
N
H
O
OH
f1 (ppm)

GI-18

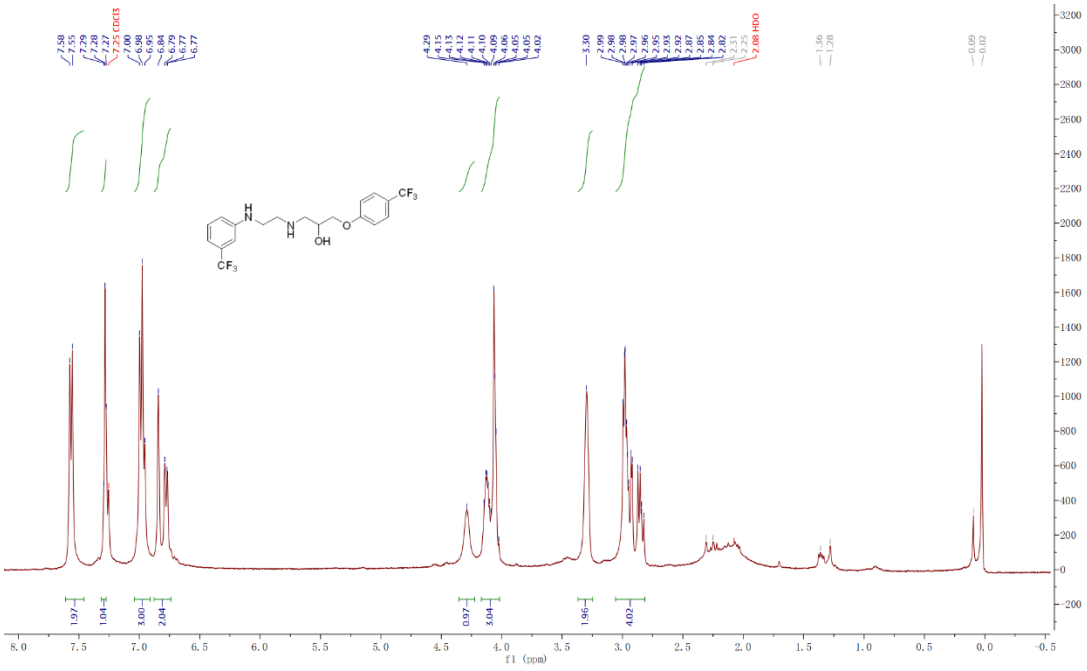
7.58
7.55
7.29
7.28
7.27
7.25 CDCl3
7.00
6.98
6.95
6.84
6.79
6.77
6.77
4.29
4.15
4.13
4.12
4.11
4.10
4.09
4.06
4.05
4.05
4.02
3.30
2.99
2.98
2.98
2.97
2.96
2.95
2.92
2.87
2.85
2.84
2.82
2.31
2.25
2.08 HDO
1.36
1.28
0.09
0.02
CF3
CF3
OH
1.97
1.04
3.00
2.04
0.97
3.04
1.96
4.02
f1 (ppm)

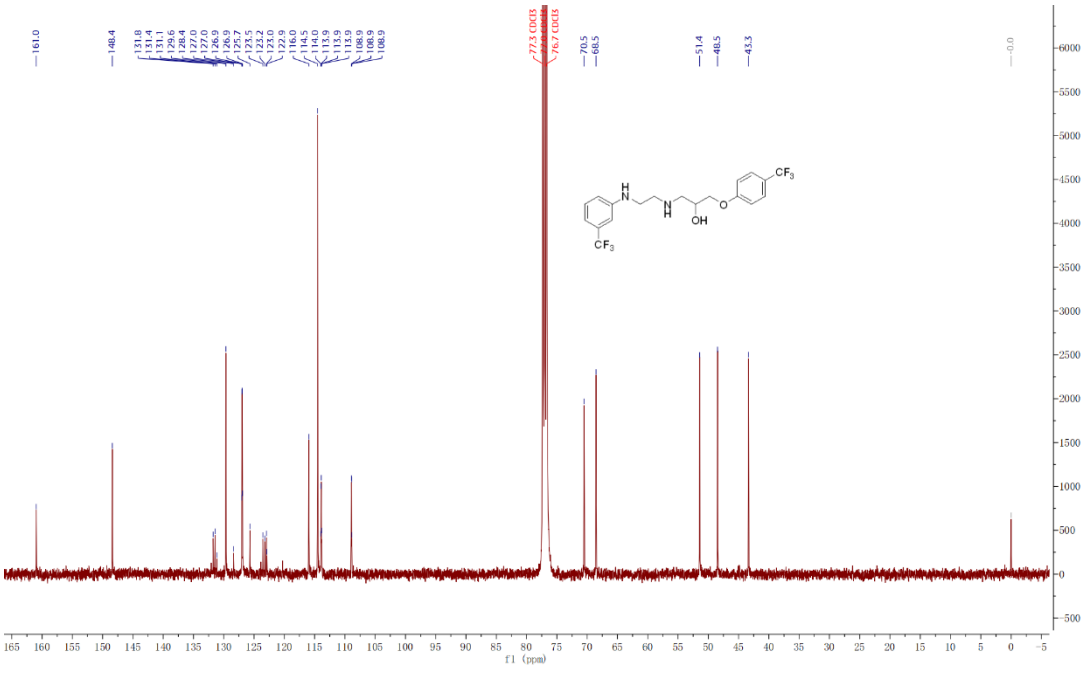
161.0
148.4
131.8
131.4
131.1
128.6
128.4
127.0
127.0
126.9
126.9
125.7
123.5
123.2
123.0
122.9
116.0
114.5
114.0
113.9
113.9
113.9
108.9
106.9
106.9
77.3 CDCl3
77.0
76.7 CDCl3
70.5
68.5
51.4
48.5
43.3
-0.0
CF3
CF3
OH
f1 (ppm)

GI-19

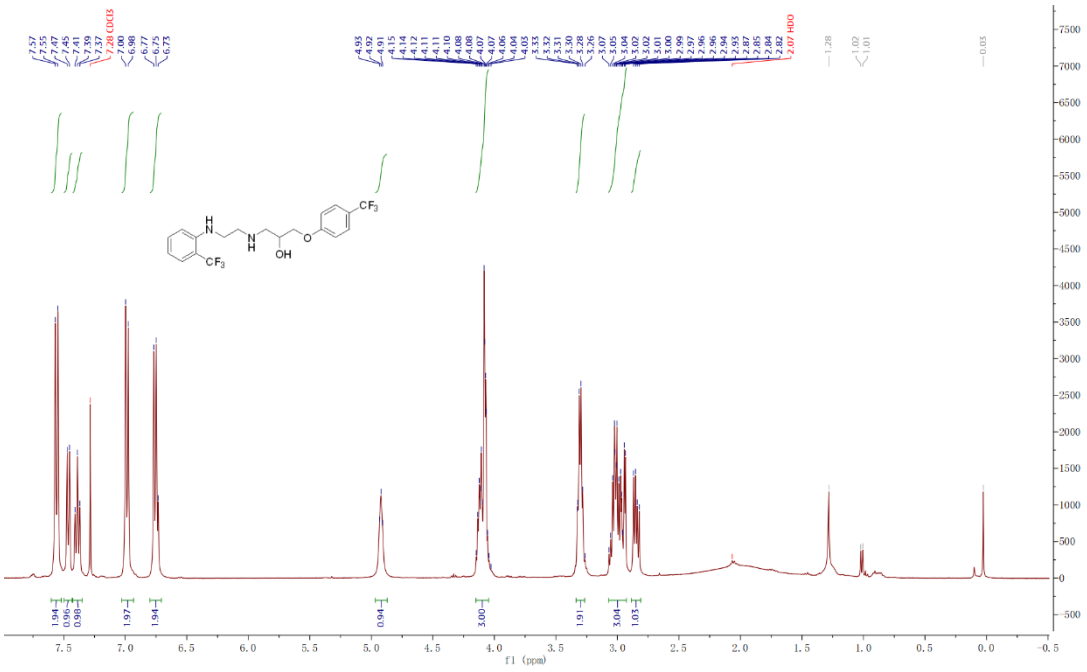

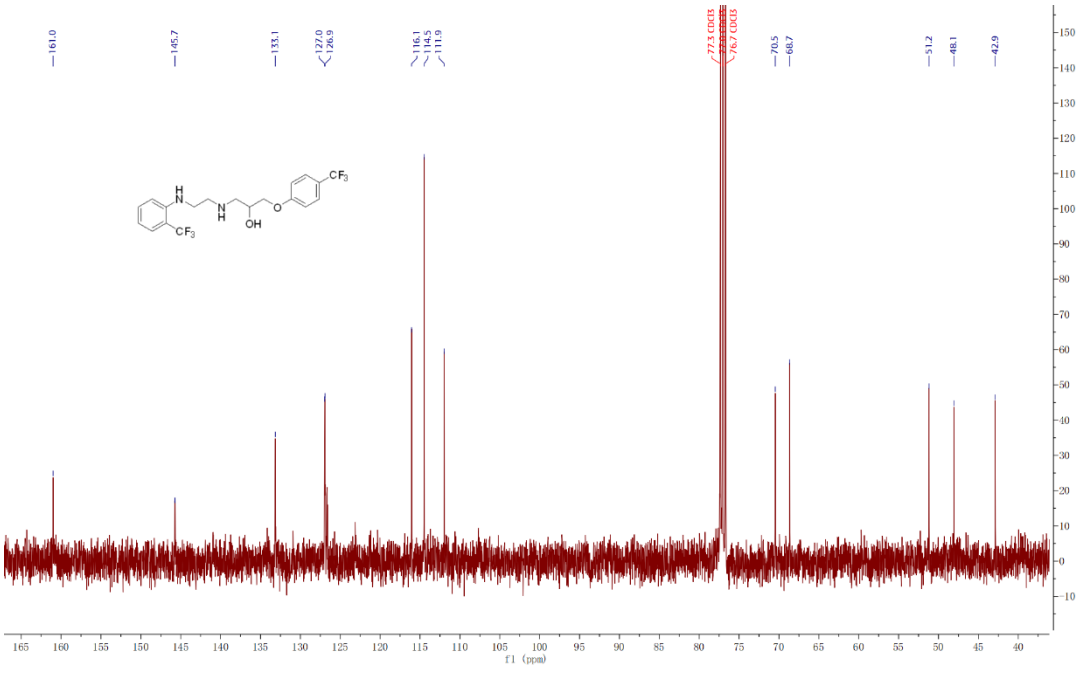

GI-20

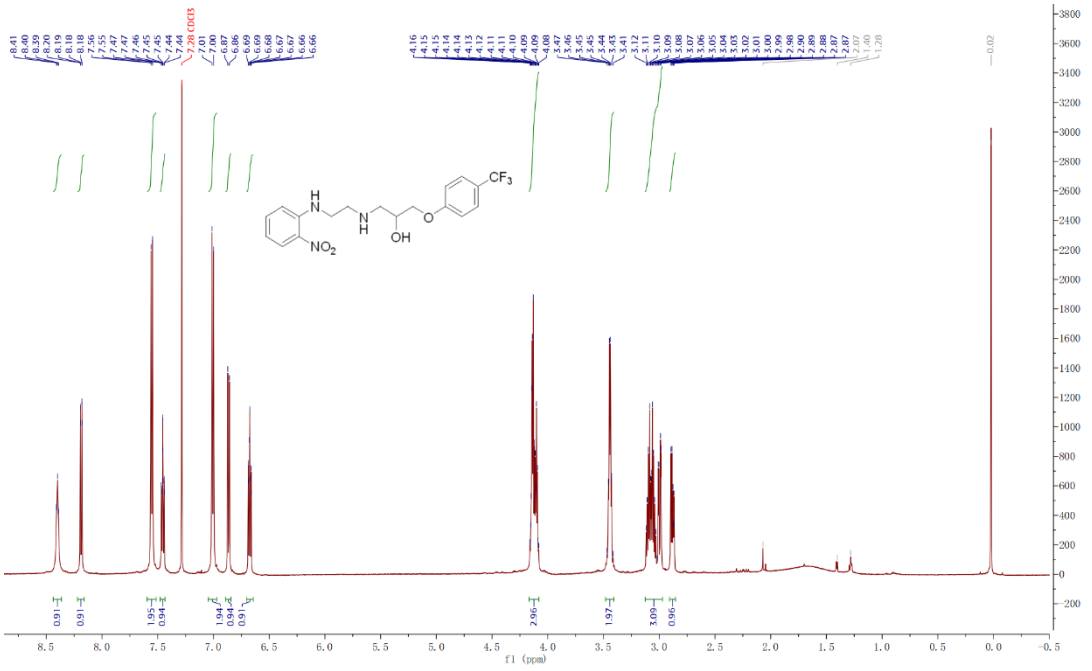

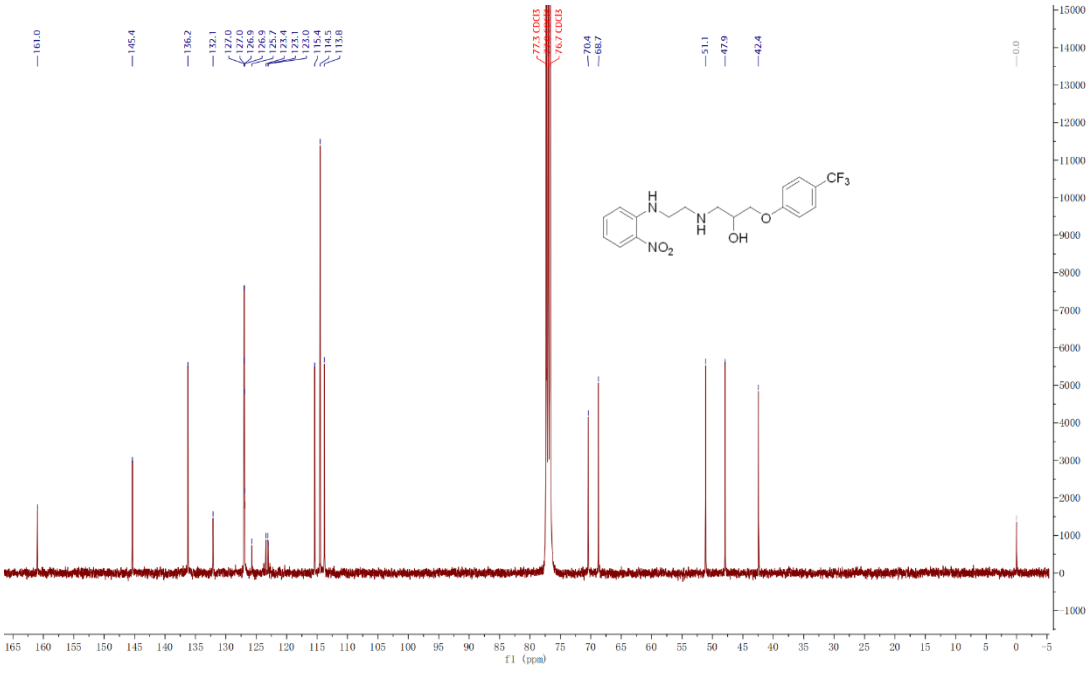

GI-21

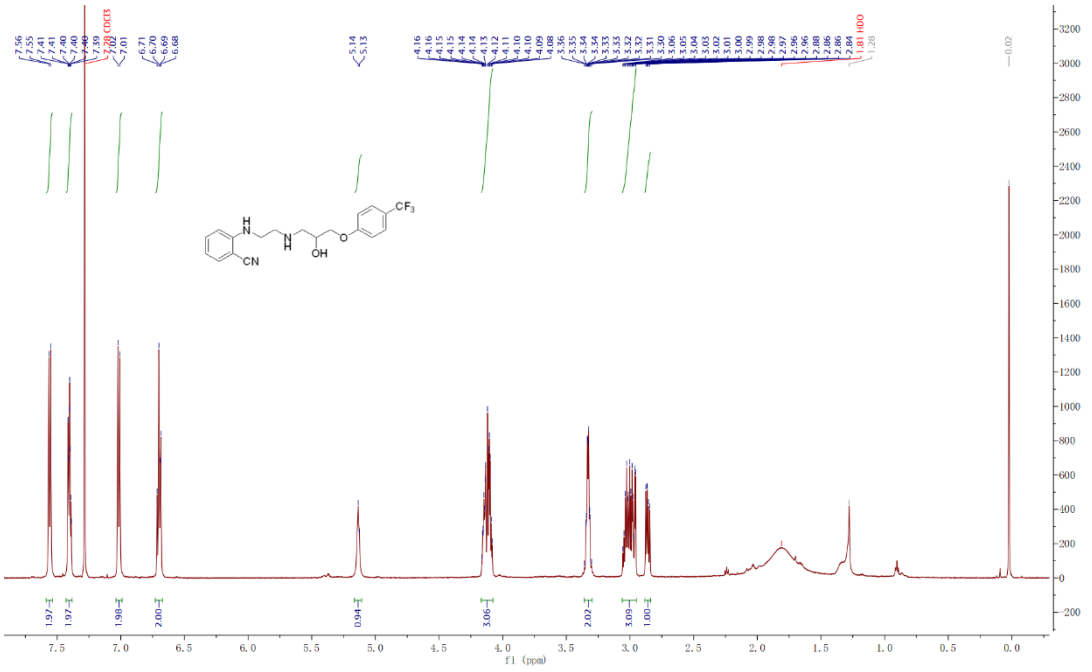
7.56
7.55
7.41
7.41
7.40
7.40
7.40
7.39
7.28 CDCl3
7.01
6.71
6.70
6.69
6.68
5.14
5.13
4.16
4.16
4.15
4.15
4.15
4.14
4.13
4.12
4.11
4.10
4.10
4.09
4.08
3.36
3.35
3.34
3.34
3.33
3.33
3.32
3.32
3.31
3.30
3.30
3.06
3.05
3.04
3.03
3.02
3.01
3.00
2.99
2.98
2.98
2.97
2.96
2.96
2.88
2.86
2.86
2.84
1.81 H2O
1.26
0.02
CF3
H
N
CN
N
H
OH
O
1.97
1.97
1.98
2.00
0.94
3.06
2.02
3.09
1.00
f1 (ppm)

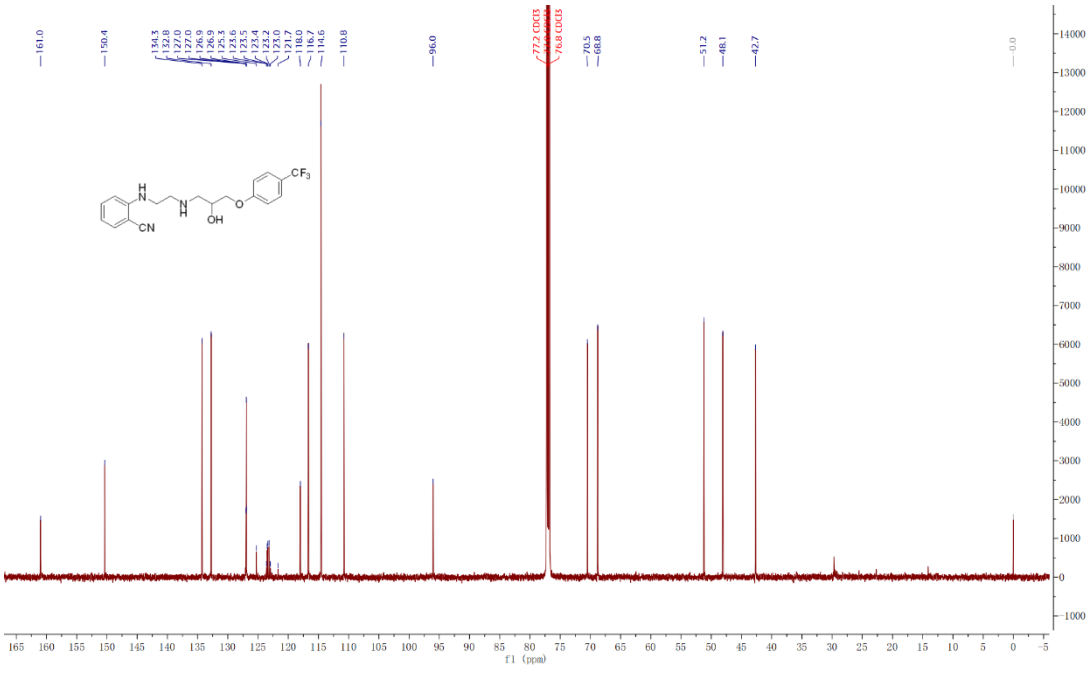
161.0
150.4
134.3
132.8
127.0
127.0
126.9
126.8
125.3
123.6
123.5
123.4
123.2
123.0
121.7
118.0
116.7
116.6
110.8
96.0
77.2 CDCl3
76.8 CDCl3
70.5
68.8
51.2
48.1
42.7
0.0
CF3
H
N
CN
N
H
OH
O
f1 (ppm)

GI-22

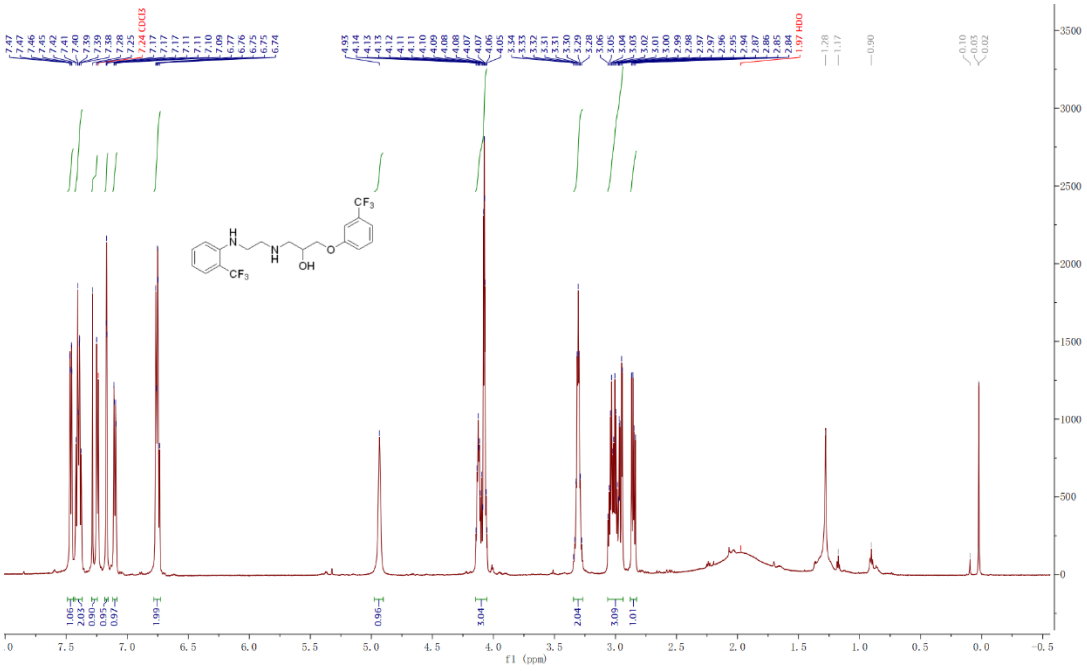

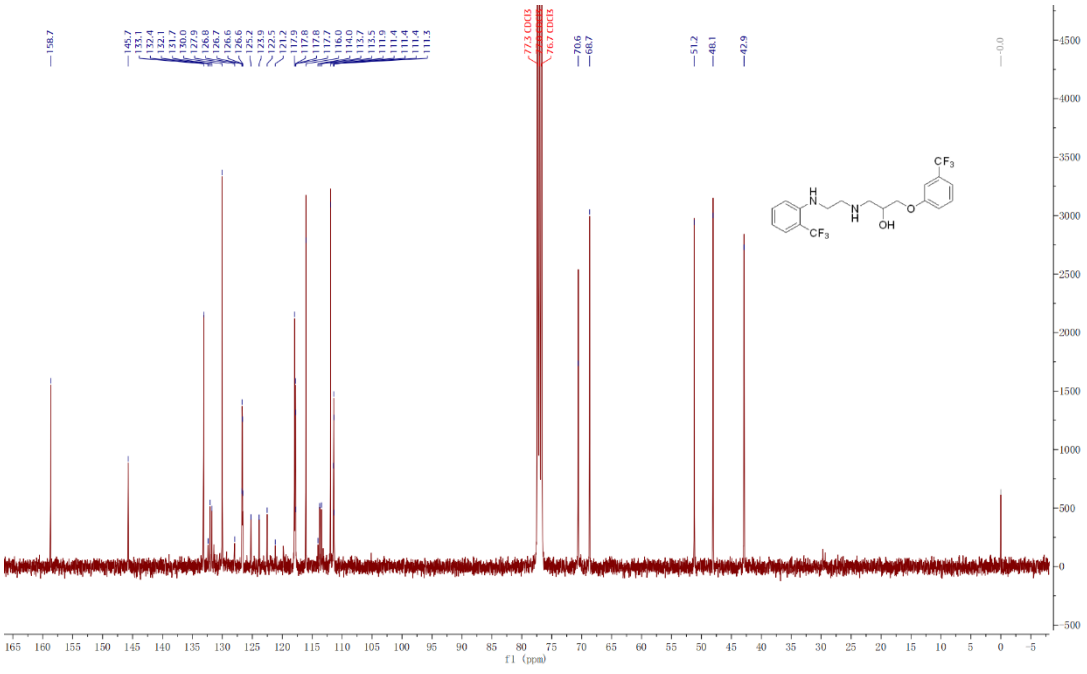

GI-23

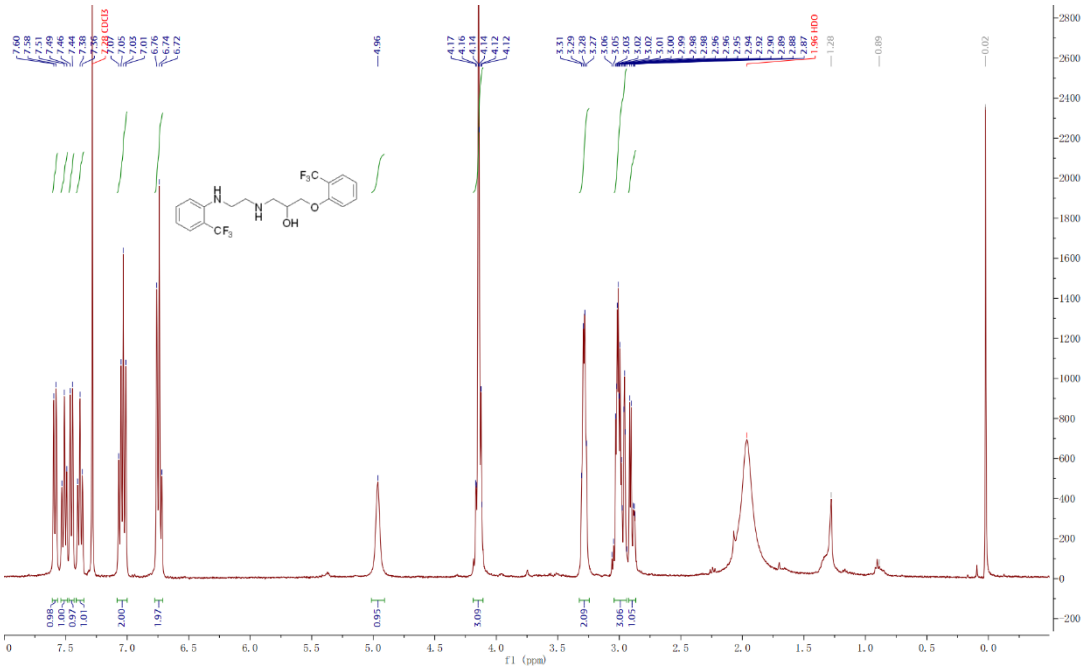

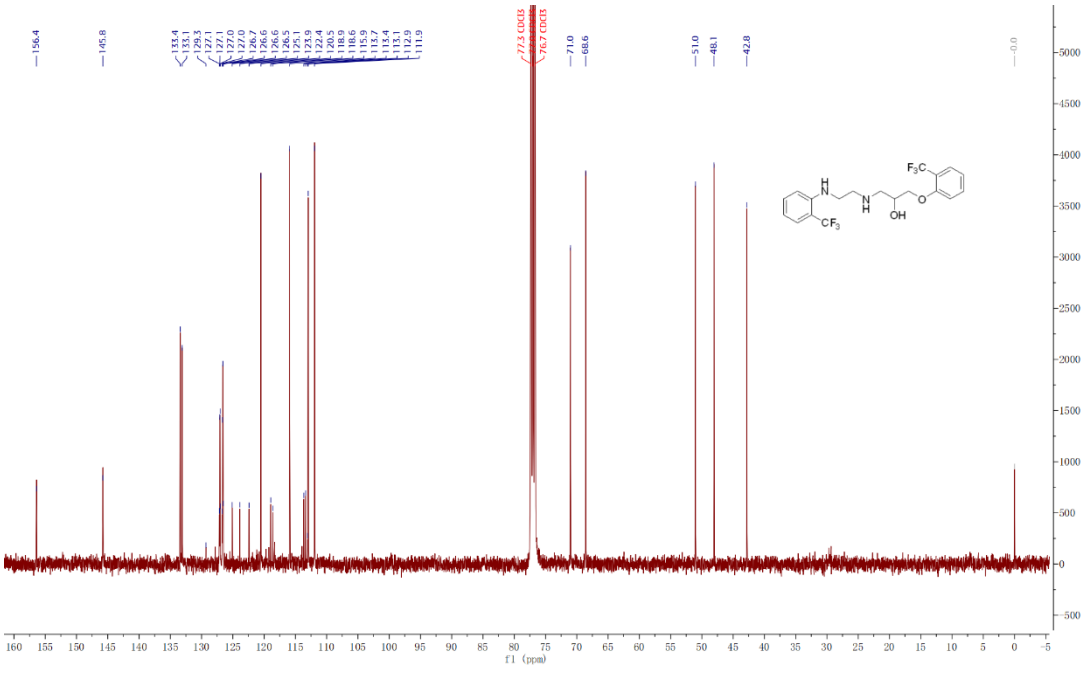

GI-24

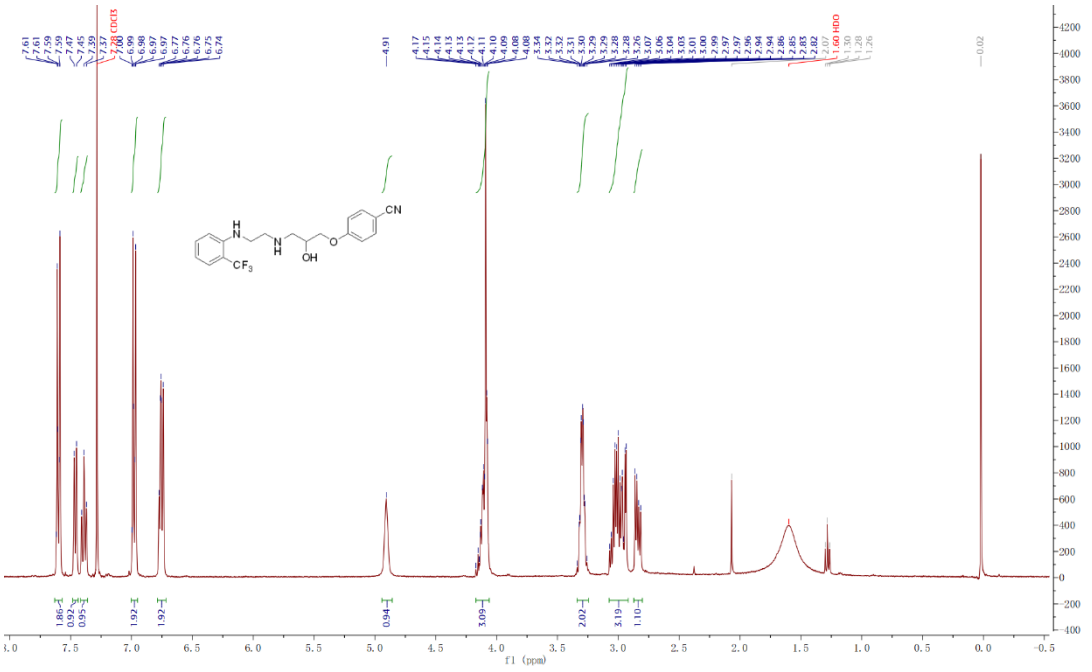

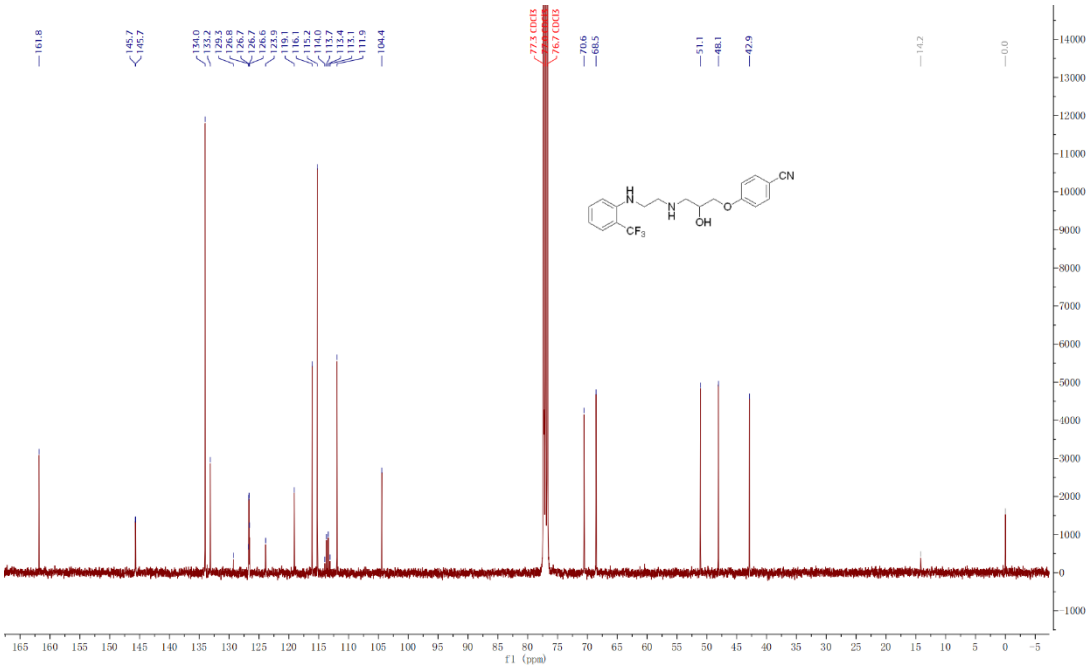

GI-25

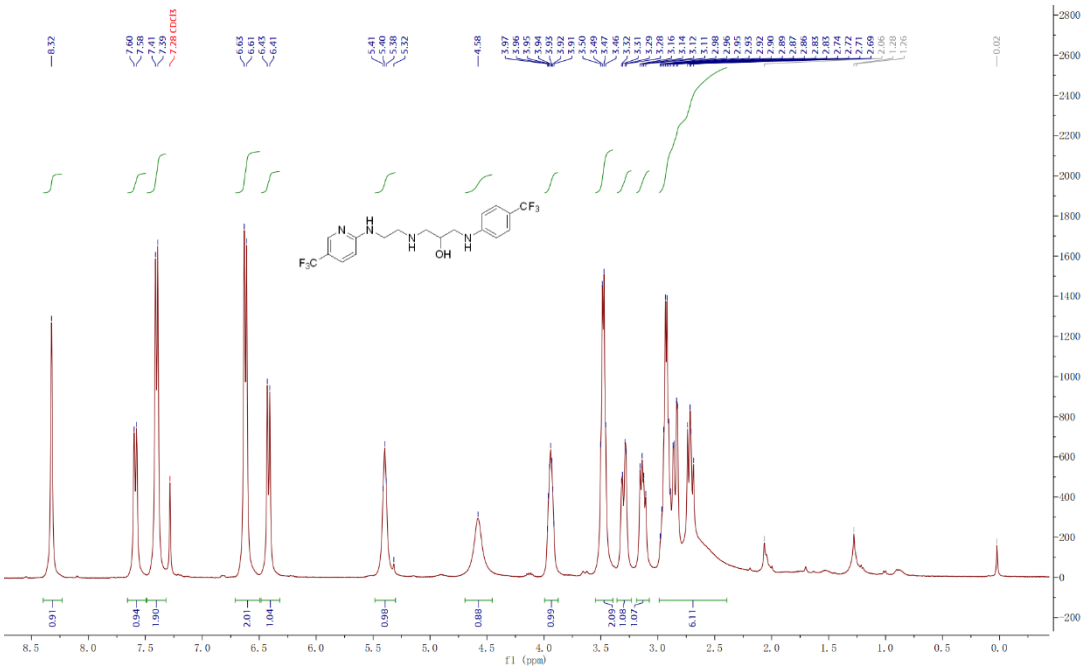

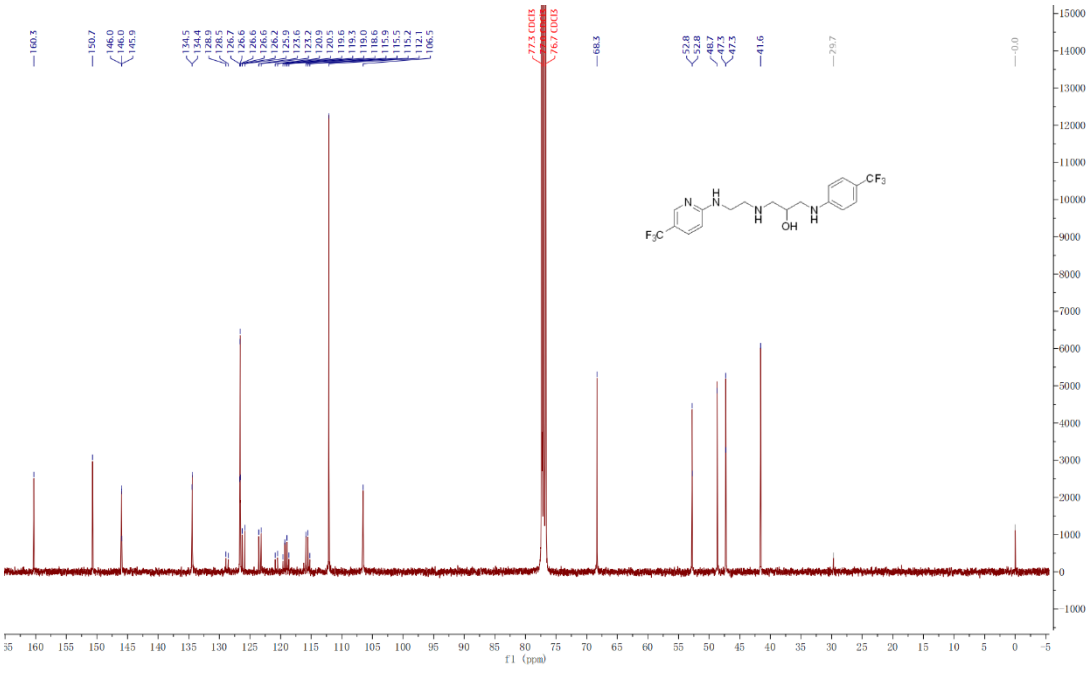

GI-26

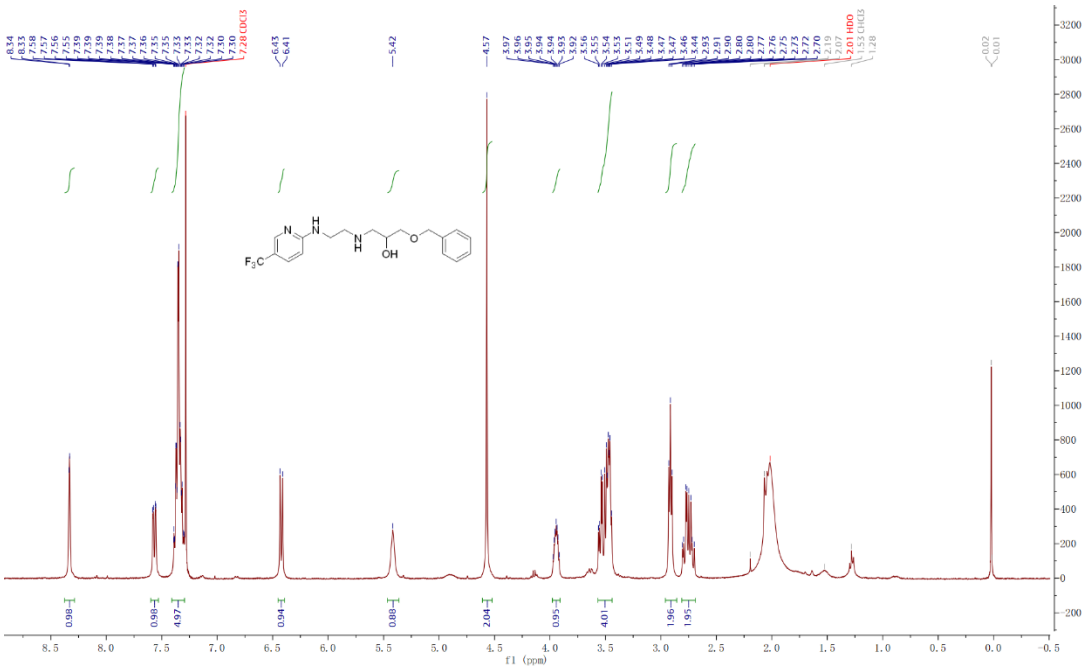

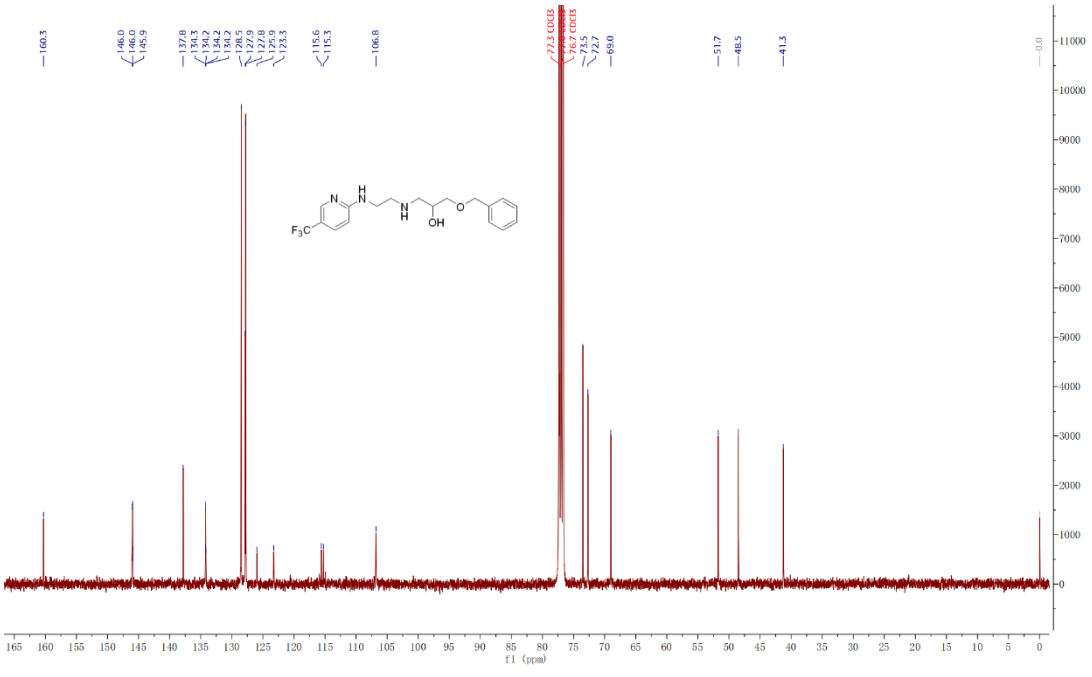

GI-27

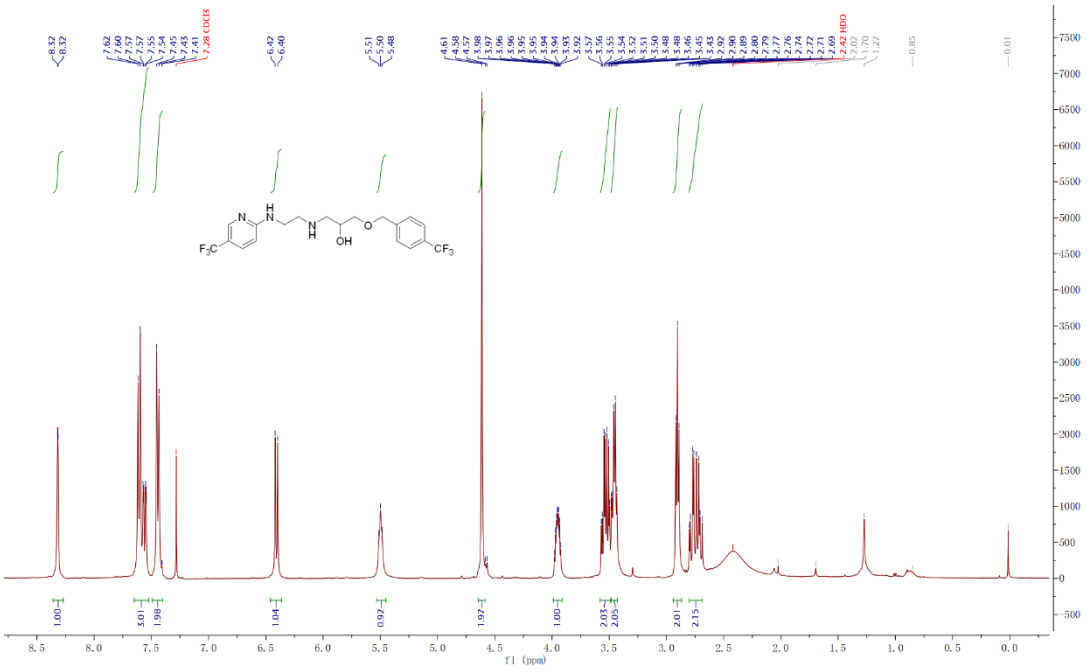

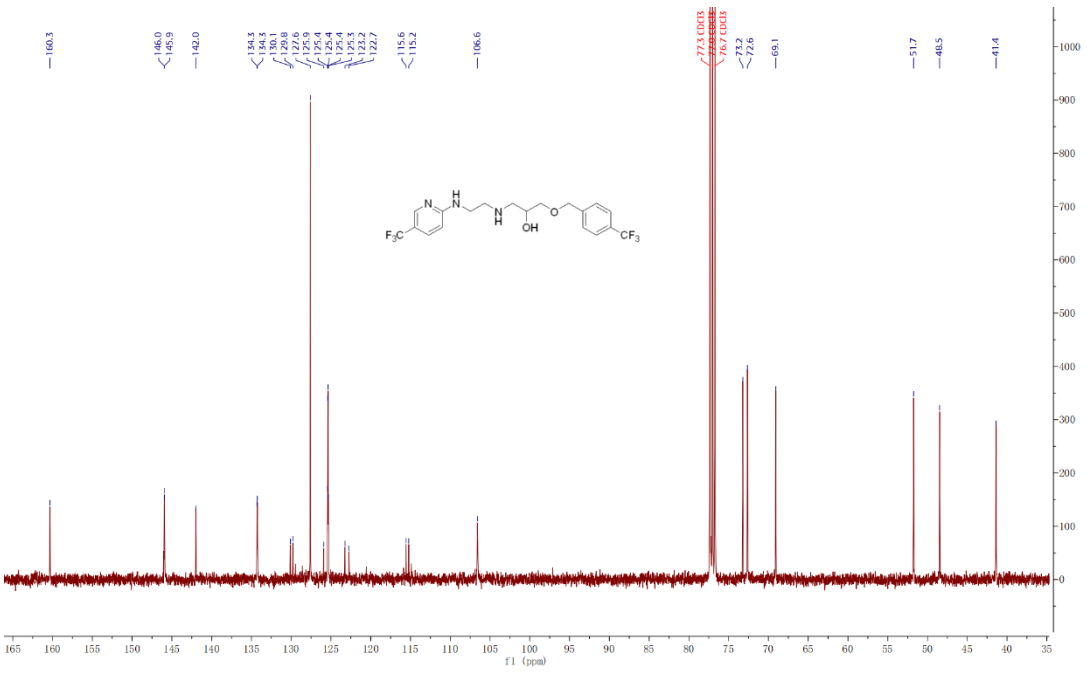

GI-28

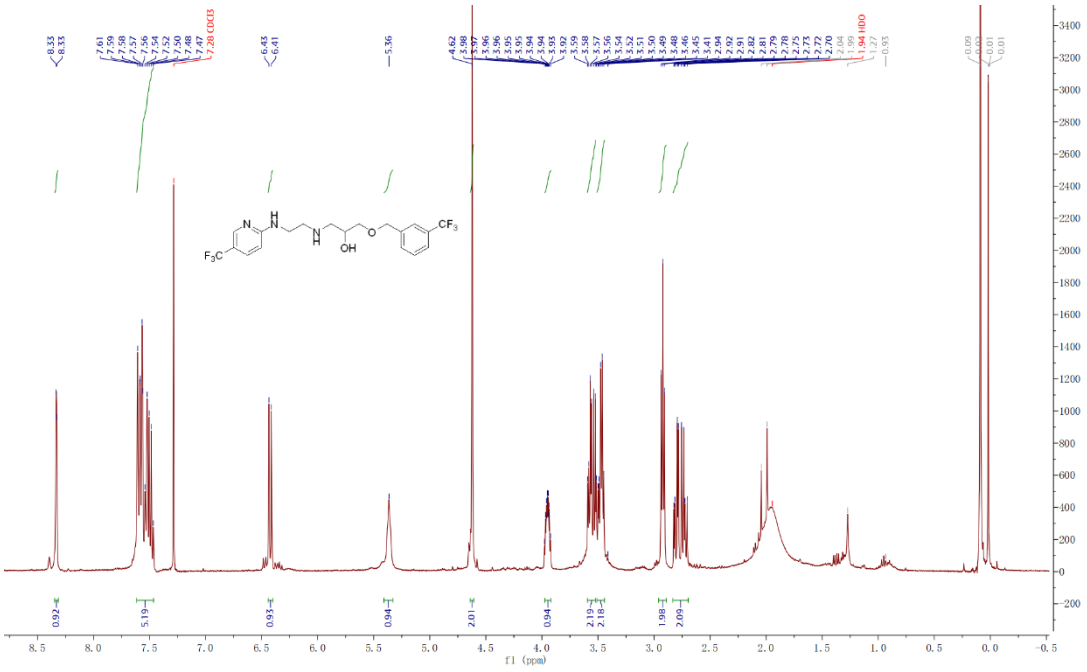

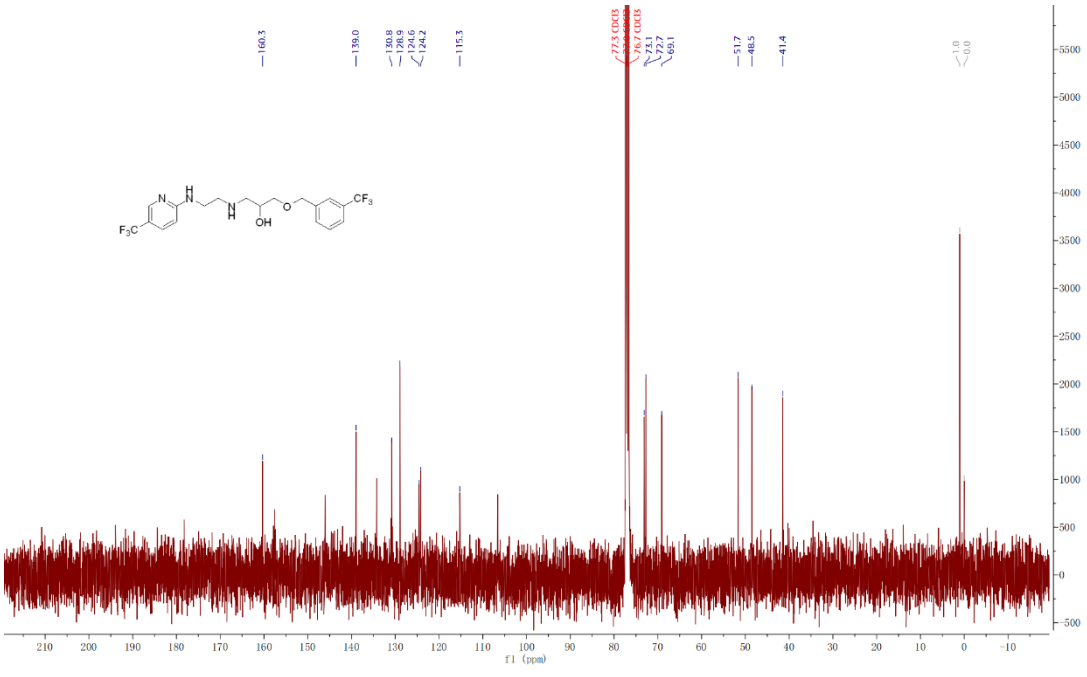

GI-29

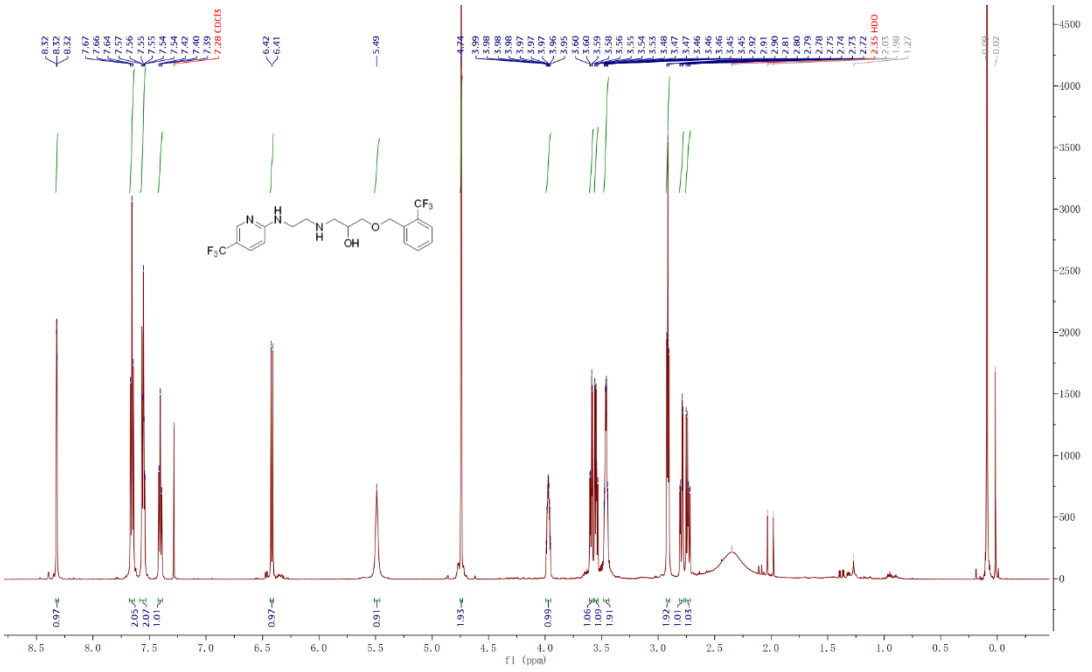

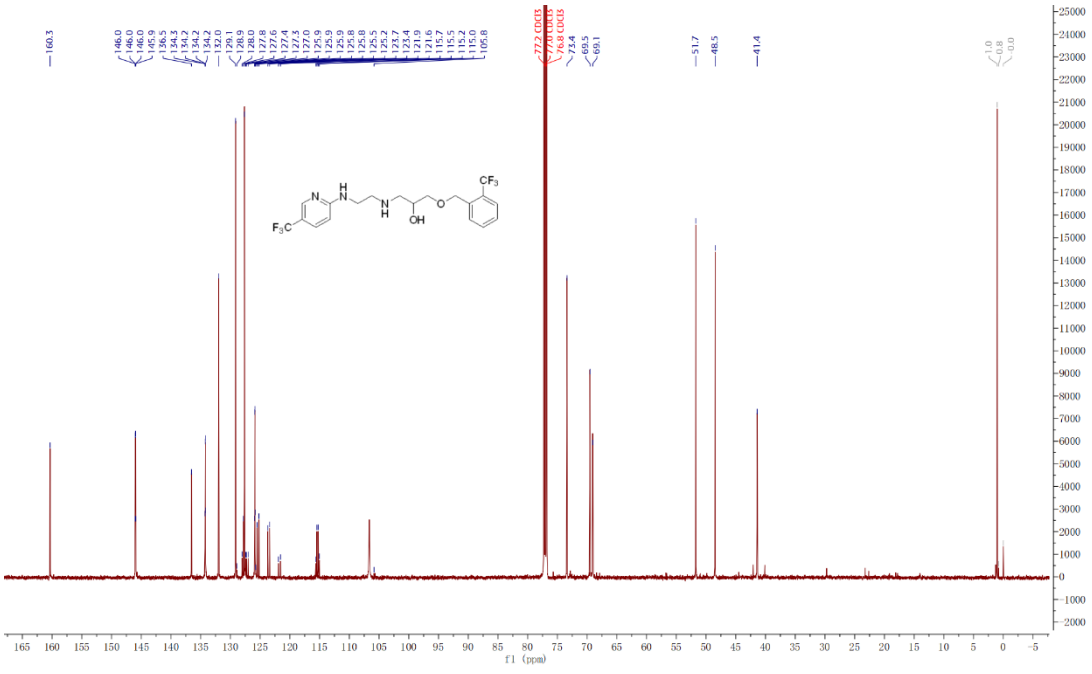

GI-30

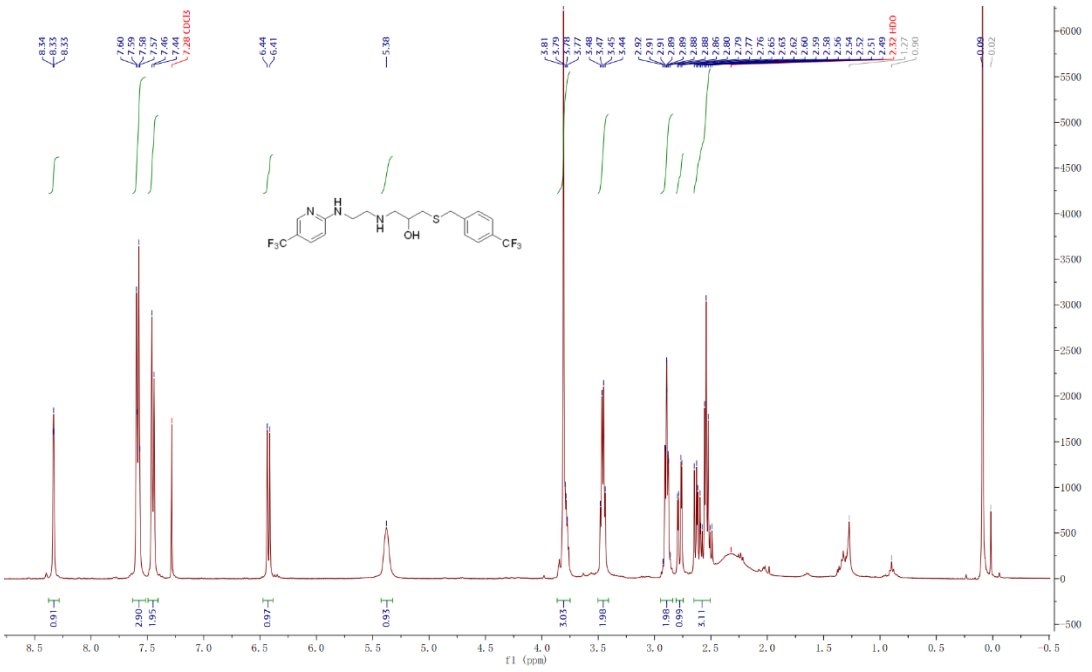
8.34
8.33
8.33
7.60
7.59
7.58
7.52
7.46
7.44
7.28 CDCl3
6.44
6.41
5.38
5.81
5.79
5.78
5.77
5.48
3.47
3.45
3.44
2.92
2.91
2.91
2.89
2.89
2.88
2.88
2.86
2.80
2.79
2.77
2.76
2.65
2.63
2.62
2.60
2.59
2.58
2.56
2.54
2.52
2.51
2.49
2.32 HDO
1.27
0.90
0.09
0.02
0.91
2.90
1.95
0.97
0.93
3.03
1.98
1.98
0.99
3.11
f1 (ppm)

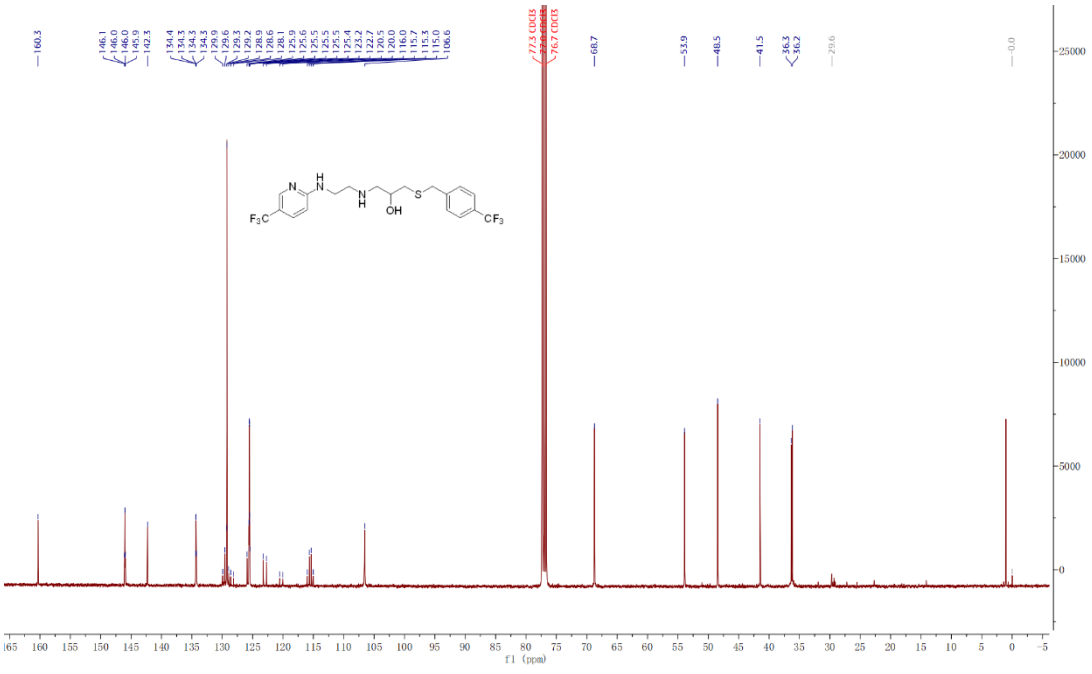
160.3
146.1
146.0
146.0
145.9
142.3
134.4
134.3
134.3
134.3
129.9
129.6
129.3
129.2
128.9
128.6
128.1
125.9
125.6
125.5
125.5
125.5
125.4
123.2
122.7
120.5
120.0
116.0
115.7
115.3
115.0
106.6
77.5 CDCl3
77.0
76.7 CDCl3
68.7
53.9
48.5
41.5
36.3
36.2
29.6
0.0
f1 (ppm)

GI-31

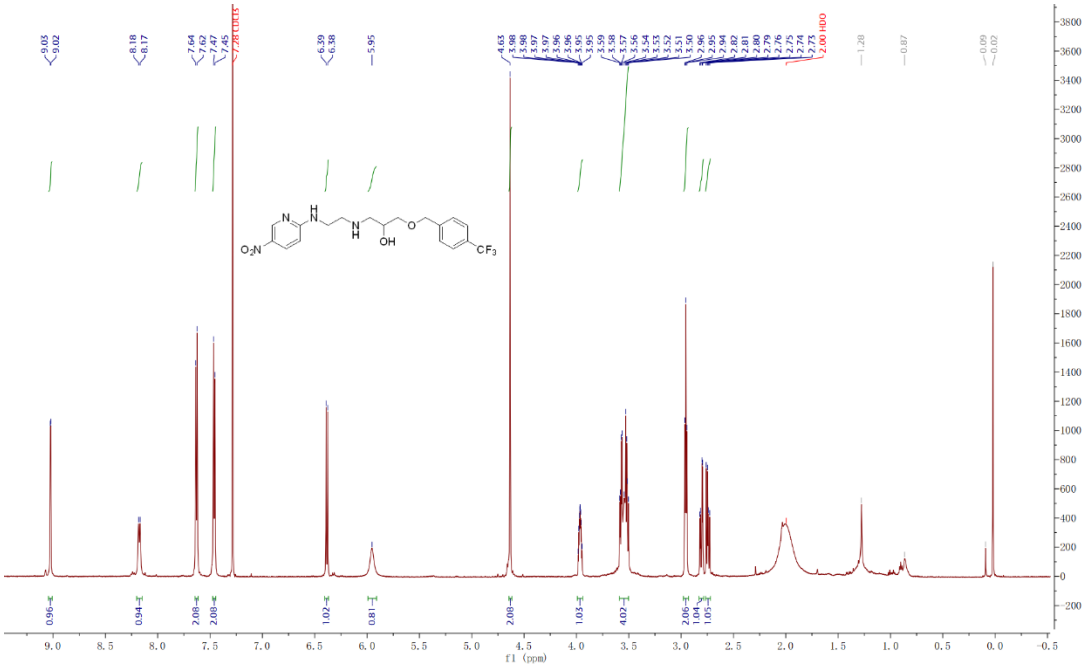
9.03
9.02
8.18
8.17
7.64
7.62
7.47
7.46
7.26 CDCl3
6.39
6.38
5.95
4.63
3.98
3.97
3.96
3.95
3.59
3.58
3.57
3.56
3.54
3.53
3.52
3.51
3.50
2.96
2.95
2.94
2.82
2.81
2.80
2.79
2.76
2.75
2.74
2.73
2.00 HDO
1.28
0.87
0.09
0.02
0.96
0.94
2.08
2.08
1.02
0.81
2.08
1.03
4.02
2.06
1.04
1.05
f1 (ppm)

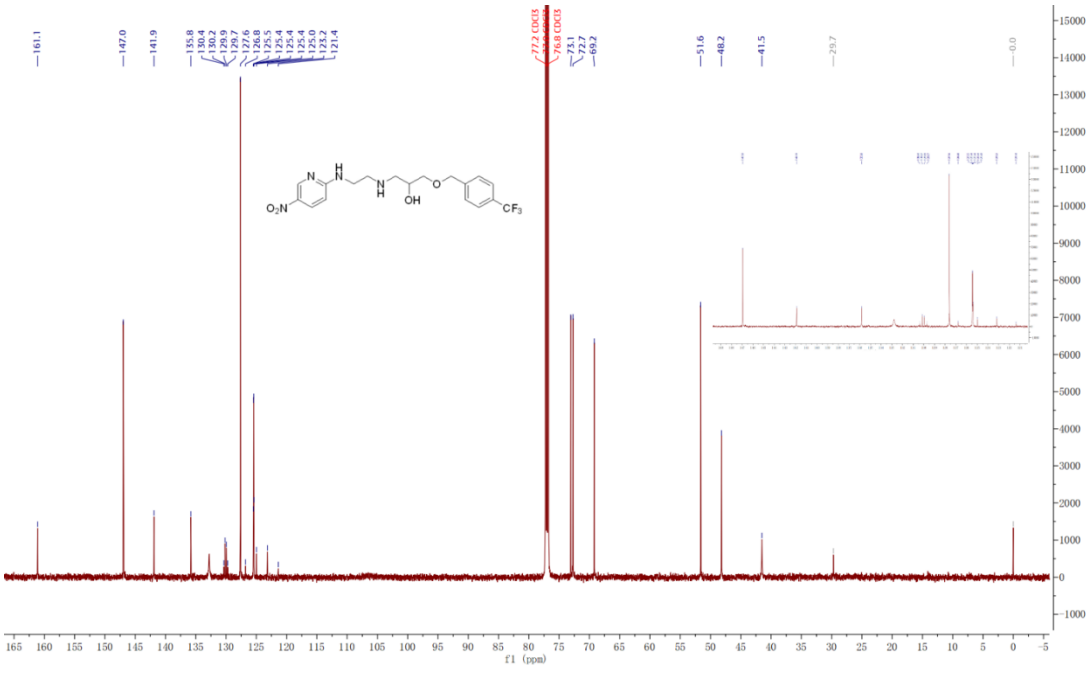
161.1
147.0
141.9
135.8
130.4
130.2
129.9
129.7
127.6
126.8
125.5
125.4
125.4
125.4
125.0
123.2
121.4
77.2 CDCl3
76.8 CDCl3
73.1
72.7
69.2
51.6
48.2
41.5
29.7
0.0
f1 (ppm)

GI-32

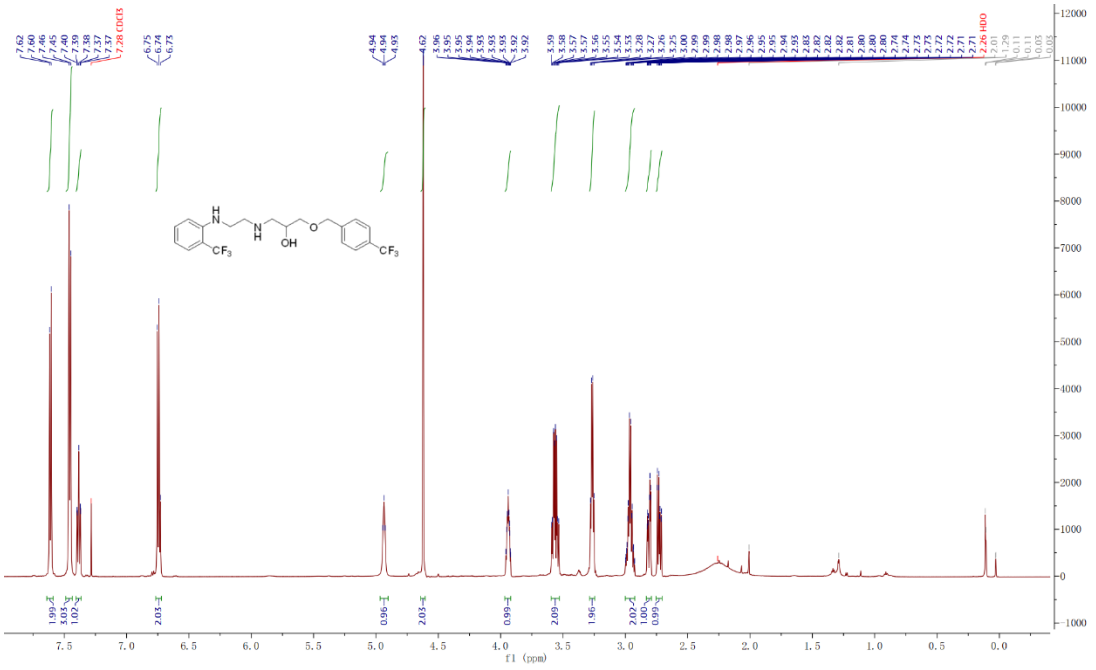

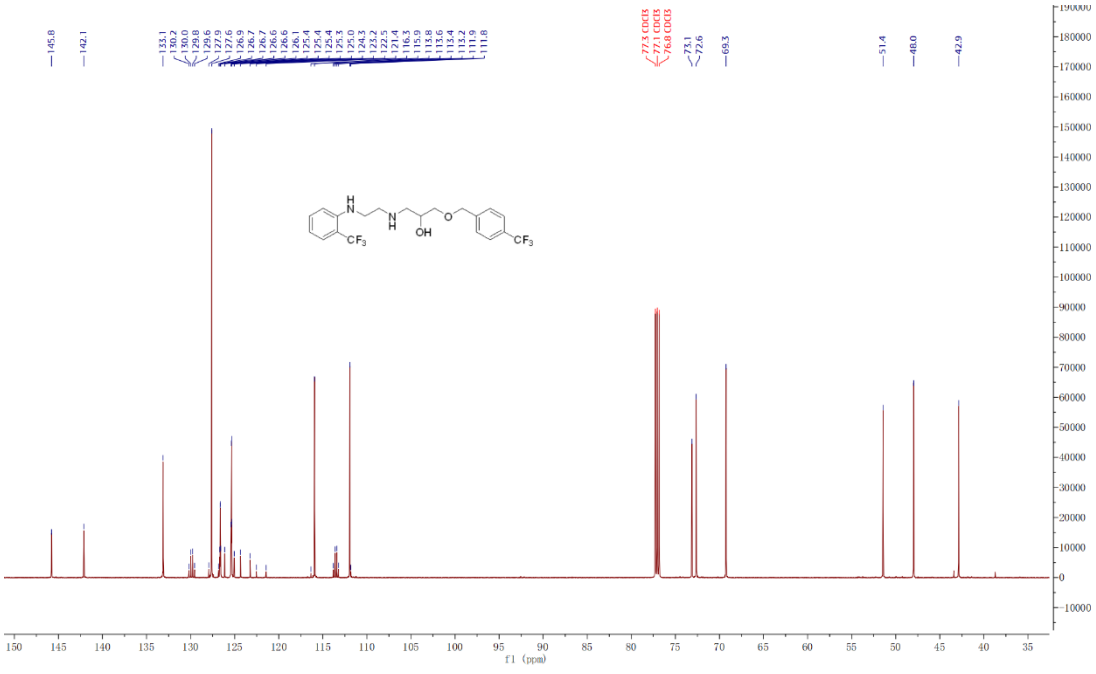

GI-33

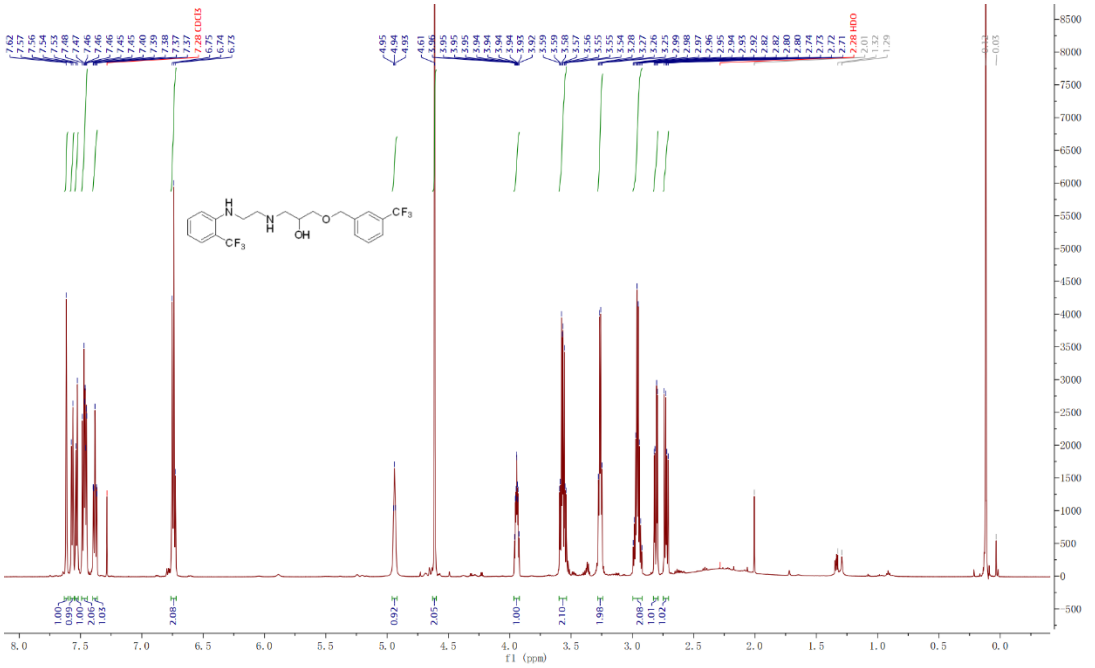

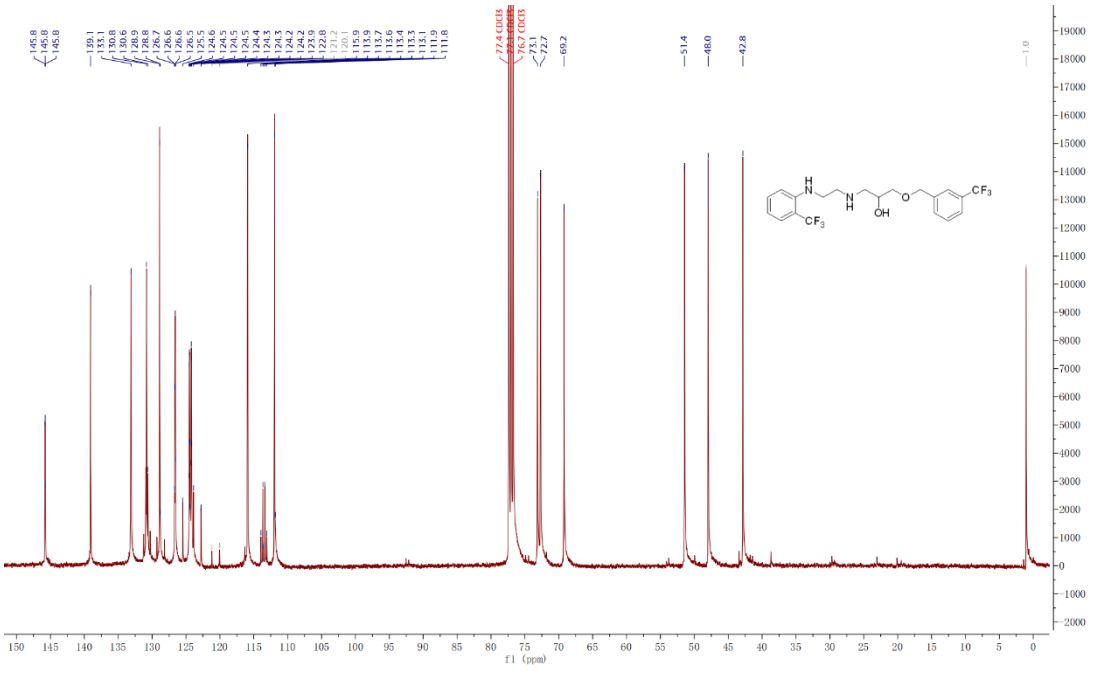

GI-34

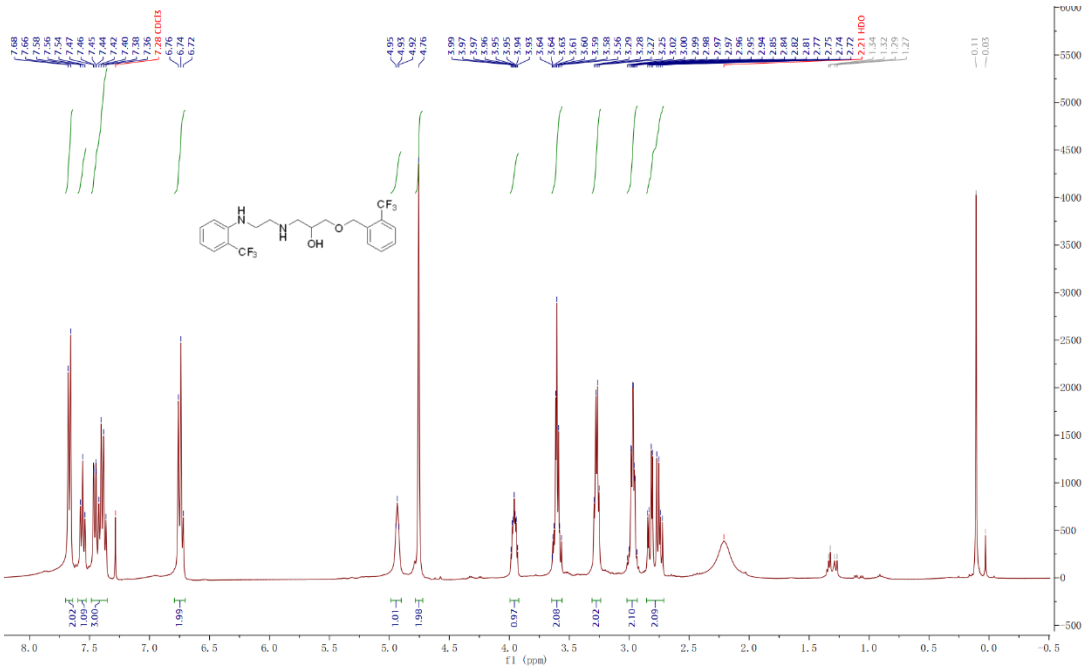

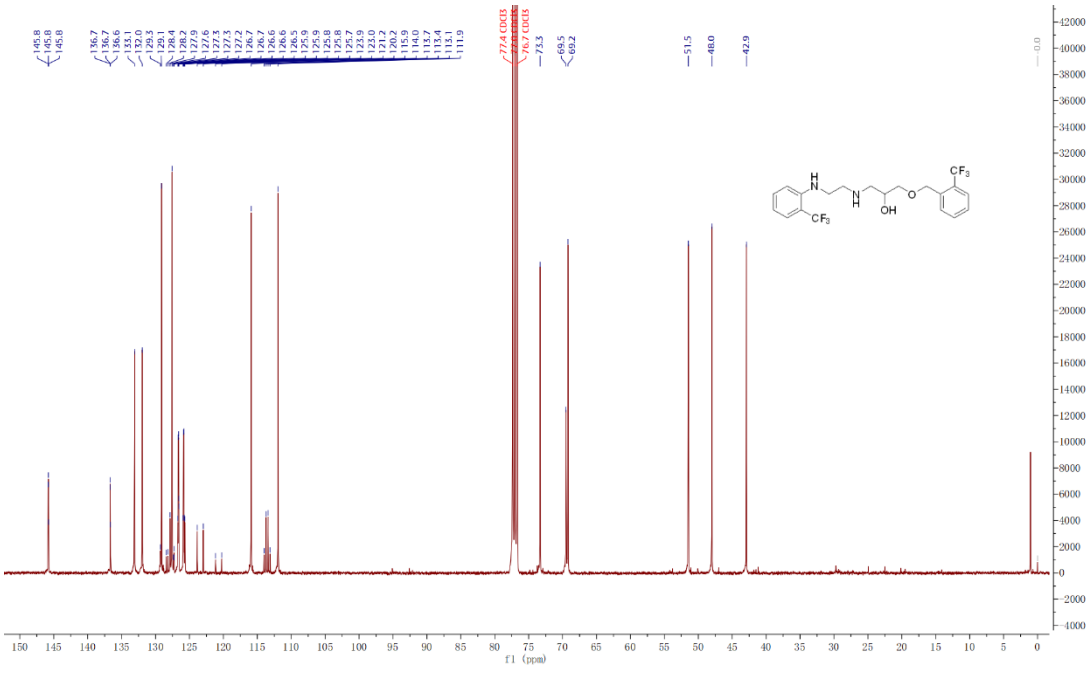

GI-35

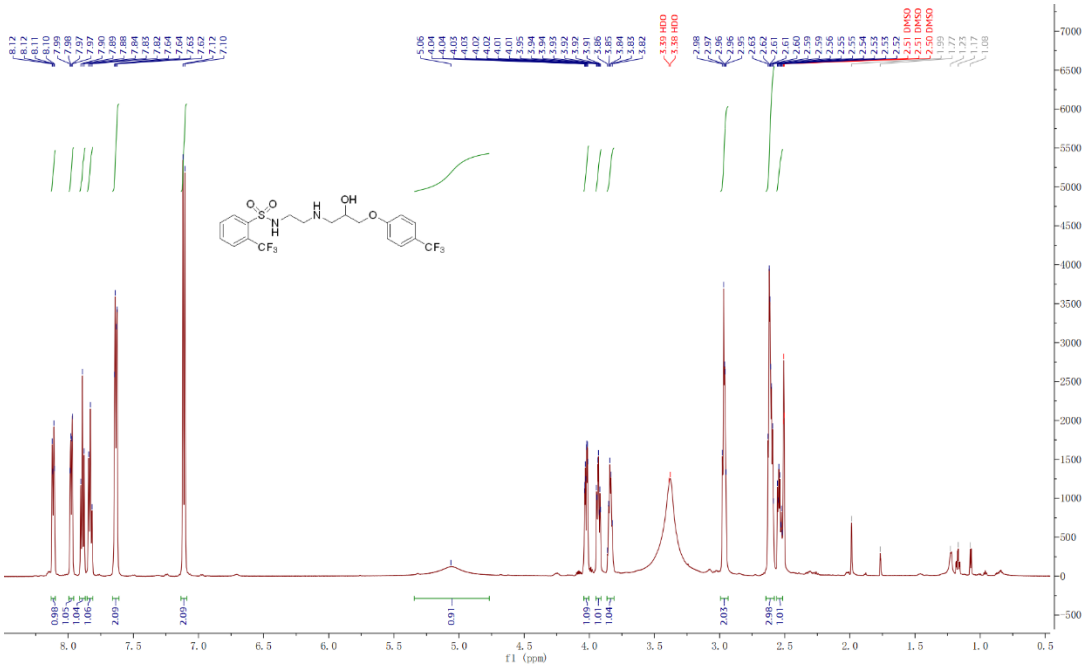

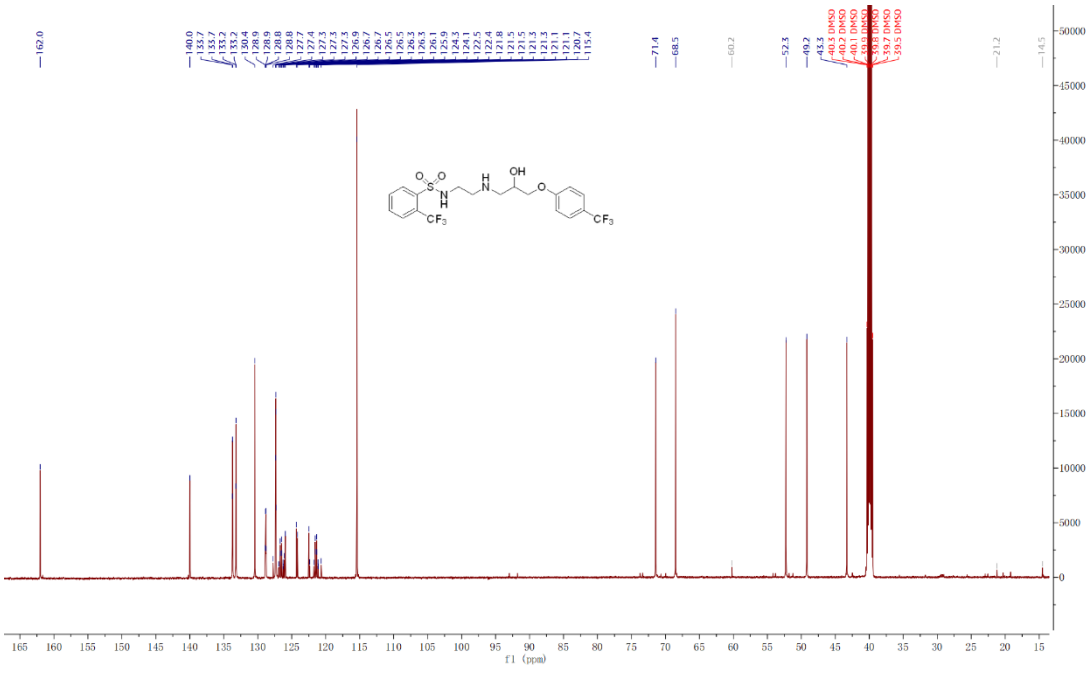

GI-36

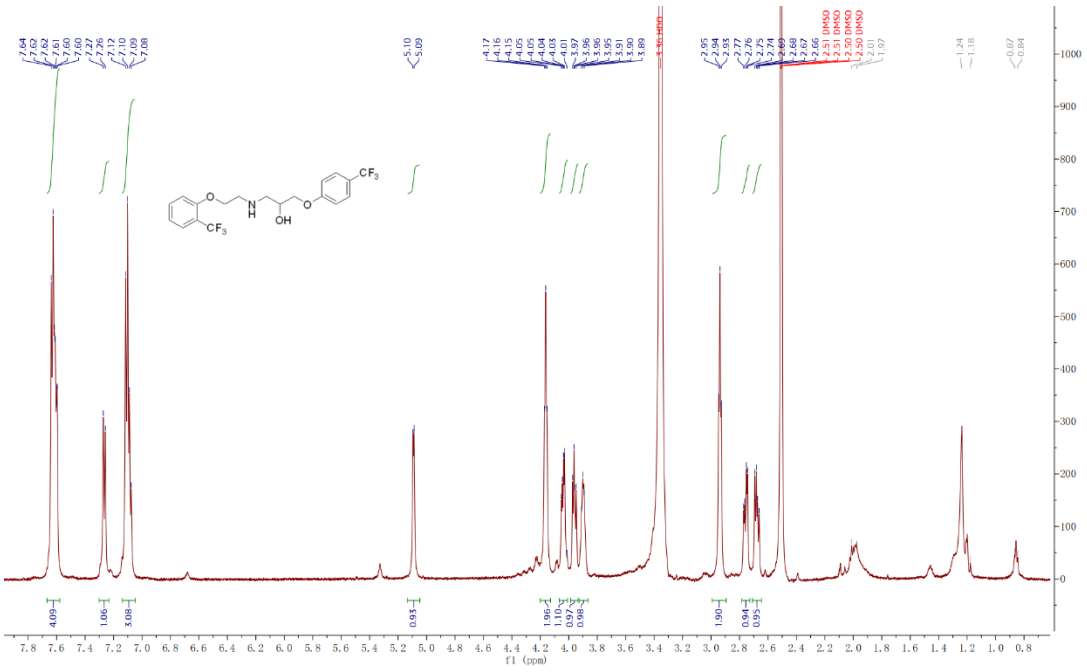

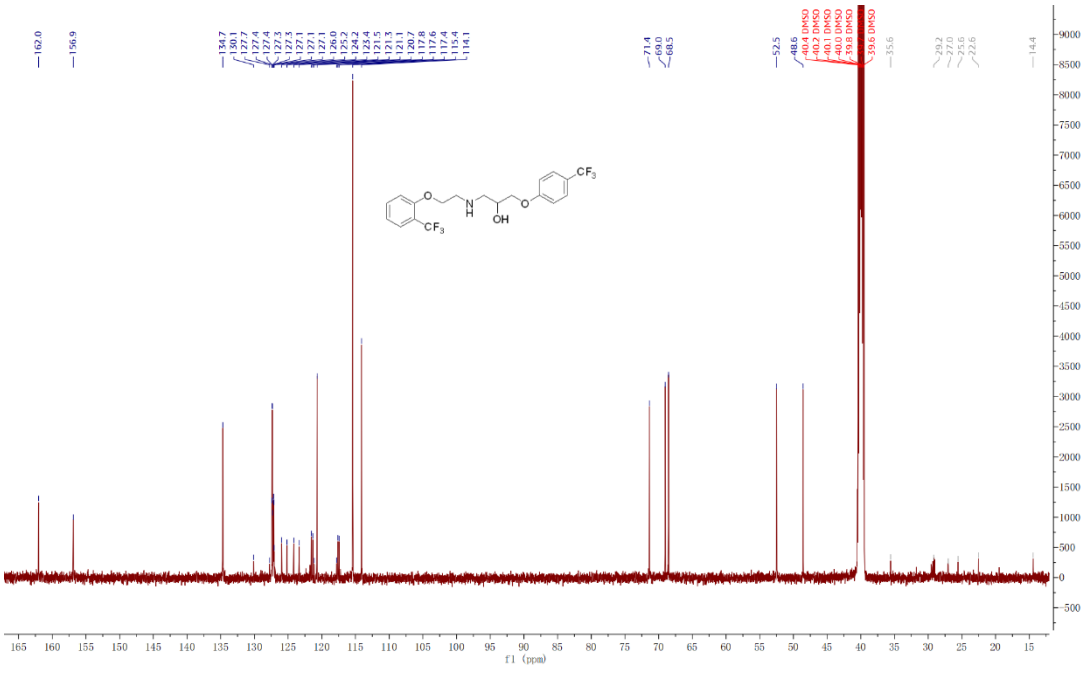

GI-37

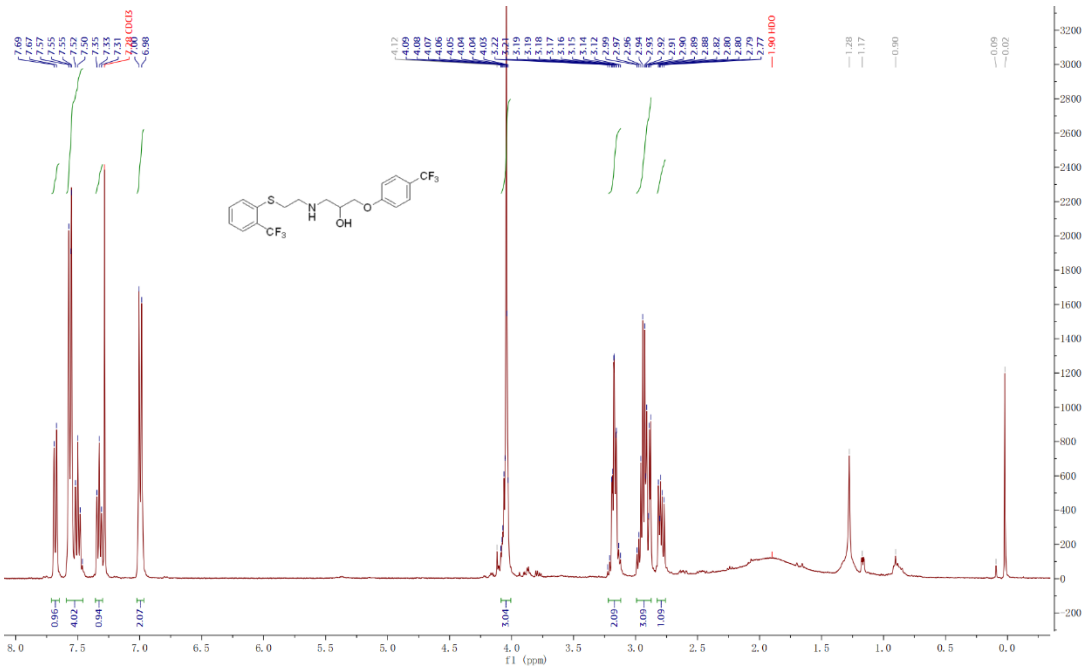

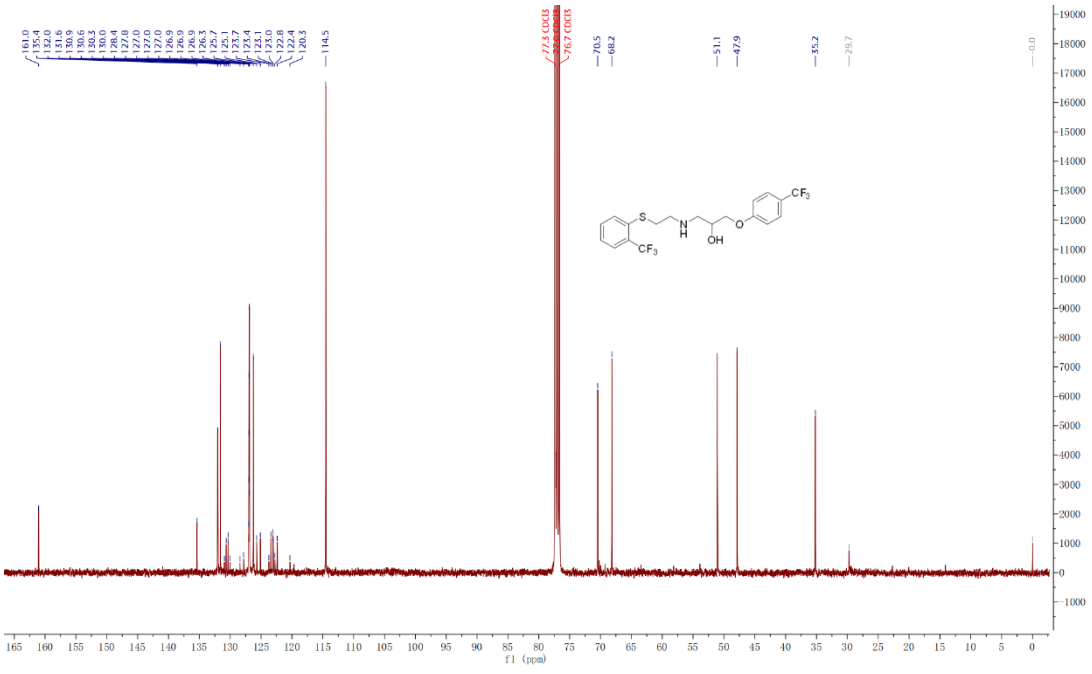

GI-38

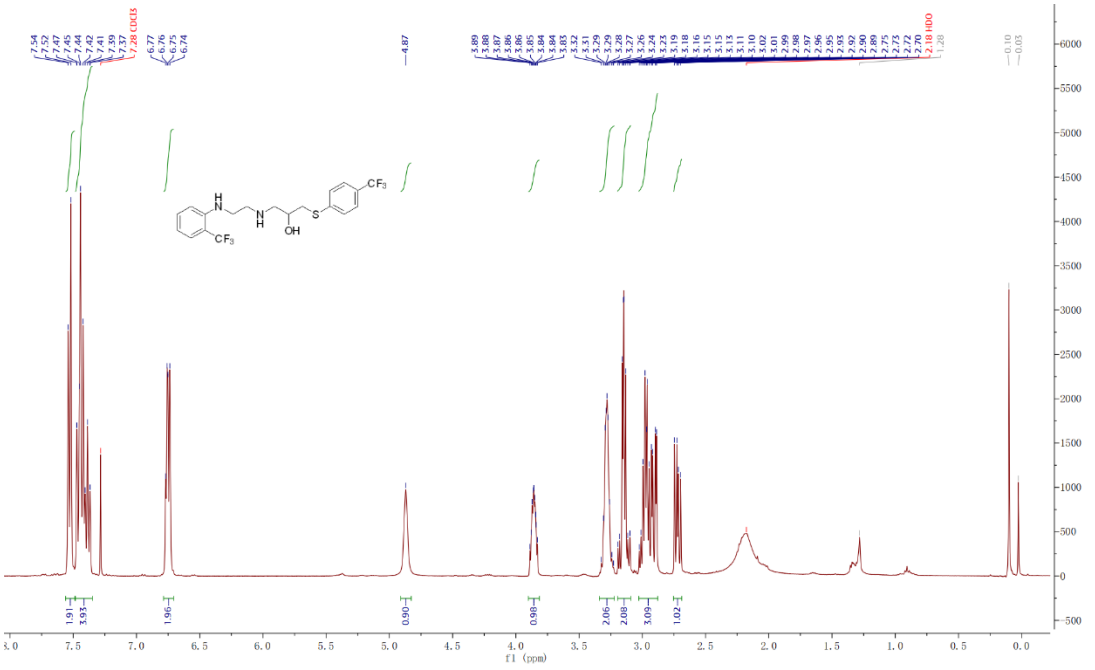

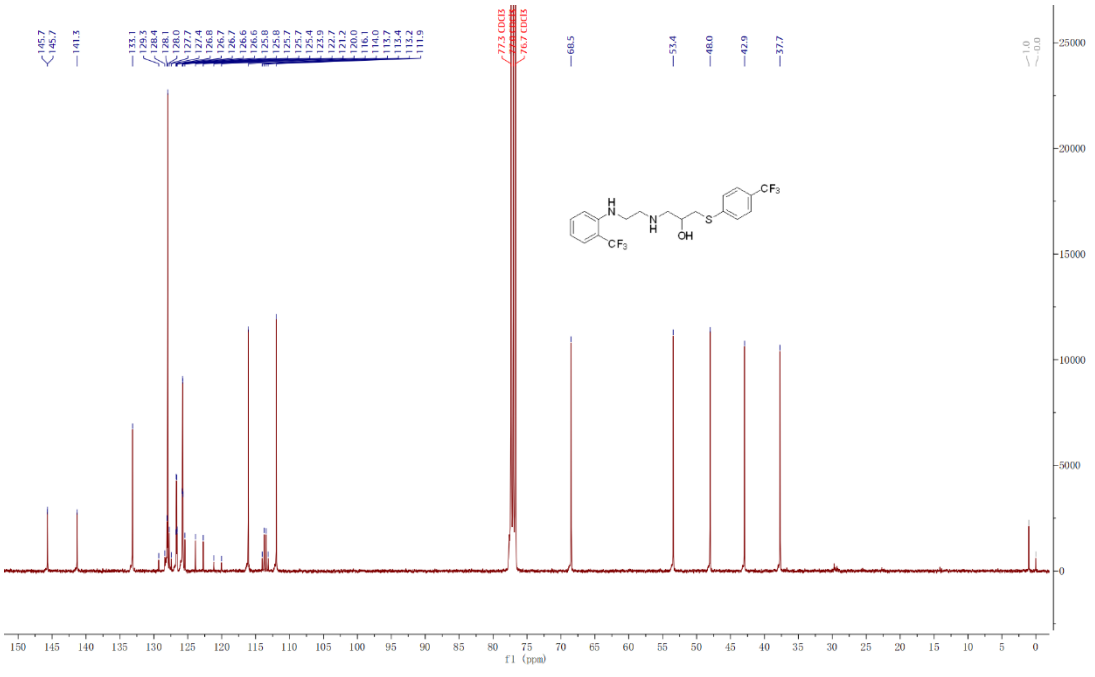

GI-39

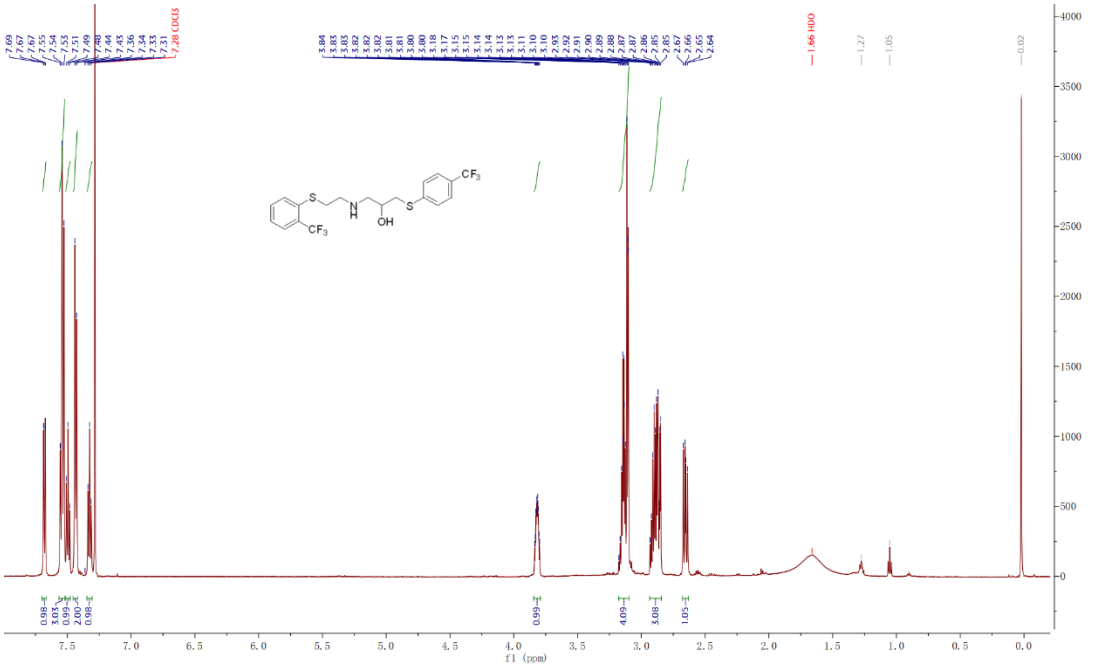
7.69
7.67
7.67
7.55
7.54
7.53
7.51
7.49
7.49
7.44
7.43
7.36
7.34
7.33
7.31
7.28 CDCl3
3.84
3.83
3.83
3.82
3.82
3.82
3.81
3.81
3.80
3.80
3.18
3.17
3.15
3.15
3.14
3.14
3.13
3.13
3.11
3.10
3.10
2.93
2.92
2.91
2.90
2.89
2.88
2.87
2.87
2.86
2.85
2.85
2.67
2.66
2.65
2.64
1.66 HDO
1.27
1.05
0.02
CF3
S
N
H
OH
S
CF3
0.98
3.03
0.95
2.00
0.98
0.99
4.09
3.08
1.05
f1 (ppm)

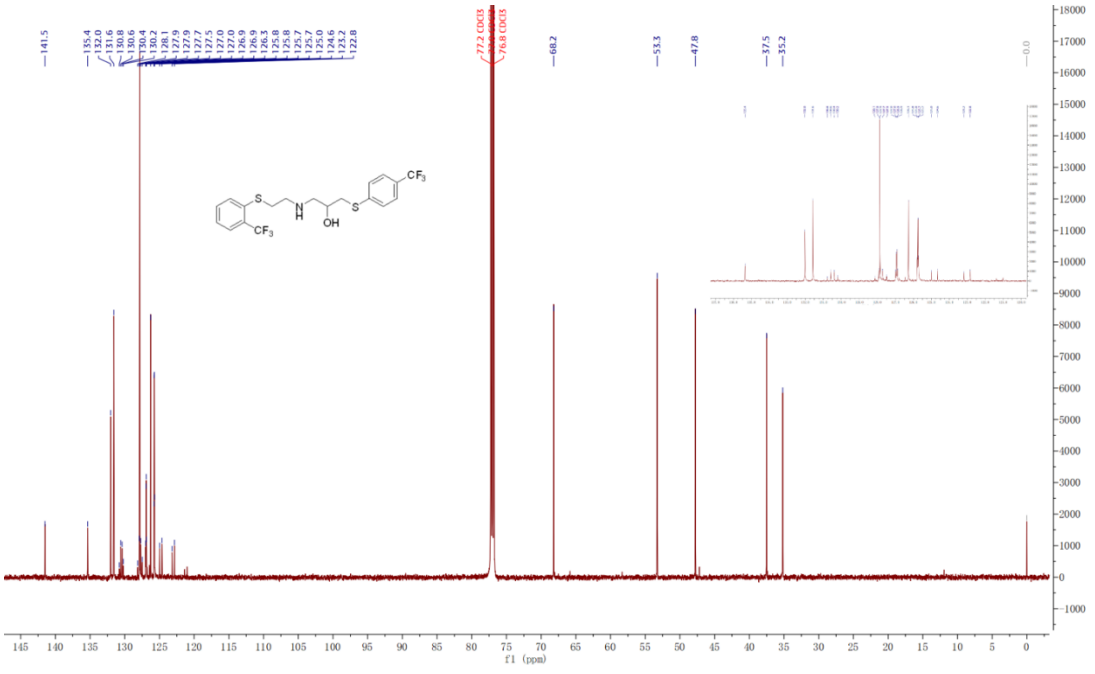
141.5
135.4
132.0
131.6
130.8
130.6
130.4
130.2
128.1
127.9
127.9
127.7
127.5
127.0
127.0
126.9
126.9
126.3
125.8
125.8
125.7
125.7
125.0
124.6
123.2
122.8
77.2 CDCl3
76.8 CDCl3
68.2
53.3
47.8
37.5
35.2
0.0
CF3
S
N
H
OH
S
CF3
f1 (ppm)

GII-1

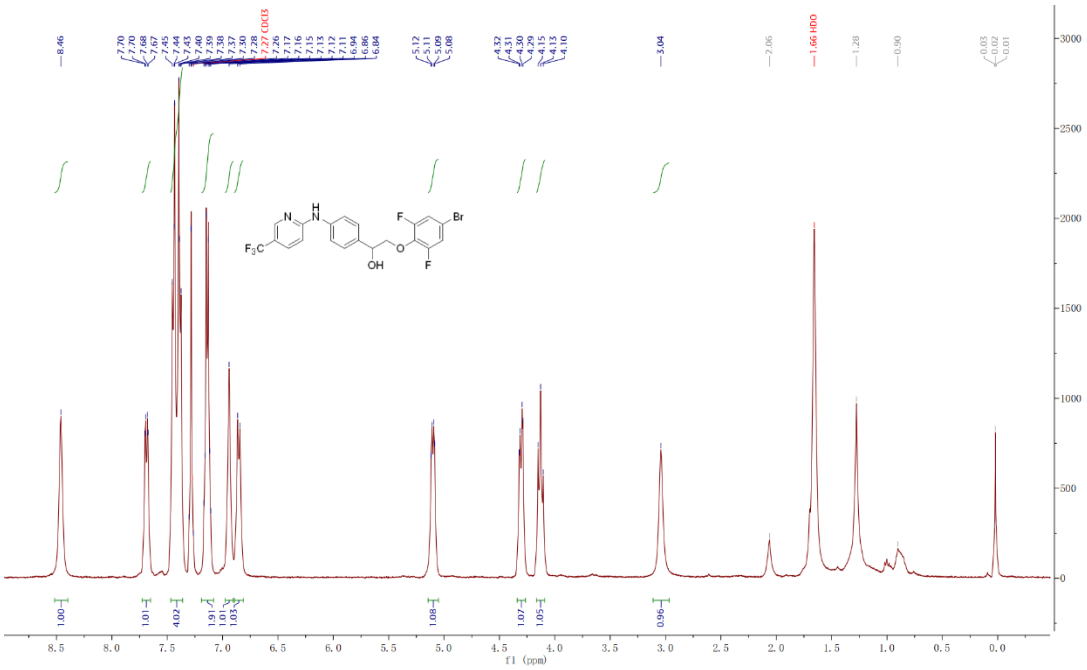
8.46
7.70
7.68
7.67
7.45
7.44
7.43
7.40
7.39
7.38
7.37
7.30
7.28
7.27 CDCl3
7.26
7.17
7.16
7.15
7.13
7.12
7.11
6.94
6.86
6.84
5.12
5.11
5.09
5.08
4.32
4.31
4.30
4.29
4.15
4.13
4.10
3.04
2.06
1.66 HDO
1.28
0.90
0.03
0.02
0.01
1.00
1.01
4.02
1.91
1.01
1.03
1.08
1.07
1.05
0.96
f1 (ppm)

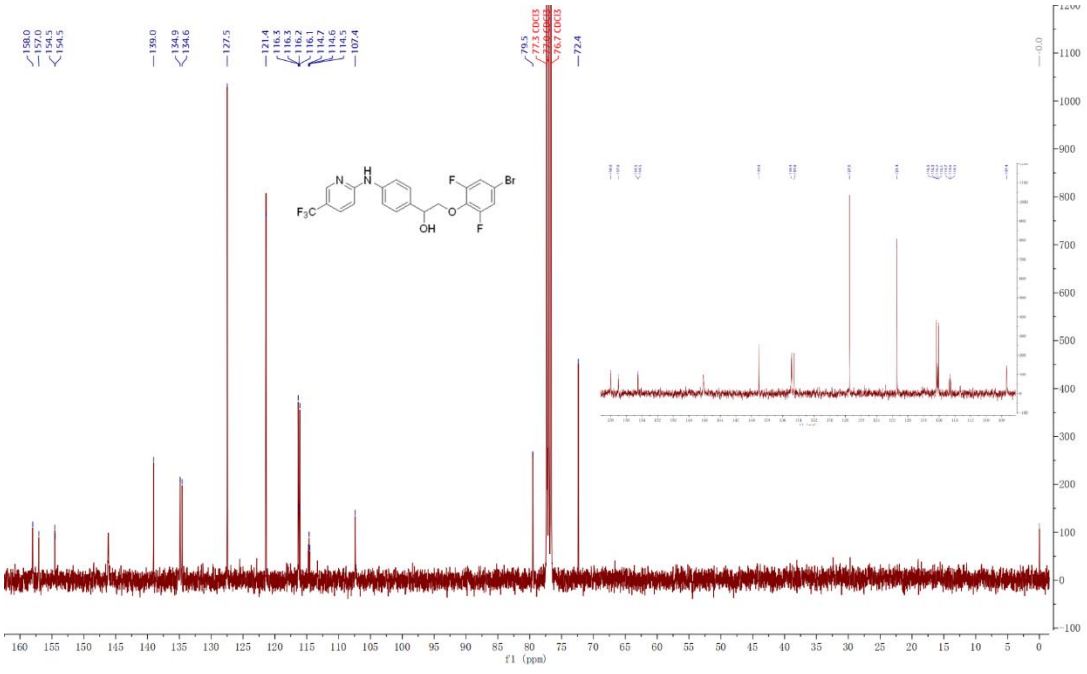
158.0
157.0
154.5
154.5
139.0
134.9
134.6
127.5
121.4
116.3
116.3
116.2
116.1
114.7
114.6
114.5
107.4
79.5
77.3 CDCl3
77.0 CDCl3
76.7 CDCl3
72.4
0.0
f1 (ppm)

GII-2

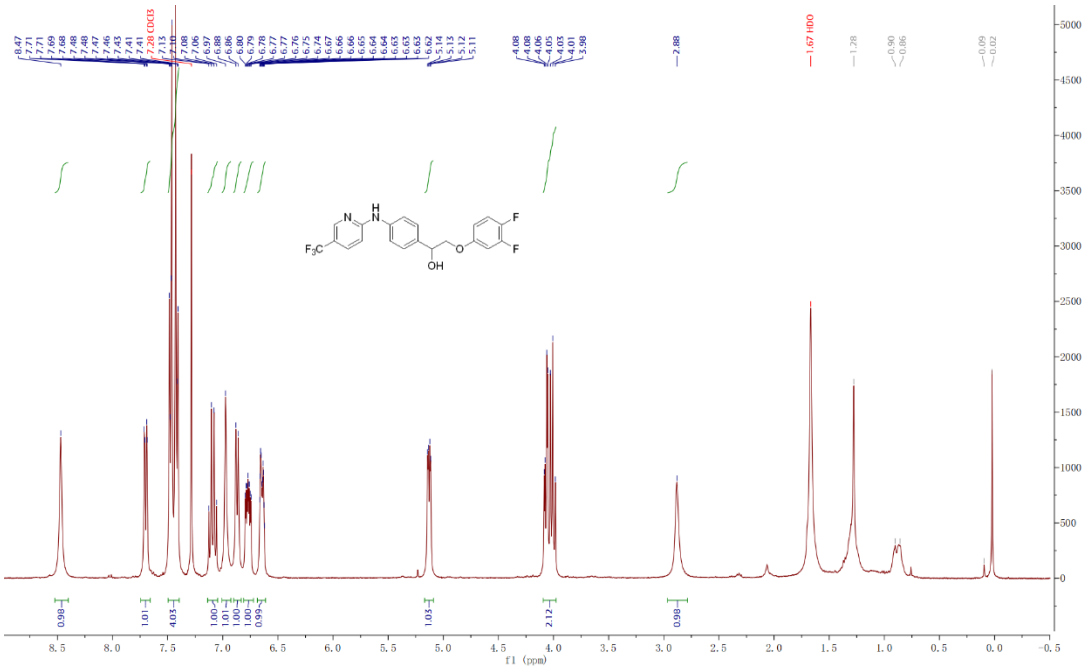

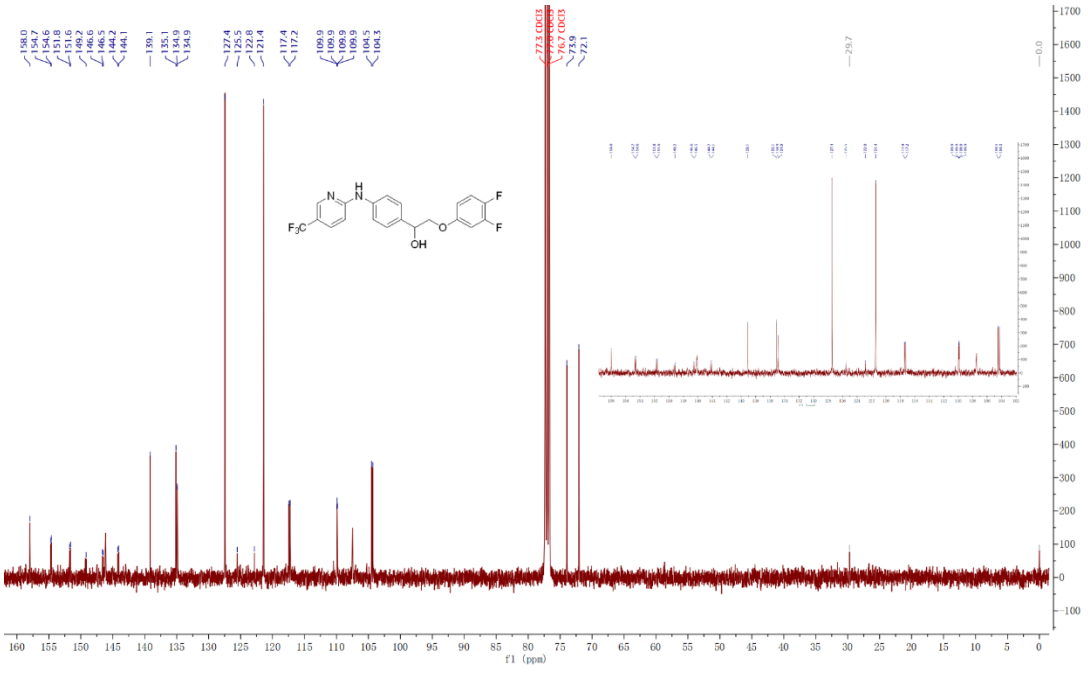

GII-3

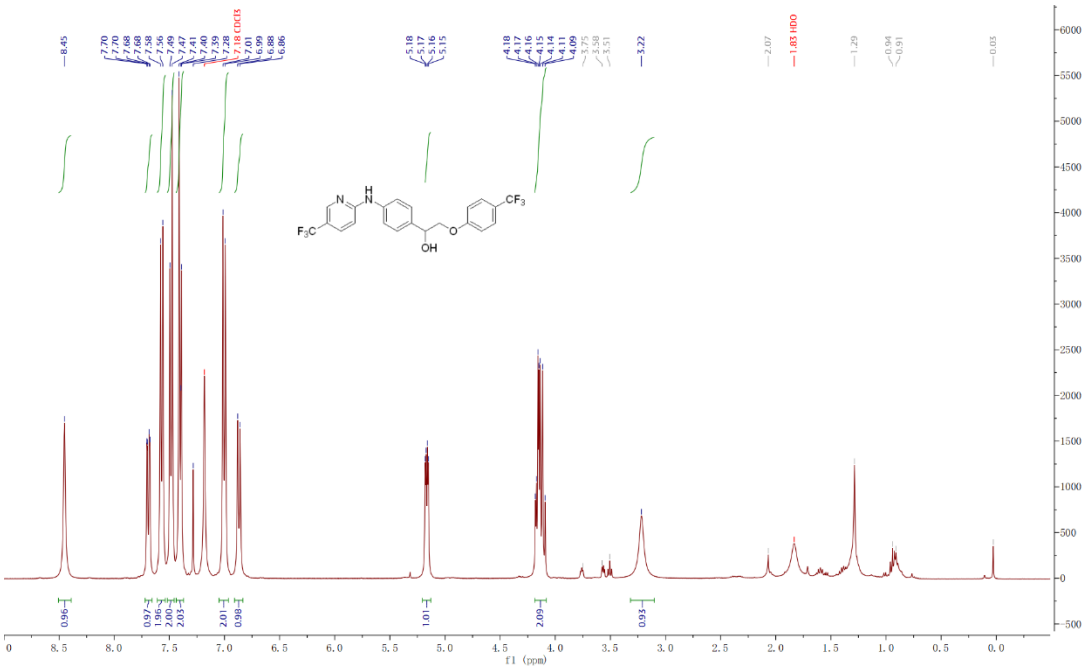
8.45
7.70
7.70
7.68
7.68
7.58
7.56
7.49
7.47
7.41
7.40
7.39
7.38
7.18 CDCl3
7.01
6.99
6.88
6.86
5.18
5.17
5.16
5.15
4.18
4.17
4.16
4.15
4.14
4.11
4.09
3.75
3.58
3.51
3.22
2.07
1.83 HDO
1.29
0.94
0.91
0.03
0.96
0.97
1.96
2.00
2.03
2.01
0.98
1.01
2.09
0.93
f1 (ppm)

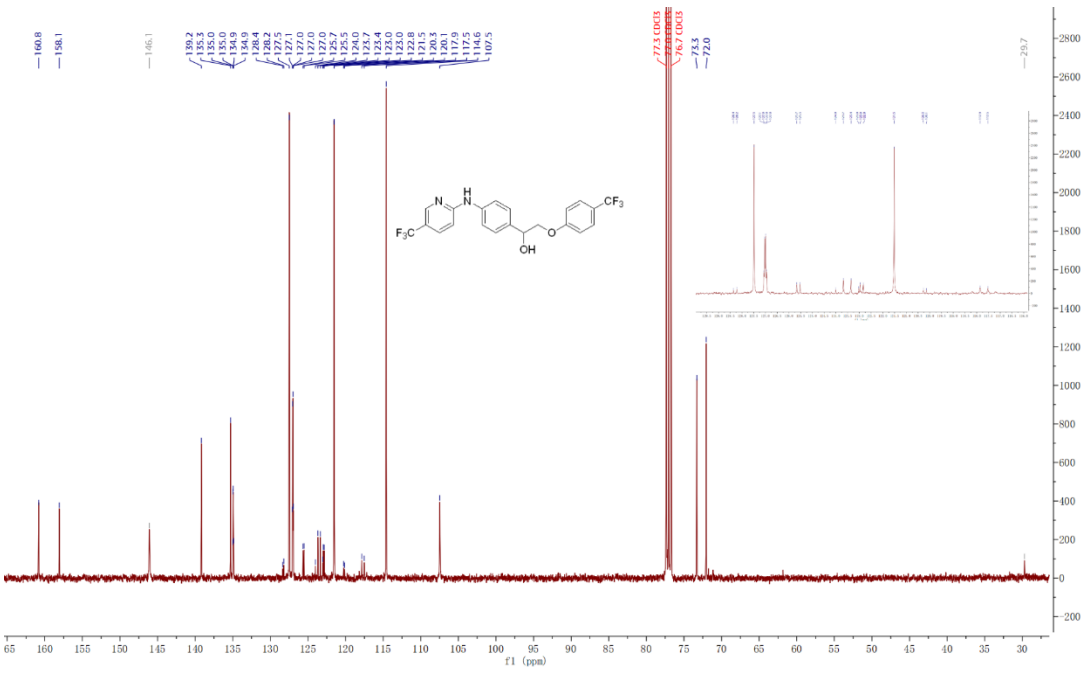
160.8
158.1
146.1
139.2
135.3
135.0
135.0
134.9
128.4
128.2
127.5
127.1
127.0
127.0
127.0
125.7
125.5
124.0
123.7
123.4
123.0
123.0
122.8
121.5
120.3
120.1
117.9
117.5
116.6
107.5
77.3 CDCl3
76.7 CDCl3
73.3
72.0
29.7
f1 (ppm)

GII-4

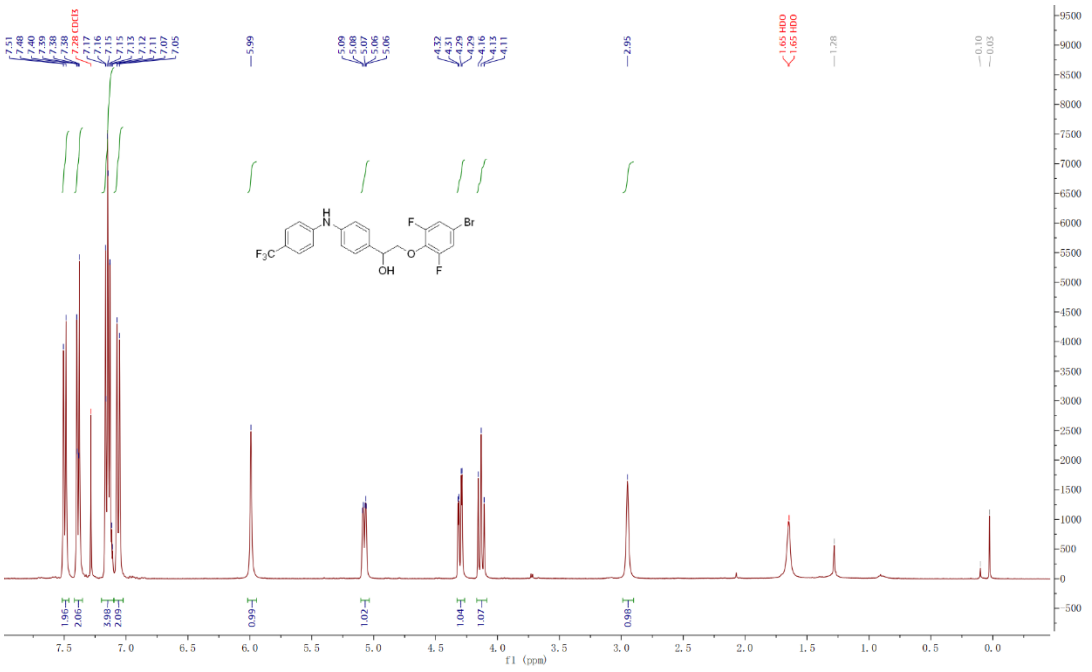
7.51
7.48
7.40
7.39
7.38
7.38
7.28 CDCl3
7.17
7.16
7.15
7.15
7.13
7.12
7.11
7.07
7.05
5.99
5.09
5.08
5.07
5.06
5.06
4.32
4.31
4.29
4.29
4.16
4.13
4.11
2.95
1.65 HDO
1.65 HDO
1.28
0.10
0.03
F3C
N
H
O
OH
F
Br
1.96
2.06
3.98
2.09
0.99
1.02
1.04
1.07
0.98
f1 (ppm)

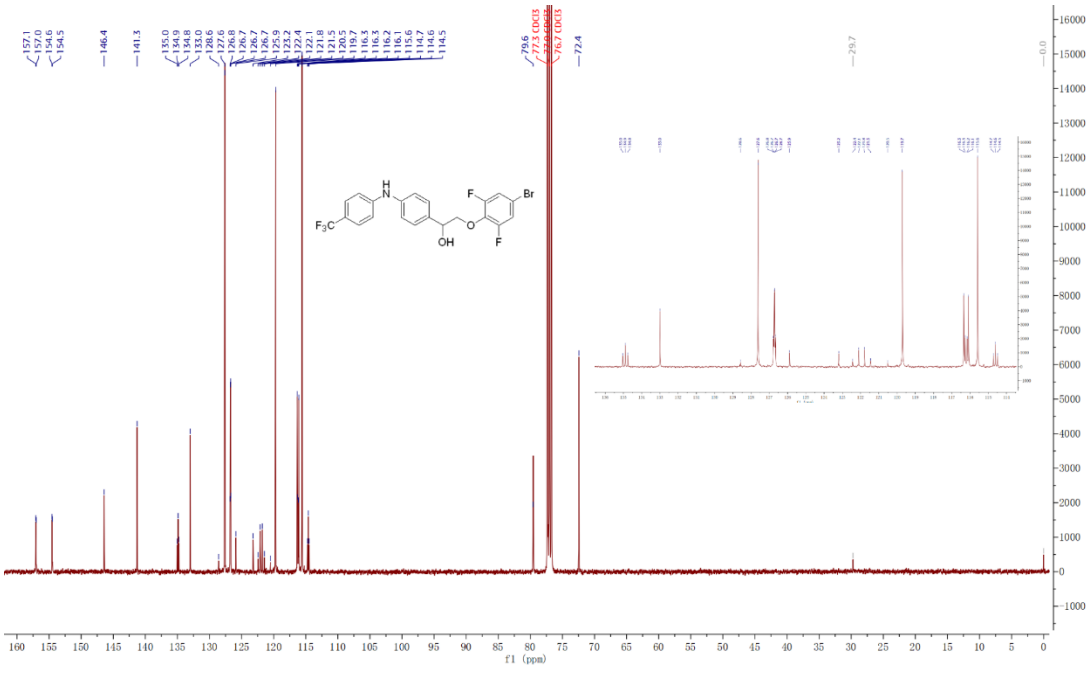
157.1
157.0
154.6
154.5
146.4
141.3
135.0
134.9
134.8
133.0
128.6
127.6
126.8
126.7
126.7
126.7
125.9
123.2
122.4
122.1
121.8
121.5
120.5
118.7
116.5
116.3
116.2
116.1
115.6
114.7
114.6
114.5
79.6
77.3 CDCl3
77.0
76.7 CDCl3
72.4
29.7
0.0
F3C
N
H
O
OH
F
Br
f1 (ppm)

GII-5

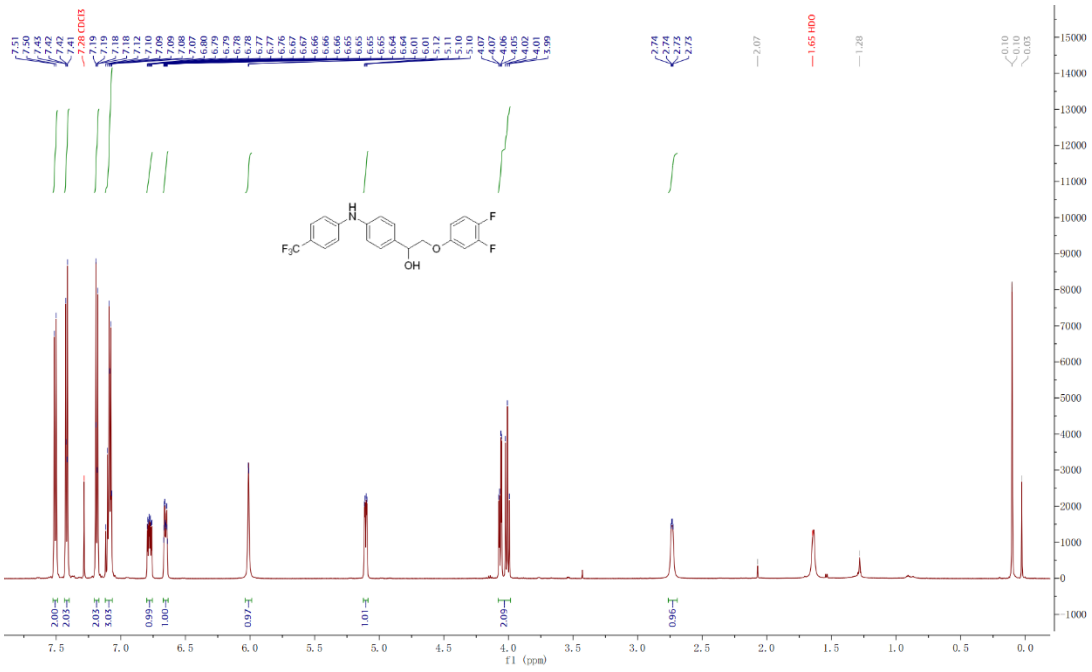

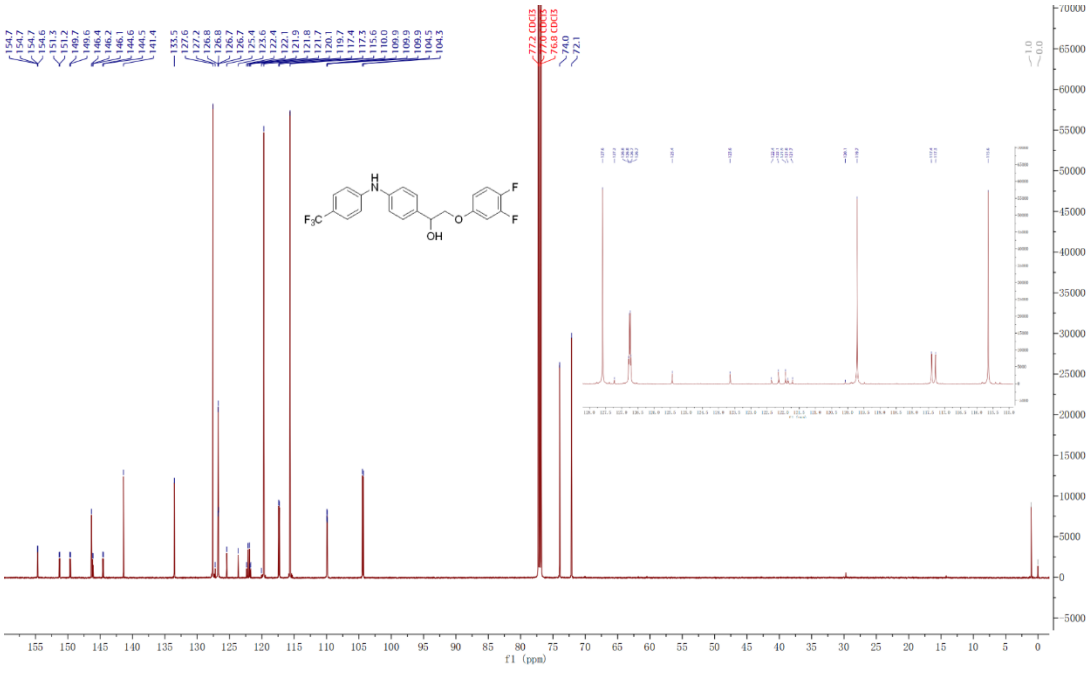

GII-6

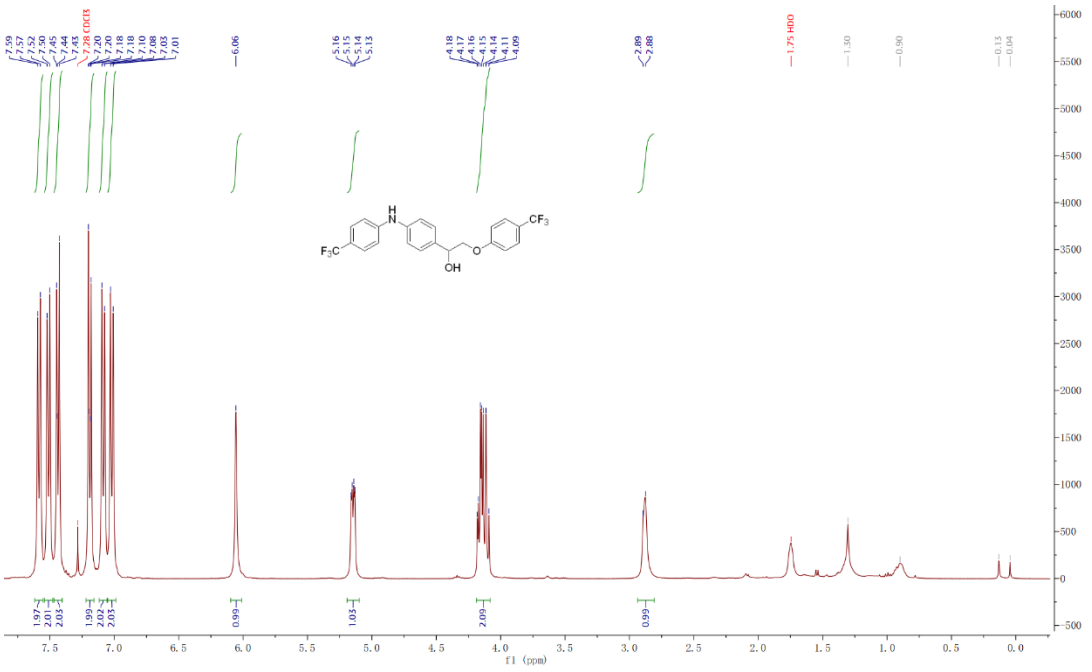
7.59
7.57
7.52
7.50
7.45
7.44
7.43
7.26 CDCl3
7.20
7.18
7.10
7.10
7.08
7.03
7.01
6.06
5.16
5.15
5.14
5.13
4.18
4.17
4.16
4.15
4.14
4.11
4.11
4.09
2.89
2.88
1.75 HDO
1.30
0.90
0.15
0.04
F3C
CF3
O
OH
1.97
2.01
2.03
1.93
2.01
2.03
0.99
1.03
2.09
0.99
f1 (ppm)

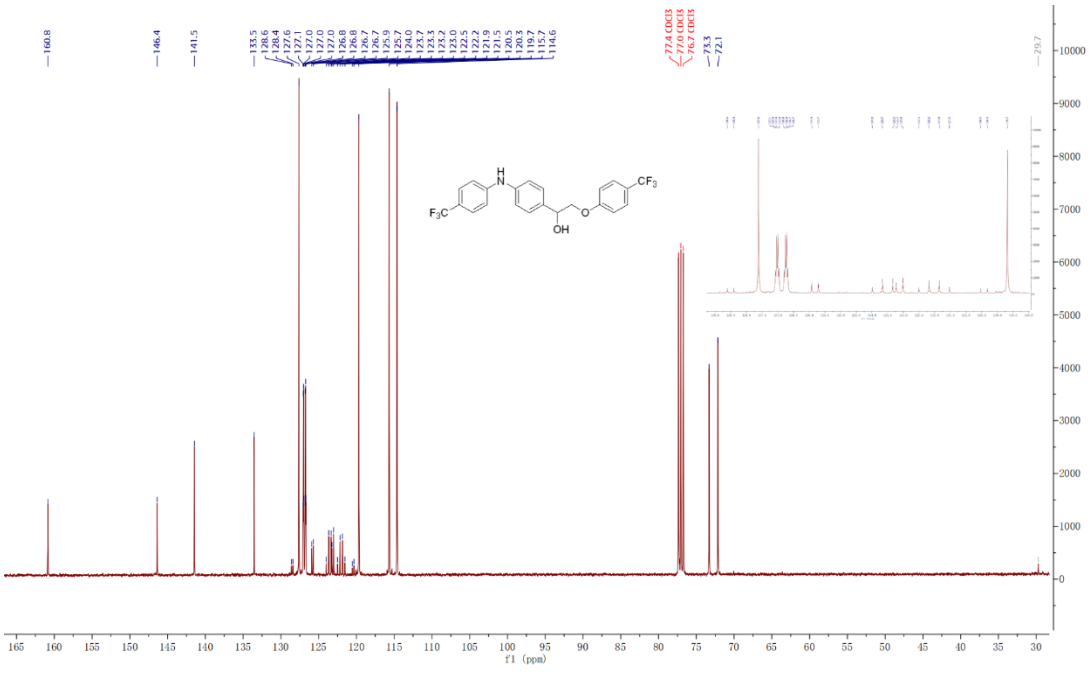
160.8
146.4
141.5
133.5
128.6
128.4
127.6
127.1
127.0
127.0
127.0
126.8
126.8
126.7
126.7
125.9
125.7
124.0
123.7
123.3
123.2
123.0
122.5
122.2
121.9
121.5
120.5
120.3
119.7
115.7
114.6
77.4 CDCl3
77.0 CDCl3
76.7 CDCl3
73.3
72.1
29.7
F3C
CF3
O
OH
f1 (ppm)

GII-7

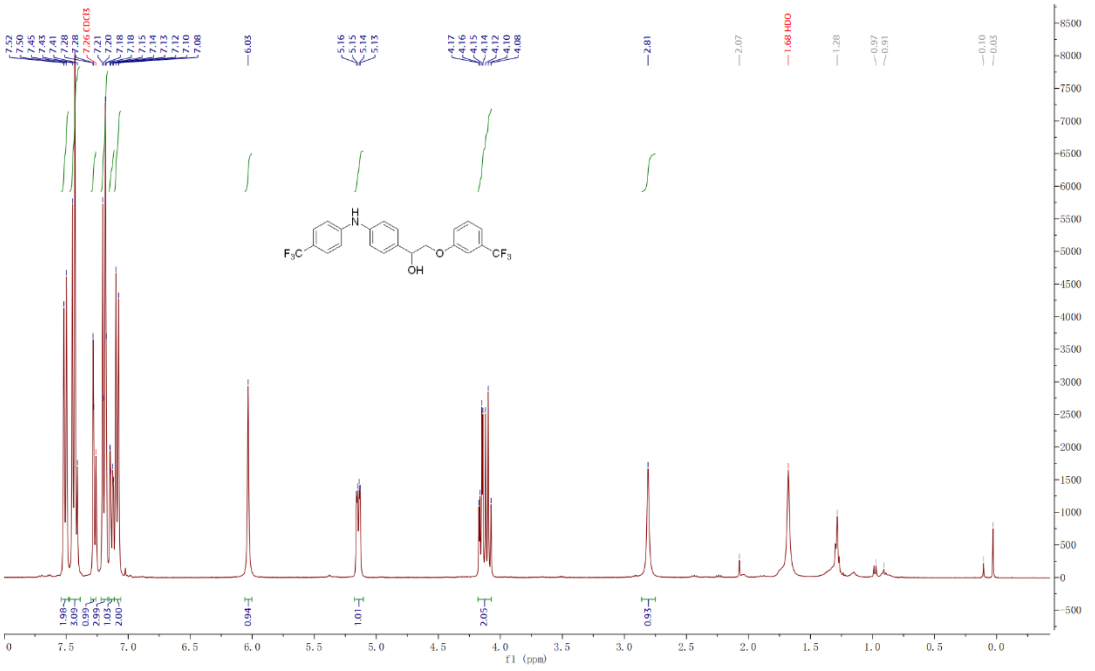
7.52
7.50
7.45
7.43
7.41
7.28
7.26 CDCl3
7.21
7.20
7.18
7.15
7.14
7.13
7.12
7.10
7.08
6.03
5.16
5.15
5.14
5.13
4.17
4.16
4.15
4.14
4.12
4.10
4.08
2.81
2.07
1.68 H2O
1.29
0.97
0.91
0.10
0.05
1.98
3.09
0.98
2.99
1.05
2.00
0.94
1.01
2.05
0.93
f1 (ppm)

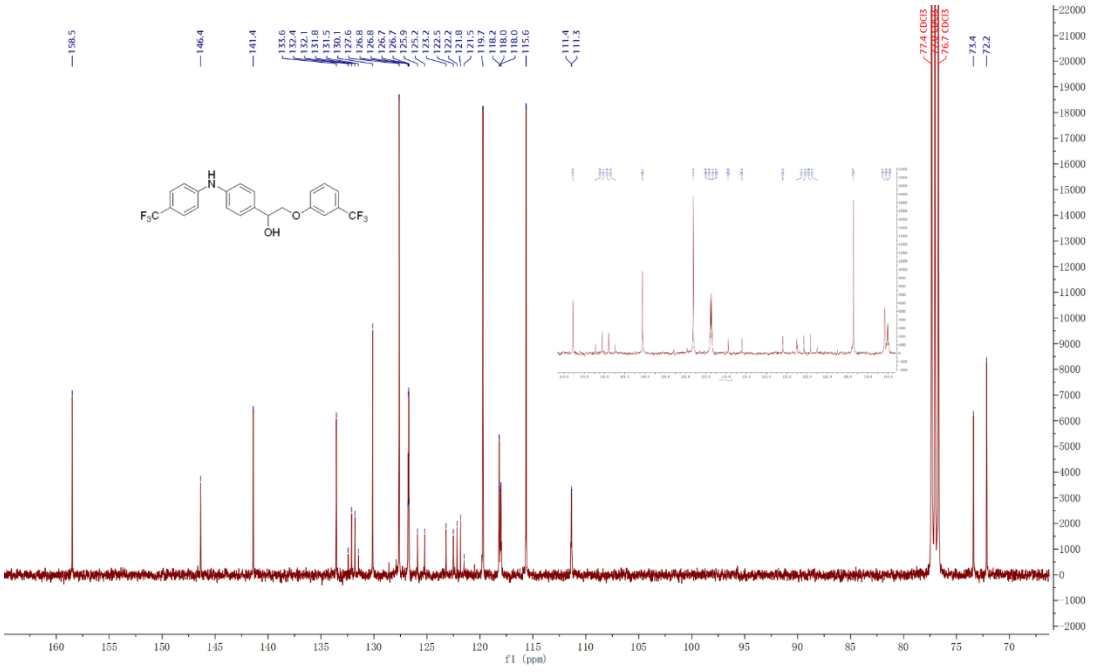
158.5
146.4
141.4
135.6
132.4
132.1
131.8
131.5
130.1
127.6
126.8
126.8
126.7
126.7
125.9
125.2
123.2
122.5
122.2
121.8
121.5
119.7
118.2
118.0
118.0
115.6
111.4
111.3
77.4 CDCl3
76.7 CDCl3
73.4
72.2
f1 (ppm)

GII-8

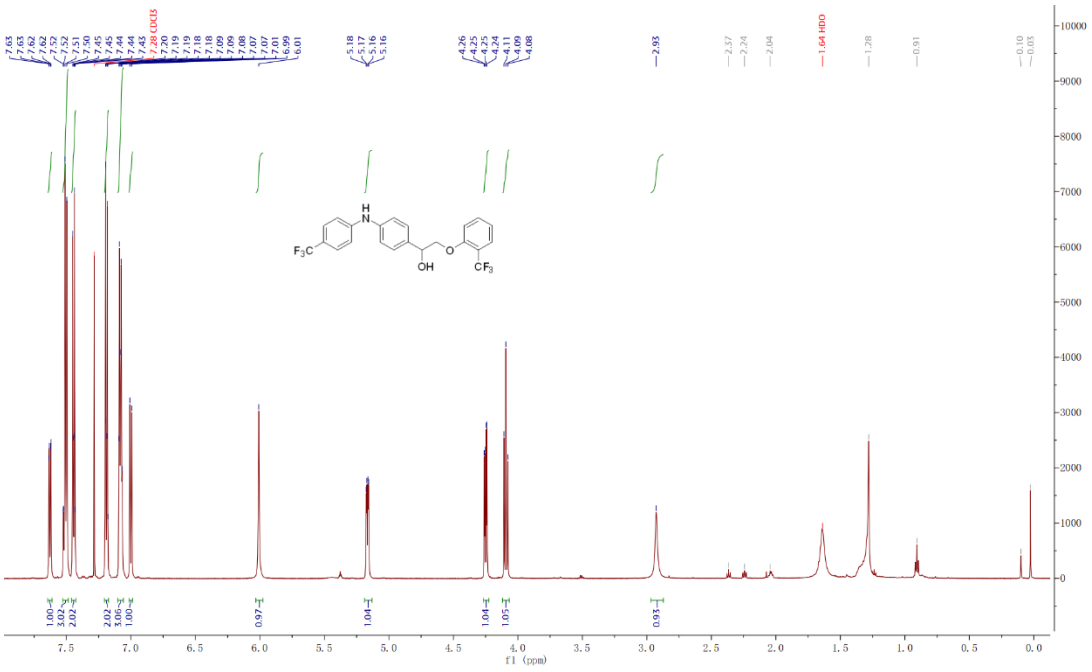

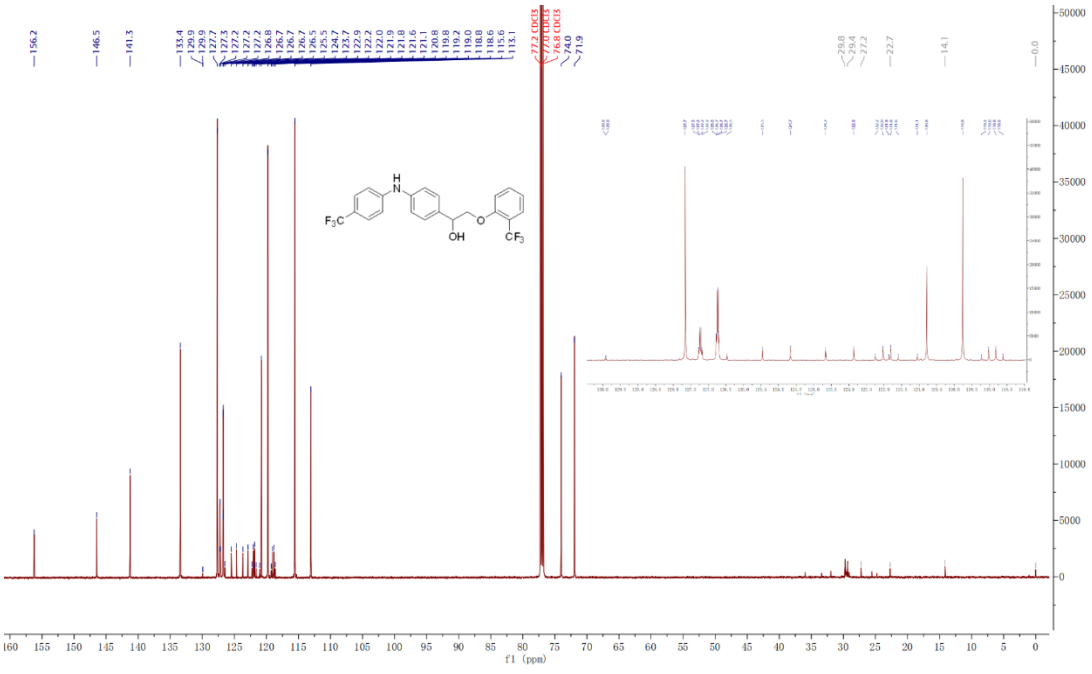

GII-9

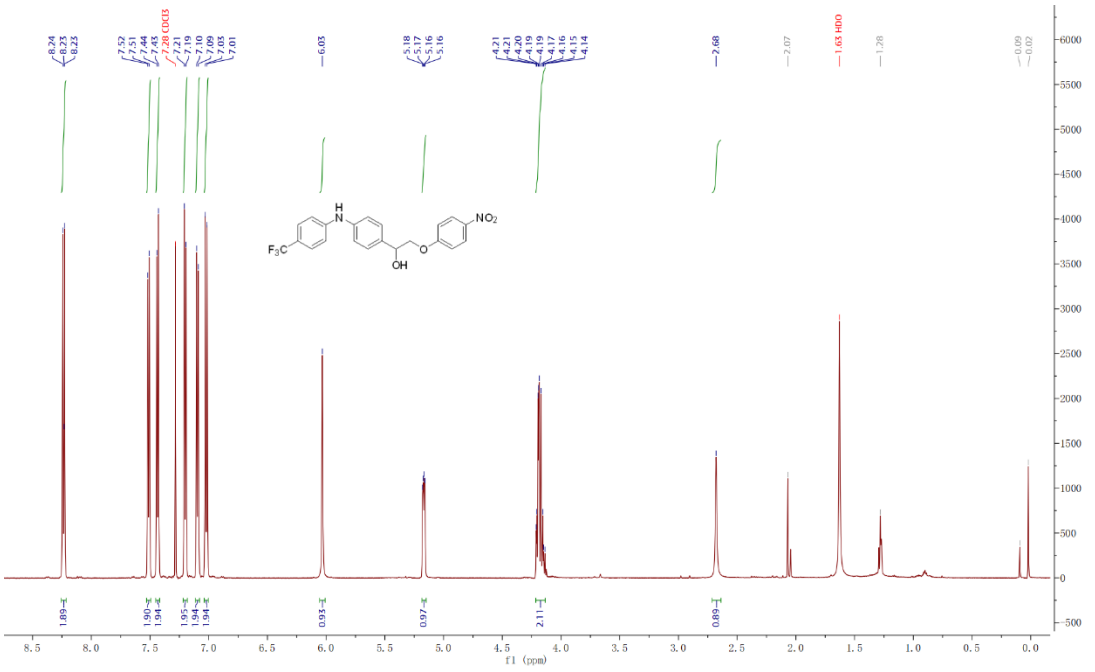
8.24
8.25
8.23
7.52
7.51
7.46
7.45
7.28 CDCl3
7.21
7.19
7.00
7.00
7.01
6.03
5.18
5.17
5.16
5.16
4.21
4.21
4.20
4.19
4.19
4.17
4.16
4.15
4.14
2.68
2.07
1.63 H2O
1.28
0.09
0.02
1.89
1.90
1.94
1.95
1.94
1.94
0.93
0.97
2.11
0.89
f1 (ppm)

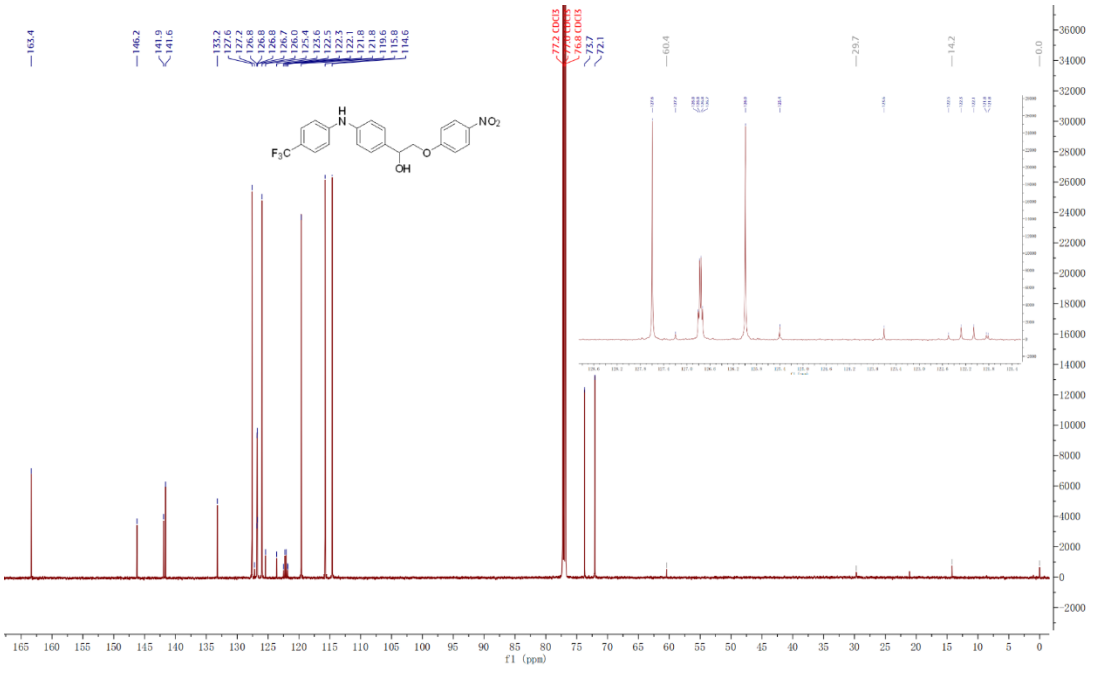
165.4
146.2
141.9
141.6
133.2
127.6
127.2
126.8
126.8
126.8
126.7
126.0
125.4
123.6
122.5
122.3
122.1
121.8
121.8
119.6
115.8
114.6
77.2 CDCl3
77.0 CDCl3
76.8 CDCl3
72.7
72.1
60.4
29.7
14.2
0.0
f1 (ppm)

GII-10

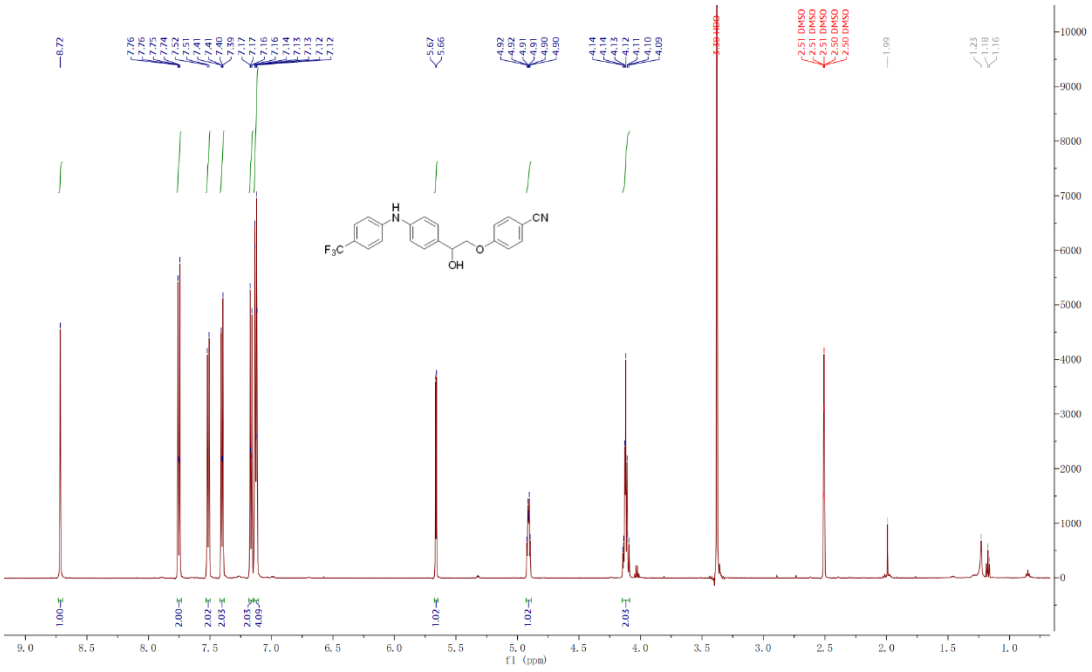

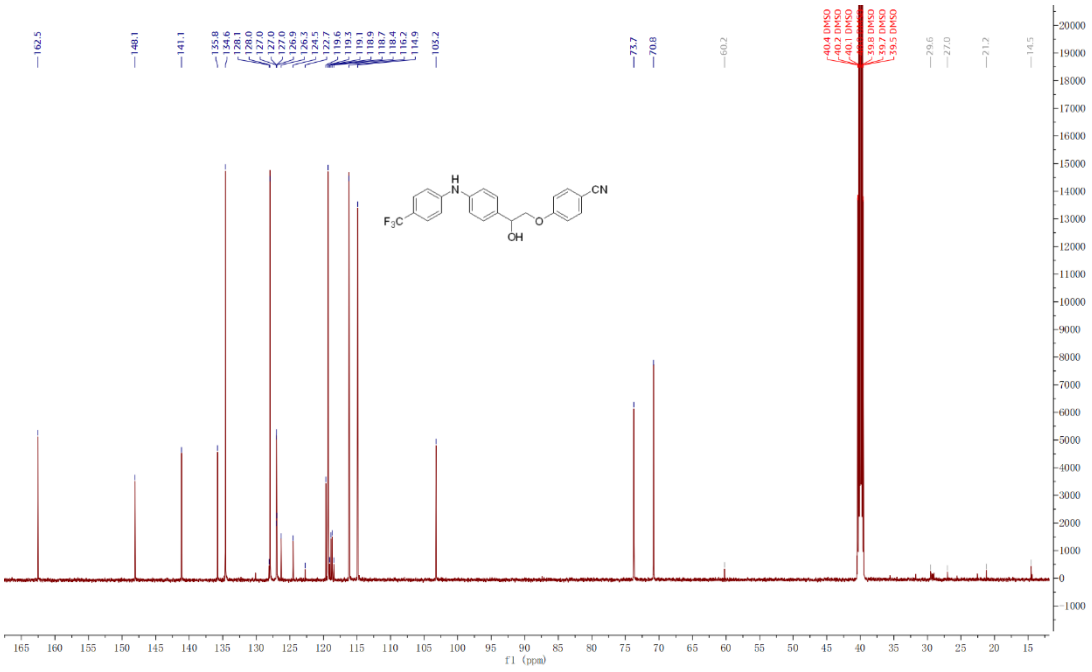

GII-11

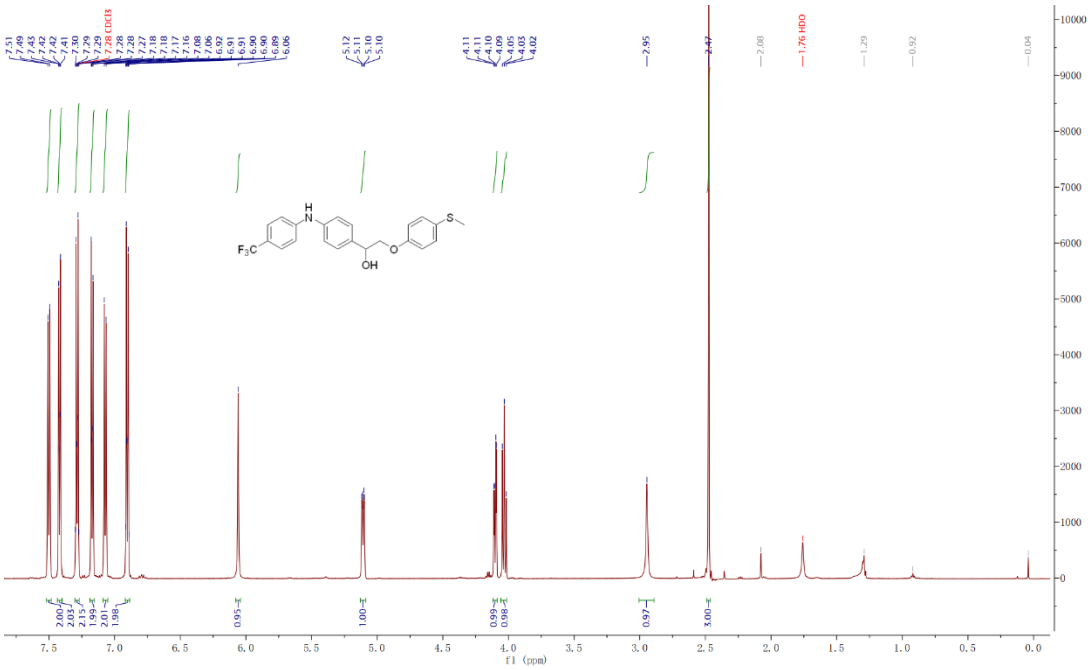
7.51
7.49
7.45
7.43
7.42
7.41
7.30
7.29
7.28 CDCl3
7.28
7.27
7.27
7.18
7.17
7.16
7.08
7.08
7.06
6.92
6.91
6.91
6.90
6.90
6.89
6.06
5.12
5.11
5.10
5.10
4.11
4.11
4.10
4.09
4.05
4.05
4.02
2.95
2.47
2.08
1.76 HDO
1.29
0.92
0.04
2.00
2.04
2.15
1.99
2.01
1.98
0.95
1.00
0.99
0.98
0.97
3.00
F3C
H
N
O
OH
S
f1 (ppm)

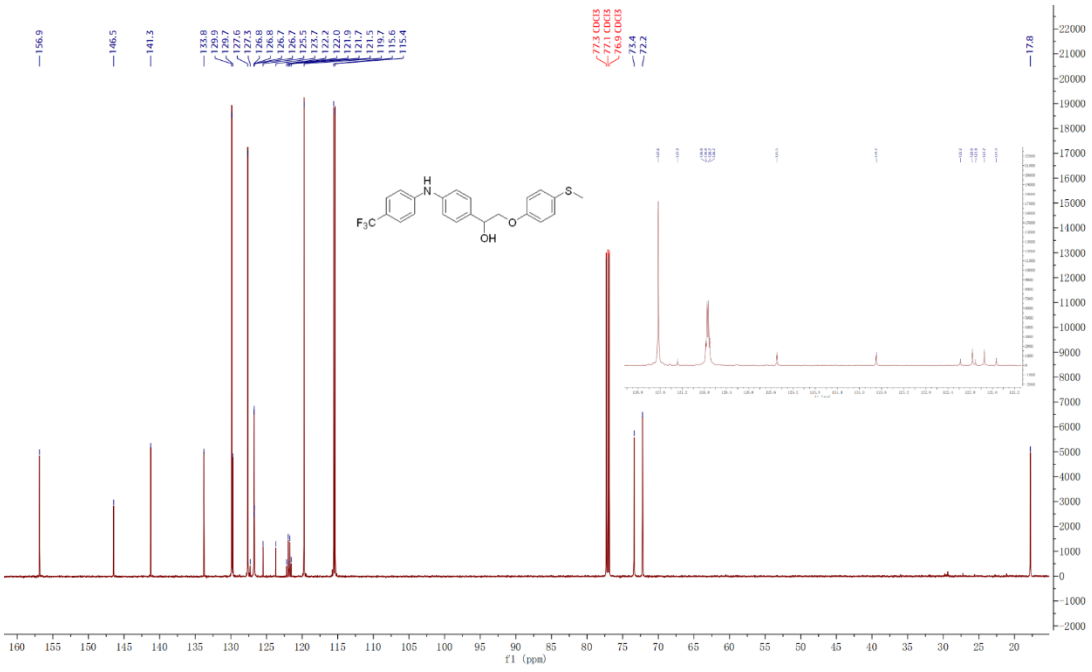
156.9
146.5
141.3
133.8
129.9
129.7
127.6
127.3
126.8
126.8
126.7
126.7
125.5
123.7
122.2
122.0
121.9
121.7
121.5
119.7
115.6
115.4
77.5 CDCl3
77.1 CDCl3
76.6 CDCl3
73.4
72.2
17.8
F3C
H
N
O
OH
S
f1 (ppm)

GII-12

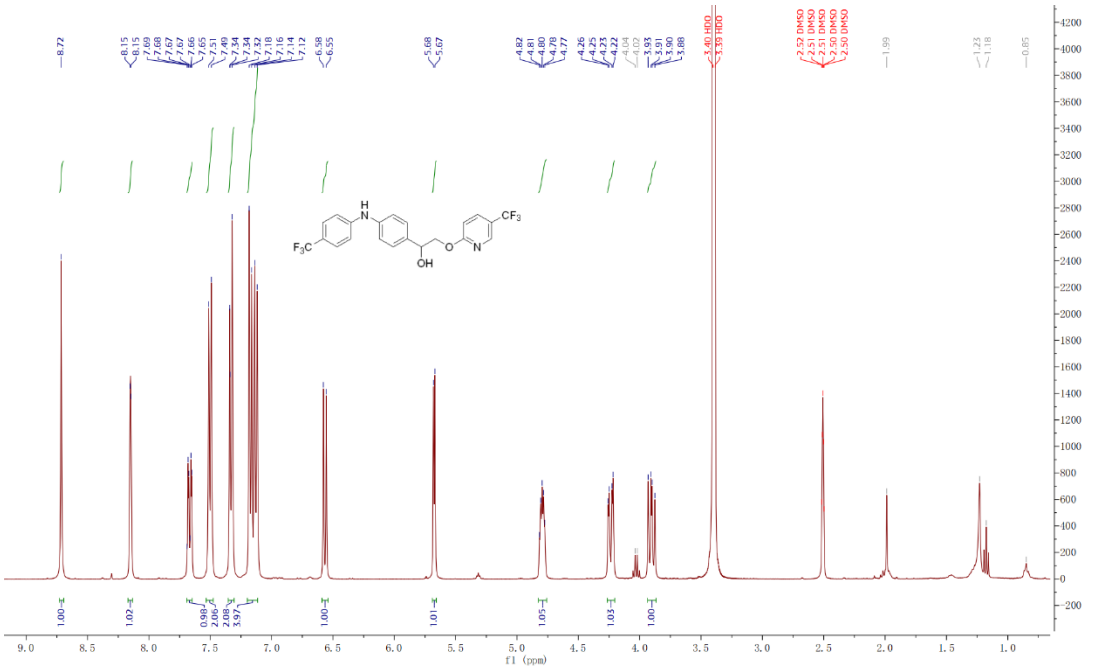
8.72
8.15
8.15
7.69
7.68
7.67
7.67
7.66
7.65
7.51
7.49
7.34
7.32
7.18
7.16
7.14
7.12
6.58
6.55
5.68
5.67
4.82
4.81
4.80
4.78
4.77
4.26
4.25
4.23
4.22
4.04
4.02
3.95
3.91
3.90
3.88
3.40 HDO
3.39 HDO
2.52 DMSO
2.51 DMSO
2.51 DMSO
2.50 DMSO
2.50 DMSO
1.99
1.23
1.18
0.85
F3C
CF3
OH
f1 (ppm)

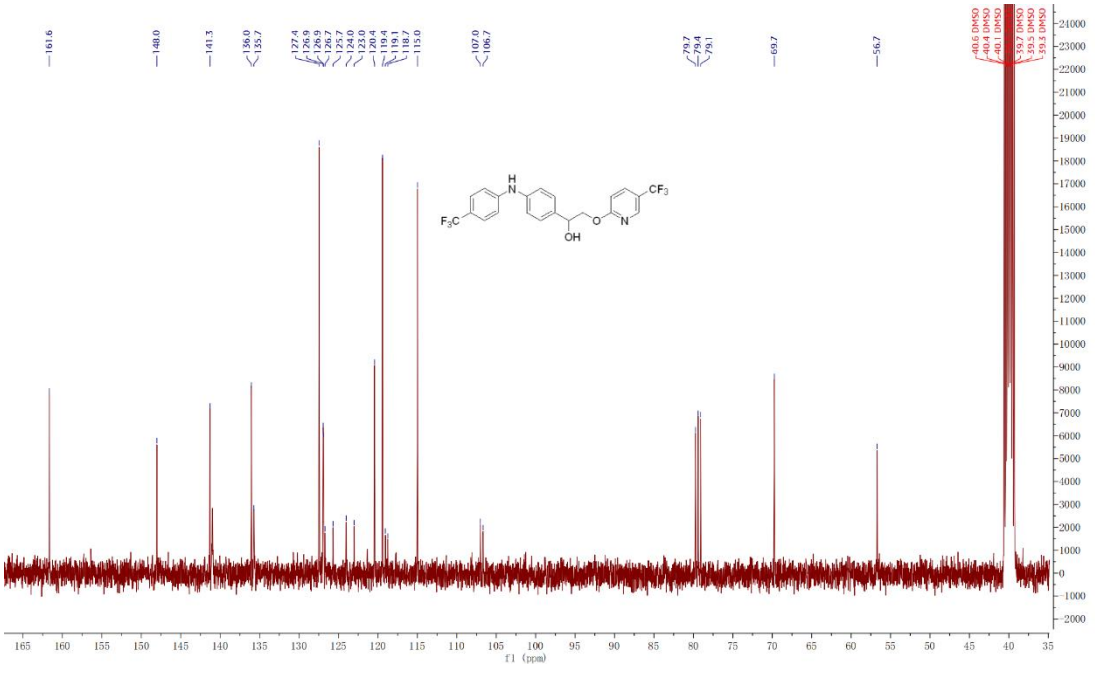
161.6
148.0
141.3
136.0
135.7
127.4
126.9
126.9
126.7
123.7
123.0
123.0
120.4
119.4
119.1
118.7
115.0
107.0
106.7
79.7
79.4
79.1
69.7
56.7
40.6 DMSO
40.4 DMSO
40.1 DMSO
39.7 DMSO
39.5 DMSO
39.3 DMSO
F3C
CF3
OH
f1 (ppm)

GII-13

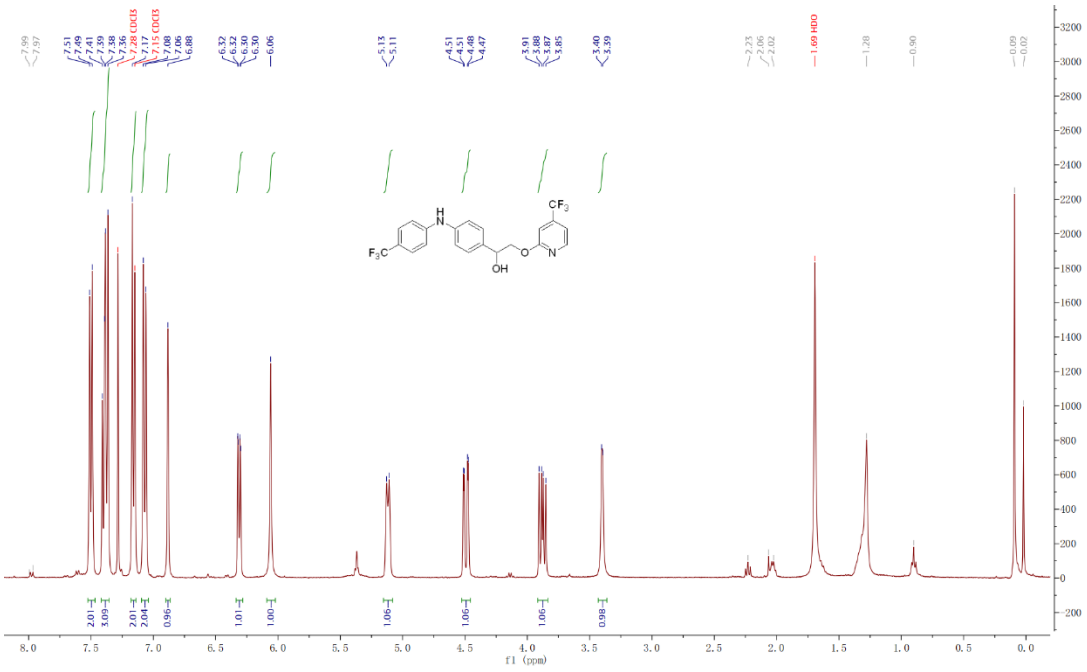
7.99
7.97
7.51
7.49
7.41
7.39
7.38
7.36
7.28 CDCl3
7.17
7.15 CDCl3
7.08
7.06
6.88
6.32
6.32
6.30
6.30
6.06
5.13
5.11
4.51
4.51
4.48
4.47
3.91
3.88
3.87
3.85
3.40
3.39
2.25
2.06
2.02
1.69 HDO
1.29
0.90
0.09
0.02
2.01
3.09
2.01
2.04
0.96
1.01
1.00
1.06
1.06
1.06
0.98
f1 (ppm)

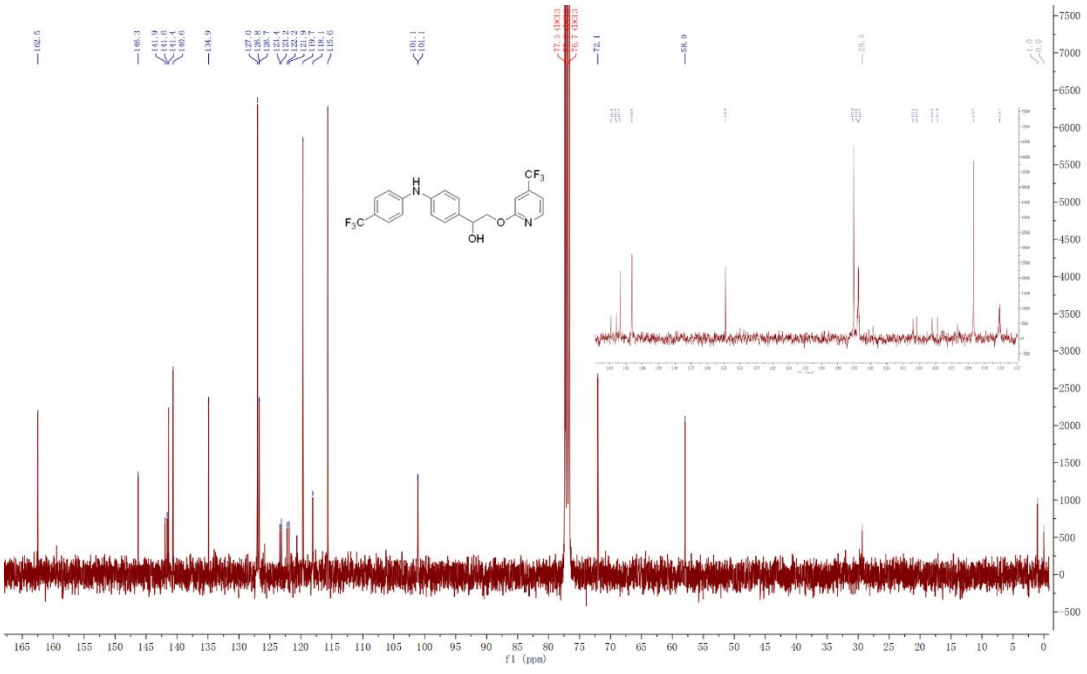
162.5
148.3
141.9
141.6
141.4
140.6
134.9
127.0
126.8
126.7
123.4
123.2
122.2
121.9
119.7
118.1
115.6
101.1
100.1
77.3 CDCl3
76.7 CDCl3
72.1
58.9
28.3
1.0
f1 (ppm)

GII-14

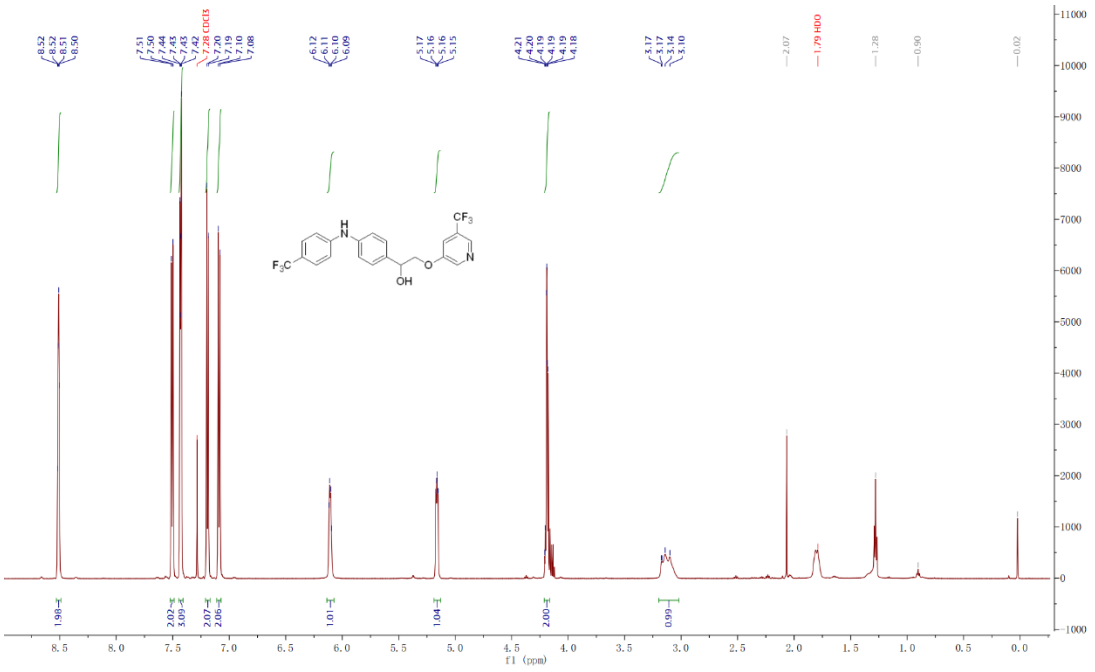
8.52
8.52
8.51
8.50
7.51
7.50
7.44
7.43
7.43
7.42
7.28 CDCl3
7.20
7.19
7.10
7.08
6.12
6.11
6.10
6.09
5.17
5.16
5.16
5.15
4.21
4.20
4.19
4.19
4.19
4.18
3.17
3.17
3.14
3.10
2.07
1.79 H2O
1.28
0.90
0.02
CF3
H
N
F3C
O
N
OH
1.98
2.02
3.09
2.07
2.06
1.01
1.04
2.00
0.99
f1 (ppm)

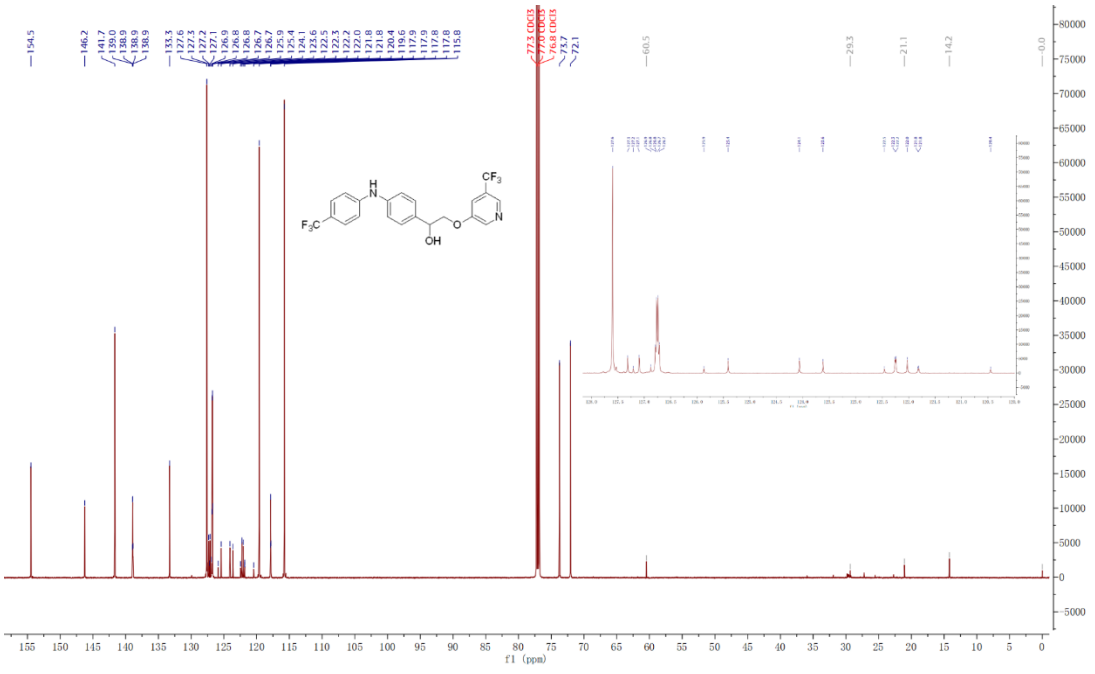
154.5
146.2
141.7
139.0
138.9
138.9
138.9
133.3
127.6
127.3
127.2
127.1
126.9
126.8
126.8
126.7
126.7
125.9
125.4
124.1
123.6
123.5
122.3
122.2
122.0
121.8
121.8
120.4
119.6
117.9
117.9
117.9
117.8
117.8
115.8
77.3 CDCl3
77.0 CDCl3
76.8 CDCl3
74.7
72.1
60.5
29.3
21.1
14.2
0.0
CF3
H
N
F3C
O
N
OH
f1 (ppm)

GII-15

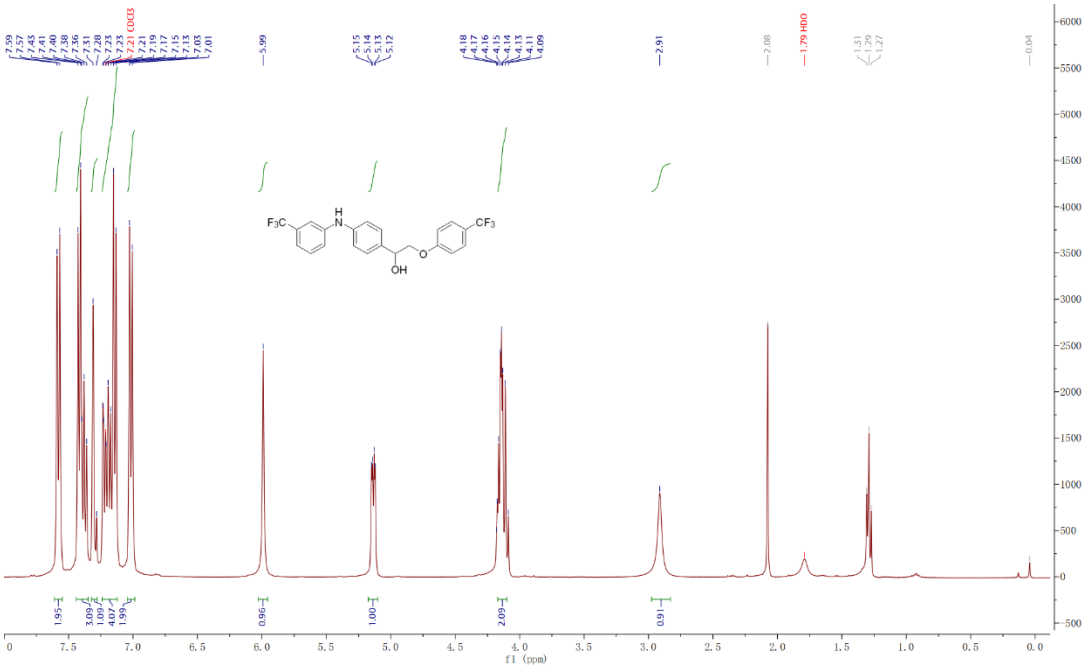
7.59
7.57
7.45
7.41
7.40
7.38
7.36
7.31
7.30
7.25
7.21 CDCl3
7.21
7.19
7.17
7.15
7.13
7.08
7.01
5.99
5.15
5.14
5.13
5.12
4.18
4.17
4.16
4.15
4.14
4.13
4.11
4.09
2.91
2.08
1.79 HDO
1.31
1.29
1.27
0.04
F3C
CF3
H
N
O
OH
1.95
3.09
1.07
4.07
1.99
0.96
1.00
2.03
0.91
f1 (ppm)

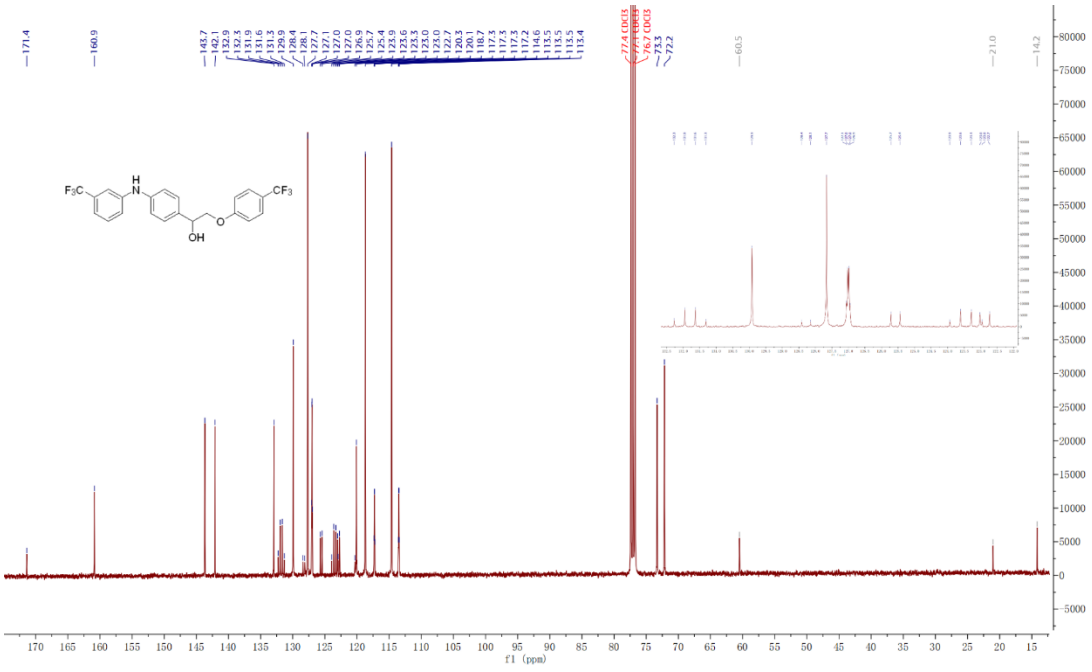
171.4
160.9
145.7
142.1
132.9
132.3
131.9
131.6
131.3
128.9
128.4
128.1
127.7
127.1
127.0
127.0
126.9
125.7
125.4
125.3
123.6
123.3
123.0
122.0
122.7
120.3
120.1
118.7
117.4
117.3
117.3
117.2
114.6
113.5
113.5
113.5
113.4
77.4 CDCl3
76.9 CDCl3
76.7 CDCl3
72.5
72.2
60.5
21.0
14.2
F3C
CF3
H
N
O
OH
f1 (ppm)

GII-16

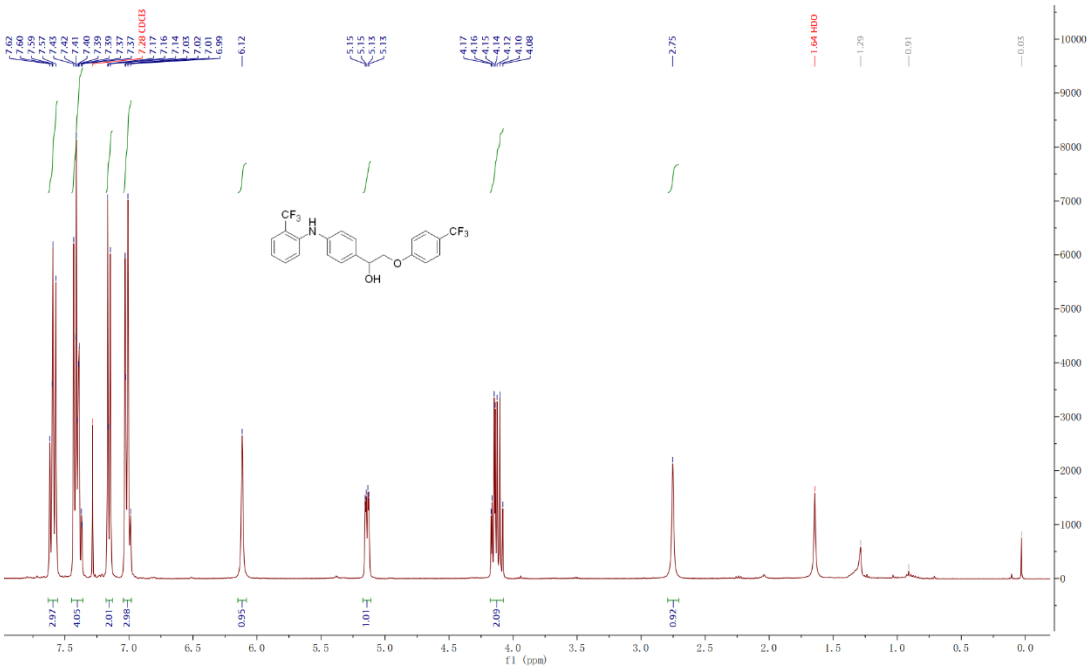
7.62
7.60
7.59
7.57
7.43
7.42
7.41
7.40
7.39
7.38
7.37
7.37
7.26 CDCl3
7.17
7.16
7.14
7.05
7.03
7.00
7.01
6.99
6.12
5.15
5.15
5.13
5.13
4.17
4.16
4.15
4.14
4.12
4.10
4.08
2.75
1.64 H2O
1.29
0.91
0.03
CF3
H
N
O
OH
CF3
2.97
4.05
2.01
2.98
0.95
1.01
2.09
0.92
f1 (ppm)

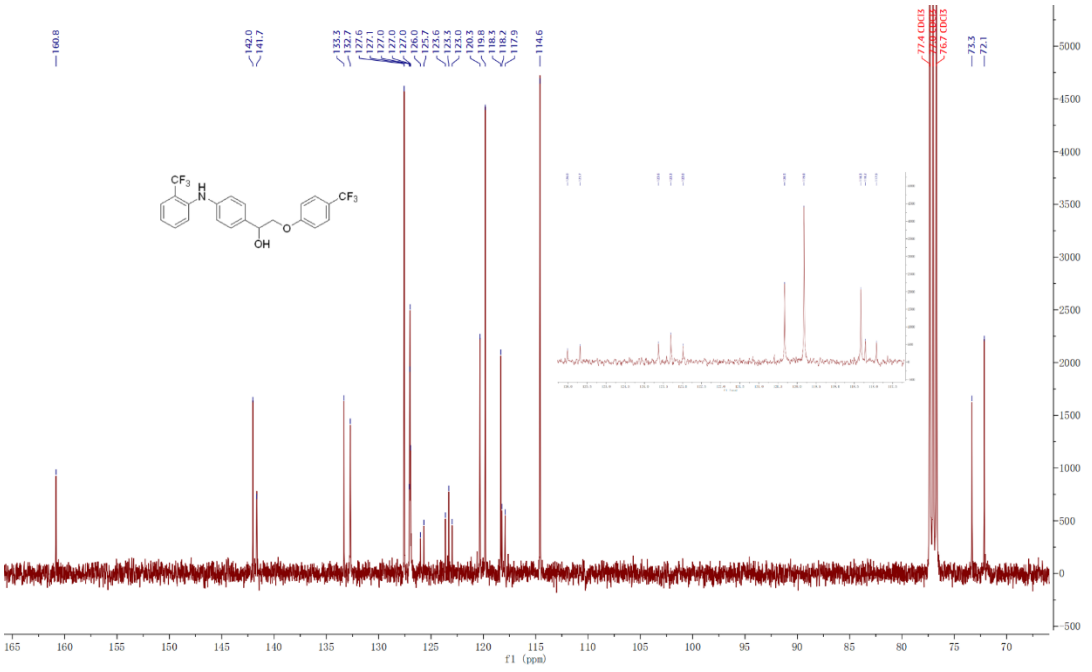
160.8
142.0
141.7
133.3
132.7
127.6
127.1
127.0
127.0
127.0
126.0
125.7
123.6
123.5
123.0
120.3
119.8
118.5
118.2
117.9
114.6
77.4 CDCl3
76.7 CDCl3
73.3
72.1
CF3
H
N
O
OH
CF3
f1 (ppm)

GII-17

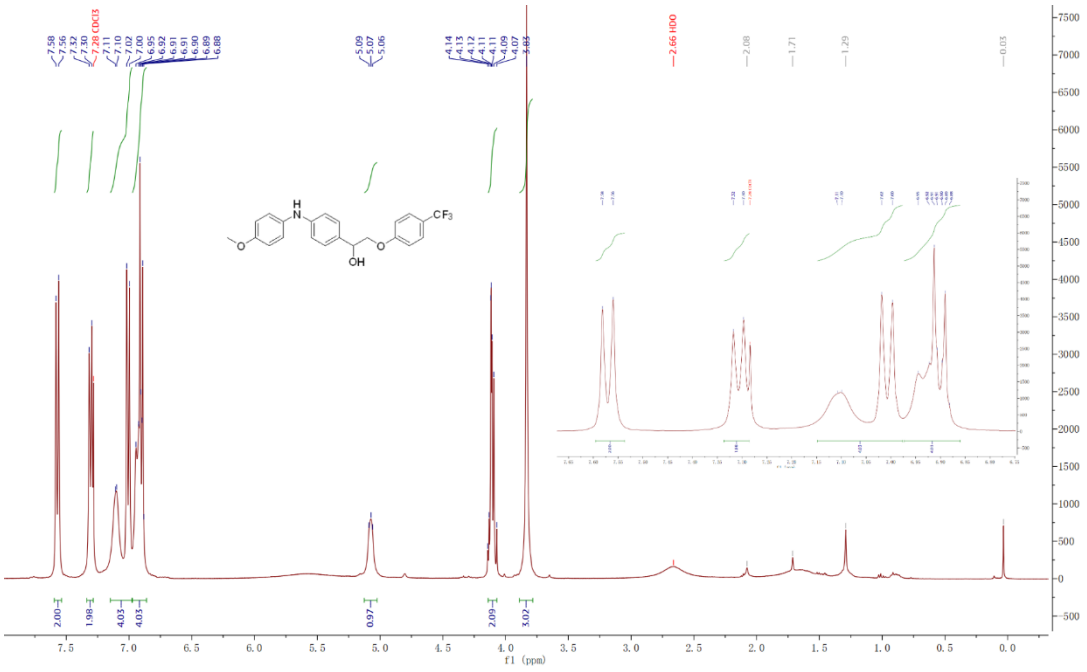
7.58
7.56
7.32
7.30
7.28 CDCl3
7.11
7.10
7.09
7.00
6.95
6.92
6.91
6.91
6.90
6.89
6.88
5.09
5.07
5.06
4.14
4.13
4.12
4.11
4.11
4.09
4.07
3.85
2.66 HDO
2.08
1.71
1.29
0.03
H
N
O
O
CF3
OH
2.00
1.98
4.03
4.03
0.97
2.09
3.02
f1 (ppm)

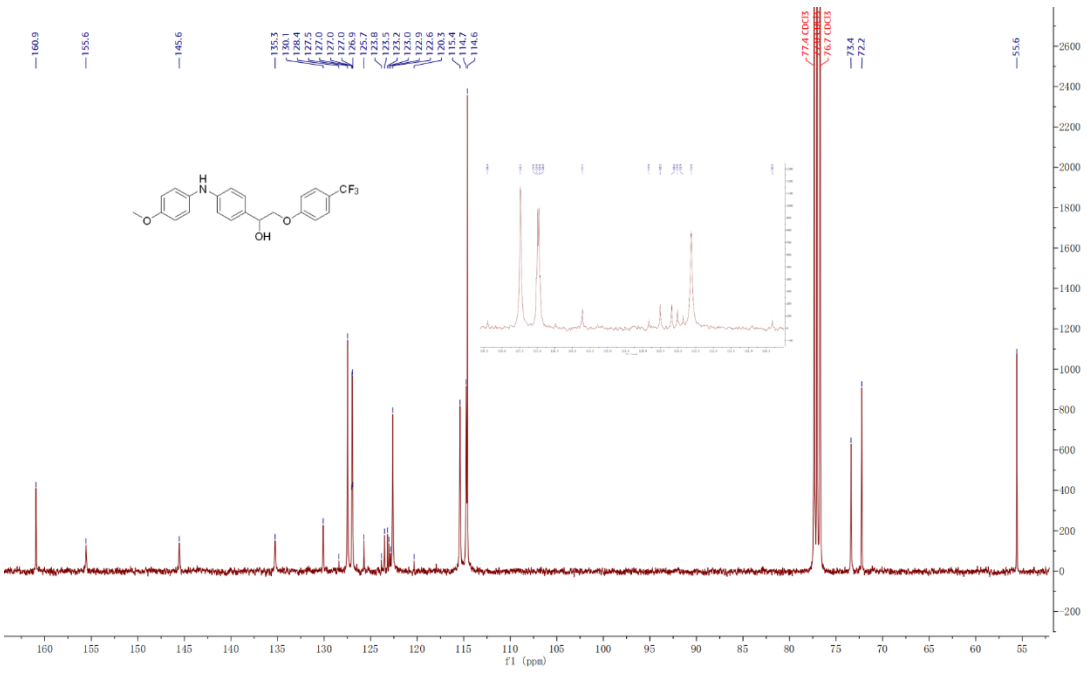
160.9
155.6
145.6
135.3
130.1
129.4
127.5
127.0
127.0
127.0
126.9
125.7
123.8
123.5
123.2
123.0
122.9
122.6
120.3
115.4
114.7
114.6
77.4 CDCl3
76.7 CDCl3
73.4
72.2
55.6
H
N
O
O
CF3
OH
f1 (ppm)

GII-18

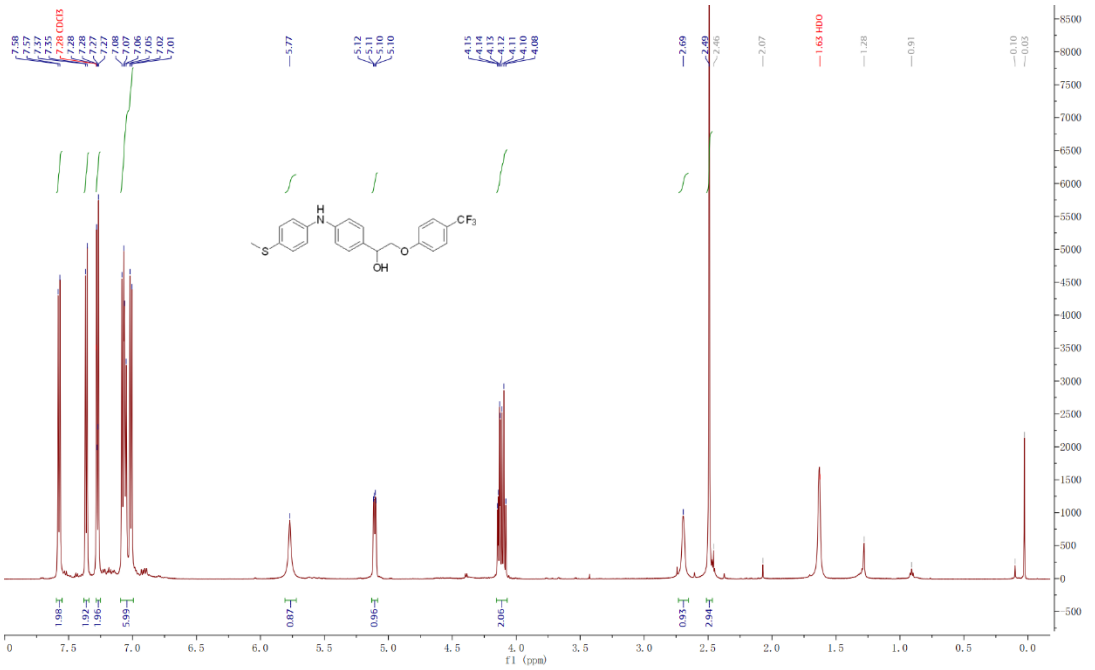
7.58
7.57
7.57
7.35
7.28 CDCl3
7.28
7.27
7.27
7.08
7.07
7.06
7.05
7.02
7.01
5.77
5.12
5.11
5.10
5.10
4.15
4.14
4.13
4.12
4.11
4.10
4.08
2.69
2.49
2.46
2.07
1.65 HDO
1.28
0.91
0.10
0.05
H
N
CF3
S
O
OH
1.98
1.92
1.96
5.99
0.87
0.96
2.06
0.93
2.94
f1 (ppm)

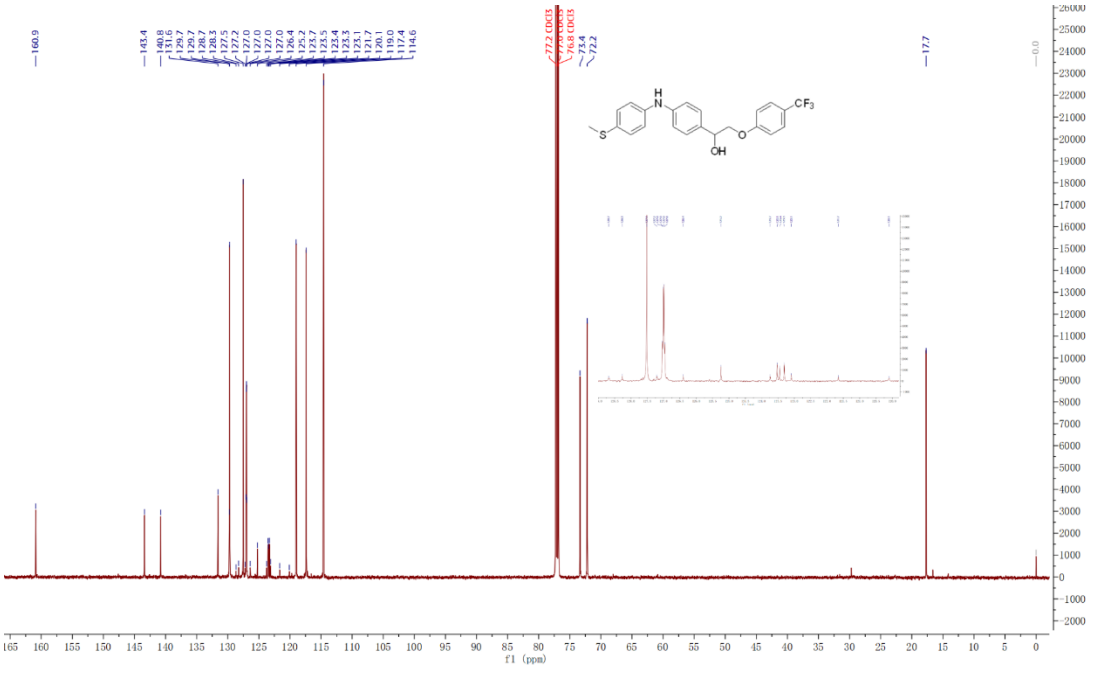
160.9
143.4
140.8
135.6
129.7
129.7
128.7
128.3
127.5
127.2
127.0
127.0
127.0
127.0
126.4
125.2
123.7
123.5
123.4
123.3
123.1
121.7
120.1
119.0
117.4
114.6
77.3 CDCl3
77.0 CDCl3
76.8 CDCl3
73.4
72.2
17.7
0.0
H
N
CF3
S
O
OH
f1 (ppm)

GII-19

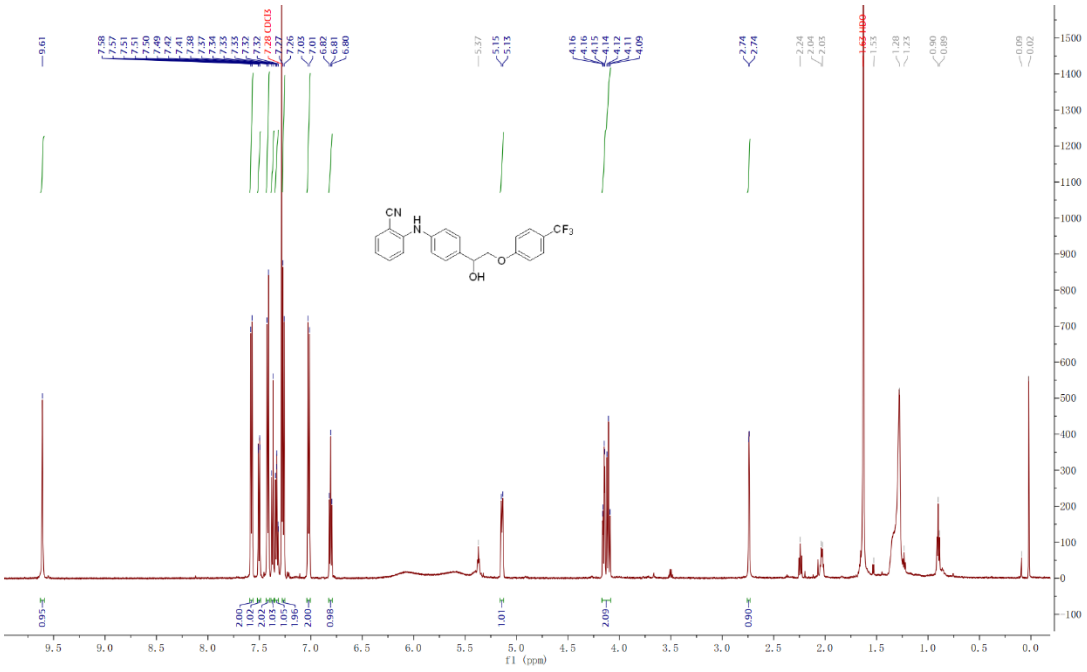

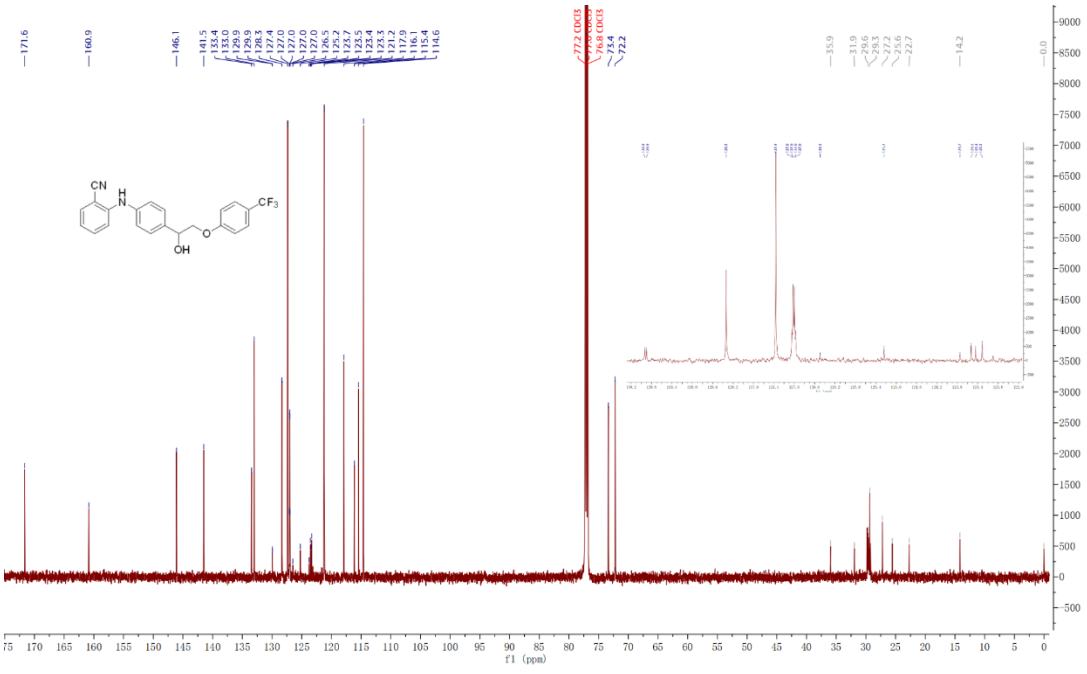

GII-20

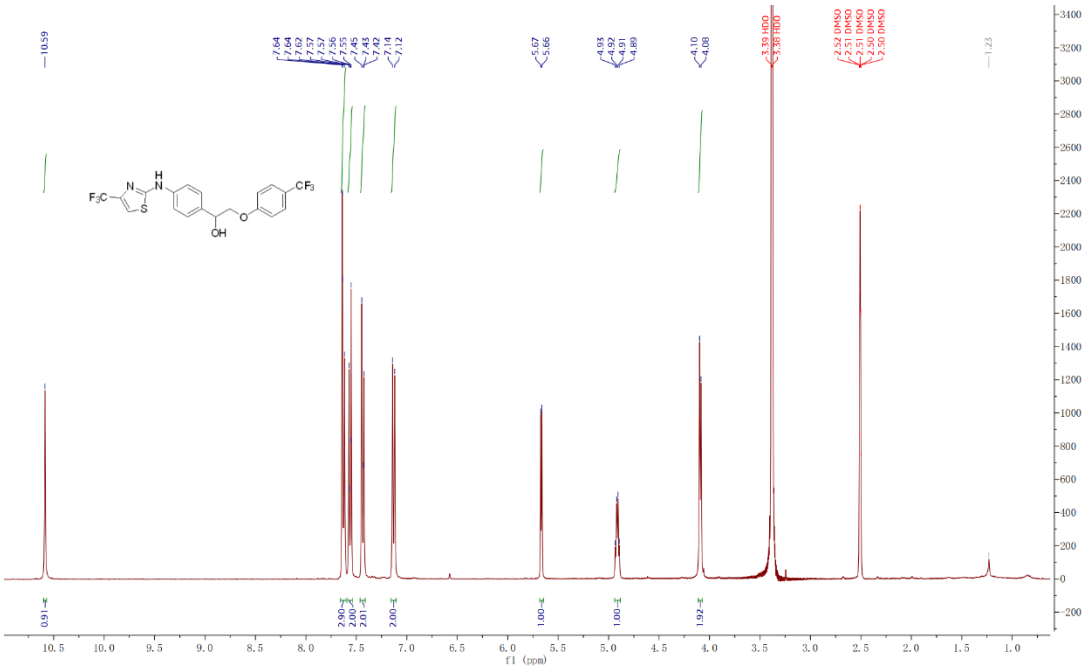
10.59
7.64
7.64
7.62
7.57
7.57
7.56
7.55
7.45
7.44
7.42
7.14
7.12
5.67
5.66
4.93
4.92
4.91
4.89
4.10
4.08
3.39 HDO
3.38 HDO
2.52 DMSO
2.51 DMSO
2.51 DMSO
2.50 DMSO
2.50 DMSO
1.25
0.91
2.90
2.00
2.01
2.00
1.00
1.00
1.92
f1 (ppm)

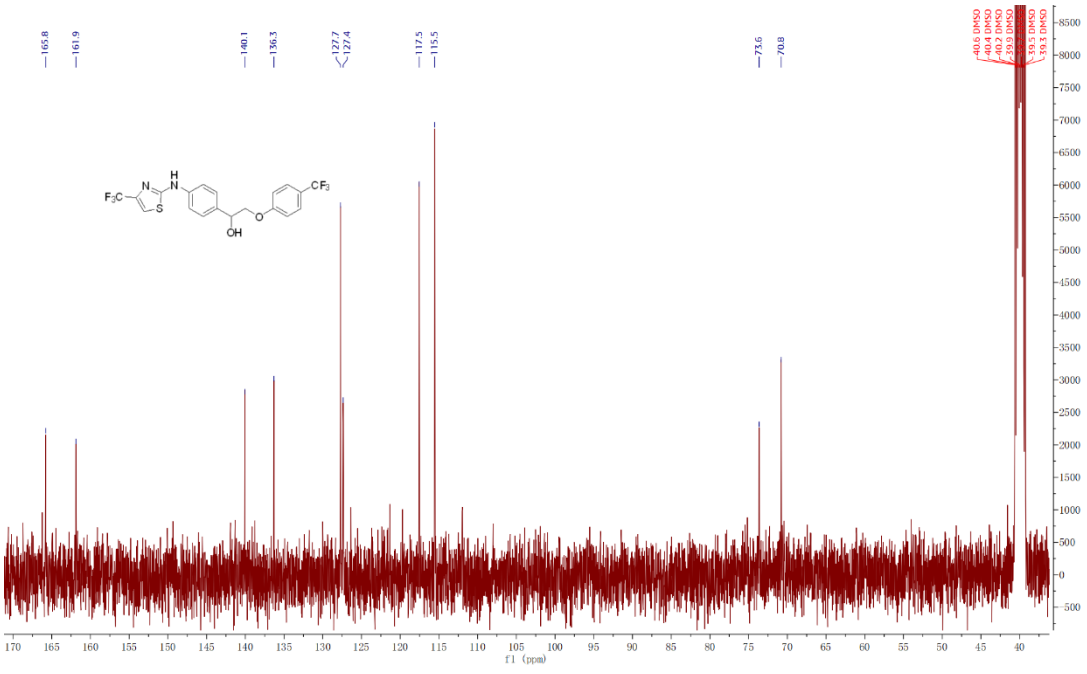
165.8
161.9
140.1
136.3
127.7
127.4
117.5
115.5
73.6
70.8
40.6 DMSO
40.4 DMSO
40.2 DMSO
39.9 DMSO
39.5 DMSO
39.3 DMSO
f1 (ppm)

GII-21

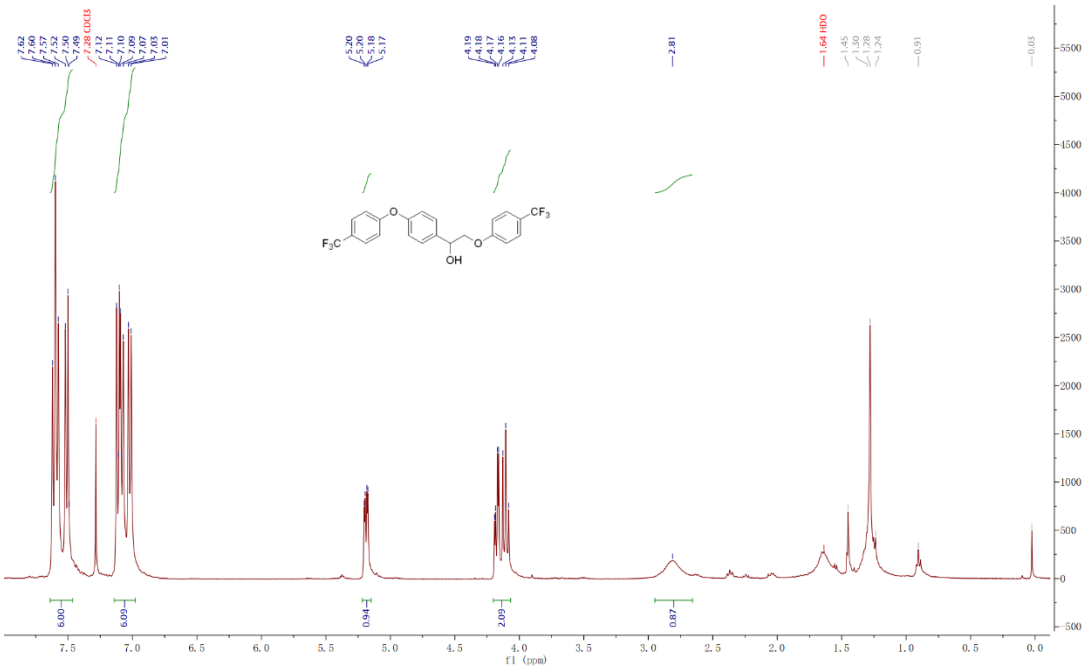
7.62
7.60
7.57
7.52
7.50
7.49
7.26 CDCl3
7.12
7.11
7.10
7.09
7.07
7.05
7.01
5.20
5.20
5.18
5.17
4.19
4.18
4.17
4.16
4.13
4.11
4.08
2.81
1.64 HDO
1.45
1.30
1.26
1.24
0.91
0.05
6.00
6.09
0.94
2.09
0.87
f1 (ppm)

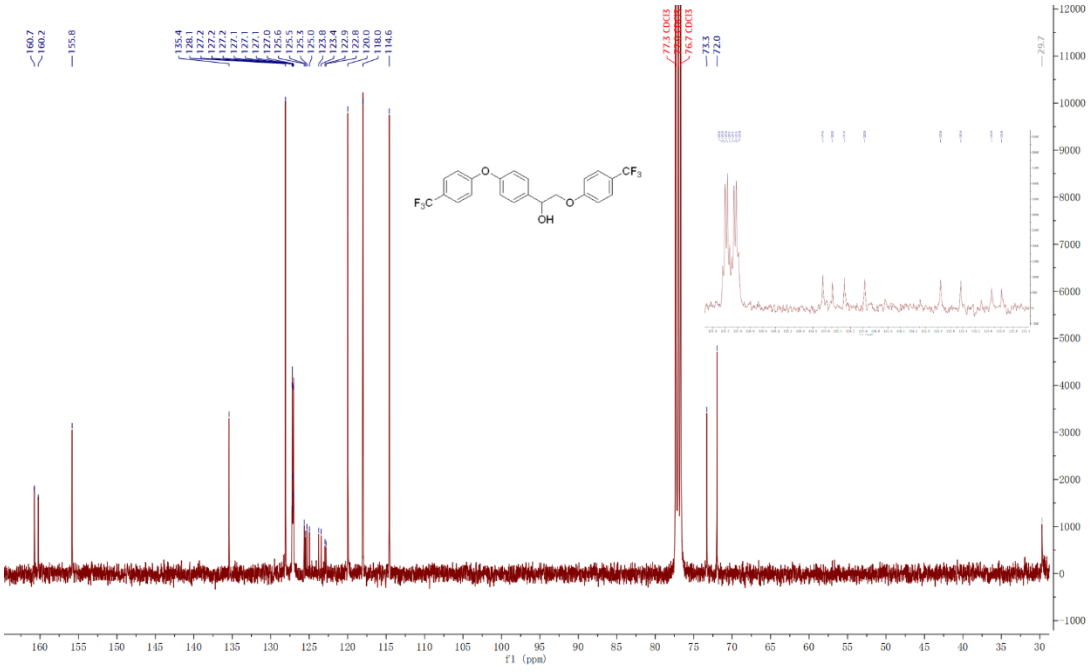
160.7
160.2
155.8
135.4
128.1
127.2
127.2
127.2
127.1
127.1
127.0
125.6
125.5
125.3
125.0
123.8
123.4
122.9
122.8
120.0
118.0
114.6
77.5 CDCl3
76.7 CDCl3
73.3
72.0
29.7
f1 (ppm)

GII-22

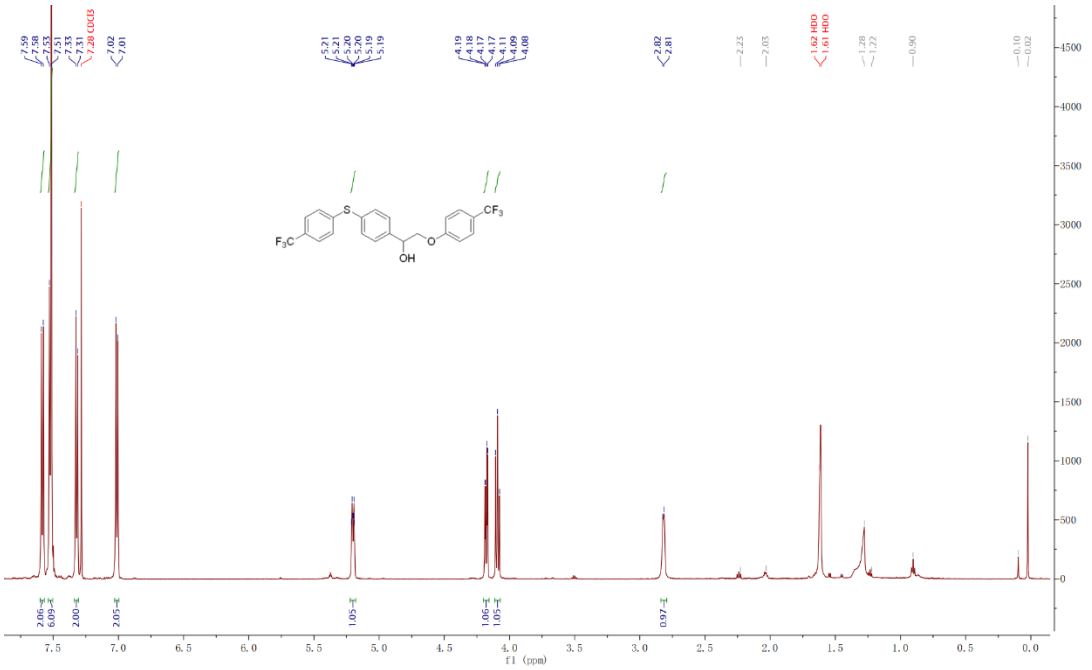
7.59
7.58
7.53
7.51
7.33
7.31
7.28 CDCl3
7.02
7.01
5.21
5.21
5.20
5.20
5.19
5.19
4.19
4.18
4.17
4.17
4.11
4.09
4.08
2.82
2.81
2.25
2.03
1.62 HDO
1.61 HDO
1.28
1.22
0.90
0.10
0.02
S
CF3
F3C
O
OH
2.06
6.09
2.00
2.05
1.05
1.06
1.05
0.97
f1 (ppm)

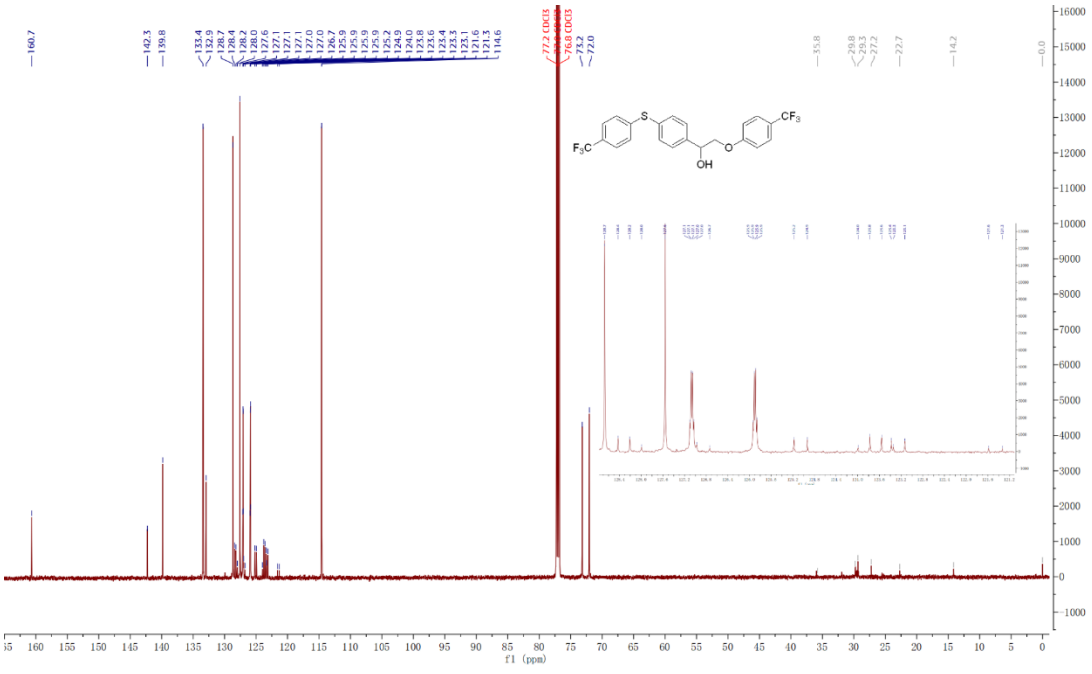
160.7
142.3
139.8
133.4
132.9
128.7
128.4
128.2
128.0
127.6
127.1
127.1
127.1
127.0
127.0
126.7
125.9
125.9
125.9
125.9
125.2
124.9
124.0
123.8
123.6
123.4
123.3
123.1
121.6
121.3
114.6
77.2 CDCl3
76.8 CDCl3
73.2
72.0
55.8
29.8
29.3
27.2
22.7
14.2
0.0
S
CF3
F3C
O
OH
f1 (ppm)

GII-23

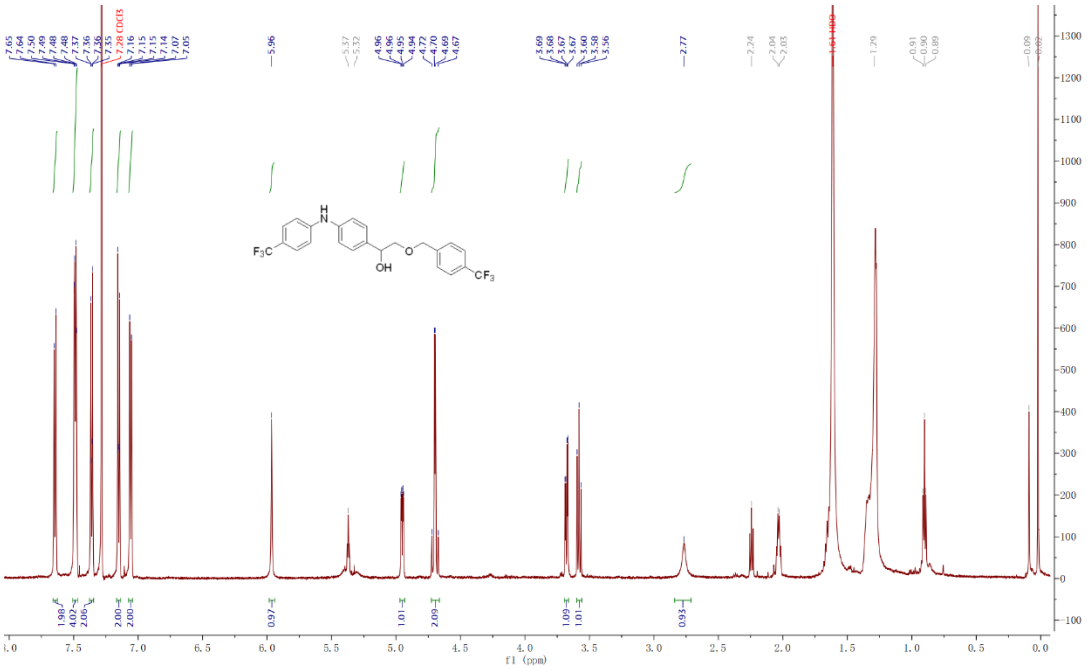
7.65
7.64
7.50
7.49
7.48
7.37
7.36
7.35
7.28 CDCl3
7.16
7.15
7.14
7.07
7.05
5.96
5.37
5.32
4.96
4.95
4.94
4.77
4.70
4.69
4.67
3.69
3.68
3.67
3.60
3.58
3.56
2.77
2.24
2.04
2.03
1.61 H2O
1.29
0.91
0.90
0.89
0.09
0.00
1.98
4.02
2.06
2.00
2.00
0.97
1.01
2.09
1.09
1.01
0.93
f1 (ppm)

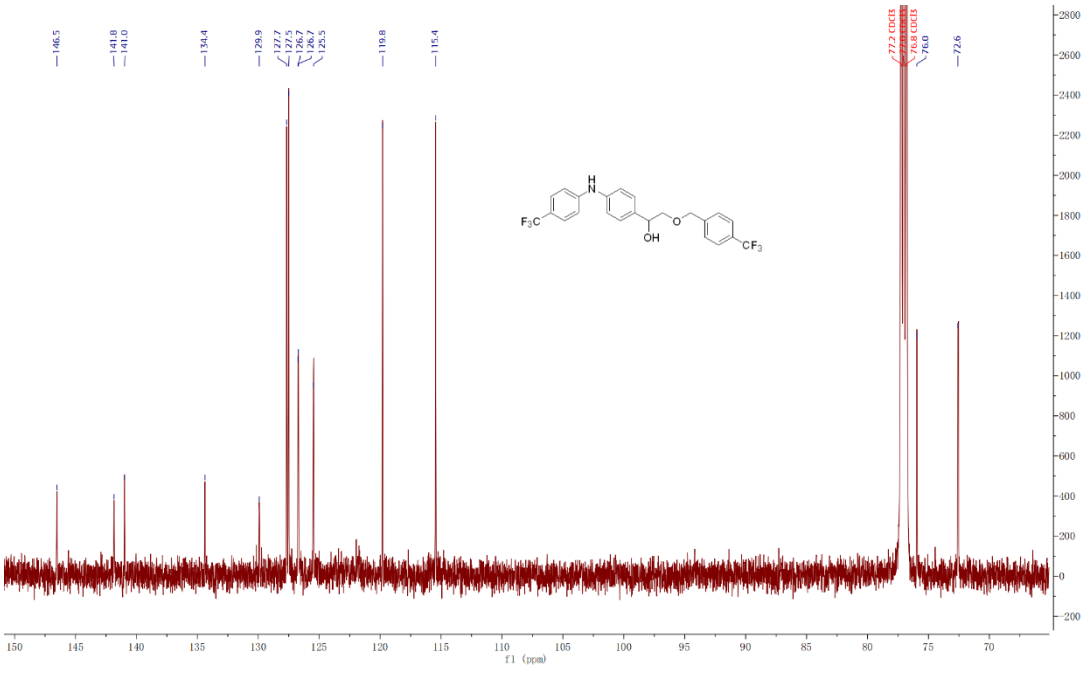
146.5
141.8
141.0
134.4
129.9
127.7
127.5
126.7
126.7
125.5
119.8
115.4
77.2 CDCl3
77.0 CDCl3
76.8 CDCl3
76.0
72.6
f1 (ppm)

GII-24

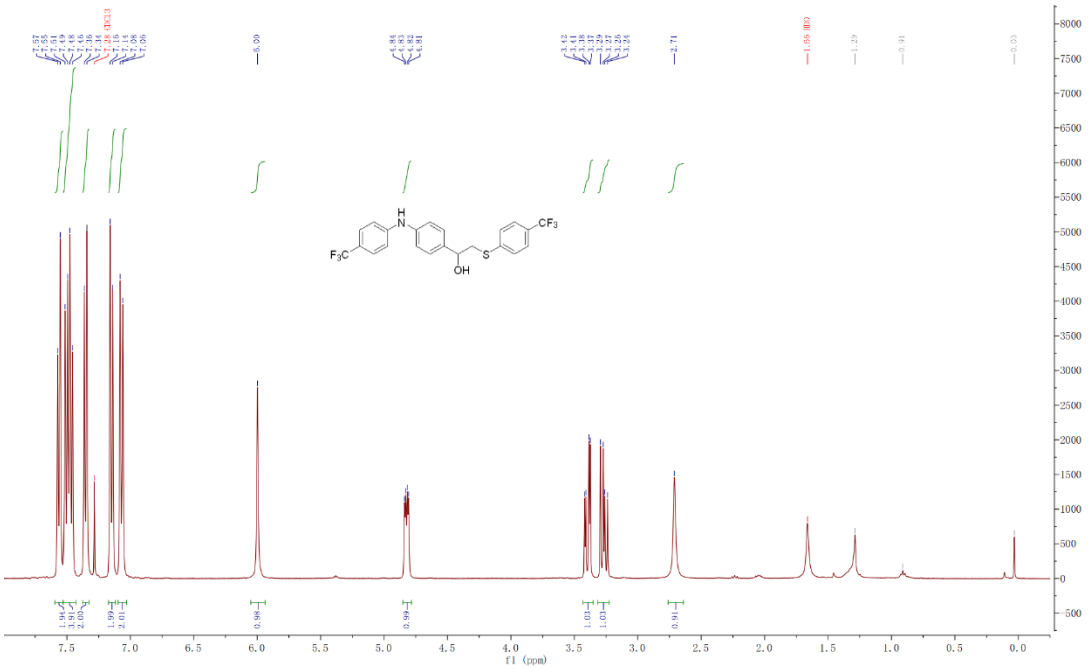

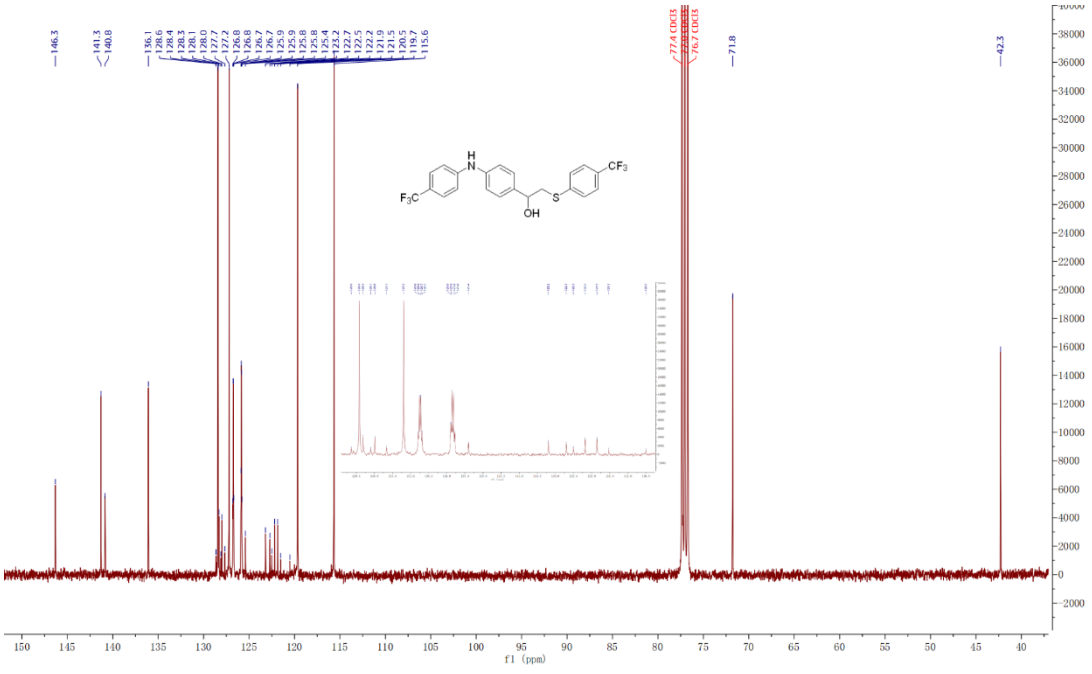

GII-25

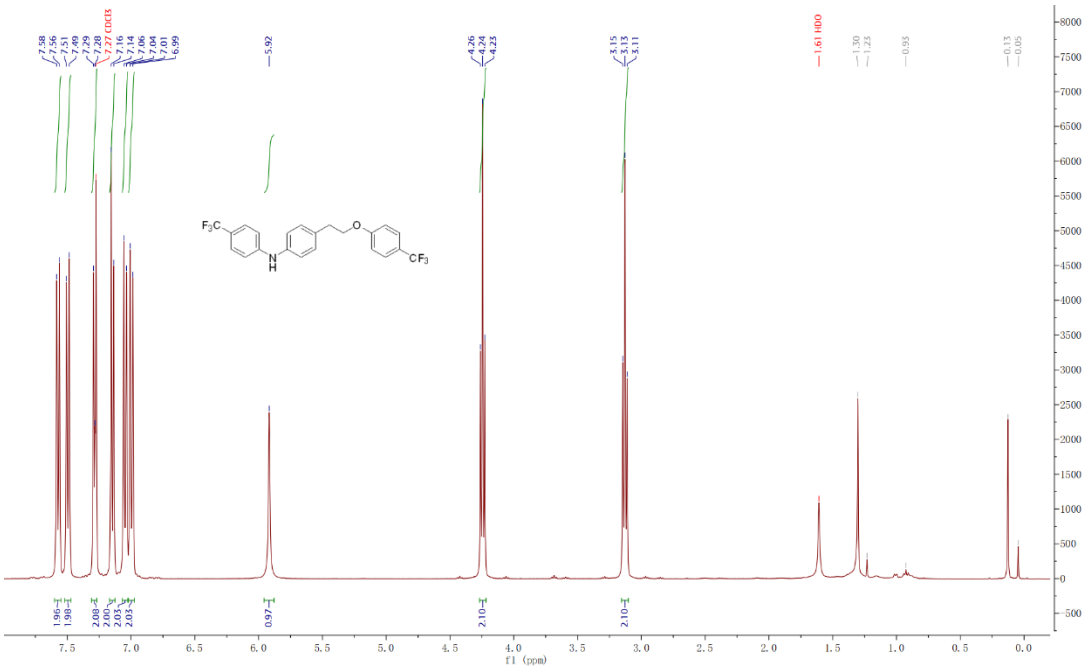
7.58
7.56
7.51
7.49
7.29
7.28
7.27 CDCl3
7.16
7.14
7.06
7.04
7.01
6.99
5.92
4.26
4.24
4.23
5.15
5.13
5.11
1.61 HDO
1.30
1.25
0.93
0.13
0.05
F3C
N
H
O
CF3
1.96
1.99
2.08
2.00
2.03
2.03
0.97
2.10
2.10
f1 (ppm)

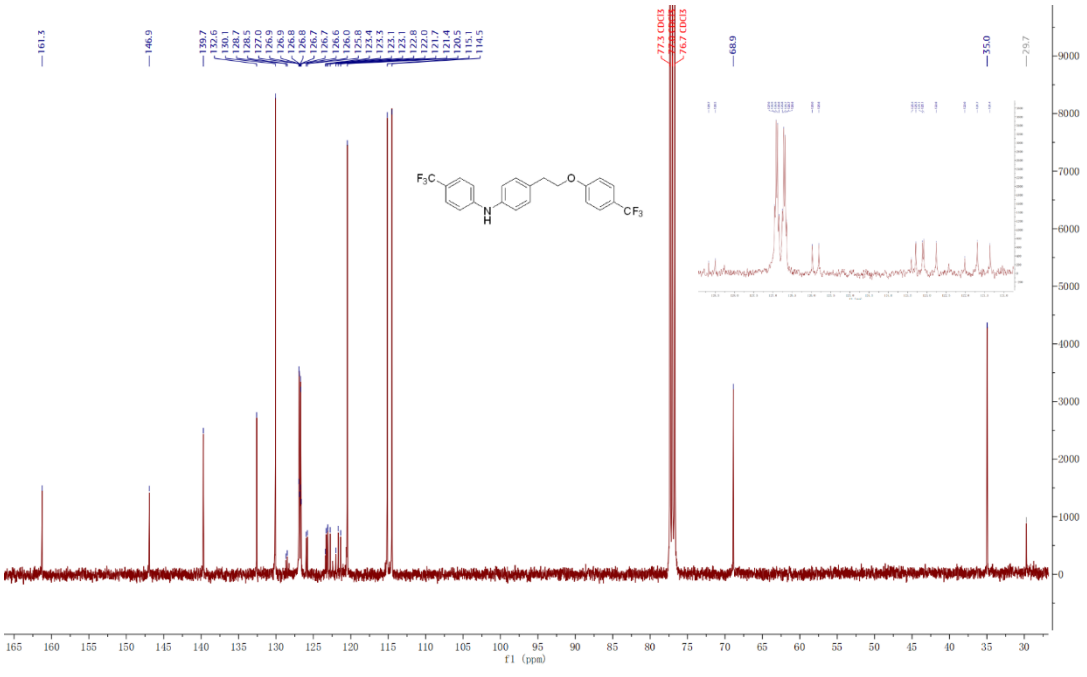
161.3
146.9
139.7
132.6
130.1
128.7
128.5
127.0
126.9
126.8
126.8
126.7
126.7
126.7
126.6
126.0
125.8
123.4
123.3
123.1
123.1
122.8
122.0
121.7
121.4
120.5
115.1
114.5
77.3 CDCl3
77.0
76.7 CDCl3
68.9
35.0
29.7
F3C
N
H
O
CF3
f1 (ppm)

GII-26

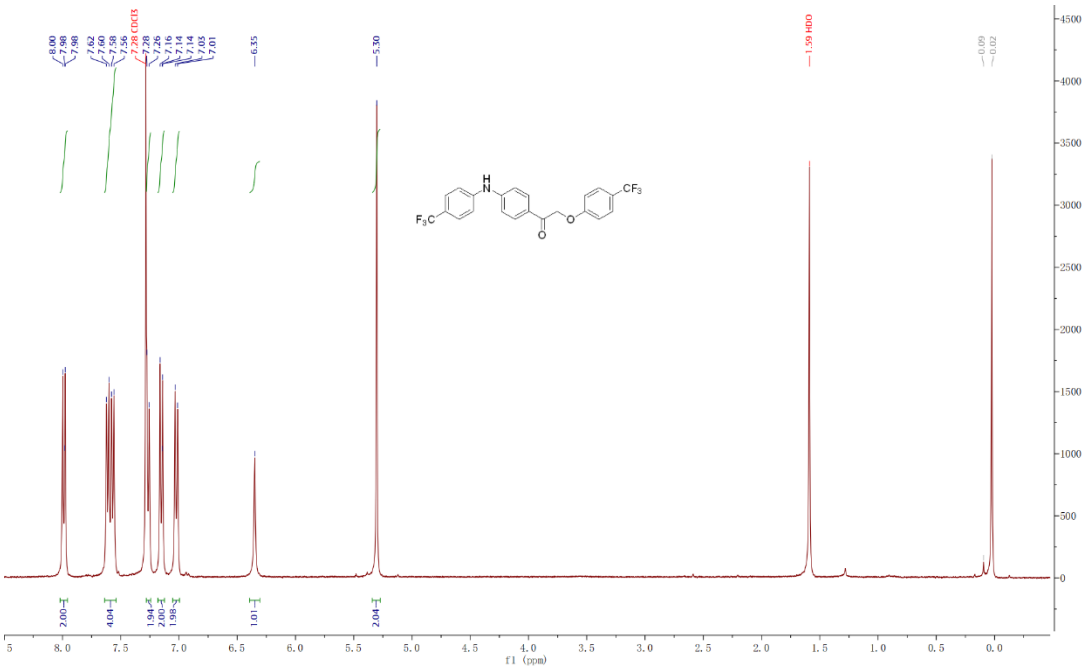
8.00
7.98
7.98
7.62
7.60
7.58
7.58
7.56
7.28 CDCl3
7.28
7.26
7.16
7.14
7.14
7.03
7.01
6.35
5.30
1.59 HDO
0.09
0.02
2.00
4.04
1.94
2.00
1.98
1.01
2.04
f1 (ppm)

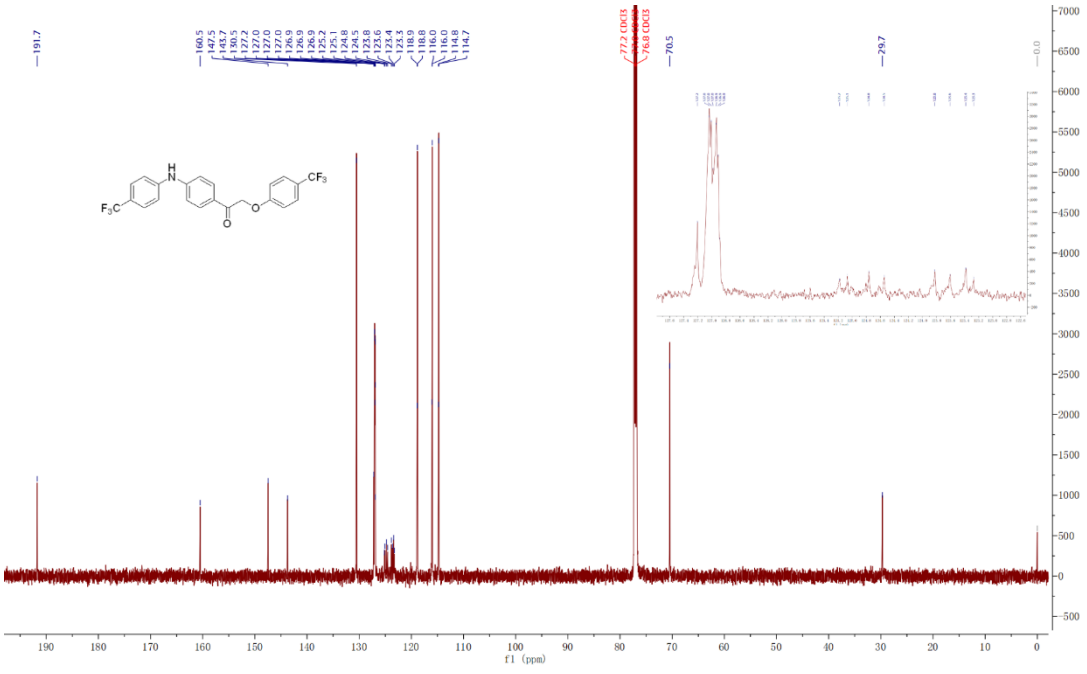
191.7
160.5
147.5
145.7
130.5
127.2
127.0
127.0
127.0
126.9
126.9
126.9
125.2
125.1
124.8
124.5
123.8
123.6
123.4
123.3
118.9
118.8
116.0
116.0
114.8
114.7
77.2 CDCl3
76.8 CDCl3
70.5
29.7
f1 (ppm)

GII-27

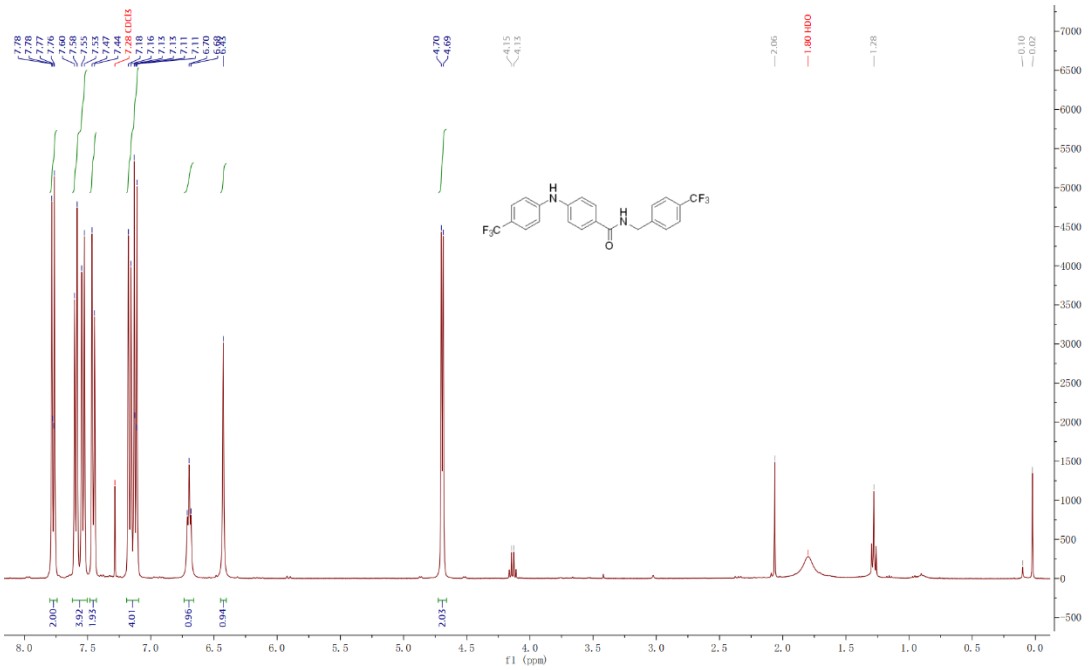
7.78
7.78
7.77
7.76
7.60
7.58
7.55
7.53
7.47
7.44
7.28 CDCl3
7.18
7.16
7.13
7.13
7.11
7.11
6.70
6.68
6.68
4.70
4.69
4.15
4.15
2.06
1.80 HDO
1.28
0.10
0.02
2.00
3.92
1.93
4.01
0.96
0.94
2.03
f1 (ppm)

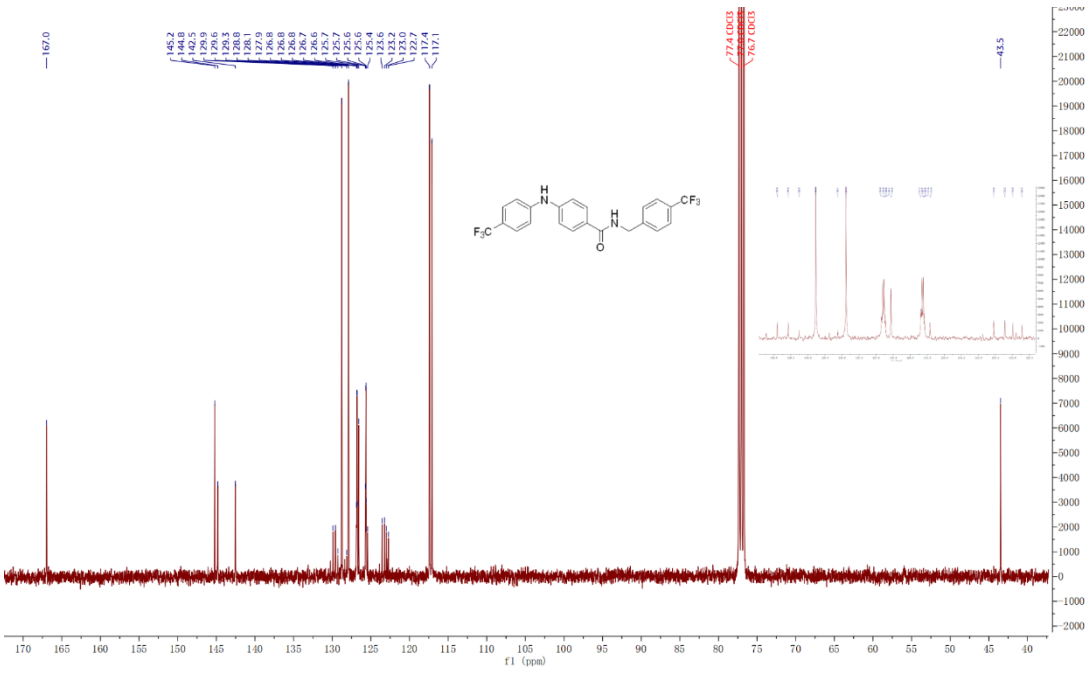
167.0
145.2
144.8
142.5
129.9
129.6
129.3
128.8
128.1
127.9
126.8
126.8
126.8
126.7
126.6
125.7
125.7
125.6
125.6
125.4
123.6
123.2
123.0
122.7
117.4
117.1
77.4 CDCl3
77.0 CDCl3
76.7 CDCl3
43.5
f1 (ppm)

GII-28

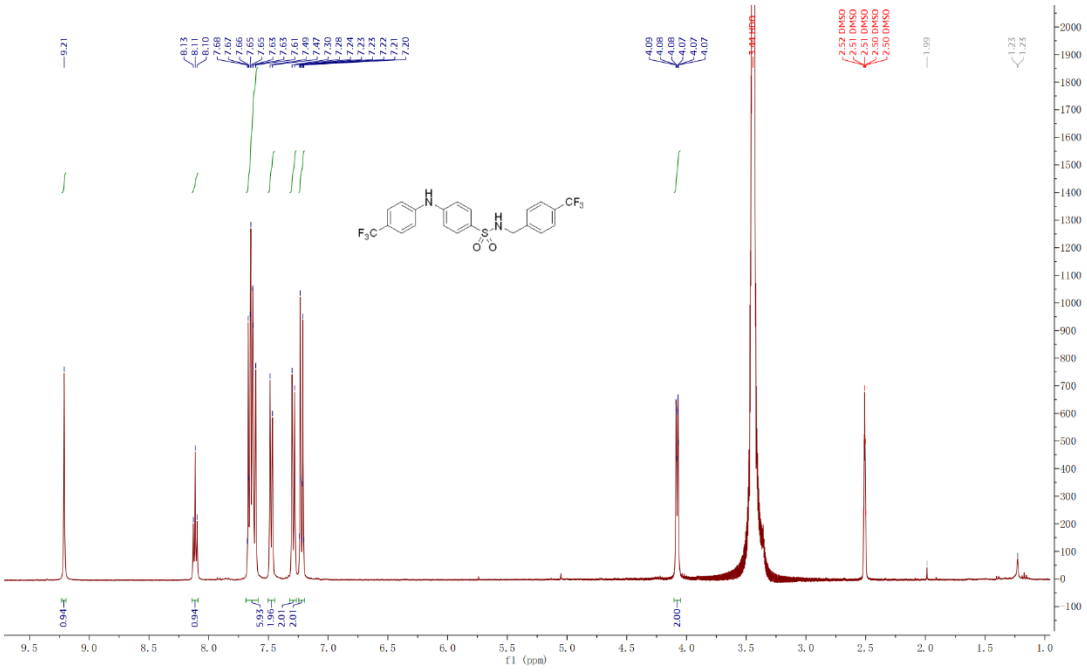

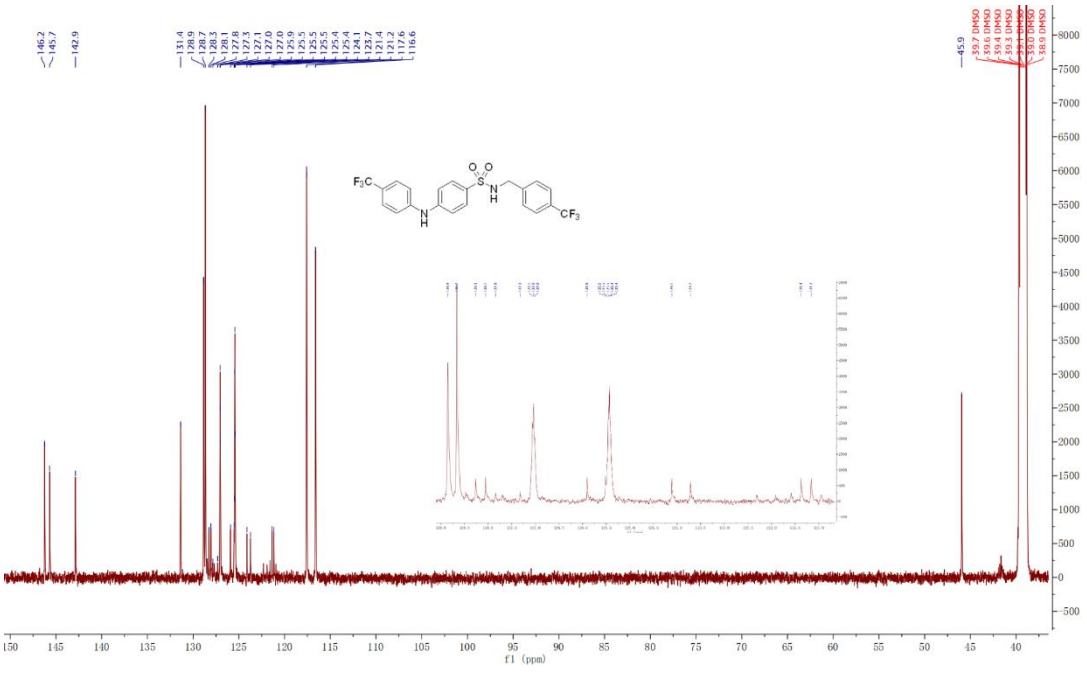

GII-29

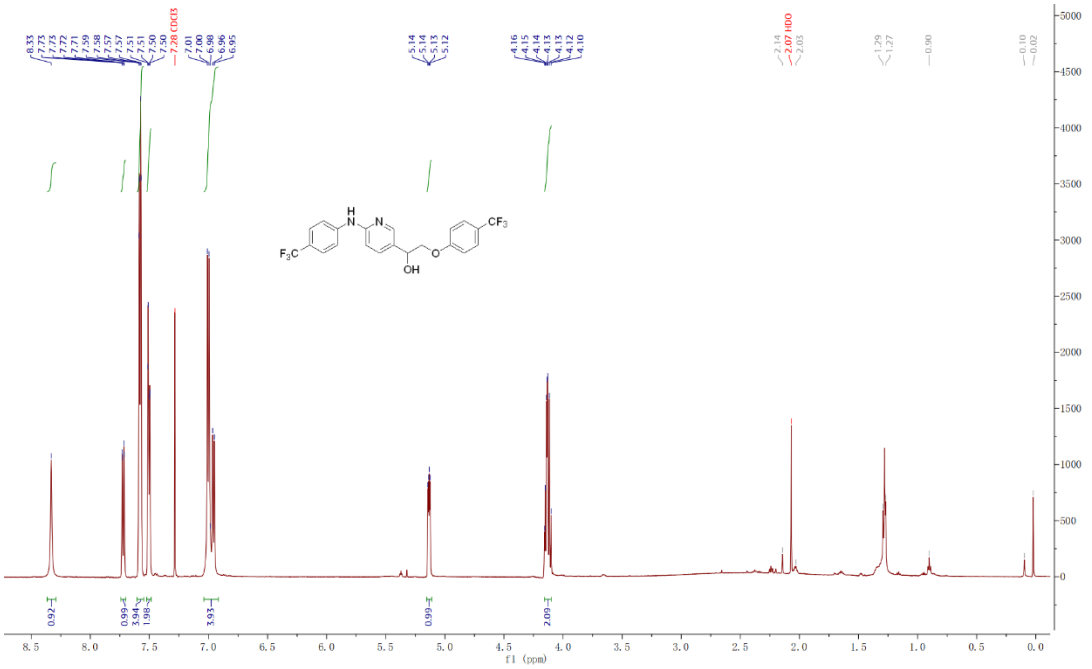
8.33
7.75
7.73
7.72
7.71
7.59
7.58
7.57
7.57
7.51
7.51
7.50
7.50
7.28 CDCl3
7.01
7.00
6.98
6.96
6.95
5.14
5.14
5.13
5.12
4.16
4.15
4.14
4.13
4.13
4.12
4.12
4.10
2.14
2.07 HDO
2.03
1.29
1.27
0.90
0.10
0.02
0.92
0.99
3.94
1.98
3.91
0.99
2.09
f1 (ppm)

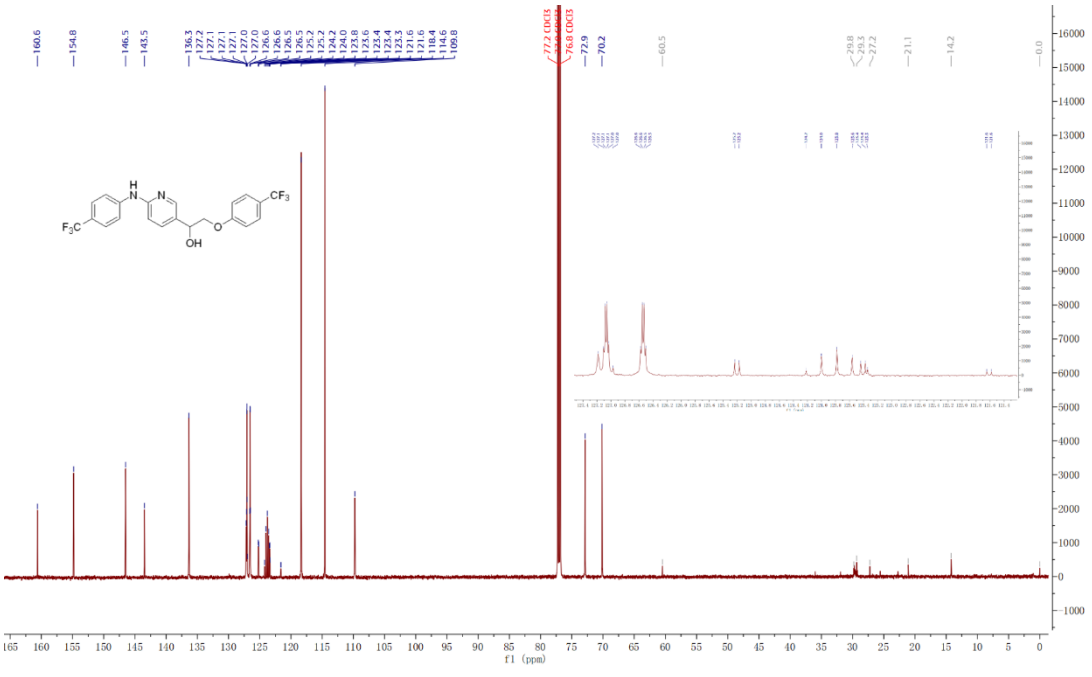
160.6
154.8
146.5
143.5
136.3
127.2
127.1
127.1
127.1
127.0
127.0
126.6
126.6
126.5
126.5
125.3
125.2
124.2
124.0
123.8
123.6
123.4
123.4
123.3
121.6
121.6
118.4
114.6
109.8
77.2 CDCl3
76.8 CDCl3
72.9
70.2
60.5
29.8
29.3
27.2
21.1
14.2
0.0
f1 (ppm)

GII-30

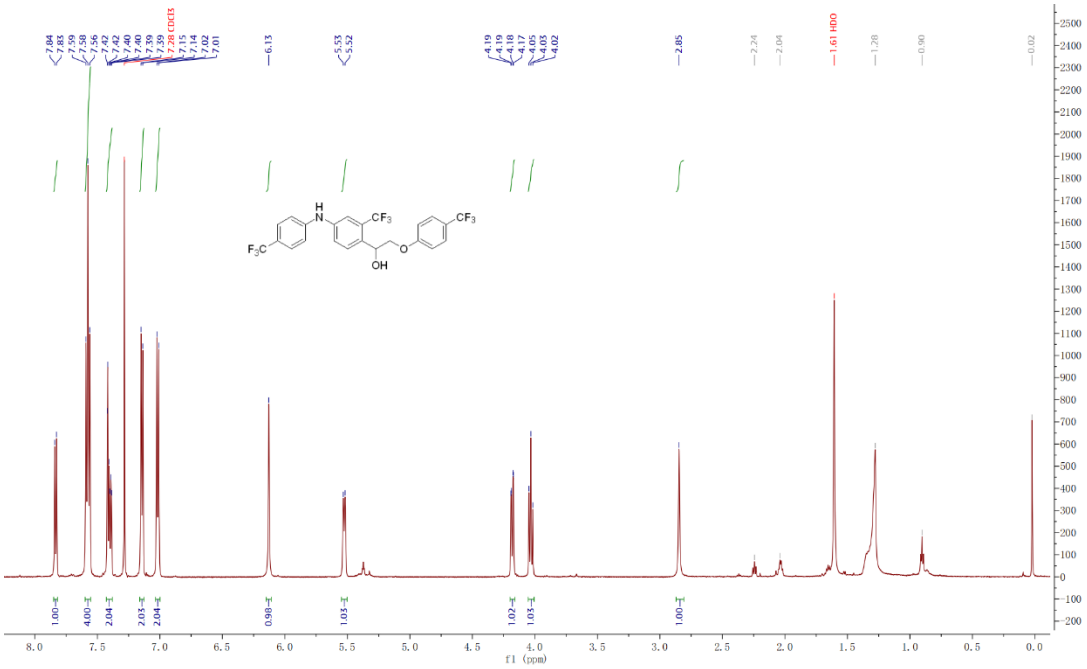
7.84
7.83
7.59
7.58
7.56
7.42
7.41
7.40
7.39
7.39
7.26 CDCl3
7.15
7.14
7.02
7.01
6.13
5.53
5.52
4.19
4.19
4.18
4.17
4.05
4.03
4.02
2.85
2.24
2.04
1.61 HDO
1.28
0.90
0.02
1.00
4.00
2.04
2.01
2.04
0.98
1.03
1.02
1.03
1.00
f1 (ppm)

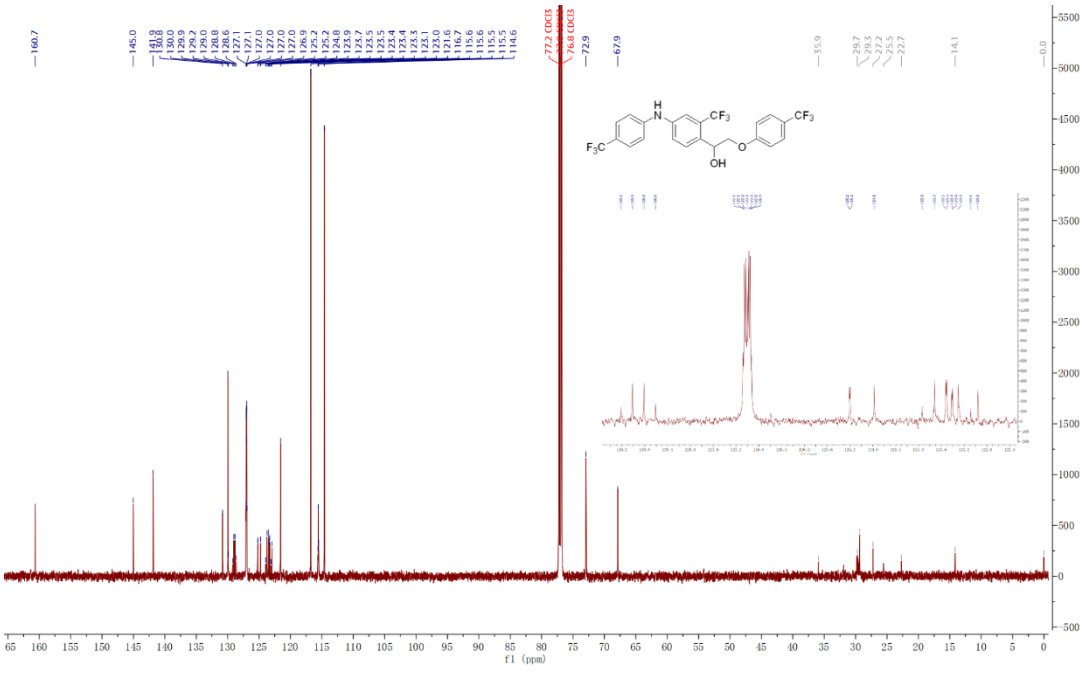
160.7
145.0
141.8
130.8
130.0
129.9
129.2
129.0
128.8
128.6
127.1
127.1
127.0
127.0
127.0
127.0
126.9
125.2
125.2
124.8
123.9
123.7
123.5
123.5
123.4
123.4
123.3
123.1
121.0
121.0
116.7
115.6
115.6
115.5
115.5
114.6
77.3 CDCl3
76.8 CDCl3
72.9
67.9
55.9
29.7
29.5
27.2
25.5
22.7
14.1
0.0
f1 (ppm)

GII-31

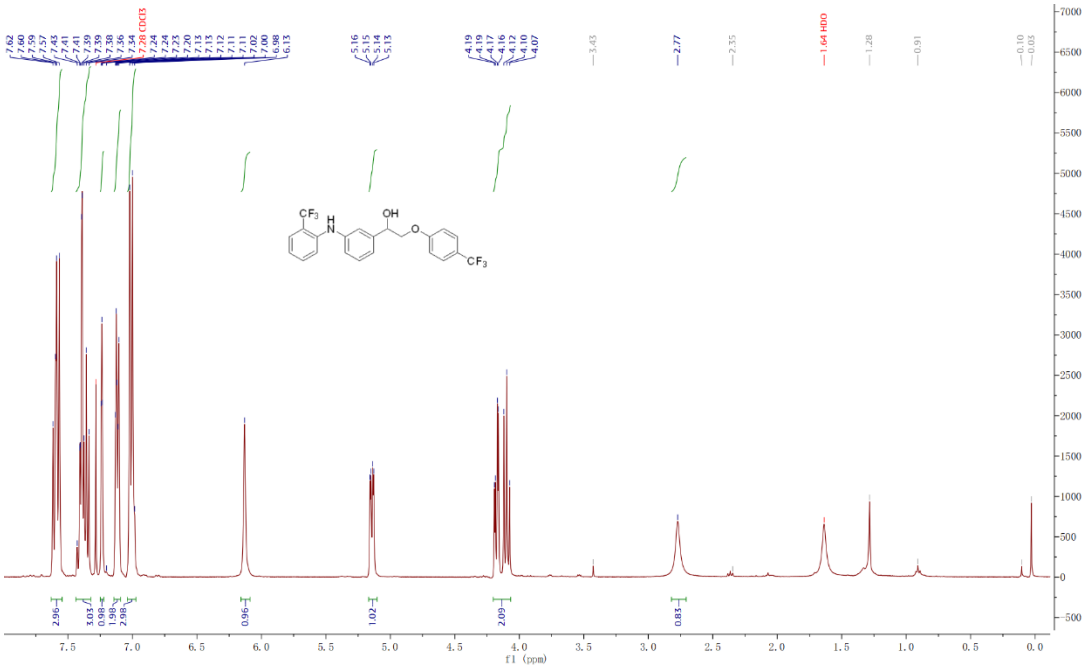
7.62
7.60
7.59
7.57
7.45
7.41
7.41
7.39
7.39
7.38
7.36
7.26 CDCl3
7.24
7.23
7.20
7.13
7.12
7.11
7.11
7.00
6.98
6.13
5.16
5.15
5.14
5.13
4.19
4.19
4.17
4.16
4.12
4.10
4.07
3.45
2.77
2.35
1.64 HDO
1.28
0.91
0.10
0.05
CF3
H
N
OH
O
CF3
2.96
3.03
0.98
1.00
2.98
0.96
1.02
2.03
0.83
f1 (ppm)

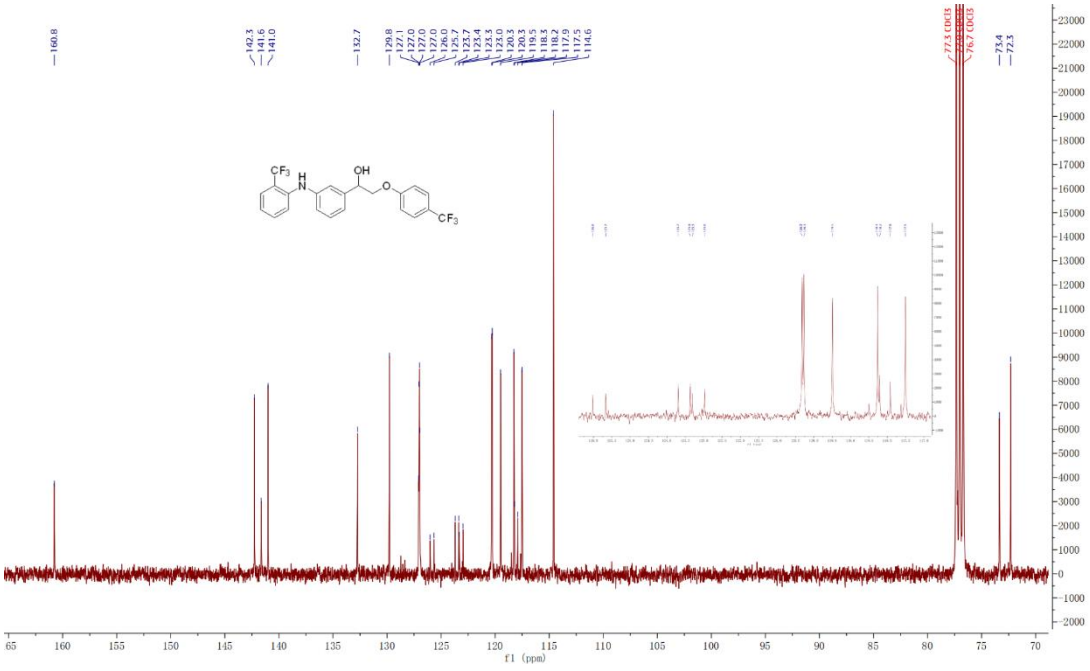
160.8
142.3
141.6
141.0
132.7
129.8
127.1
127.0
127.0
127.0
127.0
126.0
125.7
123.7
123.4
123.3
123.0
120.3
120.3
119.5
118.3
118.2
117.9
117.5
114.6
77.3 CDCl3
76.7 CDCl3
73.4
72.3
CF3
H
N
OH
O
CF3
f1 (ppm)

GII-32

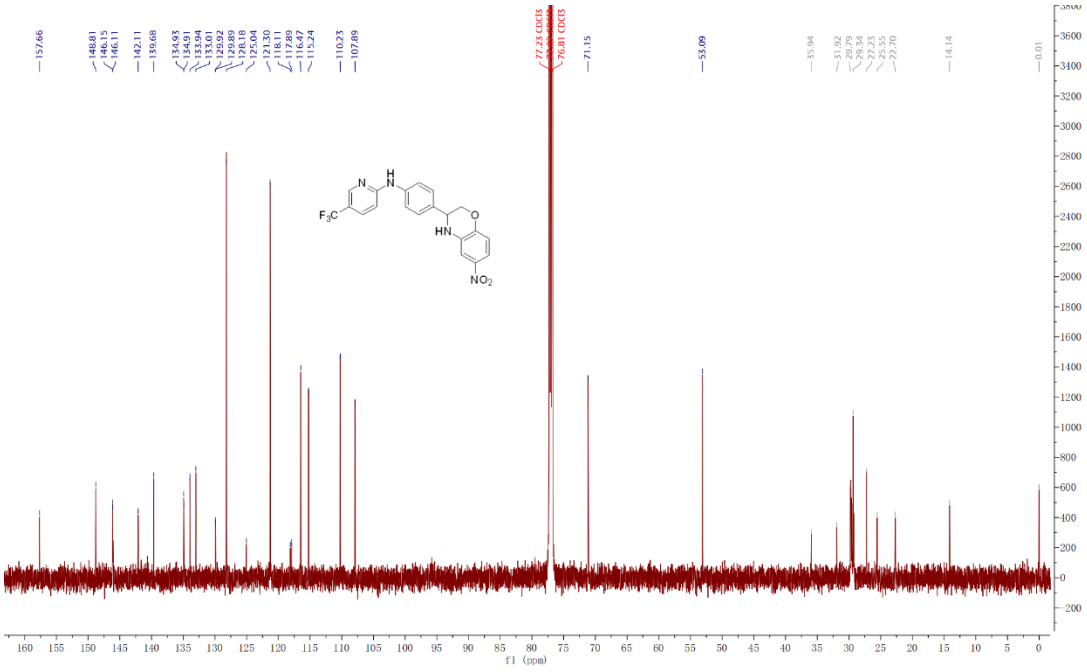
157.66
148.81
146.15
146.11
142.11
139.68
134.93
134.91
133.64
133.01
129.92
129.89
126.18
125.64
121.30
118.11
117.89
116.47
115.24
110.23
107.89
77.25 CDCl3
76.81 CDCl3
71.15
53.09
55.94
31.92
29.79
29.54
27.23
25.55
22.70
14.14
0.01
F3C
HN
NO2
f1 (ppm)

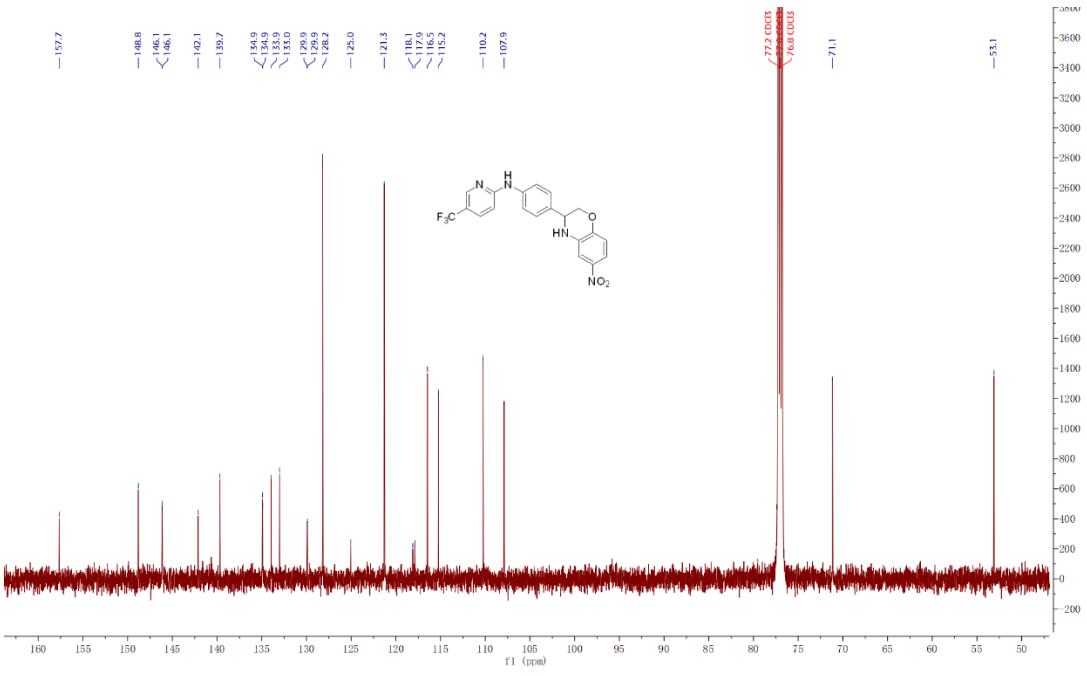
157.7
148.8
146.1
146.1
142.1
139.7
134.9
134.9
133.9
133.0
129.9
129.9
128.2
125.0
121.3
118.1
117.9
116.5
115.2
110.2
107.9
77.2 CDCl3
76.8 CDCl3
71.1
53.1
F3C
HN
NO2
f1 (ppm)

GII-33

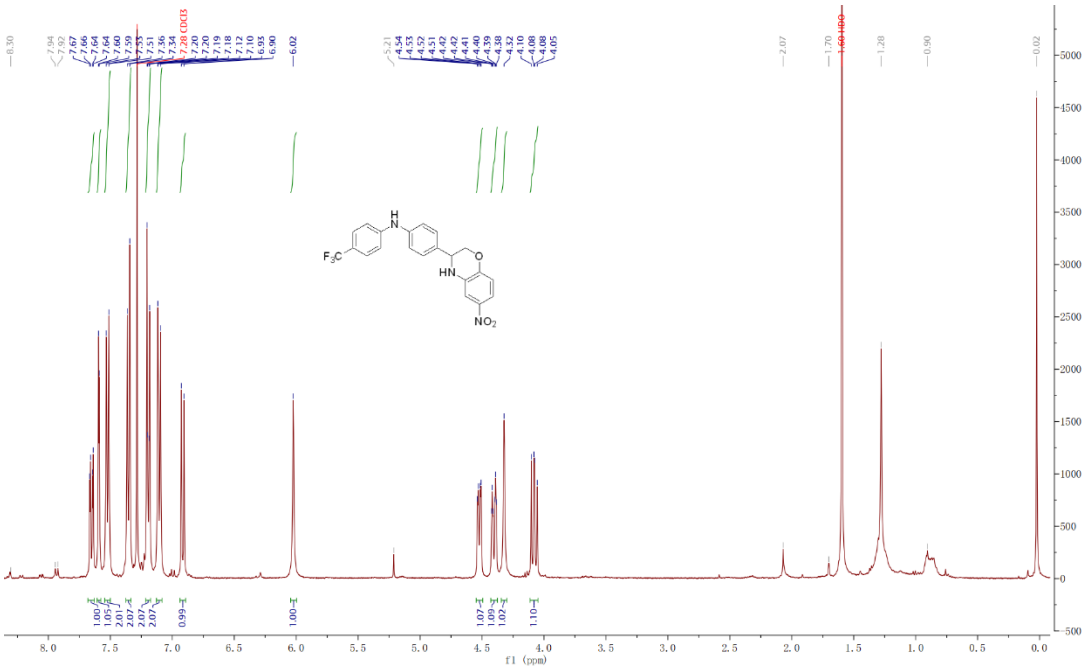

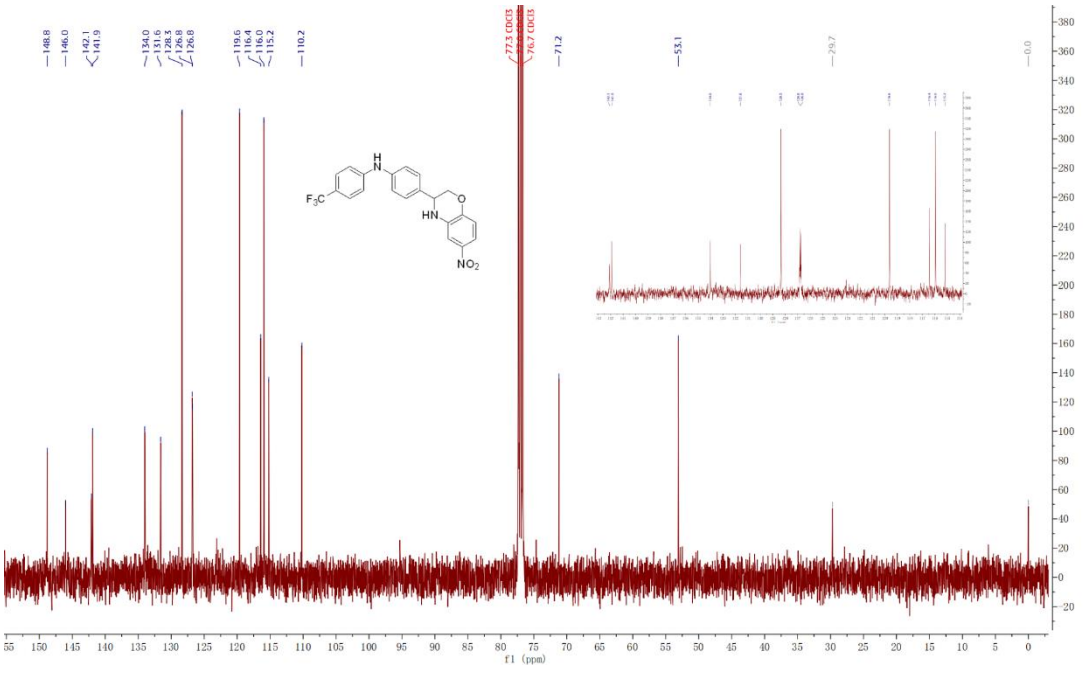

Appendix II

HPLC analysis of compounds

GI-1

Empower™ 3 SOFTWARE

Default Individual Report

SAMPLE INFORMATION

Sample Name:	NusG_A5	Acquired By:	System
Sample Type:	Unknown	Sample Set Name:	NusG_20190630_1
Vial:	1:A,5	Acq. Method Set:	NusG
Injection #:	1	Processing Method	A5
Injection Volume:	10.00 ul	Channel Name:	232.8nm
Run Time:	60.0 Minutes	Proc. Chnl. Descr.:	2998 PDA 232.8 nm (2998
Date Acquired:	30/6/2019 9:52:56 PM HKT		
Date Processed:	18/9/2022 5:15:03 AM HKT		

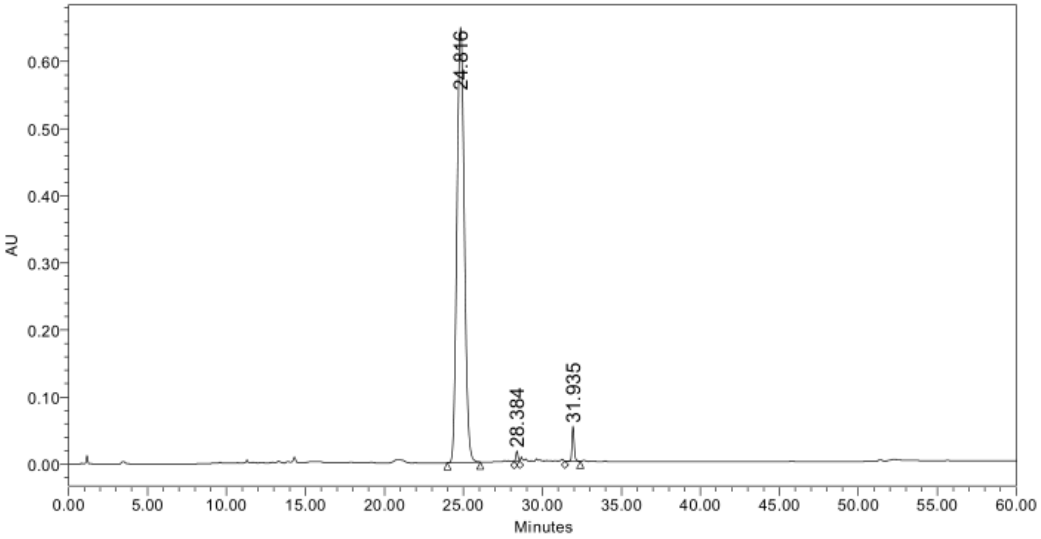

	RT	Area	% Area	Height
1	24.816	21113067	97.06	648954
2	28.384	143315	0.66	15677
3	31.935	497002	2.28	52145

GI-2

Empower 3 SOFTWARE

Default Individual Report

SAMPLE INFORMATION

Sample Name:	NusG_A2	Acquired By:	System
Sample Type:	Unknown	Sample Set Name:	NusG_20190628
Vial:	1:A,2	Acq. Method Set:	NusG
Injection #:	1	Processing Method	A2
Injection Volume:	10.00 ul	Channel Name:	309.0nm
Run Time:	63.0 Minutes	Proc. Chnl. Descr.:	2998 PDA 309.0 nm (2998
Date Acquired:	28/6/2019 4:22:40 PM HKT		
Date Processed:	18/9/2022 4:59:48 AM HKT		

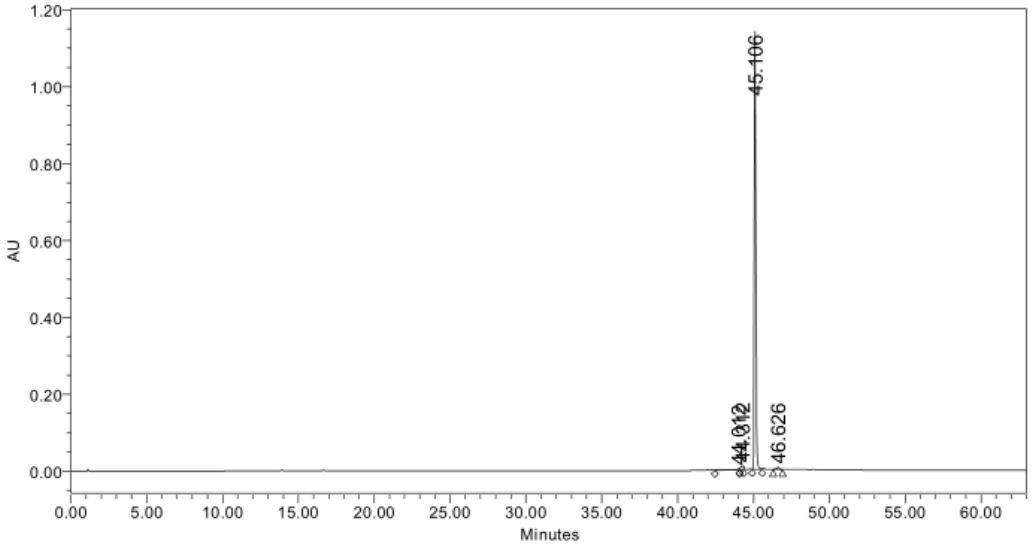

	RT	Area	% Area	Height
1	44.012	61522	0.75	2590
2	44.312	117237	1.43	10063
3	45.106	7946094	97.06	1139725
4	46.626	61946	0.76	5930

GI-3

Empower™ 3 SOFTWARE

Default Individual Report

SAMPLE INFORMATION

Sample Name:	NusG_A3	Acquired By:	System
Sample Type:	Unknown	Sample Set Name:	NusG_A3
Vial:	1:A,3	Acq. Method Set:	NusG
Injection #:	1	Processing Method	A3
Injection Volume:	10.00 ul	Channel Name:	244.6nm
Run Time:	63.0 Minutes	Proc. Chnl. Descr.:	2998 PDA 244.6 nm (2998
Date Acquired:	29/6/2019 9:01:20 PM HKT		
Date Processed:	18/9/2022 5:03:32 AM HKT		

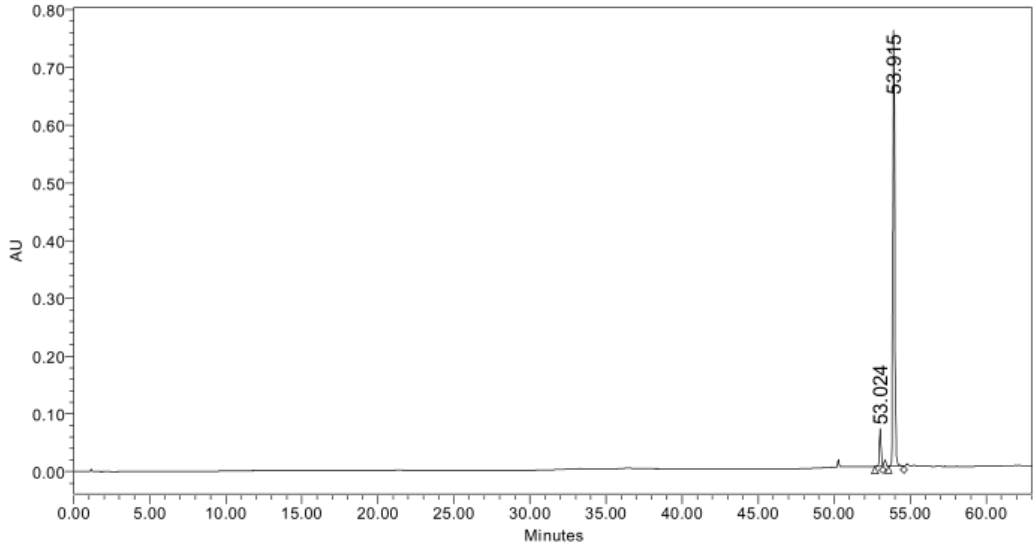

	RT	Area	% Area	Height
1	53.024	499756	7.10	65230
2	53.915	6539599	92.90	755524

GI-4

Empower™ 3 SOFTWARE

Default Individual Report

SAMPLE INFORMATION

Sample Name:	NusG_A7	Acquired By:	System
Sample Type:	Unknown	Sample Set Name:	NusG_20190701
Vial:	1:A,7	Acq. Method Set:	NusG
Injection #:	1	Processing Method	a7016
Injection Volume:	10.00 ul	Channel Name:	306.6nm
Run Time:	70.0 Minutes	Proc. Chnl. Descr.:	2998 PDA 306.6 nm (2998
Date Acquired:	1/7/2019 11:40:29 PM HKT		
Date Processed:	29/11/2022 4:26:01 AM HKT		

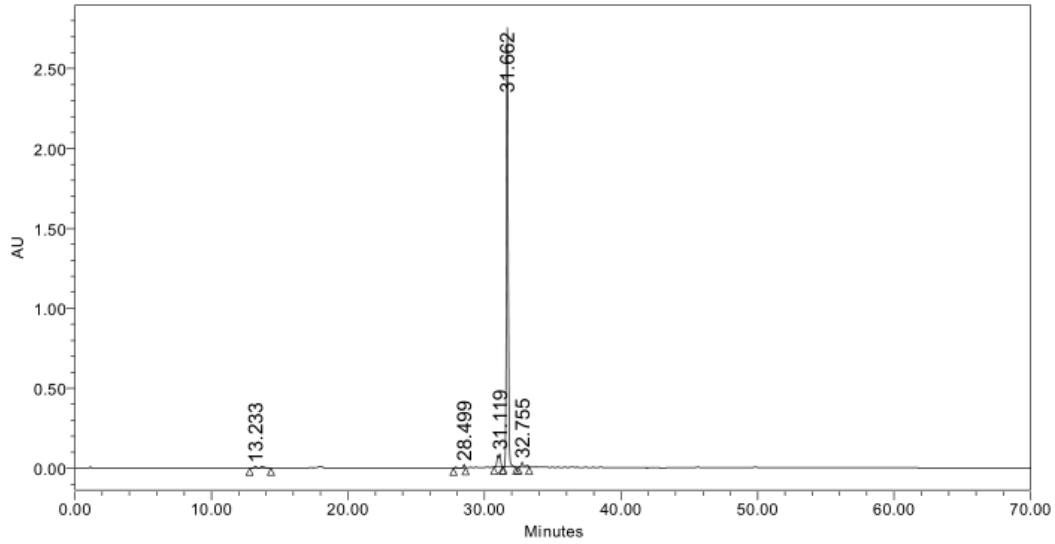

	RT	Area	% Area	Height
1	13.233	313684	1.17	11710
2	28.499	196713	0.73	19224
3	31.119	1288036	4.79	83525
4	31.662	24647615	91.70	2748774
5	32.755	433724	1.61	30285

GI-5

Empower 3 SOFTWARE

Default Individual Report

SAMPLE INFORMATION

Sample Name:	NusG_A4	Acquired By:	System
Sample Type:	Unknown	Sample Set Name:	NusG_20190630
Vial:	1:A,4	Acq. Method Set:	NusG
Injection #:	1	Processing Method	A4
Injection Volume:	10.00 ul	Channel Name:	244.6nm
Run Time:	60.0 Minutes	Proc. Chnl. Descr.:	2998 PDA 244.6 nm (2998
Date Acquired:	30/6/2019 3:51:41 PM HKT		
Date Processed:	18/9/2022 5:11:37 AM HKT		

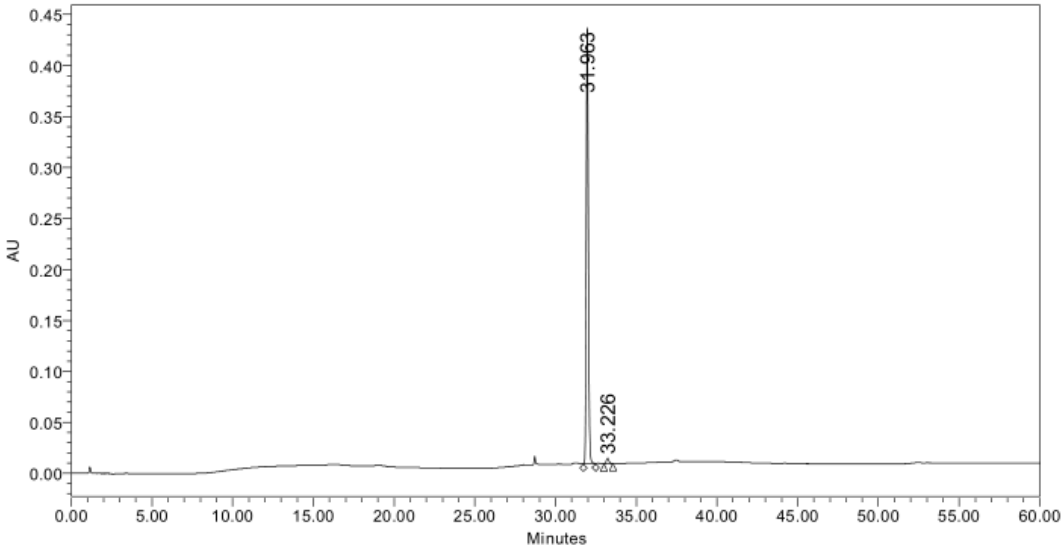

	RT	Area	% Area	Height
1	31.963	3789383	98.44	427792
2	33.226	60057	1.56	5545

GI-6

Empower 3 SOFTWARE

Default Individual Report

SAMPLE INFORMATION

Sample Name:	NusG_A6	Acquired By:	System
Sample Type:	Unknown	Sample Set Name:	NusG_20190701
Vial:	1:A,6	Acq. Method Set:	NusG
Injection #:	1	Processing Method	A6
Injection Volume:	10.00 ul	Channel Name:	242.3nm
Run Time:	70.0 Minutes	Proc. Chnl. Descr.:	2998 PDA 242.3 nm (2998
Date Acquired:	1/7/2019 10:30:08 PM HKT		
Date Processed:	19/9/2022 5:02:27 AM HKT		

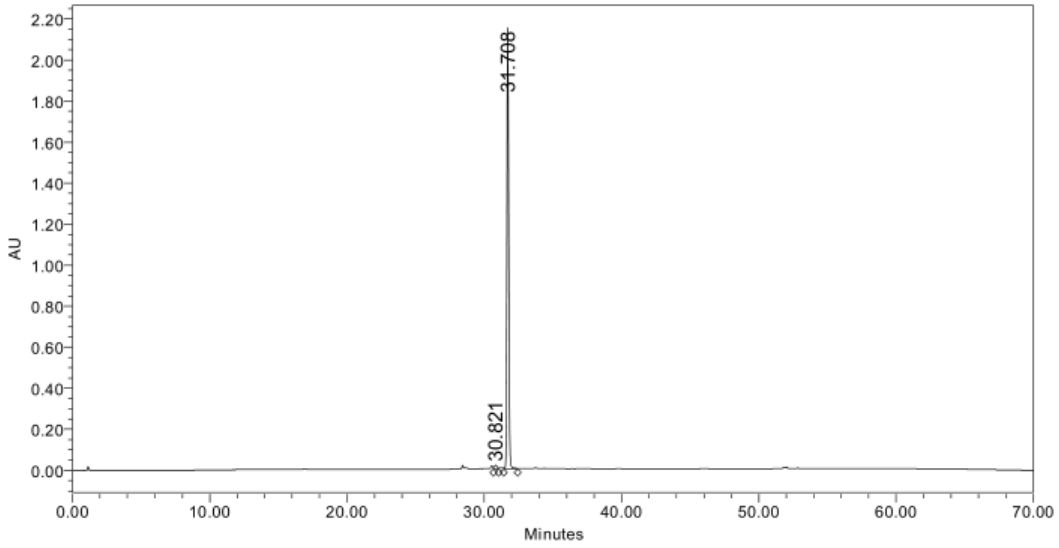

	RT	Area	% Area	Height
1	30.821	250104	1.30	18960
2	31.708	19023649	98.70	2149272

GI-7

Empower™ 3 SOFTWARE

Default Individual Report

SAMPLE INFORMATION

Sample Name:	NusG_A8	Acquired By:	System
Sample Type:	Unknown	Sample Set Name:	NusG_20190701
Vial:	1:A,8	Acq. Method Set:	NusG
Injection #:	1	Processing Method	A8
Injection Volume:	10.00 ul	Channel Name:	231.6nm
Run Time:	70.0 Minutes	Proc. Chnl. Descr.:	2998 PDA 231.6 nm (2998
Date Acquired:	2/7/2019 12:50:50 AM HKT		
Date Processed:	19/9/2022 5:08:20 AM HKT		

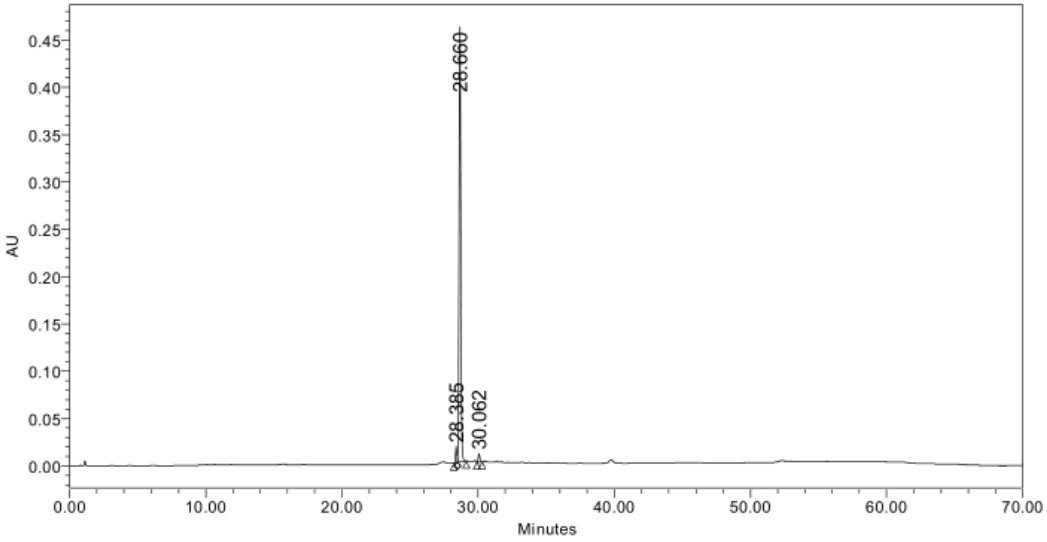

	RT	Area	% Area	Height
1	28.385	103926	2.54	17146
2	28.660	3914055	95.72	459698
3	30.062	70981	1.74	9080

GI-8

Empower™ 3 SOFTWARE

Default Individual Report

SAMPLE INFORMATION

Sample Name:	047	Acquired By:	System
Sample Type:	Standard	Sample Set Name:	0105
Vial:	1:A,1	Acq. Method Set:	NusG link
Injection #:	1	Processing Method	047b
Injection Volume:	10.00 ul	Channel Name:	254.0nm
Run Time:	40.0 Minutes	Proc. Chnl. Descr.:	2998 PDA 254.0 nm (2998
Date Acquired:	5/1/2023 4:36:38 AM HKT		
Date Processed:	5/1/2023 5:26:28 AM HKT		

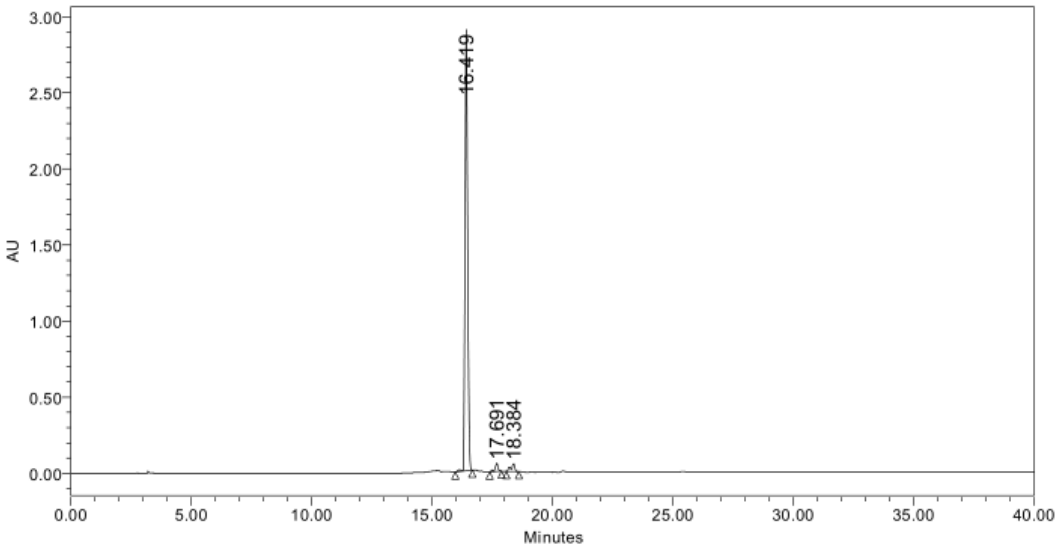

	RT	Area	% Area	Height
1	16.419	21646745	95.37	2901633
2	17.691	470992	2.08	56530
3	18.384	579274	2.55	53177

GI-9

Empower 3 SOFTWARE

Default Individual Report

SAMPLE INFORMATION

Sample Name:	NusG_C8	Acquired By:	System
Sample Type:	Unknown	Sample Set Name:	nusG_20190702
Vial:	1:B,6	Acq. Method Set:	NusG
Injection #:	1	Processing Method	c8023
Injection Volume:	10.00 ul	Channel Name:	238.7nm
Run Time:	70.0 Minutes	Proc. Chnl. Descr.:	2998 PDA 238.7 nm (2998
Date Acquired:	2/7/2019 8:37:28 AM HKT		
Date Processed:	29/11/2022 4:04:14 AM HKT		

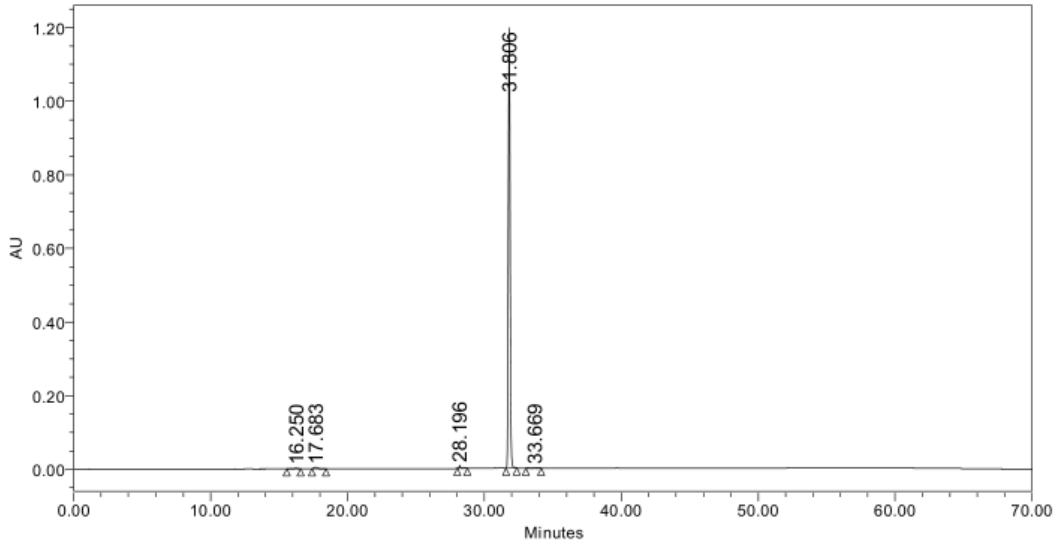

	RT	Area	% Area	Height
1	16.250	30633	0.28	1654
2	17.683	77635	0.72	3973
3	28.196	76360	0.71	8379
4	31.806	10566073	97.91	1196489
5	33.669	40818	0.38	1619

GI-10

Empower 3 SOFTWARE

Default Individual Report

SAMPLE INFORMATION

Sample Name:	NusG_C3	Acquired By:	System
Sample Type:	Unknown	Sample Set Name:	nusG_20190702
Vial:	1:B,2	Acq. Method Set:	NusG
Injection #:	1	Processing Method	c3029
Injection Volume:	10.00 ul	Channel Name:	241.1nm
Run Time:	70.0 Minutes	Proc. Chnl. Descr.:	2998 PDA 241.1 nm (2998
Date Acquired:	2/7/2019 3:56:03 AM HKT		
Date Processed:	29/11/2022 4:02:17 AM HKT		

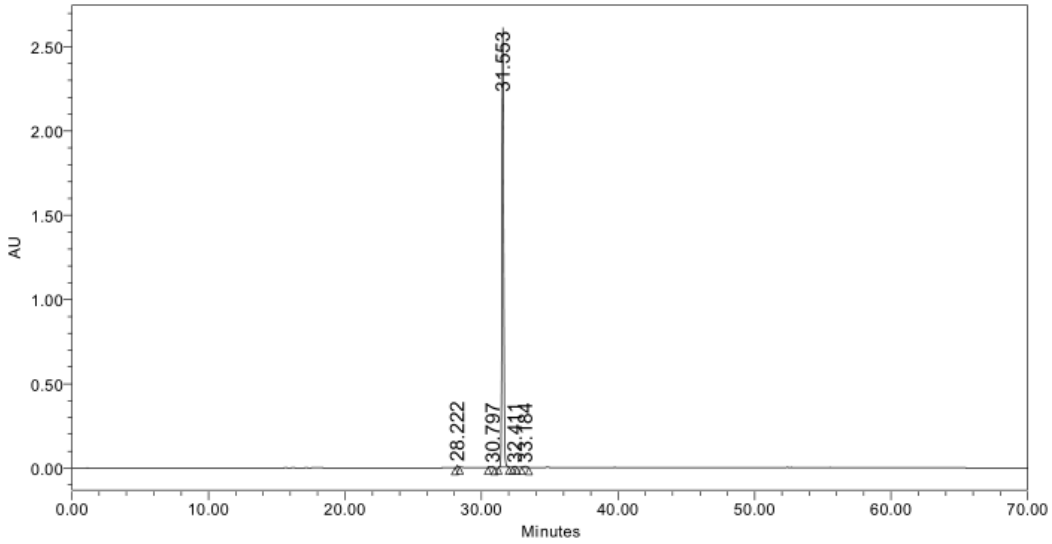

	RT	Area	% Area	Height
1	28.222	85598	0.37	14817
2	30.797	94193	0.41	6474
3	31.553	22793784	98.50	2609127
4	32.411	55602	0.24	6159
5	33.184	112498	0.49	7145

GI-11

Empower 3 SOFTWARE

Default Individual Report

SAMPLE INFORMATION

Sample Name:	NusG_C4	Acquired By:	System
Sample Type:	Unknown	Sample Set Name:	nusG_20190702
Vial:	1:B,3	Acq. Method Set:	NusG
Injection #:	1	Processing Method	c420
Injection Volume:	10.00 ul	Channel Name:	237.5nm
Run Time:	70.0 Minutes	Proc. Chnl. Descr.:	2998 PDA 237.5 nm (2998
Date Acquired:	2/7/2019 5:06:25 AM HKT		
Date Processed:	29/11/2022 4:09:49 AM HKT		

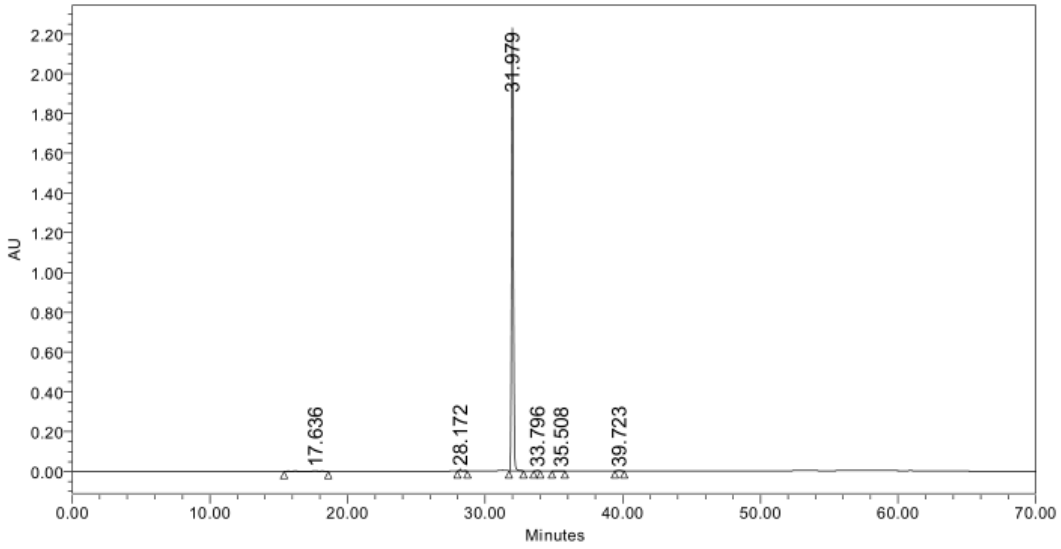

	RT	Area	% Area	Height
1	17.636	95818	0.46	2079
2	28.172	84683	0.40	9541
3	31.979	20653305	98.74	2227501
4	33.796	18871	0.09	1763
5	35.508	19505	0.09	713
6	39.723	44708	0.21	2172

GI-12

Empower 3 SOFTWARE

Default Individual Report

SAMPLE INFORMATION

Sample Name:	NusG_C5	Acquired By:	System
Sample Type:	Unknown	Sample Set Name:	nusG_20190702
Vial:	1:B,4	Acq. Method Set:	NusG
Injection #:	1	Processing Method	c5021
Injection Volume:	10.00 ul	Channel Name:	237.5nm
Run Time:	70.0 Minutes	Proc. Chnl. Descr.:	2998 PDA 237.5 nm (2998
Date Acquired:	2/7/2019 6:16:46 AM HKT		
Date Processed:	29/11/2022 4:11:59 AM HKT		

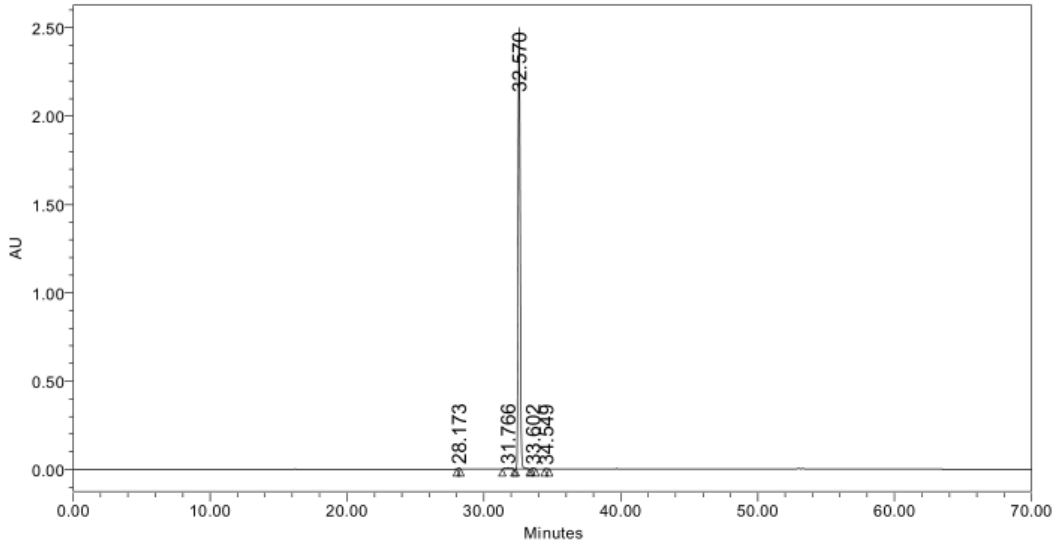

	RT	Area	% Area	Height
1	28.173	45526	0.18	7970
2	31.766	155830	0.61	6943
3	32.570	25468020	98.98	2498093
4	33.602	35230	0.14	3558
5	34.549	24861	0.10	2291

GI-13

Empower 3 SOFTWARE

Default Individual Report

SAMPLE INFORMATION

Sample Name:	NusG_C7	Acquired By:	System
Sample Type:	Unknown	Sample Set Name:	nusG_20190702
Vial:	1:B,5	Acq. Method Set:	NusG
Injection #:	1	Processing Method	c7022
Injection Volume:	10.00 ul	Channel Name:	226.9nm
Run Time:	70.0 Minutes	Proc. Chnl. Descr.:	2998 PDA 226.9 nm (2998
Date Acquired:	2/7/2019 7:27:08 AM HKT		
Date Processed:	29/11/2022 3:59:14 AM HKT		

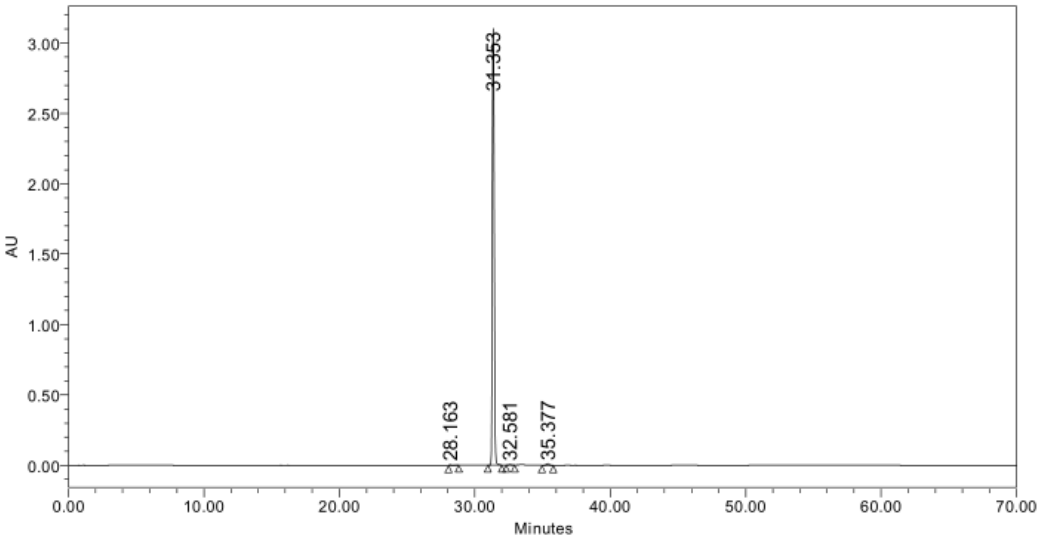

	RT	Area	% Area	Height
1	28.163	62053	0.20	5325
2	31.353	30954953	99.02	3102044
3	32.581	53292	0.17	5351
4	35.377	189725	0.61	11303

GI-14

Empower 3 SOFTWARE

Default Individual Report

SAMPLE INFORMATION

Sample Name:	NusG_C2	Acquired By:	System
Sample Type:	Unknown	Sample Set Name:	nusG_20190702
Vial:	1:B,1	Acq. Method Set:	NusG
Injection #:	1	Processing Method	C2
Injection Volume:	10.00 ul	Channel Name:	231.6nm
Run Time:	70.0 Minutes	Proc. Chnl. Descr.:	2998 PDA 231.6 nm (2998
Date Acquired:	2/7/2019 2:45:42 AM HKT		
Date Processed:	19/9/2022 5:11:45 AM HKT		

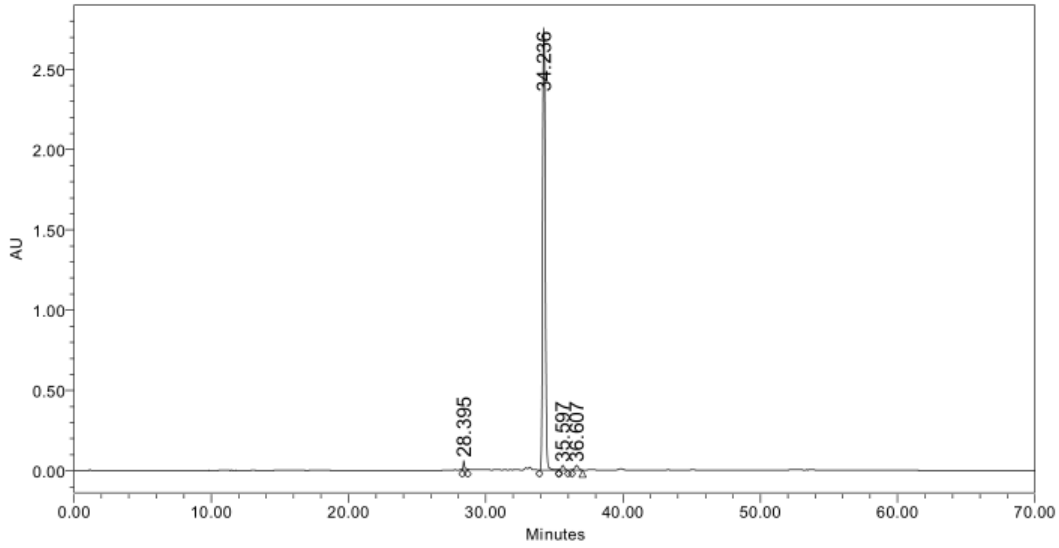

	RT	Area	% Area	Height
1	28.395	459754	1.18	59329
2	34.236	37481068	96.47	2756040
3	35.597	410606	1.06	29249
4	36.607	499246	1.29	29088

GI-15

Empower 3 SOFTWARE

Multi Sample Summary

SAMPLE INFORMATION

Sample Name:	NusG_D1	Acquired By:	System
Sample Type:	Unknown	Sample Set Name	NusG_20190702_1
Vial:	1:D,5	Acq. Method Set:	NusG
Injection #:	1	Processing Method	NusG_C2
Injection Volume:	10.00 ul	Channel Name:	NusG_C2
Run Time:	70.0 Minutes	Proc. Chnl. Descr.:	2998 PDA 254.0 nm (2998
Date Acquired:	7/3/2019 1:54:11 AM HKT		
Date Processed:	7/3/2019 6:59:55 PM HKT		

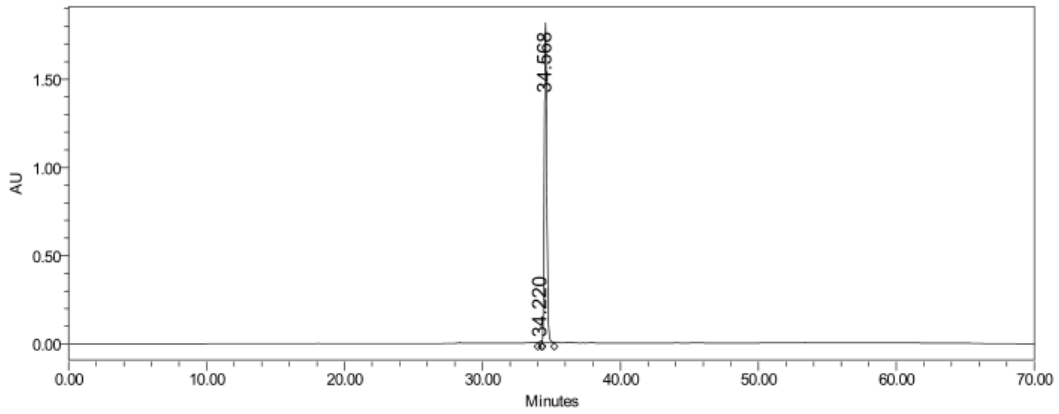

	RT	Area	% Area	Height
1	34.220	134477	0.60	12545
2	34.568	22295293	99.40	1815036

GI-16

Empower 3 SOFTWARE

Default Individual Report

SAMPLE INFORMATION

Sample Name:	NusG_D5	Acquired By:	System
Sample Type:	Unknown	Sample Set Name:	NusG_20190702_1
Vial:	1:D,8	Acq. Method Set:	NusG
Injection #:	1	Processing Method	d5029
Injection Volume:	10.00 ul	Channel Name:	287.5nm
Run Time:	70.0 Minutes	Proc. Chnl. Descr.:	2998 PDA 287.5 nm (2998
Date Acquired:	3/7/2019 5:25:15 AM HKT		
Date Processed:	29/11/2022 4:47:27 AM HKT		

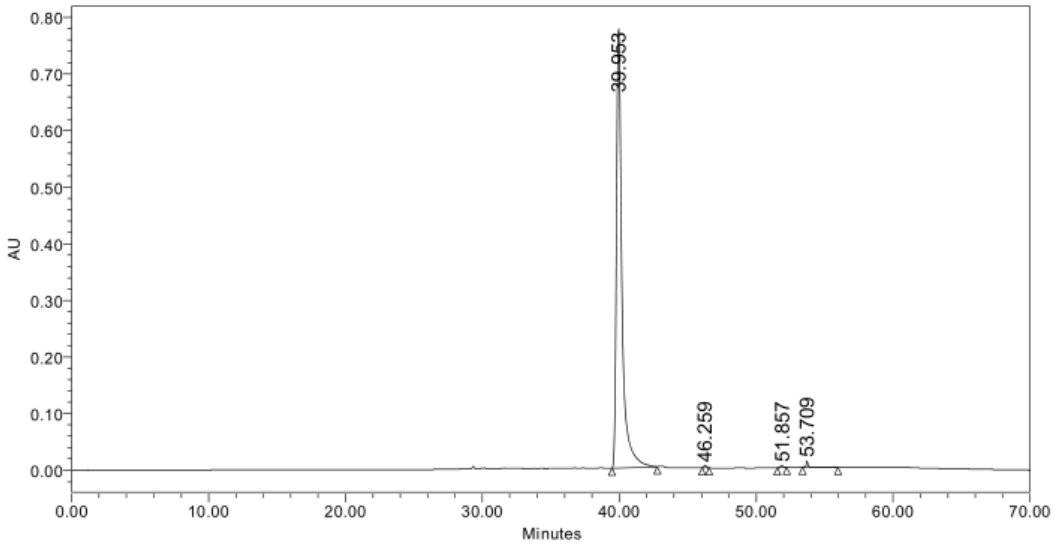

	RT	Area	% Area	Height
1	39.953	21736044	99.02	776062
2	46.259	60112	0.27	3962
3	51.857	50407	0.23	3777
4	53.709	103972	0.47	11112

GI-17

Empower 3 SOFTWARE

Default Individual Report

SAMPLE INFORMATION

Sample Name:	NusG_D2	Acquired By:	System
Sample Type:	Unknown	Sample Set Name:	NusG_20190702_1
Vial:	1:D,6	Acq. Method Set:	NusG
Injection #:	1	Processing Method	d2027
Injection Volume:	10.00 ul	Channel Name:	258.9nm
Run Time:	70.0 Minutes	Proc. Chnl. Descr.:	2998 PDA 258.9 nm (2998
Date Acquired:	3/7/2019 3:04:33 AM HKT		
Date Processed:	29/11/2022 4:49:05 AM HKT		

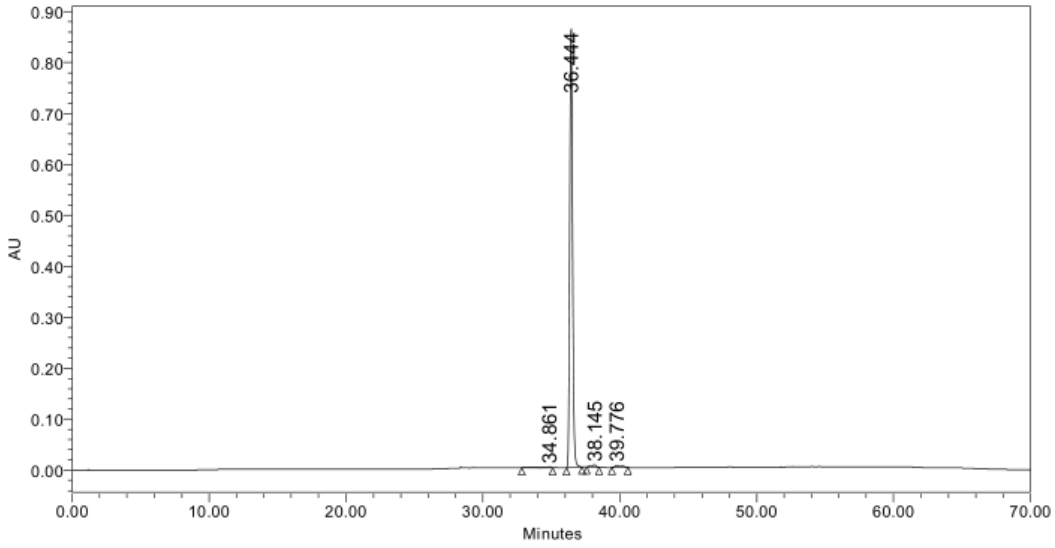

	RT	Area	% Area	Height
1	34.861	74885	0.59	1529
2	36.444	12320722	97.30	861044
3	38.145	113382	0.90	4283
4	39.776	153250	1.21	4263

GI-18

Empower 3 SOFTWARE

Default Individual Report

SAMPLE INFORMATION

Sample Name:	49	Acquired By:	System
Sample Type:	Standard	Sample Set Name:	04012023
Vial:	1:A,2	Acq. Method Set:	NusG link
Injection #:	1	Processing Method	049
Injection Volume:	10.00 ul	Channel Name:	303.0nm
Run Time:	40.0 Minutes	Proc. Chnl. Descr.:	2998 PDA 303.0 nm (2998
Date Acquired:	4/1/2023 9:28:30 AM HKT		
Date Processed:	4/1/2023 11:44:05 PM HKT		

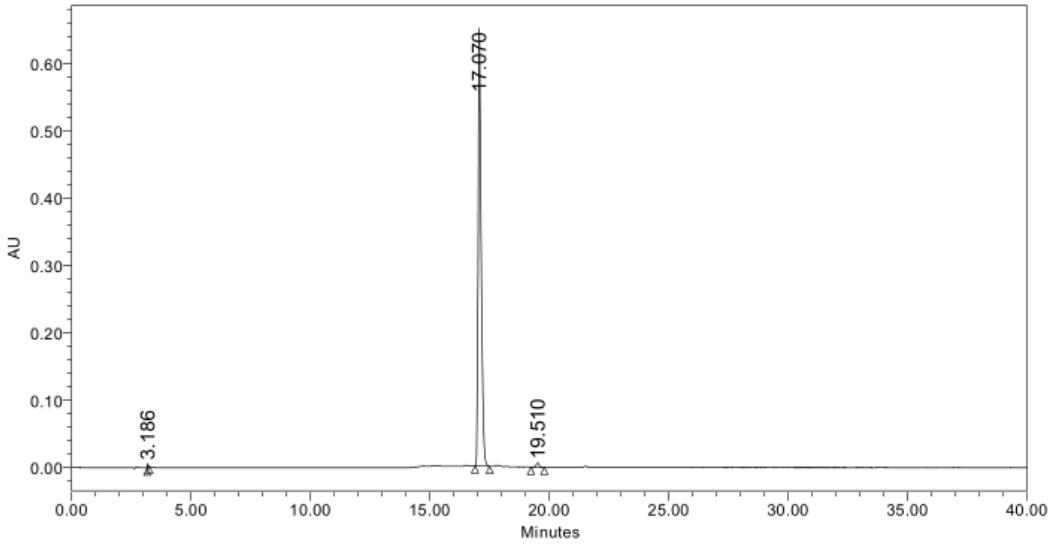

	RT	Area	% Area	Height
1	3.186	15113	0.26	6695
2	17.070	5641232	98.83	650604
3	19.510	51677	0.91	6490

GI-19

Empower 3 SOFTWARE

Default Individual Report

SAMPLE INFORMATION

Sample Name:	NusG_D3	Acquired By:	System
Sample Type:	Unknown	Sample Set Name:	NusG_20190702_1
Vial:	1:D,7	Acq. Method Set:	NusG
Injection #:	1	Processing Method	028
Injection Volume:	10.00 ul	Channel Name:	247.0nm
Run Time:	70.0 Minutes	Proc. Chnl. Descr.:	2998 PDA 247.0 nm (2998
Date Acquired:	3/7/2019 4:14:54 AM HKT		
Date Processed:	30/11/2022 3:32:39 AM HKT		

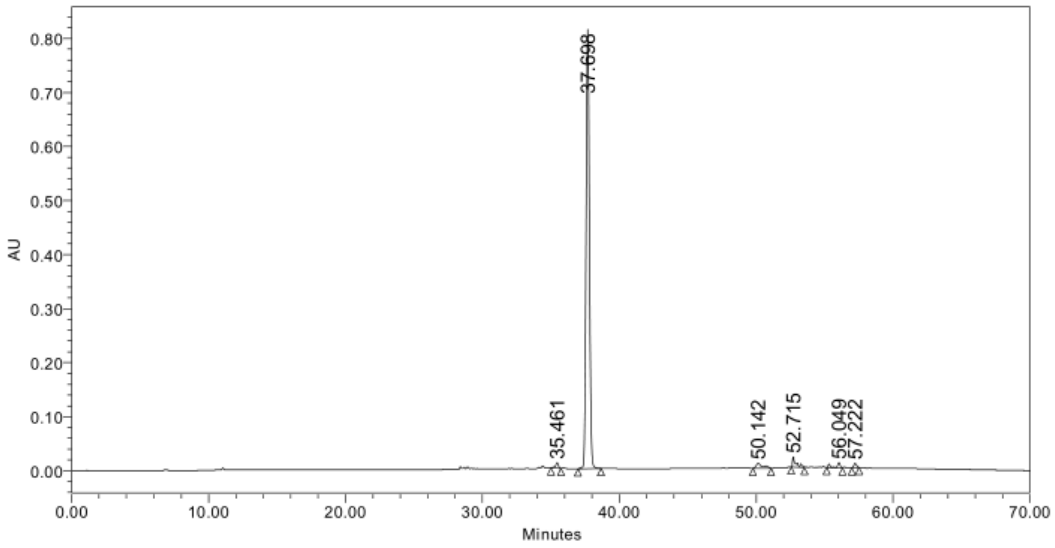

	RT	Area	% Area	Height
1	35.461	151621	1.03	10064
2	37.698	13708453	92.86	812950
3	50.142	296845	2.01	8849
4	52.715	316264	2.14	18848
5	56.049	171832	1.16	9087
6	57.222	116777	0.79	8126

GI-20

Empower 3 SOFTWARE

Default Individual Report

SAMPLE INFORMATION

Sample Name:	68	Acquired By:	System
Sample Type:	Standard	Sample Set Name:	04012023
Vial:	1:A,3	Acq. Method Set:	NusG link
Injection #:	1	Processing Method	068be
Injection Volume:	10.00 ul	Channel Name:	417.1nm
Run Time:	40.0 Minutes	Proc. Chnl. Descr.:	2998 PDA 417.1 nm (2998
Date Acquired:	4/1/2023 10:38:53 AM HKT		
Date Processed:	4/1/2023 11:47:42 PM HKT		

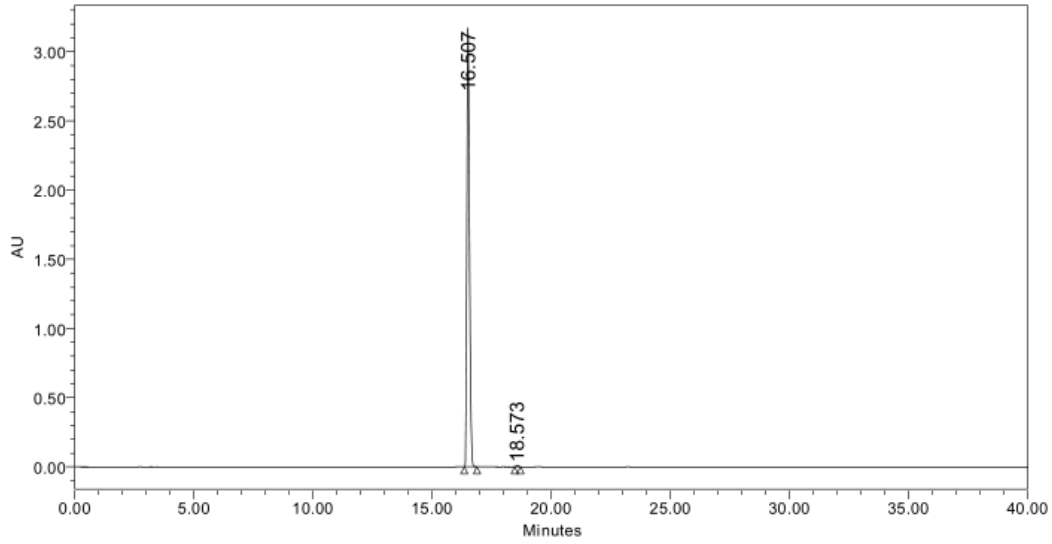

	RT	Area	% Area	Height
1	16.507	24366792	99.68	3172915
2	18.573	78485	0.32	11023

GI-21

Empower 3 SOFTWARE

Default Individual Report

SAMPLE INFORMATION

Sample Name:	87	Acquired By:	System
Sample Type:	Standard	Sample Set Name:	2510nusg
Vial:	1:A,8	Acq. Method Set:	NusG link
Injection #:	1	Processing Method	87best
Injection Volume:	10.00 ul	Channel Name:	330.5nm
Run Time:	40.0 Minutes	Proc. Chnl. Descr.:	2998 PDA 330.5 nm (2998
Date Acquired:	25/10/2022 10:00:12 AM HKT		
Date Processed:	26/10/2022 5:37:03 AM HKT		

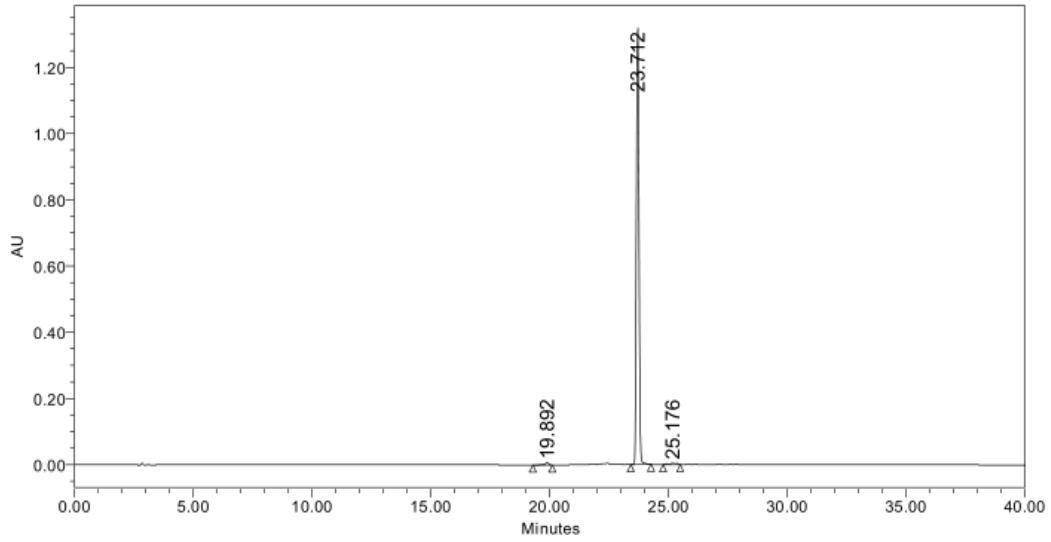

	RT	Area	% Area	Height
1	19.892	81499	0.79	7103
2	23.712	10106076	98.38	1318141
3	25.176	84709	0.82	4311

GI-22

Empower 3 SOFTWARE

Default Individual Report

SAMPLE INFORMATION

Sample Name:	45	Acquired By:	System
Sample Type:	Standard	Sample Set Name:	2510nusg
Vial:	1:A,3	Acq. Method Set:	NusG link
Injection #:	1	Processing Method	45best
Injection Volume:	10.00 ul	Channel Name:	300.6nm
Run Time:	40.0 Minutes	Proc. Chnl. Descr.:	2998 PDA 300.6 nm (2998
Date Acquired:	25/10/2022 5:58:29 AM HKT		
Date Processed:	25/10/2022 8:50:15 AM HKT		

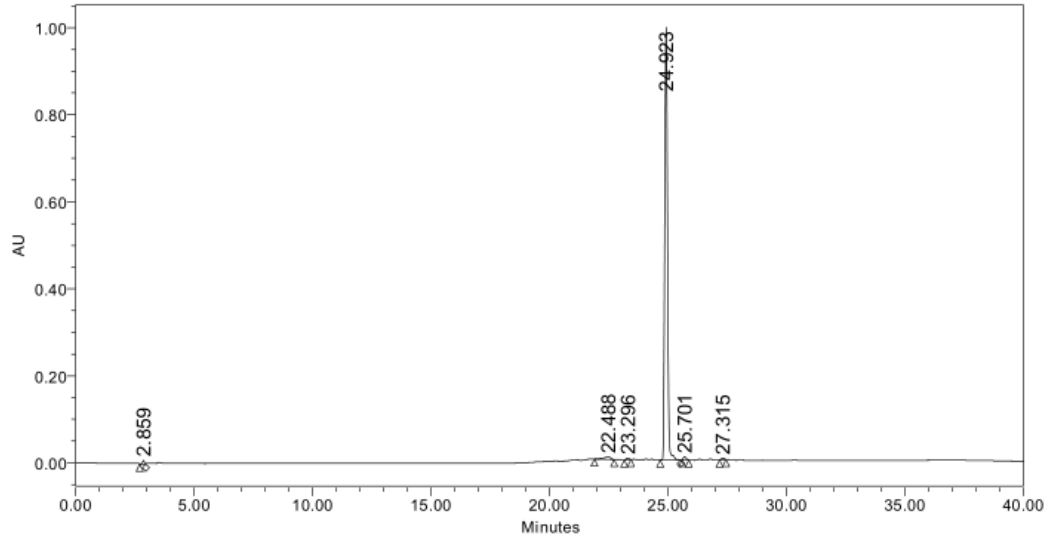

	RT	Area	% Area	Height
1	2.859	57023	0.68	9057
2	22.488	113830	1.36	5385
3	23.296	33302	0.40	4188
4	24.923	8077816	96.63	995067
5	25.701	50917	0.61	6304
6	27.315	26661	0.32	3369

GI-23

Empower 3 SOFTWARE

Default Individual Report

SAMPLE INFORMATION

Sample Name:	44	Acquired By:	System
Sample Type:	Standard	Sample Set Name:	2510nusg
Vial:	1:A,2	Acq. Method Set:	NusG link
Injection #:	1	Processing Method	44bestt
Injection Volume:	10.00 ul	Channel Name:	243.5nm
Run Time:	40.0 Minutes	Proc. Chnl. Descr.:	2998 PDA 243.5 nm (2998
Date Acquired:	25/10/2022 5:10:09 AM HKT		
Date Processed:	25/10/2022 8:47:53 AM HKT		

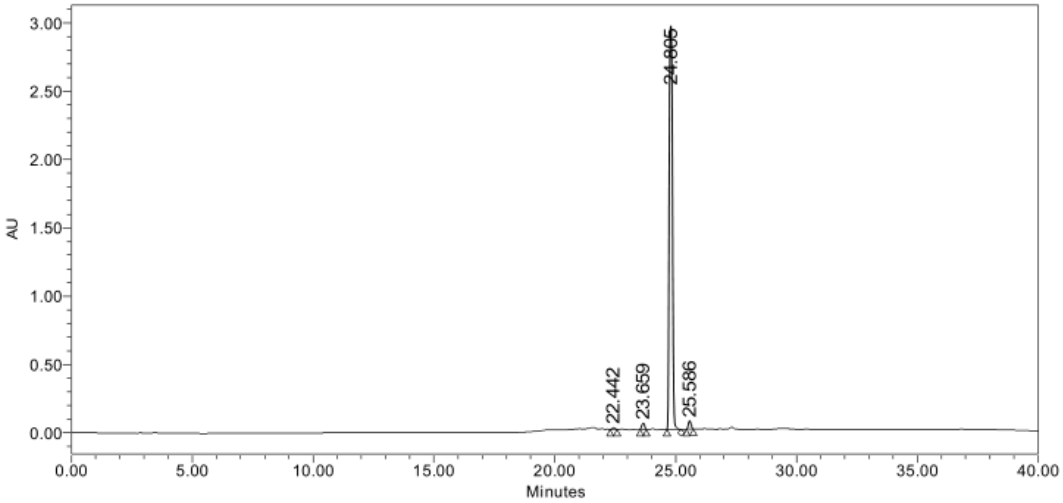

	RT	Area	% Area	Height
1	22.442	114788	0.39	14543
2	23.659	344734	1.17	46772
3	24.805	28404412	96.79	2955691
4	25.586	482942	1.65	61856

GI-24

Empower 3 SOFTWARE

Default Individual Report

SAMPLE INFORMATION

Sample Name:	86	Acquired By:	System
Sample Type:	Standard	Sample Set Name:	2510nusg
Vial:	1:A,7	Acq. Method Set:	NusG link
Injection #:	1	Processing Method	086best
Injection Volume:	10.00 ul	Channel Name:	300.6nm
Run Time:	40.0 Minutes	Proc. Chnl. Descr.:	2998 PDA 300.6 nm (2998
Date Acquired:	25/10/2022 9:11:51 AM HKT		
Date Processed:	25/10/2022 10:12:38 AM HKT		

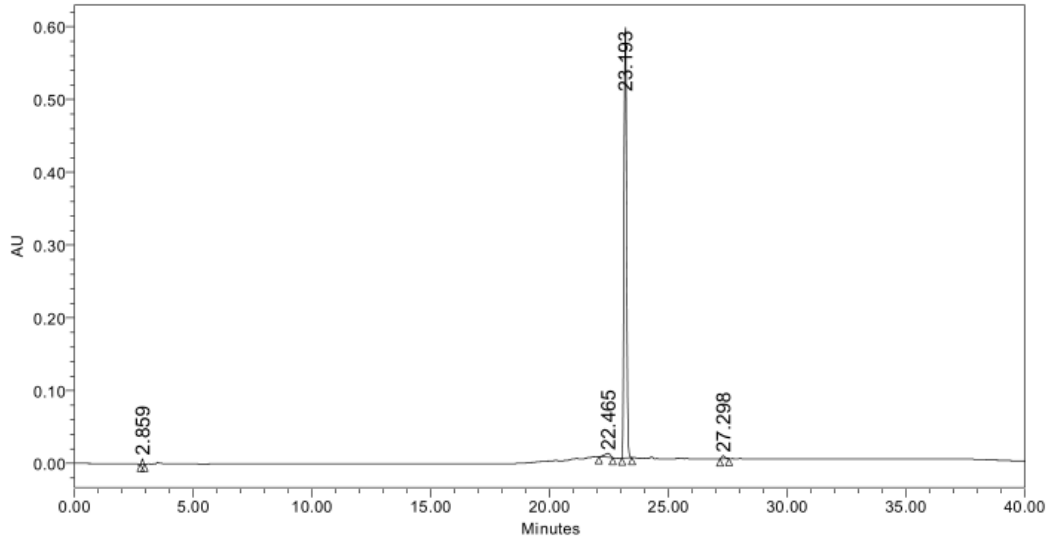

	RT	Area	% Area	Height
1	2.859	36395	0.79	7727
2	22.465	97061	2.11	5394
3	23.193	4428154	96.25	592001
4	27.298	39227	0.85	4098

GI-25

Empower 3 SOFTWARE

Multi Sample Summary

SAMPLE INFORMATION

Sample Name:	NusG_D6	Acquired By:	System
Sample Type:	Unknown	Sample Set Name	nusG_20190702
Vial:	1:C,1	Acq. Method Set:	NusG
Injection #:	1	Processing Method	NusG_A2
Injection Volume:	10.00 ul	Channel Name:	NusG_A2
Run Time:	70.0 Minutes	Proc. Chnl. Descr.:	2998 PDA 254.0 nm (2998
Date Acquired:	7/2/2019 9:47:48 AM HKT		
Date Processed:	7/3/2019 5:19:44 PM HKT		

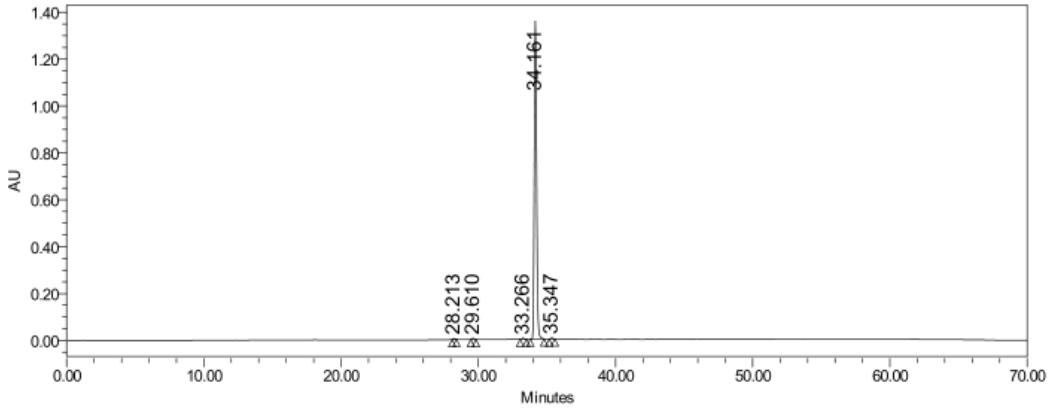

	RT	Area	% Area	Height
1	28.213	29629	0.18	5236
2	29.610	50923	0.31	6207
3	33.266	51812	0.32	4778
4	34.161	16056999	98.89	1355504
5	35.347	47807	0.29	4337

GI-26

Empower 3 SOFTWARE

Multi Sample Summary

SAMPLE INFORMATION

Sample Name:	NusG_D7	Acquired By:	System
Sample Type:	Unknown	Sample Set Name	nusG_20190702
Vial:	1:C,2	Acq. Method Set:	NusG
Injection #:	1	Processing Method	NusG_D7
Injection Volume:	10.00 ul	Channel Name:	NusG_D7
Run Time:	70.0 Minutes	Proc. Chnl. Descr.:	2998 PDA 254.0 nm (2998
Date Acquired:	7/2/2019 10:58:08 AM HKT		
Date Processed:	7/3/2019 5:26:29 PM HKT		

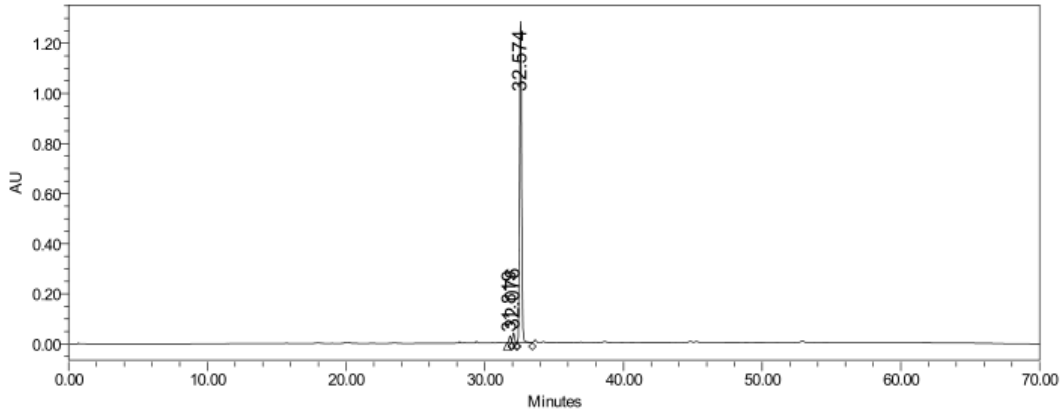

	RT	Area	% Area	Height
1	31.819	264196	1.94	27848
2	32.076	402691	2.96	39428
3	32.574	12926874	95.09	1282607

GI-27

Empower 3 SOFTWARE

Multi Sample Summary

SAMPLE INFORMATION

Sample Name:	NusG_D25	Acquired By:	System
Sample Type:	Unknown	Sample Set Name	NusG_20190702_1
Vial:	1:D,4	Acq. Method Set:	NusG
Injection #:	1	Processing Method	NusG_A2
Injection Volume:	10.00 ul	Channel Name:	NusG_A2
Run Time:	70.0 Minutes	Proc. Chnl. Descr.:	2998 PDA 254.0 nm (2998
Date Acquired:	7/3/2019 12:43:50 AM HKT		
Date Processed:	7/3/2019 6:54:03 PM HKT		

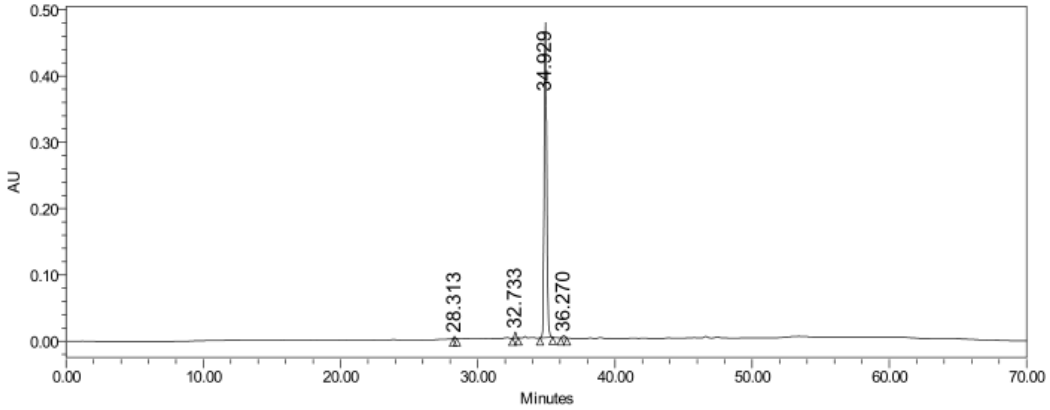

	RT	Area	% Area	Height
1	28.313	21712	0.35	4033
2	32.733	86932	1.42	9519
3	34.929	5983462	97.40	475196
4	36.270	51378	0.84	3957

GI-28

Empower 3 SOFTWARE

Default Individual Report

SAMPLE INFORMATION

Sample Name:	JIANDOWN	Acquired By:	System
Sample Type:	Standard	Sample Set Name:	U
Vial:	1:A,1	Acq. Method Set:	NusG link
Injection #:	1	Processing Method	jianup
Injection Volume:	10.00 ul	Channel Name:	249.4nm
Run Time:	40.0 Minutes	Proc. Chnl. Descr.:	2998 PDA 249.4 nm (2998
Date Acquired:	4/17/2023 11:54:21 AM HKT		
Date Processed:	4/19/2023 3:08:06 AM HKT		

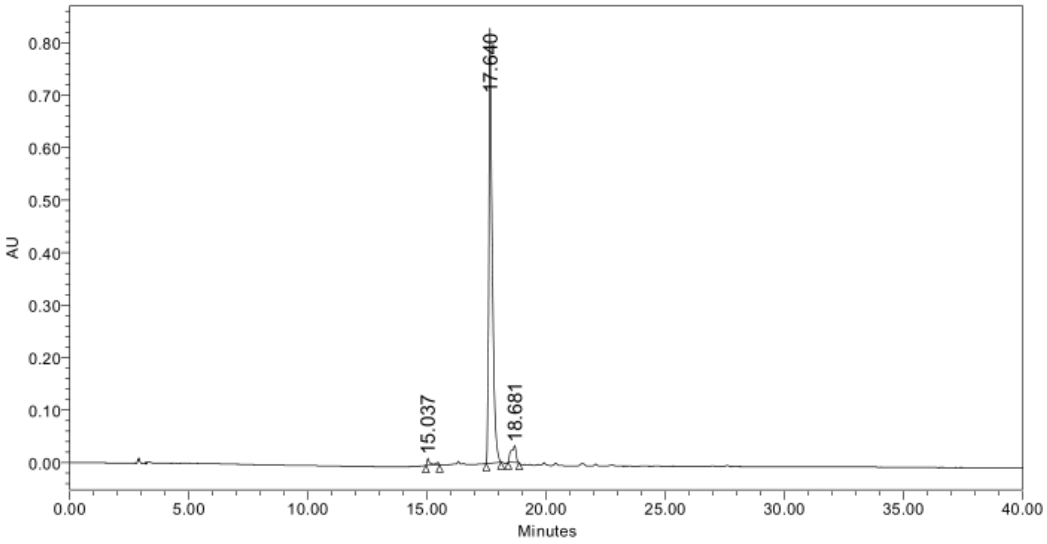

	RT	Area	% Area	Height
1	15.037	144689	1.66	13525
2	17.640	8096611	93.05	828715
3	18.681	459893	5.29	32042

GI-29

Empower 3 SOFTWARE

Default Individual Report

SAMPLE INFORMATION

Sample Name:	ling58	Acquired By:	System
Sample Type:	Standard	Sample Set Name:	11
Vial:	1:A,2	Acq. Method Set:	NusG link
Injection #:	1	Processing Method	g058lin
Injection Volume:	10.00 ul	Channel Name:	297.0nm
Run Time:	40.0 Minutes	Proc. Chnl. Descr.:	2998 PDA 297.0 nm (2998
Date Acquired:	12/4/2023 1:29:24 PM HKT		
Date Processed:	12/4/2023 10:38:53 PM HKT		

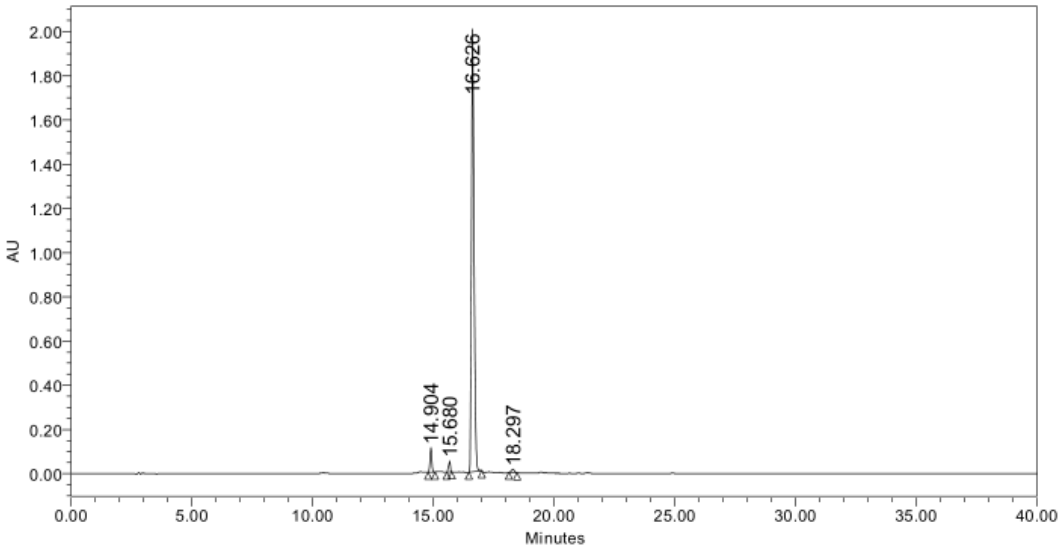

	RT	Area	% Area	Height
1	14.904	565114	3.61	110860
2	15.680	247592	1.58	49788
3	16.626	14717064	94.01	2004086
4	18.297	125001	0.80	14498

GI-30

Empower 3 SOFTWARE

Default Individual Report

SAMPLE INFORMATION

Sample Name:	64	Acquired By:	System
Sample Type:	Standard	Sample Set Name:	0411222
Vial:	1:B,4	Acq. Method Set:	NusG link
Injection #:	1	Processing Method	64
Injection Volume:	10.00 ul	Channel Name:	247.0nm@1
Run Time:	40.0 Minutes	Proc. Chnl. Descr.:	2998 PDA 247.0 nm (2998
Date Acquired:	4/11/2022 12:47:26 PM HKT		
Date Processed:	5/11/2022 4:38:47 AM HKT		

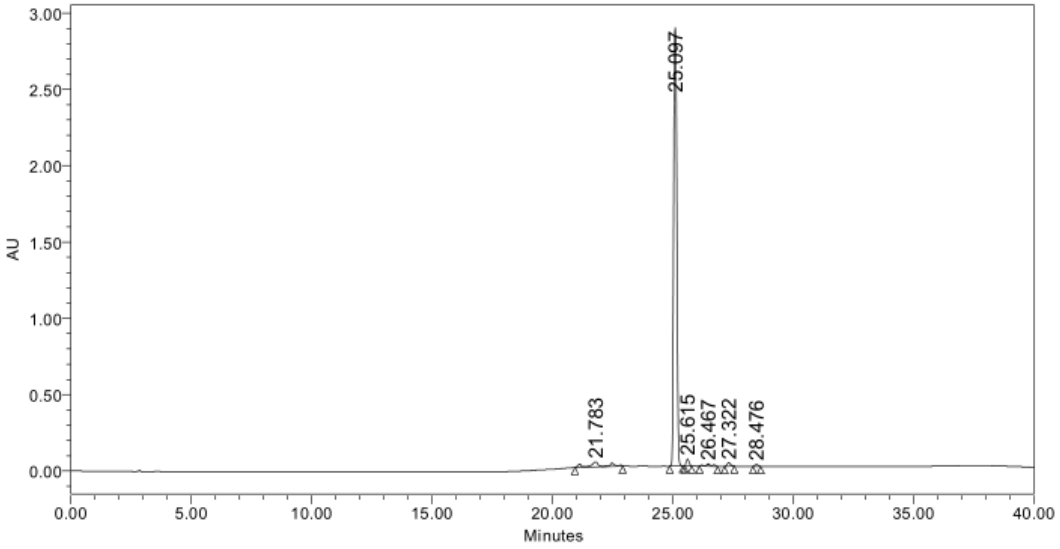

	RT	Area	% Area	Height
1	21.783	960513	3.41	30340
2	25.097	26223949	93.19	2873031
3	25.615	340404	1.21	43655
4	26.467	273025	0.97	15675
5	27.322	222204	0.79	22630
6	28.476	119678	0.43	12752

GI-31

Empower 3 SOFTWARE

Default Individual Report

SAMPLE INFORMATION

Sample Name:	48	Acquired By:	System
Sample Type:	Standard	Sample Set Name:	2510nusg
Vial:	1:A,4	Acq. Method Set:	NusG link
Injection #:	1	Processing Method	048best
Injection Volume:	10.00 ul	Channel Name:	350.9nm
Run Time:	40.0 Minutes	Proc. Chnl. Descr.:	2998 PDA 350.9 nm (2998
Date Acquired:	25/10/2022 6:46:49 AM HKT		
Date Processed:	25/10/2022 8:51:47 AM HKT		

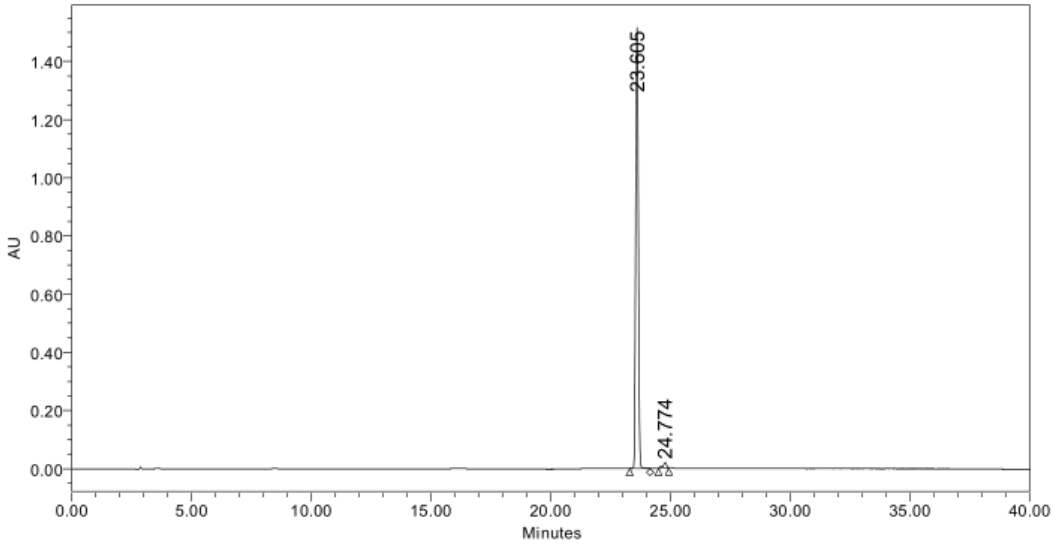

	RT	Area	% Area	Height
1	23.605	11550873	98.35	1515718
2	24.774	193416	1.65	19097

GI-32

Empower 3 SOFTWARE

Default Individual Report

SAMPLE INFORMATION

Sample Name:	46	Acquired By:	System
Sample Type:	Standard	Sample Set Name:	0411222
Vial:	1:B,2	Acq. Method Set:	NusG link
Injection #:	1	Processing Method	046
Injection Volume:	10.00 ul	Channel Name:	272.0nm
Run Time:	40.0 Minutes	Proc. Chnl. Descr.:	2998 PDA 272.0 nm (2998
Date Acquired:	4/11/2022 11:10:45 AM HKT		
Date Processed:	5/11/2022 4:46:29 AM HKT		

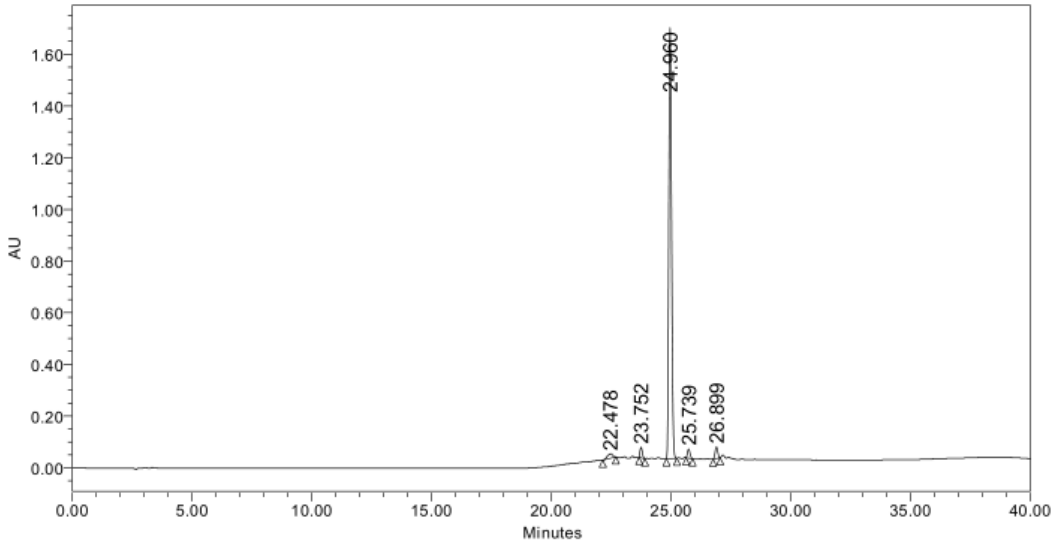

	RT	Area	% Area	Height
1	22.478	276186	1.92	16884
2	23.752	268029	1.87	40523
3	24.960	13207355	92.05	1667465
4	25.739	257512	1.79	35421
5	26.899	338772	2.36	45070

GI-33

Empower 3 SOFTWARE

Default Individual Report

SAMPLE INFORMATION

Sample Name:	62	Acquired By:	System
Sample Type:	Standard	Sample Set Name:	3122022
Vial:	1:D,1	Acq. Method Set:	NusG link
Injection #:	1	Processing Method	062
Injection Volume:	10.00 ul	Channel Name:	299.4nm
Run Time:	40.0 Minutes	Proc. Chnl. Descr.:	2998 PDA 299.4 nm (2998
Date Acquired:	3/12/2022 8:29:55 AM HKT		
Date Processed:	4/12/2022 4:49:42 AM HKT		

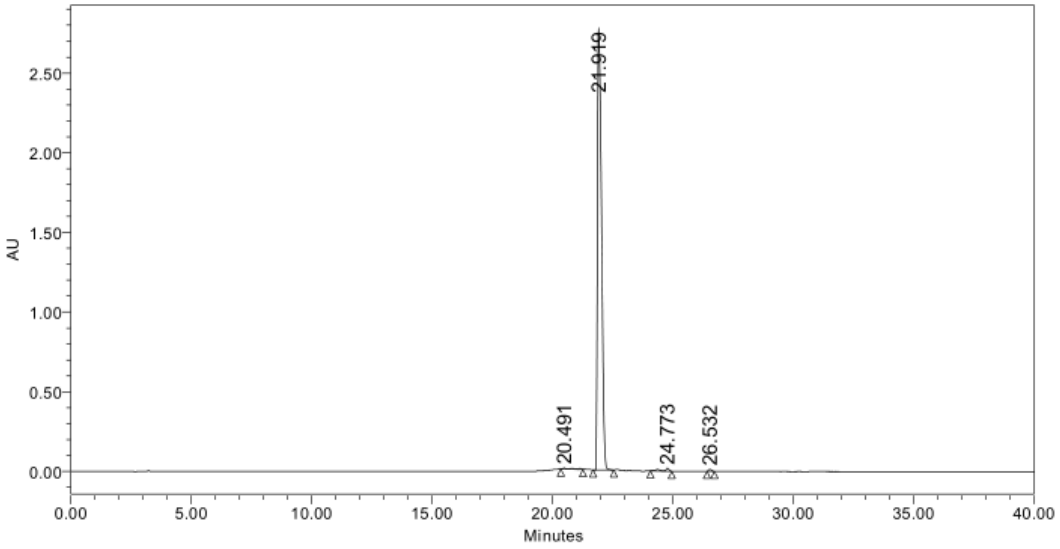

	RT	Area	% Area	Height
1	20.491	87301	0.27	6094
2	21.919	32340848	98.51	2773765
3	24.773	291187	0.89	18843
4	26.532	111001	0.34	13101

GI-34

Empower 3 SOFTWARE

Default Individual Report

SAMPLE INFORMATION

Sample Name:	61	Acquired By:	System
Sample Type:	Standard	Sample Set Name:	1129
Vial:	1:A,1	Acq. Method Set:	NusG link
Injection #:	1	Processing Method	61best
Injection Volume:	10.00 ul	Channel Name:	299.4nm
Run Time:	40.0 Minutes	Proc. Chnl. Descr.:	2998 PDA 299.4 nm (2998
Date Acquired:	29/11/2022 1:02:33 AM HKT		
Date Processed:	29/11/2022 2:54:32 AM HKT		

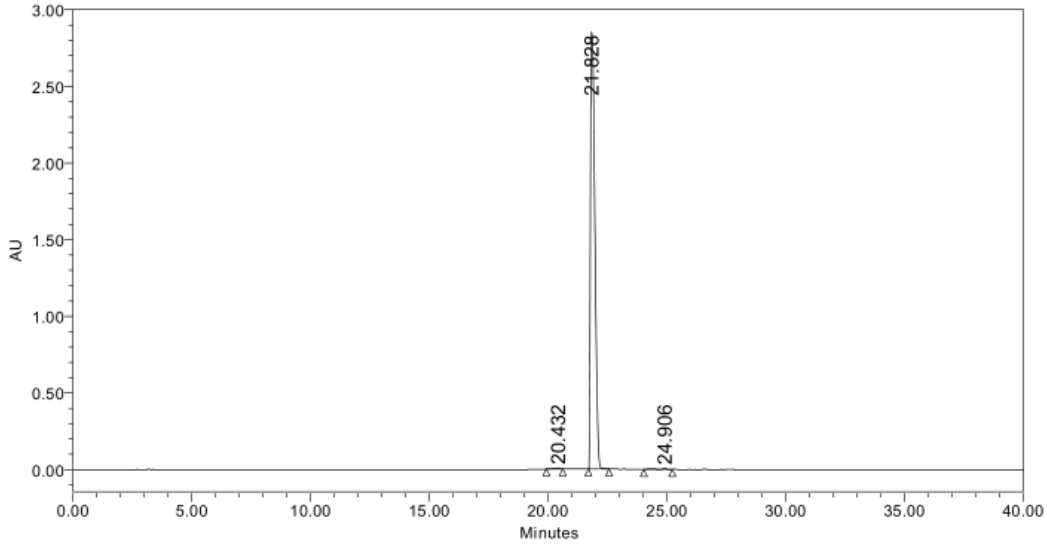

	RT	Area	% Area	Height
1	20.432	83067	0.22	8095
2	21.828	37039084	99.40	2852493
3	24.906	138823	0.37	8231

GI-35

Empower 3 SOFTWARE

Default Individual Report

SAMPLE INFORMATION

Sample Name:	56	Acquired By:	System
Sample Type:	Standard	Sample Set Name:	142
Vial:	1:A,1	Acq. Method Set:	NusG link
Injection #:	1	Processing Method	g056best
Injection Volume:	10.00 ul	Channel Name:	264.8nm
Run Time:	40.0 Minutes	Proc. Chnl. Descr.:	2998 PDA 264.8 nm (2998
Date Acquired:	14/2/2023 11:57:48 PM HKT		
Date Processed:	15/2/2023 12:47:58 AM HKT		

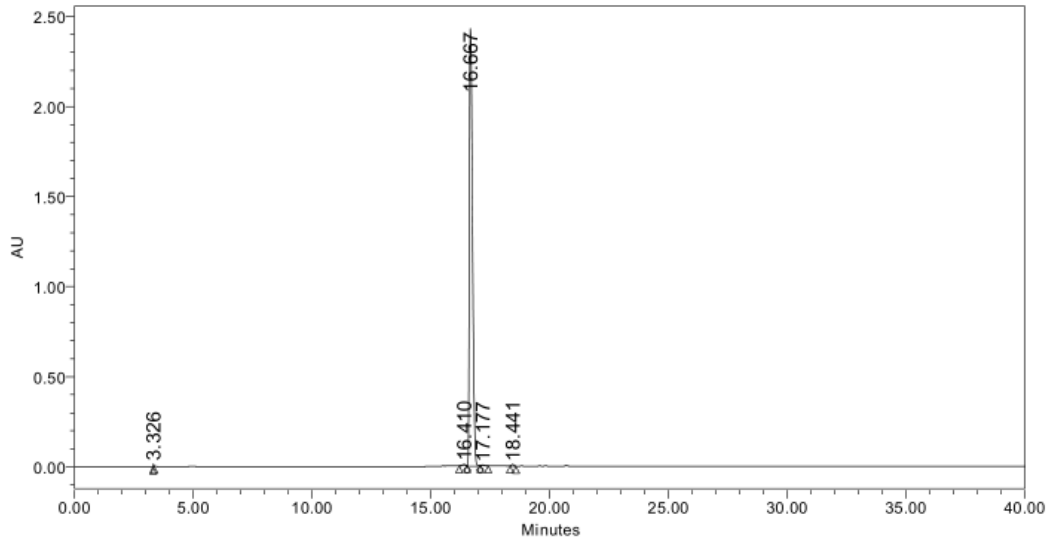

	RT	Area	% Area	Height
1	3.326	25970	0.12	14838
2	16.410	57821	0.26	6759
3	16.667	21955961	99.23	2430063
4	17.177	20895	0.09	3034
5	18.441	66291	0.30	9306

GI-36

Empower 3 SOFTWARE

Default Individual Report

SAMPLE INFORMATION

Sample Name:	057	Acquired By:	System
Sample Type:	Unknown	Sample Set Name:	17112022
Vial:	1:A,1	Acq. Method Set:	NusG link
Injection #:	1	Processing Method	057
Injection Volume:	10.00 ul	Channel Name:	273.2nm
Run Time:	40.0 Minutes	Proc. Chnl. Descr.:	2998 PDA 273.2 nm (2998
Date Acquired:	17/11/2022 2:22:32 AM HKT		
Date Processed:	17/11/2022 3:19:49 AM HKT		

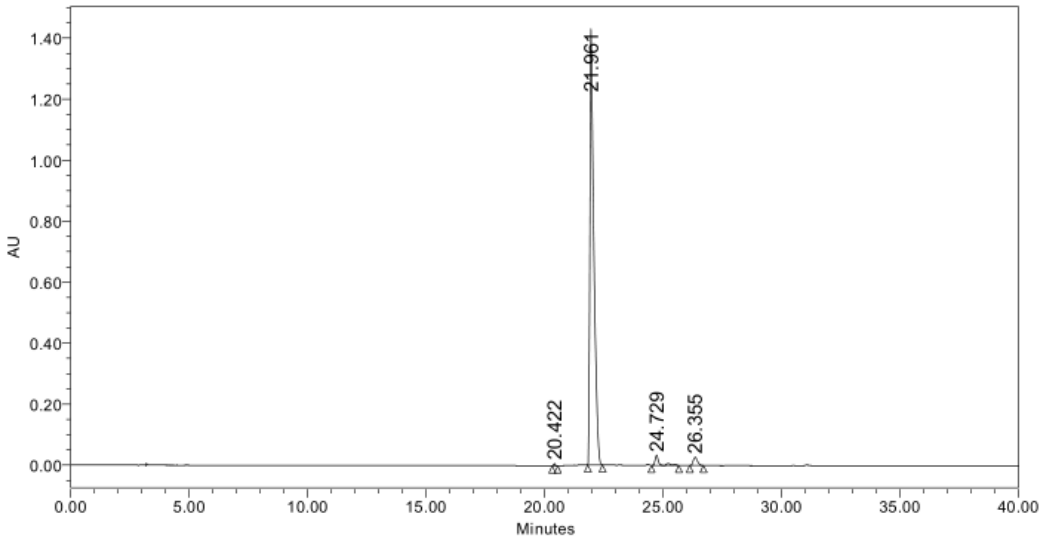

	RT	Area	% Area	Height
1	20.422	33485	0.19	7669
2	21.961	16546957	95.69	1429977
3	24.729	375376	2.17	33101
4	26.355	335971	1.94	27510

GI-37

Empower 3 SOFTWARE

Default Individual Report

SAMPLE INFORMATION

Sample Name:	59	Acquired By:	System
Sample Type:	Standard	Sample Set Name:	2610
Vial:	1:A,2	Acq. Method Set:	NusG link
Injection #:	1	Processing Method	059best
Injection Volume:	10.00 ul	Channel Name:	251.8nm
Run Time:	40.0 Minutes	Proc. Chnl. Descr.:	2998 PDA 251.8 nm (2998
Date Acquired:	26/10/2022 12:16:45 PM HKT		
Date Processed:	26/10/2022 10:05:29 PM HKT		

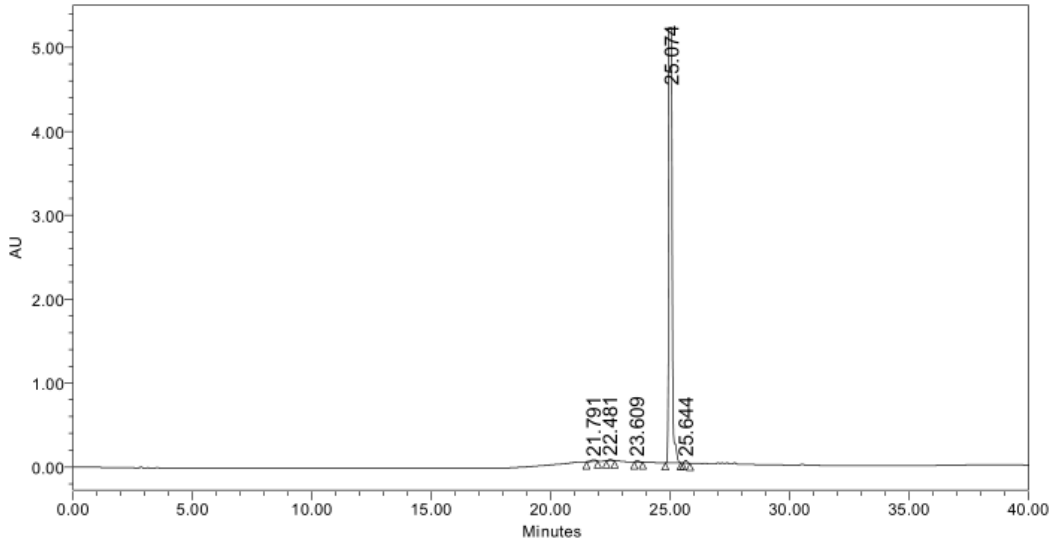

	RT	Area	% Area	Height
1	21.791	226648	0.42	15914
2	22.481	189958	0.35	18552
3	23.609	175616	0.32	20454
4	25.074	53511966	98.46	5209791
5	25.644	244580	0.45	32076

GI-38

Empower 3 SOFTWARE

Default Individual Report

SAMPLE INFORMATION

Sample Name:	060	Acquired By:	System
Sample Type:	Standard	Sample Set Name:	141120221
Vial:	1:A,1	Acq. Method Set:	NusG link
Injection #:	1	Processing Method	60BEST
Injection Volume:	10.00 ul	Channel Name:	300.2nm
Run Time:	40.0 Minutes	Proc. Chnl. Descr.:	2998 PDA 300.2 nm (2998
Date Acquired:	14/11/2022 1:05:42 AM HKT		
Date Processed:	14/11/2022 2:24:51 AM HKT		

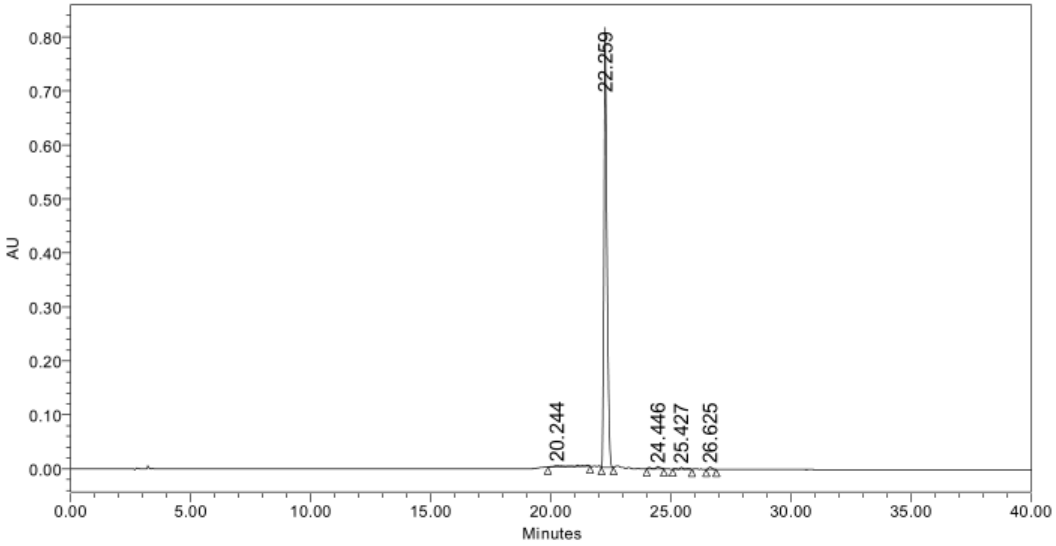

	RT	Area	% Area	Height
1	20.244	128123	1.77	2739
2	22.259	6941157	96.13	815284
3	24.446	65414	0.91	4114
4	25.427	45562	0.63	3471
5	26.625	40098	0.56	4609

GI-39

Empower 3 SOFTWARE

Default Individual Report

SAMPLE INFORMATION

Sample Name:	69	Acquired By:	System
Sample Type:	Standard	Sample Set Name:	17012023
Vial:	1:A,2	Acq. Method Set:	NusG link
Injection #:	1	Processing Method	069
Injection Volume:	10.00 ul	Channel Name:	255.3nm
Run Time:	40.0 Minutes	Proc. Chnl. Descr.:	2998 PDA 255.3 nm (2998
Date Acquired:	17/1/2023 3:52:30 AM HKT		
Date Processed:	17/1/2023 5:24:58 AM HKT		

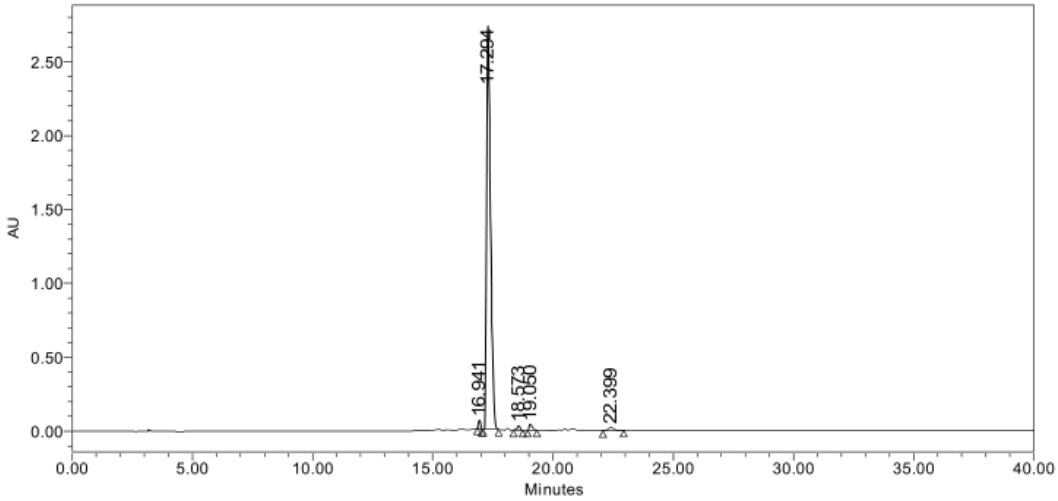

	RT	Area	% Area	Height
1	16.941	367510	1.14	57660
2	17.294	30832695	95.63	2730944
3	18.573	289808	0.90	33658
4	19.050	410318	1.27	41625
5	22.399	340111	1.05	21572

GII-1

Empower™ 3 SOFTWARE

Default Individual Report

SAMPLE INFORMATION

Sample Name:	NusG_D17	Acquired By:	System
Sample Type:	Unknown	Sample Set Name:	nusG_20190702
Vial:	1:C,6	Acq. Method Set:	NusG
Injection #:	1	Processing Method	lypd17g035
Injection Volume:	10.00 ul	Channel Name:	280.3nm
Run Time:	70.0 Minutes	Proc. Chnl. Descr.:	2998 PDA 280.3 nm (2998
Date Acquired:	2/7/2019 3:39:33 PM HKT		
Date Processed:	13/3/2023 2:32:04 AM HKT		

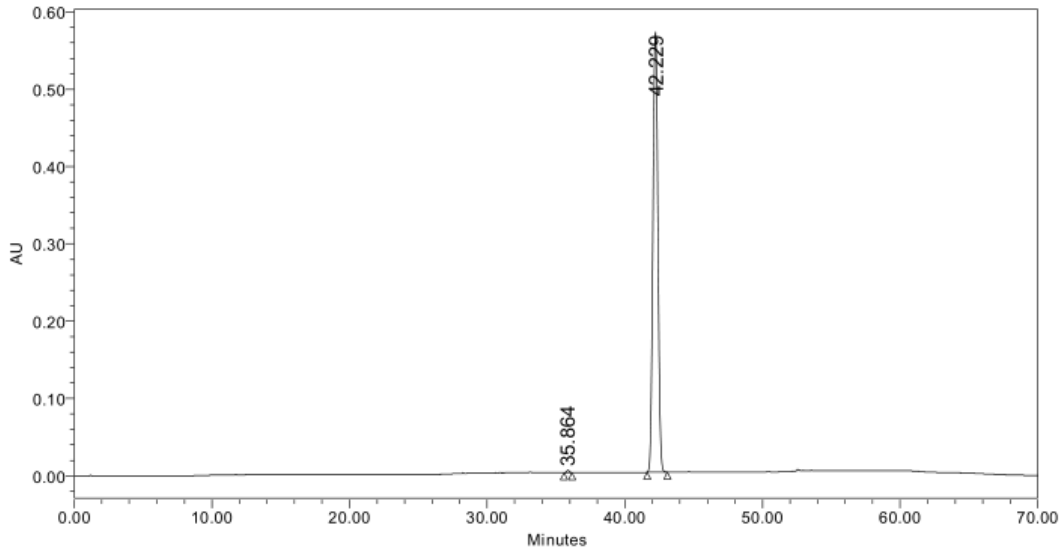

	RT	Area	% Area	Height
1	35.864	40522	0.28	3086
2	42.229	14292953	99.72	569751

GII-2

Empower 3 SOFTWARE

Default Individual Report

SAMPLE INFORMATION

Sample Name:	NusG_D18	Acquired By:	System
Sample Type:	Unknown	Sample Set Name:	nusG_20190702
Vial:	1:C,7	Acq. Method Set:	NusG
Injection #:	1	Processing Method	lypd18g036
Injection Volume:	10.00 ul	Channel Name:	279.1nm
Run Time:	70.0 Minutes	Proc. Chnl. Descr.:	2998 PDA 279.1 nm (2998
Date Acquired:	2/7/2019 4:49:53 PM HKT		
Date Processed:	13/3/2023 2:30:43 AM HKT		

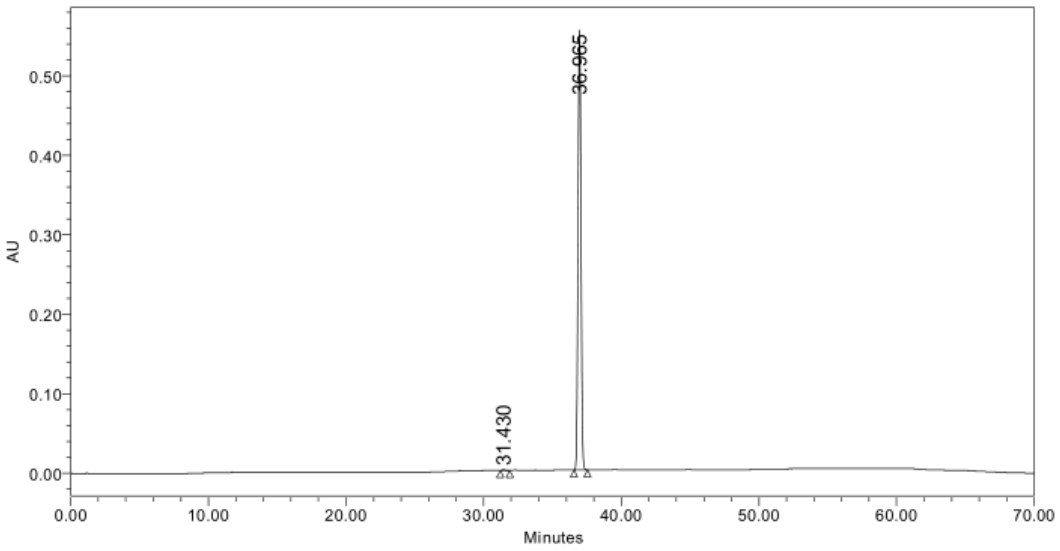

	RT	Area	% Area	Height
1	31.430	12087	0.15	1400
2	36.965	8229901	99.85	553599

GII-3

Empower 3 SOFTWARE

Default Individual Report

SAMPLE INFORMATION

Sample Name:	NusG_D8	Acquired By:	System
Sample Type:	Unknown	Sample Set Name:	nusG_20190702
Vial:	1:C,3	Acq. Method Set:	NusG
Injection #:	1	Processing Method	lypd8
Injection Volume:	10.00 ul	Channel Name:	279.1nm
Run Time:	70.0 Minutes	Proc. Chnl. Descr.:	2998 PDA 279.1 nm (2998
Date Acquired:	2/7/2019 12:08:29 PM HKT		
Date Processed:	13/3/2023 2:33:35 AM HKT		

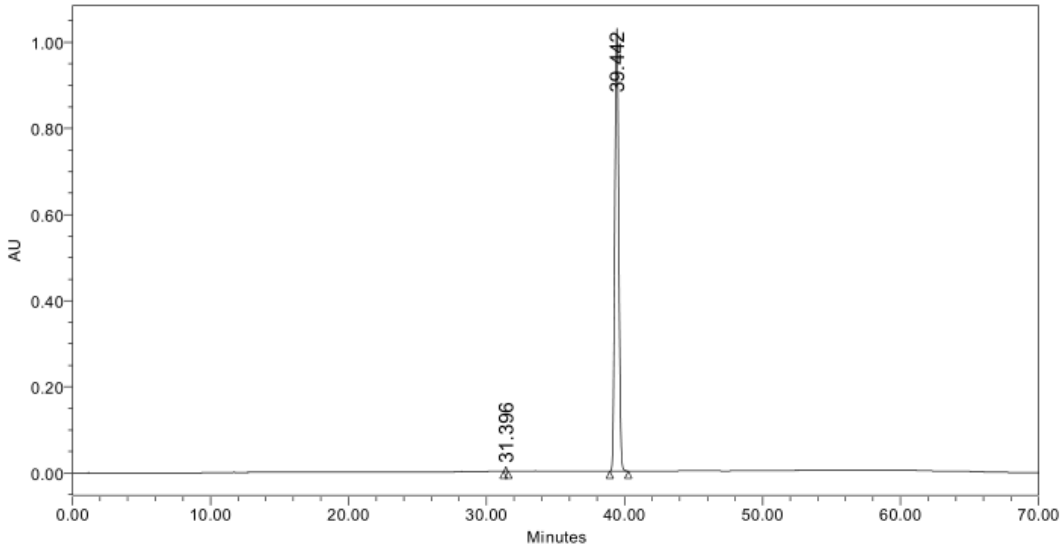

	RT	Area	% Area	Height
1	31.396	84345	0.41	10491
2	39.442	20437668	99.59	1028439

GII-4

Empower 3 SOFTWARE

Default Individual Report

SAMPLE INFORMATION

Sample Name:	GII4	Acquired By:	System
Sample Type:	Standard	Sample Set Name:	11
Vial:	1:A,1	Acq. Method Set:	NusG link
Injection #:	1	Processing Method	GII4
Injection Volume:	10.00 ul	Channel Name:	297.0nm
Run Time:	40.0 Minutes	Proc. Chnl. Descr.:	2998 PDA 297.0 nm (2998
Date Acquired:	4/20/2023 5:02:50 AM HKT		
Date Processed:	4/23/2023 4:53:17 AM HKT		

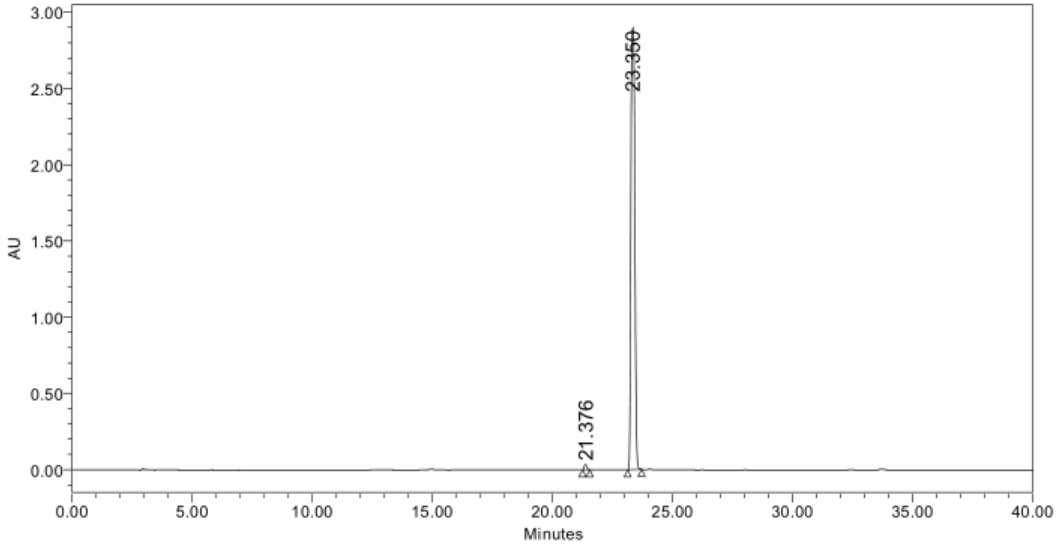

	RT	Area	% Area	Height
1	21.376	267076	0.81	35536
2	23.350	32853984	99.19	2901750

GII-5

Empower 3 SOFTWARE

Default Individual Report

SAMPLE INFORMATION

Sample Name:	GII5	Acquired By:	System
Sample Type:	Standard	Sample Set Name:	111
Vial:	1:A,2	Acq. Method Set:	NusG link
Injection #:	1	Processing Method	GII5
Injection Volume:	10.00 ul	Channel Name:	274.4nm
Run Time:	40.0 Minutes	Proc. Chnl. Descr.:	2998 PDA 274.4 nm (2998
Date Acquired:	17/4/2023 5:44:38 AM HKT		
Date Processed:	17/4/2023 7:28:24 AM HKT		

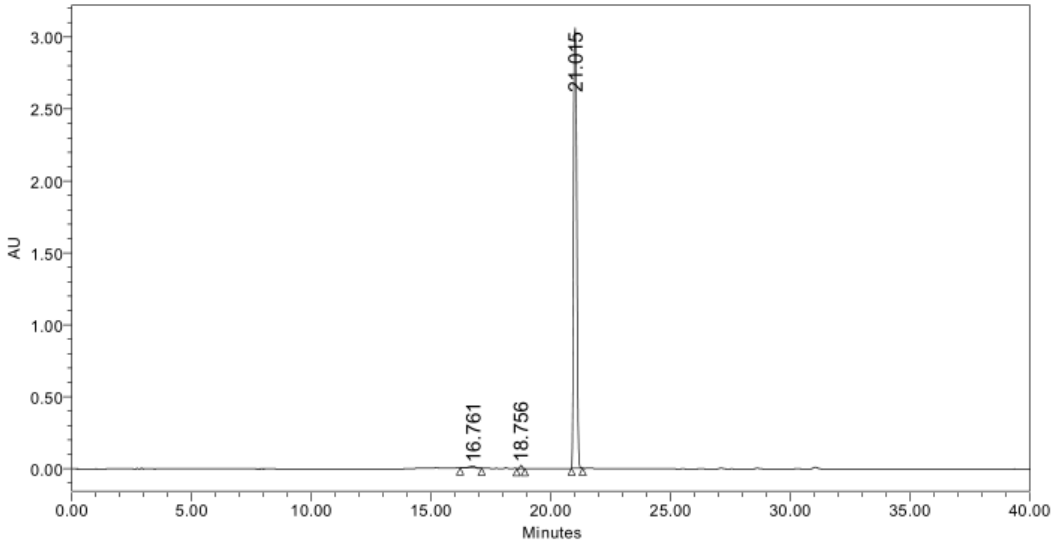

	RT	Area	% Area	Height
1	16.761	217746	0.75	12620
2	18.756	145656	0.50	21991
3	21.015	28704337	98.75	3062248

GII-6

Empower 3 SOFTWARE

Default Individual Report

SAMPLE INFORMATION

Sample Name:	033	Acquired By:	LLYM
Sample Type:	Standard	Sample Set Name:	11
Vial:	1:F,1	Acq. Method Set:	NusG link
Injection #:	1	Processing Method	033
Injection Volume:	10.00 ul	Channel Name:	333.8nm
Run Time:	40.0 Minutes	Proc. Chnl. Descr.:	2998 PDA 333.8 nm (2998
Date Acquired:	5/31/2023 7:01:28 AM HKT		
Date Processed:	5/31/2023 7:44:06 AM HKT		

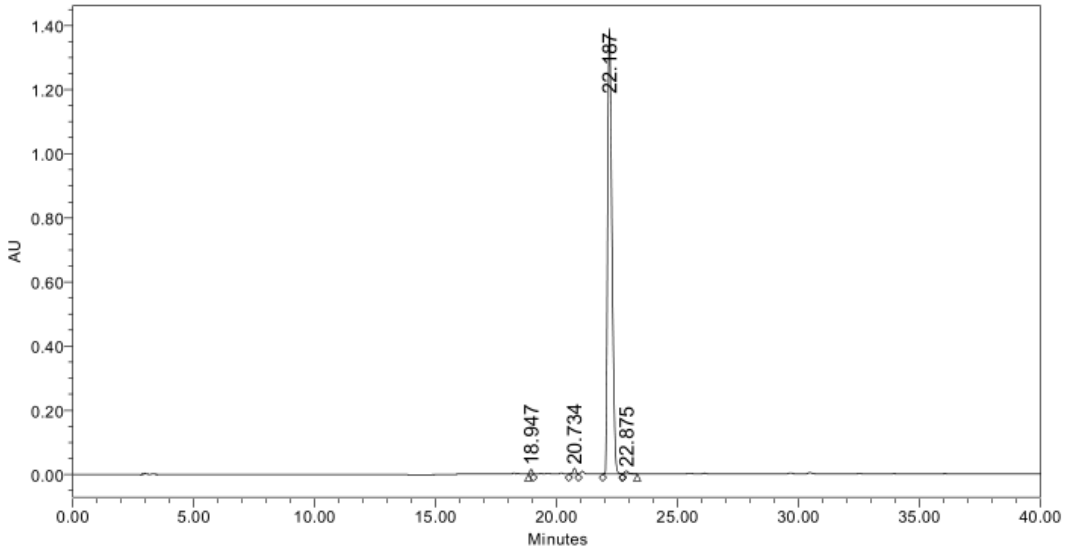

	RT	Area	% Area	Height
1	18.947	97683	0.56	14346
2	20.734	144566	0.82	17827
3	22.187	17254444	98.04	1389239
4	22.875	102145	0.58	9840

GII-7

Empower 3 SOFTWARE

Default Individual Report

SAMPLE INFORMATION

Sample Name:	D12	Acquired By:	System
Sample Type:	Standard	Sample Set Name:	D12
Vial:	1:A,1	Acq. Method Set:	NusG link
Injection #:	1	Processing Method	D12
Injection Volume:	10.00 ul	Channel Name:	282.7nm
Run Time:	40.0 Minutes	Proc. Chnl. Descr.:	2998 PDA 282.7 nm (2998
Date Acquired:	13/3/2023 3:53:48 AM HKT		
Date Processed:	13/3/2023 4:40:18 AM HKT		

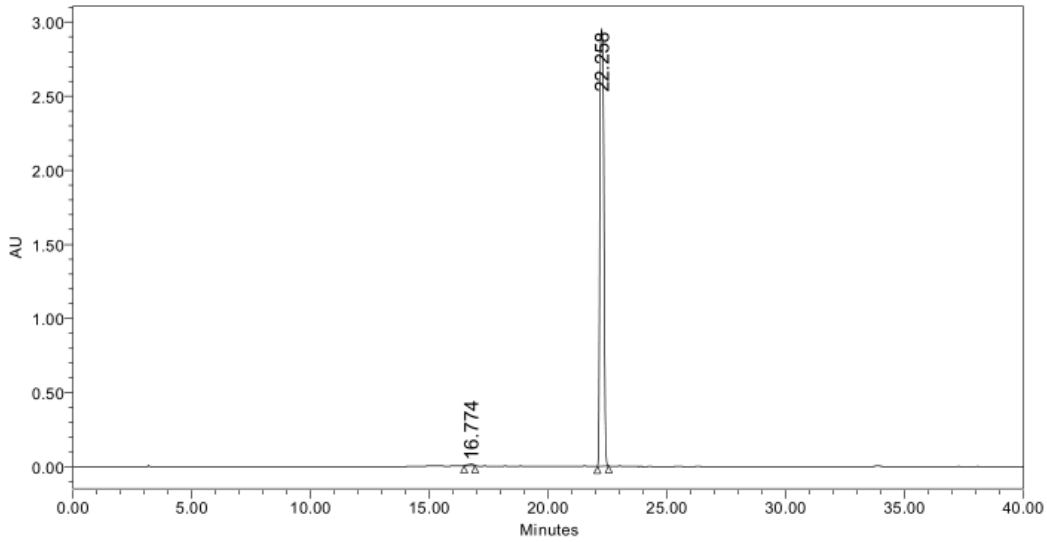

	RT	Area	% Area	Height
1	16.774	192302	0.56	11743
2	22.258	34310788	99.44	2952764

GII-8

Empower 3 SOFTWARE

Default Individual Report

SAMPLE INFORMATION

Sample Name:	d13	Acquired By:	System
Sample Type:	Standard	Sample Set Name:	07032023
Vial:	1:A,2	Acq. Method Set:	NusG link
Injection #:	1	Processing Method	d13
Injection Volume:	10.00 ul	Channel Name:	291.0nm
Run Time:	40.0 Minutes	Proc. Chnl. Descr.:	2998 PDA 291.0 nm (2998
Date Acquired:	7/3/2023 11:15:33 AM HKT		
Date Processed:	8/3/2023 1:13:05 AM HKT		

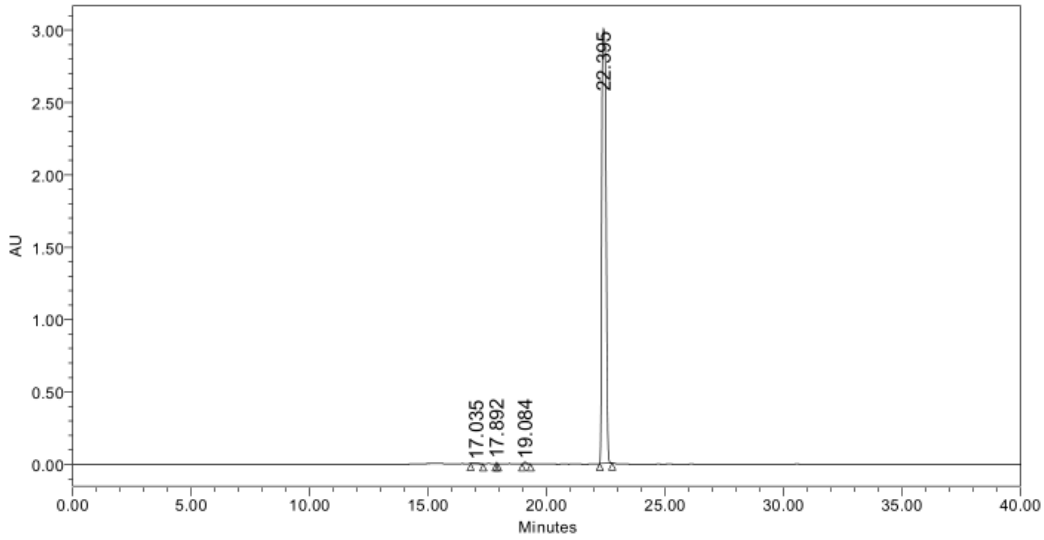

	RT	Area	% Area	Height
1	17.035	41842	0.11	3312
2	17.892	19557	0.05	14345
3	19.084	93483	0.25	13365
4	22.395	36882348	99.58	3006831

GII-9

Empower 3 SOFTWARE

Default Individual Report

SAMPLE INFORMATION

Sample Name:	D14	Acquired By:	System
Sample Type:	Standard	Sample Set Name:	1
Vial:	1:A,1	Acq. Method Set:	NusG link
Injection #:	1	Processing Method	D14
Injection Volume:	10.00 ul	Channel Name:	298.2nm
Run Time:	40.0 Minutes	Proc. Chnl. Descr.:	2998 PDA 298.2 nm (2998
Date Acquired:	9/4/2023 6:22:37 AM HKT		
Date Processed:	9/4/2023 7:21:37 AM HKT		

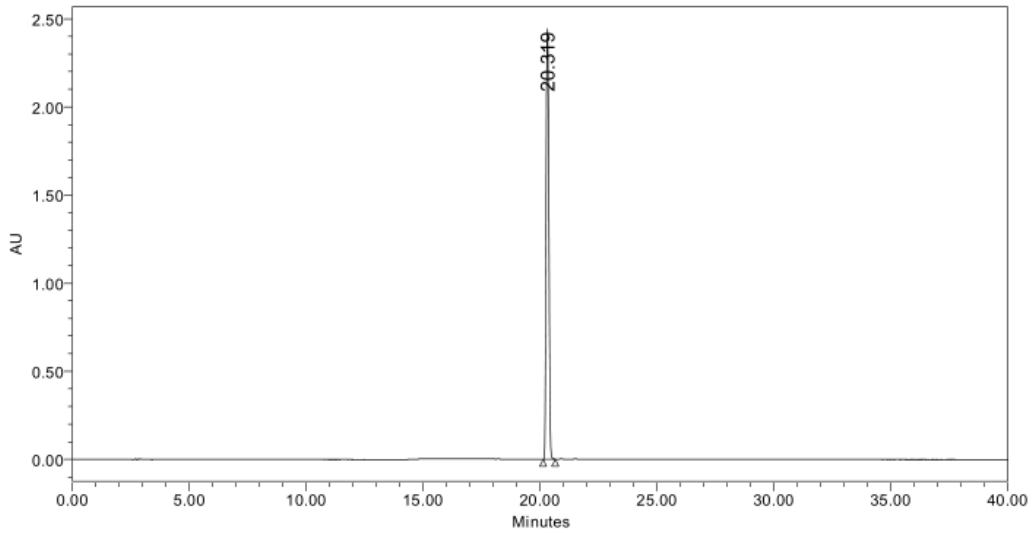

	RT	Area	% Area	Height
1	20.319	20077544	100.00	2443533

GII-10

Empower 3 SOFTWARE

Default Individual Report

SAMPLE INFORMATION

Sample Name:	d32	Acquired By:	System
Sample Type:	Standard	Sample Set Name:	03122023
Vial:	1:A,5	Acq. Method Set:	NusG link
Injection #:	1	Processing Method	D32
Injection Volume:	10.00 ul	Channel Name:	297.0nm
Run Time:	40.0 Minutes	Proc. Chnl. Descr.:	2998 PDA 297.0 nm (2998
Date Acquired:	12/3/2023 1:55:01 PM HKT		
Date Processed:	12/3/2023 10:42:58 PM HKT		

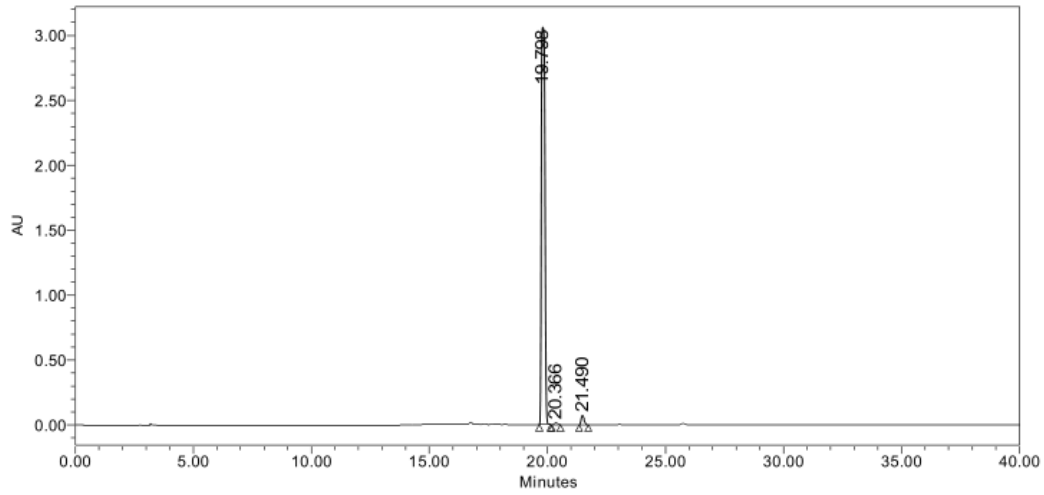

	RT	Area	% Area	Height
1	19.798	32895218	97.74	3063796
2	20.366	144250	0.43	16546
3	21.490	617026	1.83	72906

GII-11

Empower 3 SOFTWARE

Default Individual Report

SAMPLE INFORMATION

Sample Name:	rightthio	Acquired By:	System
Sample Type:	Standard	Sample Set Name:	1
Vial:	1:A,1	Acq. Method Set:	NusG link
Injection #:	1	Processing Method	RIGHTTHIO
Injection Volume:	10.00 ul	Channel Name:	310.3nm
Run Time:	40.0 Minutes	Proc. Chnl. Descr.:	2998 PDA 310.3 nm (2998
Date Acquired:	25/3/2023 10:22:16 AM HKT		
Date Processed:	26/3/2023 12:09:06 AM HKT		

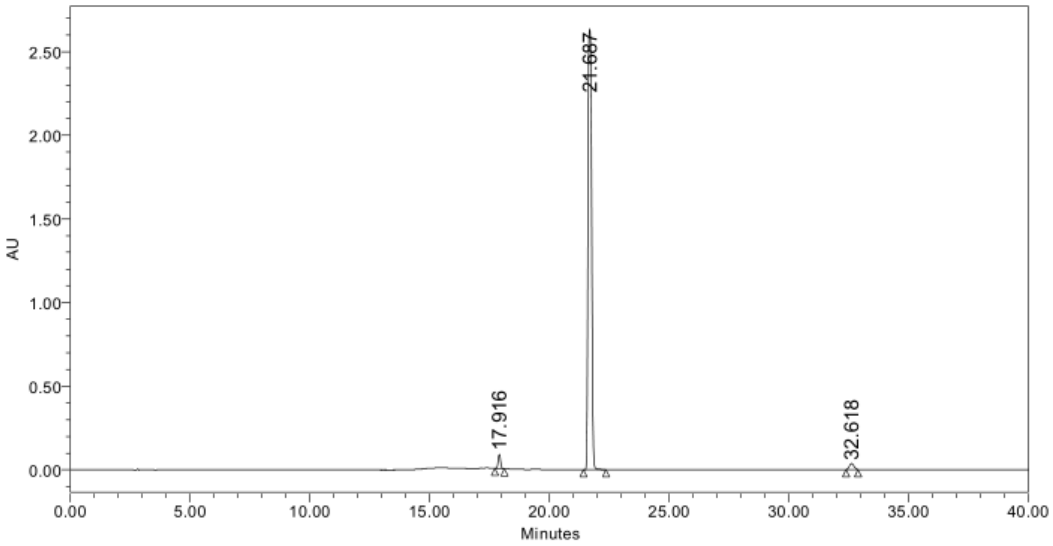

	RT	Area	% Area	Height
1	17.916	592470	2.05	86078
2	21.687	27816002	96.22	2636015
3	32.618	500245	1.73	36261

GII-12

Empower 3 SOFTWARE

Default Individual Report

SAMPLE INFORMATION

Sample Name:	D16	Acquired By:	System
Sample Type:	Standard	Sample Set Name:	1
Vial:	1:A,1	Acq. Method Set:	NusG link
Injection #:	1	Processing Method	D16
Injection Volume:	10.00 ul	Channel Name:	324.1nm
Run Time:	40.0 Minutes	Proc. Chnl. Descr.:	2998 PDA 324.1 nm (2998
Date Acquired:	9/4/2023 10:20:31 AM HKT		
Date Processed:	10/4/2023 1:29:59 AM HKT		

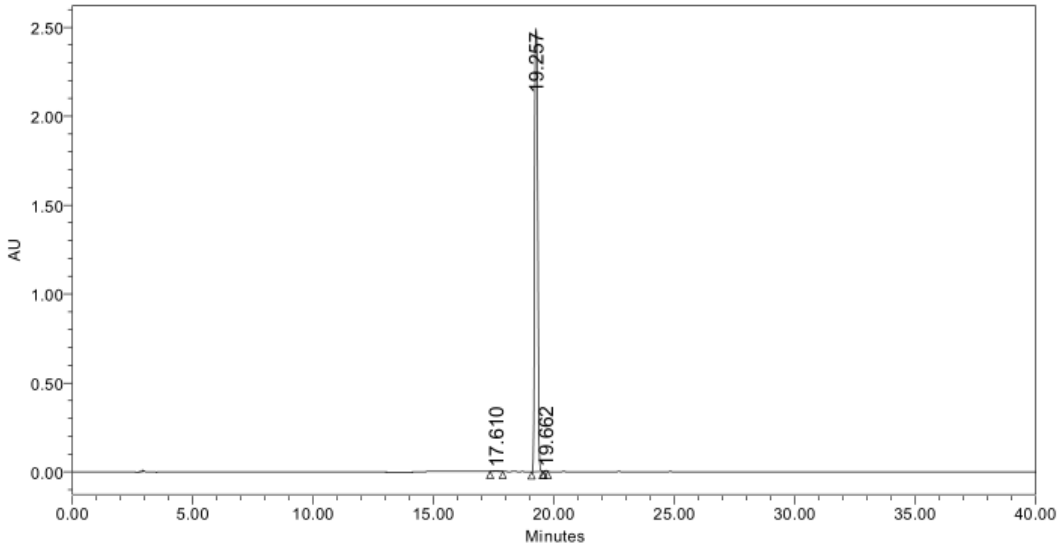

	RT	Area	% Area	Height
1	17.610	64775	0.28	4080
2	19.257	22709937	99.56	2492124
3	19.662	35548	0.16	5830

GII-13

Empower 3 SOFTWARE

Default Individual Report

SAMPLE INFORMATION

Sample Name:	D17	Acquired By:	System
Sample Type:	Standard	Sample Set Name:	11
Vial:	1:A,1	Acq. Method Set:	NusG link
Injection #:	1	Processing Method	D17
Injection Volume:	10.00 ul	Channel Name:	297.0nm
Run Time:	40.0 Minutes	Proc. Chnl. Descr.:	2998 PDA 297.0 nm (2998
Date Acquired:	1/4/2023 2:49:46 AM HKT		
Date Processed:	1/4/2023 3:52:20 AM HKT		

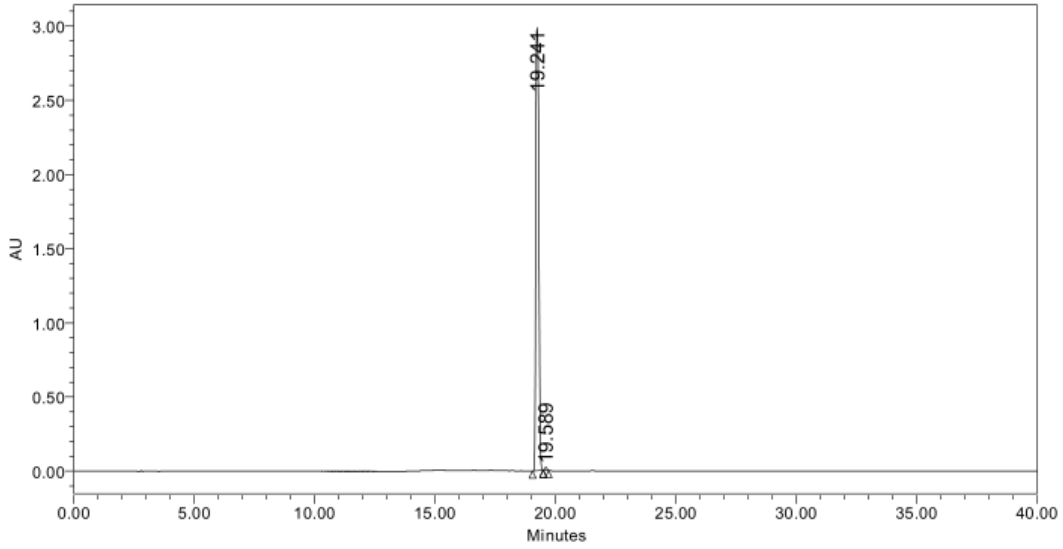

	RT	Area	% Area	Height
1	19.241	26452626	99.45	2987780
2	19.589	147415	0.55	21992

GII-14

Empower 3 SOFTWARE

Default Individual Report

SAMPLE INFORMATION

Sample Name:	PYRIDINE	Acquired By:	System
Sample Type:	Standard	Sample Set Name:	11
Vial:	1:A,6	Acq. Method Set:	NusG link
Injection #:	1	Processing Method	RIGHTPYRIDINE
Injection Volume:	10.00 ul	Channel Name:	291.0nm
Run Time:	40.0 Minutes	Proc. Chnl. Descr.:	2998 PDA 291.0 nm (2998
Date Acquired:	22/3/2023 3:57:17 PM HKT		
Date Processed:	22/3/2023 11:00:12 PM HKT		

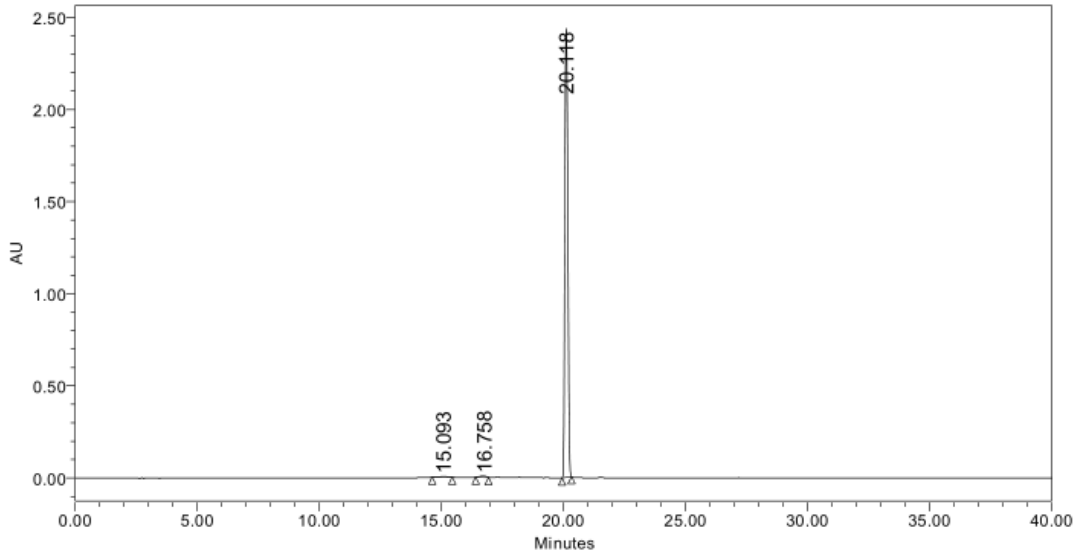

	RT	Area	% Area	Height
1	15.093	76350	0.37	3116
2	16.758	109345	0.52	5829
3	20.118	20674139	99.11	2435391

GII-15

Empower™ 3 SOFTWARE

Default Individual Report

SAMPLE INFORMATION

Sample Name:	DX	Acquired By:	System
Sample Type:	Standard	Sample Set Name:	0803
Vial:	1:A,2	Acq. Method Set:	NusG link
Injection #:	1	Processing Method	DX
Injection Volume:	10.00 ul	Channel Name:	272.0nm
Run Time:	40.0 Minutes	Proc. Chnl. Descr.:	2998 PDA 272.0 nm (2998
Date Acquired:	8/3/2023 2:33:44 AM HKT		
Date Processed:	8/3/2023 4:21:35 AM HKT		

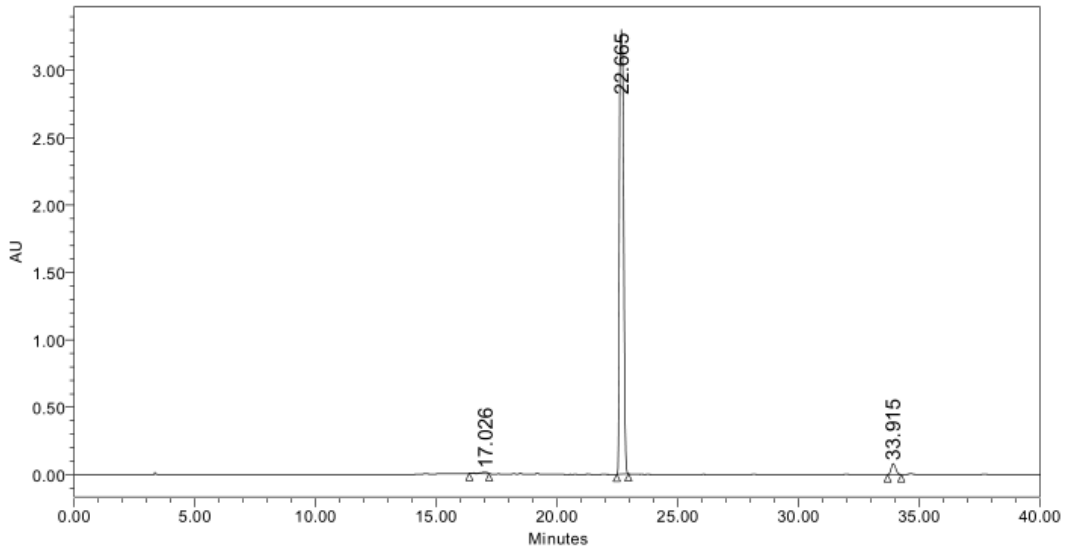

	RT	Area	% Area	Height
1	17.026	215579	0.53	10906
2	22.665	39232020	96.82	3300417
3	33.915	1071930	2.65	81078

GII-16

Empower 3 SOFTWARE

Default Individual Report

SAMPLE INFORMATION

Sample Name:	067	Acquired By:	System
Sample Type:	Standard	Sample Set Name:	03062023
Vial:	1:A,1	Acq. Method Set:	NusG link
Injection #:	1	Processing Method	g067
Injection Volume:	10.00 ul	Channel Name:	324.5nm
Run Time:	40.0 Minutes	Proc. Chnl. Descr.:	2998 PDA 324.5 nm (2998
Date Acquired:	6/3/2023 12:26:06 AM HKT		
Date Processed:	6/3/2023 4:00:25 AM HKT		

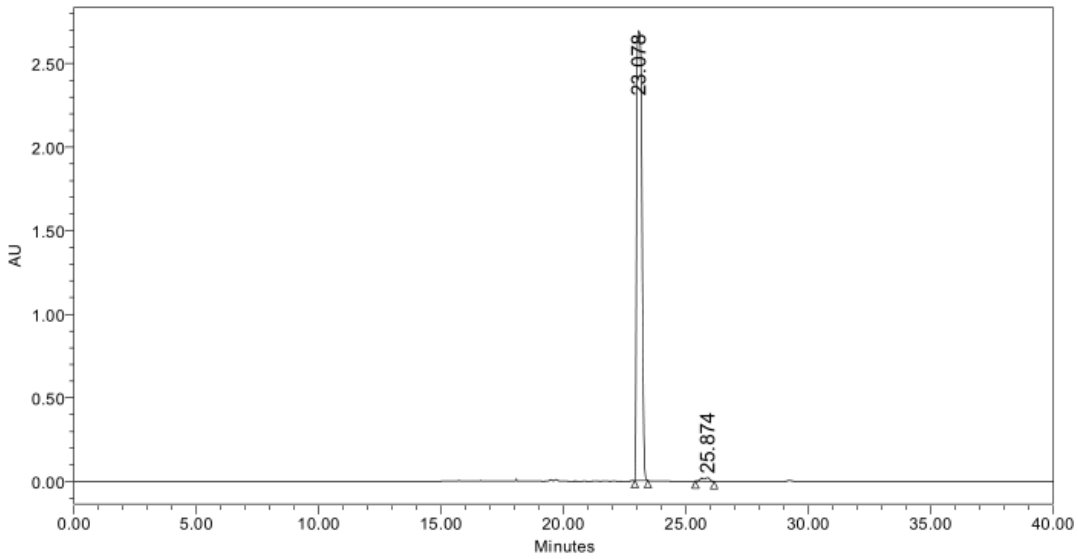

	RT	Area	% Area	Height
1	23.078	39922526	98.82	2691493
2	25.874	478157	1.18	23580

GII-17

Empower 3 SOFTWARE

Multi Sample Summary

SAMPLE INFORMATION

Sample Name:	NusG_D6	Acquired By:	System
Sample Type:	Unknown	Sample Set Name	nusG_20190702
Vial:	1:C,1	Acq. Method Set:	NusG
Injection #:	1	Processing Method	NusG_A2
Injection Volume:	10.00 ul	Channel Name:	NusG_A2
Run Time:	70.0 Minutes	Proc. Chnl. Descr.:	2998 PDA 254.0 nm (2998
Date Acquired:	7/2/2019 9:47:48 AM HKT		
Date Processed:	7/3/2019 5:19:44 PM HKT		

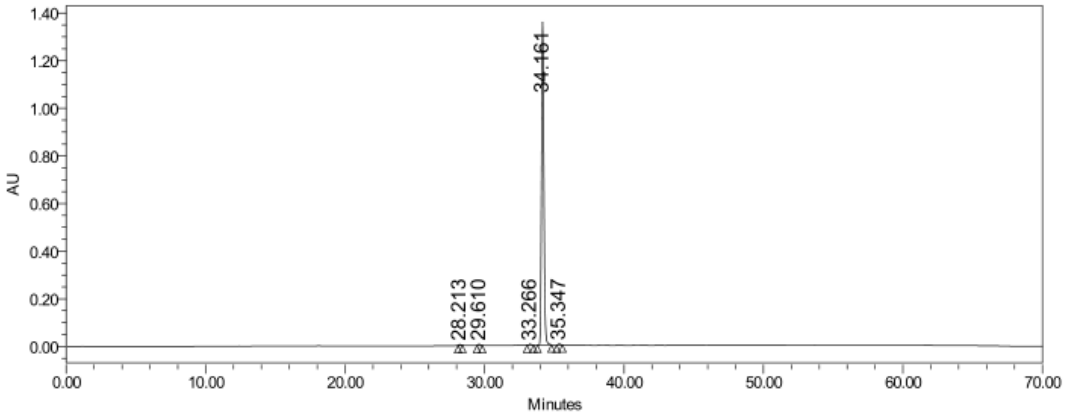

	RT	Area	% Area	Height
1	28.213	29629	0.18	5236
2	29.610	50923	0.31	6207
3	33.266	51812	0.32	4778
4	34.161	16056999	98.89	1355504
5	35.347	47807	0.29	4337

GII-18

Empower 3 SOFTWARE

Default Individual Report

SAMPLE INFORMATION

Sample Name:	LEFTthio	Acquired By:	System
Sample Type:	Standard	Sample Set Name:	111
Vial:	1:A,3	Acq. Method Set:	NusG link
Injection #:	1	Processing Method	LEFTTHIO
Injection Volume:	10.00 ul	Channel Name:	298.2nm
Run Time:	40.0 Minutes	Proc. Chnl. Descr.:	2998 PDA 298.2 nm (2998
Date Acquired:	17/4/2023 6:55:02 AM HKT		
Date Processed:	17/4/2023 10:07:00 AM HKT		

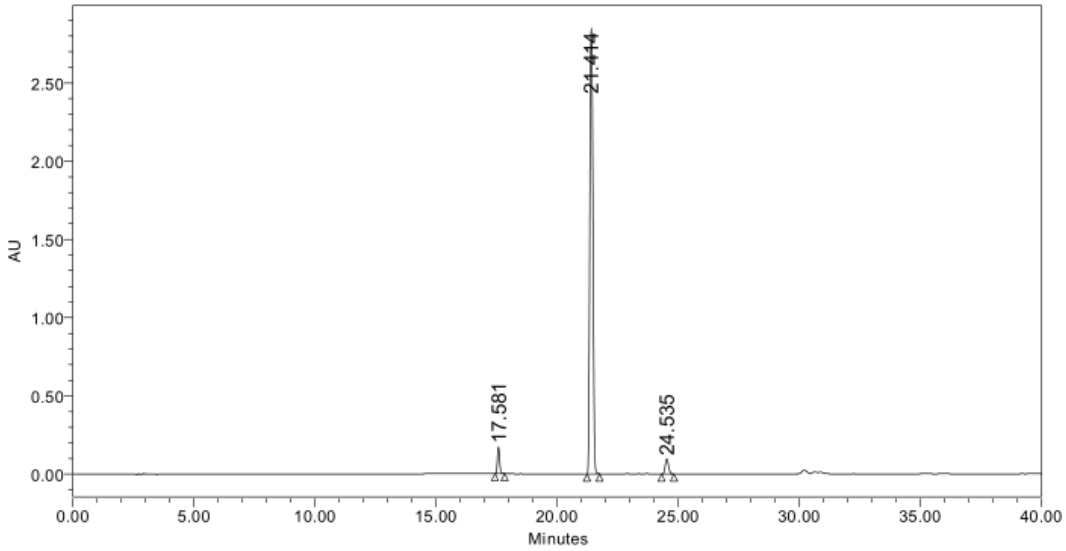

	RT	Area	% Area	Height
1	17.581	1080136	3.92	173075
2	21.414	25536927	92.71	2849618
3	24.535	929250	3.37	96081

GII-19

Empower 3 SOFTWARE

Default Individual Report

SAMPLE INFORMATION

Sample Name:	left cn	Acquired By:	System
Sample Type:	Standard	Sample Set Name:	1403
Vial:	1:A,1	Acq. Method Set:	NusG link
Injection #:	1	Processing Method	left cn
Injection Volume:	10.00 ul	Channel Name:	291.0nm
Run Time:	40.0 Minutes	Proc. Chnl. Descr.:	2998 PDA 291.0 nm (2998
Date Acquired:	14/3/2023 10:57:00 PM HKT		
Date Processed:	15/3/2023 1:38:51 AM HKT		

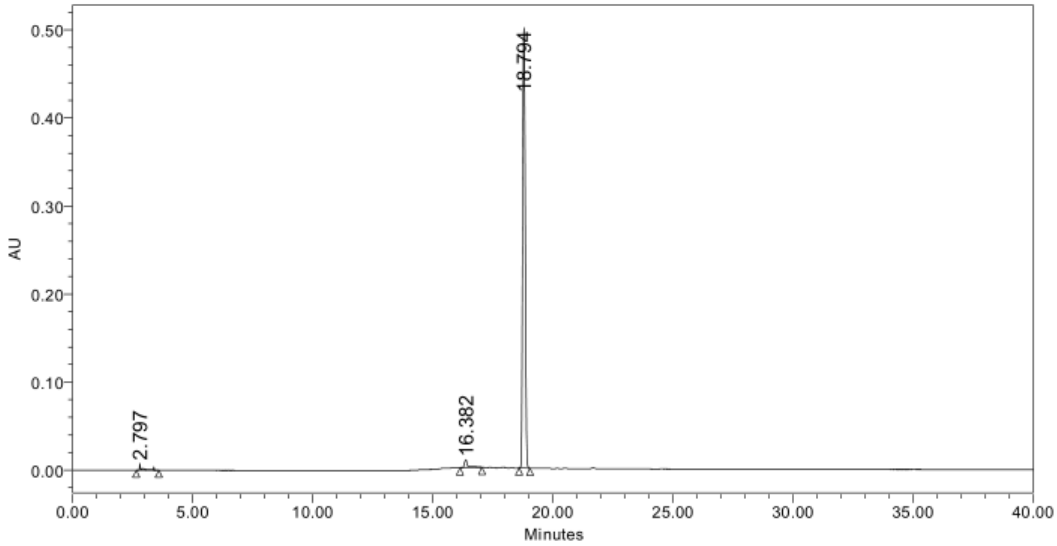

	RT	Area	% Area	Height
1	2.797	49170	1.29	7619
2	16.382	97641	2.56	8989
3	18.794	3674221	96.16	500093

GII-20

Empower 3 SOFTWARE

Default Individual Report

SAMPLE INFORMATION

Sample Name:	G088	Acquired By:	System
Sample Type:	Standard	Sample Set Name:	11
Vial:	1:A,2	Acq. Method Set:	NusG link
Injection #:	1	Processing Method	G089
Injection Volume:	10.00 ul	Channel Name:	292.2nm
Run Time:	40.0 Minutes	Proc. Chnl. Descr.:	2998 PDA 292.2 nm (2998
Date Acquired:	4/20/2023 6:13:14 AM HKT		
Date Processed:	4/23/2023 4:51:51 AM HKT		

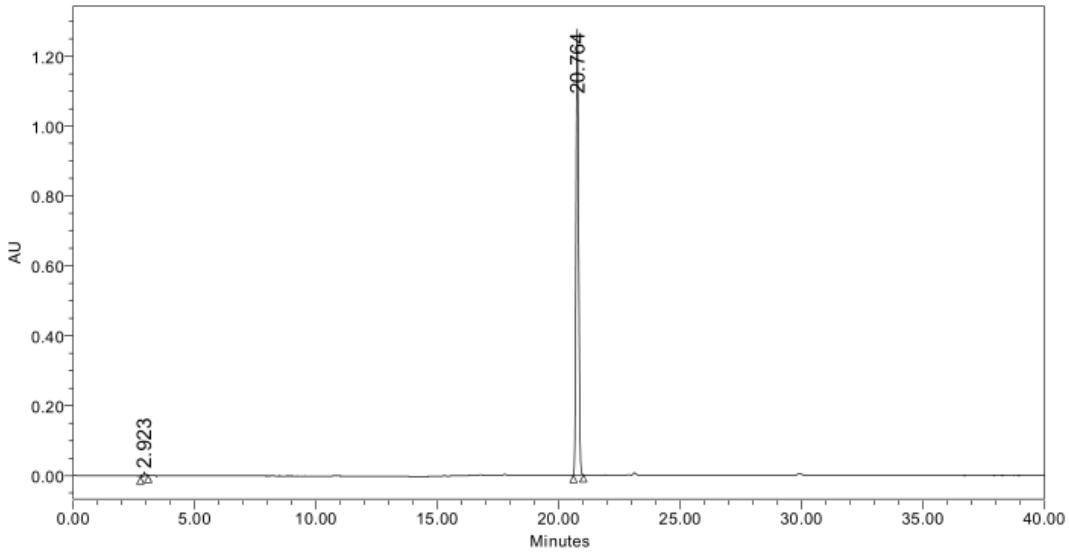

	RT	Area	% Area	Height
1	2.923	70891	0.73	11373
2	20.764	9588780	99.27	1277268

GII-21

Empower 3 SOFTWARE

Default Individual Report

SAMPLE INFORMATION

Sample Name:	d21	Acquired By:	System
Sample Type:	Standard	Sample Set Name:	1403
Vial:	1:A,2	Acq. Method Set:	NusG link
Injection #:	1	Processing Method	d211
Injection Volume:	10.00 ul	Channel Name:	251.3nm
Run Time:	40.0 Minutes	Proc. Chnl. Descr.:	2998 PDA 251.3 nm (2998
Date Acquired:	15/3/2023 12:07:24 AM HKT		
Date Processed:	15/3/2023 3:03:35 AM HKT		

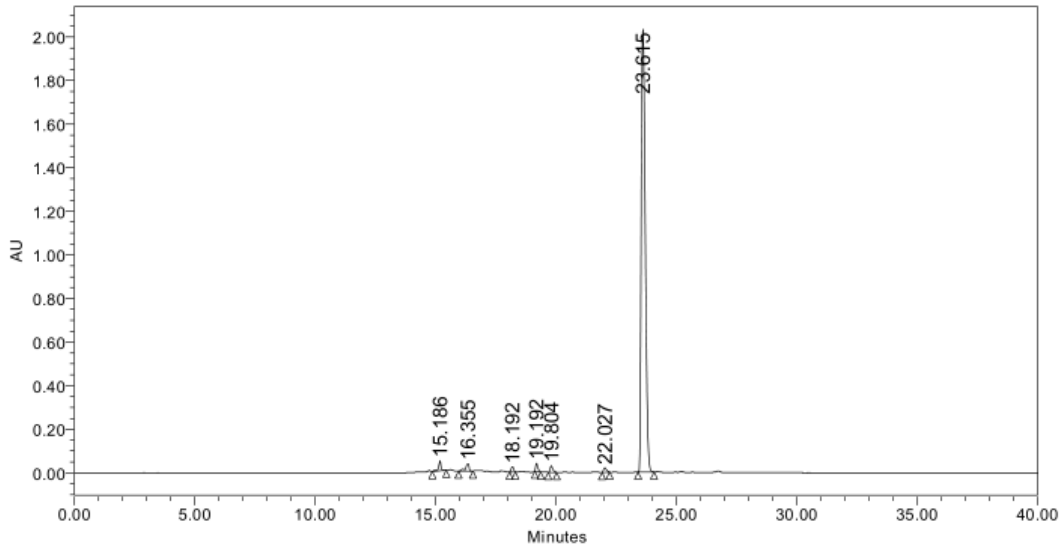

	RT	Area	% Area	Height
1	15.186	293500	1.17	46014
2	16.355	360100	1.44	33702
3	18.192	173313	0.69	23715
4	19.192	239187	0.95	38013
5	19.804	220980	0.88	30726
6	22.027	173161	0.69	20975
7	23.615	23593468	94.17	2033752

GII-22

Empower 3 SOFTWARE

Default Individual Report

SAMPLE INFORMATION

Sample Name:	left s	Acquired By:	System
Sample Type:	Standard	Sample Set Name:	03122023
Vial:	1:A,3	Acq. Method Set:	NusG link
Injection #:	1	Processing Method	LEFT S
Injection Volume:	10.00 ul	Channel Name:	251.8nm
Run Time:	40.0 Minutes	Proc. Chnl. Descr.:	2998 PDA 251.8 nm (2998
Date Acquired:	12/3/2023 11:34:12 AM HKT		
Date Processed:	12/3/2023 10:50:21 PM HKT		

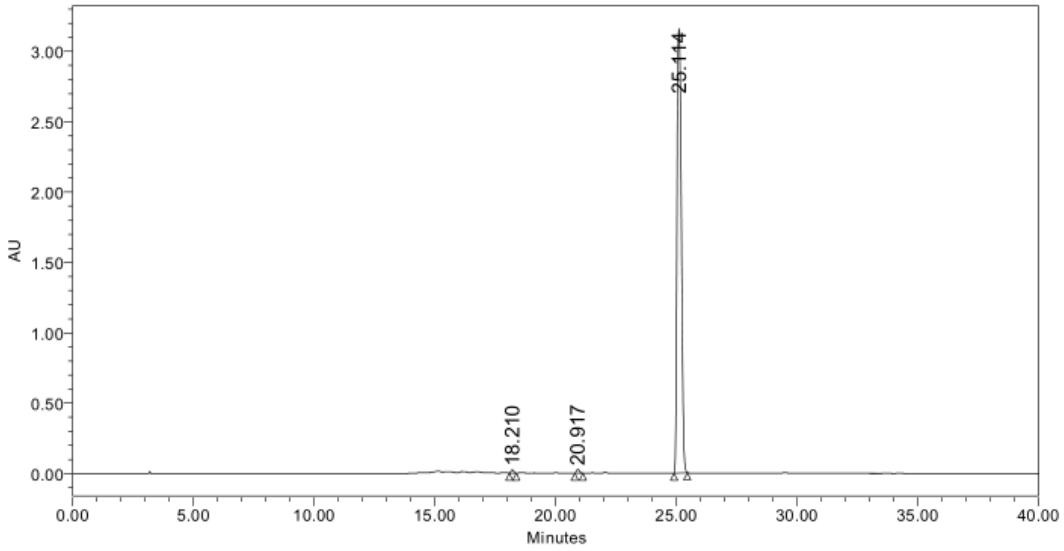

	RT	Area	% Area	Height
1	18.210	174404	0.44	23649
2	20.917	246662	0.62	29092
3	25.114	39195904	98.94	3157813

GII-23

Empower 3 SOFTWARE

Default Individual Report

SAMPLE INFORMATION

Sample Name:	d31	Acquired By:	System
Sample Type:	Standard	Sample Set Name:	1
Vial:	1:A,1	Acq. Method Set:	NusG link
Injection #:	1	Processing Method	d31
Injection Volume:	10.00 ul	Channel Name:	295.8nm
Run Time:	40.0 Minutes	Proc. Chnl. Descr.:	2998 PDA 295.8 nm (2998
Date Acquired:	29/3/2023 4:24:53 AM HKT		
Date Processed:	29/3/2023 5:08:37 AM HKT		

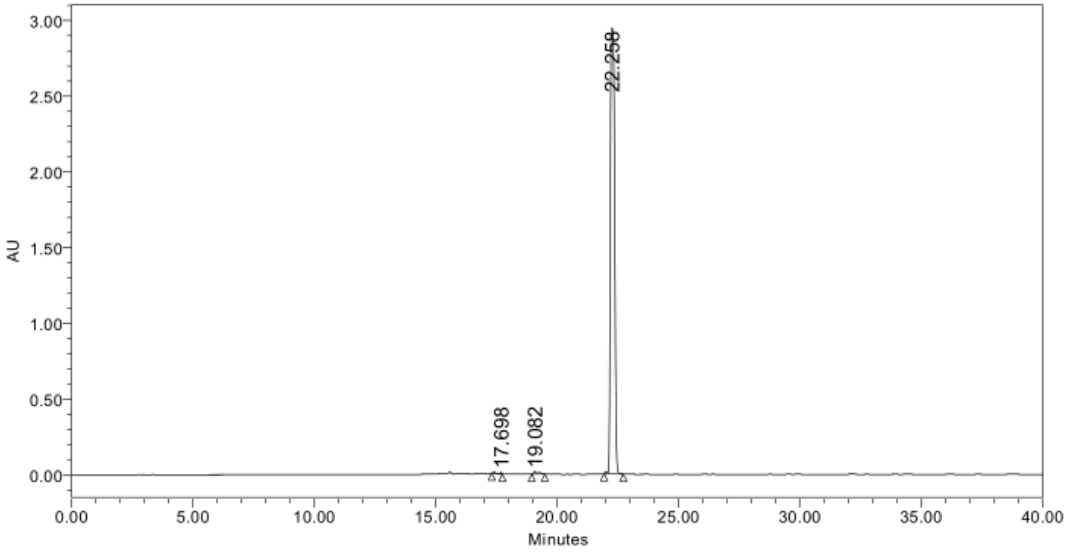

	RT	Area	% Area	Height
1	17.698	81447	0.23	13428
2	19.082	266820	0.74	19944
3	22.258	35646601	99.03	2947707

GII-24

Empower 3 SOFTWARE

Default Individual Report

SAMPLE INFORMATION

Sample Name:	d20	Acquired By:	System
Sample Type:	Standard	Sample Set Name:	1
Vial:	1:A,4	Acq. Method Set:	NusG link
Injection #:	1	Processing Method	D20
Injection Volume:	10.00 ul	Channel Name:	303.1nm
Run Time:	40.0 Minutes	Proc. Chnl. Descr.:	2998 PDA 303.1 nm (2998
Date Acquired:	25/3/2023 1:53:30 PM HKT		
Date Processed:	26/3/2023 12:03:22 AM HKT		

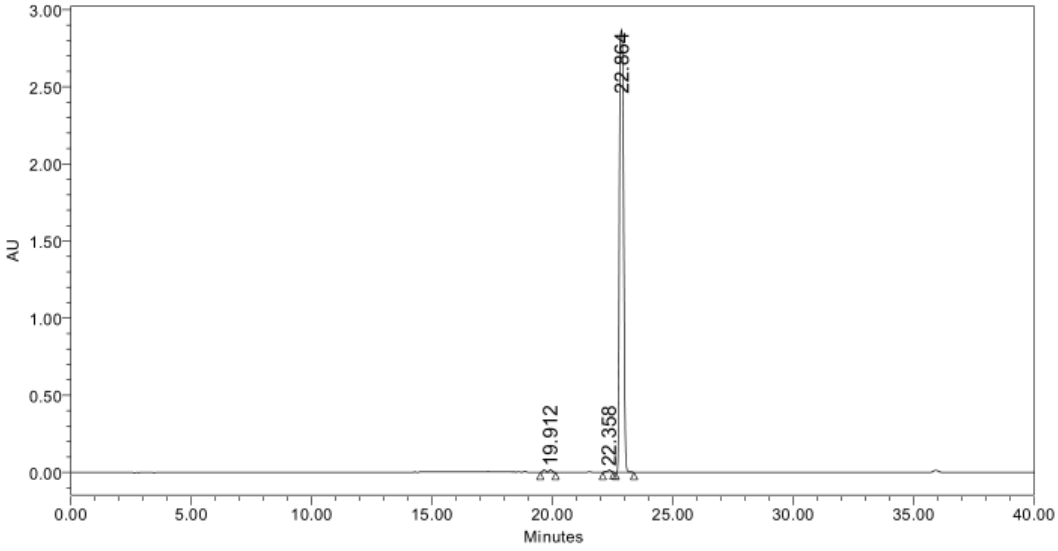

	RT	Area	% Area	Height
1	19.912	258616	0.75	16825
2	22.358	176474	0.51	14449
3	22.864	34100639	98.74	2873646

GII-25

Empower 3 SOFTWARE

Default Individual Report

SAMPLE INFORMATION

Sample Name:	nooh	Acquired By:	System
Sample Type:	Standard	Sample Set Name:	1303
Vial:	1:A,1	Acq. Method Set:	NusG link
Injection #:	1	Processing Method	nooh
Injection Volume:	10.00 ul	Channel Name:	295.8nm
Run Time:	40.0 Minutes	Proc. Chnl. Descr.:	2998 PDA 295.8 nm (2998
Date Acquired:	13/3/2023 2:36:31 AM HKT		
Date Processed:	13/3/2023 3:34:10 AM HKT		

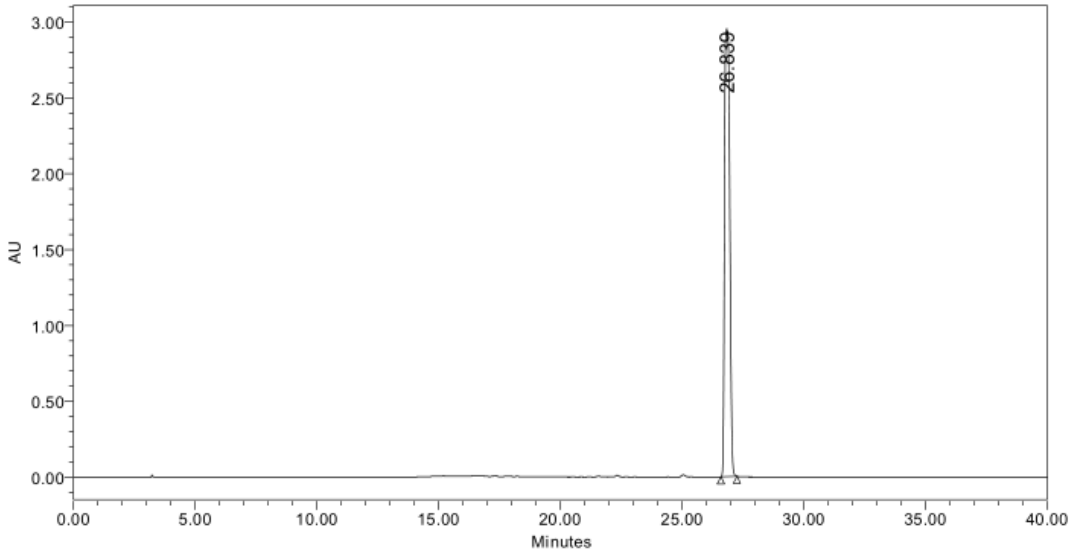

	RT	Area	% Area	Height
1	26.839	43799010	100.00	2955970

GII-26

Empower 3 SOFTWARE

Default Individual Report

SAMPLE INFORMATION

Sample Name:	gii26	Acquired By:	GUest
Sample Type:	Standard	Sample Set Name:	11
Vial:	1:B,1	Acq. Method Set:	NusG link
Injection #:	1	Processing Method	050
Injection Volume:	10.00 ul	Channel Name:	331.7nm
Run Time:	40.0 Minutes	Proc. Chnl. Descr.:	2998 PDA 331.7 nm (2998
Date Acquired:	5/27/2023 5:17:48 AM HKT		
Date Processed:	5/27/2023 7:27:32 AM HKT		

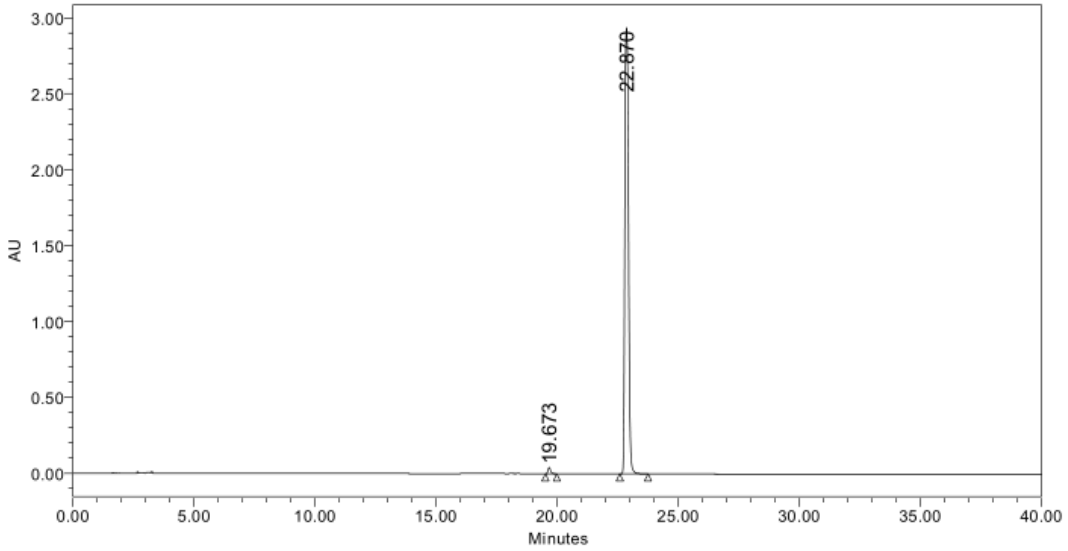

	RT	Area	% Area	Height
1	19.673	294189	0.94	41154
2	22.870	30906870	99.06	2941623

GII-27

Empower 3 SOFTWARE

Default Individual Report

SAMPLE INFORMATION

Sample Name:	D26	Acquired By:	System
Sample Type:	Standard	Sample Set Name:	111
Vial:	1:A,4	Acq. Method Set:	NusG link
Injection #:	1	Processing Method	D26
Injection Volume:	10.00 ul	Channel Name:	319.7nm
Run Time:	40.0 Minutes	Proc. Chnl. Descr.:	2998 PDA 319.7 nm (2998
Date Acquired:	17/4/2023 8:05:24 AM HKT		
Date Processed:	17/4/2023 10:05:47 AM HKT		

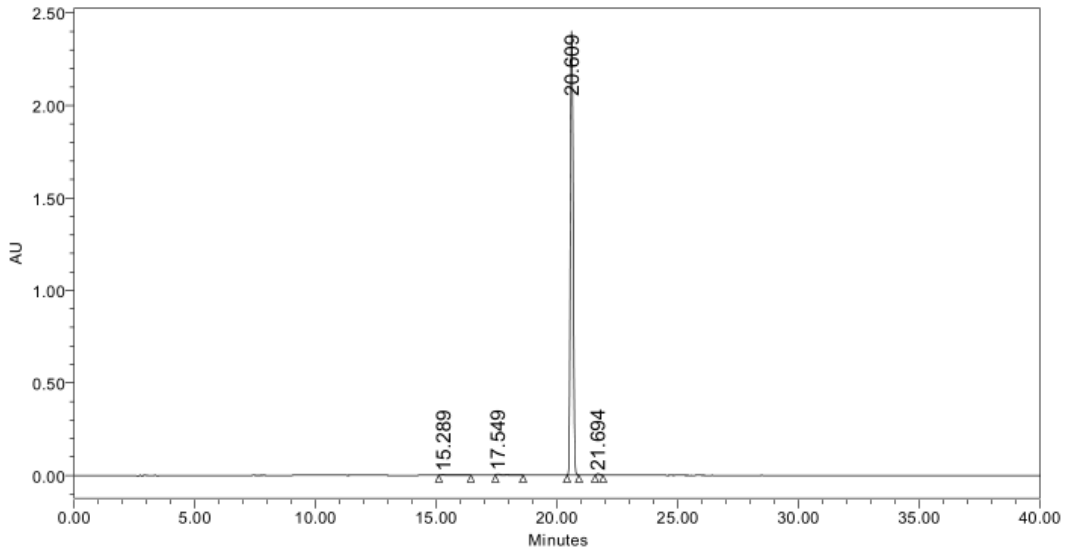

	RT	Area	% Area	Height
1	15.289	19445	0.10	783
2	17.549	61933	0.31	4184
3	20.609	19581585	99.26	2401187
4	21.694	64246	0.33	7802

GII-28

Empower 3 SOFTWARE

Default Individual Report

SAMPLE INFORMATION

Sample Name:	D27	Acquired By:	System
Sample Type:	Standard	Sample Set Name:	D27
Vial:	1:A,1	Acq. Method Set:	NusG link
Injection #:	1	Processing Method	d27
Injection Volume:	10.00 ul	Channel Name:	285.1nm
Run Time:	40.0 Minutes	Proc. Chnl. Descr.:	2998 PDA 285.1 nm (2998
Date Acquired:	13/3/2023 10:26:39 AM HKT		
Date Processed:	14/3/2023 12:19:17 AM HKT		

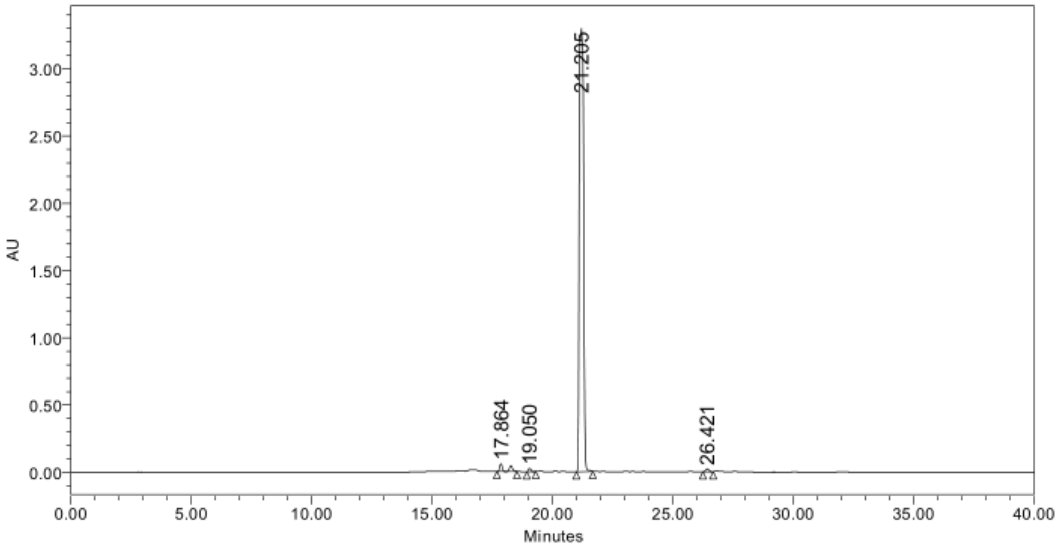

	RT	Area	% Area	Height
1	17.864	793933	1.88	59766
2	19.050	186645	0.44	25478
3	21.205	41027703	97.15	3296289
4	26.421	222014	0.53	22406

GII-29

Empower 3 SOFTWARE

Default Individual Report

SAMPLE INFORMATION

Sample Name:	middlepyridine	Acquired By:	System
Sample Type:	Standard	Sample Set Name:	1
Vial:	1:A,2	Acq. Method Set:	NusG link
Injection #:	1	Processing Method	MIDDLEPYRIDINE
Injection Volume:	10.00 ul	Channel Name:	310.2nm
Run Time:	40.0 Minutes	Proc. Chnl. Descr.:	2998 PDA 310.2 nm (2998
Date Acquired:	25/3/2023 11:32:40 AM HKT		
Date Processed:	26/3/2023 12:07:11 AM HKT		

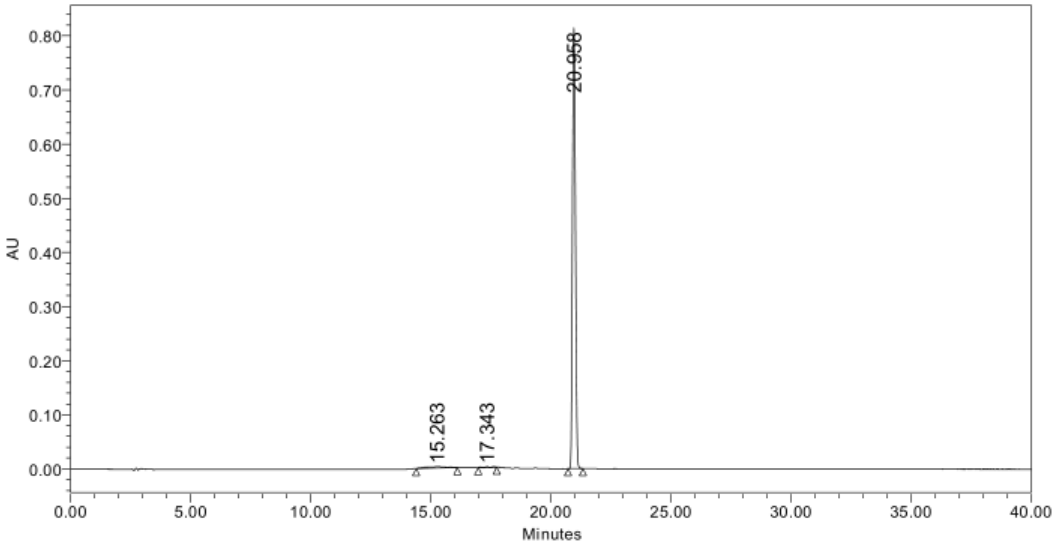

	RT	Area	% Area	Height
1	15.263	139863	1.94	2383
2	17.343	26888	0.37	1416
3	20.958	7044853	97.69	814469

GII-30

Empower 3 SOFTWARE

Default Individual Report

SAMPLE INFORMATION

Sample Name:	middlecf3	Acquired By:	System
Sample Type:	Standard	Sample Set Name:	1
Vial:	1:A,3	Acq. Method Set:	NusG link
Injection #:	1	Processing Method	MIDDLECF3
Injection Volume:	10.00 ul	Channel Name:	297.0nm
Run Time:	40.0 Minutes	Proc. Chnl. Descr.:	2998 PDA 297.0 nm (2998
Date Acquired:	25/3/2023 12:43:05 PM HKT		
Date Processed:	26/3/2023 12:05:17 AM HKT		

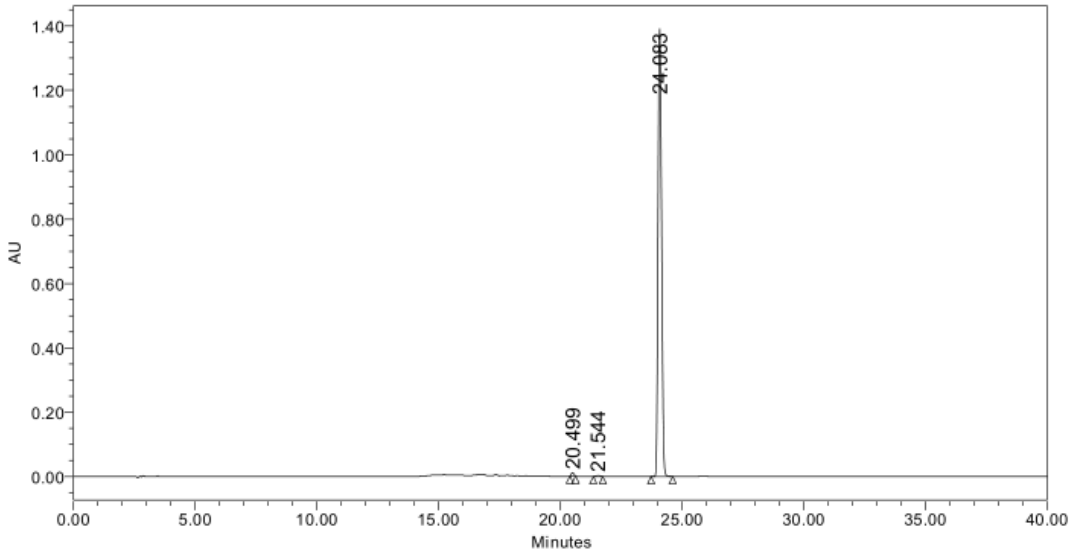

	RT	Area	% Area	Height
1	20.499	78728	0.56	10418
2	21.544	26887	0.19	3001
3	24.083	13999858	99.25	1391077

GII-31

Empower 3 SOFTWARE

Default Individual Report

SAMPLE INFORMATION

Sample Name:	G088	Acquired By:	System
Sample Type:	Standard	Sample Set Name:	11
Vial:	1:A,1	Acq. Method Set:	NusG link
Injection #:	1	Processing Method	G088
Injection Volume:	10.00 ul	Channel Name:	276.7nm
Run Time:	40.0 Minutes	Proc. Chnl. Descr.:	2998 PDA 276.7 nm (2998
Date Acquired:	4/23/2023 5:02:36 AM HKT		
Date Processed:	4/24/2023 4:12:30 AM HKT		

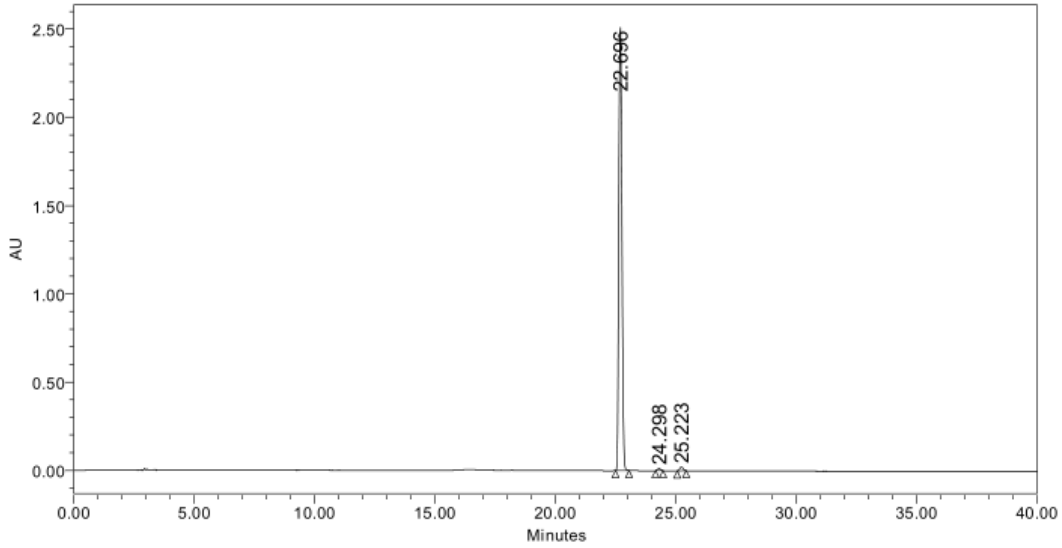

	RT	Area	% Area	Height
1	22.696	22488902	98.59	2512279
2	24.298	110837	0.49	12312
3	25.223	211090	0.93	21273

GII-32

Empower 3 SOFTWARE

Default Individual Report

SAMPLE INFORMATION

Sample Name:	D1	Acquired By:	System
Sample Type:	Standard	Sample Set Name:	1
Vial:	1:A,1	Acq. Method Set:	NusG link
Injection #:	1	Processing Method	D1
Injection Volume:	10.00 ul	Channel Name:	277.9nm
Run Time:	40.0 Minutes	Proc. Chnl. Descr.:	2998 PDA 277.9 nm (2998
Date Acquired:	24/3/2023 3:41:14 AM HKT		
Date Processed:	24/3/2023 8:42:00 AM HKT		

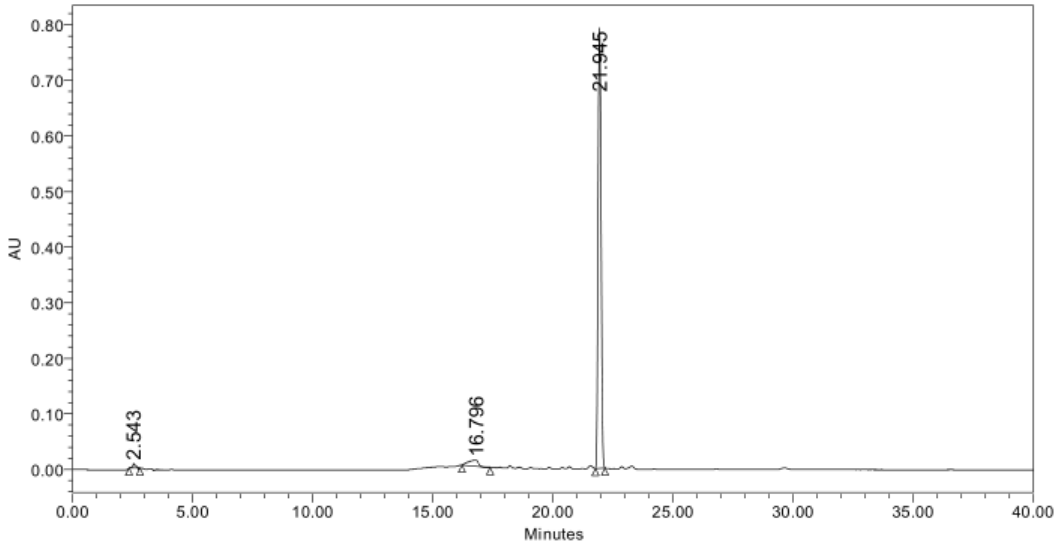

	RT	Area	% Area	Height
1	2.543	76737	1.05	8564
2	16.796	312091	4.27	10879
3	21.945	6918300	94.68	792220

GII-33

Empower 3 SOFTWARE

Default Individual Report

SAMPLE INFORMATION

Sample Name:	NusG_D23	Acquired By:	System
Sample Type:	Unknown	Sample Set Name:	NusG_20190702_1
Vial:	1:D,3	Acq. Method Set:	NusG
Injection #:	1	Processing Method	lypd23g040
Injection Volume:	10.00 ul	Channel Name:	294.6nm
Run Time:	70.0 Minutes	Proc. Chnl. Descr.:	2998 PDA 294.6 nm (2998
Date Acquired:	2/7/2019 11:33:30 PM HKT		
Date Processed:	13/3/2023 2:28:43 AM HKT		

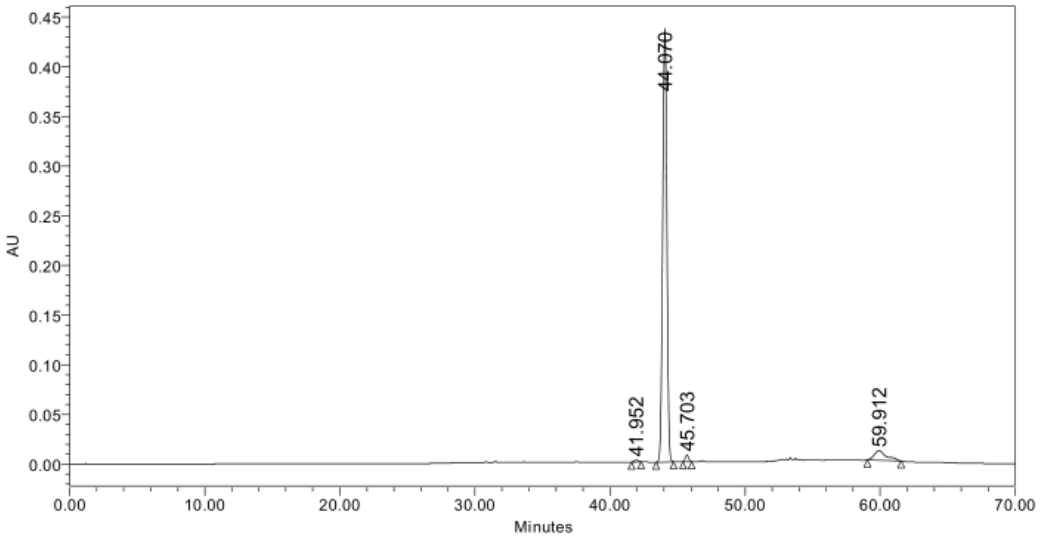

	RT	Area	% Area	Height
1	41.952	40896	0.40	1932
2	44.070	9394319	92.43	436384
3	45.703	114221	1.12	6762
4	59.912	613765	6.04	9588